Charakterisierung und strukturbasierte Optimierung von 9*H*-Pyrimido[4,5-*b*]indolen als neuartige, reversible Inhibitoren der Glykogen Synthase Kinase-3β

vorgelegt von

Stanislav Emilov Andreev

aus Sofia/Bulgarien

Tübingen

2020

Gedruckt mit Genehmigung der Mathematisch-Naturwissenschaftlichen Fakultät der Eberhard Karls Universität Tübingen.

Tag der mündlichen Qualifikation: 17.12.2020

Stellvertretender Dekan: Prof. Dr. József Fortágh

1. Berichterstatter: Prof. Dr. Pierre Koch

2. Berichterstatter: Prof. Dr. Stefan Laufer

3. Berichterstatter: Jun.-Prof. Dr. Matthias Gehringer

Die in dieser Dissertation dargelegte Arbeit wurde in der Zeit von 01.08.2015 bis 19.11.2020 am Pharmazeutischen Institut der Eberhard Karls Universität Tübingen unter der Anleitung von Prof. Dr. Pierre Koch durchgeführt.

за Тати, Чичо и Дядо

Vielen Dank an

Zusammenfassung der Arbeit

Die Glykogen Synthase Kinase-3β (GSK-3β) stellt mit mehr als 40 mutmaßlichen Substraten und einer Beteiligung in mehreren Signalwegen einen Knotenpunkt der intrazellulären Signaltransduktion dar. Eine Dysregulation dieses Enzyms wird mit verschiedenen pathologischen Zuständen in Verbindung gebracht, darunter Diabetes, Krebs, kardiovaskuläre Erkrankungen und Neurodegeneration. Im Besonderen wird dieser Kinase eine entscheidende Rolle in der Entstehung der Alzheimer-Krankheit zugeschrieben. Da für diese neurodegenerative Erkrankung aktuell keine krankheitsmodifizierenden Therapeutika zur Verfügung stehen, ist die Entwicklung neuer Inhibitoren der GSK-3β Gegenstand intensiver Forschung.

Im Rahmen dieser Arbeit sollte eine neue Strukturklasse an 9*H*-Pyrimido[4,5-*b*]indol-basierten GSK-3β-Inhibitoren charakterisiert und optimiert werden. Dies beinhaltete die Identifikation essenzieller Strukturmerkmale der Inhibitoren für eine potente Hemmung der Zielkinase, die Ableitung der wesentlichen Struktur-Aktivitäts-Beziehungen (SAR), die Untersuchung von Bindemodi sowie eine weitergehende biologische Charakterisierung hinsichtlich metabolischer Stabilität, off-Target-Effekten und in zellulären Assays. Als Ausgangspunkt diente dazu ein moderat potenter Kinom-*Screening-Hit*, der sich vom zugelassenen pan-JAK-Inhibitor Tofacitinib ableitet.

Eine neu etablierte, flexible Synthesestrategie ermöglichte eine effiziente Darstellung strukturell diverser Derivate. Diese Verbindungen wurden in einem ADP Glo^{TM} Kinase Assay evaluiert und dadurch entscheidende Strukturelemente zur Verbesserung der Hemmaktivität an der Zielkinase identifiziert. Die Bindemodi von ausgewählten Inhibitoren wurden durch Röntgenstrukturanalyse oder *in silico* Modellierung beleuchtet und für die Rationalisierung der abgeleiteten SAR sowie die Planung weiterer Optimierungsschritte herangezogen. Der strukturbasierte Optimierungsprozess resultierte schließlich in sehr potenten Inhibitoren mit IC_{50}-Werten im einstelligen nanomolaren Bereich. Flankierend wurde durch ein erfolgreiches Konzept zur Stabilisierung eines metabolischen Hotspots die Problematik einer unzureichenden mikrosomalen Stabilität adressiert. Wichtige Inhibitoren aus dieser Arbeit zeigten vielversprechende Ergebnisse in Selektivitätsscreenings und Zytotoxizitätsstudien und unterstreichen damit die Relevanz der neu etablierten Strukturklasse an GSK-3β-Inhibitoren.

Abkürzungsverzeichnis

ABL	Abelson Proto-Onkogen
AcOH	Essigsäure
ADAM	*a disintegrin and metalloprotease*
ADP	Adenosindiphosphat
AGC	Proteinkinase A, G und C
AICD	APP-Intrazellulärdomäne
Ala	Alanin
AMP-PNP	Adenylyl-imidodiphosphat
APC	Adenomatöse Polyposis Coli
aPK	atypische Proteinkinase
APP	*Amyloid Precursor Protein*
Arg	Arginin
Asp	Asparaginsäure
ATP	Adenosintriphosphat
BACE	*β-Site APP cleaving enzyme*
BCR	*Breakpoint Cluster Region* Gen
Boc	tert-Butyloxycarbonyl
CAMK	Ca2+/Calmodulin-abhängige Kinasen
CDK-5	Cyclinabhängige Kinase 5
CK	Casein Kinase
CK1	Casein Kinase 1
CMGC	**C**yclinabhängige Kinasen, **M**itogen-aktivierte Proteinkinasen, **G**lykogen-Synthase-Kinasen und **C**dk-ähnliche Kinasen

CTF	C-terminales Fragment
DC	Dünnschichtchromatographie
DCM	Dichlormethan
DC-MS	Dünnschichtchromatographie-Massenspektrometrie-Kopplung
DMSO	Dimethylsulfoxid
Dvl	*Dishevelled*
EGFR	*Epidermal growth factor receptor*
ePK	eukaryotische Proteinkinase
ESI-MS	Elektrospray-Ionisations-Massenspektrometrie
FDA	*Food and Drug Administration*
Gln	Glutamin
Glu	Glutaminsäure
Gly	Glycin
GS	Glykogen Synthase
GSK-3	Glykogen Synthase Kinase-3
His	Histidin
HLM	Humane Lebermikrosomen
HPLC	*High performance liquid chromatography*
HR	hydrophobe Region
IC_{50}	Halbmaximale inhibitorische Konzentration
IRS	Insulin-Rezeptor-Substrat
JAK	Januskinase
KDR	Kinase-Insert-Domänenrezeptor
LCMS	*Liquid chromatography mass spectrometry*

Leu	Leucin
LLC	*Limited Liability Company*
LOK	Lymphozyten-orientierte Kinase
LRP	Lipoprotein-Rezeptor verwandtes Protein
Lys	Lysin
MAP	Microtubulus-assoziiertes Protein
MKK	Mitogen-aktivierte Proteinkinase-Kinase
MCF-7	*Michigan Cancer Foundation*-7 Zelllinie
MeOH	Methanol
MLK1	Mixed-lineage Kinase 1
MRC 5	*Medical Research Council* Zellstamm
MSK2	Mitogen- und Stressaktivierte Proteinkinase 2
NFT	Neurofibrilliäre *Tangles*
NMDA	N-Methyl-D-Asparaginsäure
NMR	*Nuclear magnetic resonance*
OPLS	*Optimized Potentials for Liquid Simulations*
PCP	*Planar cell polarity*
PDGFR	*Platelet derived growth factor receptor*
PDK1	Phosphoinositid-abhängige Kinase 1
Phe	Phenylalanin
PHF	*Paired helical filament*
PI3K	Phosphoinositid-3-Kinase
PKA	Proteinkinase A
PKB	Proteinkinase B

PKI	Proteinkinaseinhibitor
Pro	Pro
rac	racemisch
RGC	Rezeptor-Guanylyl-Zyklase
Rsk	Ribosomale S6 Kinase
SAR	Struktur-Aktivitäts-Beziehung
SEM	Standardfehler des Mittelwerts
Ser	Serin
SF	*Straight filament*
S_NAr	nukleophile Substitution am Aromaten
ß-TrCP	*β-Transducin repeat containing*
STE Kinase	Sterile Kinase
Thr	Threonin
TK	Tyrosinkinase
TKL	Tyrosinkinase-ähnliche Kinase
TLC	*Thin layer chromatography*
Tos	p-Toluensulfonyl
Tyr	Tyrosin
UV	ultraviolett
Val	Valin
VEGFR	*Vascular endothelial growth factor receptor*
Wnt	zusammengesetzt für *Wingless* und Int-1
ZNS	Zentrales Nervensystem

Liste der Publikationen als Teil dieser Dissertation

Publikation I

Design, Synthesis and Biological Evaluation of 7-Chloro-9*H*-pyrimido[4,5-*b*]indole-based Glycogen Synthase Kinase-3β Inhibitors

Stanislav Andreev, Tatu Pantsar, Francesco Ansideri, Mark Kudolo, Dieter Schollmeyer, Stefan Laufer und Pierre Koch

Molecules **2019**, *24*(12), 2331

Publikation II

Discovery and Evaluation of Enantiopure 9*H*-pyrimido[4,5-*b*]indoles as Nanomolar GSK-3β Inhibitors with Improved Metabolic Stability

Stanislav Andreev, Tatu Pantsar, Ahmed El-Gokha, Francesco Ansideri, Mark Kudolo, Débora Bublitz Anton, Giulia Sita, Jenny Romasco, Christian Geibel, Michael Lämmerhofer, Márcia Ines Goettert, Andrea Tarozzi, Stefan Laufer und Pierre Koch

Int. J. Mol. Sci. **2020**, *21*(21), 7823

Publikation III

Addressing a Trapped High-Energy Water: Design and Synthesis of Highly Potent 9*H*-pyrimido[4,5-*b*]indole-based GSK-3β Inhibitors

Stanislav Andreev, Tatu Pantsar, Roberta Tesch, Niclas Kahlke, Ahmed El-Gokha, Francesco Ansideri, Lukas Grätz, Jenny Romasco, Giulia Sita, Christian Geibel, Michael Lämmerhofer, Andrea Tarozzi, Stefan Knapp, Stefan Laufer und Pierre Koch

Manuskript wurde beim Journal of Medicinal Chemistry eingereicht..

Liste weiterer Publikationen, die während dieser Forschungsperiode entstanden sind

A Diverse and Versatile Regiospecific Synthesis of Tetrasubstituted Alkylsulfanylimidazoles as p38α Mitogen-Activated Protein Kinase Inhibitors

Francesco Ansideri, Stanislav Andreev, Annette Kuhn, Wolfgang Albrecht, Stefan A. Laufer und Pierre Koch

Molecules **2018**, *23*, 221

N^1-(4-(2-(Methylthio)-1H-imidazol-5-yl)pyridin-2-yl)benzene-1,4-diamine

Ahmed El-Gokha, Francesco Ansideri, Stanislav Andreev, Dieter Schollmeyer, Stefan A. Laufer und Pierre Koch

Molbank **2019**, *2019*(1), M1048

Autorenbeiträge

Publikation I

Design, Synthesis and Biological Evaluation of 7-Chloro-9*H*-pyrimido[4,5-*b*]indole-based Glycogen Synthase Kinase-3β Inhibitors

Molecules **2019**, *24*(12), 2331

<u>Stanislav Andreev</u>

- Syntheseplanung
- Synthese und chemische Analyse von 19 Testverbindungen (95%)
- Kristallisation einer Verbindung für die Röntgenstrukturanalyse
- Koordination von nicht-synthetischen Experimenten
- Interpretation der Ergebnisse von allen biologischen Studien und nicht-synthetischen Experimenten
- Verfassen des Manuskripts

Dr. Tatu Pantsar

- *In silico*-Experimente und molekulares Modeling
- Erstellung von Grafiken für das Manuskript
- Verfassen von Teilen des Manuskripts
- Korrekturlesen des Manuskripts

Dr. Francesco Ansideri

- Durchführung des ADP Glo^{TM} Kinase Assays zur Bestimmung der IC$_{50}$-Werte der publizierten Verbindungen und Auswertung der Rohdaten

Mark Kudolo

- Durchführung der Lebermikrosomen-Studie zur Bewertung der metabolischen Stabilität ausgewählter Verbindungen und Auswertung der Rohdaten

Dr. Michael Forster

- Durchführung von vorausgegangenen synthetischen Experimenten
- Synthese und chemische Analyse von einer Testverbindung (5%)
- Korrekturlesen des Manuskripts

Dr. Dieter Schollmeyer

- Strukturaufklärung einer ausgewählten Verbindung mittels Röntgenkristallographie

Prof. Stefan Laufer

- Initiation, Koordination und Betreuung des Projekts

Prof. Pierre Koch

- Initiation, Koordination und Betreuung des Projekts
- Verfassen, Korrekturlesen und finale Freigabe des Manuskripts

Publikation II

Discovery and Evaluation of Enantiopure 9*H*-pyrimido[4,5-*b*]indoles as Nanomolar GSK-3β Inhibitors with Improved Metabolic Stability

Int. J. Mol. Sci. **2020**, *21*(21), 7823

Stanislav Andreev

- Syntheseplanung
- Synthese und chemische Analyse von 38 Testverbindungen (ca. 80%)
- Koordination von nicht-synthetischen Experimenten
- Interpretation der Ergebnisse von allen biologischen Studien und nicht-synthetischen Experimenten
- Verfassen und Korrekturlesen des Manuskripts

Dr. Tatu Pantsar

- In *silico*-Experimente und molekulares Modeling
- Erstellung von Grafiken für das Manuskript
- Verfassen von Teilen des Manuskripts
- Korrekturlesen des Manuskripts

Dr. Ahmed El-Gokha

- Syntheseplanung
- Synthese und chemische Analyse von 10 Testverbindungen (ca. 20%)
- Korrekturlesen des Manuskripts

Dr. Francesco Ansideri

- Durchführung des ADP Glo^{TM} Kinase Assays zur Bestimmung der IC_{50}-Werte der publizierten Verbindungen und Auswertung der Rohdaten

Mark Kudolo

- Durchführung Lebermikrosomen-Studie zur Bewertung der metabolischen Stabilität ausgewählter Verbindungen und Auswertung der Rohdaten

Débora Bublitz Anton

- Durchführung der Studie zur Bestimmung der Zytotoxizität ausgewählter Verbindungen in verschiedenen Wildtyp- und Krebszelllinien und Auswertung der Rohdaten

Giulia Sita

- Durchführung der Studien zur Bestimmung der intrazellulären GSK-3-Inhibition durch ausgewählte Verbindungen und zur Untersuchung der neuroprotektiven Effekte von ausgewählten Verbindungen und Auswertung der Rohdaten

Jenny Romasco

- Durchführung der Studien zur Bestimmung der intrazellulären GSK-3-Inhibition durch ausgewählte Verbindungen und zur Untersuchung der neuroprotektiven Effekte von ausgewählten Verbindungen und Auswertung der Rohdaten

Christian Geibel

- Durchführung der Studie zur Bestimmung der chiralen Reinheit ausgewählter Verbindungen und Auswertung der Rohdaten
- Korrekturlesen des Manuskripts

Prof. Michael Lämmerhofer

- Koordination und Betreuung der Studie zur Bestimmung der chiralen Reinheit

Prof. Márcia Ines Goettert

- Koordination und Betreuung der Zytotoxizitäts-Studie

Prof. Andrea Tarozzi

- Koordination und Betreuung der Studien zur Bestimmung der intrazellulären GSK3-Inhibition und zur Untersuchung der neuroprotektiven Effekte

Prof. Stefan Laufer

- Initiation, Koordination und Betreuung des Projekts

Prof. Pierre Koch

- Initiation, Koordination und Betreuung des Projekts
- Verfassen, Korrekturlesen und finale Freigabe des Manuskripts

Publikation III

Addressing a Trapped High-Energy Water: Design and Synthesis of Highly Potent 9*H*-pyrimido[4,5-*b*]indole based GSK-3β Inhibitors

Manuskript wurde beim Journal of Medicinal Chemistry eingereicht.

<u>Stanislav Andreev</u>*

- Syntheseplanung
- Synthese und chemische Analyse von 14 Testverbindungen (ca. 63%)
- Anleitung von Niclas Kahlke (Masterarbeit)
- Koordination von nicht-synthetischen Experimenten
- Interpretation der Ergebnisse von allen biologischen Studien und nicht-synthetischen Experimenten
- Verfassen und Korrekturlesen des Manuskripts

Dr. Tatu Pantsar*

- In *silico*-Experimente und molekulares Modeling
- Erstellung von Grafiken für das Manuskript
- Verfassen und Korrekturlesen des Manuskripts

*leisteten einen gleichwertigen Beitrag

Dr. Roberta Tesch

- Durchführung von Experimenten zur Ko-Kristallisation einer Verbindung mit der GSK-3β und Auswertung der Rohdaten

Niclas Kahlke

- Synthese und chemische Analyse von 3 Testverbindungen (ca. 14%)

Dr. Ahmed El-Gokha

- Syntheseplanung
- Synthese und chemische Analyse von 5 Testverbindungen (ca. 23%)

Dr. Francesco Ansideri

- Durchführung des ADP Glo^{TM} Kinase Assays zur Bestimmung der IC$_{50}$-Werte der publizierten Verbindungen und Auswertung der Rohdaten

Lukas Grätz

- Durchführung des NanoBRET^{TM} Assays zur Bestimmung der intrazellulären Bindeaffinitäten von ausgewählten Verbindungen und Auswertung der Rohdaten

Giulia Sita

- Durchführung der Studien zur Bestimmung der intrazellulären GSK-3-Inhibition durch ausgewählte Verbindungen und zur Untersuchung der neuroprotektiven Effekte von ausgewählten Verbindungen und Auswertung der Rohdaten

Jenny Romasco

- Durchführung der Studien zur Bestimmung der intrazellulären GSK-3-Inhibition durch ausgewählte Verbindungen und zur Untersuchung der neuroprotektiven Effekte von ausgewählten Verbindungen und Auswertung der Rohdaten

Christian Geibel

- Durchführung der Studie zur Bestimmung der chiralen Reinheit ausgewählter Verbindungen und Auswertung der Rohdaten

Prof. Michael Lämmerhofer

- Koordination und Betreuung der Studie zur Bestimmung der chiralen Reinheit

Prof. Andrea Tarozzi

- Koordination und Betreuung der Studien zur Bestimmung der intrazellulären GSK3-Inhibition und zur Untersuchung der neuroprotektiven Effekte

Prof. Stefan Knapp

- Koordination und Betreuung der Experimente zur Ko-Kristallisation und Röntgenstrukturanalyse

Prof. Stefan Laufer

- Initiation, Koordination und Betreuung des Projekts

Prof. Pierre Koch

- Initiation, Koordination und Betreuung des Projekts
- Verfassen, Korrekturlesen und finale Freigabe des Manuskripts

Inhaltsverzeichnis

1   Einleitung

1.1   Kinasen

Die reversiblen Phosphorylierungen von Proteinen und Lipiden stellen Schlüsselschritte der intrazellulären Signaltransduktion dar und werden von Kinasen katalysiert. Die Gesamtheit des humanen Genpools für diese Phosphotransferasen, das Kinom, setzt sich aus ungefähr 20 Lipidkinasen und inzwischen über 500 identifizierten Genen für Proteinkinasen zusammen (Abbildung 1).[1,2] Proteinkinasen übertragen das γ-Phosphat von Adenosintriphosphat (ATP) auf die Seitenketten der Aminosäuren Serin, Threonin und Tyrosin und beeinflussen so die Konformation und den Ladungszustand ihrer Substrate. Innerhalb der Proteinkinasen werden die (echten) eukaryotischen Proteinkinasen (ePK) von den atypischen Proteinkinasen (aPK) unterschieden (Abbildung 1). Letztere zeigen zwar aus biochemischer Sicht Kinaseaktivität, weisen jedoch nur eine geringe Sequenz- und Strukturähnlichkeit zu den ePK auf.[3]
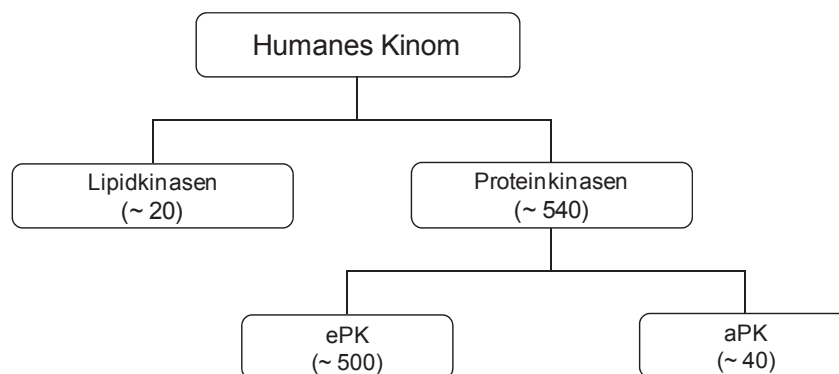
Abbildung 1.   Struktur des humanen Kinoms. Abbildung in Anlehnung an Duong-Ly *et al.*[4]

Im Folgenden sollen drei wichtige Gesichtspunkte aufgezeigt werden, die eine Kategorisierung der beachtlichen Anzahl an Proteinkinasen ermöglichen.

a) Einteilung anhand der Art der modifizierten Aminosäure

Proteinkinasen können anhand der von ihnen phosphorylierten Aminosäureseitenkette klassifiziert werden. Den über 400 Serin/Threonin-Kinasen stehen lediglich 90 Tyrosinkinasen gegenüber, die wiederum zusätzlich in membrangebundene und nicht-mebrangebundene Tyrosinkinasen unterteilt werden können. Weiterhin sind die dual-

spezifischen Proteinkinasen zu unterscheiden, die sowohl Serin- und Threonin-, als auch Tyrosinreste phosphorylieren. Prominente Beispiele für dieses sehr übersichtliche Enzymkollektiv sind die Mitogen-aktivierte Proteinkinase-Kinasen MKK1 und MKK2.[3,5]

b) Einteilung in die acht Gruppen des Proteinkinasestammbaums

Basierend auf ihrer Sequenzhomologie lassen sich die eukaryotischen Proteinkinasen in die folgenden acht Gruppen einteilen.[4]

- TK (Tyrosinkinasen)
- TKL (Tyrosinkinase-ähnliche Kinasen)
- RGC (Rezeptor-Guanylyl-Cyclasen)
- STE Kinasen
- CMGC (Cyclinabhängige Kinasen (Cdks), Mitogen-aktivierte Proteinkinasen (MAPKs), Glykogen Synthase Kinasen (GSKs) und Cdk-ähnliche Kinasen)
- CK1 (Casein kinase 1 und verwandte Kinasen)
- CAMK (Ca^{2+}/Calmodulin-abhängige Kinasen)
- AGC (Proteinkinasen A, G und C und verwandte Kinasen)

c) Unterscheidung zwischen katalytisch aktiven Kinasen und Pseudokinasen

Als dritter Gesichtspunkt soll schließlich noch das Komplement der Pseudokinasen beleuchtet werden. Diesen bisher unzureichend charakterisierten Proteinkinasen wird die vollwertige enzymatische Aktivität abgesprochen, da ihnen essentielle Strukturelemente fehlen, um den Transfer des γ-Phosphats zu katalysieren.[6] Aufgrund der konservierten Gesamtstruktur gelten diese Pseudoenzyme dennoch als Kinasen und machen etwa 10% des Kinoms aus.[3] Trotz mangelnder Enzymaktivität wird ihnen sowohl eine physiologische Relevanz als Gerüstproteine und allosterische Modulatoren aktiver Kinasen, als auch pathophysiologisches Potenzial zugesprochen.[6,7]

1.2   Proteinkinasen als Zielstrukturen für Arzneistoffe

Aufgrund des weitreichenden Einflusses zahlreicher Kinasen auf zelluläre Prozesse und Signalwege liegt vielen pathophysiologischen Veränderungen eine dysregulierte Kinaseaktivität zu Grunde. Für mehr als 180 Kinasen wird eine Krankheitsassoziation vermutet, in mehr als zwei Drittel der Fälle handelt es sich dabei um maligne Erkrankungen.[8] Proteinkinasen sind deshalb seit ca. 40 Jahren Gegenstand intensiver Forschung der pharmazeutischen Industrie und haben sich zu einem der wichtigsten Arzneistofftargets des 21. Jahrhunderts entwickelt.[9] Der Markteinführung von Imatinib (Gleevec®), dem ersten direkten Proteinkinaseinhibitor (PKI), durch die amerikanische *Food and Drug Administration* (FDA) folgten bis dato 60 weitere Wirkstoffe.[10] Von diesen wurde über die Hälfte allein in den letzten fünf Jahren zugelassen (Abbildung 2A).

Der Großteil dieser niedermolekularen Therapeutika adressiert Tyrosinkinasen (Abbildung 2B).[10] Hier kann ein Zusammenhang zur maßgeblich onkologischen Anwendung der Proteinkinaseinhibitoren erkannt werden (Abbildung 2C). In diesem Indikationsbereich adressieren PKIs häufig überaktive Kinasen, die im Rahmen von Tumorgenese und -wachstum hyperproliferative Signale transduzieren. Als Beispiele dienen die Rezeptoren für zahlreiche Wachstumfaktoren wie der *epidermal growth factor*-Rezeptor (EGFR), der *platelet-derived growth factor*-Rezeptor (PDGFR) oder *vascular endothelial growth factor*-Rezeptor (VEGFR). Diesen Rezeptoren ist gemeinsam, dass sie alle intrinsische Tyrosinkinaseaktivität aufweisen.[11]

Dennoch sind auch nicht-membranständige Tyrosinkinasen wichtige Targets für PKI. Das prominenteste Beispiel ist das BCR-ABL-Fusionsprotein. Diese konstitutiv aktive Tyrosinkinase wird von einem onkogenen Fusionsgen codiert und ist das primäre Target von Imatinib (Gleevec®) und weiteren erfolgreichen Therapeutika der chronisch-myeloischen Leukämie.[11,12]

Gleich vier von der FDA zugelassene Wirkstoffe hemmen Mitglieder der sog. Janus Kinasen (JAK), einer Familie nicht-membranständiger Rezeptortyrosinkinasen. Tofacitinib (Xeljanz®) stellt in diesem Zusammenhang eine Pioniersubstanz dar: der pan-JAK-Inhibitor ist der erste PKI, der für eine nicht-onkologische Indikation (rheumatoide Arthritis) zugelassen wurde.[10] Das Indikationsgebiet wurde inzwischen sogar um weitere immunologische Erkrankungen (Morbus Crohn und Colitis ulcerosa) erweitert.[13]
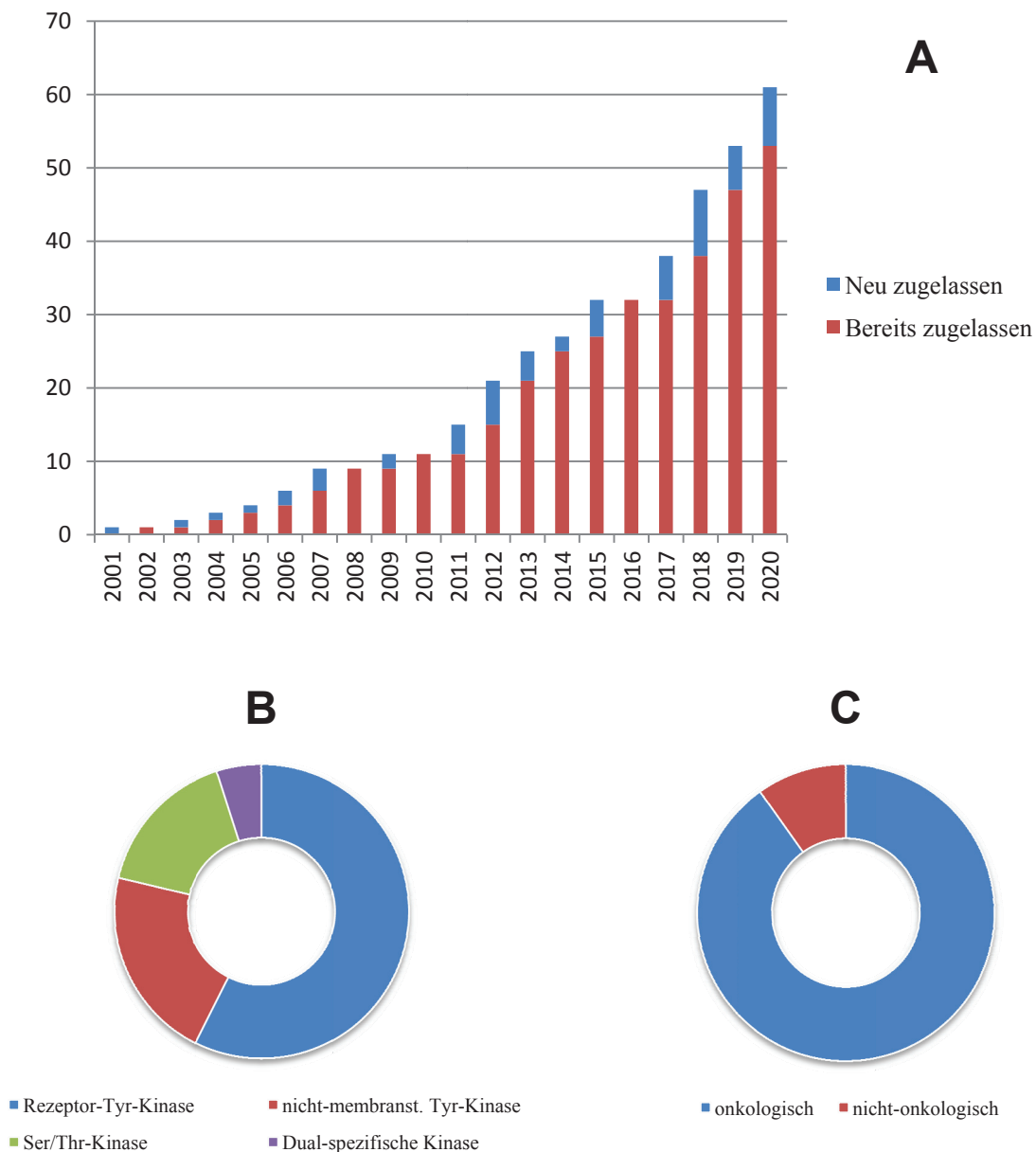
Abbildung 2. (**A**) Zulassungen an Proteinkinaseinhibitoren in den letzten zwei Jahrzehnten und Klassifizierung von Proteinkinaseinhibitoren nach Art der gehemmten Kinase (**B**) bzw. nach Indikationsgebiet (**C**).[10]

Die fortschreitende Ausweitung der Anwendungsmöglichkeiten für PKIs im nicht-onkologischen Segment deutet das therapeutische Potenzial dieser vielversprechenden, modernen Arzneistoffgruppe an. Laut der PKI Datenbank befinden sich zurzeit mehr als 150 Hemmstoffe in klinischen Studien der Phasen I-III, sodass von einer Aufrechterhaltung des positiven Trends der Zulassungen von PKIs in den nächsten Jahren auszugehen ist.[14]

Dennoch fehlen für viele der krankheitsassoziierten Kinasen weiterhin konkrete Strategien für die Entwicklung neuartiger Wirkstoffe. Dies kann einerseits in einem Mangel chemischer Substanzen, die den hohen Anforderungen an Wirkstoffkandidaten genügen, begründet liegen. Andererseits limitiert ein ungenügendes Verständnis über die zellbiologische Rolle vieler Kinasen, sowohl in physiologischem, als auch in pathophysiologischem Kontext, die Targetvalidierung und damit den Arzneistoff-entwicklungsprozess.

1.3   Die Glykogen Synthase Kinase-3

Die Glykogen Synthase Kinase-3 (GSK-3) ist ein prominentes Beispiel dieser bis jetzt unzureichend validierten Targets für PKIs. Die ubiquitär exprimierte Kinase kommt in zwei Isoformen vor (α und β) und ist aus vielerlei Hinsicht als einzigartig anzusehen.[15] Trotz jahrzehntelanger Forschung und umfassender Charakterisierung der Proteinstruktur bleiben zahlreiche Fragen bezüglich der zellbiologischen Funktionen und der Regulation dieses Enzyms ungeklärt. Dies liegt nicht zuletzt in einer überwältigenden Anzahl an vermeintlichen Substraten begründet. Sutherland definierte folgende Kriterien, um die Verifikation eines vermuteten Substrats zu erleichtern.[16]

1.   Eine aufgereinigte GSK-3-Fraktion phosphoryliert das Substrat in nennenswertem Ausmaß *in vitro* auf den Aminosäuren, die auch *in vivo* phosphoryliert werden.
2.   Eine genetische oder pharmakologische Beeinflussung der GSK-3-Aktivität *in vivo* spiegelt sich im Phosphorylierungszustand des Substrats wider.
3.   Ein(e) zelluläre(r) Funktion/Effekt des Substrats ändert sich in Abhängigkeit der GSK-3-Aktivität bzw. der Phosphorylierung. Durch Mutation der von der GSK-3 phosphorylierten Aminosäure zu Alanin ist diese(r) Funktion/Effekt nicht mehr durch die GSK-3 steuerbar.

Bisher wurden ungefähr 40 Substrate identifiziert, die zumindest zwei dieser Kriterien erfüllen.[16] Dies suggeriert einen erheblichen Einfluss der GSK-3 auf das zelluläre Signalnetzwerk und wird durch eine Beteiligung der Kinase in mindestens fünf Signalwegen reflektiert, darunter der Insulin- und Wnt-Signalweg.[17] Diese sollen im Folgenden illustriert werden, um einen Einblick in die zellulären Funktionen der GSK-3 zu gewähren.

1.3.1 Zellbiologische Funktionen

a) Insulin-Signalweg

Die GSK-3 reguliert ihr namensgebendes Substrat, die Glykogen Synthase (GS), im Rahmen des Insulin-Signalwegs. In ruhenden Zellen wird die GS hierzu von der konstitutiv aktiven GSK-3 phosphoryliert, was eine Hemmung der Glykogensynthese zur Folge hat. Die Bindung von Insulin an den Rezeptor initiiert eine Signalkaskade, die in einer Hemmung der GSK-3 mündet (Abbildung 3). Bei unterdrückter GSK-3-Aktivität kann die Glykogen Synthase schließlich durch Phosphatasen in ihre aktive Konformation überführt und damit die Glykogensynthese katalysiert werden.[18]
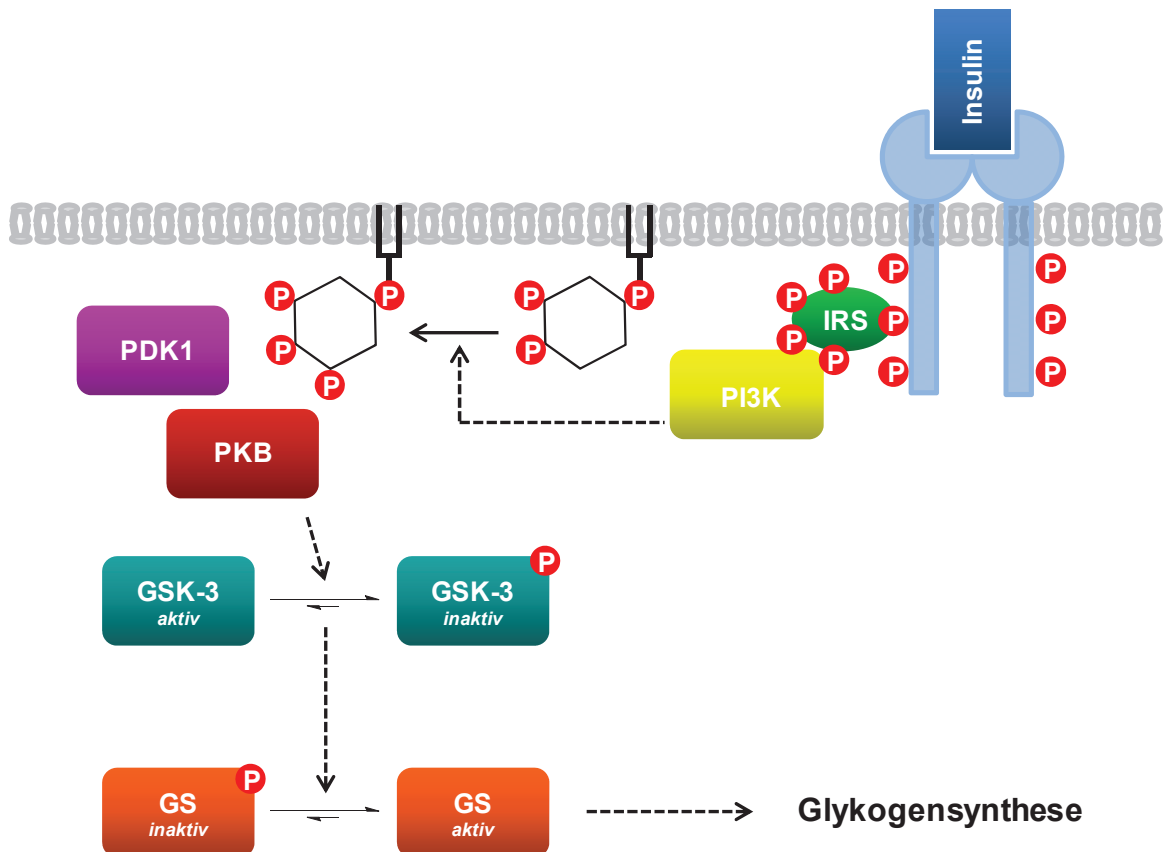
Abbildung 3. Insulin-Signalweg unter Beteiligung der GSK-3. Die Bindung von Insulin an den extrazellulären Teil des Insulinrezeptors führt zu einer Aktivierung der intrazellulären Tyrosinkinasedomäne mit anschließender Autophosphorylierung des Rezeptors, sowie Phosphorylierung der Insulin-Rezeptor-Substrate IRS1 und IRS2. Die phosphorylierten Insulin-Rezeptor-Substrate rekrutieren die Phosphoinositid-3-kinase (PI3K) durch Bindung ihrer p85 Untereinheit, sodass diese Kinase anschließend zellmembranständiges Phosphatidylinositol-4,5-bisphosphat in Phosphatidylinositol-3,4,5-trisphosphat überführen kann. Letzteres bringt die Phosphoinositid-abhängige Kinase 1 (PDK1) und die Proteinkinase B (PKB) in räumliche Nähe zueinander und erleichtert so die Aktivierung der PKB durch die PDK1. Die PKB deaktiviert schließlich die GSK-3 durch Phosphorylierung eines N-terminalen Serins (Ser21 in GSK-3α bzw. Ser9 in GSK-3β).[18] Abbildung in Anlehnung an Cohen *et al.*[18]

b) Wnt-Signalweg

Prinzipiell werden drei verschiedene Signalwege unterschieden, die durch extrazelluläre Wnt-Liganden initiiert werden können. Dies sind der kanonische Wnt-Signalweg, sowie die zwei nicht-kanonischen PCP (*planar cell polarity*)- und Wnt/Calcium-Signalwege.[19] Dabei läuft lediglich Ersterer unter Beteiligung der GSK-3 ab, wobei die zwei Isoformen in dieser Kaskade Redundanz aufweisen.[19,20] Die kanonische Wnt Kaskade reguliert die zytosolischen Spiegel des Effektorproteins β-Catenin (Abbildung 4). In ruhenden Zellen wird der β-Catenin-Spiegel durch den sog. *Destruction Complex* kontrolliert.
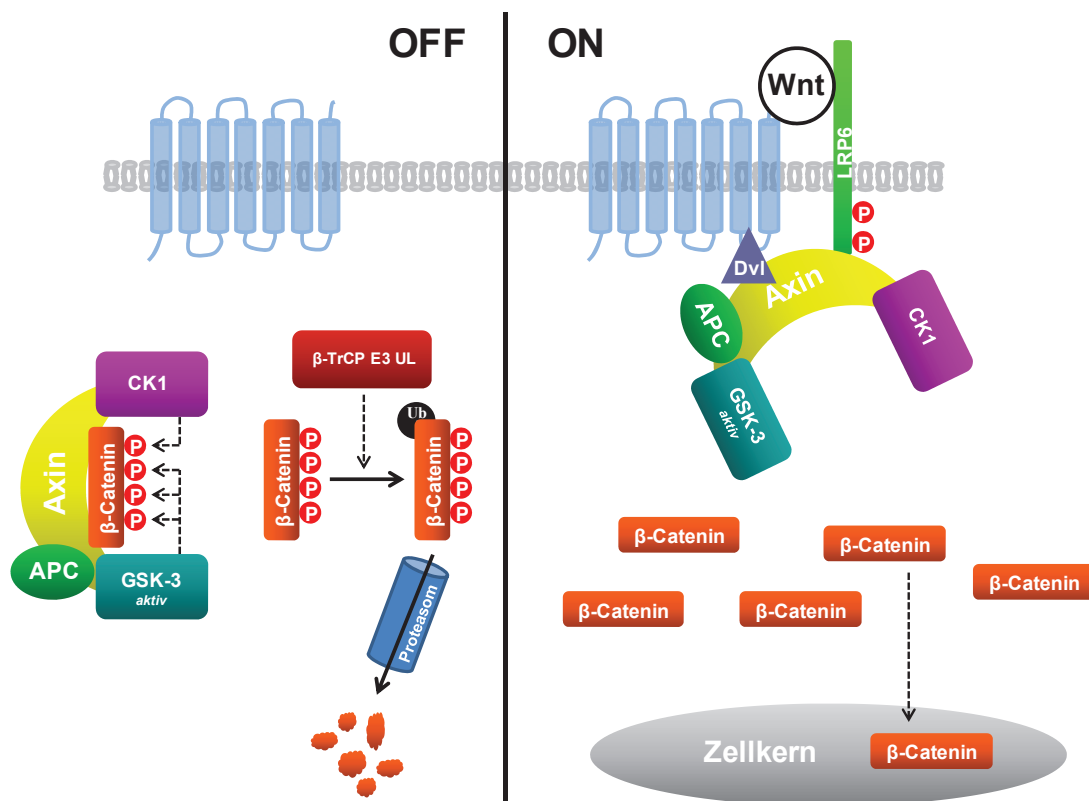
Abbildung 4. Kanonischer Wnt Signalweg. (**OFF**) Im Ruhezustand des Signalwegs ist der *Destruction Complex* aktiv: Axin-gebundenes β-Catenin wird dem *Priming* (siehe Kapitel 1.3.3) durch die CK1 folgend mehrfach durch die GSK-3 phosphoryliert. Dies bewirkt eine Rekrutierung der β-Transducin repeat containing (β-TrCP) E3 Ubiquitin Ligase, welche das β-Catenin durch Ubiquitinylierung für den proteasomalen Abbau markiert. (**ON**) Bei Rezeptoraktivierung durch Wnt Liganden wird das Effektorprotein Dishevelled (Dvl) rekrutiert und eine Assoziation von Axin an das Rezeptorsystem, sowie eine Phosphorylierung von LRP5/6 durch die Axin-gebundenen Kinasen ermöglicht. Es resultiert eine Inaktivierung des *Destruction Complex*.[21] Abbildung in Anlehnung an van Kappel *et al.*[21]

Dieser Komplex setzt sich aus dem Gerüstprotein Axin, dem Tumorsupressor Adenomatous Polyposis Coli (APC) und den konstitutiv aktiven Kinasen Casein Kinase 1 (CK1) und GSK-3 zusammen. Die Bindung von Wnt Liganden an die Frizzled-

Rezeptoren und LRP5/6-Corezeptoren bewirken intrazellulär eine Inaktivierung des *Destruction Complex*, deren Mechanismus noch nicht vollständig aufgeklärt ist. Infolgedessen kann β-Catenin intrazellulär akkumulieren und transloziert in den Zellkern, wo es als Ko-Transkriptionsfaktor die Transkription der Zielgene des Wnt-Signalwegs aktiviert.[21] Der Wnt-Signalweg und das β-Catenin sind im Rahmen einer therapeutisch angewendeten GSK-3-Inhibition besonders aus toxikologischer Sicht relevant (siehe Kapitel 1.4.2).

1.3.2 Struktur der GSK-3

Die Struktur der GSK-3β wurde 2001 durch Röntgenkristallanalyse aufgeklärt.[22,23] Durch Betrachtung der Kristallstuktur können typische Merkmale der Kinase-Architektur, aber auch einige Besonderheiten der GSK-3β erkannt werden (Abbildung 5). Initial ist die für Proteinkinasen typische zweiteilige Struktur augenscheinlich. Das Protein besteht aus einer größeren α-Helix-reichen Domäne am C-Terminus aus etwa 200 Aminosäuren und einer kleineren β-Faltblatt-reichen Domäne am N-Terminus aus etwa 80 Aminosäuren. Die N-terminale Domäne setzt sich aus sieben antiparallelen β-Faltblättern zusammen, von denen sich sechs als fassartige Tertiärstruktur anordnen. Die β-Faltblätter 5 und 6 werden von einer α-Helix unterbrochen. Mit nur zehn Aminosäuren bzw. zwei Umdrehung fällt dieses als C-Helix bekannte α-helicale Segment bei der GSK-3β deutlich kürzer aus als bei anderen Kinasen. Zwischen den β-Faltblättern 3 und 4 befindet sich ein weiteres wichtiges Element der N-terminalen Domäne, die hochkonservierte Glycin-reiche Schleife mit der Erkennungs-Sequenz GXGXXG.[22,23] Die N- und C-terminale Domäne werden durch die sog. Gelenkregion - die *Hinge Region* - verbunden, welche aus den Aminosäuren Asp133, Tyr134, Val135 und Pro136 besteht.
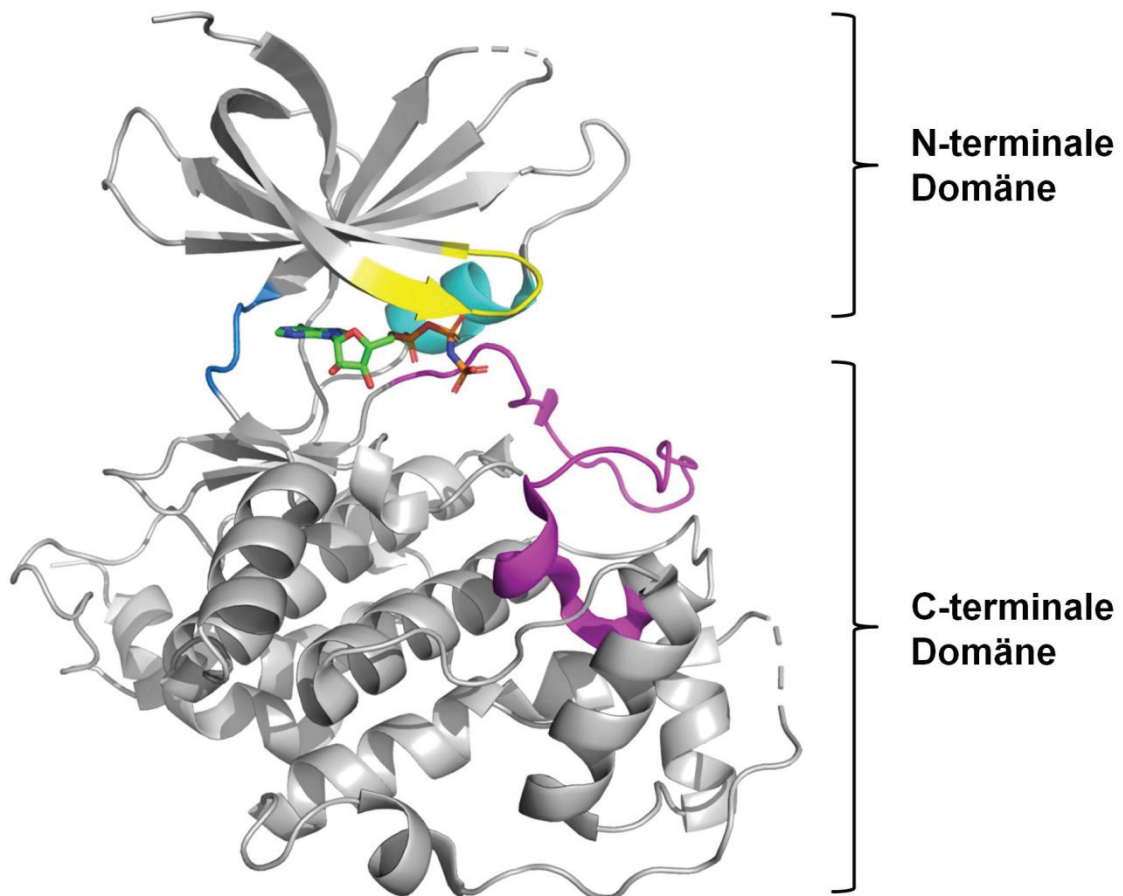
Abbildung 5. Struktur der GSK-3β in Komplex mit dem ATP-Analogon AMP-PNP (PDB ID 1PYX).[24] Das Protein ist als grauer „Cartoon" und der Ligand in grünen „Sticks" dargestellt. Wichtige Strukturelemente des Proteins sind farblich hervorgehoben: Hinge-Region (blau), Glycin-reiche Schleife (gelb), C-Helix (türkis), Aktivierungsschleife (magenta). Die Abbildung wurde mit PyMOL (Schrödinger LLC) erstellt.[25]

Die Bindestelle für ATP befindet sich zwischen den beiden Domänen und wird zur einen Seite von der Gelenkregion und zur anderen Seite von der Glycin-reichen Schleife begrenzt.[22] Sie ist hochkonserviert und kann nach dem Modell von Traxler in fünf charakteristische Subregionen unterteilt werden.[26] Der Bindemodus von ATP in der GSK-3β kann aus einer Kristallstruktur in Komplex mit dem nicht-hydrolysierbaren Analogon Adenylylimidodiphosphat (AMP-PNP) abgeleitet werden (Abbildung 6).[24] Die Adenin-Substruktur befindet sich in einer hydrophoben Umgebung und bildet eine zweizähnige Wasserstoffbrückenwechselwirkung zum Rückgrat der Aminosäuren Asp133 und Val135 der Gelenkregion aus. Eine der Hydroxylgruppen der Ribose-Einheit geht als Wasserstoffbrücken-Donator eine Interaktion mit der Carbonylgruppe des Rückgrats von Glu185 ein. Die drei Phosphatgruppen sind in zahlreiche Wechselwirkungen involviert. Insgesamt vier Sauerstoffe des Triphosphats koordinieren an zwei Magnesium-Kationen. Zusätzlich werden mehrere Wasserstoffbrücken zu den basischen Zentren von Lys85 (fünftes β-Faltblatt der N-terminalen Domäne) und von Lys183 (C-terminale Domäne)

ausgebildet. Die optimale Ausrichtung dieser Lysinseitenketten wird durch Salzbrücken zu den Carboxylat-Seitenketten der Aminosäuren Glu97 (C-Helix) bzw. Asp181 sichergestellt. Somit ermöglicht ein komplexes Netzwerk polarer Wechselwirkungen die optimale Positionierung des Triphosphats.[24]
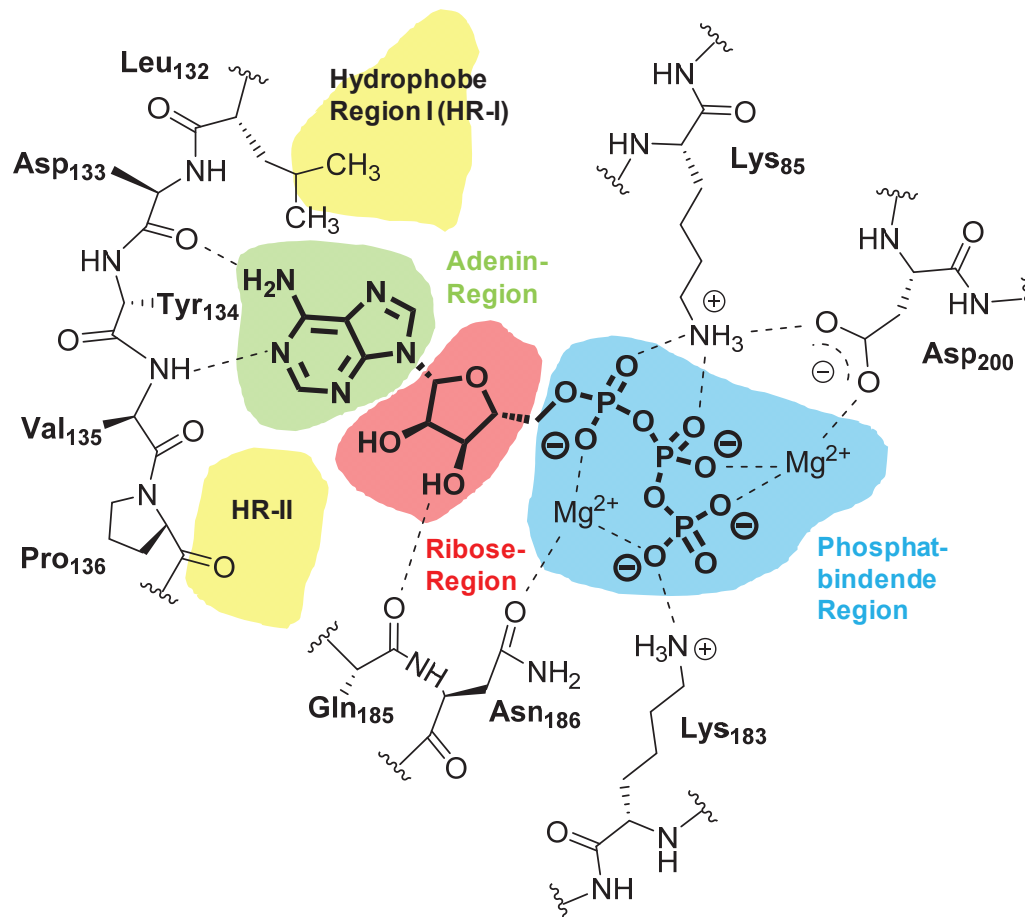
Abbildung 6. Abgeleiteter Bindemodus von Adenosintriphosphat (ATP) in der GSK-3β und Unterteilung der Bindestelle nach dem Traxler-Modell.[24,26] Adenin-Region (grün); Ribose-Region (rot), Phosphat-bindende Region (blau); hydrophobe Regionen I und II (gelb). Letztere werden vom nativen Liganden nicht besetzt. Polare Interaktionen sind als gestrichelte schwarze Linien dargestellt.

Bedeutsame Strukturelemente für die Regulation der GSK-3β, die Bindung des Substrats und den Transfer des γ-Phosphats befinden sich in der C-terminalen Domäne des Enzyms:[27,28]

- die Aktivierungsschleife, die das phosphorylierbare Tyr216 zur Regulation der Kinase und das sog. DFG-Motiv (Asp200-Phe201-Gly202) enthält
- die katalytische Schleife mit dem darin enthaltenen HRD-Motiv (His179-Arg180-Asp181) und Lys183

Für das mechanistische Verständnis der Phosphotransferkatalyse sind zwei Konformation der Kinase zu unterscheiden: die aktive und die inaktive Konformation.[4] In der aktiven Konformation ist die Aktivierungsschleife von der ATP-Bindestelle weg positioniert, sodass ein Spalt entsteht, welcher die Bindung des Substrats ermöglicht.[29] In dieser Konformation („DFG-in") ist das Asp200 des DFG-Motivs zur ATP-Bindestelle hin ausgerichtet und koordiniert dort eines der zwei Magnesium-Kationen.[4] Das Phe201 bildet hydrophobe Wechselwirkungen zur C-Helix in der N-terminalen Domäne aus.[28] Die korrekte Position dieser C-Helix ermöglicht die notwendige Salzbrücke zwischen Lys85 und Glu97.[29] Asp181 aus dem HRD-Motiv interagiert neben der Salzbrücke zu Lys183 mit der Hydroxylgruppe der zu phosphorylierenden Aminosäure im Substrat und positioniert diese für den Transfer des Phosphats. Dabei fungiert es als Base und nimmt das im Rahmen der Phosphorylierung freiwerdende Proton kurzzeitig auf.[28]

Im Gegensatz zur hoch konservierten aktiven Konformation, müssen inaktive Konformationen keine besonderen strukturellen Anforderungen erfüllen und sind deshalb innerhalb des Kinoms variabel.[29] Typischerweise wird in diesen Konformationen eine Bindung des Substrats verhindert, da die Aktivierungsschleife die entsprechende Bindestelle besetzt.[4,29] Bei vielen Kinasen werden zudem veränderte Ausrichtungen der Aminosäuren des DFG-Motivs beobachtet. Bei der klassischen „DFG-out"-Konformation sind beispielsweise die Orientierung des Phenylalanins und der Asparaginsäure vertauscht, sodass Letztere nicht mehr zur ATP-Bindestelle ausgerichtet ist.[29] Die mangelnde hydrophobe Interaktion des Phenylalanins zur C-Helix bedingt eine Fehlpositionierung dieser Helix. Die Salzbrücke zwischen Lys85 und Glu97 kann nicht mehr ausgebildet werden und die Interaktionsmuster in der ATP-Bindestelle sind derart gestört, dass die Kinase neben Substrat auch kein ATP zu binden vermag und folglich ihre katalytische Aktivität verliert.[28]

Zahlreiche Kinasen können durch Phosphorylierung von Aminosäuren in der Aktivierungsschleife von der inaktiven in die aktive Konformation überführt werden. Ihre Aktivität kann deshalb durch andere Kinasen auf einfache Weise gesteuert werden.[29,30] In diesem Zusammenhang nimmt die GSK-3 eine besondere Stellung im Kinom ein, da sie als konstitutiv aktivierte Kinase elaborierteren Regulationsmechanismen unterliegt, die im Folgenden Kapitel näher betrachtet werden sollen.[31]

1.3.3 Regulation

a) Regulation durch post-translationale Strukturmodifikationen und Priming

Die Aktivität der GSK-3 kann durch post-translationale Phosphorylierung entsprechender Aminosäuren sowohl positiv, als auch negativ beeinflusst werden. Ähnlich zu anderen Kinasen resultiert eine Phosphorylierung von Aminosäuren in der Aktivierungsschleife (Tyr279 in GSK-3α bzw. Tyr216 in GSK-3β) in einer Aktivitätssteigerung.[32,33] Das phosphorylierte Tyrosin geht dabei eine zweizähnige ionische Interaktion zu zwei Argininseitenketten (Arg220 und Arg223 in der GSK-3β) ein, welche ebenfalls in der Aktivierungsschleife lokalisiert sind.[34] Die Relevanz dieser Modifikation für die Regulation der GSK-3β ist jedoch aus verschiedenen Gründen lediglich als untergeordnet anzusehen:

- die GSK-3β zeigt in Röntgenkristallstrukturen auch in unphosphorylierter Form eine aktive Konformation.[22,23]
- während die Phosphorylierung bei verwandten Kinasen zu einer über 1000-fachen Aktivitätssteigerung führen kann, resultiert hier bei der GSK-3β nur eine moderate Erhöhung der Wechselzahl um den Faktor 5.[35]
- nach aktuellem Stand bleibt umstritten, ob die Phosphorylierung von Tyr279 bzw. Tyr216 in zellulärem Kontext tatsächlich einer regulativen Dynamik unterliegt oder doch eher irreversibel ist.[31,32,36]

Interessanterweise stellt die Phosphorylierung der GSK-3β auf Tyr216 einen Chaperon-abhängigen Autophosphorylierungsprozess dar. Durch post-translationale Proteinfaltung entsteht zunächst eine Enzymvorstufe mit Tyrosinkinaseaktivität, welche sich intramolekular phosphoryliert und damit autoaktiviert.[37] Die GSK-3β zeigt damit also Eigenschaften einer dual-spezifischen Kinase, jedoch beschränkt sich ihre Tyrosinkinaseaktivität lediglich auf die Autophosphorylierung und betrifft nicht exogene Substrate. Die voll ausgereifte GSK-3β ist schließlich eine Serin/Threonin-Kinase und (wahrscheinlich dauerhaft) auf Tyr216 phosphoryliert, was ihre Aktivität in ruhenden Zellen begründet.[32,36]

In diesem Zusammenhang gilt es eine weitere Besonderheit der GSK-3 zu beleuchten, welche eine dominantere Rolle in der Regulation des Enzyms einnimmt - das sog. *Priming*. *Priming* bzw. *Primed Phosphorylation* beschreibt die Voraussetzung der

Vorphosphorylierung von Substraten durch andere Kinasen, bevor diese schließlich durch die GSK-3 selbst prozessiert werden.[18,22] Die GSK-3 erkennt dabei vorphosphorylierte Sequenzen der Form Ser/Thr-X-X-X-(p)Ser/(p)Thr.[38] Sie modifiziert also bevorzugt Serin- und Threoninreste, die sich vier Aminosäuren entfernt von einem bereits phosphorylierten Rest befinden. Das *Priming*-Phosphat besetzt dabei eine spezielle Bindestelle, gebildet von drei basischen Aminosäuren (Arg96, Arg180 und Lys205 in GSK-3β), und induziert dadurch eine aktive Enzymkonformation.[22,23,39] Die durch die GSK-3 eingeführte Phosphatgruppe kann im Anschluss wiederum als *Priming*-Phosphat erkannt werden, sodass eine sequenzielle Mehrfachphosphorylierung resultiert.[40] Das *Priming* stellt zwar keine absolute Voraussetzung für die Phosphorylierung eines Substrats durch die GSK-3 dar, jedoch kann es diesen Prozessfach 100 bis 1000-fach beschleunigen.[41] Es ist in seiner Auswirkung auf die Enzymaktivität der Phosphorylierung von Tyr279 bzw. Tyr216 als übergeordnet anzusehen, da durch die Kopplung von Enzymaktivität und Substratselektion eine außerordentliche Spezifität sichergestellt wird. Tatsächlich liegt es nahe, dass das Tyrosin der Aktivierungsschleife durch dessen Phosphorylierung und der dadurch ermöglichten Salzbrücken zu den Argininseitenketten lediglich zu einer Ausrichtung gezwungen wird, die den Zugang zur Bindestelle des *Priming*-Phosphats und damit die Substratbindung erleichtert.[23] Darüber hinaus wird die Aktivität der GSK-3 durch unabhängige Signalkaskaden, welche die *geprimten* Substrate bereitstellen, passiv mitreguliert.[31]

Den soeben beschriebenen Aktivierungsmechanismen für die GSK-3 sind inhibierende Phosphorylierungen von Serinen im N-Terminus des Enzyms (Ser21 in GSK-3α bzw. Ser9 in GSK-3β) gegenübergestellt.[42,43] Im phosphorylierten Zustand kann die N-terminale Domäne als Pseudosubstrat fungieren, indem das Phospho-Serin die Bindestelle des *Priming*-Phosphats besetzt und somit die Bindung von *geprimten* Substraten verhindert.[23,39] Es handelt sich dabei jedoch um keine absolute Hemmung der Kinase - die kompetitive Besetzung der Bindestelle bedingt, dass hohe Konzentrationen an *geprimten* Substraten die N-terminale Domäne zu verdrängen vermögen.[39] In einem zellulären Kontext wäre dies in Form einer Akkumulation von Substraten vorstellbar, die erst ab einer bestimmten Schwellenkonzentration durch die GSK-3 prozessiert werden. Zudem bleibt die Umsetzung von Substraten, die keines *Primings* bedürfen, von diesem Hemmmechanismus unbeeinflusst.[31]

Zu guter Letzt ist anzumerken, dass der N-Terminus der GSK-3 samt der darin enthaltenen regulatorischen Serine einer Abspaltung durch die Cysteinprotease Calpain unterliegen kann, die erwartungsgemäß den eben beschriebenen Inhibitionsmechanismus aufhebt und eine Aktivierung des Enzyms bewirkt.[44]

b) Regulation durch Assoziation in Proteinkomplexen

In der Literatur sind verschiedene Formen der Interaktion der GSK-3 zu anderen Proteinen beschrieben, die für die Aktivität des Enzyms bedeutend sein können.[31] Der in Kapitel 1.3.1 beschriebene *Destruction Complex* stellt ein gut aufgeklärtes Beispiel für diese Interaktionen dar und soll deshalb im Folgenden genauer beschrieben werden.

Im Rahmen des Wnt-Signalwegs wird die Phosphorylierung von β-Catenin durch die Assoziation der GSK-3 an das Gerüstprotein Axin erleichtert. Die deutlich niedrigere intrazelluläre Axin-Konzentration, verglichen mit der GSK-3, bedingt, dass schätzungsweise weniger als 10% des zellulären GSK-3-Pools an Axin gebunden vorliegen.[45] Die Sequestrierung dieser Fraktion für den Wnt-Signalweg ist für die Regulation der Kinase aus zwei Gründen entscheidend. Einerseits stellt die Co-Lokalisation mit β-Catenin eine gezielte Umsetzung von diesem durch die sonst Substrat-promiskuitive GSK-3 sicher. Andererseits wird Axin-gebundene GSK-3 nicht von der PKB phosphoryliert und entzieht sich somit dem Einfluss des Insulin-Signalwegs.[45] Durch die Assoziation mit Axin wird folglich verhindert, dass die GSK-3 als ungewollte Schnittstelle der beiden Signalwege fungiert. Folglich kommt diesem Proteinkomplex eine entscheidende regulatorische Funktion für die Aktivität der GSK-3 zu.

c) Regulation durch intrazelluläre Lokalisation

Das intrazelluläre Verteilungsmuster der GSK-3β wurde in humanen Neuroblastomen genauer untersucht. Dabei konnte die Kinase hauptsächlich im Zytosol, aber auch im Zellkern und den Mitochondrien nachgewiesen werden. Die nukleäre und mitochondriale Fraktion zeigten eine signifikant höhere Aktivität gegenüber der zytosolischen Fraktion. Diese Beobachtungen spiegeln sinnvollerweise das Verhältnis von aktiver zu inaktiver ((p)Ser9)-GSK-3β in den jeweiligen Kompartimenten wider. Dies deutet darauf hin, dass die verschiedenen Fraktionen unterschiedlichen Regulationsmechanismen unterliegen und somit die genaue intrazelluläre Lokalisation des Enzyms ebenfalls einen entscheidenden Einfluss auf dessen Aktivität hat.[46]

1.4   Die GSK-3 als Arzneistofftarget

1.4.1 Morbus Alzheimer und GSK-3

Eine dysregulierte Aktivität der GSK-3 wird mit zahlreichen Krankheiten und pathophysiologischen Prozessen wie Typ-II Diabetes, Krebs, kardiovaskulären Erkrankungen und Neurodegeneration in Verbindung gebracht. Besonders Morbus Alzheimer spielt dabei in der krankheitsbezogenen Grundlagenforschung zur GSK-3 eine dominierende Rolle.[47] Dies liegt in der dringenden Notwendigkeit neuer Interventionsmöglichkeiten für diese häufigste Form der neurodegenerativen Erkrankungen begründet.[48]

Die verfügbaren pharmakologischen Therapiekonzepte beinhalten die Hemmstoffe der Acetylcholinesterase (Donepezil, Galantamin und Rivastigmin), sowie den NMDA-Rezeptor-Antagonisten Memantin (Abbildung 7). Der therapeutische Nutzen dieser Arzneistoffe für die Alltagsfähigkeiten und die kognitiven Fähigkeiten der Patienten ist zwar eindeutig belegt, beschränkt sich jedoch lediglich auf eine Linderung der Symptome. Somit stehen aktuell keine Pharmaka zur Verfügung, die die neuropathologischen Prozesse und damit die Progression der Krankheit beeinflussen (Leitlinie).[48]
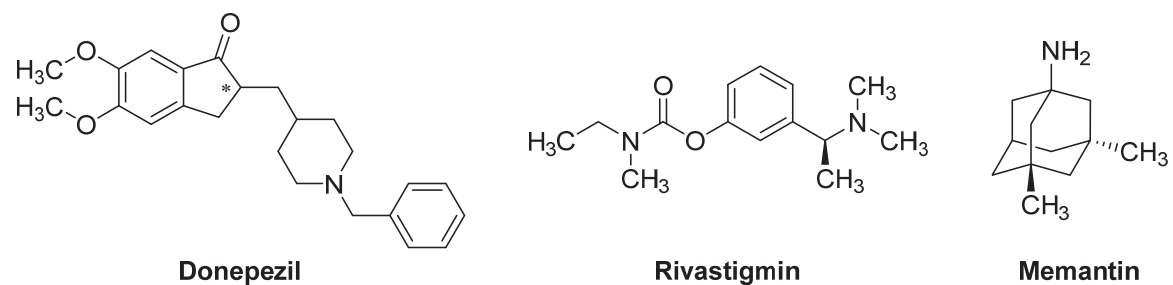
Abbildung 7. Strukturformeln ausgewählter Therapeutika für Morbus Alzheimer.

Um die Bedeutung der GSK-3 als potenzielle Zielstruktur für neuartige, krankheitsmodifizierende Therapeutika zu verstehen, müssen die pathologischen Merkmale der Alzheimer-Krankheit erfasst werden. Während sich die Neurodegeneration klinisch durch eine abnehmende Gedächtnisleistung und Kognition äußert, ist das Gehirn von Alzheimer-Patienten aus histopathologischer Sicht von zwei hochcharakteristischen Abnormalitäten geprägt: (extrazelluläre) *senile Plaques*, bestehend aus unlöslichem Aβ-Protein, und (intrazelluläre) *neurofibrilläre Tangles* (NFTs), zusammengesetzt aus hyperphosphoryliertem Tau-Protein. Obwohl die Ablagerung des Aβ-Proteins häufig als

der vorrangige Prozess der Pathogenese eingeordnet wird, scheint das Aufkommen der NFTs besser mit der Atrophie des Hirngewebes zu korrelieren.[49]

a)   Aβ-Protein (senile Plaques)

Das unlösliche Aβ-Protein, aus dem die senilen Plaques zusammengesetzt sind, hat seinen Ursprung im *Amyloid Precursor Protein* (APP). Dieses membranständige Vorläuferprotein unterliegt in seiner transmembranären Domäne einer proteolytischen Spaltung durch Sekretasen. Dabei wird zwischen der amyloidogenen und der nicht-amyloidogenen Prozessierung des APPs unterschieden, wobei Erstere das unlösliche Aβ-Protein generiert (Abbildung 8).[50]
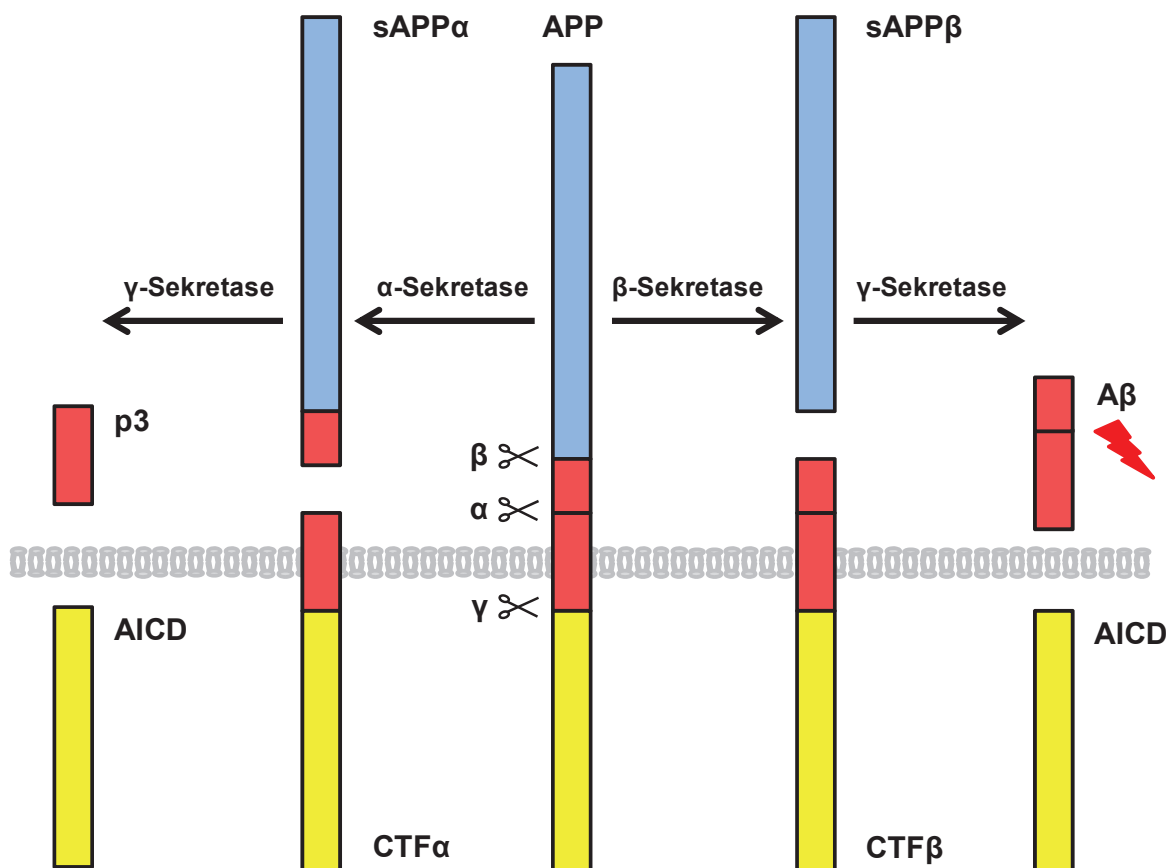
Abbildung 8. Prozessierung des Amyloid Precursor Proteins (APP). Im nicht-amyloidogenen Verlauf (links) wird das APP zunächst durch α-Sekretasen gespalten. Dabei handelt es sich um sog. *a disintegrin and metalloprotease* (ADAM) Enzyme wie ADAM9, ADAM10 und ADAM17. Die Proteolyse des APP durch diese Enzyme resultiert einerseits im löslichen Fragment sAPPα und andererseits im membrangebundenen C-terminalen Fragment (CTFα). Letzteres wird im Anschluss durch den γ-Sekretase-Proteinkomplex zum p3-Protein und der APP-Intrazellulärdomäne (AICD) geschnitten. Im amyloidogenen Verlauf (rechts) hingegen ist das APP im ersten Schritt Substrat der β-Sekretase, die die Aspartatprotease BACE1 (β-Site APP cleaving enzyme) darstellt. Analog entstehen hier die zwei Fragmente sAPPβ und CTFβ. Aus Letzterem setzt die γ-Sekretase erneut das AICD, jedoch nun auch das Aβ-Protein, frei.[50] Abbildung in Anlehnung an Nhan *et al*.[50]

Folgende Befunde sprechen in diesem Kontext für eine Etablierung eines *circulus vitiosus*, in welchem der Metabolismus des APP durch die GSK-3 zu Gunsten des amyloidogenen Verlaufs manipuliert wird und anfallendes Aβ-Protein wiederum eine Aktivierung der GSK-3 hervorrufen kann:

- Eine pharmakologische Hemmung der GSK-3 führt zu einer verringerten Entstehung von Aβ-Protein *in vitro*. Während Ly *et al*. dies auf eine Modulation der β-Sekretase-Expression durch die GSK-3β zurückführen, postulieren Phiel et al. einen Einfluss der GSK-3α auf den γ-Sekretase-Komplex.[51,52] Ly *et al*. konnten zudem im Alzheimer-Mausmodell eine Verringerung der β-Sekretase-Expression, der Aβ-Produktion und Plaque-Entstehung, sowie eine verbesserte Gedächtnisleistung unter Einwirkung eines GSK-3-Inhibitors beobachten und damit ihre *in vitro* Ergebnisse *in vivo* bestätigen.[51] Hurtado *et al*. sprechen hingegen lediglich der GSK-3α, jedoch nicht der GSK-3β, eine Rolle in der Entstehung seniler Plaques im Alzheimer-Mausmodell zu.[53]

- GSK-3β phosphoryliert das APP *in vitro*.[54] Rockenstein *et al*. fanden korrespondierend dazu im Mausmodell einen Zusammenhang zwischen der Hemmung der GSK-3β und einer verminderten Phosphorylierung des APP, sowie in der Folge erniedrigte Aβ-Spiegel.[55]

- Sofola *et al*. beobachteten in einem *in vivo* Modell in *Drosophila* außerdem positive Effekte einer pharmakologischen GSK-3-Inhibition auf die Aβ-Spiegel, die unabhängig vom Metabolismus des APP waren.[56]

- Die Behandlung muriner Neurone mit Aβ-Protein bewirkt *in vitro* eine Aktivierung der GSK-3β.[57] Dies kann auf eine Hemmung des Insulin-Signalwegs durch Interaktion von Aβ-Protein mit dem Insulin-Rezeptor zurückgeführt werden.[58,59]

- Aβ-Protein interagiert außerdem in murinen Zellen mit dem Frizzled Rezeptor und bewirkt eine Hemmung des Wnt-Signalwegs und damit eine Erniedrigung der zellulären β-Catenin-Spiegel,[60] was ebenfalls eine Aktivierung der GSK-3 impliziert.

- In einer kortikalen Zellkultur konnte die Aβ-induzierte Apoptose durch Einsatz eines GSK-3-Inhibitors vermindert werden.[61]

b)   Neurofibrilliäre Tangles (NFTs)

Das Tau-Protein gehört zu den Microtubulus-assoziierten Proteinen (MAP). Es bindet an Microtubuli und reguliert ihre Anordnung und Zusammenbau und leistet so einen Beitrag zur Stabilität des Zytoskeletts. Es liegt physiologisch als Phosphoprotein vor und enthält 2-3 mol Phosphat pro mol Protein.[62] Durch den Phosphorylierungsgrad kann die Funktion des Tau moduliert werden.[63] Die Phosphorylierung des Tau-Proteins kann eine verringerte Affinität zu den Microtubuli bewirken und entsprechend die Stabilisierung selbiger beeinträchigen.[64,65] Dies kann eine physiologische Bedeutung in der Neurogenese haben, in der ein dynamisches Microtubuli-Netzwerk erforderlich ist.[66]

Im Gehirn von Alzheimer-Patienten wurden in *post mortem* Untersuchung 3 bis 4-fach hyperphosphorylierte Tauformen gefunden.[62] Hyperphosphoryliertes Tau-Protein liegt häufig in gepaarten helikalen Filamenten (*paired helical filaments*, PHF) oder gestreckten Filamenten (*straight filaments*, SF) vor und ist aggregierter Hauptbestandteil der NFTs.[67] In diesem Zustand bindet es nicht an Tubulin und beeinflusst nicht den Zusammenbau der Microtubuli.[63] Fast die Hälfte der hyperphosphorylierten Tau-Fraktion liegt im Zytosol jedoch in nicht-polymerisierter Form vor. In dieser Form bewirkt es einen Einbruch des Microtubuli-Netzwerks, da es einerseits ihren Zusammenbau nicht unterstützt und andererseits gesundes Tau-Protein und weitere MAPs bindet und somit sequestriert. Das toxische Potential der nicht-polymerisierten Tau-Fraktion steht dabei in direktem Zusammenhang zu dessen Hyperphosphorylierung, da es durch Dephosphorylierung in ein funktionsfähiges Protein rücküberführt werden kann.[63] Jaworski *et al.* postulieren, dass es sich beim nicht-polymerisierten hyperphosphorylierten Tau um die tatsächlich neurotoxische Spezies handelt, während die Bildung der (ungiftigen) PHFs bzw. NFTs einen neuroprotektiven *escape*-Mechanismus der Zelle darstellt, um dieses durch Aggregation unschädlich zu machen.[68]

Verschiedene Kinasen, darunter GSK-3, CDK-5, CK1 und PKA, phosphorylieren Tau *in vitro* und zeigen dabei jeweils spezifische Phosphorylierungsmuster in Bezug auf die angezielten Serin- und Threonin-Seitenketten. Von diesen Kinasen phosphoryliert die GSK-3, auch bekannt als Tau Kinase 1, mindestens 36 Aminosäuren im Tau-Protein und deckt viele der Aminosäuren ab, die im „Alzheimer-Tau" phosphoryliert vorliegen.[69,70] Dabei ist auch ein Zusammenspiel von Kinasen wie z.B. der GSK-3 und CDK-5 möglich, bei dem Letztere als *priming* Kinase fungiert.[63,67] Die GSK-3β-vermittelte

Phosphorylierung von Tau beeinflusst dessen Bindung zu den Microtubuli und damit die Organisation des Netzwerks.[71] Dementsprechend stehen die Anhäufung von hyperphosphoryliertem Tau und neurofibrilliäre Veränderung in Zusammenhang mit einer erhöhten Aktivität der GSK-3β.[72,73] Da zudem die Aktivität entscheidender Tau-Phosphatasen im Gehirn von Alzheimer-Patienten herabgesetzt ist,[74,75] kann eine dysbalancierte Kinase-Phosphatase-Relation als Ursache für die Hyperphosphorylierung des Tau-Proteins angesehen werden. Eine pharmakologische Hemmung der GSK-3 bewirkt *in vivo* eine verminderte Tau-Phosphorylierung und kann positive Effekte auf die Bildung von Aggregaten und sogar die Neurodegeneration auslösen.[76-79]

Abbildung 9 bietet eine vereinfachte Übersicht über die potenziellen Einflüsse der GSK-3 in der Pathogenese des Morbus Alzheimer. Eine Schlüsselrolle dieser Kinase als molekularer Knotenpunkt in der Entstehung der neuronalen Läsionen wird augenscheinlich und unterstreicht ihre Relevanz als Angriffspunkt für eine pharmakologische Intervention.
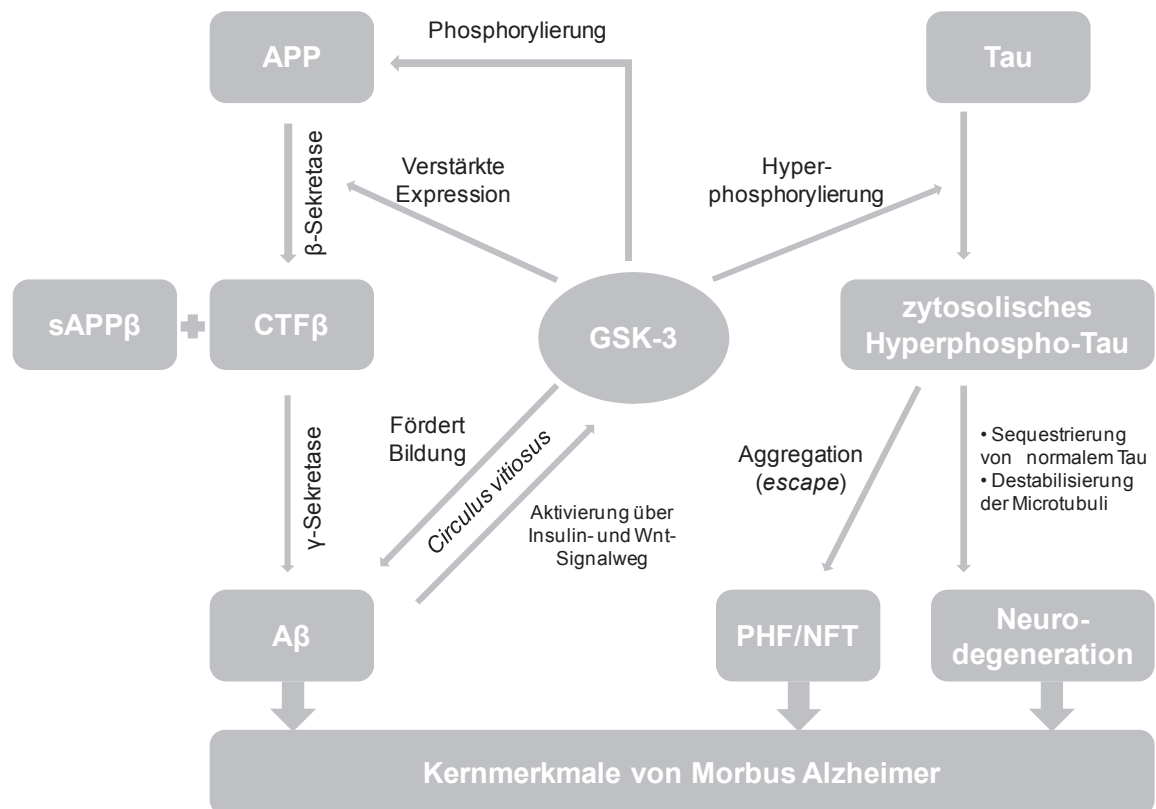
Abbildung 9. Die GSK-3 als molekularer Knotenpunkt in der Entstehung von neuronalen Läsionen als Kernmerkmale von Morbus Alzheimer.

1.4.2 Toxikologische Aspekte einer GSK-3-Hemmung

Der weitreichende zelluläre Einfluss der GSK-3 und ihre präzise Regulation lassen Zweifel an der toxikologischen Sicherheit von GSK-3-inhibierenden Therapeutika aufkommen. Dies ist beim Einsatz zur Behandlung von Morbus Alzheimer besonders relevant, da konträr zu den onkologisch eingesetzten PKIs eine Langzeitanwendung erforderlich erscheint. Im Fokus der Sicherheitsbedenken stehen dabei häufig der Wnt-Signalweg und das von ihm regulierte β-Catenin, deren onkologenes Potenzial nicht zu unterschätzen ist. So wird ein hyperaktiver Wnt-Signalweg als essenzielles Element in der Pathogenese des kolorektalen Karzinoms eingeordnet.[80]

Das toxikologische Risiko einer GSK-3-Hemmung spiegelt sich in einem Mangel an klinischen Kandidaten bzw. dem Misserfolg bislang erprobter Substanzen wider. AstraZeneca hatte beispielsweise zu Beginn des Jahrtausends mit dem Aminopyrazin AZD2858 und dem Oxindol AZD1080 zwei vielsprechende Inhibitoren in der *Pipeline* (Abbildung 10). Neben Selektivität und inhibitorischer Potenz überzeugten sie auch aus pharmakokinetischer Sicht durch ZNS-Gängigkeit und orale Bioverfügbarkeit, scheiterten jedoch bereits in tierexperimentellen Studien aufgrund ihrer nicht-tolerierbaren Nebenwirkungsprofile.[81]

AZD2858   **AZD1080**
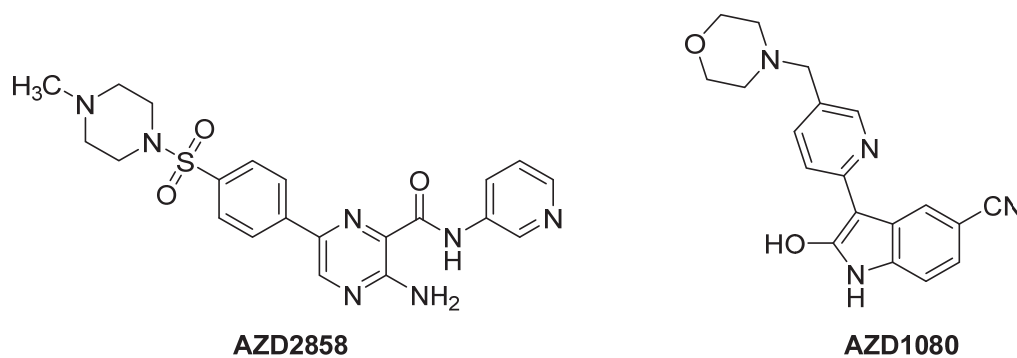
Abbildung 10. Weitentwickelte Wirkstoffkandidaten von AstraZeneca.

Die unerwarteten Nebenwirkungen von AZD2858 auf die Knochenmasse in Ratten und Hunden, die sich in verstärkter Osteoblastenproliferation und folglich osteogenen Effekten manifestierten, konnten dabei tatsächlich auf den Einfluss einer Wnt Aktivierung auf das Knochengewebe zurückgeführt werden.[81,82] AZD1080 war der erste Inhibitor, für den neben überzeugenden Effekten auf die Tau Phosphorylierung in Nagetieren sogar eine Hemmung der GSK-3 in Menschen in einer Phase-I-Studie nachgewiesen werden konnte.[83] Trotz einer gemäßigteren pharmakodynamischen Potenz

verglichen mit AZD2858, disqualifizierte sich dieser Kandidat durch nicht tolerable toxische Effekte auf die Gallenblase im Hund, von Hyperplasie bis hin zur Cholecystitis.[81]

1.4.3 Strategien zur Limitierung des Nebenwirkungsrisikos

Die Misserfolge von AstraZeneca verdeutlichen, dass die Hemmung der GSK-3 zu therapeutischen Zwecken ausgereiftere Konzepte als die schlichte hochpotente Hemmung des Enzyms erfordert. In diesem Kontext erscheinen folgende Strategien zur Limitierung von Nebenwirkungen sinnvoll:

a) Einsatz Substrat-kompetitiver Inhibitoren

Durch den Einsatz kurzkettiger, präphosphorylierter Peptide gelang es Licht-Murava *et al.* die *Priming*-Phosphat-Bindestelle (gebildet von Arg96, Arg180 und Lys205 in GSK-3β) zu adressieren und so die Substratbindestelle der GSK-3β zu besetzen. Der myristoylierte peptidische GSK-3-Inhibitor L807-mts hat die Sequenz Lys-Glu-Ala-Pro-Pro-**Ser**-Pro-Pro-Gln-**(p)Ser**-Pro und ist vom Hitzeschockfaktor 1 (HSF-1) abgeleitet. Diese Verbindung bedient sich den Autoren zufolge eines sog. *substrate-to-inhibitor*-Mechanismus: sie wird zunächst von der GSK-3 als Substrat erkannt und dementsprechend phosphoryliert, zeigt jedoch im Anschluss in ihrer Bisphosphatform durch verlangsamte Dissoziation vom Enzym. Die Effektivität dieses Konzepts spiegelt sich in einer ausgeprägten inhibitorischen Potenz mit einem IC_{50}-Wert von 1 μM wider.[84]

Substrat-kompetitive Inhibitoren dieser Art überzeugen gegenüber ATP-kompetitiven Hemmstoffen durch ein erniedrigtes Risiko für Off-Target-Effekte aufgrund der hohen Targetspezifität. Diese ergibt sich einerseits aus der Tatsache, dass die Substratbindestelle in Kinasen deutlich weniger konserviert ist als die ATP-Bindestelle. Obendrein nutzt das hier beschriebene Peptid die unikale *Priming*-Phosphat-Bindestelle der GSK-3 aus. Beide Aspekte spiegeln sich in einer überzeugenden Selektivität von L807-mts in einem Testpanel mit ca. 140 Kinasen wider.[84]

b) Expositionsminimierung durch gewebespezifisches Kinasetargeting

Ein geringeres systemisches Nebenwirkungspotenzial ist ein typischer Vorteil lokal angewendeter Pharmaka. Bei systemisch applizierten Arzneistoffen ist eine gewebsspezifische Adressierung der Zielstruktur zwar deutlich erschwert, jedoch durch

eine Konjugation an ein geeignetes Vehikel vorstellbar. Dabei wird das Wirkstoffmolekül durch einen chemischen Linker an einen Antikörper, Peptid, Kohlenhydrat o.ä. gekoppelt. Diese Vehikelsysteme binden gezielt an gewebsspezifische Rezeptoren oder Transporter und dirigieren so den Wirkstoff zu seinem intendierten Wirkort, wo er unter Spaltung des Linkers freigesetzt wird. Bhat *et al*. schlagen mit der in Abbildung 11 gezeigten Struktur eine Möglichkeit vor, um das Konzept auf AZD2858 anzuwenden.[81]
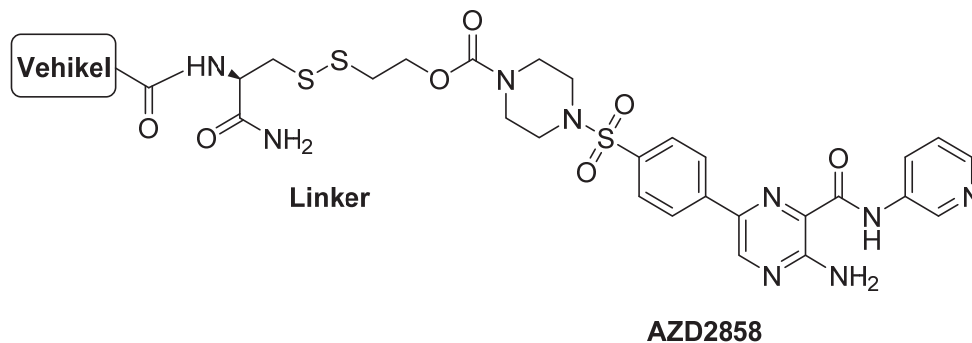
Abbildung 11. Vorschlag zur Kopplung von AZD2858 an ein Vehikel für gewebespezifisches Kinasetargeting.[81]

c) Gemäßigte GSK-3-Hemmung durch isoformselektive Hemmstoffe

Aus toxikologischer Sicht erscheint es sinnvoll, die Aktivität der GSK-3 nicht vollständig auszuschalten, sondern lediglich eine pathologische Hyperaktivität auf ein physiologisches Level abzusenken. Verschiedene Befunde aus zellphysiologischen und pharmakologischen Studien deuten an, dass eine Hemmung der Enzymaktivität um 30-50% mit einem vertretbaren Ausmaß an Nebenwirkungen, auch in Bezug auf die intrazellulären β-Catenin-Spiegel, einhergehen kann:

- Insulin und Wnt-Signale bewirken im physiologischen Kontext eine vorübergehende Hemmung der GSK-3 um 50-60%.[85]

- Knockout-Experimente in embryonalen Stammzellen zeigten die Redundanz der beiden Isoformen der Kinase im Wnt-Signalweg. Ein isoformselektiver Komplettknockout kann durch die jeweils andere Isoform kompensiert werden, sodass keine Akkumulation des onkogenen β-Catenins beobachtet wird.[20]

- Lithiumsalze sind langjährig eingesetzte Arzneistoffe zur Behandlung der affektiven Störungen.[86] Die pharmakodynamischen Effekte des Kations werden zum Teil auf eine Hemmung der GSK-3 zurückgeführt. Lithium hemmt die GSK-3 sowohl direkt durch Kompetition mit Magnesium und wahrscheinlich auch indirekt

durch Hemmung von Phosphatasen, die die GSK-3 durch Dephosphorylierung auf Ser21 in GSK-3α bzw. Ser9 in GSK-3β aktivieren.[87] Therapeutische Serumkonzentrationen (~ 1 mM) bewirken in Mäusen ähnlich ausgeprägte Effekte wie ein heterozygoter GSK-3β-Knockout (GSK-3β^{+/-}).[88] Daraus kann abgeleitet werden, dass eine Lithium-Therapie mit einer ca. 25%igen Hemmung der GSK-3 einhergeht.[89] Auch wenn im Mausmodell unter diesen Bedingungen ein Anstieg der β-Catenin-Spiegel beobachtet wird, ist aus der langjährigen Anwendung von Lithium kein onkogenes Risiko bekannt.[86,88]

In diesem Zusammenhang wird deutlich, eine isoformselektive Hemmung der GSK-3 (und damit eine maximal 50%ige Hemmung des Gesamtpools) einen geeigneten Kompromiss zwischen einem ausreichenden biologischen Effekt und einer toxikologischen Risikominimierung darstellen kann. Das rationale Design der dafür notwendigen Inhibitoren setzt ein detailliertes Verständnis für die (nur marginalen) strukturellen Unterschiede der beiden Isoformen voraus, die deshalb im folgenden Kapitel genauer beleuchtet werden sollen.

1.4.4 Isoformselektive GSK-3-Hemmung

Bei Betrachtung der Gesamtsequenz beider Isoformen der GSK-3 zeigen diese lediglich eine Übereinstimmung von 67%. Diese resultiert jedoch hauptsächlich aus signifikanten Unterschieden in den C- und N-terminalen Enden der Peptidkette. Einerseits stimmen die C-terminalen 76 Aminosäuren lediglich zu 36% überein, andererseits besitzt die α-Isoform am N-Terminus eine zusätzliche 4 kDa schwere Glycin-reiche Verlängerung.[90]

Die selektivitätsgerichtete Optimierung eines klassischen ATP-kompetitiven *Scaffolds* erfordert die Identifikation adressierbarer struktureller Unterschiede in der ATP-Bindetasche. In diesem Bereich liegt eine Identität von etwa 95% vor, da sich die beiden Isoformen dort lediglich in einer einzigen Aminosäure unterscheiden. Dabei handelt es sich um das Asp133 der Gelenkregion (β-Isoform), welches eine Wasserstoffbrücke zur Adenin-Teilstruktur des ATPs eingeht (s. Abbildung 6 in Kapitel 1.3.2). In der α-Isoform befindet sich an dieser Position das Glu196, welches sich von Asp133 lediglich durch eine um eine Methylengruppe verlängerte Seitenkette unterscheidet.[27] Da diese

Seitenkette von der ATP-Bindestelle weg ausgerichtet ist, gestaltet sich eine direkte Adressierung durch einen ATP-kompetitiven Liganden nahezu unmöglich.

Der strukturelle Vergleich der beiden Isoformen in Bezug auf die Sekundär- und Tertiärstruktur wird zusätzlich durch das Fehlen einer Kristallstruktur der α-Isoform erschwert, sodass bis kürzlich die Auswirkungen des eben beschriebenen Aminosäureaustauschs in der Gelenkregion unklar waren. Wagner *et al.* gelang es jedoch mit Hilfe eines Homologiemodells für die GSK-3α einige entscheidende topologische Unterschiede in der ATP-Bindestelle der beiden Isoformen aufzuklären.[27] Im Rahmen ihrer Untersuchungen entdeckten die Autoren ein charakteristisches Netzwerk an Wasserstoffbrücken an der Rückseite der Gelenkregion der GSK-3β, welches u.a. von den Seitenketten des Asp133 aus der Gelenkregion, sowie des Arg113 und des Glu80 aus der N-terminalen Domäne gebildet wird. Die entsprechenden Aminosäuren in der GSK-3α sind Glu196, Arg176 und Glu143. Ein Vergleich beider Isoformen durch moleculardynamische Simulationen legt nahe, dass dieses Netzwerk in der GSK-3α deutlich flüchtiger und instabiler ist. Dies führten die Autoren auf suboptimale Abstände zwischen den Seitenketten der relevanten Aminosäuren zurück, die sich auf Grund der zusätzlichen Methylengruppe des Glu196 verglichen mit dem Asp133 der β-Isoform ergeben.[27]

Um einen möglichen Einfluss dieses Wasserstoffbrückennetzwerks auf die Topologie der ATP-Bindestelle zu untersuchen, erzeugten die Autoren eine Asp133Glu-Mutante der GSK-3β, die die Röntgenkristallanalyse eines zumindest α-Isoform-*ähnlichen* Proteins ermöglichte. Durch Vergleich der Kristallstrukturen der GSK-3β und ihrer Asp133Glu-Mutante können geringfügige Unterschiede in zwei hydrophoben Taschen aufgedeckt werden. So ist einerseits die hydrophobe Region I in der GSK-3β großräumiger und tiefer, andererseits ist eine hydrophobe Tasche oberhalb der Adenin-bindenden Region in der GSK-3α-ähnlichen Mutante etwas voluminöser und weitläufiger (Abbildung 12). Die beiden Substanzen BRD0705 und BRD3731 zeigen in diesem Kontext beispielhaft wie diese Selektivitätstaschen durch Dekoration eines trizyklischen *Scaffolds* mit geeigneten raumfordernden Substituenten adressiert werden können, um isoformpräferentielle Inhibitoren zu generieren. Während BRD0705 ihre Präferenz für GSK-3α durch Besetzung der hydrophoben Tasche oberhalb der Adenin-Region mittels des Ethylsubstituenten am Stereozentrum erlangen kann, wird der voluminöse Neopentyl-Rest in BRD3731 in der größeren hydrophoben Region I der GSK-3β gut toleriert.[27]

Die recht ausgeprägte Selektivität der beiden Verbindungen am isolierten Enzym translatierte zwar im zellulären Kontext in eine nur noch ca. 5-fache Selektivität für die jeweilige Isoform. Dieser Faktor erwies sich jedoch in verschiedenen Zellmodellen bereits als ausreichend, um vorteilhafte Effekte auf die unerwünschte β-Catenin-Stabilisierung im Vergleich mit einem unselektiven Inhibitor zu bewirken.[27] Die Verbindungen liefern somit einen *Proof-of-Concept*, dass eine isoformselektive Hemmung das β-Catenin-vermittelte Nebenwirkungspotenzial einer pharmakologischen GSK-3-Inhibition minimieren kann.
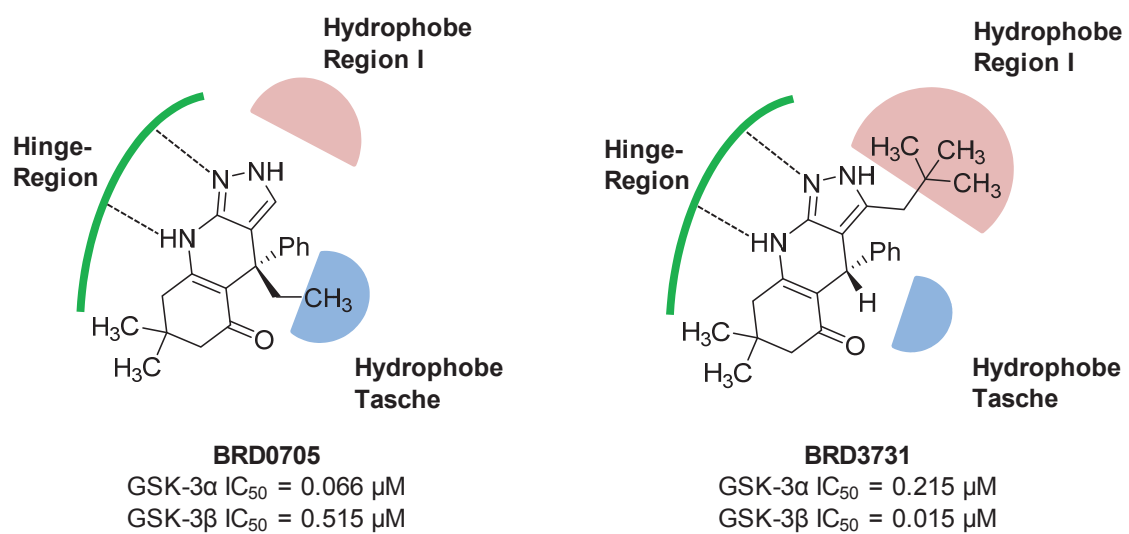
Abbildung 12. Adressierung der Selektivitätstaschen durch die isoformpräferentiellen Inhibitoren BRD0705 und BRD3731.[27]

2   Zielsetzung

Der Ursprung der hier dargelegten Arbeit liegt in Verbindung **1**, welche durch zwei unabhängige *Kinom-Screenings* als moderat potenter Inhibitor der GSK-3β identifiziert wurde. Diese Substanz leitet sich vom pan-JAK-Inhibitor Tofacitinib ab (s. Kapitel 1.2), unterscheidet sich jedoch strukturell von diesem durch den anellierten Chlor-substituierten Aromaten (Schema 1). Diesem Strukturmerkmal kommt für die Hemmung der GSK-3β entscheidende Bedeutung zu, da für Tofacitinib keine relevanten Off-Target-Effekte auf der GSK-3β bekannt sind.[91-93]
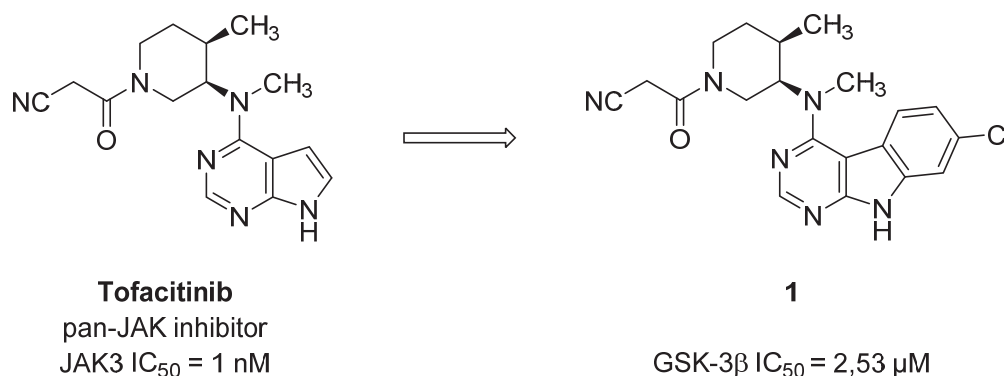
Schema 1. Strukturformeln von Tofacitinib und Verbindung **1**.[94]

Verbindung **1** stellt somit den ersten Vertreter einer neuen Klasse an Inhibitoren der GSK-3β dar, zeigt jedoch hinsichtlich ihres vermeintlich ATP-kompetitiven Hemmmechanismus eine unzureichende biologische Potenz. Ausgehend von diesem moderat potenten GSK-3β-Inhibitor sollte im Rahmen der hier dargelegten Arbeit eine Substanzbibliothek an 9*H*-Pyrimido[4,5-*b*]indol-basierten Verbindungen erstellt werden, um diese neue Klasse an Kinaseinhibitoren in den folgenden Punkten zu charakterisieren und dadurch für die Hemmung der GSK-3β zu optimieren:

(A) Identifikation der essentiellen Strukturelemente für eine potente Hemmung der Zielkinase

(B) Ableitung der wesentlichen Struktur-Aktivitäts-Beziehungen (SAR)

(C) Untersuchung der Bindemodi von ausgewählten Verbindungen an der Zielkinase

(D) Weitergehende biologische Charakterisierung vielversprechender Kandidaten hinsichtlich metabolischer Stabilität, off-Target-Effekten und in zellulären Assays

3   Ergebnisse und Diskussion

3.1   Identifikation und Modifikation der Leitstruktur

Verbindung **1** enthält das von Tofacitinib abstammende, enantiomerenreine 3-((3*R*,4*R*)-4-methyl-3-(methylamino)piperidin-1-yl)-3-oxopropannitril-Motiv (**1a**, Abbildung 13). Diese charakteristische Teilstruktur ist entscheidend für die Aktivität und Selektivität von Tofacitinib für die Familie der Janus-Kinasen, jedoch auf Grund der Methylgruppe in der 4-Position des Piperidins und der eindeutig definierten Stereokonfiguration nur über eine aufwendige Syntheseroute zugänglich.[95]
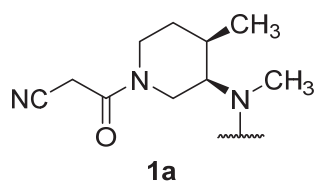
Abbildung 13. Das charakteristische 3-((3*R*,4*R*)-4-methyl-3-(methylamino)piperidin-1-yl)-3-oxopropannitril-Motiv **1a** von Tofacitinib und Verbindung **1**.

Bereits in einer frühen Phase dieses Projekts wurde das Motiv **1a** durch eine vereinfachte 3-(3-(Methylamino)piperidin-1-yl)-3-oxopropanenitril-Teilstruktur ohne Methylgruppe in der 4-Position des Piperidins ersetzt (**2**) (Schema 2). Verbindung **2** enthält entsprechend nur noch ein Stereozentrum und ist über eine deutlich vereinfachte Syntheseroute zugänglich (siehe Kapitel 3.2, sowie Details in **Publikation I**). Sie zeigte darüber hinaus (als Racemat) eine ähnliche Hemmaktivität auf der GSK-3β wie **1** und wurde aufgrund dessen frühzeitig als Leitstruktur für die Entwicklung der in dieser Arbeit dargestellten Verbindungen definiert (Schema 2). Ausgehend von diesem Templat wurden vielseitige strukturelle Modifikationen angestrebt, um die Identifikation essenzieller Strukturelemente und die Ableitung von SARs zu ermöglichen.

2
GSK-3β IC$_{50}$ = 1,86 µM

Derivate in dieser Arbeit
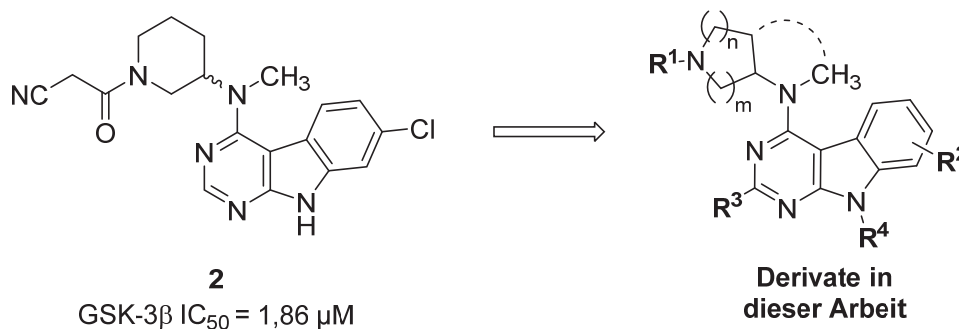
Schema 2. Entwicklung von neuartigen GSK-3β-Inhibitoren abgeleitet von Leitstruktur **2**.

Schema 3 bietet eine detaillierte Übersicht über die beabsichtigten Modifikationen an Leitstruktur **2**. Diese zielten sowohl auf die aliphatische Seitenkette des Moleküls, als auch auf das Substitutionsmuster des 9*H*-Pyrimido[4,5-*b*]indol-Grundgerüsts ab.
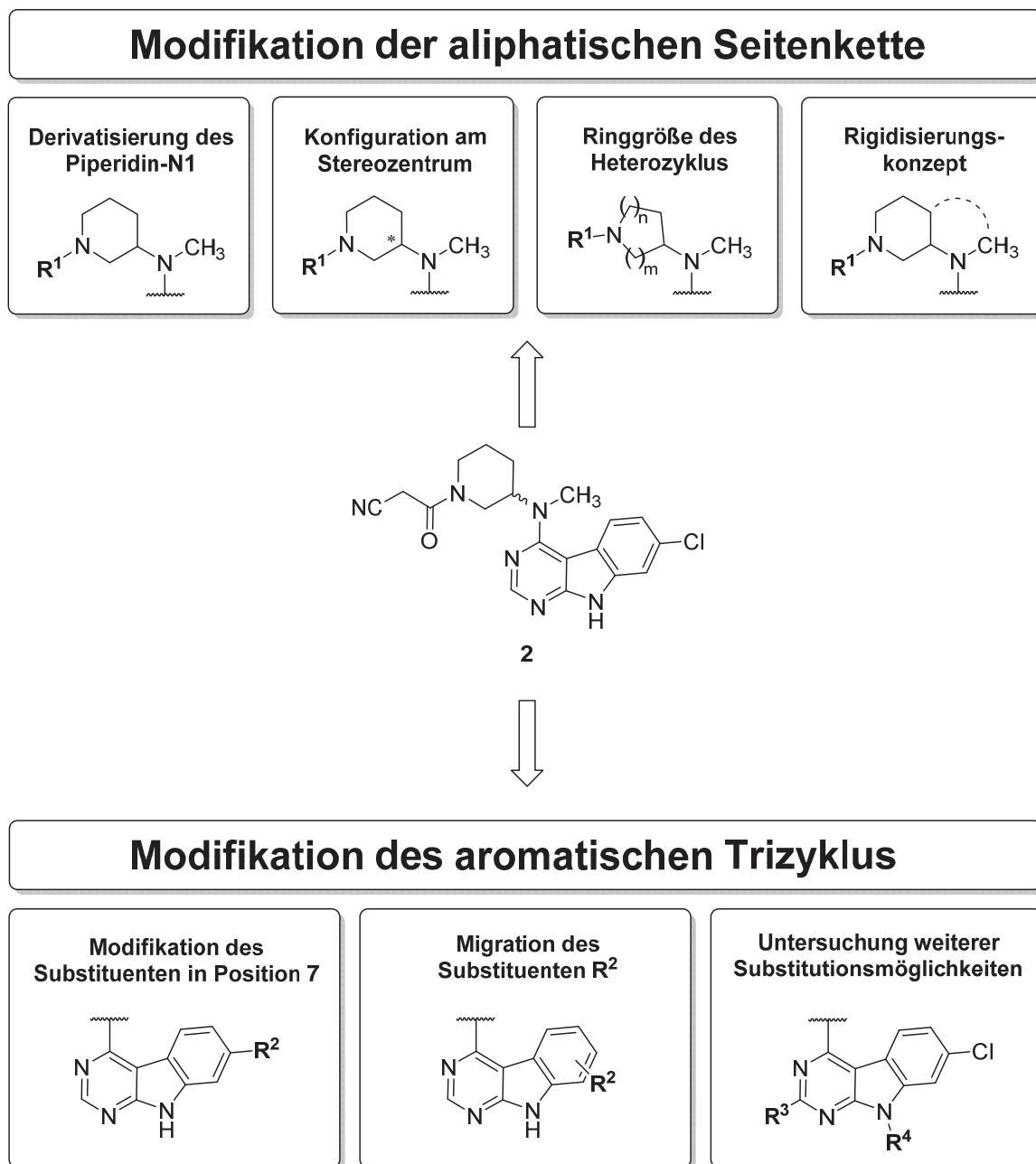
Schema 3. Angestrebte Strukturmodifikationen an Leitstruktur **2**.

3.2   Überblick über die Synthesestrategie

Die Umsetzung der beabsichtigten Modifikationen erforderte die Etablierung einer versatilen Syntheseroute zur effizienten Darstellung der gewünschten neuartigen Verbindungen. In einer konvergenten Herangehensweise wurden hierzu zunächst 4-Chlor-9-tosyl-9*H*-pyrimido[4,5-*b*]indole, sowie separat aliphatische Seitenketten als reaktive Stickstoff-Nukleophile synthetisiert (Schema 4). Diese konnten dann durch nukleophile aromatische Substitution (S$_N$Ar) variabel kombiniert werden, was eine einfache Derivatisierung und schnelles Aufstellen von SARs ermöglichte.

A

X = F oder Cl

4-5 Schritte

(**A**) Synthese der 4-Chlor-9-tosyl-9*H*-pyrimido[4,5-*b*]indole. Art und Position von **R²** wird durch das initial eingesetzte, kommerziell verfügbare Halonitrobenzol-Derivat definiert. (**Publikation II**)

B

2 Schritte

(**B**) Synthese von zyklischen aliphatischen Seitenketten mit Boc-Schutzgruppe ausgehend von kommerziell verfügbaren Ketonen. (**Publikation I**)

C

4 Schritte

(**C**) Synthese der rigidisierten Seitenkette mit vorinstalliertem Cyanethyl-Substituenten. (**Publikation I**)

D

R
S

(**D**) Kommerziell verfügbare *N*-Boc-3-aminopiperidine zur Darstellung von enantiomerenreinen Testverbindungen. (**Publikation II**)

Schema 4. Herkunft essenzieller Intermediate zur Darstellung der Testverbindungen dieser Arbeit.

Das Substitutionsmuster des trizyklischen Grundgerüsts (**R²** und **R³**) wurde dabei bereits früh in der Synthese der entsprechenden 4-Chlor-9-tosyl-9*H*-pyrimido[4,5-*b*]indole definiert (Schema 4A).

Die ringoffenen Seitenketten mit variierenden Ringgrößen wurden ausgehend von den entsprechenden kommerziell verfügbaren heterozyklischen Ketonen synthetisiert (Schema 4B). Dabei wurde auf eine Boc-Schutzgruppe für den innerzyklischen Stickstoff

zurückgegriffen und diese erst in einem späten Schritt der Syntheseroute entfernt. Die Umsetzung des Rigidisierungskonzepts gelang durch eine alternative synthetische Herangehensweise ausgehend vom aromatischen 6-Azaindol und erforderte entsprechend einen Hydrierungsschritt zur vollständigen Absättigung des bizyklischen Systems (Schema 4C). Die Darstellung enantiomerenreiner Derivate wurde durch den Einsatz der entsprechenden *N*-Boc-3-aminopiperidine realisiert (Schema 4D).

Die in Schema 4 dargestellten Intermediate wurden schließlich durch eine S_NAr miteinander verknüpft (Schema 5). In diesem Schlüsselschritt wurde eine saubere Umsetzung durch den Einsatz der Tosyl-Schutzgruppe sichergestellt. Sie erhöhte einerseits durch den elektronenziehenden Effekt die Reaktivität des Pyrimidin-Rings und verhinderte andererseits unerwünschte Nebenreaktionen in Zusammenhang mit dem Indol-Stickstoff. Auf die aromatische Substitutionsreaktion folgten typischerweise sequenzielle Entschützung-Prozeduren zur Entfernung der Tosyl- und der Boc-Schutzgruppe. Dies ermöglichte im Anschluss eine effiziente Derivatisierung des innerzyklischen Stickstoff-Atoms der Seitenkette mit variierenden Resten R^1. In wenigen Fällen war es zudem möglich in den finalen Schritten der Route alternative Substituenten R^2 (–C≡N, –C≡CH oder –Aryl) durch Palladium-katalysierte Kreuzkupplungsreaktionen oder eine Methylgruppe auf dem Indol-Stickstoff (R^4) durch Alkylierung am trizyklischen Grundgerüst einzuführen (siehe **Publikationen I und III**).
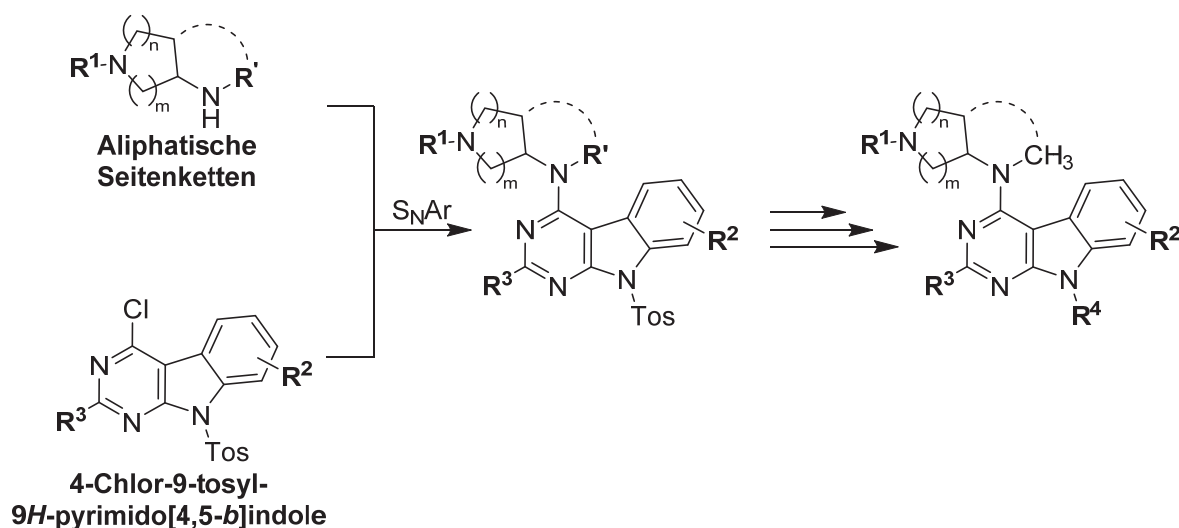
Schema 5. Grundlegende Strategie zur Darstellung der Testverbindungen dieser Arbeit.

3.3   Initiale SAR und Strukturierung des Projekts

Ausgehend von Leitstruktur **2** konzentrierten sich anfängliche Modifikationen auf die aliphatische Seitenkette, wohingegen die trizyklische 7-Chlor-9*H*-pyrimido[4,5-*b*]indol-Teilstruktur zunächst nicht verändert wurde. Dabei wurden frühzeitig die SAR der Carbonyl- und Nitrilgruppe, sowie der Einfluss der Stereokonfiguration untersucht. Die daraus hervorgegangenen Verbindungen **2-5** sind mit ihren Hemmwerten in Tabelle 1 gelistet. Die Einführung eines Cyanethyl-Rests anstelle des ursprünglichen Cyanacetyl-Substituenten (**3**) erbrachte eine 2,5-fach potentere Verbindung und damit den ersten nanomolaren Inhibitor des Projekts. Diese Verbindung stellte gleichzeitig den ersten Vertreter einer Serie an tertiären alizyklischen Aminen (im Folgenden als „Amin-Serie" bezeichnet) dar.

Tabelle 1: Initiale SAR

			IC$_{50}$ (GSK-3β) ± SEM [nM] ^{a}				
2		*rac*	1862 ± 113	**3**		*rac*	764 ± 203
		R	476 ± 36			*R*	712 ± 176
		S	≥ 10.000			*S*	489 ± 119
4			1710 ± 521	**5**			≥ 10.000

^{a} Die IC$_{50}$-Werte wurden in einem ADP Glo^{TM} Kinase Assay (Promega) bestimmt. Angegeben sind Mittelwerte von mindestens zwei unabhängigen Experimenten ± SEM. Das Assay-Protokoll ist in der *Support. Information* der **Publikationen II** und **III** beschrieben.

Im weiteren Vorgehen wurde der Einfluss der Nitrilgruppe auf die Aktivität der Inhibitoren **2** und **3** untersucht. Während die Propanoyl-substituierte Verbindung **4** eine ähnliche Aktivität wie ihr Cyanacetyl-Analogon **2** zeigte, ging der Austausch des Cyanethyl-Rests durch den korrespondierenden Propyl-Substituenten (**5**) mit einem vollständigen Verlust der inhibitorischen Potenz einher. Somit stellte sich die

Nitrilgruppe als essentiell für die Aktivität von Inhibitor **3** heraus, wohingegen sie für die Potenz von Inhibitor **2** entbehrlich erschien.

Die Evaluierung der enantiomerenreinen Isomere von **2** und **3** im Kinase-Assay lieferte ähnlich uneinheitliche Ergebnisse. So konnte im Falle von Inhibitor **2** das *R*-Enantiomer eindeutig als Eutomer identifiziert werden. Im Gegensatz dazu wurden für die Enantiomere von **3** nur marginale Aktivitätsunterschiede festgestellt.

Die frühzeitigen Trends, die trotz der strukturellen Ähnlichkeit von **2** und **3** in Bezug auf den Einfluss der Nitrilgruppe und der Stereokonfiguration beobachtet wurden, deuteten auf nicht identische Bindemodi dieser Inhibitoren an der GSK-3β hin. Diese können mitunter auf Unterschiede in der Flexibilität des Cyanacetyl- und Cyanethyl-Substituenten zurückgeführt werden. Sie bildeten eine maßgebliche Grundlage für eine frühzeitige Unterteilung der Verbindungsklasse in zwei verschiedene Serien („Amid-Serie" und „Amin-Serie") entsprechend der Art des Substituenten auf dem Piperidin-Stickstoff (Acyl- oder Alkyl). Diese Substrukturierung des Projekts wurde auch bei der Publikations-Strategie der Ergebnisse dieser Arbeit zugrunde gelegt: während die Optimierung und biologische Evaluation der Amin-Serie in den **Publikationen I** und **III** beschrieben wird, liegt der Fokus in **Publikation II** auf den Verbindungen der Amid-Serie. In den folgenden Kapiteln werden die wichtigsten Erkenntnisse der Veröffentlichungen wiedergegeben und dabei Parallelen, als auch Unterschiede der Serien ausgearbeitet und zueinander in Kontext gestellt. Auf diese Art soll trotz strukturbasierter Unterteilung des Projekts ein Gesamtüberblick über die Ergebnisse dieser Arbeit ermöglicht werden.
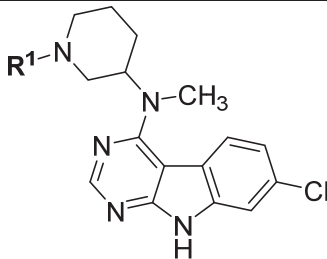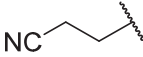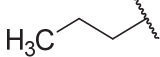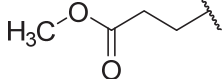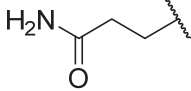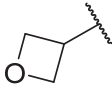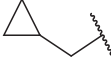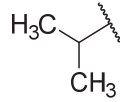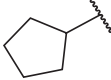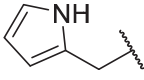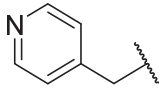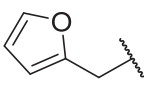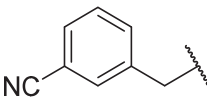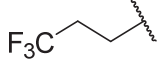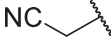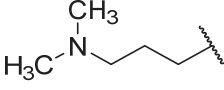
3.4   Optimierung und SAR der Amin-Serie

3.4.1 Aliphatische Seitenkette

Die Optimierung und Struktur-Wirkungs-Beziehungen der aliphatischen Seitenkette der Amin-Serie sind zu einem großen Teil in **Publikation I** beschrieben. Der Piperidin-Stickstoff stellte auf Grund seiner Reaktivität als Nukleophil ein geeignetes Zentrum für die Einführung diverser Alkylreste dar. Ausgehend vom freien sekundären Amin **6** wurde durch Michael-Additionen, nucleophile Substitutionen oder reduktive Aminierungen ein SAR-informatives Kollektiv an tertiären alizyklischen Aminen generiert (Tabelle 2). Die durchgeführten Modifikationen umfassten dabei die Einführung aliphatischer (**5**, **11** und **19**), aromatischer (**16**), alizyklischer (**10** und **12**) und heterozyklischer (**9**, **13-15**) Substituenten. Zusätzlich sollten durch geeignete Verbindungen gezielt Informationen über die Rolle der Nitril-Gruppe gewonnen werden. Dazu wurde diese Funktionalität einerseits durch alternative Wasserstoffbrückenakzeptoren (**7** und **8**) bzw. durch eine CF_3-Gruppe (**17**) ersetzt und andererseits ihr Abstand zum Piperidin-Stickstoff verkleinert (**18**). Unerwarteterweise gingen sämtliche dieser Veränderungen mit deutlichen Einbußen in der Hemmaktivität auf der Zielkinase einher. Diese identifizierten Aktivitätsklippen werden detailliert in **Publikation I** diskutiert. Sie ermöglichten wichtige Rückschlüsse über die Bedeutung des Cyanethyl-Substituenten, von denen die Wichtigsten an dieser Stelle wiedergegeben werden sollen:

- Die Nitril-Gruppe hat essentielle Bedeutung für die Aktivität von Inhibitor **3**. Dies ist wahrscheinlich auf die Ausbildung einer Wasserstoffbrücke zurückzuführen, da dies die am häufigsten beobachtete Interaktion für Nitril-Gruppen im Rahmen von Protein-Ligand-Komplexen darstellt.[96]

- Der Austausch der Nitril-Gruppe durch alternative Wasserstoffbrücken-akzeptoren wie einem Methylester (**7**), einem primären Amid (**8**), einem Cyanobenzyl-Rest (**16**) oder Heteroaromaten (**14-15**) ist mit einem vollständigen Verlust der inhibitorischen Potenz verbunden. Darüber hinaus wird der Wechsel von einer C_2- zu einer C_1-Einheit zwischen Nitril-Gruppe und Piperidin-Stickstoff (**18**) ebenfalls nicht toleriert. Folglich wird im Falle der vermuteten Ausbildung einer Wasserstoffbrücke selbige durch die einzigartige stabförmige Geometrie der Nitril-Gruppe, sowie durch ihre optimale Positionierung durch den C_2-Spacer, ermöglicht.
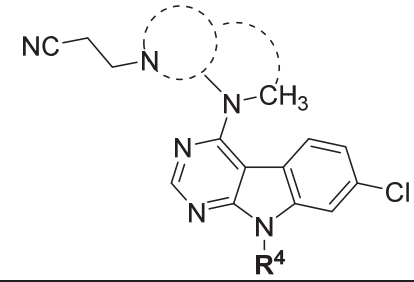
Tabelle 2: Alkylsubstituenten am Piperidin-Stickstoff

IC_{50} (GSK-3β) $\pm$ SEM [nM] [a]

3	NC~~~	764 ± 203	**5**	H_3C~~~	≥ 10.000
6 [b]	H~~~	≥ 10.000	**7**	H_3CO-C(=O)~~~	≥ 10.000
8	H_2N-C(=O)~~~	≥ 10.000	**9** [b]	oxetanyl~~~	≥ 10.000
10	cyclopropyl~~~	≥ 10.000	**11**	H_3C-CH(CH_3)~~~	≥ 10.000
12	cyclopentyl~~~	≥ 10.000	**13** [b]	pyrrolyl~~~	≥ 10.000
14	pyridyl~~~	≥ 10.000	**15**	furyl~~~	≥ 10.000
16	NC-phenyl~~~	≥ 10.000	**17**	F_3C~~~	≥ 10.000
18	NC~~~	≥ 10.000	**19**	H_3C-N(CH_3)~~~	3557 ± 664

[a] Die IC_{50}-Werte wurden in einem ADP Glo^{TM} Kinase Assay (Promega) bestimmt. Angegeben sind Mittelwerte von mindestens zwei unabhängigen Experimenten $\pm$ SEM; [b] nicht publiziert.

Basierend auf den erhobenen Daten wurde der essenzielle Cyanethyl-Substituent in den darauffolgenden Optimierungsschritten beibehalten. Weitere Untersuchungen fokussierten sich schließlich auf die Feinabstimmung der Orientierung dieses Substituenten. Dabei gingen bereits kleinste Veränderungen wie der Austausch des Piperidins durch ein Pyrrolidin (**21**) oder Azepan (**22**) mit einem 10- bzw. 2-fachen Aktivitätsverlust einher (Tabelle 3). Im Gegensatz dazu konnte durch eine Rigidisierung des aliphatischen Gerüsts (**23**) eine bioaktive Konformation der Seitenkette stabilisiert werden, was sich in einem deutlich verbesserten IC_{50}-Wert von 130 nM widerspiegelte.

Tabelle 3: Modifikationen unter Beibehaltung des Cyanethyl-Substituenten

	Seitenkette	R^4	IC_{50} (GSK-3β) $\pm$ SEM [nM] [a]
3		H	764 ± 203
20		CH_3	≥ 10.000
21		H	7017 ± 1077
22		H	1535 ± 284
23		H	130 ± 8

[a] Die IC_{50}-Werte wurden in einem ADP Glo[TM] Kinase Assay (Promega) bestimmt. Angegeben sind Mittelwerte von mindestens zwei unabhängigen Experimenten $\pm$ SEM.

Der hierfür benötigte aliphatische Bizyklus wurde dabei durch eine separate Syntheseroute ausgehend von 6-Azazindol zugänglich gemacht und ähnlich zu den anderen aliphatischen Seitenketten in einer S_NAr eingeführt (s. Kapitel 3.2 und **Publikation I**). In diesem Kontext gilt es die zwei Stereozentren des Moleküls zu berücksichtigen, die prinzipiell die Existenz von vier Stereoisomeren begründen. Jedoch verlief die katalytische Hydrierung des Boc-geschützten Azaindols, in welchem diese Stereozentren generiert werden, überwiegend selektiv für eines der zwei Enantiomerenpaare. Dies konnte durch röntgenkristallografische Experimente mit Inhibitor **23** sichergestellt werden, welche lediglich die Anwesenheit des *cis*-konfigurierten Enantiomerenpaars zeigten (Abbildung 14, experimentelle Daten zur Kristallstruktur in **Publikation I**).
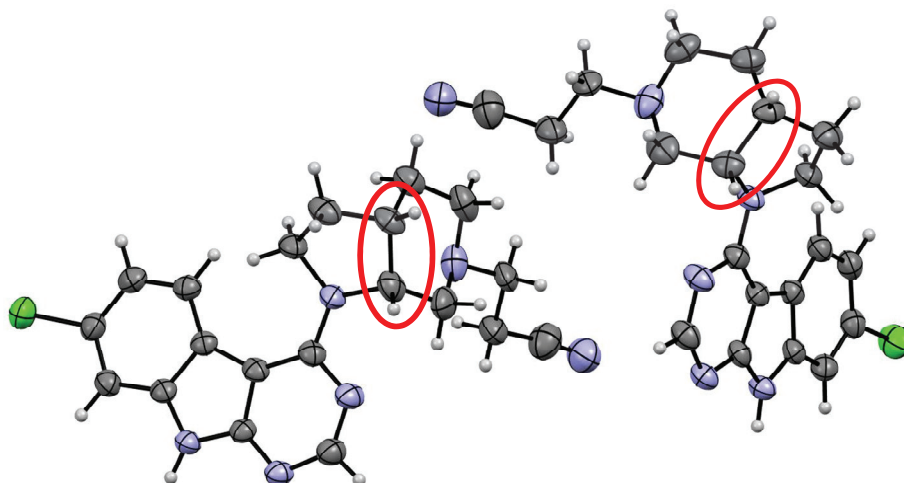
Abbildung 14. Strukturaufklärung von Inhibitor **23** mittels Röntgenkristallographie. Es liegen das (3a*S*/7a*R*)-Enantiomer (links) und das (3a*R*/7a*S*)-Enantiomer (rechts) vor. Die vicinalen Protonen an den Stereozentren (rot eingekreist) sind zueinander *cis*-ständig.

Zusammenfassend lässt sich festhalten, dass das eingesetzte 3-(Octahydro-6*H*-pyrrolo[2,3-*c*]pyridin-6-yl)propannitril-Motiv eine nahezu 15-fache Aktivitätssteigerung verglichen mit dem korrespondieren Motiv der Leitstruktur **2** erbrachte. Es stellt den Endpunkt der Optimierungsarbeit an der aliphatischen Seitenkette im Rahmen der Amin-Serie dar. Die potenten Inhibitoren **3** und **23** wurden durch zusätzliche Experimente weitergehend evaluiert, darunter Untersuchungen zur metabolischen Stabilität, ATP-Kompetition und JAK3-Hemmung. Die entsprechenden Ergebnisse werden in Kapitel 3.4.3 diskutiert.
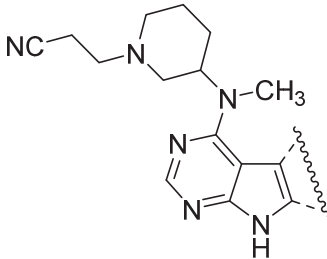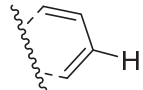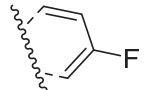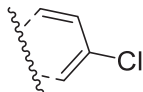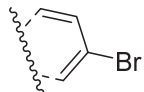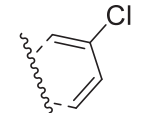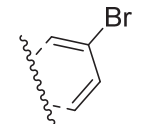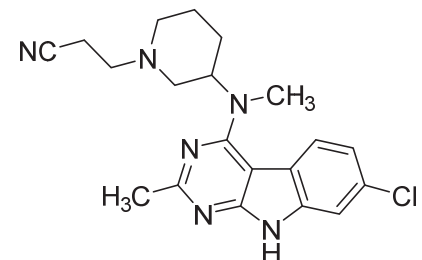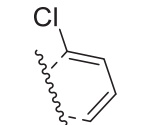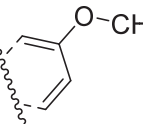
3.4.2 Trizyklisches Grundgerüst

Parallel zur Ausoptimierung der aliphatischen Seitenkette folgten in einem weiteren Teilprojekt der vorliegenden Arbeit Modifikationen am trizyklischen 9*H*-Pyrimido[4,5-*b*]indol-Grundgerüst. Diese Optimierungen sind größtenteils in **Publikation III** beschrieben. Aufgrund der synthetisch einfachen Zugänglichkeit der entsprechenden Verbindungen, wurden die Veränderungen am trizyklischen Grundgerüst zunächst unter Beibehaltung der ringoffenen Seitenkette durchgeführt (Tabelle 4).

Der Fokus lag dabei vorerst auf der Untersuchung von Halogensubstituenten auf dem terminalen Phenylring des Grundgerüsts. Die Einführung alternativer Halogene in der 7-Position des 9*H*-Pyrimido[4,5-*b*]indols sowie die Entfernung des Chlor-Atoms wurden generell gut toleriert. In den meisten Fällen resultierten hierbei ähnlich aktive Inhibitoren mit IC_{50}-Werten im dreistelligen nanomolaren Bereich (siehe **24-26**). Lediglich das iodsubstituierte Derivat **27** zeigte eine marginal niedrigere Potenz. Konträr dazu verursachte die Verschiebung des Chlor-Atoms in die 6- oder 5-Position (**28** und **30**) bzw. des Bromatoms in die 6-Position (**29**) des Trizyklus deutliche Einbußen in der biologischen Aktivität. Die Einführung einer Methoxygruppe in der 6-Position (**31**) oder einer Methylgruppe in der 2-Position (**32**) des Grundgerüsts gingen sogar mit einem vollständigen Verlust der Hemmaktivität einher.

Um weitere strukturelle Optimierungen am trizyklischen Grundgerüst zu rationalisieren, wurden in Zusammenarbeit mit dem Arbeitskreis Prof. Knapp der Goethe-Universität Frankfurt am Main Experimente zur Ko-Kristallisation ausgewählter Inhibitoren mit der GSK-3β mit anschließender Röntgenstrukturanalyse initiiert. Für diese Zwecke sollten bevorzugt die Eutomere ausgewählter potenter Inhibitoren verwendet werden. Wie bereits in Kapitel 3.3 beschrieben, konnten für Inhibitor **3** nur marginale Aktivitätsunterschiede zwischen den reinen Enantiomeren und dem racemischen Gemisch festgestellt werden. Dabei wurde dennoch das *S*-konfigurierte Enantiomer als Eutomer identifiziert. Diese Trends konnten durch das korrespondierende Set an 7-bromsubstituierten Verbindungen (siehe **26**) bestätigt werden. Die Ko-Kristallisation gelang mit Verbindung *(S)*-**3** und ermöglichte die Aufklärung des Bindemodus dieses Inhibitors in der ATP-Bindetasche der GSK-3β (Abbildung 15, experimentelle Daten zur Kristallstruktur in **Publikation III**).

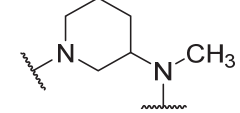**Tabelle 4**: Substitutionsmuster am 9*H*-Pyrimido[4,5-*b*]indol-Grundgerüst

IC$_{50}$ (GSK-3β) ± SEM [nM] ^{a}			
24 ^{c} (Phenyl, H)	480 ± 76	**25** ^{c} (F)	973 ± 276
3 (Cl) *rac* / *R* / *S*	764 ± 203 / 712 ± 176 / 489 ± 191	**26** (Br) *rac* ^{c} / *R* / *S*	388 ± 80 / 408 ± 99 / 319 ± 66
27 (I)	1382 ± 394	**28** (Cl)	3811 ± 118
29 (Br)	6096 ± 654		
30 (Cl)	8042 ± 617	**32**	≥ 10.000
31 ^{b} (O–CH$_3$)	≥ 10.000		

^{a} Die IC$_{50}$-Werte wurden in einem ADP Glo^{TM} Kinase Assay (Promega) bestimmt. Angegeben sind Mittelwerte von mindestens zwei unabhängigen Experimenten ± SEM; ^{b} nicht publiziert; ^{c} Projektbeitrag von Dr. Ahmed El-Gokha.

Das trizyklische 9*H*-Pyrimido[4,5-*b*]indol-Grundgerüst fungiert als Hinge-Bindungsmotiv und bildet zwei Wasserstoffbrückenbindungen zum Rückgrat der Hinge-Aminosäuren Asp133 und Val135 aus. Zusätzlich kann eine Kristallwasservermittelte Interaktion zwischen dem N-3 des Pyrimidinrings und der Carbonylgruppe von Pro136 festgestellt werden. Der dritte aromatische Ring und sowie der Chlor-Substituent sind in Richtung der hydrophoben Region I ausgerichtet. Der Piperidin-Ring der aliphatischen Seitenkette ist in der Ribose-Region positioniert. Für die Nitril-Gruppe des Cyanethyl-Substituenten kann wie vermutet eine Wasserstoffbrücke zwischen dem negativ polarisierten Nitril-Stickstoff und der Amino-Gruppe der Seitenkette von Lys85 beobachtet werden.
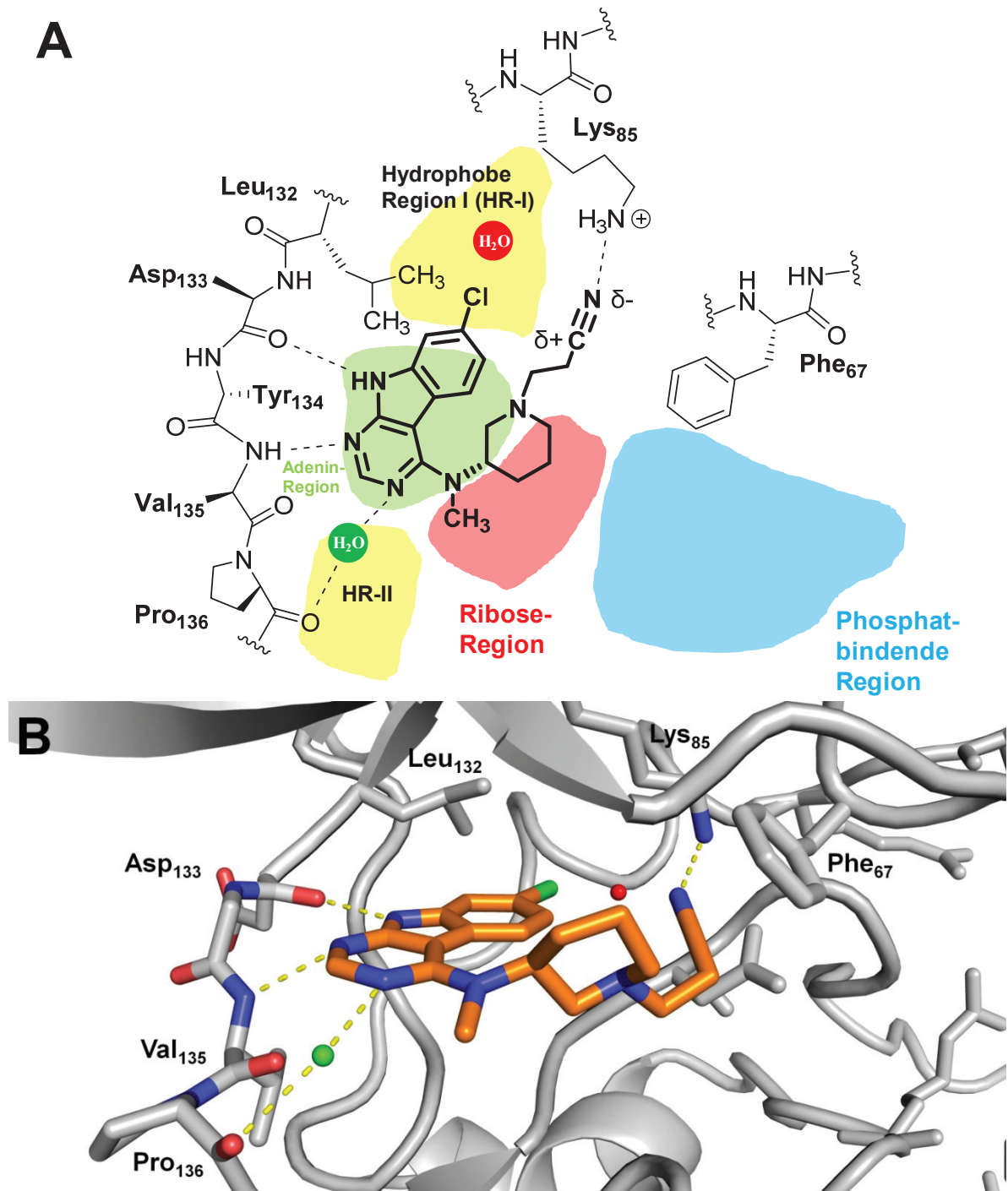
Abbildung 15. Bindemodus von *(S)*-**3** in der ATP-Bindestelle der GSK-3β abgeleitet aus der erhaltenen Röntgenkristallstruktur. Ausgewählte Kristallwassermoleküle sind als Kreise bzw. Kugeln dargestellt und entsprechend ihrer Bewertung durch WaterMap eingefärbt (grün – geringe freie Enthalpie; rot – hohe freie Enthalpie); (**A**) Schematische Darstellung;   Wasserstoffbrücken-bindungen sind als gestrichelte schwarze Linien dargestellt. (**B**) Dreidimensionale Darstellung; das Protein ist als grauer „Cartoon", der Ligand in orangefarbenen „Sticks" und Wasserstoffbrücken-bindungen als gestrichelte gelbe Linien dargestellt. Die dreidimensionale Darstellung wurde mit PyMOL (Schrödinger LLC) erstellt.[25]

Der in der Kristallstruktur beobachtete Bindemodus von Inhibitor *(S)*-**3** in der ATP-Binde-tasche der GSK-3β ermöglicht es, essenzielle SAR der Verbindungsklasse zu rationalisieren:
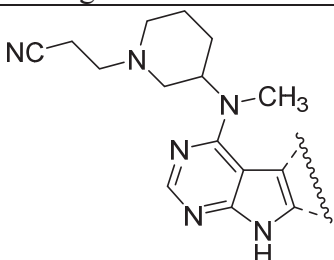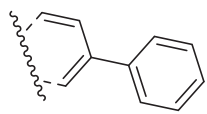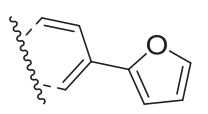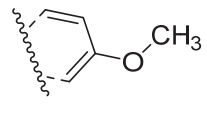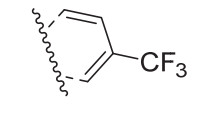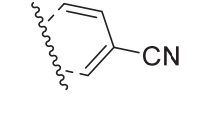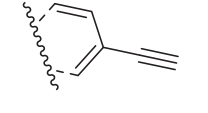
- die herausragende Aktivität von Inhibitor **3** lässt sich auf die Ausbildung der Wasserstoffbrückenbindung zwischen der Nitril-Gruppe und der Seitenkette des Lys85 zurückführen

- Die Ausbildung dieser Interaktion erfordert eine optimale Positionierung der Nitril-Gruppe, welche durch den Piperidin-Ring und die Flexibilität des C_2-Spacers ermöglicht wird.

- Die beobachtete Anordnung der aliphatischen Seitenkette würde durch größere Substituenten in der 5- und 6-Position des 9*H*-Pyrimido[4,5-*b*]indols sterisch beeinträchtigt werden. Die deutlich erniedrigte Aktivität von **28**-**31** (Tabelle 4) kann somit plausibel auf einen intramolekularen Zusammenstoß beim Einnehmen der beobachteten Konformation zurückgeführt werden.

- Ähnlich würde die Einführung eines Substituenten in der 2-Position des Pyrimidins für diesen Bindemodus einen Zusammenstoß des Inhibitors mit der Hinge-Region des Enzyms bedeuten. Entsprechend wird bereits eine Methyl-Gruppe in dieser Position nicht toleriert (siehe **32**, Tabelle 4).

- Der Indolstickstoff trägt als Wasserstoffbrücken-Donator entscheidend zur Verankerung des Inhibitors an der Hinge-Region bei. Eine Methyl-Gruppe auf diesem Stickstoff führt somit verständlicherweise zum vollständigen Verlust der Aktivität (siehe **20**, Tabelle 3).

Bei einer genaueren Begutachtung der ATP-Bindetasche der GSK-3β wurde ein eingeschlossenes Wassermolekül in der HR-I erkannt. Dies motivierte die ganzheitliche Untersuchung der Bindetasche mit dem *in silico*-Tool WaterMap der Schrödinger Suite in Zusammenarbeit mit Dr. Tatu Pantsar.[97,98] Diese Software ermöglicht es, die freie Enthalpie (Δ*G*) von Wassermolekülen in Proteinstrukturen basierend auf einer moleculardynamischen Simulationen abzuschätzen. So wurde beispielsweise das Kristallwassermolekül, welches eine polare Interaktion zwischen *(S)*-**3** und Pro136 vermittelt, mit einer geschätzten freien Enthalpie von +0,13 kJ/mol von WaterMap als (vergleichsweise) energetisch günstig bewertet. Im Gegensatz dazu wurde das eingeschlossene Wassermolekül in der hydrophoben Region I mit einer geschätzten freien Enthalpie von 6,71 kJ/mol als hochenergetisch und damit sehr ungünstig beurteilt

(Abbildung 15). Eine Adressierung dieses Wassermoleküls erschien deshalb als eine vielversprechende Strategie, um die Bindeaffinität des betrachteten Liganden zu erhöhen.

Dazu wurden im nachfolgenden Schritt geeignete Substituenten in der 7-Position des 9*H*-pyrimido[4,5-*b*]indols untersucht (Tabelle 5). Anfängliche Versuche zielten auf eine vollständige Ausfüllung der hydrophoben Tasche durch voluminöse Substituenten ab, um eine Verdrängung des Wassermoleküls zu bewirken. Die Einführung von aromatischen Ringen (**33** und **34**) oder einem Methoxy-Rest (**35**) resultierte dabei allerdings in deutlich niederpotenteren Inhibitoren. Der Einsatz einer CF₃-Gruppe (**36**) verursachte sogar einen vollständigen Verlust der Hemmaktivität. Diese Ergebnisse offenbarten (deutlicher als die Halogenserie in Tabelle 4) ausgeprägte Limitationen in Bezug auf die Größe der eingesetzten Substituenten. Ein Vergleich der van-der-Waals-Radii des Chlor- und Iod-Atoms, sowie der CF₃-Gruppe in der 7-Position verdeutlichte, dass eine passgenaue Unterbringung dieser Substituenten in der hydrophoben Region I im Besonderen von ihrer räumlichen Breite mitbestimmt wird (siehe *Supporting Information* von **Publikation III**).

Tabelle 5: Optimierung des Substituenten in der 7-Position

IC$_{50}$ (GSK-3β) ± SEM [nM] [a]

33		5112 ± 270	**34**		5299 ± 145
35 [b]		8690 ± 57	**36** [b]		≥ 10.000
37		1204 ± 146	**38**		*rac* [c] 23 ± 8 *S* 6 ± 3
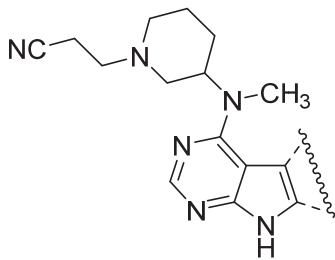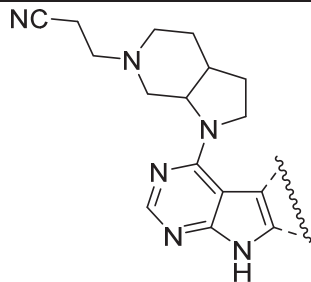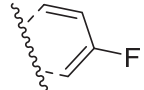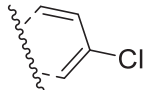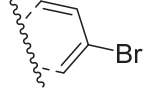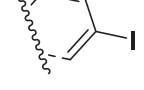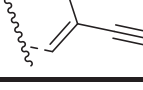
[a] Die IC$_{50}$-Werte wurden in einem ADP Glo^{TM} Kinase Assay (Promega) bestimmt. Angegeben sind Mittelwerte von mindestens zwei unabhängigen Experimenten ± SEM; [b] Projektbeitrag von Dr. Ahmed El-Gokha; [c] Die Verbindung wurde von Niclas Kahlke im Rahmen einer projektzugehörigen Masterarbeit synthetisiert.

Als Konsequenz aus den beobachteten Limitationen wurden für weitergehende Modifikation lineare Substituenten mit schmalem Radius selektiert. Die Verdrängung eines hochenergetischen Wassermoleküls mittels einer Nitril-Gruppe ist bereits in der Literatur beschrieben.[99,100] Entgegen der Erwartungen stellte sich diese Strategie in diesem Fall jedoch als nicht erfolgreich heraus, da die 7-Cyano-substituierte Verbindung **37** einen Aktivitätsverlust zeigte. Schlussendlich konnte durch die Einführung eines Ethinyl-Substituenten (**38**) eine erhebliche Verstärkung der Hemmaktivität erreicht werden. Für Inhibitor **38** wurde mit 23 nM ein um den Faktor 33 besserer Hemmwert verglichen mit dem chlorsubstituierten Analogon **3** ermittelt. Darüber hinaus zeigte sich für diese Verbindung auch ein verstärkter Einfluss der Stereokonfiguration am Piperidin auf die Aktivität: das *S*-Enantiomer von **38** zeigte einen IC_{50}-Wert von 6 nM, was sogar einer ungefähr 80-fach verbesserten Hemmaktivität verglichen mit *(S)*-**3** entspricht.

Als finaler Schritt in der Optimierung der Amin-Serie galt es schließlich zu evaluieren, ob das bereits für Inhibitor **3** beschriebene Rigidisierungskonzept auch auf andere Derivate der Serie erfolgreich angewendet werden kann. Für diese Untersuchungen wurden die in Position 7 halogenierten Analoga **25-27** sowie das Ethinyl-Derivat **38** ausgewählt. Erwartungsgemäß konnte durch die Rigidisierung der aliphatischen Seitenkette für die Mehrheit dieser Verbindungen eine beträchtliche (5 bis 10-fache) Verbesserung der inhibitorischen Potenz erzielt werden (Tabelle 6). Insbesondere ist dabei hervorzuheben, dass mit dem rigidisierten Ethinyl-Derivat **42** ein weiterer Hemmstoff mit einem IC_{50}-Wert im einstelligen nanomolaren Bereich identifiziert und damit der ausgeprägte Effekt des Ethinyl-Substituenten bestätigt werden konnte.

Tabelle 6: Einfluss der Rigidisierung auf die Hemmaktivität ausgewählter Inhibitoren

	IC$_{50}$ (GSK-3β) ± SEM [nM] [a]		
F	**25** [b]	973 ± 276	**39** [c]	2668 ± 1488
Cl	**3**	764 ± 203	**23**	130 ± 8
Br	**26** [b]	388 ± 80	**40**	66 ± 15
I	**27**	1382 ± 394	**41** [c]	132 ± 36
≡	**38** [c]	23 ± 8	**42**	2 ± 0

[a] Die IC$_{50}$-Werte wurden in einem ADP Glo^{TM} Kinase Assay (Promega) bestimmt. Angegeben sind Mittelwerte von mindestens zwei unabhängigen Experimenten ± SEM; [b] Projektbeitrag von Dr. Ahmed El-Gokha; [c] Die Verbindung wurde von Niclas Kahlke im Rahmen einer projektzugehörigen Masterarbeit synthetisiert.

3.4.3 Weitergehende biologische Untersuchungen

a) ATP-Kompetition und JAK3-Hemmung

Zum Zeitpunkt der Veröffentlichung von **Publikation I** lag die Röntgenkristallstruktur von Inhibitor *(S)*-3 im Komplex mit der GSK-3β nicht vor. Es wurde lediglich von einer Bindung von Inhibitor **3** in der ATP-Bindetasche des Enzyms ausgegangen. Um diese Vermutung zu stützten, wurde Inhibitor **3** auf ATP-Kompetition untersucht (siehe *Supporting Information* von **Publikation I**). Dazu wurden IC_{50}-Werte der Verbindung bei verschiedenen ATP-Konzentrationen bestimmt. Dabei offenbarte sich ein erheblicher Abfall der inhibitorischen Potenz bei erhöhten ATP-Konzentrationen (Tabelle 7), was die Hypothese eines ATP-kompetitiven Bindemodus bestätigte.

Tabelle 7: ATP-Kompetition von Inhibitor **3** [a]			
ATP-Konz. [µM]	25	100	500
IC_{50} [nM]	764 ± 203	2684	9260

[a] Die IC_{50}-Werte wurden in einem ADP Glo[TM] Kinase Assay (Promega) bestimmt, n = 1 für 100 µM und 500 µM ATP.

b) Kinom-Selektivität von *(S)*-38 und 42

Die Inhibitoren *(S)*-38 und **42** eigneten sich auf Grund der hohen Potenz für eine Untersuchung ihrer Selektivität im Kinom. Um diese abzuschätzen wurde ein Kollektiv von 57 Kinasen gewählt und jeweils die prozentuale Hemmung, die bei einer Inhibitor-Konzentration von 500 nM resultiert, bestimmt. Neben der am stärksten gehemmten GSK-3β wurden dabei nur wenige weitere Kinasen zu mehr als 50% gehemmt (Tabelle 8). Die Ergebnisse deuten somit ein ordentliches Selektivitätsprofil der untersuchten Inhibitoren im Kinom an. Interessanterweise wurden die nahezu identischen Off-Targets grundsätzlich durch **42** stärker als durch *(S)*-38 gehemmt. Die erhobenen Daten lassen entsprechend vermuten, dass die Rigidisierung der aliphatischen Seitenkette auch im Falle der Off-Targets eine Erhöhung der inhibitorischen Potenz bewirkt.

Tabelle 8: Selektivität von *(S)*-38 und 42 in einem Kollektiv von 57 Kinasen		
Kinase	Hemmung durch *(S)*-38 (%)	Hemmung durch 42 (%)
GSK-3β	97	vollständig
Fyn	84	94
LOK	81	89
KDR	78	92
Rsk1	72	88
Lyn	69	75
Pim-1	64	72
MSK2	< 50	67
MLK1	< 50	61

[a] Kommerziell durchgeführte Untersuchung mit 57 humanen Kinasen. Aufgelistet sind alle Kinasen, die bei einer Inhibitor-Konzentration von 500 nM zu mehr als 50% gehemmt wurden.

c)   Mikrosomale Stabilität

Zur Bewertung der metabolischen Stabilität der Inhibitoren 3 und 23 wurden diese mit humanen Lebermikrosomen (HLM) inkubiert. Der Abbau der Verbindungen und die Entstehung von Metaboliten wurden über einen Zeitraum von 120 min beobachtet und mittels Flüssigchromatographie-Massenspektrometrie-Kopplung (LCMS) untersucht (Tabellen 9 und 10) (durchgeführt von Mark Kudolo aus dem Arbeitskreis Prof: Laufer, für Details siehe *Supporting Information* von **Publikation I**). Dabei konnte für beide Inhibitoren eine ausgeprägte Biotransformation beobachtet werden, die sich in kurzen HLM-Halbwertszeiten von maximal 30 min widerspiegelte. Am Endpunkt des Experiments konnten lediglich 25% von 3 und 8% von 23 als intakt detektiert werden.

Alizyklische Amine wie Piperidin, Piperazin und Morpholin stellen zwar wichtige Strukturmotive in zahlreichen Arzneistoffen dar, sind jedoch gleichzeitig als relevante Zielstrukturen für CYP450-Enzyme bekannt. Die typischen Angriffspunkte der Monooxygenasen sind dabei das Stickstoffatom, sowie die benachbarten α-Kohlenstoffatome. Entsprechend resultieren Modifikationen wie *N*-Oxidationen, *N*-Desalkylierungen, Ringoxidationen oder Ringöffnungen.[101,102] Folglich liegt nahe, dass die beobachtete metabolische Labilität von 3 und 23 auf die enthaltenen Cyanethyl-substituierten Heterozyklen zurückzuführen ist. Übereinstimmend mit dieser Hypothese wurden die korrespondierenden sekundären Amine, die durch *N*-Desalkylierung des Cyanethyl-Substituenten entstehen, als wahrscheinliche Metaboliten (m/z 316 für 3 bzw. 328 für 23) identifiziert.

Tabelle 9: Mikrosomaler Abbau von Inhibitor **3**

3
HLM t$_{1/2}$ = 30 min
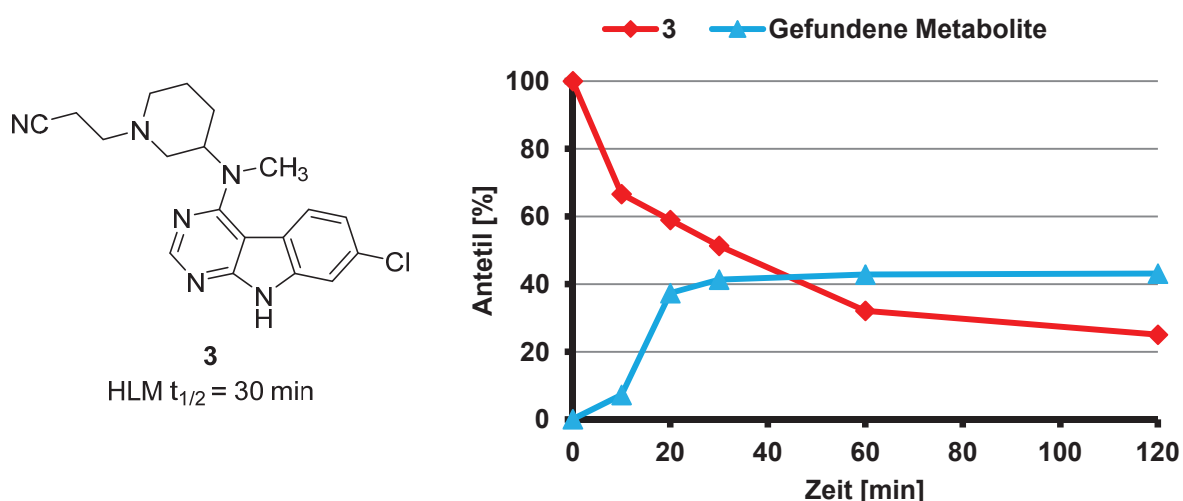
m/z der Hauptmetabolite (Anteil)	**316** (11%)	**385** (5%)	**394** (26%)
vermutete Modifikation	Desalkylierung (Elimination des Cyanethyl-Substituenten)	Monooxygenierung/ Hydroxylierung	nicht aufgeklärt

Tabelle 10: Mikrosomaler Abbau von Inhibitor **23**

23
HLM t$_{1/2}$ = 25 min
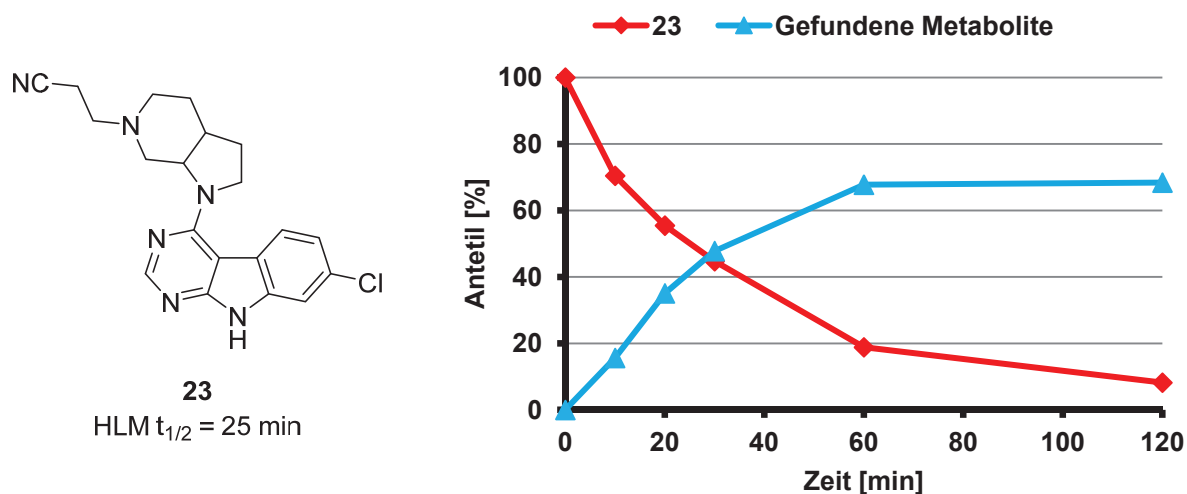
m/z der Hauptmetabolite (Anteil)	**328** (26%)	**379** (18%)	**379** (5%)	**395** (25%)
vermutete Modifikation	Desalkylierung (Elimination des Cyanethyl-Substituenten)	nicht aufgeklärt	nicht aufgeklärt	α-Carbonyl-Bildung (Lactam)

Im Falle der ringoffenen Verbindung **3** wurde das unsubstituierte sekundäre Amin (**6**, m/z 316) in Kapitel 3.4.1 bereits als inaktives Derivat beschrieben. Hinsichtlich der SAR der Amin-Serie in Bezug auf den Cyanethyl-Substituenten, ist auch für Inhibitor **23** von einem substanziellen Aktivitätsverlust im Rahmen der metabolischen *N*-Desalkylierung auszugehen. Somit offenbarte die durchgeführte Lebermikrosomen-Studie unzufriedenstellende pharmakokinetische Eigenschaften der entwickelten Inhibitoren, welche es im weiteren Verlauf der vorgelegten Arbeit zu adressieren galt (siehe Kapitel 3.5).
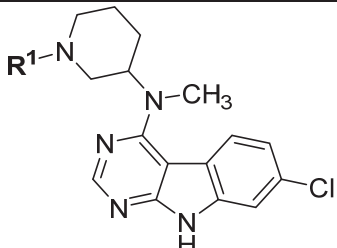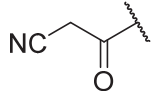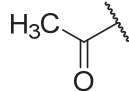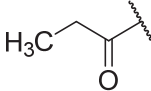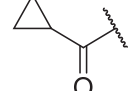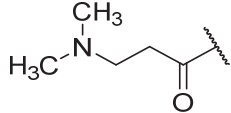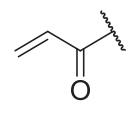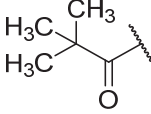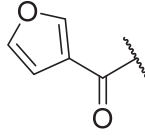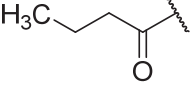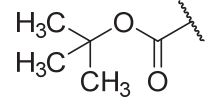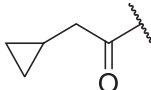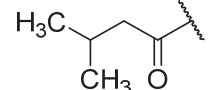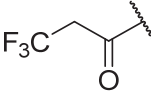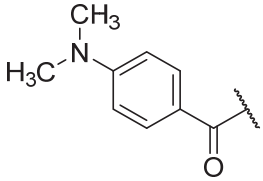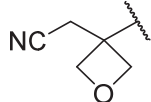
3.5   Optimierung und SAR der Amid-Serie (Publikation II)

Wie im letzten Kapitel beschrieben, konnten die im Rahmen dieser Arbeit entwickelten GSK-3β-Inhibitoren der Amin-Serie insbesondere in Bezug auf ihre inhibitorische Potenz überzeugen. Sie zeigten jedoch eine unzureichende metabolische Stabilität in Inkubationen mit humanen Lebermikrosomen, welche mitunter auf eine Abspaltung des für die Hemmaktivität essenziellen Cyanethyl-Substituenten zurückgeführt werden kann. Der vermutete Zusammenhang zwischen der metabolischen Labilität und dem Strukturmotiv des tertiären alizyklischen Amins motivierte die Einführung einer Amidbindung am Piperidin-Stickstoff als Konzept zur Stabilisierung des metabolischen Hotspots.

Zur Umsetzung dieser Strategie wurde die Leitstruktur **2** erneut in den Fokus gerückt und als Startpunkt für die Entwicklung und Optimierung einer Serie Amid-basierter GSK-3β-Inhibitoren gewählt, welche in **Publikation II** beschrieben werden.

Ähnlich zur Amin-Serie stellte der Piperidin-Stickstoff ein reaktives Zentrum für die Einführung verschiedener (Acyl-)Substituenten dar, welche durch typische Amidkupplungs-Protokolle unter Einsatz von aktivierten Carbonsäuren realisiert wurde. Der Fokus lag dabei überwiegend auf der Untersuchung von (apolaren) Kohlenwasserstoff-Resten (Tabelle 11). In diesem Kollektiv konnte ein Trend bezüglich der Hemmaktivität und der Größe der eingeführten Substituenten festgestellt werden, welcher in **Publikation II** genauer diskutiert wird. Dabei stellten sich besonders kurze, sterisch wenig anspruchsvolle Reste wie die ursprüngliche Cyanacetyl-Gruppe (**2**), aber auch Propanoyl- (**4**) und Acetyl- (**43**) als optimale Acyl-Substituenten auf dem Piperidin-Stickstoff heraus. Interessanterweise konnte somit für die Amid-Serie, gegensätzlich zur Amin-Serie, keine direkte Abhängigkeit der inhibitorischen Potenz von der Nitril-Gruppe beobachtet werden. Stattdessen ließ sich hinsichtlich des inaktiven Propyl-Derivates **5** (siehe Kapitel 3.3) ein entscheidender Beitrag der Carbonyl-Gruppe feststellen. Dieser Befund wird durch die verminderte Aktivität von Verbindung **55** gestützt, da bereits der bioisostere Austausch der Carbonyl-Gruppe durch einen Oxetan-Ring nicht toleriert wurde.[103] Basierend auf den Ergebnissen der beschriebenen Reihe wurde der ursprüngliche Cyanacetyl-, sowie die Propanoyl-Substituent im Rahmen weiterer Strukturmodifikationen beibehalten.
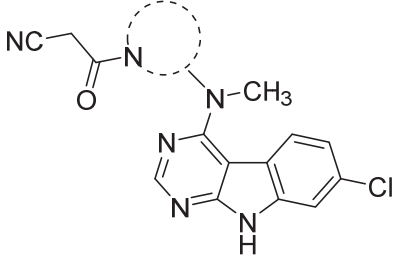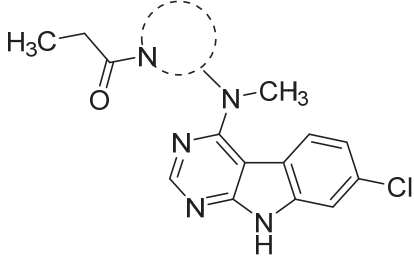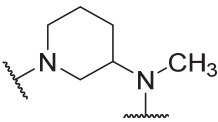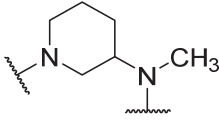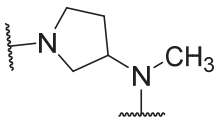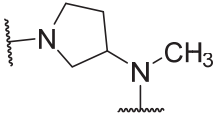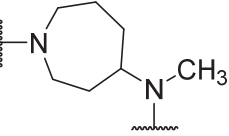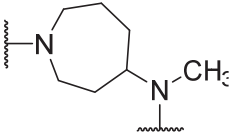
Tabelle 11: Substituenten am Piperidin-Stickstoff (Amid-Serie)

		IC$_{50}$ (GSK-3β) ± SEM [nM] [a]			
2		1862 ± 113	**43**		1571 ± 295
4		1710 ± 521	**44**		3494 ± 655
45		3828 ± 78	**46**		3921 ± 557
47		4394 ± 93	**48**		5462 ± 1029
49		7069 ± 1025	**50**		≥ 10.000
51		≥ 10.000	**52**		≥ 10.000
53		≥ 10.000	**54**		≥ 10.000
55		6,701 [b]			

[a] Die IC$_{50}$-Werte wurden in einem ADP Glo^{TM} Kinase Assay (Promega) bestimmt. Angegeben sind Mittelwerte von mindestens zwei unabhängigen Experimenten ± SEM; [b] n = 1.

Analog zu den Befunden aus der Amin-Serie konnte auch im Falle der Cyanacetyl- und Propanoyl-substituierten Verbindungen kein substantieller Vorteil bei der Untersuchung eines Pyrrolidin- oder Azepan-Rings als alternative gesättigte Heterozyklen festgestellt werden (Tabelle 12). Schlussfolgernd wurde auch für die Amid-Serie der Piperidin-Ring als bevorzugtes Strukturelement ausgewählt und im Folgenden unverändert belassen.

Tabelle 12: Modifikationen am alizyklischen Gerüst (Amid-Serie)
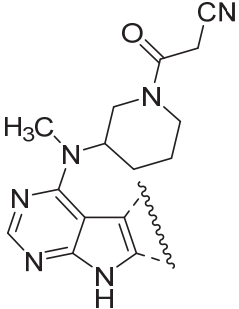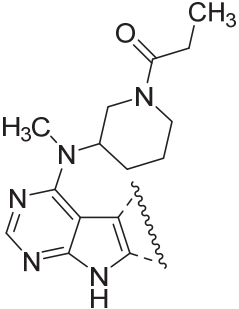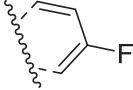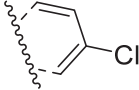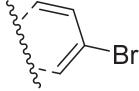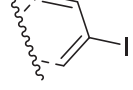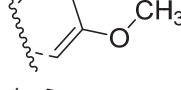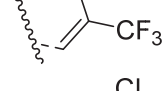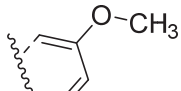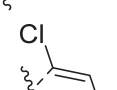
		IC$_{50}$ (GSK-3β) ± SEM [nM] [a]			
2		1862 ± 113	**4**		1710 ± 521
56 [b]		6093 ± 1809	**57** [b]		9356 ± 1076
58 [b]		1008 ± 28	**59** [b,c]		6472

[a] Die IC$_{50}$-Werte wurden in einem ADP Glo^{TM} Kinase Assay (Promega) bestimmt. Angegeben sind Mittelwerte von mindestens zwei unabhängigen Experimenten ± SEM; [b] nicht publiziert; [c] Die Verbindung wurde von Florian Wittlinger im Rahmen einer projektzugehörigen Masterarbeit synthetisiert, n = 1.

In den darauffolgenden Optimierungsschritten am 9*H*-Pyrimido[4,5-*b*]indol-Gerüst wurden ähnliche Modifikationen wie in der Amin-Serie vorgenommen (Tabelle 13). Dabei ist insbesondere die Einführung von Substituenten (Chlor-, Brom- oder Methoxy-) in der 6-Position des Trizyklus hervorzuheben (**66/74**, **67/75** und **68/76**), welche konträr zur Amin-Serie gut toleriert wurde und in Derivaten mit ähnlichen inhibitorischen Potenzen wie die 7-substituierten Analoga **2/4** und **62/72** resultierte. Die Einführung einer Methylgruppe in der Position 2 des Pyrimidins in **2** führte hingegen analog zu Verbindung **32** zu einem vollständigen Verlust der biologischen Aktivität (**79**, Strukturformel im Anhang der Arbeit gezeigt). Die Ergebnisse der Verbindungen mit modifizierten Substitutionsmustern am trizyklischen Gerüst werden in **Publikation II** detailliert diskutiert.

Tabelle 13: Substitutionsmuster des trizyklischen Gerüsts (Amid-Serie)

Aryl	Nr.		IC$_{50}$ (GSK-3β) ± SEM [nM] [a]	Nr.		IC$_{50}$ (GSK-3β) ± SEM [nM] [a]
(phenyl)	**60** [b]		1732 ± 26	**70**		4576 ± 740
F	**61** [b]		1790 ± 184	**71**		4808 ± 608
Cl	**2**	*rac*	1862 ± 113	**4**		1710 ± 521
		R	476 ± 36			
		S	≥ 10.000			
Br	**62**	*rac* [b]	1415 ± 158	**72**	*rac*	707 ± 22
		R	840 ± 74		*R*	360 ± 51
		S	≥ 10.000			
I	**63**		940 ± 172	**73**		3754 ± 652
O–CH$_3$	**64** [b]		≥ 10.000	-		- [c]
CF$_3$	**65** [b]		≥ 10.000	-		- [c]
Cl	**66**		2295 ± 70	**74**		1254 ± 27
Br	**67**		2010 ± 200	**75**		1271 ± 474
O–CH$_3$	**68**		2535 ± 111	**76**		1175 ± 34
Cl	**69**		8202 ± 1273	**77**		≥ 10.000

[a] Die IC$_{50}$-Werte wurden in einem ADP Glo^{TM} Kinase Assay (Promega) bestimmt. Angegeben sind Mittelwerte von mindestens zwei unabhängigen Experimenten ± SEM; [b] Projektbeitrag von Dr. Ahmed El-Gokha; [c] nicht untersucht.

In Bezug auf den Substituenten am Piperidin-Stickstoff (Cyanacetyl- oder Propanoyl-) konnte aus dieser Serie vielseitig dekorierter 9*H*-Pyrimido[4,5-*b*]indole kein eindeutiger Favorit identifiziert werden. Jedoch gelang es durch die Synthese der reinen Enantiomere ausgewählter Inhibitoren aus diesem Kollektiv einen entscheidenden Aktivitätsgewinn zu erzielen. So zeigten analog zur bereits in Kapitel 3.3 diskutierten Leitstruktur **2** auch die *R*-Enantiomere der 7-Brom-substituierten Derivate **62** und **72** IC$_{50}$-Werte im nanomolaren Bereich und damit ähnliche inhibitorische Potenzen wie ihre korrespondierenden Analoga aus der Amin-Serie (Verbindungen **3** und **26**, Tabelle 4). Die Eutomere *(R)*-**2** und *(R)*-**72** wurden deshalb als potenteste Vertreter der Amid-Serie für weitergehende Charakterisierungen, insbesondere der Untersuchung ihrer mikrosomalen Stabilität, selektiert.

3.5.1 Weitergehende biologische Untersuchungen

a) Modellierung des Bindemodus durch molekulardynamische Simulationen

Zur Modellierung der Bindemodi der Inhibitoren *(R)*-**2** und *(R)*-**72** in der ATP-Bindetasche der GSK-3β wurden in Zusammenarbeit mit Dr. Tatu Pantsar 1 µs molekulardynamische Simulationen in Maestro (Schrödinger Release 2019-3/4, Schrödinger LLC, New York, NY, US) unter Verwendung einer publizierten Kristallstruktur (PDB ID: 4PTC) durchgeführt.[104] Die Details zu diesen *in silico* Experimenten sind in **Publikation II** beschrieben. Auf Grund ähnlicher Ergebnisse beider Inhibitoren im Rahmen der Simulationen, wird im Folgenden lediglich der Bindemodus von *(R)*-**72** beispielhaft veranschaulicht. In Abbildung 16A ist dazu schematisch eine repräsentative Momentaufnahme des während der Simulation beobachteten Bindemodus dargestellt.

Im Einklang mit der Röntgenkristallstruktur von Inhibitor *(S)*-**3** konnte in den molekulardynamischen Simulationen die Ausbildung von stabilen Wasserstoffbrücken zwischen dem trizyklischen 9*H*-Pyrimido[4,5-*b*]indol-Grundgerüst sowie eine Ausrichtung des Halogens in Position 7 zur hydrophoben Region I festgestellt werden. Ebenfalls tritt die Kristallwasser-vermittelte Interaktion zwischen dem N-3 de Pyrimidins und Pro136, wenn auch mit recht geringer Ereignishäufigkeit von 12%, auf.

Jedoch wird beim Vergleich des modellierten Bindemodus von *(R)*-72 und des kristallografisch bestimmten Bindemodus von *(S)*-3 eine unterschiedliche Positionierung des Piperidinrings augenscheinlich, was maßgeblich auf die entgegengesetzte räumliche Anordnung am Stereozentrum zurückgeführt werden kann (Abbildungen 16B und 16C). So ragt das Piperidin im Falle von *(R)*-72 in eine kleine lipophile Tasche am Boden der ATP-Bindestelle, was in einer gänzlich anderen Ausrichtung des Propanoyl-Substituenten verglichen mit dem Cyanethyl-Substituenten von *(S)*-3 resultiert. Dabei geht die Carbonyl-Gruppe von *(R)*-72 zwar keine direkten Wechselwirkungen mit dem Enzym ein, jedoch kann die Ausbildung von Kristallwasservermittelte Wasserstoffbrücken zu Ser66 und Asp200 mit Ereignishäufigkeiten von 42% bzw. 32% beobachtet werden.

Die nicht identischen Konformationen der aliphatischen Seitenkette im aufgeklärten Bindemodus von *(S)*-3 und dem modellierten Bindemodus von *(R)*-72 können als Grundlage dienen, um die z.T. uneinheitlichen SARs der Amin- und Amid-Serie zu rationalisieren. Beide Bindemodi werden wesentlich von der Konfiguration des Stereozentrums mitbestimmt. So erscheint es sinnvoll, dass im Falle der Amin-Serie die *S*-Enantiomere einheitlich eine etwas bessere Hemmaktivität zeigen, während in der Amid-Serie die *R*-Enantiomere eindeutig als Eutomere identifiziert werden konnten. Da außerdem im Falle von *(R)*-72 der Substituent am Piperidin-Stickstoff in der modellierten Konformation der gesamten Seitenkette nicht mit Lys83 wechselwirken kann, ist es verständlich, dass eine Nitril-Gruppe für die Hemmaktivität dieser Amid-basierten Verbindung nicht zwingend erforderlich ist. Für diese Inhibitoren spielt hingegen die Carbonyl-Gruppe eine relevante Rolle für die inhibitorische Potenz, was durch die beobachtete Ausbildung von Kristallwasservermittelten polaren Interaktionen zum Enzym erklärt werden könnte.

b) *Evaluation in zellulären Assays*

Das zytotoxische Potential von *(R)*-72 wurde in Zusammenarbeit mit den Arbeitskreisen von Prof. Goettert und Prof. Tarozzi auf verschiedenen Zelltypen untersucht (siehe *Supporting Information* von **Publikation II**). Sowohl auf Wildtyp-Zelllinien (*Chinese hamster ovary* Zelllinie und humane Lungenfibroblasten Zelllinie MRC 5), als auch auf Krebszelllinien (humane Neuroblastom-Zelllinine SH-SY5Y, hepatozelluläre-Karzinom-Zelllinie HepG2 und humane Brustadenokarzinom-Zelllinie MCF-7) zeigte der Inhibitor selbst bei einer hohen Konzentration von 10 μM nur ein minimales zytotoxisches

Potential. Zudem übte dieser Inhibitor in neuronalen SH-SY5Y-Zellen neuroprotektive Effekte gegen oxidativen Stress in Form von Wasserstoffperoxid (100 µM) aus.
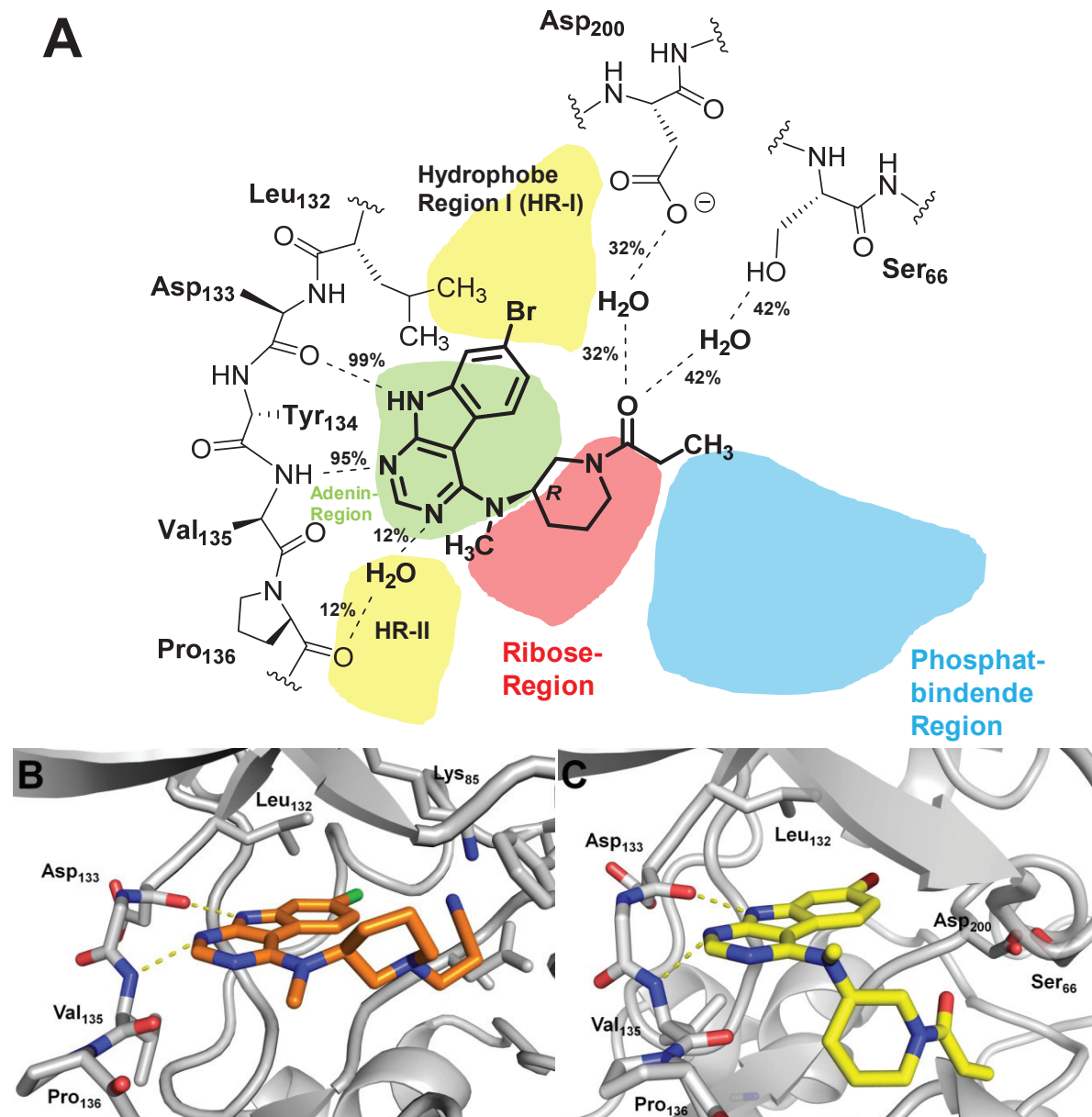
Abbildung 16. (**A**) Schematische Darstellung des modellierten Bindemodus von *(R)*-**72** in der ATP-Bindestelle der GSK-3β abgeleitet aus der 1 µs molekulardynamischen Simulation (Moment-aufnahme bei 880 ns). Wasserstoffbrückenbindungen sind als gestrichelte Linien und unter Angabe ihrer Ereignishäufigkeit (%) während der Simulation dargestellt. Dreidimensionale Darstellungen des aufgeklärten Bindemodus von *(S)*-**3** (in orangefarbenen „Sticks" in **B**) und des modellierten Bindemodus von *(R)*-**72** (in gelben „Sticks" in **C**); das Protein ist als grauer „Cartoon" und die Wasserstoffbrückenbindungen zur Hinge-Region als gestrichelte gelbe Linien dargestellt. Die dreidimensionalen Darstellungen wurden mit PyMOL (Schrödinger LLC) erstellt.[25]

c) Mikrosomale Stabilität

Im Rahmen der Evaluation der mikrosomalen Stabilität zeichneten sich für *(R)-2* und *(R)-72* deutlich verbesserte metabolische Profile verglichen mit **3** und **23** ab (Tabellen 14 und 15). Beide Verbindungen zeigten eine deutlich niedrigere Zerfallsrate, sodass zum Endpunkt der Untersuchung *(R)-2* zu 58% und *(R)-72* sogar zu 68% in intakter Form vorgefunden wurden. Die massenspektrometrischen Daten der gefundenen Metaboliten deuten mehrheitlich auf Hydroxylierungen hin (m/z 399 für *(R)-2* bzw. 432 für *(R)-72*). Dabei ist hervorzuheben, dass im Falle dieser Amid-Derivate keine Metaboliten detektiert wurden, die auf eine Abspaltung des Substituenten am Piperidin-Stickstoff deuten. Sowohl die verringerte Zerfallsrate als auch die Auswertung der Metaboliten bestätigen somit die beabsichtigte Stabilisierung des metabolischen Hotspots.

Tabelle 14: Mikrosomaler Abbau von Inhibitor *(R)-2*

m/z der Hauptmetabolite (Anteil)	**399** (2%)	**399** (10%)	**390** (8%)
vermutete Modifikation	Monooxygenierung/ Hydroxylierung	Monooxygenierung/ Hydroxylierung	nicht aufgeklärt
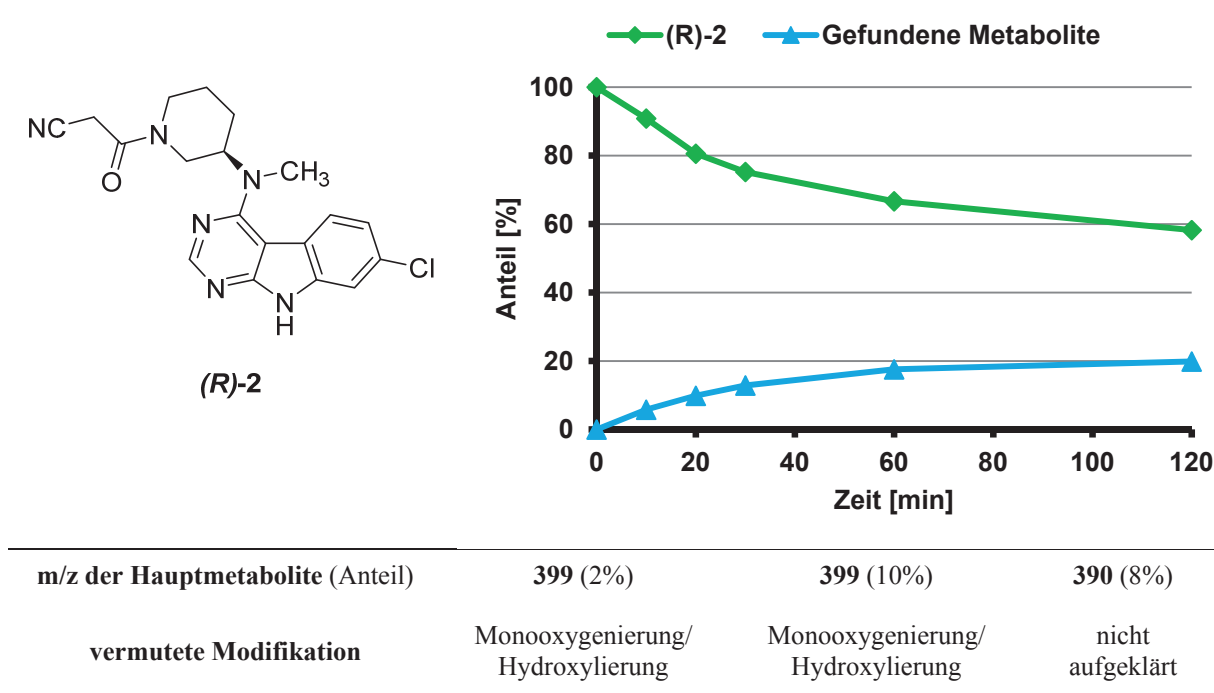
Tabelle 15: Mikrosomaler Abbau von Inhibitor *(R)*-72
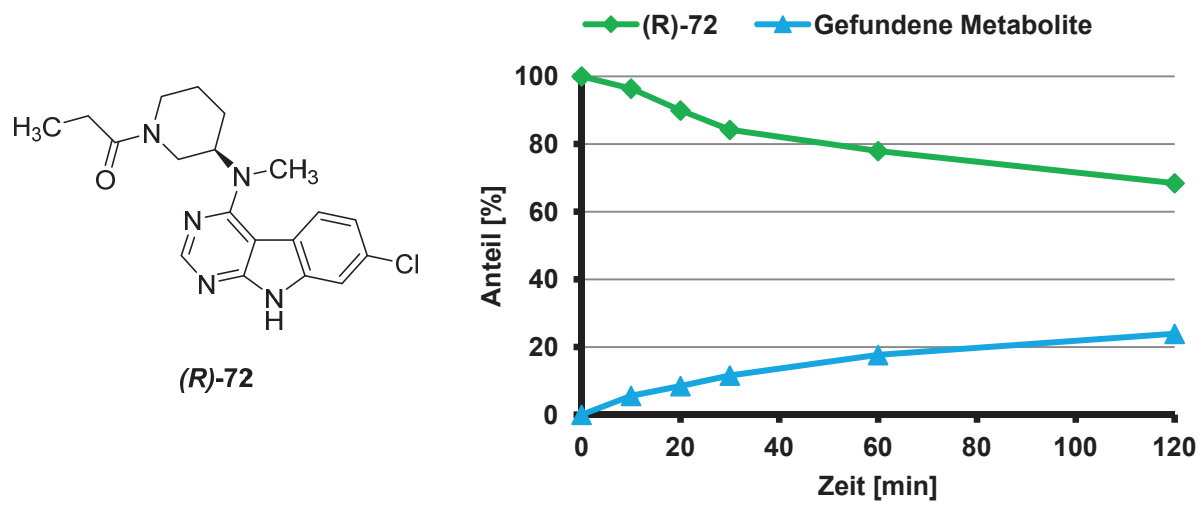
m/z der Hauptmetabolite (Anteil)	**432** (10%)	**434** (5%)	**432** (8%)
vermutete Modifikation	Monooxygenierung/ Hydroxylierung	nicht aufgeklärt	zweifache Monooxygenierung/ Hydroxylierung

4   Zusammenfassung

Ziel der vorliegenden Arbeit war die Charakterisierung und Optimierung einer neuen Klasse an 9*H*-Pyrimido[4,5-*b*]indol-basierten Inhibitoren der GSK-3β. Auf die strukturelle Vereinfachung des *Screening-Hits* 1 zur Leitstruktur 2 (siehe Kapitel 3.1) folgte basierend auf initial abgeleiteten SARs zunächst eine Unterteilung der Verbindungsklasse in eine Amin- und eine Amid-Serie. Die Etablierung einer flexiblen und variablen Synthesestrategie ermöglichte anschließend einen effizienten Aufbau einer Bibliothek strukturell diverser Verbindungen mit dem primären Ziel, diese neue Strukturklasse auf eine hochpotente Hemmung der Zielkinase zu optimieren.

Eine deutliche Erhöhung der inhibitorischen Potenz konnte insbesondere im Rahmen der Optimierung der Amin-Serie erreicht werden. Die folgenden drei Strukturmodifikationen spielten in diesem Zusammenhang eine Schlüsselrolle:

- Die Einführung eines Cyanethyl-Substituenten am Piperidin-Stickstoff
- Die Rigidisierung der aliphatischen Seitenkette durch ein Octahydro-1*H*-pyrrolo[2,3-*c*]pyridin-Gerüst
- Der Austausch des Chlor-Substituenten in Position 7 des 9*H*-Pyrimido[4,5-*b*]indol-Gerüsts durch einen Ethinyl-Substituenten

Durch ihre Kombination konnte die Hemmaktivität der Verbindungsklasse um bis zu drei Zehnerpotenzen verbessert werden (Schema 6, links), sodass ein hochpotenter Inhibitor mit einem IC_{50}-Wert von 2 nM resultierte (42).

In weiteren biologischen Untersuchungen wurde allerdings für ausgewählte Inhibitoren der Amin-Serie eine unzureichende mikrosomale Stabilität festgestellt, die strukturell auf das tertiäre alizyklische Amin der aliphatischen Seitenkette zurückgeführt werden konnte. Die Stabilisierung dieses metabolischen Hotspots wurde durch die Einführung einer Amidbindung am Piperidin-Stickstoff beabsichtigt, was zur Weiterentwicklung der Amid-Serie motivierte. Diese Optimierungsarbeit mündete u.A. in Inhibitor *(R)*-**72**, welcher durch folgende Strukturmerkmale gekennzeichnet ist (Schema 6, rechts):

- ein Propanoyl-Substituent am Piperidin-Strickstoff
- *(R)*-Konfiguration am Stereozentrum
- ein Brom-Substituent in Position 7 des 9*H*-Pyrimido[4,5-*b*]indol-Gerüsts

Neben einem IC$_{50}$-Wert von 360 nM überzeugte diese Verbindung vor allem durch eine deutlich niedrigere Zerfallsrate in der Lebermikrosomen-Studie und bestätigte die beabsichtigte Stabilisierung des metabolisch labilen Strukturmotivs.
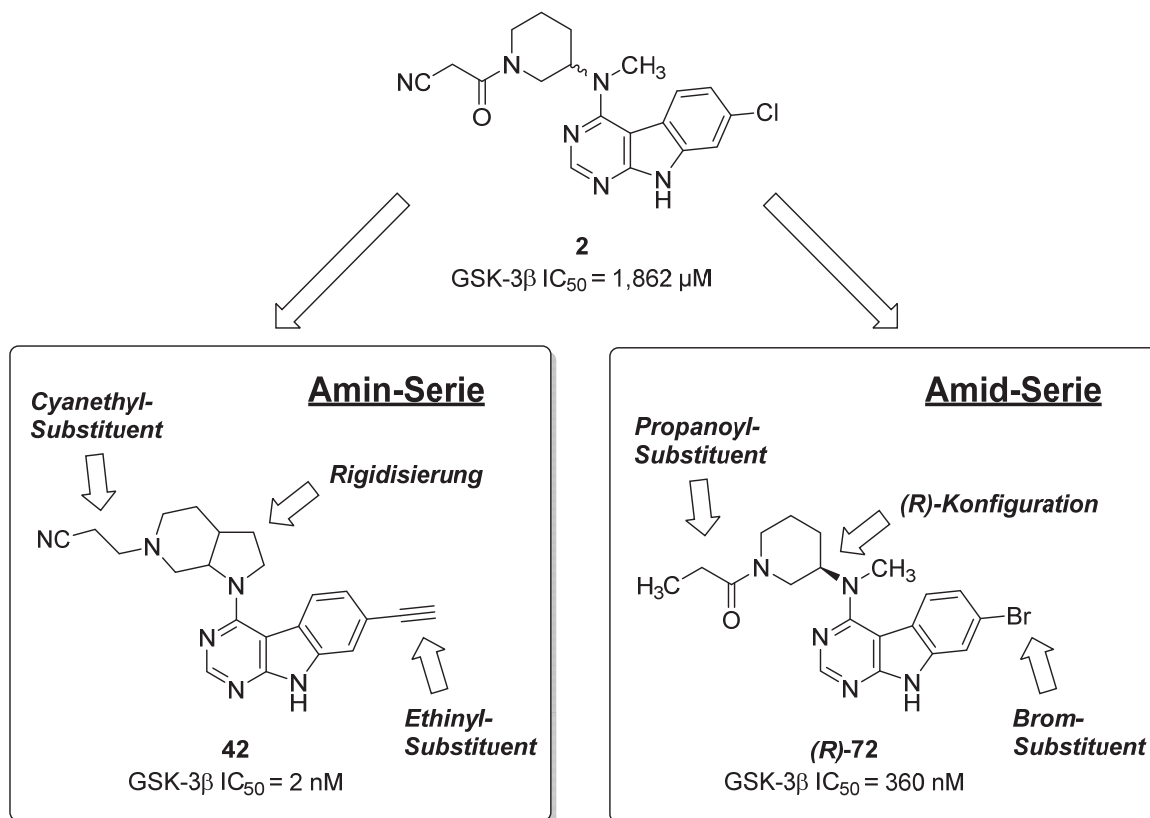
Schema 6. Weiterentwicklung von Leitstruktur **2** zu den potentesten Vertretern der Amin- und der Amid-Serie.

Im Rahmen der gezielten Entwicklung dieser Inhibitoren wurden die SARs der beiden Serien umfangreich untersucht und teilweise deutliche Unterschiede erkannt. Tabelle 16 bietet im Rahmen dieser Zusammenfassung eine umfassende Gegenüberstellung der Ergebnisse der SAR-Studien. Darüber hinaus wurden die Bindemodi von Vertretern beider Serien in der ATP-Bindetasche der GSK-3β beleuchtet. So wurde der Bindemodus von Inhibitor *(S)*-**3** durch Röntgenstrukturanalyse vollständig aufgeklärt und der Bindemodus von Inhibitor *(R)*-**72** (und weiteren) durch molekulardynamische Simulationen *in silico* modelliert. Während in beiden Fällen das 9*H*-Pyrimido[4,5-*b*]indol als Hinge-Bindungs-Motiv fungierte und der Halogensubstituent in Position 7 zur hydrophoben Region I ausgerichtet war, wurden für die aliphatische Seitenkette und den Substituenten auf dem Piperidin-Ring deutlich unterschiedliche Konformationen und Interaktionsmuster beobachtet. Daraus schlussfolgernd konnten die uneinheitlichen SARs der beiden untersuchten Serien plausibel rationalisiert werden.

Tabelle 16: SAR von 9*H*-Pyrimido[4,5-*b*]indol-basierten
Inhibitoren der GSK-3β im Rahmen dieser Arbeit
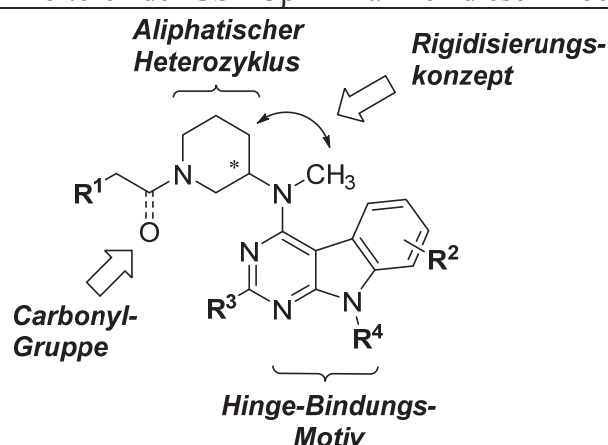
Strukturmerkmal	Amin-Serie	Amid-Serie
Carbonyl-Gruppe	(nicht vorhanden)	• C=O essentiell für die Hemmaktivität • bioisosteres Oxetan wird nicht toleriert • metab. Stabilität ↑↑
R^1	• –C≡N essentiell für die Hemmaktivität	• kurze, sterisch wenig anspruchsvolle Reste bevorzugt (**R^1** = –H, –CH$_3$, –C≡N)
R^2	• Substituenten in Position 5 oder 6 verursachen Aktivitätsverlust • kleinere Halogene (–F, –Cl, –Br) werden in Position 7 toleriert • –C≡CH in Position 7 bewirkt einen Aktivitätsgewinn um nahezu zwei Zehnerpotenzen	• Substituenten in Position 7 **und** 6 werden toleriert (bevorzugt –Cl und –Br)
R^3	Einführung von –CH$_3$ wird nicht toleriert	
Hinge-Bindungs-Motiv (R^4)	• H-Brücken-Donator erforderlich • Einführung von –CH$_3$ wird entspr. nicht toleriert	-
Stereo-konfiguration	*S > R*	*R > S*
Aliphatischer Heterozyklus	Piperidin-Ring bevorzugt	
Rigidisierungs-konzept	• bewirkt in den meisten Fällen einen Aktivitätsgewinn um Faktor 5-10	-

Zusätzlich zur Untersuchung der mikrosomalen Stabilität wurden ausgewählte Hemmstoffe weitergehend biologisch evaluiert und überzeugten dabei durch vielversprechende Selektivitätsdaten bzw. ein günstiges Zytotoxizitätsprofil. Zudem ist durch den mittels Röntgenstrukturanalyse aufgekärten Bindemodus ersichtlich, dass das 9*H*-Pyrimido[4,5-*b*]indol-*Scaffold* eine strukturelle Adressierung der hydrophoben Region I ermöglicht, was eine geeignete Strategie zur Identifikation isoformselektiver Inhibitoren darstellen kann. Die vielversprechenden Ergebnisse dieser Arbeit verdeutlichen somit die Relevanz der neu etablierten Strukturklasse und bilden eine solide Grundlage für zukünftige medizinalchemische und pharmakologische Studien zur Weiterentwicklung und Charakterisierung der 9*H*-Pyrimido[4,5-*b*]indol-basierten GSK-3(β)-Inhibitoren.

5   Experimenteller Teil

5.1   Allgemeine Information

Alle verwendeten Reagenzien und Lösemittel wurden kommerziell bezogen und ohne weitere Aufreinigung verwendet.

Die Dünnschichtchromatographie (DC) wurden auf DC Kieselgel 60 F_{254} Aluminium-Platten von Merck (Darmstadt, Deutschland) oder auf Alugram Sil G/UV$_{254}$ Platten von Macherey-Nagel (Düren, Deutschland) durchgeführt. Die Banden wurden unter UV-Licht (254 nm) detektiert.

Die Hochleistungsflüssigkeitschromatographie (HPLC) wurde auf einem HP1090 LC series II System von Hewlett-Packard oder einem 1100 series System von Agilent Technologies (Santa Clara, CA, USA), jeweils ausgestattet mit einer Binärpumpe, einem Autosampler, einem Dioden-Array-Detektor (Detektion bei 254 und 230 nm) und einer Phenomenex Luna 5μ C8 RP Säule (150 mm x 4,6 mm) von Phenomenex (Torrance, CA, USA), durchgeführt. Die mobilen Phasen A (HPLC MeOH) und B (0,01M aq. KH_2PO_4 eingestellt auf pH 2,3) wurden in einer Flussrate von 1,5 mL/min und mit folgendem Gradienten bewegt: Phase A über acht Minuten von 40 auf 85%, Phase A für fünf Minuten konstant bei 85%, Phase A über zwei Minuten von 85% auf 40%, Phase A für eine Minute kostant bei 40%, volle Zeitspanne eines Runs folglich 16 Minuten.

Die Flashchromatographie wurde auf einer PuriFlash 430 von Interchim (Montluçon, Frankreich) durchgeführt. Als Vorsäulengel wurde Geduran Si60 63-200 micron von Merck (Darmstadt, Deutschland) verwendet. Als Trennsäulen wurden selbstgepackte Säulen mit Davisil LC60A 20-34 micron von Grace Davison (Columbia, USA) oder vorgepackte Säulen von Interchim (Montluçon, Frankreich) verwendet. Die mobilen Phase sind für jede aufgereinigte Verbindung in der experimentellen Vorschrift beschrieben.

Die Kernresonanzspektroskopie (NMR) wurde auf Avance 200, 300 und 400 MHz Geräten von Bruker (Billerica, MA, USA) durchgeführt. Die Spektren wurden auf die verwendeten deuterierten Lösemittel kalibriert. Die Signale sind in ppm angegeben und bezogen auf Tetramethylsilan ($\delta = 0$).

Die Massenspektrometrie wurde auf einer DC-MS gekoppelten Expression CMS Apparatur von Advion (Ithaca, NY, USA), ausgestattet mit einer Advion Plate Express TLC plate reader von Advion (Ithaca, NY, USA) und einer PU-980 intelligent HPLC

Pumpe von Jasco (Tokio, Japan) durchgeführt. Die Analyten wurden mit LCMS MeOH von der DC Platte eluiert und mittels Elektrospray-Ionisation ionisiert. Die Apparatur wurde im ESI (+) Modus (Kapillartemperatur 250 °C, Kapillarspannung 180 V, Gastemperatur 250 °C und ESI Spannung 3500 V) und im ESI (–) Modus (Kapillartemperatur 250 °C, Kapillarspannung 180 V, Gastemperatur 250 °C und ESI Spannung 3500 V) betrieben.

5.2   Synthese unpublizierter Verbindungen

Die im Folgenden beschriebenen Verbindungen wurden ausgehend von 7-Chlor-*N*-methyl-*N*-(piperidin-3-yl)-9*H*-pyrimido[4,5-*b*]indol-4-amin (**6**) bzw 6-Methoxy-*N*-methyl-*N*-(piperidin-3-yl)-9*H*-pyrimido[4,5-*b*]indol-4-amin synthetisiert. Die Substituenten am Piperidin-Stickstoff wurden dabei durch eine reduktive Aminierung von geeigneten Carbonylverbindungen (**9** und **13**) oder durch Michael-Addition (**31**) entsprechend den in **Publikation I** beschriebenen synthetischen Protokollen eingeführt.

5.2.1   7-Chlor-*N*-methyl-*N*-(1-(oxetan-3-yl)piperidin-3-yl)-9*H*-pyrimido[4,5-*b*]indol-4-amin (**9**)
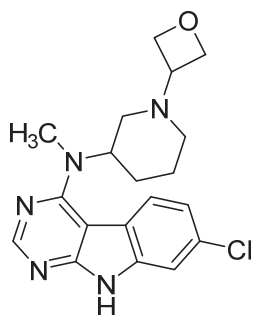
7-Chlor-*N*-methyl-*N*-(piperidin-3-yl)-9*H*-pyrimido[4,5-*b*]indol-4-amin (30.0 mg, 0.10 mmol) wurden in trockenem DCM (4,5 mL) über etwas Na$_2$SO$_4$ (35 mg) gerührt. 3-Oxetanon (24.0 mg, 0.33 mmol), AcOH (11.4 mg, 0.19 mmol) und Na(OAc)$_3$BH (40.3 mg, 0.19 mmol) wurden zugefügt und der Ansatz bei RT und unter N$_2$-Atmosphäre für 2 h gerührt. Der Ansatz wurde mit DCM verdünnt und mit gesättigter NaHCO$_3$-Lösung (4 x 15 mL) gewaschen. Die organische Phase wurde über Na$_2$SO$_4$ getrocknet und am Rotationsverdampfer eingeengt. Der Rückstand wurde säulenchromatographisch augefereingt (SiO$_2$, DCM:MeOH Gradientenelution von 96:4 zu 93:7). Ausbeute: 22 mg (62%). ^{1}H NMR (300 MHz, DMSO-*d$_6$*) δ 12.21 (s, 1H), 8.40 (s, 1H), 7.80 (d, *J* = 8.6 Hz, 1H), 7.48 (d, *J* = 1.9 Hz, 1H), 7.27 (dd, *J* = 8.6, 2.0 Hz, 1H), 4.59 – 4.37 (m, 5H), 3.50 – 3.41 (m, 1H), 3.15 (s, 3H), 2.88 – 2.77 (m, 1H), 2.71 – 2.62 (m, 1H), 2.19 – 2.06 (m, 1H), 1.92 – 1.68 (m, 4H), 1.65 – 1.47 (m, 1H); ^{13}C NMR (101 MHz, DMSO-*d$_6$*) δ 159.4, 157.5, 153.7, 137.4, 129.1, 123.8, 120.3, 118.5, 110.8, 97.1, 74.6, 74.6, 58.6, 54.5, 52.3, 49.1, 32.8, 27.2, 24.1; ESI-MS (m/z) 372.0 [M+H]$^+$, 393.9 [M+Na]$^+$, 370.0 [M-H]$^-$; HPLC: t$_r$ = 3,560 min.

5.2.2   N-(1-((1H-pyrrol-2-yl)methyl)piperidin-3-yl)-7-chlor-N-methyl-9H-pyrimido[4,5-b]indol-4-amin (13)
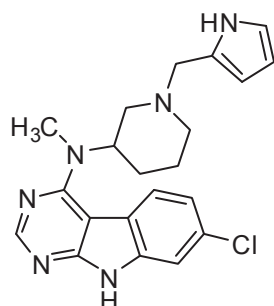
7-Chlor-N-methyl-N-(piperidin-3-yl)-9H-pyrimido[4,5-b]indol-4-amin (70.0 mg, 0.22 mmol) und Pyrrol-2-carbaldehyd (25.2 mg, 0.27 mmol) wurden in trockenem DCM (10 mL) über etwas Na$_2$SO$_4$ (40 mg) gerührt. AcOH (26.6 mg, 0.44 mmol) und Na(OAc)$_3$BH (70.5 mg, 0.33 mmol) wurden zugefügt und der Ansatz bei RT und unter N$_2$-Atmosphäre gerührt. Nach 1,5 h wurde mittels HPLC eine Umsetzung von ca. 80 % nachgewiesen. Trockenes DCM (5 mL) wurde zugefügt, um verdampfte Mengen wiederherzustellen. Nach 3,5 h wurde mittels HPLC weiterhin eine unvollstädnige Umsetzung beobachtet, sodass mehr Na(OAc)$_3$BH (14.1 mg, 0.07 mmol) zugegeben wurde. Die Reaktion wurde nach weiteren 1,5 h Rühren gestoppt. Der Ansatz wurde mit DCM verdünnt und mit gesättigter NaHCO$_3$-Lösung (5 x 15 mL) gewaschen. Die organische Phase wurde über Na$_2$SO$_4$ getrocknet und am Rotationsverdampfer eingeengt. Der Rückstand wurde säulenchromatographisch augefereingt (SiO$_2$, DCM:(2N NH$_3$ in MeOH) Gradientenelution von 95:5 zu 92:8. Ausbeute: 66 mg (75%). ^{1}H NMR (300 MHz, DMSO-d_6) δ 12.20 (s, 1H), 10.68 (s, 1H), 8.38 (s, 1H), 7.63 (d, J = 8.7 Hz, 1H), 7.47 (d, J = 2.0 Hz, 1H), 7.26 (dd, J = 8.6, 2.1 Hz, 1H), 6.63 (dd, J = 4.1, 2.5 Hz, 1H), 5.94 – 5.84 (m, 2H), 4.47 – 4.33 (m, 1H), 3.48 (d, J = 13.4 Hz, 1H), 3.38 (d, J = 13.4 Hz, 1H), 3.12 (s, 3H), 3.00 – 2.89 (m, 1H), 2.84 – 2.75 (m, 1H), 2.28 – 2.17 (m, 1H), 1.94 – 1.62 (m, 4H), 1.60 – 1.41 (m, 1H); ^{13}C NMR (50 MHz, DMSO-d_6) δ 159.4, 157.4, 153.8, 137.3, 129.1, 127.6, 123.7, 120.6, 118.5, 117.2, 110.8, 107.5, 107.0, 97.1, 55.7, 55.1, 54.9, 52.6, 32.5, 27.5, 24.4; ESI-MS: (m/z) 395,1 [M+H]$^+$, 417.0 [M+Na]$^+$, 392,9 [M-H]$^-$; HPLC: t$_r$ = 4.877 min.

5.2.3   3-(3-((6-Methoxy-9H-pyrimido[4,5-b]indol-4-yl)(methyl)amino)piperidin-1-yl)propannitril (31)
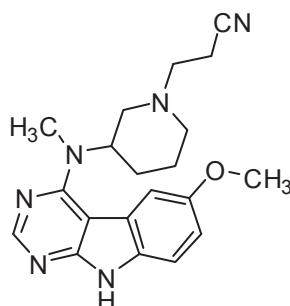
6-Methoxy-N-methyl-N-(piperidin-3-yl)-9H-pyrimido[4,5-b]indol-4-amin (60.0 mg, 0.19 mmol) und Acrylnitril (22.5 mg, 0.42 mmol) wurden in HPLC MeOH (17 mL) über Nacht bei RT gerührt. Der Ansatz wurde am Rotationsverdampfer eingeengt und der Rückstand säulenchromatographisch augefereingt (SiO$_2$, DCM:MeOH 95:5). Ausbeute: 54 mg (73%); ^{1}H NMR (400 MHz, DMSO-d_6) δ 11.91 (s, 1H), 8.38 (s, 1H), 7.40 (d, J = 8.7 Hz, 1H), 7.23 (d, J = 2.1 Hz, 1H), 7.05 (dd, J = 8.7, 2.3 Hz, 1H), 4.44 – 4.30 (m, 1H), 3.85 (s, 3H), 3.13 (s, 3H), 2.98 – 2.88 (m, 1H), 2.88 – 2.80 (m, 1H), 2.70 – 2.54 (m, 4H), 2.45 – 2.35 (m, 1H), 2.00 – 1.71 (m, 4H), 1.60 – 1.46 (m, 1H); ^{13}C NMR (101 MHz, DMSO-d_6) δ 159.9, 157.2, 153.9, 153.2, 131.2, 119.9, 113.2, 111.8, 106.1, 98.1, 55.5, 55.0, 52.9, 51.8, 32.4, 27.3, 24.3, 14.6; ESI-MS: (m/z) 365,3 [M+H]$^+$, 387.4 [M+Na]$^+$, 363,3 [M-H]$^-$; HPLC: t$_r$ = 2.040 min.

6   Literaturverzeichnis

1.   Kanev, G. K.; de Graaf, C.; de Esch, I. J. P.; Leurs, R.; Würdinger, T.; Westerman, B. A.; Kooistra, A. J. The Landscape of Atypical and Eukaryotic Protein Kinases. *Trends in Pharmacological Sciences* **2019**, *40*, 818-832.

2.   Heath, C. M.; Stahl, P. D.; Barbieri, M. A. Lipid kinases play crucial and multiple roles in membrane trafficking and signaling. *Histol Histopathol* **2003,** *18*, 989-998.

3.   Manning, G.; Whyte, D. B.; Martinez, R.; Hunter, T.; Sudarsanam, S. The Protein Kinase Complement of the Human Genome. *Science* **2002,** *298*, 1912-1934.

4.   Duong-Ly, K. C.; Peterson, J. R. The Human Kinome and Kinase Inhibition. *Current Protocols in Pharmacology* **2013,** *60*, 2.9.1-2.9.14.

5.   Dhanasekaran, N.; Reddy, E. P. Signaling by dual specificity kinases. *Oncogene* **1998,** *17*, 1447-1455.

6.   Byrne, D. P.; Foulkes, D. M.; Eyers, P. A. Pseudokinases: update on their functions and evaluation as new drug targets. *Future Medicinal Chemistry* **2017,** *9*, 245-265.

7.   Kwon, A.; Scott, S.; Taujale, R.; Yeung, W.; Kochut, K. J.; Eyers, P. A.; Kannan, N. Tracing the origin and evolution of pseudokinases across the tree of life. *Science Signaling* **2019,** *12*, eaav3810.

8.   Kinase-Disease   Associations.   Online   verfügbar: https://www.cellsignal.de/contents/resources-reference-tables/kinase-disease-associations/science-tables-kinase-disease/ (aufgerufen am 27.10.2020).

9.   Cohen, P. Protein kinases — the major drug targets of the twenty-first century? *Nature Reviews Drug Discovery* **2002,** *1*, 309-315.

10.   Roskoski, R. FDA-approved small molecule protein kinase inhibitors. Online verfügbar: http://www.brimr.org/PKI/PKIs.htm (aufgerufen am 27.10.2020).

11.   Bhullar, K. S.; Lagarón, N. O.; McGowan, E. M.; Parmar, I.; Jha, A.; Hubbard, B. P.; Rupasinghe, H. P. V. Kinase-targeted cancer therapies: progress, challenges and future directions. *Molecular Cancer* **2018,** *17*, 48.

12.   Soverini, S.; Mancini, M.; Bavaro, L.; Cavo, M.; Martinelli, G. Chronic myeloid leukemia: the paradigm of targeting oncogenic tyrosine kinase signaling and counteracting resistance for successful cancer therapy. *Molecular Cancer* **2018,** *17*, 49.

13.   Xeljanz: Highlights of prescribing information. Online verfügbar: https://www.accessdata.fda.gov/drugsatfda_docs/label/2018/203214s018lbl.pdf (aufgerufen am 16.11.2020).

14.   Carles, F.; Bourg, S.; Meyer, C.; Bonnet, P. PKIDB: A Curated, Annotated and Updated Database of Protein Kinase Inhibitors in Clinical Trials. *Molecules* **2018,** *23*, 908.

15.   Kaidanovich-Beilin, O.; Woodgett, J. GSK-3: Functional Insights from Cell Biology and Animal Models. *Frontiers in Molecular Neuroscience* **2011,** *4*.

16.   Sutherland, C. What Are the *bona fide* GSK3 Substrates? *International Journal of Alzheimer's Disease* **2011,** *2011*, 505607.

17.   Patel, P.; Woodgett, J. R. Chapter Eight - Glycogen Synthase Kinase 3: A Kinase for All Pathways? *Current Topics in Developmental Biology* **2017,** *123*, 277-302.

18.   Cohen, P.; Frame, S. The renaissance of GSK3. *Nature Reviews Molecular Cell Biology* **2001,** *2*, 769-776.

19.   Komiya, Y.; Habas, R. Wnt signal transduction pathways. *Organogenesis* **2008,** *4*, 68-75.

20.   Doble, B. W.; Patel, S.; Wood, G. A.; Kockeritz, L. K.; Woodgett, J. R. Functional Redundancy of GSK-3α and GSK-3β in Wnt/β-Catenin Signaling Shown by Using an Allelic Series of Embryonic Stem Cell Lines. *Developmental Cell* **2007,** *12*, 957-971.

21.   van Kappel, E. C.; Maurice, M. M. Molecular regulation and pharmacological targeting of the β-catenin destruction complex. *British Journal of Pharmacology* **2017,** *174*, 4575-4588.

22.   ter Haar, E.; Coll, J. T.; Austen, D. A.; Hsiao, H.-M.; Swenson, L.; Jain, J. Structure of GSK3β reveals a primed phosphorylation mechanism. *Nature Structural Biology* **2001,** *8*, 593-596.

23.   Dajani, R.; Fraser, E.; Roe, S. M.; Young, N.; Good, V.; Dale, T. C.; Pearl, L. H. Crystal Structure of Glycogen Synthase Kinase 3β: Structural Basis for Phosphate-Primed Substrate Specificity and Autoinhibition. *Cell* **2001,** *105*, 721-732.

24.   Bertrand, J. A.; Thieffine, S.; Vulpetti, A.; Cristiani, C.; Valsasina, B.; Knapp, S.; Kalisz, H. M.; Flocco, M. Structural Characterization of the GSK-3β Active Site Using Selective and Non-selective ATP-mimetic Inhibitors. *Journal of Molecular Biology* **2003,** *333*, 393-407.

25.   Schrodinger, L. The PyMOL Molecular Graphics System, Version 2.0 (2019).

26.   Traxler, P.; Furet, P. Strategies toward the Design of Novel and Selective Protein Tyrosine Kinase Inhibitors. *Pharmacology & Therapeutics* **1999,** *82*, 195-206.

27.   Wagner, F. F.; Benajiba, L.; Campbell, A. J.; Weïwer, M.; Sacher, J. R.; Gale, J. P.; Ross, L.; Puissant, A.; Alexe, G.; Conway, A.; Back, M.; Pikman, Y.; Galinsky, I.; DeAngelo, D. J.; Stone, R. M.; Kaya, T.; Shi, X.; Robers, M. B.; Machleidt, T.; Wilkinson, J.; Hermine, O.; Kung, A.; Stein, A. J.; Lakshminarasimhan, D.; Hemann, M. T.; Scolnick, E.; Zhang, Y.-L.; Pan, J. Q.; Stegmaier, K.; Holson, E. B. Exploiting an Asp-Glu "switch" in glycogen synthase kinase 3 to design paralog-selective inhibitors for use in acute myeloid leukemia. *Science Translational Medicine* **2018,** *10*, eaam8460.

28.   Fabbro, D.; Cowan-Jacob, S. W.; Moebitz, H. Ten things you should know about protein kinases: IUPHAR Review 14. *British Journal of Pharmacology* **2015,** *172*, 2675-2700.

29.   Modi, V.; Dunbrack, R. L. Defining a new nomenclature for the structures of active and inactive kinases. *Proceedings of the National Academy of Sciences* **2019,** *116*, 6818-6827.

30.   Xu, Q.; Malecka, K. L.; Fink, L.; Jordan, E. J.; Duffy, E.; Kolander, S.; Peterson, J. R.; Dunbrack, R. L. Identifying three-dimensional structures of autophosphorylation complexes in crystals of protein kinases. *Science Signaling* **2015,** *8*, rs13.

31.   Beurel, E.; Grieco, S. F.; Jope, R. S. Glycogen synthase kinase-3 (GSK3): regulation, actions, and diseases. *Pharmacology & therapeutics* **2015,** *148*, 114-131.

32.   Hughes, K.; Nikolakaki, E.; Plyte, S. E.; Totty, N. F.; Woodgett, J. R. Modulation of the glycogen synthase kinase-3 family by tyrosine phosphorylation. *The EMBO Journal* **1993,** *12*, 803-808.

33.   Frame, S.; Cohen, P. GSK3 takes centre stage more than 20 years after its discovery. *Biochemical Journal* **2001,** *359*, 1-16.

34.   Bax, B.; Carter, P. S.; Lewis, C.; Guy, A. R.; Bridges, A.; Tanner, R.; Pettman, G.; Mannix, C.; Culbert, A. A.; Brown, M. J. B.; Smith, D. G.; Reith, A. D. The Structure of Phosphorylated GSK-3β Complexed with a Peptide, FRATtide, that Inhibits β-Catenin Phosphorylation. *Structure* **2001,** *9*, 1143-1152.

35.   Dajani, R.; Fraser, E.; Roe, S. M.; Yeo, M.; Good, V. M.; Thompson, V.; Dale, T. C.; Pearl, L. H. Structural basis for recruitment of glycogen synthase kinase 3β to the axin—APC scaffold complex. *The EMBO Journal* **2003,** *22*, 494-501.

36.   Cole, A.; Frame, S.; Cohen, P. Further evidence that the tyrosine phosphorylation of glycogen synthase kinase-3 (GSK3) in mammalian cells is an autophosphorylation event. *Biochemical Journal* **2004,** *377*, 249-255.

37.   Lochhead, P. A.; Kinstrie, R.; Sibbet, G.; Rawjee, T.; Morrice, N.; Cleghon, V. A Chaperone-Dependent GSK3β Transitional Intermediate Mediates Activation-Loop Autophosphorylation. *Molecular Cell* **2006,** *24*, 627-633.

38.   Fiol, C. J.; Mahrenholz, A. M.; Wang, Y.; Roeske, R. W.; Roach, P. J. Formation of protein kinase recognition sites by covalent modification of the substrate. Molecular mechanism for the synergistic action of casein kinase II and glycogen synthase kinase 3. *Journal of Biological Chemistry* **1987,** *262*, 14042-14048.

39.   Frame, S.; Cohen, P.; Biondi, R. M. A Common Phosphate Binding Site Explains the Unique Substrate Specificity of GSK3 and Its Inactivation by Phosphorylation. *Molecular Cell* **2001,** *7*, 1321-1327.

40.   Fiol, C. J.; Wang, A.; Roeske, R. W.; Roach, P. J. Ordered multisite protein phosphorylation. Analysis of glycogen synthase kinase 3 action using model peptide substrates. *Journal of Biological Chemistry* **1990,** *265*, 6061-6065.

41.   Thomas, G. M.; Frame, S.; Goedert, M.; Nathke, I.; Polakis, P.; Cohen, P. A GSK3-binding peptide from FRAT1 selectively inhibits the GSK3-catalysed phosphorylation of Axin and β-catenin. *FEBS Letters* **1999,** *458*, 247-251.

42.   Sutherland, C.; Leighton, I. A.; Cohen, P. Inactivation of glycogen synthase kinase-3β by phosphorylation: new kinase connections in insulin and growth-factor signalling. *Biochemical Journal* **1993,** *296*, 15-19.

43.   Sutherland, C.; Cohen, P. The α-isoform of glycogen synthase kinase-3 from rabbit skeletal muscle is inactivated by p70 S6 kinase or MAP kinase-activated protein kinase-1 in vitro. *FEBS Letters* **1994,** *338*, 37-42.

44.   Goñi-Oliver, P.; Lucas, J. J.; Avila, J.; Hernández, F. N-terminal Cleavage of GSK-3 by Calpain: a new form of GSK-3 regulation. *Journal of Biological Chemistry* **2007,** *282*, 22406-22413.

45.   Ng, S. S.; Mahmoudi, T.; Danenberg, E.; Bejaoui, I.; de Lau, W.; Korswagen, H. C.; Schutte, M.; Clevers, H. Phosphatidylinositol 3-Kinase Signaling Does Not Activate the Wnt Cascade. *Journal of Biological Chemistry* **2009,** *284*, 35308-35313.

46.   Bijur, G. N.; Jope, R. S. Glycogen synthase kinase-3β is highly activated in nuclei and mitochondria. *NeuroReport* **2003,** *14*, 2415-2419.

47.   Phukan, S.; Babu, V.; Kannoji, A.; Hariharan, R.; Balaji, V. GSK3β: role in therapeutic landscape and development of modulators. *British Journal of Pharmacology* **2010,** *160*, 1-19.

48.   S3-Leitlinie Demenzen. *Arbeitsgemeinschaft der Wissenschaftlichen Medizinischen Fachgesellschaften e.V. (AWMF)* **2016,** *AWMF-Register-Nr. 038-013.*

49.   Josephs, K. A.; Whitwell, J. L.; Ahmed, Z.; Shiung, M. M.; Weigand, S. D.; Knopman, D. S.; Boeve, B. F.; Parisi, J. E.; Petersen, R. C.; Dickson, D. W.; Jack Jr, C. R. β-amyloid burden is not associated with rates of brain atrophy. *Annals of Neurology* **2008,** *63*, 204-212.

50.   Nhan, H. S.; Chiang, K.; Koo, E. H. The multifaceted nature of amyloid precursor protein and its proteolytic fragments: friends and foes. *Acta Neuropathologica* **2015,** *129*, 1-19.

51.   Ly, P. T. T.; Wu, Y.; Zou, H.; Wang, R.; Zhou, W.; Kinoshita, A.; Zhang, M.; Yang, Y.; Cai, F.; Woodgett, J.; Song, W. Inhibition of GSK3β-mediated BACE1 expression reduces Alzheimer-associated phenotypes. *The Journal of Clinical Investigation* **2013,** *123*, 224-235.

52.   Phiel, C. J.; Wilson, C. A.; Lee, V. M. Y.; Klein, P. S. GSK-3α regulates production of Alzheimer's disease amyloid-β peptides. *Nature* **2003,** *423*, 435-439.

53.   Hurtado, D. E.; Molina-Porcel, L.; Carroll, J. C.; MacDonald, C.; Aboagye, A. K.; Trojanowski, J. Q.; Lee, V. M.-Y. Selectively Silencing GSK-3 Isoforms Reduces Plaques and Tangles in Mouse Models of Alzheimer's Disease. *The Journal of Neuroscience* **2012,** *32*, 7392-7402.

54.   Aplin, A. E.; Gibb, G. M.; Jacobsen, J. S.; Gallo, J.-M.; Anderton, B. H. In Vitro Phosphorylation of the Cytoplasmic Domain of the Amyloid Precursor Protein by Glycogen Synthase Kinase-3β. *Journal of Neurochemistry* **1996,** *67*, 699-707.

55.   Rockenstein, E.; Torrance, M.; Adame, A.; Mante, M.; Bar-on, P.; Rose, J. B.; Crews, L.; Masliah, E. Neuroprotective Effects of Regulators of the Glycogen Synthase Kinase-3β Signaling Pathway in a Transgenic Model of Alzheimer's Disease Are Associated with Reduced Amyloid Precursor Protein Phosphorylation. *The Journal of Neuroscience* **2007,** *27*, 1981-1991.

56.   Sofola, O.; Kerr, F.; Rogers, I.; Killick, R.; Augustin, H.; Gandy, C.; Allen, M. J.; Hardy, J.; Lovestone, S.; Partridge, L. Inhibition of GSK-3 Ameliorates Aβ Pathology in an Adult-Onset Drosophila Model of Alzheimer's Disease. *PLOS Genetics* **2010,** *6*, e1001087.

57.   Takashima, A.; Noguchi, K.; Michel, G.; Mercken, M.; Hoshi, M.; Ishiguro, K.; Imahori, K. Exposure of rat hippocampal neurons to amyloid β peptide (25–35) induces the inactivation of phosphatidyl inositol-3 kinase and the activation of tau protein kinase I/glycogen synthase kinase-3β. *Neuroscience Letters* **1996,** *203*, 33-36.

58.   Xie, L.; Helmerhorst, E.; Taddei, K.; Plewright, B.; van Bronswijk, W.; Martins, R. Alzheimer's β-Amyloid Peptides Compete for Insulin Binding to the Insulin Receptor. *The Journal of Neuroscience* **2002,** *22*, RC221.

59.   Townsend, M.; Mehta, T.; Selkoe, D. J. Soluble Aβ Inhibits Specific Signal Transduction Cascades Common to the Insulin Receptor Pathway. *Journal of Biological Chemistry* **2007,** *282*, 33305-33312.

60.   Magdesian, M. H.; Carvalho, M. M. V. F.; Mendes, F. A.; Saraiva, L. M.; Juliano, M. A.; Juliano, L.; Garcia-Abreu, J.; Ferreira, S. T. Amyloid-β Binds to the Extracellular Cysteine-rich Domain of Frizzled and Inhibits Wnt/β-Catenin Signaling. *Journal of Biological Chemistry* **2008,** *283*, 9359-9368.

61.   Koh, S.-H.; Noh, M. Y.; Kim, S. H. Amyloid-beta-induced neurotoxicity is reduced by inhibition of glycogen synthase kinase-3. *Brain Research* **2008,** *1188*, 254-262.

62.   Köpke, E.; Tung, Y. C.; Shaikh, S.; Alonso, A. C.; Iqbal, K.; Grundke-Iqbal, I. Microtubule-associated protein tau. Abnormal phosphorylation of a non-paired helical filament pool in Alzheimer disease. *Journal of Biological Chemistry* **1993,** *268*, 24374-24384.

63.   Iqbal, K.; Liu, F.; Gong, C.-X.; Alonso, A. d. C.; Grundke-Iqbal, I. Mechanisms of tau-induced neurodegeneration. *Acta Neuropathologica* **2009,** *118*, 53-69.

64.   Drechsel, D. N.; Hyman, A. A.; Cobb, M. H.; Kirschner, M. W. Modulation of the dynamic instability of tubulin assembly by the microtubule-associated protein tau. *Molecular Biology of the Cell* **1992,** *3*, 1141-1154.

65.   Sengupta, A.; Kabat, J.; Novak, M.; Wu, Q.; Grundke-Iqbal, I.; Iqbal, K. Phosphorylation of Tau at Both Thr 231 and Ser 262 Is Required for Maximal Inhibition of Its Binding to Microtubules. *Archives of Biochemistry and Biophysics* **1998,** *357*, 299-309.

66.   Fuster-Matanzo, A.; Llorens-Martín, M.; Jurado-Arjona, J.; Avila, J.; Hernández, F. Tau Protein and Adult Hippocampal Neurogenesis. *Frontiers in Neuroscience* **2012,** *6*.

67.   Llorens-Marítin, M.; Jurado, J.; Hernández, F.; Ávila, J. GSK-3β, a pivotal kinase in Alzheimer disease. *Frontiers in Molecular Neuroscience* **2014,** *7*.

68.   Jaworski, T.; Kügler, S.; Van Leuven, F. Modeling of Tau-Mediated Synaptic and Neuronal Degeneration in Alzheimer's Disease. *International Journal of Alzheimer's Disease* **2010,** *2010*, 573138.

69.   Hanger, D. P.; Byers, H. L.; Wray, S.; Leung, K.-Y.; Saxton, M. J.; Seereeram, A.; Reynolds, C. H.; Ward, M. A.; Anderton, B. H. Novel Phosphorylation Sites in Tau from Alzheimer Brain Support a Role for Casein Kinase 1 in Disease Pathogenesis. *Journal of Biological Chemistry* **2007,** *282*, 23645-23654.

70.   Hanger, D. P.; Anderton, B. H.; Noble, W. Tau phosphorylation: the therapeutic challenge for neurodegenerative disease. *Trends in Molecular Medicine* **2009,** *15*, 112-119.

71.   Wagner, U.; Utton, M.; Gallo, J. M.; Miller, C. C. Cellular phosphorylation of tau by GSK-3 beta influences tau binding to microtubules and microtubule organisation. *Journal of Cell Science* **1996,** *109*, 1537-1543.

72.   Pei, J.-J.; Braak, E.; Braak, H.; Grundke-Iqbal, I.; Iqbal, K.; Winblad, B.; Cowburn, R. F. Distribution of Active Glycogen Synthase Kinase 3β (GSK-3β) in Brains Staged for Alzheimer Disease Neurofibrillary Changes. *Journal of Neuropathology & Experimental Neurology* **1999,** *58*, 1010-1019.

73.   Leroy, K.; Yilmaz, Z.; Brion, J.-P. Increased level of active GSK-3β in Alzheimer's disease and accumulation in argyrophilic grains and in neurones at different stages of neurofibrillary degeneration. *Neuropathology and Applied Neurobiology* **2007,** *33*, 43-55.

74.   Gong, C.-X.; Singh, T. J.; Grundke-Iqbal, I.; Iqbal, K. Phosphoprotein Phosphatase Activities in Alzheimer Disease Brain. *Journal of Neurochemistry* **1993,** *61*, 921-927.

75.   Gong, C.-X.; Shaikh, S.; Wang, J.-Z.; Zaidi, T.; Grundke-Iqbal, I.; Iqbal, K. Phosphatase Activity Toward Abnormally Phosphorylated τ: Decrease in Alzheimer Disease Brain. *Journal of Neurochemistry* **1995,** *65*, 732-738.

76.   Pérez, M.; Hernández, F.; Lim, F.; Díaz-Nido, J.; Avila, J. Chronic lithium treatment decreases mutant tau protein aggregation in a transgenic mouse model. *Journal of Alzheimer's Disease* **2003,** *5*, 301-308.

77.   Caccamo, A.; Oddo, S.; Tran, L. X.; LaFerla, F. M. Lithium Reduces Tau Phosphorylation but Not Aβ or Working Memory Deficits in a Transgenic Model with Both Plaques and Tangles. *The American Journal of Pathology* **2007,** *170*, 1669-1675.

78.   Noble, W.; Planel, E.; Zehr, C.; Olm, V.; Meyerson, J.; Suleman, F.; Gaynor, K.; Wang, L.; LaFrancois, J.; Feinstein, B.; Burns, M.; Krishnamurthy, P.; Wen, Y.; Bhat, R.; Lewis, J.; Dickson, D.; Duff, K.; Iversen, L. L. Inhibition of Glycogen Synthase Kinase-3 by Lithium Correlates with Reduced Tauopathy and Degeneration in vivo. *Proceedings of the National Academy of Sciences of the United States of America* **2005,** *102*, 6990-6995.

79.   Leroy, K.; Ando, K.; Héraud, C.; Yilmaz, Z.; Authelet, M.; Boeynaems, J.-M.; Buée, L.; De Decker, R.; Brion, J.-P. Lithium Treatment Arrests the Development of Neurofibrillary Tangles in Mutant Tau Transgenic Mice with Advanced Neurofibrillary Pathology. *Journal of Alzheimer's Disease* **2010,** *19*, 705-719.

80.   Schatoff, E. M.; Leach, B. I.; Dow, L. E. WNT Signaling and Colorectal Cancer. *Current Colorectal Cancer Reports* **2017,** *13*, 101-110.

81.   Bhat, R. V.; Andersson, U.; Andersson, S.; Knerr, L.; Bauer, U.; Sundgren-Andersson, A. K. The Conundrum of GSK3 Inhibitors: Is it the Dawn of a New Beginning? *Journal of Alzheimer's Disease* **2018,** *64*, S547-S554.

82.   Krishnan, V.; Bryant, H. U.; MacDougald, O. A. Regulation of bone mass by Wnt signaling. *The Journal of Clinical Investigation* **2006,** *116*, 1202-1209.

83.   Georgievska, B.; Sandin, J.; Doherty, J.; Mörtberg, A.; Neelissen, J.; Andersson, A.; Gruber, S.; Nilsson, Y.; Schött, P.; Arvidsson, P. I.; Hellberg, S.; Osswald, G.; Berg, S.; Fälting, J.; Bhat, R. V. AZD1080, a novel GSK3 inhibitor, rescues synaptic plasticity deficits in rodent brain and exhibits peripheral target engagement in humans. *Journal of Neurochemistry* **2013,** *125*, 446-456.

84.   Licht-Murava, A.; Paz, R.; Vaks, L.; Avrahami, L.; Plotkin, B.; Eisenstein, M.; Eldar-Finkelman, H. A unique type of GSK-3 inhibitor brings new opportunities to the clinic. *Science Signaling* **2016,** *9*, ra110.

85.   Woodgett, J. R. Physiological roles of glycogen synthase kinase-3: potential as a therapeutic target for diabetes and other disorders. *Current Drug Targets - Immune, Endocrine and Metabolic Disorders* **2003,** *3*, 281-290.

86.   Vestergaard, P.; Licht, R. W. 50 Years with Lithium Treatment in Affective Disorders: Present Problems and Priorities. *The World Journal of Biological Psychiatry* **2001,** *2*, 18-26.

87.   Jope, R. S. Lithium and GSK-3: one inhibitor, two inhibitory actions, multiple outcomes. *Trends in Pharmacological Sciences* **2003,** *24*, 441-443.

88.   O'Brien, W. T.; Harper, A. D.; Jové, F.; Woodgett, J. R.; Maretto, S.; Piccolo, S.; Klein, P. S. Glycogen Synthase Kinase-3β Haploinsufficiency Mimics the Behavioral and Molecular Effects of Lithium. *The Journal of Neuroscience* **2004,** *24*, 6791-6798.

89.   Martinez, A.; Perez, D. I. GSK-3 Inhibitors: A Ray of Hope for the Treatment of Alzheimer's Disease? *Journal of Alzheimer's Disease* **2008,** *15*, 181-191.

90.   Woodgett, J. R. Molecular cloning and expression of glycogen synthase kinase-3/factor A. *The EMBO journal* **1990,** *9*, 2431-2438.

91.   Changelian, P. S.; Flanagan, M. E.; Ball, D. J.; Kent, C. R.; Magnuson, K. S.; Martin, W. H.; Rizzuti, B. J.; Sawyer, P. S.; Perry, B. D.; Brissette, W. H.; McCurdy, S. P.; Kudlacz, E. M.; Conklyn, M. J.; Elliott, E. A.; Koslov, E. R.; Fisher, M. B.; Strelevitz, T. J.; Yoon, K.; Whipple, D. A.; Sun, J.; Munchhof, M. J.; Doty, J. L.; Casavant, J. M.; Blumenkopf, T. A.; Hines, M.; Brown, M. F.; Lillie, B. M.; Subramanyam, C.; Shang-Poa, C.; Milici, A. J.; Beckius, G. E.; Moyer, J. D.; Su, C.; Woodworth, T. G.; Gaweco, A. S.; Beals, C. R.; Littman, B. H.; Fisher, D. A.; Smith, J. F.; Zagouras, P.; Magna, H. A.; Saltarelli, M. J.; Johnson, K. S.; Nelms, L. F.; Des Etages, S. G.; Hayes, L. S.; Kawabata, T. T.; Finco-Kent, D.; Baker, D. L.; Larson, M.; Si, M.-S.; Paniagua, R.;

Higgins, J.; Holm, B.; Reitz, B.; Zhou, Y.-J.; Morris, R. E.; O'Shea, J. J.; Borie, D. C. Prevention of Organ Allograft Rejection by a Specific Janus Kinase 3 Inhibitor. *Science* **2003,** *302*, 875-878.

92.   Karaman, M. W.; Herrgard, S.; Treiber, D. K.; Gallant, P.; Atteridge, C. E.; Campbell, B. T.; Chan, K. W.; Ciceri, P.; Davis, M. I.; Edeen, P. T.; Faraoni, R.; Floyd, M.; Hunt, J. P.; Lockhart, D. J.; Milanov, Z. V.; Morrison, M. J.; Pallares, G.; Patel, H. K.; Pritchard, S.; Wodicka, L. M.; Zarrinkar, P. P. A quantitative analysis of kinase inhibitor selectivity. *Nature Biotechnology* **2008,** *26*, 127-132.

93.   Davis, M. I.; Hunt, J. P.; Herrgard, S.; Ciceri, P.; Wodicka, L. M.; Pallares, G.; Hocker, M.; Treiber, D. K.; Zarrinkar, P. P. Comprehensive analysis of kinase inhibitor selectivity. *Nature Biotechnology* **2011,** *29*, 1046-1051.

94.   Flanagan, M. E.; Blumenkopf, T. A.; Brissette, W. H.; Brown, M. F.; Casavant, J. M.; Shang-Poa, C.; Doty, J. L.; Elliott, E. A.; Fisher, M. B.; Hines, M.; Kent, C.; Kudlacz, E. M.; Lillie, B. M.; Magnuson, K. S.; McCurdy, S. P.; Munchhof, M. J.; Perry, B. D.; Sawyer, P. S.; Strelevitz, T. J.; Subramanyam, C.; Sun, J.; Whipple, D. A.; Changelian, P. S. Discovery of CP-690,550: A Potent and Selective Janus Kinase (JAK) Inhibitor for the Treatment of Autoimmune Diseases and Organ Transplant Rejection. *Journal of Medicinal Chemistry* **2010,** *53*, 8468-8484.

95.   Jiang, J.-k.; Ghoreschi, K.; Deflorian, F.; Chen, Z.; Perreira, M.; Pesu, M.; Smith, J.; Nguyen, D.-T.; Liu, E. H.; Leister, W.; Costanzi, S.; O'Shea, J. J.; Thomas, C. J. Examining the Chirality, Conformation and Selective Kinase Inhibition of 3-((3R,4R)-4-methyl-3-(methyl(7H-pyrrolo[2,3-d]pyrimidin-4-yl)amino)piperidin-1-yl)-3-oxopropanenitrile (CP-690,550). *Journal of Medicinal Chemistry* **2008,** *51*, 8012-8018.

96.   Wang, Y.; Du, Y.; Huang, N. A survey of the role of nitrile groups in protein–ligand interactions. *Future Medicinal Chemistry* **2018,** *10*, 2713-2728.

97.   Abel, R.; Young, T.; Farid, R.; Berne, B. J.; Friesner, R. A. Role of the Active-Site Solvent in the Thermodynamics of Factor Xa Ligand Binding. *Journal of the American Chemical Society* **2008,** *130*, 2817-2831.

98.   Young, T.; Abel, R.; Kim, B.; Berne, B. J.; Friesner, R. A. Motifs for molecular recognition exploiting hydrophobic enclosure in protein–ligand binding. *Proceedings of the National Academy of Sciences* **2007,** *104*, 808-813.

99.   Desroy, N.; Housseman, C.; Bock, X.; Joncour, A.; Bienvenu, N.; Cherel, L.; Labeguere, V.; Rondet, E.; Peixoto, C.; Grassot, J.-M.; Picolet, O.; Annoot, D.; Triballeau, N.; Monjardet, A.; Wakselman, E.; Roncoroni, V.; Le Tallec, S.; Blanque, R.; Cottereaux, C.; Vandervoort, N.; Christophe, T.; Mollat, P.; Lamers, M.; Auberval, M.; Hrvacic, B.; Ralic, J.; Oste, L.; van der Aar, E.; Brys, R.; Heckmann, B. Discovery of 2-[[2-Ethyl-6-[4-[2-(3-hydroxyazetidin-1-yl)-2-oxoethyl]piperazin-1-yl]-8-methylimidazo[1,2-a]pyridin-3-yl]methylamino]-4-(4-fluorophenyl)thiazole-5-carbonitrile (GLPG1690), a First-in-Class Autotaxin Inhibitor Undergoing Clinical

Evaluation for the Treatment of Idiopathic Pulmonary Fibrosis. *Journal of Medicinal Chemistry* **2017,** *60*, 3580-3590.

100.   Kung, P.-P.; Sinnema, P.-J.; Richardson, P.; Hickey, M. J.; Gajiwala, K. S.; Wang, F.; Huang, B.; McClellan, G.; Wang, J.; Maegley, K.; Bergqvist, S.; Mehta, P. P.; Kania, R. Design strategies to target crystallographic waters applied to the Hsp90 molecular chaperone. *Bioorganic & Medicinal Chemistry Letters* **2011,** *21*, 3557-3562.

101.   Gorrod, J. W.; Aislaitner, G. The metabolism of alicyclic amines to reactive iminium ion intermediates. *European Journal of Drug Metabolism and Pharmacokinetics* **1994,** *19*, 209-217.

102.   Bolleddula, J.; DeMent, K.; Driscoll, J. P.; Worboys, P.; Brassil, P. J.; Bourdet, D. L. Biotransformation and bioactivation reactions of alicyclic amines in drug molecules. *Drug Metabolism Reviews* **2014,** *46*, 379-419.

103.   Wuitschik, G.; Carreira, E. M.; Wagner, B.; Fischer, H.; Parrilla, I.; Schuler, F.; Rogers-Evans, M.; Müller, K. Oxetanes in Drug Discovery: Structural and Synthetic Insights. *Journal of Medicinal Chemistry* **2010,** *53*, 3227-3246.

104.   Sivaprakasam, P.; Han, X.; Civiello, R. L.; Jacutin-Porte, S.; Kish, K.; Pokross, M.; Lewis, H. A.; Ahmed, N.; Szapiel, N.; Newitt, J. A.; Baldwin, E. T.; Xiao, H.; Krause, C. M.; Park, H.; Nophsker, M.; Lippy, J. S.; Burton, C. R.; Langley, D. R.; Macor, J. E.; Dubowchik, G. M. Discovery of new acylaminopyridines as GSK-3 inhibitors by a structure guided in-depth exploration of chemical space around a pyrrolopyridinone core. *Bioorganic & Medicinal Chemistry Letters* **2015,** *25*, 1856-1863.

7 Anhang

7.1   Publikation I

**Design, Synthesis and Biological Evaluation of
7-Chloro-9*H*-pyrimido[4,5-*b*]indole-based Glycogen Synthase Kinase-3β Inhibitors**

Stanislav Andreev, Tatu Pantsar, Francesco Ansideri, Mark Kudolo,

Dieter Schollmeyer, Stefan Laufer und Pierre Koch

Article

Design, Synthesis and Biological Evaluation of 7-Chloro-9*H*-pyrimido[4,5-*b*]indole-based Glycogen Synthase Kinase-3β Inhibitors

Stanislav Andreev [1], Tatu Pantsar [2,3], Francesco Ansideri [1], Mark Kudolo [1], Michael Forster [1], Dieter Schollmeyer [4], Stefan A. Laufer [1] and Pierre Koch [1,5,*]

[1] Institute of Pharmaceutical Sciences, Department of Medicinal and Pharmaceutical Chemistry, Eberhard Karls University Tübingen, Auf der Morgenstelle 8, 72076 Tübingen, Germany; stanislav.andreev@uni-tuebingen.de (S.A.); francesco.ansideri@uni-tuebingen.de (F.A.); Mark.Kudolo@uni-tuebingen.de (M.K.); Michael.forster@uni-tuebingen.de (M.F.); Stefan.laufer@uni-tuebingen.de (S.A.L.)

[2] Department of Internal Medicine VIII, University Hospital Tübingen, Otfried-Müller-Str. 14, 72076 Tübingen, Germany; tatu.pantsar@uef.fi

[3] School of Pharmacy, University of Eastern Finland, P.O. Box 1627, 70211 Kuopio, Finland

[4] Department of Organic Chemistry, Johannes Gutenberg University Mainz, Duesbergweg 10-14, 55099 Mainz, Germany; scholli@uni-mainz.de

[5] Department of Pharmaceutical/Medicinal Chemistry II, Institute of Pharmacy, University of Regensburg, Universitätsstraße 31, 93053 Regensburg, Germany

* Correspondence: pierre.koch@uni-tuebingen.de; Tel.: +49-7071-29-74579

check for updates

Abstract: Glycogen synthase kinase-3β (GSK-3β) represents a relevant drug target for the treatment of neurodegenerative pathologies including Alzheimer's disease. We herein report on the optimization of a novel class of GSK-3β inhibitors based on the tofacitinib-derived screen hit 3-((3*R*,4*R*)-3-((7-chloro-9*H*-pyrimido[4,5-*b*]indol-4-yl)(methyl)amino)-4-methylpiperidin-1-yl)-3-oxopropanenitrile (**1**). We synthesized a series of 19 novel 7-chloro-9*H*-pyrimido[4,5-*b*]indole-based derivatives and studied their structure–activity relationships with focus on the cyanoacetyl piperidine moiety. We unveiled the crucial role of the nitrile group and its importance for the activity of this compound series. A successful rigidization approach afforded 3-(3a*RS*,7a*SR*)-(1-(7-chloro-9*H*-pyrimido[4,5-*b*]indol-4-yl)octahydro-6*H*-pyrrolo[2,3-*c*]pyridin-6-yl)-propanenitrile (**24**), which displayed an IC$_{50}$ value of 130 nM on GSK-3β and was further characterized by its metabolic stability. Finally, we disclosed the putative binding modes of the most potent inhibitors within the ATP binding site of GSK-3β by 1 μs molecular dynamics simulations.

Keywords: Glycogen synthase kinase-3β; 7-chloro-9*H*-pyrimido[4,5-*b*]indole; protein kinase; kinase inhibitor; tofacitinib

1. Introduction

The human kinome represents a collective of over 500 genes dedicated to the sophisticated signaling networks in human cells [1]. With the majority of protein kinases being catalytically active, hence capable of transferring the γ-phosphate group from ATP/GTP to their protein substrates, this enzyme group is assumed to modify up to 30% of the intracellular proteome by phosphorylation [2]. While certain kinases target a limited number of substrates and consequently play a distinct role in cell signaling, others act as multitasking players in the cell circuitry. With over 30 proposed substrates glycogen synthase kinase-3 (GSK-3) clearly joins the ranks of the latter class [3]. Its name

is attributed to the inhibition on glycogen synthesis within the frame of intracellular insulin signal transduction [4–6], yet not fully reflects the wide-ranging tasks of GSK-3 within the cell. The two isoforms of this serine/threonine kinase, namely GSK-3α and GSK-3β, differ in their C- and N-termini, while their kinase domains are highly conserved and characterized by 98% homology [7]. Despite their similarities, knock-out experiments in mice as well as numerous pharmacological studies have questioned the complete redundancy of these two paralogs [8–11].

GSK-3 is ubiquitously expressed and involved in at least five different signaling pathways (Insulin, Wnt, Notch, Hedgehog and TGF-β). This raises the question on how proper regulation mechanisms guarantee the flawless functionality of this enzyme [12]. A dysregulated GSK-3 activity has been linked to the development of several pathologies such as cancer, diabetes, CNS disorders, and neurodegeneration [11]. Thus, being a potential therapeutic target, GSK-3 has received attention of pharmaceutical research. Despite decades of extensive research efforts, several questions regarding the intracellular impact of this kinase, the mechanisms ensuring its regulation as well as its validity as a drug target remain unanswered. This has caused a strong demand for chemical agents, which can serve as chemical probes in pharmacological and biochemical studies and also as starting points for the development of clinical candidates.

In this context, we herein present a novel class of 7-chloro-9*H*-pyrimido[4,5-*b*]indole-based GSK-3β inhibitors. The compound series is derived from the pan-Janus kinase (JAK) inhibitor tofacitinib (Scheme 1), formerly known as CP-690,550. The main target of tofacitinib is JAK3 [13]. This non-receptor tyrosine kinase is expressed exclusively in lymphoid cells, where it transduces the signals of γ-common cytokines in the course of the JAK-STAT signaling pathway [13,14]. A pharmacological intervention in this pathway with tofacitinib is used in the treatment of immunological disorders such as rheumatoid or psoriatic arthritis [15]. In the course of a kinome-wide screening campaign of our in-house compound library, the tofacitinib-derived 7-chloro-9*H*-pyrimido[4,5-*b*]indole **1** was identified as a GSK-3β inhibitor in the single-digit micromolar range (Scheme 1). Interestingly, GSK-3β and JAK3 are located in different branches of the phylogenetic kinome tree. They are structurally diverse, even their kinase domains display low homology (identity 22.6%) (Figure S1, Supplementary Materials).
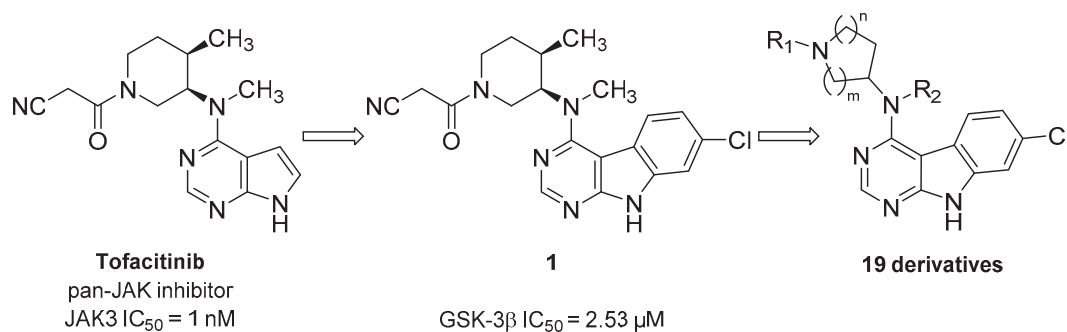
Scheme 1. Development of glycogen synthase kinase-3β (GSK-3β) inhibitors derived from the pan-Janus kinase (JAK) inhibitor tofacitinib.

In this work, we describe a medicinal chemistry strategy consisting of the design, synthetic preparation and biological evaluation of a series of compounds dedicated to an optimization of hit **1** towards GSK-3β inhibition. Interpretation of the biological data combined with in silico approaches provides insight into structure–activity relationships (SARs) and the putative binding mode of this novel class of GSK-3β inhibitors. Finally, the most promising inhibitors were further characterized by their metabolic stability in human liver microsomes (HLM) and inhibitory activity on JAK3, which is the main target of tofacitinib.

2. Results and Discussion

2.1. Biological Evaluation

The binding mode of JAK3 in complex with tofacitinib (PDB ID: 3LXK) has been resolved (Figure 1) [16]. The 7*H*-pyrrolo[2,3-*d*]pyrimidine moiety of tofacitinib forms a bidentate hydrogen bond to the hinge residues Glu903 and Leu905, whereas the N-3 atom of the pyrimidine ring displays an interaction with a crystal water molecule. The ribose region of the kinase accommodates the piperidine ring of the inhibitor, allowing the exocyclic methyl group to occupy a miniscule lipophilic cavity in the bottom of the catalytic cleft formed by Ala966, Cys909, and Leu956. Consequently, this positioning of the methyl group leads to an orientation of the nitrile residue towards the glycine-rich loop.
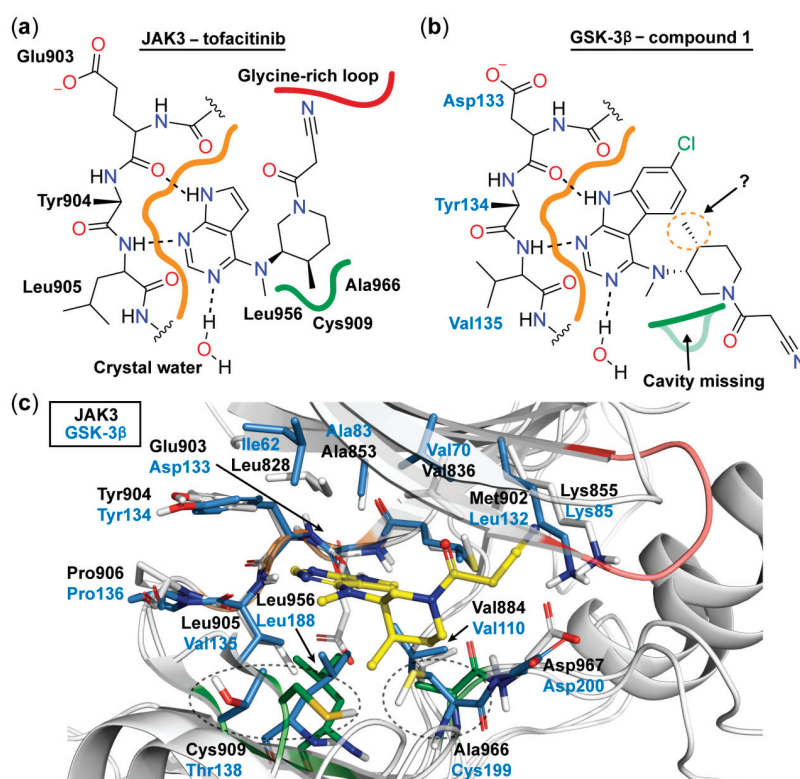
Figure 1. Schematic 2D representation of the binding mode of tofacitinib to JAK3 derived from its co-crystal structure (PDB ID: 3LXK) [16] (**a**) and the expected binding mode of **1** to GSK-3β (**b**). The lipophilic cavity is highlighted with green and the hinge region with orange. Hydrogen bonds are depicted as dashed lines. (**c**) 3D superposition based on the hinge regions of GSK-3β (PDB ID: 4PTC) and JAK3 (PDB ID: 3LXK) shows a high conservation of the residues in the ATP binding site [17]. The lipophilic cavity is missing in GSK-3β, as the spatial orientation of the Thr138 is totally different compared to the Cys909 in JAK3 and the residue Cys199 is bulkier than the Ala966 found in JAK3. Moreover, this Cys199 would clash with tofacitinib (yellow) in its JAK3 binding conformation. Residues near to tofacitinib are depicted as sticks. The stick coloring is the following: GSK-3β, blue; JAK3, grey; JAK3 residues forming the lipophilic cavity, green. The cartoon coloring is the following: hinge regions, orange; lipophilic cavity residues, green; JAK3 glycine-rich loop, red.

Taking into account the high conservation of the ATP binding site, we expected a similar hydrogen bonding pattern to occur for the 7-chloro-9*H*-pyrimido[4,5-*b*]indole substructure in **1** with the hinge region of GSK-3β (Figure 1). Therefore, we decided to leave the chlorinated tricycle unmodified and set the focus of our optimization study on the aliphatic piperidine side chain. The distinct configuration of the two stereocenters within this moiety is a prerequisite for potent JAK3 inhibition and requires laborious steps in the enantiopure preparation of tofacitinib and hit **1**, respectively [18]. However, in
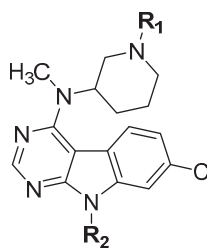
contrast to JAK3, GSK-3β lacks a comparable lipophilic cavity in the bottom of its ATP binding site (Figure 1), which questioned the necessity of the corresponding exocyclic methyl group. This motivated us to prepare **14a** (Table 1). This compound, lacking the methyl substituent, has one stereocenter less and was prepared as racemic mixture. This approach simplified the synthetic preparation significantly. The racemic **14a** was found to exhibit a similar inhibitory activity on GSK-3β as **1**, justifying the selected approach, and was therefore chosen as a starting point for the development of further derivatives.
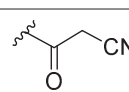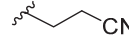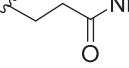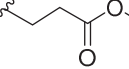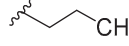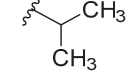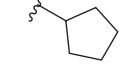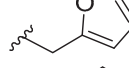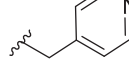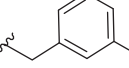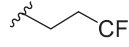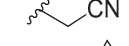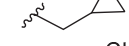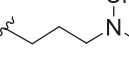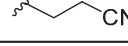
At first, we evaluated the importance of the carbonyl group within the cyanoacetamide moiety. Tertiary amine **14b**, which lacks the carbonyl group of **14a**, exhibited a 2.5-fold increase in activity. The molecular structures of **14b** and its amide counterpart display critical differences in their chemical properties. The loss of a possible hydrogen bond acceptor, a highly increased basicity of the piperidine nitrogen, as well as an enhanced flexibility of the cyanoethyl substituent provide putative explanations for the enhanced biological activity. With regard to this affinity shift into the nanomolar range this tertiary amine was assigned as the lead compound of this optimization study.

Next, we installed a methyl group on the indole nitrogen of **14b**. The resulting compound **14o**, uncapable of donating a hydrogen bond with its indole nitrogen, was inactive on GSK-3β. This negative outcome supported our hypothesis concerning the hydrogen bonding interactions of the 7-chloro-9*H*-pyrimido[4,5-*b*]indole scaffold to the hinge backbone of GSK-3β.

With this data in hand, our attention was refocused on the piperidine ring to assess the effects of the substituent **R₁** (Table 1). In order to examine the chemical space around the cyanoethyl moiety of the lead compound **14b**, we prepared a series of diverse tertiary amines (**14c–n**). Our initial approaches consisted of the application of linear and branched lipophilic substituents such as propyl (**14e**), isopropyl (**14f**), cyclopentyl (**14g**), and cyclopropylmethyl (**14m**). The corresponding compounds displayed a severe decrease in activity on GSK-3β, which clearly indicates that aliphatic hydrocarbon substituents are not tolerated in this position. Within this inactive quartet, it is worth highlighting compound **14e**, whose propyl substituent maintains similar steric properties as in **14b**, however, **14e** lacks the nitrile group. Therefore, the significantly decreased activity of **14e** accentuates the importance of this functional group.

In order to disclose the vital role of the nitrile group for the activity of **14b**, we considered the following effects which can originate from its functionality. First, owing to the polarization of the triple bond, its nitrogen can serve as hydrogen bond acceptor. Such interactions have been observed in a number of nitrile-containing pharmaceuticals [19,20]. To evaluate this hypothesis, diverse substituents containing hydrogen bond acceptors, assigned to mimic the crucial nitrile group, were introduced on the piperidine nitrogen. These included both (hetero)aromatic rings like furane, pyridine or cyanobenzene in compounds **14h–j**, as well as carbonyl group-containing moieties (**14c** and **14d**). Surprisingly, all of these modifications were associated with a dramatic decrease in activity. Even compound **14n**, bearing a dimethylaminopropyl substituent, showed remarkably reduced GSK-3β inhibition.

Table 1. Structures, biological activity and calculated pK$_a$ values of piperidine derivatives **14a–o**.

Cpd.	R$_1$	R$_2$	IC$_{50}$ (μM) Mean ± SEM GSK-3β [a]	pK$_a$ [c]
14a		-H	1.862 ± 0.113	-
14b		-H	0.764 ± 0.203 [b]	5.5
14c		-H	>10	6.8
14d		-H	>10	6.8
14e		-H	>10	7.5
14f		-H	>10	8.3
14g		-H	>10	8.0
14h		-H	>10	6.9
14i		-H	>10	6.2
14j		-H	>10	6.3
14k		-H	>10	5.7
14l		-H	>10	2.5
14m		-H	>10	7.8
14n		-H	3.557 ± 0.664	7.2
14o		-CH$_3$	>10	n.d. [d]

[a] IC$_{50}$ values were determined in an ADP Glo kinase assay [21,22], *n* = 2; [b] *n* = 5; [c] pK$_a$ value for the piperidine nitrogen calculated with Jaguar (Schrödinger LLC) (for details see Materials and Methods); [d] not determined.

At first glance, these findings might lead to the assumption of a hydrogen bond interaction being improbable for the nitrile group. However, the uniqueness of this functionality in terms of its rod-shaped geometry, resulting from the sp-hybridization of the carbon-nitrogen bond, must clearly be considered when interpreting these results. Most probably, the geometric and/or steric configuration of the other applied hydrogen bond-accepting substituents were not tolerated by the target enzyme.

Furthermore, taking into account that a nitrile group can significantly lower the electron density of atoms in its close proximity, we investigated the impact of the substituents on the basicity of the

piperidine nitrogen. To this end, we calculated pK$_a$ values for the piperidine nitrogen in compounds **14b–j** and **14m–n** (Table 1). The majority of pK$_a$ values for this tertiary amine collective falls in the range between 6.8 and 8.3 predicting a significant degree of protonation of the nitrogen at pH 7.4. In contrast, **14b** was assigned with a significantly lower value of 5.5, which thoroughly reflects the electron withdrawing effects of the nitrile group and suggests a dominating presence of the uncharged free base under the physiological pH. This can be of great relevance for the binding of **14b** to GSK-3β. For instance, if the lone pair of the piperidine nitrogen is directed towards positively charged residues of the enzyme, a protonation would result in repulsion.
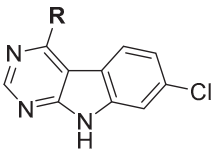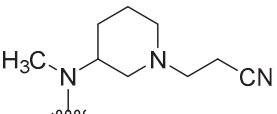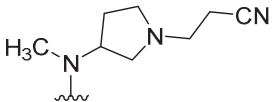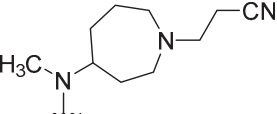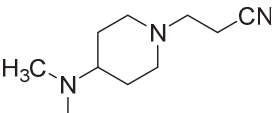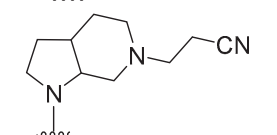
In this context, we hypothesized that the lowered pK$_a$ and therefrom resulting unprotonated piperidine nitrogen might be an explanation for the significantly higher affinity of **14b**. To pursue this theory, we installed proper substituents on the piperidine nitrogen with the aim to lower the pK$_a$ in a similar manner. A bioisosteric replacement of the nitrile with a highly electron withdrawing trifluoromethyl group afforded compound **14k**. In contrast, the nitrile group was maintained in compound **14l**, but is located closer to the piperidine nitrogen than in **14b**, amplifying its influence on the basicity. Even though the pK$_a$ values of these molecules are in agreement with the original intentions (5.7 and 2.5, respectively), both derivatives were found to be inactive in the kinase assay. These negative results allowed us the conclusion that the protonation state of the piperidine nitrogen cannot solely determine the nanomolar activity of **14b**. Additionally, the drop in activity seen with **14l** points out that a specific distance between the nitrile group and the piperidine nitrogen is of utmost importance and once more emphasizes the cyanoethyl residue as preferred substituent in this position.

The outcomes with the above described set of derivatives encouraged us to keep the essential cyanoethyl moiety intact during the upcoming optimization steps. Taking into account that a proper position of the nitrile group was revealed a prerequisite for binding affinity, we attempted to fine-tune the orientation of the cyanoethyl substituent by modifications of the piperidine ring.

Alteration of the heterocyclic ring size to a pyrrolidine or azepane as well as relocation of the inner cyclic nitrogen within the piperidine delivered compounds **15–17**. These modifications resulted in marginal shifts in the orientation of the essential cyanoethyl substituent. However, the derivatives **15–17** did not conserve the nanomolar activity of the parent compound **14b**, which highlighted the original piperidine as the optimal scaffold within this series to properly orientate the cyanoethyl moiety. Therefore, we decided to return to this saturated heterocycle and considered rigidization approaches with the idea of stabilizing a bioactive conformation of this moiety. The bicyclic octahydro-1*H*-pyrrolo[2,3-*c*]pyridine side chain present in compound **24** was chosen for its chemical feasibility. This compound displayed an IC$_{50}$ value of 130 nM, which equals a 6-fold increase in potency compared to its unrigidized counterpart **14b**. It is worth noticing, that the extended hydrocarbon scaffold of **24** results in an expanded lipophilic surface area of the molecule, which enables the possibility of its improved inhibition to be driven by entropic effects. However, this is not reflected by the calculated lipophilic ligand efficiency (cLLE) values of this series (Table 2). In turn, it appears plausible that the cyanoethyl substituent is forced into a favorable direction due to the restricted rotation of the piperidine ring.

Table 2. Structures, biological activity and AlogP-derived lipophilic ligand efficiencies (cLLE) of compounds **14b**, **15–17** and **24**.

Cpd.	R	IC$_{50}$ (µM) Mean ± SEM GSK-3β [a]	pIC$_{50}$	AlogP [d]	cLLE [e]
14b		0.764 ± 0.203 b	6.12	3.25	2.87
15		7.017 ± 1.077	5.15	2.67	2.48
16		1.535 ± 0.284	5.81	3.31	2.50
17		13.335 ± 4.393	4.88	2.73	2.15
24		0.130 ± 0.008 c	6.89	3.15	3.74

[a] IC$_{50}$ values were determined in an ADP Glo assay [21,22], *n* = 2; [b] *n* = 5; [c] *n* = 3; [d] calculated with Canvas (Schrödinger LLC) [23]; [e] cLLE = pIC$_{50}$ − AlogP.

2.2. Molecular Modelling

For the better understanding of the binding and interactions of our compounds to GSK-3β, we conducted 1 µs molecular dynamics (MD) simulations for the most potent compounds **14b** and **24** (for full movies and raw data see Supplementary Materials).

Throughout the simulations, the 7-chloro-9*H*-pyrimido[4,5-*b*]indole scaffold of both ligands exhibits stable interactions with the backbone of the hinge residues Asp133 and Val135 (Figure 2), while the halogen-substituted third aromatic ring of the scaffold is pointing towards the hydrophobic region I of the kinase.
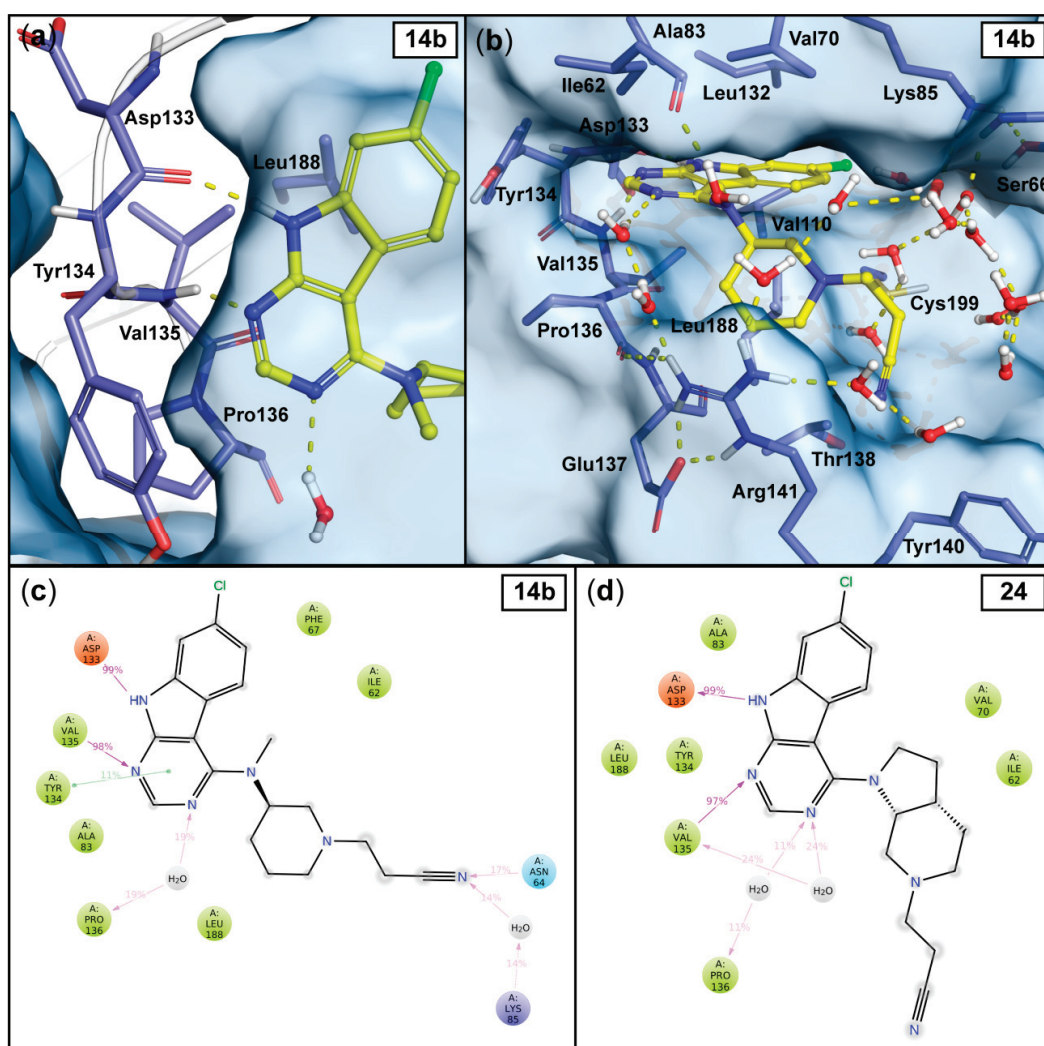
Figure 2. Observed interactions in the 1 μs MD simulations with the most potent compounds **14b** and **24**. The output conformation of compound **14b** (at 1000 ns) illustrates the stable hinge interactions with the Asp133 and Val135 and to the solvent (similar in **24**) (**a**), as well as the solvent exposure of the cyanoethyl moiety (**b**). Hydrogen bonds are depicted as yellow dashed lines and the water molecules within 4Å from the ligand are shown. The simulation interaction frequencies of compound **14b** (**c**) and compound **24** (**d**) were analyzed using the stabilized part of the simulations: 50–1000 ns and 30–1000 ns for **14b** and **24**, respectively (see Figure 3c–d). Interactions that appeared with more than 10% frequency are shown; hydrogen bonds are depicted as purple arrows, π–π interactions are depicted as green lines.
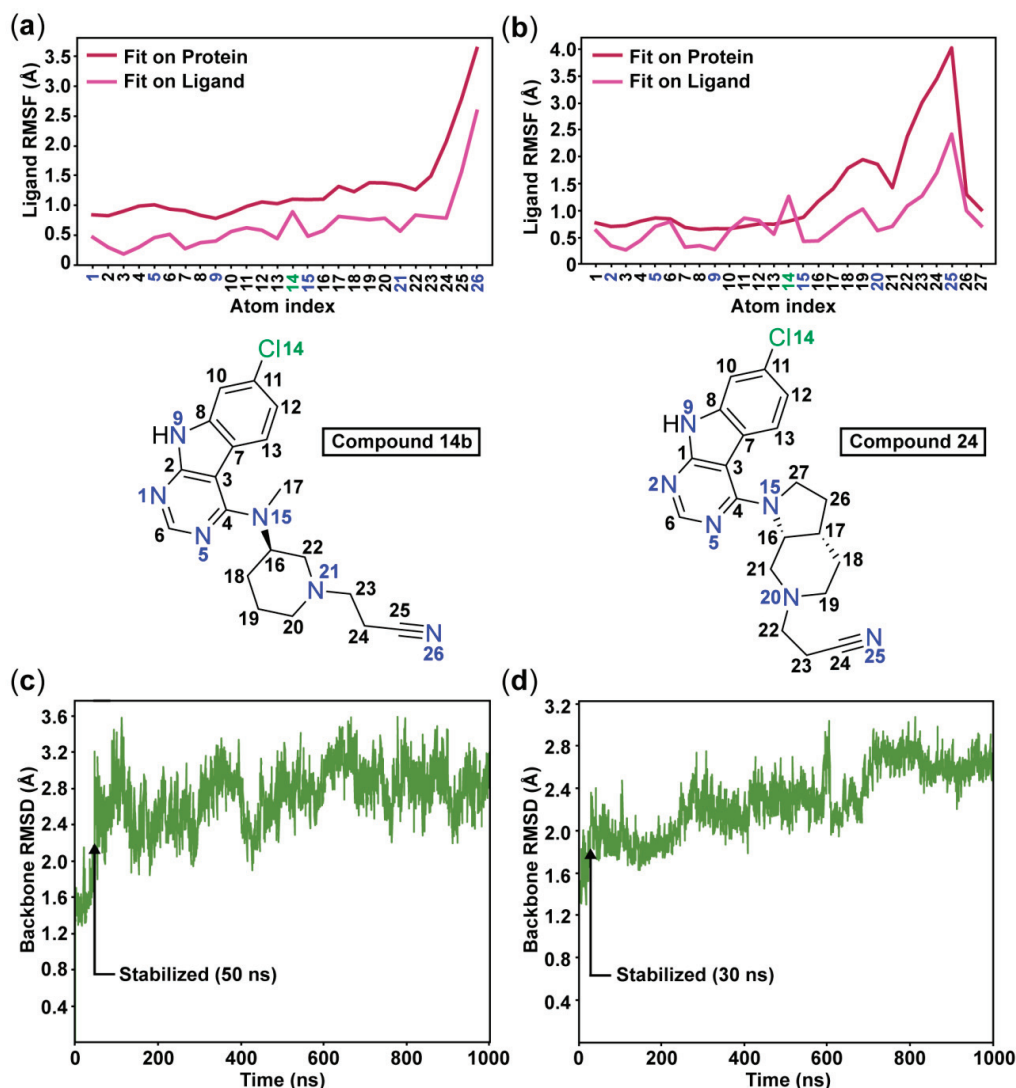
Figure 3. The root-mean-square fluctuations (RMSF) of the ligands **14b** (**a**) and **24** (**b**) illustrate the high flexibility of the cyanoethyl moieties throughout the simulations. The root-mean-square deviation (RMSD) of the protein shows that the simulations stabilize after 50 ns with compound **14b** (**c**) and after 30 ns with compound **24** (**d**).

In analogy to the observed crystal water interaction in the tofacitinib-JAK3 complex (see Figure 1), relatively stable water interactions were evident for the N-3 atom in the pyrimidine ring of our inhibitors (Figure 2). Additionally, a π–π interaction between this pyrimidine ring and the side chain of hinge residue Tyr134 appears in 11% frequency with **14b**. As expected, the sugar pocket is occupied by the piperidine heterocycle in case of **14b** or the octahydro-1*H*-pyrrolo[2,3-*c*]pyridine bicycle in case of **24**. While the hinge binding motifs of **14b** and **24** appear stable throughout the simulations, the cyanoethyl substituent is highly dynamic. These observations are well reflected by the ligand root-mean-square fluctuation (RMSF) for both ligands (Figure 3a–b). As far as the nitrile group is concerned, no single stable and specific interaction is observed. Rather a proper accommodation of the nitrile in the water interaction network is evident for both **14b** and **24**. A water-mediated interaction towards Lys85 as well as a direct hydrogen bond to Asn64 occurs in case of **14b**, however with relatively low frequencies (Figure 2c–d).

To disclose potential differences in the binding mode of the enantiomers of compound **24**, we conducted a 1 μs MD simulation also for the other enantiomer of **24** (3a*R*, 7a*S*). As comparable behavior

between the enantiomers was observed (Figure S2, Supplementary Materials), we expect a similar binding mode to occur with compound **24** regardless of the enantiomer.

Overall, examples of nitrile groups functioning as hydrogen bond acceptors in ligand–protein complexes are described in literature including well-characterized examples of direct contacts to asparagine residues, as well as interactions mediated through water bridges [19,20]. Therefore, the interactions observed in the simulations appear plausible despite their low frequencies. Finally, although we used the most recent state-of-the-art force field for drug-like small molecules, OPLS3e [24], a potential inaccuracy in the characterization of the cyanoethyl group by the force field needs to be considered (e.g., lack of polarization).

2.3. ATP competition, JAK3 Inhibition, and Metabolic Stability

To extend the biological profile of this novel class of 7-chloro-9*H*-pyrimido[4,5-*b*]indole-based GSK-3β inhibitors, we tested the lead compound **14b** for its ATP competition in our ADP Glo assay system. An incubation of **14b** with an increased concentration of ATP (100 μM and 500 μM) resulted in a reduced inhibition potential for GSK-3β. The corresponding IC_{50} values were determined as 2.684 μM and 9.260 μM, respectively (Table S1 and Figure S3, Supplementary Materials). This suggests an ATP-competitive type of inhibition, which supports our theory of a binding mode within the ATP site of the kinase.

Furthermore, **14b** and **24** were examined for their inhibitory activity on the possible off-target JAK3, as this class of GSK-3β inhibitors is derived from the pan-JAK inhibitor tofacitinib. However, both compounds displayed no significant inhibition of JAK3 in an enzyme-linked immunosorbent assay (Table S2, Supplementary Materials) [25].

In a HLM stability assay, **14b** and **24** were intensively degraded during a timeframe of 120 min (25% and 8% remaining parent compound at the endpoint of the experiment, respectively; for details see Tables S3 and S4 as well as Figures S4 and S5, Supplementary Materials). The corresponding unsubstituted piperidines were observed as prominent metabolites.

2.4. Chemistry

Our synthetic strategy to access the majority of the herein presented 7-chloro-9*H*-pyrimido[4,5-*b*]indole-based GSK-3β inhibitors featured a convergent approach consisting of the preparation of the key intermediate 4,7-dichloro-9-tosyl-9*H*-pyrimido[4,5-*b*]indole (**10**) as well as the separate synthesis of appropriate alicyclic amine side chains (**4a–d**) (Scheme 2). Both building blocks were then fused via a nucleophilic aromatic substitution (S$_N$Ar), with successive deprotection and derivatization procedures to afford the final compounds **14a–n** and **15–17**.
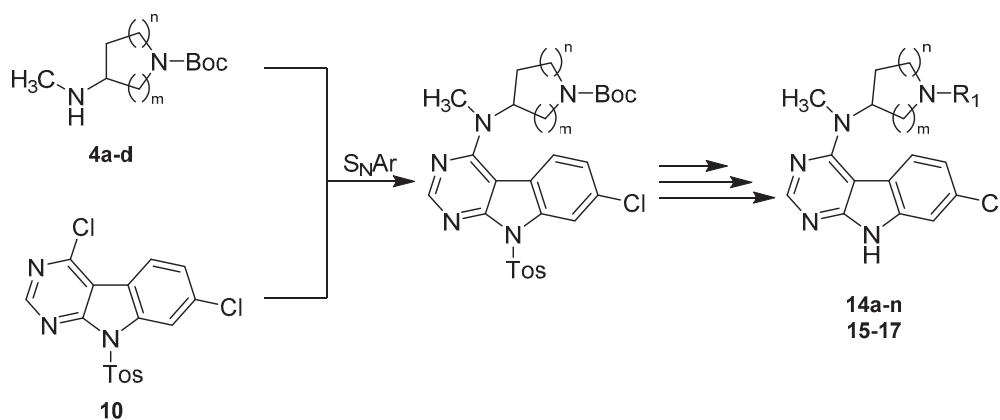
Scheme 2. Synthetic strategy towards 7-chloro-9*H*-pyrimido[4,5-*b*]indole-based GSK-3β inhibitors.

The preparation of alicyclic secondary amine side chains **4a–d** was achieved in two steps via benzyl protected amines **3a–d** adapting the strategy of Le Bourdonnec et al. (Scheme 3) [26]. The commercially

available *N*-Boc protected cyclic ketones **2a–d** were reductively aminated with *N,N*-benzylmethylamine to give tertiary amines **3a–d** in moderate to high yields. Sodium triacetoxyborohydride was used as reductive agent facilitating a convenient one-pot procedure. Hydrogenolytic benzyl cleavage with a palladium catalyst gave secondary amines **4a–d** in nearly quantitative yields.

2a: m=1; n=1
2b: m=1; n=2
2c: m=2; n=2
2d: m=2; n=1

3a: m=1; n=1
3b: m=1; n=2
3c: m=2; n=2
3d: m=2; n=1

4a: m=1; n=1
4b: m=1; n=2
4c: m=2; n=2
4d: m=2; n=1
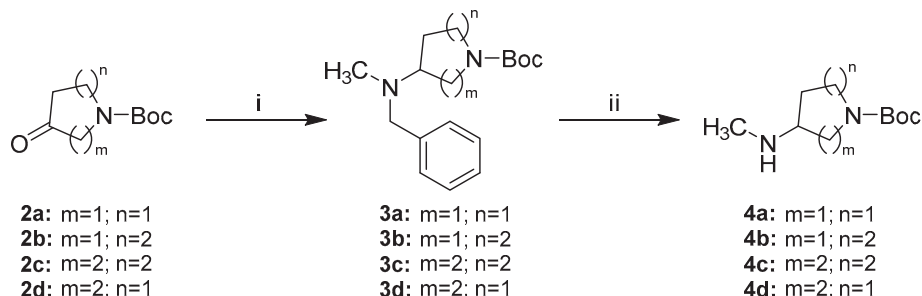
Scheme 3. Synthetic route to alicyclic secondary amine side chains **4a–d**. Reagents and conditions: (**i**) *N,N*-benzylmethylamine, Na(OAc)$_3$BH, AcOH, DCM, rt, (69–86%); (**ii**) H$_2$ (5 bar), Pd/C, MeOH or EtOAc/MeOH 3:2, rt in case of **4a–4c** or Pd/C and Pd(OH)$_2$/C, MeOH, rt in case of **4d**, (96–98%).

Synthetic literature provides numerous examples for the preparation of 9*H*-pyrimido[4,5-*b*]indoles with varying substituents on the non-heteroaromatic ring [27–31]. These typically include four-step procedures starting from appropriately decorated o-halonitrobenzenes, as the substitution pattern of the non-heteroaromatic ring is defined by this starting material. Modifying the protocols published by Reader et al. [31], we prepared key intermediate 4,7-dichloro-9-tosyl-9*H*-pyrimido[4,5-*b*]indole (**10**) starting from 1,4-dichloro-2-nitrobenzene (**5**) (Scheme 4).
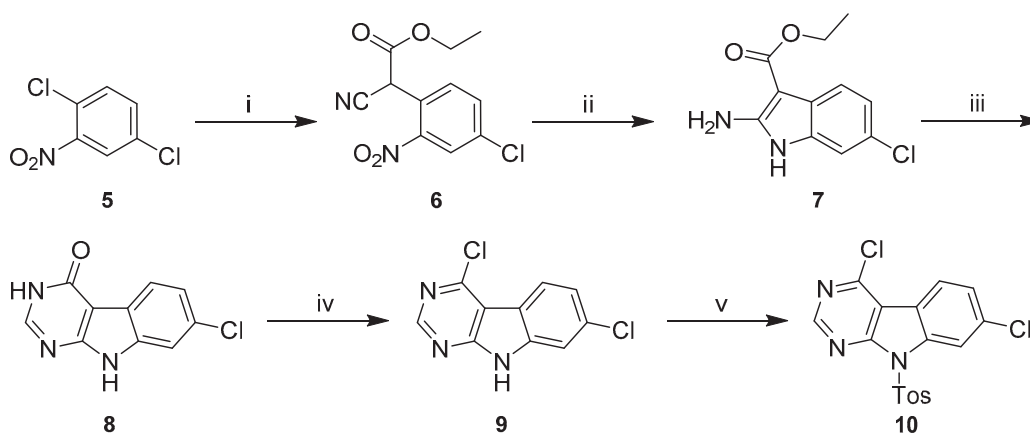
Scheme 4. Synthetic route to 4,7-dichloro-9-tosyl-9*H*-pyrimido[4,5-*b*]indole (**10**). Reagents and conditions: (**i**) ethyl-2-cyanoacetate, NaH, DMF, 0 °C to 80 °C, (quant.); (**ii**) Zn, AcOH, 90 °C, (93%); (**iii**) NH$_4$HCO$_2$, formamide, 160 °C, (86%); (**iv**) POCl$_3$, chlorobenzene, rt to 80 °C, (51%); (**v**) p-toluenesulfonyl chloride, NaH, THF, rt, (99%).

In the initial step the commercially available **5** underwent an S$_N$Ar with the sodium salt of ethyl-2-cyanoacetate, generated in situ with sodium hydride. The resulting intermediate **6** was then subjected to reductive conditions using elemental zinc in acetic acid. The crude product obtained in this cyclization reaction was a mixture of two compounds, which we assume to be the desired 2-aminoindole **7** and the corresponding 1-hydroxy derivative, in analogy to some closely related structures described by Showalter et al. [27]. Treatment of this mixture with formamide under forcing conditions resulted predominantly in **8**, whose carbonyl function was chlorinated with stochiometric amounts of POCl$_3$ in chlorobenzene following the methodology described by Arnott et al. [32].

First attempts of a direct reaction of **9** with the alicyclic amine side chains gave unsatisfactory results, in the form of either prolonged reaction times or significant by-product formation, owing to

harsh thermal conditions. The installation of a toluenesulfonyl (Tos) protecting group on the indole nitrogen in **10** significantly enhanced the reactivity of the pyrimidine ring and therefore allowed a clean nucleophilic substitution under relatively mild conditions in DMF and presence of DIPEA (Scheme 5). The sulfonamide protecting group was removed subsequently under basic conditions. A modification of the protocol described by Xu et al. using a high excess of K*t*BuO (7 eq.) instead of refluxing conditions allowed a fast deprotection at room temperature [33]. This approach gave intermediates **12a–d** in satisfying purity and yields (64–77% over three steps), justifying the synthetic detour associated with the protection of the indole nitrogen. **12a–d** were treated with TFA in DCM to convert them into the corresponding secondary amines **13a–d** [34]. These intermediates were then properly decorated by amide coupling, reductive amination [34], nucleophilic substitution [35] or Michael-addition [36] to give final compounds **14a–n** and **15–17** listed in Tables 1 and 2, respectively. For the synthesis of **14o**, lead structure **14b** was methylated on its indole nitrogen applying a common procedure.
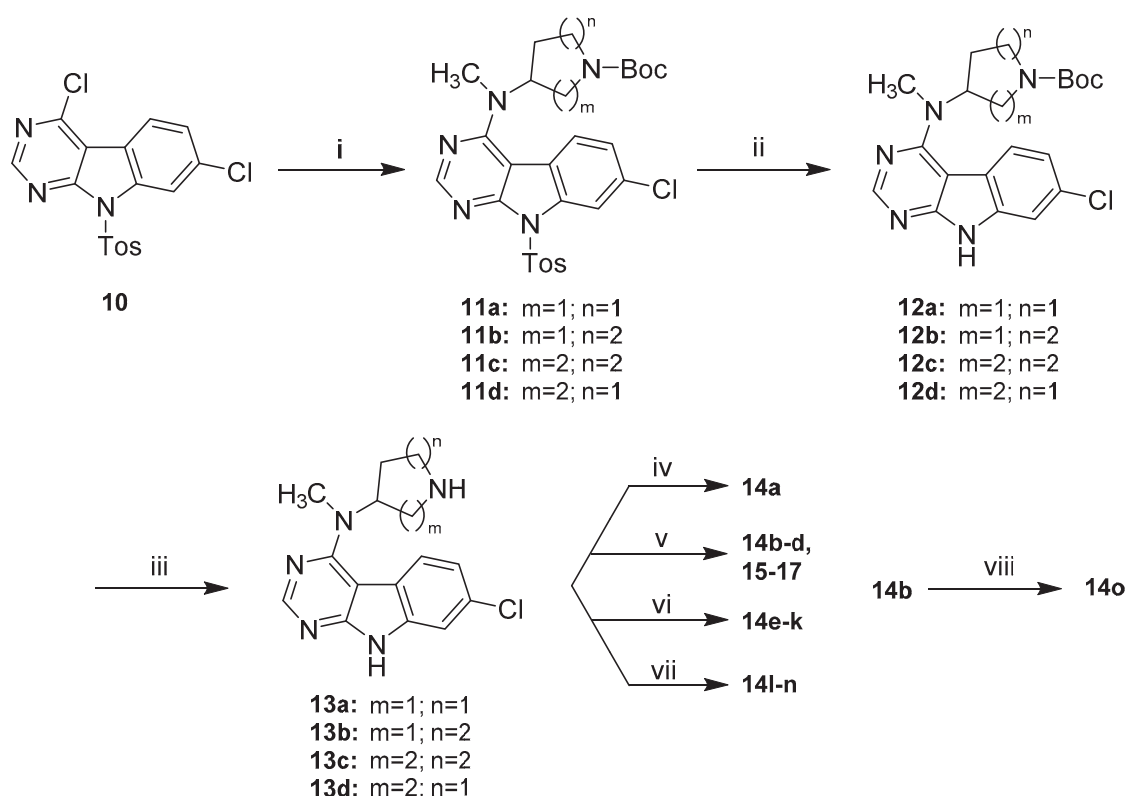
Scheme 5. Synthetic route to final compounds **14a–o** listed with their structures in Table 1 and **15–17** listed with their structures in Table 2. Reagents and conditions: (**i**) **4a–d**, DIPEA, DMF, 80 °C, (93% to quant.); (**ii**) K*t*BuO, THF, rt, (65–78%); (**iii**) TFA, DCM, rt, (74–99%); (**iv**) **13b**, cyanoacetic acid, PyBOP, DIPEA, DCM, rt, (59%); (**v**) **13a–d**, acrylonitrile, MeOH, rt in case of **14b** and **15–17** or **13b**, corresponding acrylic acid derivative, MeOH, rt in case of **14c–d**, (63–89%); (**vi**) **13b**, corresponding aldehyde or ketone, AcOH, Na(OAc)₃BH, DCM, rt, (43–74%); (**vii**) **13b**, bromoacetonitrile, Et₃N, DMF, rt in case of **14l** or **13b**, (bromomethyl)cyclopropane, Et₃N, MeCN, 60 °C in case of **14m** or **13b**, 3-chloro-*N,N*-dimethylpropan-1-amine ·HCl, Et₃N, MeCN, 90 °C in case of **14n**, (39–91%); (**viii**) methyl iodide, NaH, THF, rt, (60%).

For the preparation of the rigidized precursor **22** (Scheme 6) we followed a different synthetic approach compared to the aforementioned secondary amines **4a–d**. The use of 6-azaindole (**18**) as starting material allowed a selective, high-yielding protection of the pyrrole ring nitrogen with Boc anhydride in THF. The key step of this synthetic route was the following hydrogenation which we achieved under comparably mild conditions using Adam's catalyst in glacial acetic acid giving the free piperidine base **20** [37].
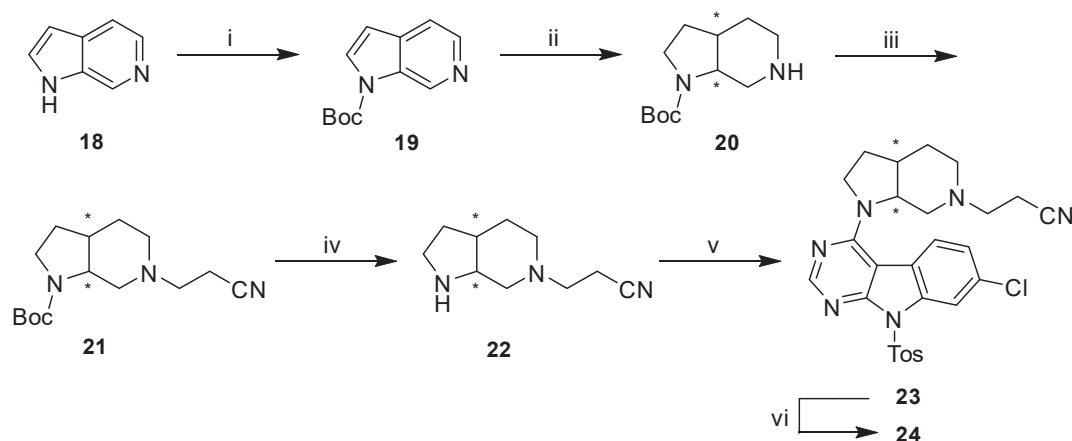
Scheme 6. Synthetic route to final compound **24**. Reagents and conditions: (**i**) Boc$_2$O, THF, 0 °C to rt, (92%); (**ii**) H$_2$ (5 bar), PtO$_2$, AcOH, rt, (88%); (**iii**) acrylonitrile, MeOH, rt, (83%); (**iv**) 4N HCl in dioxane, DCM, rt, (83%); (**v**) **10**, DIPEA, DMF, 80 °C, (64%); (**vi**) K*t*BuO, THF, rt, (55%).

In order to decrease the number of subsequent steps the crucial cyanoethyl moiety was directly installed on the piperidine nitrogen rather than an orthogonal protecting group. This conversion was readily achieved by Michael-addition with acrylonitrile in MeOH (**21**). Finally, acidic conditions were applied to cleave the protecting carbamate yielding **22** [38], which was reacted with **10** under similar S$_N$Ar conditions with subsequent basic detosylation to afford final compound **24**.

In order to define the stereochemistry at the two stereocenters of the octahydro-1*H*-pyrrolo[2,3-*c*]pyridine ring, which were generated during the hydrogenation of Boc-protected azaindole **19**, single crystal analysis of **24** was performed (for details, see Table S5, Supplementary Materials). As expected, X-ray data confirmed that solely a mixture of the (3a*R*, 7a*S*) and (3a*S*, 7a*R*) enantiomers of **24** was obtained (Figure 4).
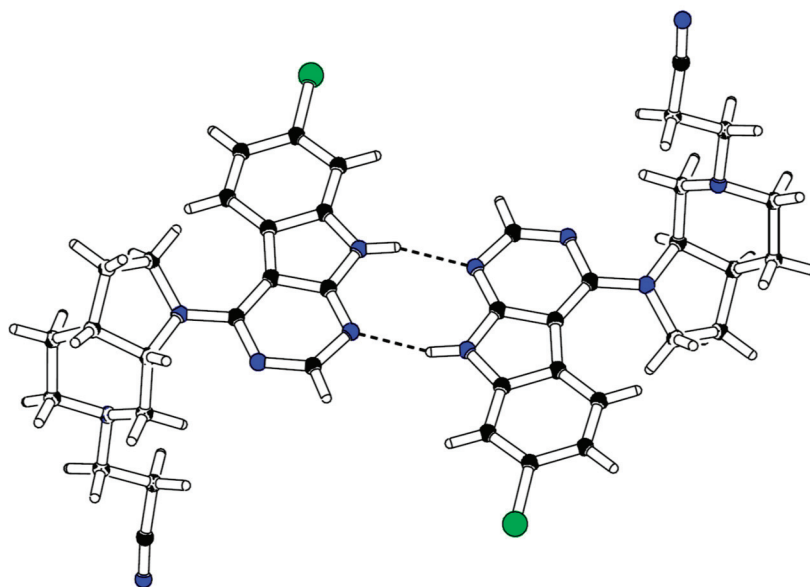
Figure 4. X-ray crystal structure of compound **24**.

3. Conclusions

Starting from the micromolar GSK-3β screen hit **1**, we prepared a series of tofacitinib-derived 7-chloro-9*H*-pyrimido-[4,5-*b*]indole-based compounds. We characterized these compounds in their biological activity in an ADP Glo GSK-3β assay. A switch from amides to tertiary amines proved beneficial for the binding affinity regarding the substituent on the piperidine nitrogen. Moreover, a

cyanoethyl substituent revealed to be an essential structural feature within this series. We examined the role of the nitrile group in detail and assume that it undergoes crucial hydrogen bonding interactions. We derived a putative binding mode for the most potent inhibitors **14b** and **24** from 1 μs molecular dynamics simulations. Most importantly, these inhibitors displayed no significant inhibition of the off-target JAK3. However, we observed a lack of metabolic stability in our HLM experiments, which is currently addressed in further optimization studies regarding this novel class of GSK-3β inhibitors.

4. Materials and Methods

4.1. Comparison of JAK3 and GSK-3β

The location of JAK3 and GSK3β in the phylogenetic tree of the human kinome was visualized by KinMap [39]. The sequence alignment was conducted to annotated kinase domains of the Uniprot entries P52333 (JAK3) and P49841 (GSK3B) with Clustal Omega (1.2.4) [40–42].

4.2. Molecular Modelling

All the modelling was conducted with Maestro Small-Molecule Drug Discovery Suite 2019-1 (Schrödinger, LLC, New York, NY, USA). The figures and the supplementary movies were prepared with PyMOL 2.2.3 (Schrödinger, LLC).

4.2.1. pK$_a$ Calculations

We used the Jaguar pK$_a$ module (Schrödinger, LLC) for the pK$_a$ predictions [43–45]. The calculations were conducted with default settings, except the conformational search step was omitted, as for the input conformation we used the lowest energy structure obtained from QM Conformer & Tautomer Predictor tool (Schrödinger, LLC). In brief, the QM Conformer & Tautomer Predictor workflow is the following. First, the proton donor and acceptor atoms are identified, and protons are redistributed among these to form a list of tautomers (protons can also be added to or subtracted from the input molecule). The generated tautomers were next ranked by their semiempirical PM3 heat of formation, and the high-energy tautomers were then discarded. For the surviving tautomers, a set of conformers were generated with MacroModel and the high-energy structures were eliminated by their semiempirical PM3 heat of formation. Subsequently, DFT geometry optimizations were performed on the surviving structures, using the B3LYP-D3/LACVP** level of theory. Finally, the structures were ranked using single-point energies at the M06-2X/cc-pVTZ(-f) calculated at the optimal geometries from the previous step.

4.2.2. MD Simulations

For the simulations, we used the GSK-3β crystal structure PDB ID: 4PTC [17]. First, the structure (protein–co-crystallized ligand) was prepared by Protein Preparation Wizard [46] (default settings) using OPLS3e force field [24]. Next, the co-crystallized ligand was replaced by the compound **14b** or **24**, using the QM Conformer & Tautomer Predictor (for details see 4.2.1) output conformation of the compounds (second lowest energy structure for **14b**, Boltzmann population: 20.0%; lowest energy structure for **24**, Boltzmann population: 15.6%; lowest energy structure for **24** (3a*R*, 7a*S*), Boltzmann population: 13.0%). The MD simulations were conducted with Desmond [47] using OPLS3e force field [24], except the charges derived from the QM Conformer & Tautomer Predictor were applied for the ligands. The systems were solvated in a cubic box (edges 13 Å from the protein) and neutralized with counterions (Cl$^-$) with 0.15 M KCl salt. The water was described with TIP3P water model [48]. The final systems consisted of 67,285 (**14b**) and 71,836 (**24**, both enantiomers) atoms. Prior to the 1000 ns production simulations, the default relaxation protocol of Desmond was conducted. The final simulations were conducted in NPT ensemble (310 K, thermostat: Nosé-Hoover chain; 1.01325 bar, barostat: Martyna–Tobias–Klein) with the default timestep of 2 fs and cut-off radius of 9.0 Å for Coulombic interactions.

4.3. Chemistry

4.3.1. General Information

All solvents and reagents were commercially obtained and used without additional purification. High performance liquid chromatography (HPLC) was performed on an Hewlett Packard HP1090 series II HPLC system (Hewlett-Packard, Palo Alto, CA, USA) or an Agilent 1100 series HPLC system (Agilent, Santa Clara, CA, USA) equipped with a Phenomenex Luna 5 µm C8(2) 100 Å RP column (150 × 4.6 mm) (Phenomenex, Torrance, CA, USA) and a diode array detector detecting at 230 nm and 254 nm. The method consisted of elution using mobile phase A (MeOH) and mobile phase B (aqueous 0.01M KH_2PO_4 buffer, pH 2.3) in a flow of 1.5 mL/min and the gradient as follows: mobile phase A 40% to 85% during 8 min, mobile phase A 85% constant for 5 min, mobile phase A 85% to 40% during 1 min, mobile phase A 40% constant for 2 min; complete run time 16 min; injection volume 5 µL. Purity of final compounds was determined at 254 nm. Gas chromatography-mass spectrometry (GC-MS) was performed on a Hewlett-Packard HP 6890 Series GC System equipped with an HP 5973 mass selective detector (electron impact ionization) (Hewlett-Packard, Palo Alto, CA, USA). Helium 6.0 was used as carrier gas with a flow of 1.2 mL/min. In *method A* a Zebron ZB-5 column (30 m × 0.25 mm; 0.25 µm film thickness) (Phenomenex, Torrance, CA, USA) was used with the following temperature gradient: hold 160 °C for 1 min, from 160 °C to 240 °C during 8 min, hold 240 °C for 3 min, from 240 °C to 270 °C during 3 min, hold 270 °C for 3 min, from 270 °C to 300 °C during 3 min, hold 300 °C for 12 min; complete run time 33 min. In *method B* an Agilent J&W DB-5ms (30 m × 0.25 mm; 0.25 µm film thickness) (Agilent, Santa Clara, CA, USA) was used with the following temperature gradient: hold 100 °C for 5 min, from 100 °C to 320 °C during 22 min, hold 320 °C for 5 min; complete run time 32 min. Electrospray ionization mass spectrometry (ESI-MS) was performed on an Advion expression[s] CMS TLC-ESI-MS coupling system (Advion, Ithaca, NY, USA) operating in ESI+ mode (capillary temperature 250 °C, capillary voltage 180V, source gas temperature 250 °C, ESI voltage 3500V) and ESI-mode (capillary temperature 250 °C, capillary voltage 180V, source gas temperature 250 °C, ESI voltage 2500V), elution with MeOH. Flash column chromatography was performed on an Interchim puriflash 430 or XS 420 (Interchim, Montluçon, France) on Grace Davison Discovery Sciences Davisil Chromatographic Silica Media LC60A (20–45 µm) (Grace Davison Discovery Sciences, MD, USA) or Interchim puriflash prepacked silica columns (SIHP-JP, 30 µm) (Interchim, Montluçon, France) and Merck Geduran Si60 63–200 µm silica gel (Merck, Darmstadt, Germany) for pre-columns. Mobile phases are described in the detailed procedures. Nuclear magnetic resonance (NMR) analysis was performed on 200, 300, and 400 MHz Bruker Avance spectrometers (Bruker, Billerica, MA, USA). Spectra were calibrated to residual peaks of utilized solvents, chemical shifts are reported in parts per million (ppm) relative to tetramethylsilane ($\delta = 0$). Compounds with amide substituents (Boc protected intermediates and compounds **1** and **14a**) often displayed mixtures of amide bond rotamers in their NMR spectra. Thin layer chromatography (TLC) was performed on silica gel coated aluminum sheets (Merck TLC Silica gel F_{254}, Merck, Darmstadt, Germany or Macherey-Nagel Alugram Sil G/UV_{254}, Macherey-Nagel, Düren, Germany) with visualization under UV light at 254 nm or by ninhydrin stain.

4.3.2. General Procedures

General Procedure A for the Preparation of Intermediates **3a–d** by Reductive Amination

The corresponding cyclic ketone (**2a–d**) (1 eq.) was dissolved in dry DCM. Glacial AcOH (1.1–1.15 eq.) and *N,N*-benzylmethylamine (1.1–1.25 eq.) were added, followed by portion-wise addition of Na(OAc)$_3$BH (1.5–1.6 eq.). The mixture was stirred at rt, under N_2 atmosphere and over Na_2SO_4 (0.5–1 g) overnight. In case of incomplete consumption of the ketone, additional amine and reductive agent were added to the mixture. After complete conversion, saturated $NaHCO_3$ solution was added and phases were separated. The aqueous layer was extracted thrice with DCM. Combined

organic layers were dried over Na_2SO_4 and concentrated under reduced pressure. The residue was purified by flash column chromatography.

General Procedure B for the Preparation of Intermediates **11a–d** by S_NAr

The appropriate secondary amine (**4a–d**) (1.25–1.4 eq.) and DIPEA (3 eq.) were added to a suspension of **10** (1 eq.) in dry DMF. The mixture was stirred at 70–80 °C overnight and poured into ice-cold water after completion. Saturated NH_4Cl solution was added and the formed precipitate filtered, washed with cold water and dried over P_2O_5 in vacuo.

General Procedure C for the Preparation of Intermediates **12a–d** by Deprotection of Tosyl Protecting Group

The corresponding intermediate (**11a–d**) (1 eq.) was dissolved in THF (dry or HPLC grade) and K*t*BuO (7 eq.) was added. The mixture was stirred at rt and under N_2 atmosphere for 0.5 h to 2 h. Saturated NH_4Cl solution was added and the aqueous phase extracted three to four times with EtOAc. Combined organic layers were dried over Na_2SO_4. Volatiles were removed under reduced pressure and the residue purified by flash column chromatography.

General Procedure D for the Preparation of Intermediates **13a–d** by Deprotection of Boc Protecting Group

The appropriate Boc protected amine (**12a–d**) was dissolved or suspended in dry DCM and stirred. Subsequently trifluoroacetic acid (TFA) was added resulting in a 17% (*V/V*) solution which was stirred at rt for 0.5 h to 1.5 h. Volatiles were removed under reduced pressure and the highly acidic residue neutralized by addition of saturated $NaHCO_3$ solution (30 mL). The high polarity of products required repetitive extraction with EtOAc and addition of MeOH to improve solubility. Combined organic layers were washed thrice with saturated $NaHCO_3$ solution and dried over Na_2SO_4. Volatiles were removed under reduced pressure and the residue purified by flash column chromatography or directly used in the next step.

General Procedure E for the Preparation of Final Compounds **14e–k** by Reductive Amination

Intermediate **13b** (1 eq.), glacial AcOH (2 eq.) and the corresponding aldehyde or ketone (1.2–40 eq.) were stirred in dry DCM. $Na(OAc)_3BH$ (1.5–2.0 eq.) was added and the reaction stirred at rt, under N_2 atmosphere and over some Na_2SO_4 (~ 50 mg) for 2 h to 6 h. When reaction control by HPLC indicated sufficient conversion, the mixture was diluted with DCM, washed four times with saturated $NaHCO_3$ solution, dried over Na_2SO_4 and concentrated under reduced pressure. The residue was purified by flash column chromatography.

4.3.3. Detailed Procedures

Preparation of **1**

3-((3*R*,4*R*)-3-((7-Chloro-9*H*-pyrimido[4,5-*b*]indol-4-yl)(methyl)amino)-4-methylpiperidin-1-yl)-3-oxopropanenitrile (**1**). 4,7-Dichloro-9*H*-pyrimido[4,5-*b*]indole (**9**) (50.0 mg, 0.21 mmol) and 3-((3*R*,4*R*)-4-methyl-3-(methylamino)piperidin-1-yl)-3-oxopropanenitrile hydrochloride [49] (48.7 mg, 0.21 mmol) were suspended in a mixture of dry dioxane (1 mL) and dry DMF (0.1 mL). DIPEA (67.9 mg, 0.53 mmol) was added and the mixture stirred under microwave irradiation (120 °C, 130W) in a sealed tube for 26 h. Volatiles were removed under reduced pressure. Purification of the residue by flash column chromatography (SiO₂, 1.EtOAc:*i*PrOH 8:1, 2.DCM:MeOH 95:5) gave 24 mg of a light brown solid (29% yield); NMR shows a 3:1 mixture of amide bond rotamers, ¹H-NMR (400 MHz, acetone-*d₆*) δ 11.30 (s, 1H), 8.55–8.38 (m, 1H), 7.81 (d, *J* = 8.5 Hz, 1H), 7.62 (s, 1H), 7.33 (d, *J* = 8.4 Hz, 1H), 4.85–4.74 (m, 0.75H), 4.27–4.17 (m, 0.25H), 4.11–3.64 (m, 6H), 3.19 (s, 2.25H), 3.05 (s, 0.75H), 2.51–2.31 (m, 1H), 2.01–1.79 (m, 2H), 1.24 (d, *J* = 6.8 Hz, 0.75H), 1.15 (d, *J* = 6.9 Hz, 2.25H); ¹³C-NMR

(101 MHz, acetone-*d*$_6$) δ 164.5, 164.0, 161.0, 158.8, 155.3, 138.7, 131.4, 124.5, 122.0, 119.6, 116.0, 112.2, 100.0, 56.1, 53.3, 48.4, 46.6, 46.2, 34.1, 34.0, 32.9, 32.5, 32.2, 26.0, 25.7, 14.9; ESI-MS: (*m/z*) 396.9 [M + H]$^+$, 418.9 [M + Na]$^+$, 394.9 [M − H]$^-$; HPLC: t$_r$ = 7.201 min (100.0% purity).

Detailed Procedures for the Preparation of Intermediates **3a–d**

tert-Butyl-3-(benzyl(methyl)amino)pyrrolidine-1-carboxylate (**3a**). **3a** was prepared from *N*-Boc-pyrrolidin-3-one (**2a**) (1.5 g, 8.10 mmol), *N,N*-benzylmethylamine (1.1 g, 8.91 mmol), glacial AcOH (534.9 mg, 8.91 mmol) and Na(OAc)$_3$BH (2.6 g, 12.15 mmol) in dry DCM (17 mL) according to general procedure A. Purification by flash column chromatography (SiO$_2$, n-hexane:EtOAc 3:1) gave 1.8 g of a yellow oil (76% yield); ^{1}H-NMR (300 MHz, CDCl$_3$) δ 7.38–7.22 (m, 5H, overlap with CHCl$_3$ signal), 3.79–3.46 (m, 4H), 3.36–3.15 (m, 2H), 3.11–2.94 (m, 1H), 2.16 (s, 3H), 2.14–2.05 (m, 1H), 1.98–1.79 (m, 1H), 1.48 (s, 9H); ^{13}C-NMR (75 MHz, CDCl$_3$) δ 154.6, 138.7, 138.6, 129.2, 129.0, 128.4, 127.2, 79.3, 64.0, 63.2, 60.5, 50.0, 49.6, 45.2, 44.8, 39.8, 30.1, 29.1, 28.6; GC-MS *method A*: t$_r$ = 8.792 min, (*m/z*) 290 [M].

tert-Butyl-3-(benzyl(methyl)amino)piperidine-1-carboxylate (**3b**). **3b** was prepared from *N*-Boc-piperidin-3-one (**2b**) (2.5 g, 12.55 mmol), *N,N*-benzylmethylamine (2.0 g, 16.31 mmol), glacial acetic acid (904.1 mg, 15.06 mmol) and Na(OAc)$_3$BH (4.3 g, 20.08 mmol) in dry DCM (30 mL) according to general procedure A. After stirring overnight reaction control indicated incomplete conversion, therefore a second portion of *N,N*-benzylmethylamine (494.1 mg, 4.08 mmol) and Na(OAc)$_3$BH (1.1 g, 5.02 mmol) was added and stirring continued for 1 h. Purification by flash column chromatography (SiO$_2$, petroleum ether:EtOAc 3:1) gave 2.6 g of a yellow oil (69% yield); ^{1}H-NMR (300 MHz, CDCl$_3$) δ 7.32–7.07 (m, 5H, overlap with CHCl$_3$ signal), 4.35–3.78 (m, 2H), 3.59 (d, *J* = 13.5 Hz, 1H), 3.51 (d, *J* = 13.4 Hz, 1H), 2.74–2.49 (m, 2H), 2.46–2.31 (m, 1H), 2.15 (s, 3H), 1.96– 1.82 (m, 1H), 1.70–1.57 (m, 1H), 1.48–1.29 (m, 11H); ^{13}C-NMR (75 MHz, CDCl$_3$) δ 155.0, 139.7, 128.8, 128.3, 126.9, 79.4, 59.4, 58.4, 46.2 (br), 44.4 (br), 38.0, 28.5, 27.6 (br), 24.7 (br).

tert-Butyl-4-(benzyl(methyl)amino)azepane-1-carboxylate (**3c**). **3c** was prepared from *N*-Boc-hexahydro-1*H*-azepin-4-one (**2c**) (2.25 g, 10.55 mmol), *N,N*-benzylmethylamine (1.5 g, 12.66 mmol), glacial AcOH (696.9 mg, 11.61 mmol) and Na(OAc)$_3$BH (3.4 g, 15.83 mmol) in dry DCM (25 mL) according to general procedure A. After stirring overnight reaction control indicated incomplete conversion, therefore a second portion of *N,N*-benzylmethylamine (639.2 mg, 5.27 mmol) and Na(OAc)$_3$BH (1.1 g, 5.27 mmol) was added and stirring continued for 1 d. Purification by flash column chromatography (SiO$_2$, n-hexane:EtOAc 3:1) gave 2.7 g of a yellow oil (81% yield); ^{1}H-NMR (300 MHz, CDCl$_3$) δ 7.36–7.20 (m, 5H, overlap with CHCl$_3$ signal), 3.66–3.39 (m, 4H), 3.32–3.17 (m, 2H), 2.67–2.56 (m, 1H), 2.21–2.16 (m, 3H), 2.10–1.80 (m, 3H), 1.78–1.41 (m, 12H); ^{13}C-NMR (75 MHz, CDCl$_3$) δ 155.6, 140.0, 140.0, 128.7, 128.3, 126.9, 126.9, 79.2, 63.2, 63.1, 57.8, 57.7, 46.8, 46.4, 44.3, 44.0, 37.6, 30.3, 29.9, 29.8, 28.6, 25.9.

tert-Butyl-4-(benzyl(methyl)amino)piperidine-1-carboxylate (**3d**). **3d** was prepared from *N*-Boc-piperidin-4-one (**2d**) (2.75 g, 13.80 mmol), *N,N*-benzylmethylamine (1.8 g, 15.18 mmol), glacial AcOH (911.7 mg, 15.18 mmol) and Na(OAc)$_3$BH (4.4 g, 20.70 mmol) in dry DCM (30 mL) according to general procedure A. The reaction mixture was stirred over molecular sieves instead of Na$_2$SO$_4$, which was separated by filtration before stopping the reaction with saturated NaHCO$_3$. Purification by flash column chromatography (SiO$_2$, petroleum ether:EtOAc:3.5N NH$_3$ in MeOH 25:73:2) gave 3.6 g of a white solid (86% yield) ^{1}H-NMR (200 MHz, CDCl$_3$) δ 7.37–7.17 (m, 5H, overlap with CHCl$_3$ signal), 4.28–4.04 (m, 2H), 3.59 (s, 2H), 2.80–2.50 (m, 3H), 2.21 (s, 3H), 1.90–1.73 (m, 2H), 1.62–1.43 (m, 11H); ^{13}C-NMR (50 MHz, CDCl$_3$) δ 154.9, 139.5, 128.9, 128.4, 127.1, 79.6, 60.9, 58.1, 43.6, 37.7, 28.6, 28.0; GC-MS *method A*: t$_r$ = 9.663 min, (*m/z*) 304 [M].

Detailed Procedures for the Preparation of Intermediates **4a–d**

tert-Butyl-3-(methylamino)pyrrolidine-1-carboxylate (**4a**). **3a** (1.6 g, 5.51 mmol) was dissolved in HPLC grade MeOH (30 mL) and Pd/C 10% (*m/m*) (532.0 mg) was added. The suspension was stirred in a

reactor charged with 5 bar of H_2 pressure at rt for 4 h and then filtered over a pad of celite rinsing with fresh solvent. The filtrate was concentrated under reduced pressure to give 1.1 g of a green oil (96% crude yield), which was used in the next step without further purification; ^{1}H-NMR (400 MHz, $CDCl_3$) δ 3.48–3.19 (m, 3H), 3.17–2.93 (m, 2H), 2.33 (s, 3H), 2.00–1.88 (m, 1H), 1.67–1.54 (m, 1H), 1.38–1.33 (m, 9H), 1.30 (br s, 1H); ^{13}C-NMR (101 MHz, $CDCl_3$) δ 154.6, 79.0, 59.5, 58.7, 51.6, 51.1, 44.3, 44.0, 34.7, 31.7, 31.0, 28.5; GC-MS *method A*: t_r = 3.039 min, (*m/z*) 200 [M].

tert-Butyl-3-(methylamino)piperidine-1-carboxylate (**4b**). **3b** (2.2 g, 7.16 mmol) was dissolved in a solvent mixture of EtOAc (27 mL) and MeOH (18 mL). Pd/C 10% (*m/m*) (727.0 mg) was added and the mixture stirred in a reactor charged with 5 bar of H_2 pressure at rt for 3 h. The mixture was filtered over a pad of celite rinsing with fresh solvent. The filtrate was concentrated under reduced pressure to give 1.5 g of a green oil (96% crude yield), which was used in the next step without further purification; ^{1}H-NMR (400 MHz, $CDCl_3$) δ 4.18–3.67 (m, 2H), 2.99–2.51 (m, 2H), 2.49–2.37 (m, 4H), 1.95–1.85 (m, 1H), 1.70–1.60 (m, 1H), 1.49–1.37 (m, 10H), 1.35–1.21 (m, 2H); ^{13}C-NMR (101 MHz, $CDCl_3$) δ 155.0, 79.5, 55.6, 48.8 (br), 44.3 (br), 33.9, 31.3, 28.6, 23.6 (br). GC-MS *method B*: t_r = 11.729 min, (*m/z*) 214 [M].

tert-Butyl-4-(methylamino)azepane-1-carboxylate (**4c**). **3c** (662.0 mg, 2.08 mmol) was dissolved in a solvent mixture of EtOAc (9 mL) and MeOH (6 mL). Pd/C 10% (*m/m*) (220.7 mg) was added and the mixture stirred in a reactor charged with 5 bar of H_2 pressure at rt for 3 h. The mixture was filtered over a pad of celite rinsing with fresh solvent. The filtrate was concentrated under reduced pressure to give 463 mg of a green oil (98% crude yield), which was used in the next step without further purification; ^{1}H-NMR (400 MHz, $CDCl_3$) δ 3.54–3.36 (m, 2H), 3.36–3.09 (m, 2H), 2.51–2.41 (m, 1H), 2.36 (s, 3H), 1.97–1.87 (m, 1H), 1.87–1.72 (m, 2H), 1.59–1.31 (m, 13H); ^{13}C-NMR (101 MHz, $CDCl_3$) δ 155.6, 79.2, 60.2, 59.8, 46.6, 46.0, 43.3, 42.8, 34.8, 34.5, 34.2, 33.2, 32.5, 28.6, 24.8, 24.4. GC-MS *method B*: t_r = 13.406 min, (*m/z*) 228 [M].

tert-Butyl-4-(methylamino)piperidine-1-carboxylate (**4d**). **3d** (5.7 g, 18.72 mmol) was dissolved in MeOH (150 mL). Pd/C 10% (*m/m*) (600 mg) and $Pd(OH)_2$/C 20% (*m/m*) (300 mg) were added and the mixture stirred in a reactor charged with 5 bar of H_2 pressure at rt overnight. The mixture was filtered over a pad of celite rinsing with fresh solvent. The filtrate was concentrated under reduced pressure to give 3.9 g of a green oil (97% crude yield), which was used in the next step without further purification; 1H-NMR (200 MHz, $CDCl_3$) δ 4.17–3.83 (m, 2H), 2.88–2.65 (m, 2H), 2.55–2.42 (m, 1H), 2.40 (s, 3H), 1.92–1.74 (m, 2H), 1.42 (s, 9H), 1.33–1.04 (m, 2H); ^{13}C-NMR (50 MHz, $CDCl_3$) δ 155.0, 79.5, 56.8, 42.6 (br), 33.5, 32.2, 28.5; GC-MS *method A*: t_r = 3.499 min, (*m/z*) 214 [M].

Detailed Procedures for the Preparation of 4,7-dichloro-9-tosyl-9*H*-pyrimido[4,5-*b*]indole (**10**)

Ethyl-2-(4-chloro-2-nitrophenyl)-2-cyanoacetate (**6**). A solution of ethyl-2-cyanoacetate (12.4 g, 109.38 mmol) in dry DMF (10 mL) was drop-added to a stirring, ice-cooled suspension of NaH (4.4 g of a 60% dispersion in mineral oil, 109.38 mmol) in dry DMF (20 mL). After complete addition, the dropping funnel was purged with additional dry DMF (5 mL) and ice-cooling was removed. After stirring at rt for 0.5 h, a solution of 1,4-dichloro-2-nitrobenzene (**5**) (10.0 g, 52.08 mmol) in dry DMF (10 mL) was drop-added. The stirring mixture was subsequently heated to 80 °C for 0.5 h, when reaction control via HPLC indicated complete conversion. The mixture was left to cool to rt and acidified with 10% $HCl_{(aq)}$ (50 mL). EtOAc (100 mL) was added, phases were separated and the aqueous layer extracted with additional EtOAc (3 × 30 mL). Combined organic layers were washed with saturated NaCl solution (5 × 50 mL) and dried over Na_2SO_4. The mixture was concentrated under reduced pressure and the liquid residue treated with ice-cold water and stirred with ice-cooling. The resulting yellow precipitate was triturated with the ice-cold water, filtered washing with ice-cold water and dried over P_2O_5 in vacuo. 14.5 g of a yellow solid (> 100% crude yield) that may contain traces of excessive ethyl-2-cyanoacetate, but was used in the next step without further purification; ^{1}H-NMR (200 MHz, DMSO-d_6) δ 8.35 (d, *J* = 2.0 Hz, 1H), 8.02 (dd, *J* = 8.2, 2.1 Hz, 1H), 7.78 (d, *J* = 8.2 Hz, 1H), 6.27 (s, 1H), 4.22 (q, *J* = 7.1 Hz, 2H), 1.19 (t, *J* = 7.1 Hz, 3H); ^{13}C-NMR (50 MHz, DMSO-d_6) δ 163.7,

147.4, 135.2, 134.9, 134.6, 126.0, 124.5, 115.0, 63.1, 40.7, 13.8; ESI-MS: (*m/z*) 266.9 [M − H]⁻; HPLC: t$_r$ = 6.655 min.

Ethyl-2-amino-6-chloro-1*H*-indole-3-carboxylate (**7**). **6** (7.0 g, 26.06 mmol) was dissolved in glacial AcOH (60 mL). The solution was stirred at 85 °C and Zinc dust (20.4 g, 312.72 mmol) was added in ten portions. The suspension was stirred at 85 °C for 75 min when reaction control via HPLC indicated complete consumption of the starting material. After cooling to rt, Zn dust was filtered off rinsing with AcOH (or EtOAc, alternatively) and the filtrate was concentrated under reduced pressure to leave a liquid residue. Careful addition of saturated NaHCO₃ solution neutralized residual AcOH resulting in a precipitate which was filtered off, washed with water and dried over P₂O₅ in vacuo. 5.8 g of a red-brown solid (93% crude yield), which was used in the next step without further purification. A small batch was purified by flash column chromatography (SiO₂, DCM/MeOH 97.5:2.5) for analytical purposes. ¹H-NMR shows a mixture of products, which are assumed to be the title compound and the corresponding 1-hydroxyindole [27]; HPLC: t$_r$ = 8.042 min.

7-Chloro-3,9-dihydro-4*H*-pyrimido[4,5-*b*]indol-4-one (**8**). **7** (5.7 g, 23.88 mmol) and NH₄HCO₂ (1.7 g, 27.46 mmol) were suspended in formamide (50 mL) and stirred at 160 °C for 28 h with reflux cooling when reaction control via HPLC indicated nearly full consumption of the starting material. After cooling to rt the mixture was poured into ice-cold water resulting in a precipitate which was filtered, washed thoroughly with ice-cold water and dried over P₂O₅ in vacuo. 4.5 g of a green-brown solid (86% crude yield), which was used in the next step without further purification; ¹H-NMR (200 MHz, DMSO-*d₆*) δ 12.32 (br s, 2H), 8.15 (s, 1H), 7.95 (d, *J* = 8.5 Hz, 1H), 7.48 (d, *J* = 1.4 Hz, 1H), 7.25 (dd, *J* = 8.5, 1.5 Hz, 1H); ¹³C-NMR (50 MHz, DMSO-*d₆*) δ 158.0, 154.3, 148.0, 136.0, 128.4, 121.8, 121.4, 120.9, 111.4, 100.0; ESI-MS: (*m/z*) 217.9 [M − H]⁻; HPLC: t$_r$ = 5.489 min.

4,7-Dichloro-9*H*-pyrimido[4,5-*b*]indole (**9**). **8** (4.5 g, 20.44 mmol) was suspended in chlorobenzene (30 mL) and DIPEA (4.0 g, 30.66 mmol) was added. The mixture was stirred at rt and under N₂ atmosphere when POCl₃ (4.4 g, 28.62 mmol) was added carefully dropwise. After stirring at rt for 1 h, the mixture was heated to 80 °C for additional 4.5 h with reflux cooling when HPLC indicated complete consumption of the starting material. The mixture was left to cool down and dropped carefully into stirring water (300 mL) at rt resulting in a brown precipitate. Saturated NaHCO₃ solution was added carefully and the suspension left to stir overnight for neutralization. The precipitate was filtered, washed with water and dried over P₂O₅ in vacuo. 4.2 g of a brown solid (87% crude yield), which was purified by the following recrystallization procedure: 2 g of crude 4,7-dichloro-9*H*-pyrimido[4,5-*b*]indole were suspended in boiling toluene (650 mL) and stirred for 0.5 h. The hot suspension was filtered rinsing the brown filter cake with fresh hot toluene. The filtrate was concentrated under reduced pressure resulting in precipitation of the product. The suspension was cooled and subsequently the precipitate was filtered, washed with cold toluene and dried under reduced pressure giving 1.2 g of a yellow solid (59% recrystallization yield, 51% total yield); ¹H-NMR (200 MHz, DMSO-*d₆*) δ 12.85 (s, 1H), 8.76 (s, 1H), 8.14 (d, *J* = 8.5 Hz, 1H), 7.57 (d, *J* = 1.9 Hz, 1H), 7.37 (dd, *J* = 8.5, 1.9 Hz, 1H); ¹³C-NMR (50 MHz, DMSO-*d₆*) δ 156.3, 154.2, 151.3, 139.1, 132.7, 123.6, 121.9, 116.5, 112.0, 110.7; ESI-MS: (*m/z*) 235.7 [M − H]⁻; HPLC: t$_r$ = 8.590 min.

4,7-Dichloro-9-tosyl-9*H*-pyrimido[4,5-*b*]indole (**10**). NaH (151.2 mg of a 60% dispersion in mineral oil, 3.78 mmol) was added in three portions to a stirring suspension of 4,7-dichloro-9*H*-pyrimido[4,5-*b*]indole (**9**) (600.0 mg, 2.52 mmol) in dry THF (20 mL). p-Toluenesulfonyl chloride (576.6 mg, 3.02 mmol) was added after 20 min and stirring continued for another 0.5 h at rt and under N₂ atmosphere when TLC indicated complete consumption of the starting material. The mixture was poured into ice-cold water and saturated NH₄Cl solution (60 mL) was added. The precipitate was filtered, washed with cold water and dried over P₂O₅ in vacuo. 982 mg of a yellow solid (99% crude yield), which was directly used in the next step without further purification; ESI-MS: (*m/z*) 390.0 [M − H]⁻.

Detailed Procedures for the Preparation of Intermediates **11a–d**

tert-Butyl-3-((7-chloro-9-tosyl-9*H*-pyrimido[4,5-*b*]indol-4-yl)(methyl)amino)pyrrolidine-1-carboxylate (**11a**). **11a** was prepared from **10** (1.0 g, 2.55 mmol), **4a** (638.4 mg, 3.19 mmol) and DIPEA (988.8 mg, 7.65 mmol) in dry DMF (25 mL) according to general procedure B. 1.4 g of a beige solid (>100% crude yield), which was used in the next step without further purification. A small batch was purified by flash column chromatography (SiO$_2$, DCM:MeOH 97.5:2.5) for analytical purposes; ^{1}H-NMR (300 MHz, CDCl$_3$) δ 8.64 (s, 1H), 8.54 (d, *J* = 1.8 Hz, 1H), 8.10 (d, *J* = 8.1 Hz, 2H), 7.63 (d, *J* = 8.5 Hz, 1H), 7.40 (dd, *J* = 8.5, 1.9 Hz, 1H), 7.27 (d, 2H, overlap with CHCl$_3$ signal), 4.93–4.74 (m, 1H), 3.94–3.75 (m, 1H), 3.71–3.53 (m, 1H), 3.48–3.29 (m, 2H), 3.10 (s, 3H), 2.37 (s, 3H), 2.33–2.06 (m, 2H), 1.46 (s, 9H); ^{13}C-NMR (50 MHz, CDCl$_3$) δ 161.2, 157.2, 154.5, 154.3, 145.8, 136.2, 135.3, 132.9, 129.8, 128.1, 124.5, 123.3, 119.9, 114.7, 102.0, 79.6, 58.0, 57.4, 47.8, 44.7, 44.3, 35.2, 28.7, 28.6, 28.0, 21.7; ESI-MS: (*m/z*) 578.1 [M + Na]$^+$, 554.3 [M − H]$^-$; HPLC: t$_r$ = 11.123 min.

tert-Butyl-3-((7-chloro-9-tosyl-9*H*-pyrimido[4,5-*b*]indol-4-yl)(methyl)amino)piperidine-1-carboxylate (**11b**). **11b** was prepared from **10** (430.0 mg, 1.10 mmol), **4b** (328.9 mg, 1.54 mmol) and DIPEA (425.1 mg, 3.29 mmol) in dry DMF (12 mL) according to general procedure B. 580 mg of a beige solid (93% crude yield), which was used in the next step without further purification. A small batch was purified by flash column chromatography (SiO$_2$, DCM:MeOH 97.5:2.5) for analytical purposes; ^{1}H-NMR (300 MHz, CDCl$_3$) δ 8.60 (s, 1H), 8.52 (d, *J* = 1.9 Hz, 1H), 8.09 (d, *J* = 8.4 Hz, 2H), 7.60 (d, *J* = 8.1 Hz, 1H), 7.38 (dd, *J* = 8.5, 1.9 Hz, 1H), 7.25 (d, *J* = 8.1 Hz, 2H, overlap with CHCl$_3$ signal), 4.49–3.96 (m, 3H), 3.10 (s, 3H), 3.08–2.98 (m, 1H), 2.76–2.61 (m, 1H), 2.35 (s, 3H), 2.00–1.71 (m, 3H), 1.63–1.50 (m, 1H), 1.39 (s, 9H); ESI-MS: (*m/z*) 569.9 [M + H]$^+$, 591.9 [M + Na]$^+$, 568.0 [M − H]$^-$; HPLC: t$_r$ = 11.456 min.

tert-Butyl-4-((7-chloro-9-tosyl-9*H*-pyrimido[4,5-*b*]indol-4-yl)(methyl)amino)azepane-1-carboxylate (**11c**). **11c** was prepared from **10** (465.0 mg, 1.19 mmol), **4c** (338.4 mg, 1.48 mmol) and DIPEA (459.7 mg, 3.56 mmol) in dry DMF (14 mL) according to general procedure B. 682 mg of a beige solid (98% crude yield), which was used in the next step without further purification. A small batch was purified by flash column chromatography (SiO$_2$, DCM:MeOH 97.5:2.5) for analytical purposes; ^{1}H-NMR (400 MHz, DMSO-*d$_6$*) δ 8.49 (s, 1H), 8.36 (d, *J* = 1.9 Hz, 1H), 8.07–8.01 (m, 2H), 7.79–7.73 (m, 1H), 7.52 (dd, *J* = 8.6, 1.6 Hz, 1H), 7.40 (d, *J* = 8.2 Hz, 2H), 4.28–4.18 (m, 1H), 3.49–3.35 (m, 2H), 3.29–3.12 (m, 2H), 3.04 (s, 3H), 2.33 (s, 3H), 1.96–1.76 (m, 5H), 1.67–1.53 (m, 1H), 1.36–1.28 (m, 9H); ESI-MS: (*m/z*) 606.0 [M + Na]$^+$, 582.1 [M − H]$^-$; HPLC: t$_r$ = 11.827 min.

tert-Butyl-4-((7-chloro-9-tosyl-9*H*-pyrimido[4,5-*b*]indol-4-yl)(methyl)amino)piperidine-1-carboxylate (**11d**). **11d** was prepared from **10** (200.0 mg, 0.51 mmol), **4d** (142.1 mg, 0.66 mmol) and DIPEA (197.7 mg, 1.53 mmol) in dry DMF (5.5 mL) according to general procedure B. Beige solid (>100% crude yield), which was used in the next step without further purification. A small batch was purified by flash column chromatography (SiO$_2$, petroleum ether:EtOAc gradient elution from 9:1 to 4:6) for analytical purposes; ^{1}H-NMR (200 MHz, CDCl$_3$) δ 8.59 (s, 1H), 8.52 (d, *J* = 1.8 Hz, 1H), 8.09 (d, *J* = 8.3 Hz, 2H), 7.54 (d, *J* = 8.6 Hz, 1H), 7.37 (dd, *J* = 8.5, 1.9 Hz, 1H), 7.26 (d, *J* = 8.2 Hz, 2H, overlap with CHCl$_3$ signal), 4.49–4.33 (m, 1H), 4.33–4.16 (m, 2H), 3.07 (s, 3H), 2.94–2.68 (m, 2H), 2.36 (s, 3H), 1.92–1.72 (m, 4H), 1.47 (s, 9H); ^{13}C-NMR (50 MHz, CDCl$_3$) δ 160.1, 157.4, 154.8, 154.1, 145.8, 136.2, 135.5, 132.7, 129.8, 128.2, 124.4, 123.1, 120.5, 114.8, 100.8, 80.0, 56.6, 43.4 (br), 33.4, 29.0, 28.6, 21.8. ESI-MS: (*m/z*) 592.0 [M + Na]$^+$, 568.0 [M − H]$^-$; HPLC: t$_r$ = 11.988 min.

Detailed Procedures for the Preparation of Intermediates **12a–d**

tert-Butyl-3-((7-chloro-9*H*-pyrimido[4,5-*b*]indol-4-yl)(methyl)amino)pyrrolidine-1-carboxylate (**12a**). **12a** was prepared from **11a** (697.0 mg, 1.26 mmol) and K*t*BuO (986.1 mg, 8.79 mmol) in dry THF (40 mL) according to general procedure C in a reaction time of 1.5 h. Purification by flash column chromatography (SiO$_2$, DCM:MeOH gradient elution from 97.5:2.5 to 93:7) gave 394 mg of a beige solid (78% yield); ^{1}H-NMR (300 MHz, CDCl$_3$) δ 11.68 (br s, 1H), 8.65–8.51 (m, 1H), 7.74 (d, *J* = 8.6 Hz,

1H), 7.53 (d, *J* = 1.8 Hz, 1H), 7.29 (dd, 1H, overlap with CHCl$_3$ signal), 5.23–5.02 (m, 1H), 3.99–3.80 (m, 1H), 3.78–3.37 (m, 3H), 3.30 (s, 3H), 2.39–2.14 (m, 2H), 1.49 (s, 9H); ^{13}C-NMR (50 MHz, DMSO-*d$_6$*) δ 160.2, 157.4, 153.7, 153. 6, 137.5, 129.5, 124.0, 120.6, 118.3, 110.9, 98.1, 78.4, 56.8, 56.2, 47.0, 44.4, 44.1, 34.1, 28.2, 27.9, 27.0; ESI-MS: (*m/z*) 424.2 [M + Na]$^+$, 400.2 [M − H]$^-$; HPLC: t$_r$ = 9.653 min.

tert-Butyl-3-((7-chloro-9*H*-pyrimido[4,5-*b*]indol-4-yl)(methyl)amino)piperidine-1-carboxylate (**12b**). **12b** was prepared from **11b** (580.0 mg, 1.02 mmol) and K*t*BuO (799.1 mg, 7.12 mmol) in dry THF (32 mL) according to general procedure C in a reaction time of 1 h. Purification by flash column chromatography (SiO$_2$, DCM:MeOH gradient elution from 97.5:2.5 to 93:7) gave 320 mg of a beige solid (76% yield); ^{1}H-NMR (200 MHz, CDCl$_3$) δ 12.25 (br s, 1H), 8.57 (s, 1H), 7.70 (d, *J* = 8.6 Hz, 1H), 7.50 (d, *J* = 1.8 Hz, 1H), 7.24 (dd, 1H, overlap with CHCl$_3$ signal), 4.59–3.95 (m, 3H), 3.26 (s, 3H), 3.17–2.96 (m, 1H), 2.84–2.56 (m, 1H), 2.19–1.55 (m, 4H), 1.43 (s, 9H); ^{13}C-NMR (50 MHz, CDCl$_3$) δ 160.2, 157.2, 155.0, 152.5, 137.5, 131.1, 123.7, 121.5, 118.8, 111.6, 98.7, 80.0, 55.2, 46.8, 44.1, 33.4, 28.5, 28.2, 25.0; ESI-MS: (*m/z*) 438.0 [M + Na]$^+$, 413.9 [M − H]$^-$; HPLC: t$_r$ = 9.001 min.

tert-Butyl-4-((7-chloro-9*H*-pyrimido[4,5-*b*]indol-4-yl)(methyl)amino)azepane-1-carboxylate (**12c**). **12c** was prepared from **11c** (682.0 mg, 1.17 mmol) and K*t*BuO (917.0 mg, 8.17 mmol) in dry THF (40 mL) following general procedure C in a reaction time of 0.75 h. Purification by flash column chromatography (SiO$_2$, DCM:MeOH gradient elution from 97.5:2.5 to 93:7) gave 392 mg of a beige solid (78% yield); ^{1}H-NMR (400 MHz, CDCl$_3$) δ 12.43 (br s, 1H), 8.55 (s, 1H), 7.69–7.62 (m, 1H), 7.50–7.45 (m, 1H), 7.25–7.20 (m, 1H), 4.64–4.52 (m, 1H), 3.88–3.78 (m, 0.5H), 3.72–3.63 (m, 0.5H), 3.57–3.38 (m, 2H), 3.28–3.15 (m, 4H), 2.11–1.67 (m, 6H), 1.47 (s, 9H); ^{13}C-NMR (101 MHz, CDCl$_3$) δ 159.9, 157.3, 155.7, 152.7, 137.5, 130.9, 123.5, 121.3, 119.0, 111.6, 98.4, 79.6, 58.9, 58.4, 46.9, 46.0, 43.6, 43.5, 33.1, 32.3, 31.82, 31.79, 31.5, 28.7, 25.43, 25.36; ESI-MS: (*m/z*) 430.0 [M + H]$^+$, 452.0 [M + Na]$^+$, 428.0 [M − H]$^-$; HPLC: t$_r$ = 9.734 min.

tert-Butyl-4-((7-chloro-9*H*-pyrimido[4,5-*b*]indol-4-yl)(methyl)amino)piperidine-1-carboxylate (**12d**). **12d** was prepared from **11d** (290.8 mg, 0.51 mmol) and K*t*BuO (400.7 mg, 3.57 mmol) in HPLC grade THF (32 mL) according to general procedure C in a reaction time of 2 h. Purification by flash column chromatography (SiO$_2$, DCM:MeOH gradient elution from 97.5:2.5 to 93:7) gave 138 mg of an off-white solid (65% yield); ^{1}H-NMR (400 MHz, CDCl$_3$) δ 12.09 (s, 1H), 8.56 (s, 1H), 7.67 (d, *J* = 8.6 Hz, 1H), 7.48 (d, *J* = 1.9 Hz, 1H), 7.24 (dd, *J* = 8.6, 1.9 Hz, 1H), 4.70–4.58 (m, 1H), 4.46–4.11 (m, 2H), 3.23 (s, 3H), 2.99–2.75 (m, 2H), 1.96–1.80 (m, 4H), 1.50 (s, 9H); ^{13}C-NMR (50 MHz, CDCl$_3$) δ 160.0, 157.2, 154.9, 152.5, 137.5, 130.9, 123.4, 121.2, 118.9, 111.6, 98.3, 79.9, 55.9, 43.6, 33.2, 29.1, 28.6; ESI-MS: (*m/z*) 416.1 [M + H]$^+$, 438.1 [M + Na]$^+$, 414.1 [M − H]$^-$; HPLC: t$_r$ = 10.236 min.

Detailed Procedures for the Preparation of Intermediates **13a–d**

7-Chloro-*N*-methyl-*N*-(pyrrolidin-3-yl)-9*H*-pyrimido[4,5-*b*]indol-4-amine (**13a**). **13a** was prepared from **12a** (340.0 mg, 0.85 mmol) and TFA (1.8 mL) in dry DCM (9 mL) according to general procedure D. 220 mg of a beige solid (86% yield), which was used in the next step without further purification; ^{1}H-NMR (300 MHz, DMSO-*d$_6$*) δ 8.40 (s, 1H), 7.83 (d, *J* = 8.6 Hz, 1H), 7.48 (d, *J* = 2.0 Hz, 1H), 7.27 (dd, *J* = 8.6, 2.0 Hz, 1H), 4.97–4.85 (m, 1H), 3.17 (s, 3H), 3.14–3.07 (m, 1H), 3.00–2.75 (m, 3H), 2.12–1.98 (m, 1H), 1.94–1.80 (m, 1H). Both N-H not detected due to hydrogen bonding; ^{13}C-NMR (75 MHz, DMSO-*d$_6$*) δ 160.1, 157.4, 153.7, 137.4, 129.2, 123.8, 120.4, 118.6, 110.8, 97.6, 58.8, 49.2, 46.4, 33.4, 29.0; ESI-MS: (*m/z*) 301.9 [M + H]$^+$, 299.9 [M − H]$^-$, HPLC: t$_r$ = 3.556 min.

7-Chloro-*N*-methyl-*N*-(piperidin-3-yl)-9*H*-pyrimido[4,5-*b*]indol-4-amine (**13b**). **13b** was prepared from **12b** (314.0 mg, 0.76 mmol) and TFA (1.7 mL) in dry DCM (8.5 mL) according to general procedure D in a reaction time of 1 h. 236 mg of a beige solid (99% yield), which was used in the next step without further purification; ^{1}H-NMR (300 MHz, MeOD) δ 8.34 (s, 1H), 7.75 (d, *J* = 8.6 Hz, 1H), 7.49 (d, *J* = 1.9 Hz, 1H), 7.26 (dd, *J* = 8.6, 2.0 Hz, 1H), 4.48 (tt, *J* = 11.2, 4.0 Hz, 1H), 3.25 (s, 3H), 3.17–3.08 (m, 1H), 3.05–2.96 (m, 1H), 2.96–2.86 (m, 1H), 2.63–2.49 (m, 1H), 2.16–1.85 (m, 3H), 1.78–1.60 (m, 1H); ^{13}C-NMR

(50 MHz, DMSO-d_6) δ 159.6, 157.5, 153.7, 137.4, 129.1, 123.8, 120.4, 118.7, 110.8, 97.1, 55.7, 48.6, 45.5, 32.7, 28.2, 26.4; ESI-MS: (*m/z*) 316.0 [M + H]$^+$, 338.0 [M + Na]$^+$, 313.9 [M − H]$^-$; HPLC: t$_r$ = 3.815 min.

N-(Azepan-4-yl)-7-chloro-*N*-methyl-9*H*-pyrimido[4,5-*b*]indol-4-amine (**13c**). **13c** was prepared from **12c** (125.0 mg, 0.29 mmol) and TFA (1 mL) in dry DCM (5 mL) according to general procedure D in a reaction time of 1.5 h. Purification by flash column chromatography (SiO$_2$, DCM:2N NH$_3$ in MeOH 9:1) gave 71 mg of a beige solid (74% yield); ^{1}H-NMR (400 MHz, CDCl$_3$) δ 8.53 (s, 1H), 7.66 (d, *J* = 8.6 Hz, 1H), 7.44 (d, *J* = 1.6 Hz, 1H), 7.20 (dd, *J* = 8.6, 1.8 Hz, 1H), 4.75–4.66 (m, 1H), 3.23 (s, 3H), 3.12–2.99 (m, 2H), 2.96–2.87 (m, 2H), 2.13–1.96 (m, 4H), 1.95–1.85 (m, 1H), 1.78–1.66 (m, 1H). Both N-H not detected due to hydrogen bonding; ^{13}C-NMR (101 MHz, CDCl$_3$) δ 160.1, 157.8, 153.1, 137.5, 130.7, 123.5, 121.1, 119.2, 111.5, 98.5, 58.6, 48.9, 46.1, 35.0, 32.7, 31.6, 27.6; ESI-MS: (*m/z*) 329.9 [M + H]$^+$, 328.0 [M − H]$^-$; HPLC: t$_r$ = 3.401 min.

7-Chloro-*N*-methyl-*N*-(piperidin-4-yl)-9*H*-pyrimido[4,5-*b*]indol-4-amine (**13d**). **13d** was prepared from **12d** (105.0 mg, 0.25 mmol) and TFA (0.6 mL) in dry DCM (3 mL) according to general procedure D in a reaction time of 1 h. 73 mg of a beige solid (92% yield) which was used in the next step without further purification; ^{1}H-NMR (400 MHz, MeOD) δ 8.34 (s, 1H), 7.73 (d, *J* = 8.6 Hz, 1H), 7.50 (d, *J* = 1.9 Hz, 1H), 7.26 (dd, *J* = 8.6, 2.0 Hz, 1H), 4.55–4.46 (m, 1H), 3.23 (s, 3H), 3.21–3.13 (m, 2H), 2.76–2.66 (m, 2H), 2.02–1.90 (m, 2H), 1.90–1.83 (m, 2H); ESI-MS: (*m/z*) 316.0 [M + H]$^+$, 314.0 [M − H]$^-$; HPLC: t$_r$ = 3.485 min.

Detailed Procedures for the Preparation of Compounds **14a–o**

3-(3-((7-Chloro-9*H*-pyrimido[4,5-*b*]indol-4-yl)(methyl)amino)piperidin-1-yl)-3-oxopropanenitrile (**14a**). Cyanoacetic acid (23.1 mg, 0.27 mmol) and PyBOP (141.4 mg, 0.27 mmol) were dissolved in dry DCM (5 mL) and stirred at rt and under N$_2$ atmosphere for 20 min. A suspension of **13b** (71.5 mg, 0.23 mmol) and DIPEA (87.8 mg, 0.68 mmol) in dry DCM (5 mL) was added and the mixture stirred at rt and under N$_2$ atmosphere for 1.5 h. The mixture was then diluted with DCM, washed with saturated NaHCO$_3$ solution (4 × 15 mL), dried over Na$_2$SO$_4$ and concentrated under reduced pressure. Purification of the residue by flash column chromatography (SiO$_2$, 1. DCM:MeOH gradient elution from 95:5 to 92.5:7.5, 2. DCM:EtOH gradient elution from 96.5:3.5 to 93:7) gave 51 mg of a white solid (59% yield); NMR shows a 7:3 mixture of amide bond rotamers, ^{1}H (400 MHz, CDCl$_3$) δ 12.59 (br s, 1H), 8.51–8.30 (m, 1H), 7.67–7.48 (m, 1H), 7.41–7.30 (m, 1H), 7.21–7.09 (m, 1H), 4.90–4.78 (m, 0.3H), 4.70–4.58 (m, 0.7H), 4.45–4.23 (m, 1H), 4.22–4.11 (m, 0.7H), 4.04–3.79 (m, 1.4H), 3.78–3.69 (m, 0.3H), 3.66–3.54 (m, 0.6H), 3.30–3.12 (m, 4H), 3.05–2.94 (m, 0.3H), 2.70–2.56 (m, 0.7H), 2.26–1.88 (m, 3H), 1.86–1.64 (m, 1H); ^{13}C-NMR (101 MHz, CDCl$_3$) δ 161.2, 160.6, 159.8, 157.2, 156.7, 152.5, 152.0, 137.5, 137.4, 131.24, 131.17, 123.6, 123.5, 121.5, 121.4, 118.41, 118.35, 114.7, 114.1, 111.7, 111.6, 98.5, 77.4, 55.5, 54.6, 48.2, 46.9, 45.4, 43.5, 34.9, 34.0, 28.7, 27.6, 25.40, 25.37, 25.2, 24.8; ESI-MS: (*m/z*) 383.1 [M + H]$^+$, 405.1[M + Na]$^+$, 380.9 [M − H]$^-$; HPLC: t$_r$ = 6.202 min (100.0% purity).

3-(3-((7-Chloro-9*H*-pyrimido[4,5-*b*]indol-4-yl)(methyl)amino)piperidin-1-yl)propanenitrile (**14b**). **13b** (125.0 mg, 0.40 mmol) and acrylonitrile (46.2 mg, 0.87 mmol) were stirred in dry MeOH (35 mL) at rt and under N$_2$ atmosphere overnight. Volatiles were removed under reduced pressure. Purification of the residue by flash column chromatography (SiO$_2$, DCM:MeOH gradient elution from 95.5:4.5 to 93.5:6.5) gave 92 mg of a white solid (63% yield); ^{1}H-NMR (400 MHz, DMSO-d_6) δ 12.22 (s, 1H), 8.40 (s, 1H), 7.78 (d, *J* = 8.6 Hz, 1H), 7.48 (s, 1H), 7.34 (d, *J* = 8.4 Hz, 1H), 4.56–4.33 (m, 1H), 3.14 (s, 3H), 3.11–3.03 (m, 1H), 2.92–2.81 (m, 1H), 2.78–2.68 (m, 2H), 2.68–2.58 (m, 2H), 2.44–2.32 (m, 1H), 2.02–1.88 (m, 1H), 1.84–1.63 (m, 3H), 1.59–1.41 (m, 1H); ^{13}C-NMR (101 MHz, DMSO-d_6) δ 159.4, 157.4, 153.7, 137.3, 129.1, 123.8, 120.6, 120.0, 118.5, 110.8, 97.0, 55.7, 54.7, 53.0, 52.2, 32.5, 27.2, 24.3, 15.0. ESI-MS: (*m/z*) 369.1 [M + H]$^+$, 391.0 [M + Na]$^+$, 366.9 [M − H]$^-$; HPLC: t$_r$ = 3.695 min (100.0% purity).

3-(3-((7-Chloro-9*H*-pyrimido[4,5-*b*]indol-4-yl)(methyl)amino)piperidin-1-yl)propanamide (**14c**). **13b** (65.0 mg, 0.21 mmol) and acrylamide (16.1 mg, 0.23 mmol) were stirred in dry MeOH (11 mL) at rt and

under N$_2$ atmosphere overnight. Additional acrylamide (16.1 mg, 0.23 mmol) was added and stirring at rt continued for 5 days. Volatiles were removed under reduced pressure. Purification of the residue by flash column chromatography (SiO$_2$, DCM:2N NH$_3$ in MeOH gradient elution from 92:8 to 9:1) gave 65 mg of a white solid (82% yield); ^{1}H-NMR (400 MHz, DMSO-d_6) δ 12.21 (s, 1H), 8.39 (s, 1H), 7.76 (d, *J* = 8.7 Hz, 1H), 7.48 (d, *J* = 2.0 Hz, 1H), 7.34 (br s, 1H), 7.30 (dd, *J* = 8.6, 2.0 Hz, 1H), 6.78 (br s, 1H), 4.50–4.34 (m, 1H), 3.15 (s, 3H), 3.05–2.96 (m, 1H), 2.87–2.77 (m, 1H), 2.65–2.52 (m, 2H), 2.35–2.18 (m, 3H), 1.96–1.85 (m, 1H), 1.84–1.65 (m, 3H), 1.58–1.42 (m, 1H); ^{13}C-NMR (101 MHz, DMSO-d_6) δ 173.2, 159.4, 157.4, 153.7, 137.3, 129.1, 123.8, 120.5, 118.5, 110.8, 97.0, 55.9, 54.8, 54.2, 52.7, 33.0, 32.6, 27.4, 24.4; ESI-MS: (*m/z*) 387.4 [M + H]$^+$, 409.4 [M + Na]$^+$, 385.3 [M − H]$^−$; HPLC: t$_r$ = 3.872 min (100.0% purity).

Methyl-3-(3-((7-chloro-9*H*-pyrimido[4,5-*b*]indol-4-yl)(methyl)amino)piperidin-1-yl)propanoate (**14d**). **13b** (65.0 mg, 0.21 mmol) and methyl acrylate (19.5 mg, 0.23 mmol) were stirred in dry MeOH (11 mL) at rt and under N$_2$ atmosphere for 3 h. Additional methyl acrylate (4.4 mg, 0.05 mmol) was added and stirring at rt continued for 1 h. Volatiles were removed under reduced pressure. Purification of the residue by flash column chromatography (SiO$_2$, DCM:MeOH gradient elution from 96:4 to 92:8) gave 74 mg of a beige solid (89% yield); ^{1}H-NMR (400 MHz, DMSO-d_6) δ 12.21 (s, 1H), 8.39 (s, 1H), 7.75 (d, *J* = 8.7 Hz, 1H), 7.47 (d, *J* = 2.0 Hz, 1H), 7.28 (dd, *J* = 8.6, 2.0 Hz, 1H), 4.45–4.34 (m, 1H), 3.55 (s, 3H), 3.14 (s, 3H), 3.00–2.92 (m, 1H), 2.84–2.75 (m, 1H), 2.62 (t, *J* = 6.9 Hz, 2H), 2.53–2.46 (m, 2H, overlap with DMSO-d_5 signal), 2.36–2.26 (m, 1H), 1.95–1.85 (m, 1H), 1.83–1.65 (m, 3H), 1.55–1.41 (m, 1H); ^{13}C-NMR (101 MHz, DMSO-d_6) δ 172.4, 159.4, 157.4, 153.7, 137.3, 129.1, 123.8, 120.4, 118.5, 110.8, 97.0, 55.9, 54.8, 53.3, 52.5, 51.1, 32.6, 31.6, 27.3, 24.4; ESI-MS: (*m/z*) 402.5 [M + H]$^+$, 424.6 [M + Na]$^+$, 400.3 [M − H]$^-$; HPLC: t$_r$ = 4.363 min (100.0% purity).

7-Chloro-*N*-methyl-*N*-(1-propylpiperidin-3-yl)-9*H*-pyrimido[4,5-*b*]indol-4-amine (**14e**). **14e** was prepared from **13b** (65.0 mg, 0.21 mmol), propionaldehyde (17.9 mg, 0.31 mmol), glacial AcOH (24.7 mg, 0.41 mmol) and Na(OAc)$_3$BH (87.2 mg, 0.41 mmol) in dry DCM (10 mL) according to general procedure E in a reaction time of 2 h. Purification by flash column chromatography (SiO$_2$, 1. DCM:2N NH$_3$ in MeOH gradient elution from 95:5 to 92:8, 2. DCM:2N NH$_3$ in MeOH gradient elution from 94:6 to 91.5:8.5) gave 46 mg of a white solid (62% yield); ^{1}H-NMR (400 MHz, DMSO-d_6) δ 2.21 (s, 1H), 8.39 (s, 1H), 7.78 (d, *J* = 8.7 Hz, 1H), 7.47 (d, *J* = 2.0 Hz, 1H), 7.23 (dd, *J* = 8.6, 2.0 Hz, 1H), 4.48–4.37 (m, 1H), 3.14 (s, 3H), 3.00–2.91 (m, 1H), 2.84–2.76 (m, 1H), 2.33–2.17 (m, 3H), 1.87–1.66 (m, 4H), 1.58–1.39 (m, 3H), 0.84 (t, *J* = 7.3 Hz, 3H); ^{13}C-NMR (101 MHz, DMSO-d_6) δ 159.4, 157.4, 153.7, 137.3, 129.1, 123.8, 120.3, 118.6, 110.8, 97.0, 60.0, 56.3, 54.9, 52.9, 32.6, 27.6, 24.5, 19.6, 11.7; ESI-MS: (*m/z*) 358.2 [M + H]$^+$, 380.1 [M + Na]$^+$, 356.2 [M − H]$^-$; HPLC: t$_r$ = 4.200 min (99.3% purity).

7-Chloro-*N*-(1-isopropylpiperidin-3-yl)-*N*-methyl-9*H*-pyrimido[4,5-*b*]indol-4-amine (**14f**). **14f** was prepared from **13b** (62.0 mg, 0.20 mmol), acetone (228.1 mg, 3.93 mmol), glacial AcOH (23.6 mg, 0.39 mmol) and Na(OAc)$_3$BH (83.2 mg, 0.39 mmol) in dry DCM (10 mL) according to general procedure E in a reaction time of 5 h. A second portion of acetone (228.1 mg, 3.93 mmol) was added after 3 h. Purification by flash column chromatography (SiO$_2$, DCM:2N NH$_3$ in MeOH 95:5 to 92.5:7.5) gave 30 mg of a beige solid (43% yield); ^{1}H-NMR (400 MHz, DMSO-d_6) δ 12.20 (s, 1H), 8.39 (s, 1H), 7.79 (d, *J* = 8.7 Hz, 1H), 7.47 (d, *J* = 2.0 Hz, 1H), 7.24 (dd, *J* = 8.6, 2.0 Hz, 1H), 4.46–4.35 (m, 1H), 3.16 (s, 3H), 2.96–2.86 (m, 1H), 2.79–2.66 (m, 2H), 2.48–2.41 (m, 1H), 2.16–2.03 (m, 1H), 1.86–1.67 (m, 3H), 1.55–1.41 (m, 1H), 1.05–0.92 (m, 6H); ^{13}C-NMR (50 MHz, DMSO-d_6) δ 159.4, 157.4, 153.8, 137.3, 129.1, 123.9, 120.3, 118.6, 110.8, 97.0, 55.5, 54.0, 51.3, 48.1, 32.7, 28.0, 24.8, 18.1, 17.7; ESI-MS: (*m/z*) 357.8 [M + H]$^+$, 355.8 [M − H]$^-$; HPLC: t$_r$ = 4.291 min (99.0% purity).

7-Chloro-*N*-(1-cyclopentylpiperidin-3-yl)-*N*-methyl-9*H*-pyrimido[4,5-*b*]indol-4-amine (**14g**). **14g** was prepared from **13b** (60.0 mg, 0.19 mmol), cyclopentanone (63.9 mg, 0.76 mmol), glacial AcOH (22.8 mg, 0.38 mmol) and Na(OAc)$_3$BH (80.5 mg, 0.38 mmol) in dry DCM (10 mL) according to general procedure E in a reaction time of 3 h. Purification by flash column chromatography (SiO$_2$, DCM:2N NH$_3$ MeOH gradient elution from 96:4 to 93:7) gave 54 mg of a white solid (74% yield); ^{1}H-NMR (400

MHz, DMSO-d_6) δ 12.21 (s, 1H), 8.38 (s, 1H), 7.79 (d, J = 8.7 Hz, 1H), 7.47 (d, J = 1.9 Hz, 1H), 7.24 (dd, J = 8.6, 2.0 Hz, 1H), 4.47–4.35 (m, 1H), 3.14 (s, 3H), 3.09–3.01 (m, 1H), 2.94–2.84 (m, 1H), 2.58–2.52 (m, 1H, overlap with DMSO-d_5), 2.30–2.17 (m, 1H), 1.93–1.67 (m, 6H), 1.64–1.39 (m, 5H), 1.38–1.25 (m, 2H); ^{13}C-NMR (101 MHz, DMSO-d_6) δ 159.4, 157.4, 153.7, 137.3, 129.1, 123.8, 120.2, 118.6, 110.8, 96.9, 66.7, 55.0, 54.8, 51.5, 32.6, 29.8, 29.6, 27.6, 24.5, 23.6; ESI-MS: (*m/z*) 383.8 [M + H]$^+$, 381.8 [M − H]$^-$; HPLC: t$_r$ = 4.839 min (100.0% purity).

7-Chloro-*N*-(1-(furan-2-ylmethyl)piperidin-3-yl)-*N*-methyl-9*H*-pyrimido[4,5-*b*]indol-4-amine (14h). **14h** was prepared from **13b** (80.0 mg, 0.25 mmol), furan-2-carbaldehyde (30.4 mg, 0.32 mmol), glacial AcOH (30.4 mg, 0.51 mmol) and Na(OAc)$_3$BH (80.5 mg, 0.38 mmol) in dry DCM (10 mL) according to general procedure E in a reaction time of 6.5 h. Purification by flash column chromatography (SiO$_2$, 1.DCM:MeOH gradient elution from 96:4 to 92.5:7.5, 2.DCM:MeOH gradient elution from 96:4 to 92:8) gave 55 mg of an off-white solid (55% yield); ^{1}H-NMR (300 MHz, CDCl$_3$) δ 11.76 (br s, 1H), 8.54 (s, 1H), 7.63 (d, J = 8.6 Hz, 1H), 7.49–7.37 (m, 2H), 7.21 (dd, J = 8.6, 1.8 Hz, 1H), 6.39–6.31 (m, 1H), 6.30–6.22 (m, 1H), 4.69–4.50 (m, 1H), 3.71 (d, J = 14.2 Hz, 1H), 3.64 (d, J = 14.2 Hz, 1H), 3.28–3.14 (m, 4H), 3.03–2.92 (m, 1H), 2.50–2.37 (m, 1H), 2.14–2.02 (m, 1H), 2.00–1.90 (m, 1H), 1.88–1.71 (m, 3H); ^{13}C-NMR (50 MHz, CDCl$_3$) δ 160.3, 157.6, 153.1, 151.4, 142.5, 137.3, 130.8, 123.7, 121.3, 119.0, 111.4, 110.4, 109.4, 98.7, 56.1, 55.7, 54.9, 53.2, 33.2, 28.0, 24.7.; ESI-MS: (*m/z*) 396.1 [M + H]$^+$, 418.1 [M + Na]$^+$, 393.9 [M − H]$^-$; HPLC: t$_r$ = 4.781 min (99.7% purity).

7-Chloro-*N*-methyl-*N*-(1-(pyridin-4-ylmethyl)piperidin-3-yl)-9*H*-pyrimido[4,5-*b*]indol-4-amine (14i). **14i** was prepared from **13b** (75.0 mg, 0.24 mmol), pyridin-4-carbaldehyde (38.2 mg, 0.36 mmol), glacial AcOH (28.5 mg, 0.48 mmol) and Na(OAc)$_3$BH (100.7 mg, 0.48 mmol) in dry DCM (10 mL) according to general procedure E in a reaction time of 2.5 h. Purification by flash column chromatography (SiO$_2$, DCM:MeOH gradient elution from 95:5 to 90.5:9.5) gave 71 mg of a white solid (73% yield); ^{1}H-NMR (400 MHz, DMSO-d_6) δ 12.22 (s, 1H), 8.49 (d, J = 5.7 Hz, 2H), 8.37 (s, 1H), 7.69 (d, J = 8.6 Hz, 1H), 7.48 (d, J = 1.8 Hz, 1H), 7.32 (d, J = 5.6 Hz, 2H), 7.22 (dd, J = 8.6, 1.8 Hz, 1H), 4.54–4.41 (m, 1H), 3.59–3.48 (m, 2H), 3.13 (s, 3H), 2.98–2.88 (m, 1H), 2.80–2.70 (m, 1H), 2.37–2.27 (m, 1H), 2.00–1.89 (m, 1H), 1.86–1.65 (m, 3H), 1.62–1.48 (m, 1H); ^{13}C-NMR (50 MHz, DMSO-d_6) δ 159.4, 157.5, 153.7, 149.5, 147.5, 137.4, 129.2, 123.8, 123.7, 120.3, 118.5, 110.9, 97.0, 60.8, 55.9, 54.8, 52.8, 32.8, 27.2, 24.4; ESI-MS: (*m/z*) 407.4 [M + H]$^+$, 405.2 [M − H]$^-$; HPLC: t$_r$ = 6.121 min (99.5% purity).

3-((3-((7-Chloro-9*H*-pyrimido[4,5-*b*]indol-4-yl)(methyl)amino)piperidin-1-yl)methyl)benzonitrile (14j). **14j** was prepared from **13b** (25.0 mg, 0.08 mmol), 3-formylbenzonitrile (31.1 mg, 0.24 mmol), glacial AcOH (9.5 mg, 0.16 mmol) and Na(OAc)$_3$BH (33.6 mg, 0.16 mmol) in dry DCM (4 mL) according to general procedure E in a reaction time of 4 h. Purification by flash column chromatography (SiO$_2$, DCM:MeOH gradient elution from 96:4 to 93:7) gave 20 mg of a white solid (59% yield); ^{1}H-NMR (400 MHz, DMSO-d_6) δ 12.20 (s, 1H), 8.37 (s, 1H), 7.77 (br s, 1H), 7.75–7.64 (m, 3H), 7.54 (t, J = 7.7 Hz, 1H), 7.47 (d, J = 2.0 Hz, 1H), 7.21 (dd, J = 8.6, 2.0 Hz, 1H), 4.54–4.41 (m, 1H), 3.61 (d, J = 13.7 Hz, 1H), 3.54 (d, J = 13.7 Hz, 1H), 3.14 (s, 3H), 3.01–2.91 (m, 1H), 2.82–2.72 (m, 1H), 2.37–2.26 (m, 1H), 2.02–1.90 (m, 1H), 1.84–1.67 (m, 3H), 1.61–1.48 (m, 1H); ^{13}C-NMR (50 MHz, DMSO-d_6) δ 159.4, 157.4, 153.7, 140.2, 137.4, 133.7, 132.1, 130.9, 129.4, 129.2, 123.8, 120.3, 118.9, 118.5, 111.2, 110.9, 97.0, 61.0, 55.6, 54.8, 52.8, 32.8, 27.2, 24.4; ESI-MS: (*m/z*) 431.2 [M + H]$^+$, 453.2 [M + Na]$^+$, 429.2 [M − H]$^-$; HPLC: t$_r$ = 4.879 min (100.0% purity).

7-Chloro-*N*-methyl-*N*-(1-(3,3,3-trifluoropropyl)piperidin-3-yl)-9*H*-pyrimido[4,5-*b*]indol-4-amine (14k). **14k** was prepared from **13b** (55.0 mg, 0.17 mmol), trifluoropropanal (97.6 mg, 0.87 mmol), glacial AcOH (20.9 mg, 0.35 mmol) and Na(OAc)$_3$BH (73.8 mg, 0.35 mmol) in dry DCM (10 mL) according to general procedure E in a reaction time of 3 h. Purification by flash column chromatography (SiO$_2$, DCM:MeOH gradient elution from 97.5:2.5 to 92.5:7.5) gave 38 mg of a white solid (53% yield); ^{1}H-NMR (400 MHz, DMSO-d_6) δ 12.20 (s, 1H), 8.39 (s, 1H), 7.76 (d, J = 8.7 Hz, 1H), 7.48 (d, J = 2.0 Hz, 1H), 7.26 (dd, J = 8.6, 2.0 Hz, 1H), 4.49–4.37 (m, 1H), 3.15 (s, 3H), 3.03–2.96 (m, 1H), 2.88–2.79 (m, 1H), 2.61–2.53 (m, 2H),

2.51–2.41 (m, 2H, overlapping with DMSO-d_5), 2.37–2.26 (m, 1H), 1.96–1.87 (m, 1H), 1.86–1.67 (m, 3H), 1.59–1.45 (m, 1H); ^{13}C-NMR (101 MHz, DMSO-d_6) δ 159.4, 157.4, 153.7, 137.3, 129.1, 127.2 (q, *J* = 276.9 Hz), 123.7, 120.3, 118.5, 110.8, 97.0, 55.8, 54.7, 52.4, 50.4 (q), 32.6, 30.4 (q, *J* = 26.3 Hz), 27.2, 24.3; ESI-MS: (*m/z*) 412.3 [M + H]$^+$, 434.4 [M + Na]$^+$, 410.3 [M − H]$^-$; HPLC: t$_r$ = 7.463 min (97.2% purity).

2-(3-((7-Chloro-9*H*-pyrimido[4,5-*b*]indol-4-yl)(methyl)amino)piperidin-1-yl)acetonitrile (**14l**). **13b** (40.0 mg, 0.13 mmol) was dissolved in dry DMF (2 mL). 2-Bromoacetonitrile (16.7 mg, 0.14 mmol) and Et$_3$N (38.5 mg, 0.38 mmol) were added and the mixture stirred at rt for 1.5 h. Saturated NaHCO$_3$ solution (5 mL) was added and the mixture extracted with EtOAc (6 × 2 mL). Combined organic layers were diluted with additional EtOAc, washed with saturated NaHCO$_3$ solution (3 × 20 mL), dried over Na$_2$SO$_4$ and concentrated under reduced pressure. Purification of the residue by flash column chromatography (SiO$_2$, DCM:MeOH 96:4) gave 41 mg of a beige solid (91% yield); ^{1}H-NMR (400 MHz, DMSO-d_6) δ 12.22 (s, 1H), 8.41 (s, 1H), 7.76 (d, *J* = 8.6 Hz, 1H), 7.48 (d, *J* = 1.9 Hz, 1H), 7.27 (dd, *J* = 8.6, 2.0 Hz, 1H), 4.52–4.41 (m, 1H), 3.75 (s, 2H), 3.18 (s, 3H), 2.95–2.87 (m, 1H), 2.81–2.72 (m, 1H), 2.48–2.42 (m, 1H), 2.20–2.09 (m, 1H), 1.95–1.72 (m, 3H), 1.66–1.53 (m, 1H); ^{13}C-NMR (101 MHz, DMSO-d_6) δ 159.5, 157.4, 153.7, 137.4, 129.2, 123.8, 120.4, 118.4, 115.8, 110.8, 97.2, 54.4, 54.1, 51.3, 45.3, 32.8, 26.6, 24.1; ESI-MS: (*m/z*) 355.0 [M + H]$^+$, 376.9 [M + Na]$^+$, 352.9 [M − H]$^-$; HPLC: t$_r$ = 8.358 min (99.4% purity).

7-Chloro-*N*-(1-(cyclopropylmethyl)piperidin-3-yl)-*N*-methyl-9*H*-pyrimido[4,5-*b*]indol-4-amine (**14m**). (Bromomethyl)cyclopropane (34.4 mg, 0.25 mmol) and Et$_3$N (33.6 mg, 0.33 mmol) were added to a suspension of **13b** (70.0 mg, 0.22 mmol) in HPLC grade acetonitrile (10 mL). The mixture was stirred at 60 °C for 2 days and then concentrated under reduced pressure. Purification of the residue by flash column chromatography (SiO$_2$, DCM:2N NH$_3$ in MeOH gradient elution from 98:2 to 91.5:8.5) gave 64 mg of a white solid (78% yield); ^{1}H-NMR (400 MHz, DMSO-d_6) δ 12.22 (s, 1H), 8.39 (s, 1H), 7.80 (d, *J* = 8.7 Hz, 1H), 7.47 (d, *J* = 2.0 Hz, 1H), 7.25 (dd, *J* = 8.6, 2.0 Hz, 1H), 4.49–4.38 (m, 1H), 3.14 (s, 3H), 3.12–3.06 (m, 1H), 2.94–2.87 (m, 1H), 2.30–2.12 (m, 3H), 1.92–1.65 (m, 4H), 1.60–1.45 (m, 1H), 0.91–0.78 (m, 1H), 0.51–0.36 (m, 2H), 0.13–0.00 (m, 2H); ^{13}C-NMR (101 MHz, DMSO-d_6) δ 159.4, 157.4, 153.7, 137.3, 129.1, 123.8, 120.3, 118.6, 110.8, 97.0, 62.9, 56.1, 54.9, 52.8, 32.5, 27.6, 24.4, 8.3, 3.8, 3.6; ESI-MS: (*m/z*) 370.1 [M + H]$^+$, 392.1 [M + Na]$^+$, 368.2 [M − H]$^-$; HPLC: t$_r$ = 4.318 min (100.0% purity).

7-Chloro-*N*-(1-(3-(dimethylamino)propyl)piperidin-3-yl)-*N*-methyl-9*H*-pyrimido[4,5-*b*]indol-4-amine (**14n**). **13b** (100.0 mg, 0.32 mmol) and 3-chloro-*N*,*N*-dimethylpropan-1-amine hydrochloride (65.1 mg, 0.41 mmol) were suspended in HPLC grade acetonitrile (15 mL). Et$_3$N (96.1 mg, 0.95 mmol) was added. The mixture was stirred at 90 °C for 2–3 days and then concentrated under reduced pressure. Purification of the residue by flash column chromatography (SiO$_2$, DCM:2N NH$_3$ in MeOH 9:1) gave 50 mg of an off-white solid (39% yield); ^{1}H-NMR (300 MHz, CDCl$_3$) δ 12.07 (br s, 1H), 8.54 (s, 1H), 7.69 (d, *J* = 8.6 Hz, 1H), 7.44 (d, *J* = 1.0 Hz, 1H), 7.21 (dd, *J* = 8.6, 1.2 Hz, 1H), 4.66–4.51 (m, 1H), 3.23 (s, 3H), 3.18–3.10 (m, 1H), 2.99–2.90 (m, 1H), 2.53–2.20 (m, 11H), 2.02–1.66 (m, 7H); ^{13}C-NMR (101 MHz, CDCl$_3$) δ 160.3, 157.8, 153.2, 137.5, 130.8, 123.7, 121.2, 119.2, 111.4, 98.6, 58.0, 57.0, 56.8, 55.6, 53.8, 45.3, 33.1, 28.5, 25.0, 24.9; ESI-MS: (*m/z*) 401.4 [M + H]$^+$, 399.4 [M − H]$^-$; HPLC: t$_r$ = 4.318 min.

3-(3-((7-Chloro-9-methyl-9*H*-pyrimido[4,5-*b*]indol-4-yl)(methyl)amino)piperidin-1-yl)propanenitrile (**14o**). NaH (8.1 mg of a 60% dispersion in mineral oil, 0.20 mmol) was added to a stirring suspension of **14b** (50.0 mg, 0.14 mmol) in dry THF (10 mL). The mixture was stirred at rt and under N$_2$ atmosphere for 0.5 h. Methyl iodide (0.5 mL of a freshly prepared 0.4M solution in THF, 0.20 mmol) was drop-added and the mixture stirred for 20 h at rt and under N$_2$ atmosphere. Dimethylamine (0.075 mL of a 2M solution in THF, 0.15 mmol) was added to quench excessive methyl iodide and stirring continued for 1 h. Saturated NH$_4$Cl solution (15 mL) was added to stop the reaction and the mixture then basified with saturated NaHCO$_3$ solution. EtOAc was added and phases were separated. The organic layer was washed with saturated NaHCO$_3$ solution (2 × 20 mL), dried over Na$_2$SO$_4$ and concentrated under reduced pressure. Purification of the residue by flash column chromatography (SiO$_2$, DCM:MeOH 96.7:3.3 to 93.5:6.5) gave 31 mg of a light beige solid (60% yield); ^{1}H-NMR (400

MHz, DMSO-d_6) δ 8.46 (s, 1H), 7.83–7.74 (m, 2H), 7.38 (dd, J = 8.6, 1.3 Hz, 1H), 4.49–4.39 (m, 1H), 3.83 (s, 3H), 3.14 (s, 3H), 3.11–3.03 (m, 1H), 2.90–2.82 (m, 1H), 2.76–2.59 (m, 4H), 2.43–2.34 (m, 1H), 2.00–1.89 (m, 1H), 1.81–1.66 (m, 3H), 1.55–1.42 (m, 1H); ^{13}C-NMR (101 MHz, DMSO-d_6) δ 159.3, 156.8, 153.5, 138.5, 129.5, 123.7, 120.8, 120.0, 118.0, 109.7, 96.7, 55.6, 54.9, 53.0, 52.2, 32.6, 27.9, 27.2, 24.3, 15.0; ESI-MS: (*m/z*) 383.0 [M + H]$^+$, 405.0 [M + Na]$^+$; HPLC: t_r = 4.740 min (100.0% purity).

Detailed Procedures for the Preparation of Compounds **15–17**

3-(3-((7-Chloro-9*H*-pyrimido[4,5-*b*]indol-4-yl)(methyl)amino)pyrrolidin-1-yl)propanenitrile (**15**). **13a** (60.0 mg, 0.20 mmol) and acrylonitrile (23.2 mg, 0.44 mmol) were stirred in dry MeOH (17 mL) at rt overnight. Volatiles were removed under reduced pressure. Purification of the residue by flash column chromatography (SiO$_2$, DCM:MeOH 96:4 to 93:7) gave 51 mg of an off-white solid (72% yield); ^{1}H-NMR (400 MHz, DMSO-d_6) δ 12.22 (s, 1H), 8.41 (s, 1H), 7.84 (d, J = 8.6 Hz, 1H), 7.48 (d, J = 1.9 Hz, 1H), 7.29 (dd, J = 8.6, 1.9 Hz, 1H), 5.11–5.01 (m, 1H), 3.24 (s, 3H), 2.98–2.86 (m, 2H), 2.78–2.57 (m, 5H), 2.43–2.33 (m, 1H), 2.27–2.16 (m, 1H), 2.05–1.94 (m, 1H); ^{13}C-NMR (101 MHz, DMSO-d_6) δ 160.0, 157.3, 153.7, 137.4, 129.2, 123.8, 120.4, 119.8, 118.5, 110.8, 97.6, 56.8, 56.2, 52.9, 50.3, 33.3, 27.8, 16.5; ESI-MS: (*m/z*) 355.0 [M + H]$^+$, 377.0 [M + Na]$^+$, 353.0 [M − H]$^-$; HPLC: t_r = 3.414 min (100.0% purity).

3-(4-((7-Chloro-9*H*-pyrimido[4,5-*b*]indol-4-yl)(methyl)amino)azepan-1-yl)propanenitrile (**16**). **13c** (65.0 mg, 0.20 mmol) and acrylonitrile (23.0 mg, 0.43 mmol) were stirred in HPLC grade MeOH (20 mL) at rt and under N$_2$ overnight. Additional acrylonitrile was added repeatedly, but conversion seized at ~ 80% as calculated by HPLC. Volatiles were removed under reduced pressure. Purification of the residue by flash column chromatography (SiO$_2$, DCM:MeOH 95:5) gave 50 mg of a beige solid (66% yield); ^{1}H-NMR (400 MHz, CDCl$_3$) δ 12.59 (br s, 1H), 8.53 (s, 1H), 7.65 (d, J = 8.5 Hz, 1H), 7.44 (s, 1H), 7.21 (d, J = 8.5 Hz, 1H), 4.74–4.62 (m, 1H), 3.22 (s, 3H), 2.91 (t, J = 6.8 Hz, 2H), 2.87–2.71 (m, 4H), 2.52 (t, J = 6.6 Hz, 2H), 2.13–1.87 (m, 5H), 1.80–1.67 (m, 1H); ^{13}C-NMR (101 MHz, CDCl$_3$) δ 160.0, 157.7, 153.0, 137.4, 130.8, 123.5, 121.1, 119.1, 119.0, 111.5, 98.4, 58.4, 54.8, 54.0, 51.7, 32.9, 32.5, 30.9, 25.7, 16.8; ESI-MS: (*m/z*) 405.1 [M + Na]$^+$, 381.1 [M − H]$^-$; HPLC: t_r = 3.102 min (98.4% purity).

3-(4-((7-Chloro-9*H*-pyrimido[4,5-*b*]indol-4-yl)(methyl)amino)piperidin-1-yl)propanenitrile (**17**). **13d** (34.0 mg, 0.11 mmol) and acrylonitrile (8.6 mg, 0.16 mmol) were stirred in dry MeOH (10 mL) at rt and under N$_2$ atmosphere overnight. Volatiles were removed under reduced pressure. Purification of the residue by flash column chromatography (SiO$_2$, DCM:MeOH 97:3 to 95:5) gave 31 mg of a pale yellow solid (78% yield); ^{1}H-NMR (200 MHz, DMSO-d_6) δ 12.19 (s, 1H), 8.39 (s, 1H), 7.74 (d, J = 8.7 Hz, 1H), 7.48 (d, J = 1.9 Hz, 1H), 7.26 (dd, J = 8.6, 2.0 Hz, 1H), 4.41–4.19 (m, 1H), 3.14 (s, 3H), 3.07–2.91 (m, 2H), 2.73–2.53 (m, 4H), 2.19–1.65 (m, 6H); ^{13}C-NMR (50 MHz, DMSO-d_6) δ 159.6, 157.5, 153.8, 137.4, 129.2, 123.7, 120.4, 120.1, 118.6, 110.9, 97.2, 55.5, 52.7, 52.2, 32.5, 28.3, 15.2; ESI-MS: (*m/z*) 369.0 [M + H]$^-$; 391.0 [M + Na]$^+$, 367.0 [M − H]$^-$; HPLC: t_r = 3.474 min (100.0% purity).

Detailed Procedures for the Preparation of Intermediates **19–23** and Compound **24**

tert-Butyl-1*H*-pyrrolo[2,3-*c*]pyridine-1-carboxylate (**19**). A solution of 1*H*-pyrrolo[2,3-*c*]pyridine (**18**) (500.0 mg, 4.23 mmol) in dry THF (5 mL) was stirred under N$_2$ atmosphere and with ice-cooling. Boc anhydride (1108.4 mg, 5.08 mmol) was added dropwise. The mixture was left to warm to rt and stirred overnight under N$_2$ atmosphere. After diluting with EtOAc the mixture was washed with saturated NaHCO$_3$ solution (2 × 20 mL) and saturated NaCl solution (20 mL), dried over Na$_2$SO$_4$ and concentrated under reduced pressure. Purification of the residue by flash column chromatography (SiO$_2$, DCM:MeOH 97.5:2.5) gave 846 mg of a yellow oil (92% yield); ^{1}H-NMR (300 MHz, DMSO-d_6) δ 9.25 (s, 1H), 8.34 (d, J = 5.3 Hz, 1H), 7.86 (d, J = 3.6 Hz, 1H), 7.63 (dd, J = 5.3, 1.1 Hz, 1H), 6.77 (dd, J = 3.6, 0.6 Hz, 1H), 1.64 (s, 9H); ^{13}C-NMR (75 MHz, DMSO-d_6) δ 148.4, 141.7, 136.5, 135.5, 131.5, 129.5, 115.7, 106.5, 84.8, 27.6; HPLC: t_r = 2.259 min.

tert-Butyl-octahydro-1*H*-pyrrolo[2,3-*c*]pyridine-1-carboxylate (**20**). **19** (746.0 mg, 3.42 mmol) was dissolved in glacial AcOH (50 mL) and PtO$_2$ (150.0 mg, 20% (*m/m*)) was added. The mixture was stirred

in a reactor charged with 5 bar of H_2 pressure at rt for 35 h, then diluted with EtOAc and filtered over a pad of celite rinsing with EtOAc. The filtrate was concentrated under reduced pressure, redissolved in DCM and washed with saturated $NaHCO_3$ solution (2 × 20 mL) adding saturated NaCl solution to improve phase separation. Combined aqueous layers were re-extracted with DCM (25 mL). Combined organic layers were dried over Na_2SO_4 and concentrated under reduced pressure to give 680 mg of a yellow oil (88% crude yield), which was used in the next step without further purification; GC-MS *method A*: t_r = 4.974 min, (*m/z*) 226 [M].

tert-Butyl-6-(2-cyanoethyl)octahydro-1*H*-pyrrolo[2,3-*c*]pyridine-1-carboxylate (**21**). **20** (340.0 mg, 1.50 mmol) was dissolved in HPLC grade MeOH (50 mL) and acrylonitrile (175.4 mg, 3.31 mmol) was added. The mixture was stirred at rt and under N_2 atmosphere overnight. Volatiles were removed under reduced pressure. Purification of the residue by flash column chromatography (SiO_2, petroleum ether:EtOAc 35:65) gave 350 mg of a yellow oil (83% yield); ^{1}H-NMR (300 MHz, $CDCl_3$) δ 3.91–3.73 (m, 1H), 3.43–3.18 (m, 2H), 2.99–2.86 (m, 1H), 2.65 (t, *J* = 7.2 Hz, 2H), 2.60–2.48 (m, 1H), 2.44 (t, *J* = 6.8 Hz, 2H), 2.33–1.54 (m, 7H), 1.40 (s, 9H); ^{13}C-NMR (75 MHz, $CDCl_3$) δ 154.5, 154.3, 118.9, 118.8, 79.3, 79.1, 55.0, 53.8, 53.4, 53.1, 49.2, 48.6, 45.4, 44.9, 35.1, 34.5, 28.5, 26.7, 25.8, 25.7, 25.5, 15.8; GC-MS *method A*: t_r = 8.701 min, (*m/z*) 279 [M].

3-(Octahydro-6*H*-pyrrolo[2,3-*c*]pyridin-6-yl)propanenitrile (**22**). **21** (300.0 mg, 1.07 mmol) was dissolved in dry DCM (6 mL) under Ar atmosphere. 4N HCl in dioxane (2.7 mL) was added to the stirring solution resulting in a waxy precipitate. The reaction progress was monitored by a ninhydrin stained TLC. After full consumption of **21**, demineralized water was added to dissolve the waxy precipitate. The pH of the aqueous layer was adjusted to 14 with 50% NaOH(aq). Phases were separated and the aqueous layer was extracted with DCM (15 × 15 mL). Combined organic layers were dried over Na_2SO_4 and concentrated under reduced pressure. 160 mg of an orange oil (83% yield), which was used in the next step without further purification. A partial hydrolysis of the nitrile group to an amide group was observed in the NMR spectra of the crude product. A small batch was purified by flash column chromatography for analytical purposes (SiO_2, DCM:2N NH_3 in MeOH 9:1); ^{1}H-NMR (400 MHz, $CDCl_3$) δ 3.82–3.52 (m, 1H), 3.22–3.13 (m, 1H), 3.12–3.05 (m, 1H), 3.04–2.95 (m, 1H), 2.94–2.88 (m, 1H), 2.72–2.60 (m, 3H), 2.49 (t, *J* = 6.9 Hz, 2H), 2.45–2.38 (m, 1H), 2.16–2.07 (m, 1H), 2.01–1.93 (m, 1H), 1.91–1.82 (m, 1H), 1.64–1.54 (m, 2H), 1.49–1.40 (m, 1H); ^{13}C-NMR (75 MHz, $CDCl_3$) δ 118.9, 57.8, 53.7, 53.3, 51.9, 44.2, 35.8, 31.2, 27.1, 16.0; GC-MS method B: t_r = 14.130 min, (*m/z*) 179 [M].

3-(1-(7-Chloro-9-tosyl-9*H*-pyrimido[4,5-*b*]indol-4-yl)octahydro-6*H*-pyrrolo[2,3-c]pyridin-6-yl)propa-nenitrile (**23**). **10** (200.0 mg, 0.51 mmol), **22** (109.7 mg, 0.61 mmol) and DIPEA (210.9 mg, 1.63 mmol) were mixed with dry DMF (6 mL). The mixture was stirred at 80 °C for 1 h and was then left to cool to rt. Saturated NaCl solution (15 mL) was added and the mixture extracted with EtOAc (3 × 25 mL). Combined organic layers were washed with saturated NaCl solution (3 × 20 mL), dried over Na_2SO_4 and concentrated under reduced pressure. Purification of the residue by flash column chromatography (SiO_2, petroleum ether:(EtOAc + MeOH 95 + 5) 4:6) gave 175 mg of a beige solid (64% yield); ^{1}H-NMR (300 MHz, $CDCl_3$) δ 8.56–8.48 (m, 2H), 8.10 (d, *J* = 8.4 Hz, 2H), 7.77 (br s, 1H), 7.36 (dd, *J* = 8.5, 1.2 Hz, 1H), 7.27 (d, 2H, overlapping with $CHCl_3$ signal), 4.65–4.48 (m, 1H), 4.24–4.06 (m, 1H), 3.53–3.41 (m, 1H), 3.17–3.01 (m, 1H), 2.82–2.52 (m, 4H), 2.49–2.27 (m, 7H), 1.98–1.69 (m, 4H); ^{13}C-NMR (75 MHz, $CDCl_3$) δ 158.0, 156.9, 154.2, 145.7, 136.0, 135.6, 132.2, 129.8, 128.2, 124.2, 123.5, 120.7, 118.8, 114.5, 100.3, 57.5, 53.5, 53.4, 50.8, 34.6, 29.8, 26.8, 21.8, 15.8. Signal overlap assumed at 50.8; ESI-MS: (*m/z*) 534.9 [M + H]+, 556.8 [M + Na]+, 532.9 [M − H]-; HPLC: t_r = 7.197 min.

3-(3a*RS*,7a*SR*)-(1-(7-Chloro-9*H*-pyrimido[4,5-*b*]indol-4-yl)octahydro-6*H*-pyrrolo[2,3-c]pyridin-6-yl)-propanenitrile (**24**). **23** (150.0 mg, 0.28 mmol) was dissolved in dry THF (10 mL) and K*t*BuO (220.2 mg, 1.96 mmol) was added. The mixture was stirred at rt and under N_2 atmosphere for 75 min. Saturated NaCl solution (25 mL) was added and the mixture extracted with EtOAc (3 × 25 mL). Combined organic layers were dried over Na_2SO_4 and concentrated under reduced pressure. Purification of the

residue by flash column chromatography (SiO$_2$, DCM:MeOH 95:5) gave 59 mg of a light beige solid (55% yield); ^{1}H-NMR (300 MHz, pyridine-d_5) δ 13.68 (br s, 1H), 8.84 (s, 1H), 8.23 (d, *J* = 8.8 Hz, 1H), 7.81 (d, *J* = 2.0 Hz, 1H), 7.52 (dd, *J* = 8.7, 2.0 Hz, 1H), 4.95–4.86 (m, 1H), 4.42–4.22 (m, 1H), 4.03–3.86 (m, 1H), 3.18–3.02 (m, 1H), 2.74–2.53 (m, 5H), 2.50–2.25 (m, 3H), 1.98–1.62 (m, 4H); ^{13}C-NMR (101 MHz, DMSO-d_6) δ 156.9, 156.6, 153.8, 137.3, 128.7, 123.8, 120.3, 119.9, 118.5, 110.7, 96.0, 56.6, 53.2, 52.9, 49.1, 48.4, 34.1, 26.7, 25.5, 14.9; ESI-MS: (*m/z*) 381.2 [M + H]$^+$, 403.2 [M + Na]$^+$, 379.2 [M − H]$^−$; HPLC: t$_r$ = 4.362 min (99.9% purity). Crystals suitable for X-ray determination were obtained by slow evaporation of a solution of **24** in methanol and chloroform at 298 K under atmospheric pressure. CCDC 1,917,242 contains the supplementary crystallographic data. These data can be obtained free of charge via http://www.ccdc.cam.ac.uk/conts/retrieving.html.

References

1. Manning, G.; Whyte, D.B.; Martinez, R.; Hunter, T.; Sudarsanam, S. The protein kinase complement of the human genome. *Science* **2002**, *298*, 1912–1934. [CrossRef] [PubMed]

2. Manning, G.; Genomic Overview of Protein Kinases; WormBook. The C. Elegans Research Community, WormBook. Available online: http://www.wormbook.org (accessed on 13 December 2005). [CrossRef]

3. Sutherland, C. What Are the Bona fide GSK3 Substrates? *Int. J. Alzheimer's Dis.* **2011**, *2011*, 23.

4. Embi, N.; Rylatt, D.B.; Cohen, P. Glycogen synthase kinase-3 from rabbit skeletal muscle. *Eur. J. Biochem.* **1980**, *107*, 519–527. [CrossRef] [PubMed]

5. Wang, Y.; Roach, P.J. Inactivation of rabbit muscle glycogen synthase by glycogen synthase kinase-3. Dominant role of the phosphorylation of Ser-640 (site-3a). *J. Biol. Chem.* **1993**, *268*, 23876–23880. [PubMed]

6. Cohen, P.; Frame, S. The renaissance of GSK3. *Nat. Rev. Mol. Cell Biol.* **2001**, *2*, 769–776. [CrossRef]

7. Woodgett, J.R. Molecular cloning and expression of glycogen synthase kinase-3/factor A. *Embo. J.* **1990**, *9*, 2431–2438. [CrossRef] [PubMed]

8. MacAulay, K.; Doble, B.W.; Patel, S.; Hansotia, T.; Sinclair, E.M.; Drucker, D.J.; Nagy, A.; Woodgett, J.R. Glycogen Synthase Kinase 3α-Specific Regulation of Murine Hepatic Glycogen Metabolism. *Cell Metab.* **2007**, *6*, 329–337. [CrossRef]

9. Hoeflich, K.P.; Luo, J.; Rubie, E.A.; Tsao, M.-S.; Jin, O.; Woodgett, J.R. Requirement for glycogen synthase kinase-3β in cell survival and NF-κB activation. *Nature* **2000**, *406*, 86–90. [CrossRef]

10. Kerkela, R.; Kockeritz, L.; MacAulay, K.; Zhou, J.; Doble, B.W.; Beahm, C.; Greytak, S.; Woulfe, K.; Trivedi, C.M.; Woodgett, J.R.; et al. Deletion of GSK-3β in mice leads to hypertrophic cardiomyopathy secondary to cardiomyoblast hyperproliferation. *J. Clin. Investig.* **2008**, *118*, 3609–3618. [CrossRef]

11. Beurel, E.; Grieco, S.F.; Jope, R.S. Glycogen synthase kinase-3 (GSK3): Regulation, actions, and diseases. *Pharmacol. Ther.* **2015**, *148*, 114–131. [CrossRef]

12. Patel, P.; Woodgett, J.R. Chapter eight—Glycogen synthase kinase 3: A kinase for all pathways? In *Current Topics in Developmental Biology*; Jenny, A., Ed.; Academic Press: Cambridge, MA, USA, 2017; Volume 123, pp. 277–302.

13. Flanagan, M.E.; Blumenkopf, T.A.; Brissette, W.H.; Brown, M.F.; Casavant, J.M.; Shang-Poa, C.; Doty, J.L.; Elliott, E.A.; Fisher, M.B.; Hines, M.; et al. Discovery of CP-690,550: A potent and selective Janus kinase (JAK) inhibitor for the treatment of autoimmune diseases and organ transplant rejection. *J. Med. Chem.* **2010**, *53*, 8468–8484. [CrossRef] [PubMed]

14. Clark, J.D.; Flanagan, M.E.; Telliez, J.B. Discovery and Development of Janus Kinase (JAK) inhibitors for inflammatory diseases. *J. Med. Chem.* **2014**, *57*, 5023–5038. [CrossRef] [PubMed]

15. Xeljanz: Highlights of Prescribing Information. Available online: https://www.accessdata.fda.gov/drugsatfda_docs/label/2018/203214s018lbl.pdf (accessed on 19 March 2019).

16. Chrencik, J.E.; Patny, A.; Leung, I.K.; Korniski, B.; Emmons, T.L.; Hall, T.; Weinberg, R.A.; Gormley, J.A.; Williams, J.M.; Day, J.E.; et al. Structural and thermodynamic characterization of the TYK2 and JAK3 kinase domains in complex with CP-690550 and CMP-6. *J. Mol. Biol.* **2010**, *400*, 413–433. [CrossRef] [PubMed]

17. Sivaprakasam, P.; Han, X.; Civiello, R.L.; Jacutin-Porte, S.; Kish, K.; Pokross, M.; Lewis, H.A.; Ahmed, N.; Szapiel, N.; Newitt, J.A.; et al. Discovery of new acylaminopyridines as GSK-3 inhibitors by a structure guided in-depth exploration of chemical space around a pyrrolopyridinone core. *Bioorg. Med. Chem. Lett.* **2015**, *25*, 1856–1863. [CrossRef] [PubMed]

18. Jiang, J.K.; Ghoreschi, K.; Deflorian, F.; Chen, Z.; Perreira, M.; Pesu, M.; Smith, J.; Nguyen, D.T.; Liu, E.H.; Leister, W.; et al. Examining the chirality, conformation and selective kinase inhibition of 3-((3*R*,4*R*)-4-methyl-3-(methyl(7*H*-pyrrolo[2,3-*d*]pyrimidin-4-yl)amino)piperidin-1-yl)-3-oxopropanenitrile (CP-690,550). *J. Med. Chem.* **2008**, *51*, 8012–8018. [CrossRef]

19. Fleming, F.F.; Yao, L.; Ravikumar, P.C.; Funk, L.; Shook, B.C. Nitrile-containing pharmaceuticals: Efficacious roles of the nitrile pharmacophore. *J. Med. Chem.* **2010**, *53*, 7902–7917. [CrossRef] [PubMed]

20. Wang, Y.; Du, Y.; Huang, N. A survey of the role of nitrile groups in protein–ligand interactions. *Future Med. Chem.* **2018**, *10*, 2713–2728. [CrossRef]

21. Heider, F.; Ansideri, F.; Tesch, R.; Pantsar, T.; Haun, U.; Döring, E.; Kudolo, M.; Poso, A.; Albrecht, W.; Laufer, S.A.; et al. Pyridinylimidazoles as dual glycogen synthase kinase 3β/p38α mitogen-activated protein kinase inhibitors. *Eur. J. Med. Chem.* **2019**, *175*, 309–329. [CrossRef]

22. Zegzouti, H.; Zdanovskaia, M.; Hsiao, K.; Goueli, S.A. ADP-Glo: A bioluminescent and homogeneous ADP monitoring assay for kinases. *Assay Drug Dev. Technol.* **2009**, *7*, 560–572. [CrossRef]

23. Ghose, A.K.; Viswanadhan, V.N.; Wendoloski, J.J. Prediction of hydrophobic (lipophilic) properties of small organic molecules using fragmental methods: An analysis of ALOGP and CLOGP methods. *J. Phys. Chem. A* **1998**, *102*, 3762–3772. [CrossRef]

24. Roos, K.; Wu, C.; Damm, W.; Reboul, M.; Stevenson, J.M.; Lu, C.; Dahlgren, M.K.; Mondal, S.; Chen, W.; Wang, L.; et al. OPLS3e: Extending force field coverage for drug-like small molecules. *J. Chem. Theory Comput.* **2019**, *15*, 1863–1874. [CrossRef] [PubMed]

25. Bauer, S.M.; Gehringer, M.; Laufer, S.A. A direct enzyme-linked immunosorbent assay (ELISA) for the quantitative evaluation of Janus Kinase 3 (JAK3) inhibitors. *Anal. Methods* **2014**, *6*, 8817–8822. [CrossRef]

26. Bourdonnec, B.L.; Leister, L.K.; Ajello, C.A.; Cassel, J.A.; Seida, P.R.; O'Hare, H.; Gu, M.; Chu, G.-H.; Tuthill, P.A.; DeHaven, R.N.; et al. Discovery of a series of aminopiperidines as novel iNOS inhibitors. *Bioorg. Med. Chem. Lett.* **2008**, *18*, 336–343. [CrossRef] [PubMed]

27. Showalter, H.D.H.; Bridges, A.J.; Zhou, H.; Sercel, A.D.; McMichael, A.; Fry, D.W. Tyrosine kinase inhibitors. 16. 6,5,6-tricyclic benzothieno[3,2-*d*]pyrimidines and pyrimido[5,4-*b*]- and -[4,5-*b*]indoles as potent inhibitors of the epidermal growth factor receptor tyrosine kinase. *J. Med. Chem.* **1999**, *42*, 5464–5474. [CrossRef] [PubMed]

28. Tichý, M.; Pohl, R.; Xu, H.Y.; Chen, Y.-L.; Yokokawa, F.; Shi, P.-Y.; Hocek, M. Synthesis and antiviral activity of 4,6-disubstituted pyrimido[4,5-*b*]indole ribonucleosides. *Bioorg. Med. Chem.* **2012**, *20*, 6123–6133. [CrossRef] [PubMed]

29. Tichý, M.; Pohl, R.; Tloušt'ová, E.; Weber, J.; Bahador, G.; Lee, Y.-J.; Hocek, M. Synthesis and biological activity of benzo-fused 7-deazaadenosine analogues. 5- and 6-substituted 4-amino- or 4-alkylpyrimido[4,5-*b*]indole ribonucleosides. *Bioorg. Med. Chem.* **2013**, *21*, 5362–5372. [CrossRef] [PubMed]

30. Zhao, Y.; Bai, L.; Liu, L.; McEachern, D.; Stuckey, J.A.; Meagher, J.L.; Yang, C.-Y.; Ran, X.; Zhou, B.; Hu, Y.; et al. Structure-based discovery of 4-(6-methoxy-2-methyl-4-(quinolin-4-yl)-9*H*-pyrimido[4,5-*b*]indol-7-yl)-3,5-dimethylisoxazole (cd161) as a potent and orally bioavailable bet bromodomain inhibitor. *J. Med. Chem.* **2017**, *60*, 3887–3901. [CrossRef] [PubMed]

31. Reader, J.C.; Matthews, T.P.; Klair, S.; Cheung, K.-M.J.; Scanlon, J.; Proisy, N.; Addison, G.; Ellard, J.; Piton, N.; Taylor, S.; et al. Structure-guided evolution of potent and selective chk1 inhibitors through scaffold morphing. *J. Med. Chem.* **2011**, *54*, 8328–8342. [CrossRef]

32. Arnott, E.A.; Chan, L.C.; Cox, B.G.; Meyrick, B.; Phillips, A. POCl$_3$ chlorination of 4-quinazolones. *J. Org. Chem.* **2011**, *76*, 1653–1661. [CrossRef]

33. Xu, H.; Fan, L.-L. One-pot *N*-arylation of indoles directly from *N*-arylsulfonylindoles via consecutive deprotection and S_NAr reactions with activated aryl halides. *Chem. Pharm. Bull.* **2009**, *57*, 321–323. [CrossRef]

34. Kulagowski, J.J.; Blair, W.; Bull, R.J.; Chang, C.; Deshmukh, G.; Dyke, H.J.; Eigenbrot, C.; Ghilardi, N.; Gibbons, P.; Harrison, T.K.; et al. Identification of Imidazo-pyrrolopyridines as novel and potent JAK1 inhibitors. *J. Med. Chem.* **2012**, *55*, 5901–5921. [CrossRef] [PubMed]

35. Guo, Q.; Yu, C.; Zhang, C.; Li, Y.; Wang, T.; Huang, Z.; Wang, X.; Zhou, W.; Li, Y.; Qin, Z.; et al. Highly selective, potent, and oral mtor inhibitor for treatment of cancer as autophagy inducer. *J. Med. Chem.* **2018**, *61*, 881–904. [CrossRef] [PubMed]

36. Gehringer, M.; Pfaffenrot, E.; Bauer, S.; Laufer, S.A. Design and Synthesis of tricyclic jak3 inhibitors with picomolar affinities as novel molecular probes. *ChemMedChem* **2014**, *9*, 277–281. [CrossRef] [PubMed]

37. Hopkins, B.T.; Scott, D.; Conlon, P.; Jenkins, T.J.; Powell, N.; Guan, B.; Curervo, J.H.; Wang, D.; Taveras, A. Heterocyclic tyrosine kinase inhibitors. Patent WO2012058645A1, 3 May 2012.

38. Thorarensen, A.; Dowty, M.E.; Banker, M.E.; Juba, B.; Jussif, J.; Lin, T.; Vincent, F.; Czerwinski, R.M.; Casimiro-Garcia, A.; Unwalla, R.; et al. Design of a janus kinase 3 (JAK3) specific inhibitor 1-((2*S*,5*R*)-5-((7*H*-Pyrrolo[2,3-*d*]pyrimidin-4-yl)amino)-2-methylpiperidin-1-yl)prop-2-en-1-one (PF-06651600) allowing for the interrogation of JAK3 signaling in humans. *J. Med. Chem.* **2017**, *60*, 1971–1993. [CrossRef] [PubMed]

39. Eid, S.; Turk, S.; Volkamer, A.; Rippmann, F.; Fulle, S. KinMap: A web-based tool for interactive navigation through human kinome data. *BMC Bioinf.* **2017**, *18*, 16. [CrossRef] [PubMed]

40. Bateman, A.; Martin, M.J.; Orchard, S.; Magrane, M.; Alpi, E.; Bely, B.; Bingley, M.; Britto, R.; Bursteinas, B.; Busiello, G.; et al. UniProt: A worldwide hub of protein knowledge. *Nucleic Acids Res.* **2019**, *47*, D506–D515.

41. Sievers, F.; Higgins, D.G. Clustal omega for making accurate alignments of many protein sequences. *Protein Sci.* **2018**, *27*, 135–145. [CrossRef]

42. Sievers, F.; Wilm, A.; Dineen, D.; Gibson, T.J.; Karplus, K.; Li, W.Z.; Lopez, R.; McWilliam, H.; Remmert, M.; Soding, J.; et al. Fast, scalable generation of high-quality protein multiple sequence alignments using Clustal Omega. *Mol. Syst. Biol.* **2011**, *7*, 539. [CrossRef]

43. Bochevarov, A.D.; Watson, M.A.; Greenwood, J.R.; Philipp, D.M. Multiconformation, density functional theory-based pk$_a$ prediction in application to large, flexible organic molecules with diverse functional groups. *J. Chem. Theory Comput.* **2016**, *12*, 6001–6019. [CrossRef]

44. Klicić, J.J.; Friesner, R.A.; Liu, S.-Y.; Guida, W.C. Accurate prediction of acidity constants in aqueous solution via density functional theory and self-consistent reaction field methods. *J. Phys. Chem. A* **2002**, *106*, 1327–1335. [CrossRef]

45. Yu, H.S.; Watson, M.A.; Bochevarov, A.D. Weighted averaging scheme and local atomic descriptor for pk$_a$ prediction based on density functional theory. *J. Chem. Inf. Model.* **2018**, *58*, 271–286. [CrossRef] [PubMed]

46. Sastry, G.M.; Adzhigirey, M.; Day, T.; Annabhimoju, R.; Sherman, W. Protein and ligand preparation: Parameters, protocols, and influence on virtual screening enrichments. *J. Comput.-Aided Mol. Des.* **2013**, *27*, 221–234. [CrossRef] [PubMed]

47. Bowers, K.J.; Edmond, C.; Xu, H.; Dror, R.O.; Eastwood, M.P.; Gregerson, B.A.; Klepeis, J.L.; Kolossvary, I.; Moraes, M.A.; Sacerdoti, F.D.; et al. Scalable algorithms for molecular dynamics simulations on commodity clusters. In Proceedings of the ACM/IEEE Conference on Supercomputing (SC06), Tampa, FL, USA, 11–17 November 2006; IEEE: Tampa, FL, USA, 2006.

48. Jorgensen, W.L.; Chandrasekhar, J.; Madura, J.D.; Impey, R.W.; Klein, M.L. Comparison of simple potential functions for simulating liquid water. *J. Chem. Phys.* **1983**, *79*, 926–935. [CrossRef]
49. Gehringer, M.; Forster, M.; Pfaffenrot, E.; Bauer, S.M.; Laufer, S.A. Novel hinge-binding motifs for janus kinase 3 inhibitors: A comprehensive structure–activity relationship study on tofacitinib bioisosteres. *Chem. Med. Chem.* **2014**, *9*, 2516–2527. [CrossRef]

Sample Availability: Samples of the compounds are not available from the authors.

Supplementary Materials

Design, Synthesis and Biological Evaluation of 7-Chloro-9*H*-pyrimido[4,5-*b*]indole-based Glycogen Synthase Kinase-3β inhibitors.

Stanislav Andreev [1]**, Tatu Pantsar** [2,3]**, Francesco Ansideri** [1]**, Mark Kudolo** [1]**, Michael Forster** [1]**, Dieter Schollmeyer** [4]**, Stefan A. Laufer** [1] **and Pierre Koch** [1,5,*]

[1] Institute of Pharmaceutical Sciences, Department of Medicinal and Pharmaceutical Chemistry, Eberhard Karls University Tübingen, Auf der Morgenstelle 8, 72076 Tübingen, Germany

[2] Department of Internal Medicine VIII, University Hospital Tübingen, Otfried-Müller-Str. 14, 72076 Tübingen, Germany

[3] School of Pharmacy, University of Eastern Finland, P.O. Box 1627, 70211 Kuopio, Finland

[4] Department of Organic Chemistry, Johannes Gutenberg University Mainz, Duesbergweg 10-14, 55099 Mainz, Germany

[5] Department of Pharmaceutical / Medicinal Chemistry II, Institute of Pharmacy, University of Regensburg, Universitätsstraße 31, 93053 Regensburg, Germany

* Correspondence: pierre.koch@uni-tuebingen.de; Tel.: +49-7071-29-74579.

Table of Contents

Comparison of JAK3 and GSK-3β

(a)

(b)

Kinase domain alignment of JAK3 and GSK3B

Glycine-rich loop
```
JAK3   LKYISQLGKGNFGSVELCRYDPLGDNTGALVAVKQLQHSGPDQQRDFQREIQILKALHSD 881
GSK3B  YTDTKVIGNGSFGVVYQAKL----CDSGELVAIKKVLQD---KRFKNRELQIMRKLDHC 107
       .  . :*:.*.** *   .:        ::* ***:*:: :.     :*  :**:**:: *.
```

Hinge
```
JAK3   FIVKYRGVSYGPGRQ----SLRLVMEYLPSGCLRDFLQ--RHRARLDASRLLLYSSQICK 935
GSK3B  NIVRLRYFFYSSGEKKDEVYLNLVLDYVPETVYRVARHYSRAKQTLPVIYVKLYMYQLFR 167
       **:* * .*. *.:      *.**::*:*.*.   *    :  *:  *  .  : **  *: :
```

DFG
```
JAK3   GMEYLGSRRCVHRDLAARNILVESE-AHVKIADFGLAKLLPLDKDYYVVREPGQSPIFWY 994
GSK3B  SLAYIHSFGICHRDIKPQNLLLDPDTAVLKLCDFGSAKQLVRGEPNVSY----ICSRYYR 223
       .: *: *    ***:  :*:*:: : * :*:.*** ** *  .:        .  ::
```

```
JAK3   APES-LSDNIFSRQSDVWSFGVVLYELFTYCDK-----SCSPSAEFLRMMGCERDVPALC 1048
GSK3B  APELIFGATDYTSSIDVWSAGCVLAELLLGQPIFPGDSGVDQLVEIIKVLGTPTRE---- 279
       ***  :. . :: . **** * ** **:        . . .*:::::*
```

```
JAK3   RLLELLEEGQRLPAPPACPAEVHELMKLCWAPSPQ--DRPSFSALGPQLD-----MLWSG 1101
GSK3B  QI--------REMNPNYTEFKFPQIKAHPWTKVFRPRTPPEAIALCSRLLEYTPTARLTP 331
       ::         *   *     :. :: *:  :   *. ** :*        :
```

```
JAK3   SRGCETHAFT 1111        * = identical residue
GSK3B  LEACAHSFF- 340         : = residues with strongly similar properties
       ..*     *             . = residues with weakly similar properties
```

Figure S1. (**a**) The locations of JAK3 and GSK-3β in the phylogenetic tree of the human kinome. (**b**) Sequence alignment of the kinase domains of JAK3 (residues: 822-1111; Uniprot: P52333) and GSK-3β (residues 56-340; Uniprot: P49841).

MD Simulation of the (3a*R*, 7a*S*)-Enantiomer of Compound 24
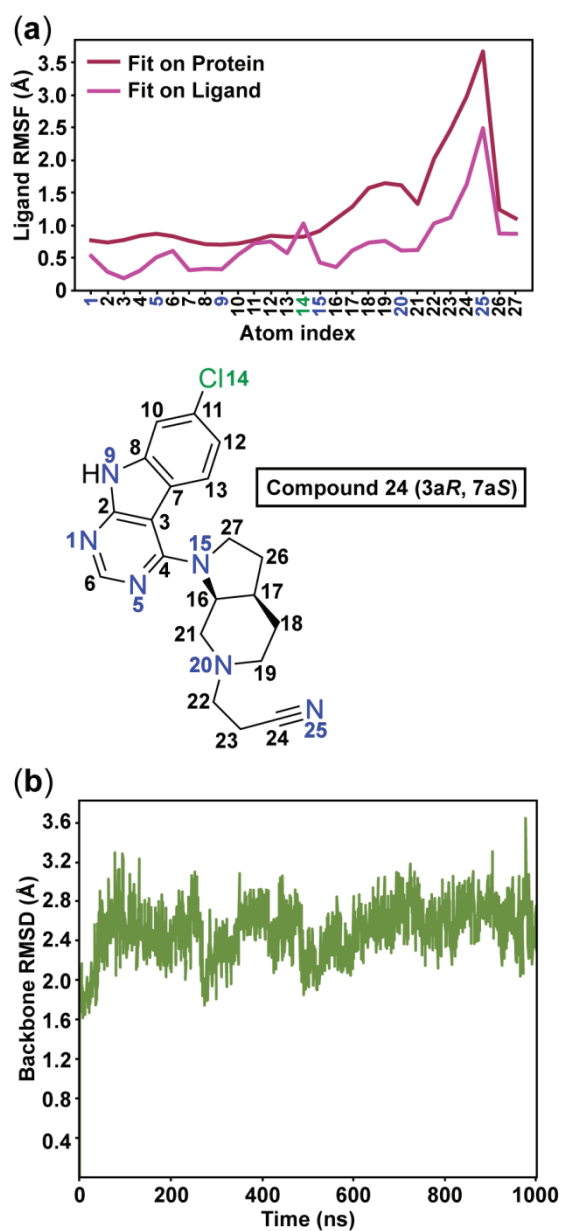
Figure S2. The root-mean-square fluctuation (RMSF) of the ligand **24** (enantiomer (3a*R*, 7a*S*)) (**a**) illustrates a similar flexibility as seen with enantiomer (3a*S*, 7a*R*) (see main text Figure 3b). The root-mean-square deviation (RMSD) of the protein shows that the simulation is stabilized.

ATP Binding Competition of Compound 14b

Compound **14b** was analyzed for its competition with ATP in an ADP Glo GSK-3β assay. To this end, a dilution series of **14b** was incubated with 25 μM, 100 μM and 500 μM of ATP and corresponding IC_{50} values were determined. Results and inhibition curves are listed in Table S1 and Figure S3.

Table S1. IC_{50} values for compound **14b** in the ATP binding competition experiment.

ATP concentration [μM]	GSK-3β IC_{50} [μM] [a]
25	0.764 ± 0.203 [b]
100	2.684
500	9.260

[a] IC_{50} values were determined in an ADP Glo kinase assay, $n = 1$; [b] $n = 5$.
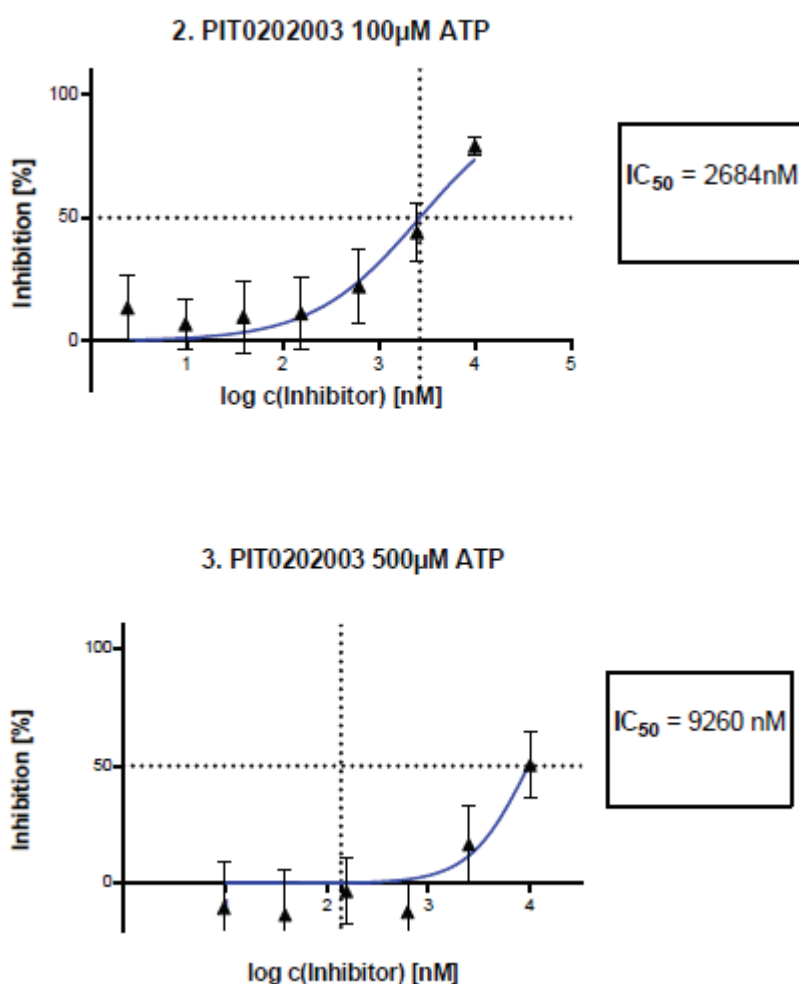
Figure S3. Inhibition curves of compound **14b** in the presence of 100 μM and 500 μM ATP.

JAK3 Inhibition by Compounds 14b and 24

Compound **14b** and **24** were analyzed for their inhibitory activity on JAK3 in an enzyme-linked immunosorbent assay (ELISA). Single point measurements at compound concentrations of 5 μM were conducted. Results are listed in Table S2.

Table S2. JAK3 inhibition of **14b** and **24** in the ELISA.

Cpd.	JAK3 inhibition [%] [a]
14b	17.8 ± 6.3
24	31.8 ± 3.8

[a] $n = 3$.

Metabolism in Human Liver Microsomes (HLM) of Compounds 14b and 24

Microsomes from liver, pooled from human (male and female) (Lot: SLBQ7487V) were purchased from Merck (Schnelldorf, Germany). The substrate (compounds **14b** and **24**, respectively) (100 μM), an NADPH-regenerating system (5 mM Glucose-6-phosphate, 5 U/mL Glucose-6-phosphate dehydrogenase and 1 mM $NADP^+$) and 4 mM $MgCl_2 \cdot 6\ H_2O$ in 0.1 M Tris buffer (pH 7.4) were preincubated for 5 min at 37°C and 750 rpm on a shaker. The reaction was started by the addition of HLM and then split into aliquots (50 μL). The reaction was quenched at seven time points (0, 10, 20, 30, 60 and 120 min) by addition of 100 μL internal standard (30 μM in MeCN). The samples were vortexed for 30 s and centrifuged (19,800 relative centrifugal force/4°C/10 min). The supernatant was directly used for LC-MS analysis (see below). All incubations were conducted in triplicates. A limit of 1% organic solvent was not exceeded. Propranolol was used as a positive control. Heat inactivated microsomes served as negative control.

The metabolite formation was analyzed with an Alliance 2695 Separations Module (Waters GmbH, Eschborn). The chromatographic separation was performed on a Waters Symmetry C18 column (150 x 4.6 mm; 5 μm) using the gradient listed in Table S3.

Sample temperature:	4°C
Column temperature:	40°C
Injection volume:	10 μL
Flow rate:	0.4 mL/min

Table S3. Chromatographic gradient for separation of metabolism analytes.

Time [min]	Solvent A [%] (90% H_2O, 10% MeCN, 0.1% formic acid)	Solvent B [%] (MeCN, 0.1% formic acid)
0	90	10
2	90	10
5	50	50
7	50	50
7.01	90	10
13	90	10

The detection was performed on a Micromass Quattro micro triple quadrupole mass spectrometer (Waters GmbH, Eschborn) using the electrospray ionization in the positive-mode.

Spray voltage:	4.5 kV
Desolvation temperature:	250°C
Desolvation gas flow:	600 L/h.
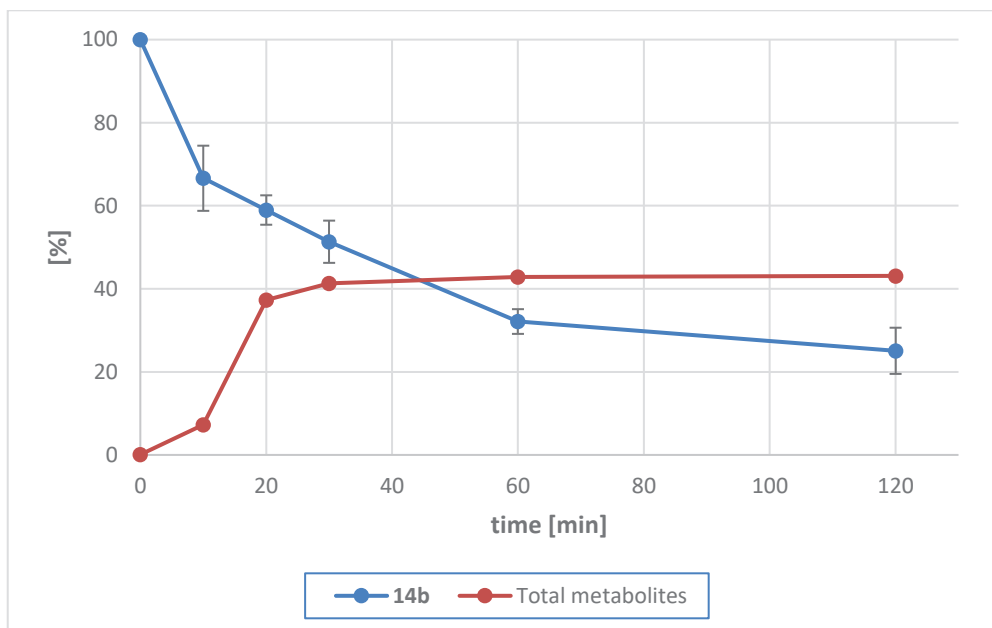
Figure S4. Degradation of compound **14b** during HLM experiment.
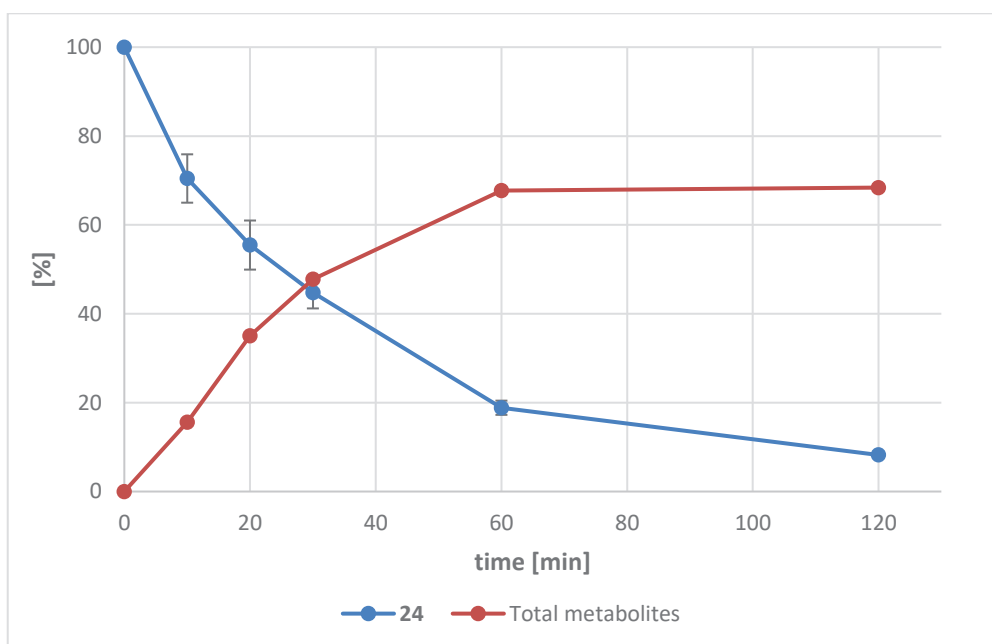
Figure S5. Degradation of compound **24** during HLM experiment.

Structure Determination of Compound 24

Diffraction data were collected at 193 K with a STOE IPDS-2T diffractometer with Mo Kα radiation. Data for atomic coordinates, thermal parameters and reflections can be obtained from the Cambridge Crystallographic Data Centre under the CCDC Nr. 1917242.

Table S5. Data collection and refinement statistics.

Data collection	
Space group	P 2$_1$/c (monoclinic)
Cell dimensions	determinate from 10604 reflections with 2.6°< θ < 28.4°
a,b,c ($\mathring{A}$)	6.7253(5), 17.8510(10), 15.3209(10)$\mathring{A}$
β (°)	90.065(5)°
V ($\mathring{A}^3$), z	1839.3(2), 4
Crystal size (mm³)	0.1 x 0.1 x 0.81 (colorless needle)
Range of Measurement	2° ≤ θ ≤ 28°, -8 ≤ h ≤ 8 -23 ≤ k ≤ 20 -20 ≤ l ≤ 16
No. of reflections:	
Measured	9417
Unique	4356 (R$_{int}$ = 0.0322)
Observed ($|F|/\sigma(F) > 4.0$)	3156
Refinement	
Nr. of parameters	263
wR2	0.1420
R1(observed), R(all)	0.0534, 0.0872
Goodness of Fit	1.029
Max. deviation of parameters	0.001 * e.s.d.
Max. Peak final	
diff. Fourier synthesis (e $\mathring{A}^{-3}$)	0.22,-0.35

7.2 Publikation II

Discovery and Evaluation of Enantiopure 9*H*-pyrimido[4,5-*b*]indoles as Nanomolar GSK-3β Inhibitors with Improved Metabolic Stability

Stanislav Andreev, Tatu Pantsar, Ahmed El-Gokha, Francesco Ansideri, Mark Kudolo, Débora Bublitz Anton, Giulia Sita, Jenny Romasco, Christian Geibel, Michael Lämmerhofer, Márcia Ines Goettert, Andrea Tarozzi, Stefan Laufer und Pierre Koch

Int. J. Mol. Sci. **2020**, *21*(21), 7823

Article

Discovery and Evaluation of Enantiopure 9*H*-pyrimido[4,5-*b*]indoles as Nanomolar GSK-3β Inhibitors with Improved Metabolic Stability

Stanislav Andreev [1], **Tatu Pantsar** [1,2], **Ahmed El-Gokha** [1,3], **Francesco Ansideri** [1], **Mark Kudolo** [1], **Débora Bublitz Anton** [4], **Giulia Sita** [5], **Jenny Romasco** [6], **Christian Geibel** [7], **Michael Lämmerhofer** [7], **Márcia Ines Goettert** [4], **Andrea Tarozzi** [6], **Stefan A. Laufer** [1] and **Pierre Koch** [1,8,*]

[1]   Institute of Pharmaceutical Sciences, Department of Medicinal and Pharmaceutical Chemistry, Eberhard Karls University Tübingen, Auf der Morgenstelle 8, 72076 Tübingen, Germany; stanislav.andreev@uni-tuebingen.de (S.A.); tatu.pantsar@uni-tuebingen.de (T.P.); ahmed.abdelaleem@science.menofia.edu.eg (A.E.-G.); francesco.ansideri@uni-tuebingen.de (F.A.); mark.kudolo@uni-tuebingen.de (M.K.); stefan.laufer@uni-tuebingen.de (S.A.L.)

[2]   School of Pharmacy, Faculty of Health Sciences, University of Eastern Finland, P.O. Box 1627, 70211 Kuopio, Finland

[3]   Chemistry Department, Faculty of Science, Menoufia University, Gamal Abdel-Nasser Street, Shebin El-Kom 32511, Egypt

[4]   Cell Culture Laboratory, Postgraduate Program in Biotechnology, University of Vale do Taquari (Univates), Lajeado 95914-014, Brazil; debora.anton@univates.br (D.B.A.); marcia.goettert@univates.br (M.I.G.)

[5]   Department of Pharmacy and Biotechnology, Alma Mater Studiorum, University of Bologna, Via Irnerio, 48, 40126 Bologna, Italy; giulia.sita2@unibo.it

[6]   Department for Life Quality Studies, Alma Mater Studiorum, University of Bologna, Corso D'Augusto, 237, 47921 Rimini, Italy; jenny.romasco@unibo.it (J.R.); andrea.tarozzi@unibo.it (A.T.)

[7]   Institute of Pharmaceutical Sciences, Department of Pharmaceutical (Bio-)Analysis, Eberhard Karls University Tübingen, Auf der Morgenstelle 8, 72076 Tübingen, Germany; christian.geibel@uni-tuebingen.de (C.G.); michael.laemmerhofer@uni-tuebingen.de (M.L.)

[8]   Department of Pharmaceutical/Medicinal Chemistry II, Institute of Pharmacy, University of Regensburg, Universitätsstraße 31, 93053 Regensburg, Germany

*   Correspondence: pierre.koch@uni-tuebingen.de; Tel.: +49-(941)-943-2847

check for updates

Abstract: Glycogen synthase kinase-3β (GSK-3β) is a potential target in the field of Alzheimer's disease drug discovery. We recently reported a new class of 9*H*-pyrimido[4,5-*b*]indole-based GSK-3β inhibitors, of which 3-(3-((7-chloro-9*H*-pyrimido[4,5-*b*]indol-4-yl)(methyl)amino)piperidin-1-yl)propanenitrile (**1**) demonstrated promising inhibitory potency. However, this compound underwent rapid degradation by human liver microsomes. Starting from **1**, we prepared a series of amide-based derivatives and studied their structure–activity relationships against GSK-3β supported by 1 µs molecular dynamics simulations. The biological potency of this series was substantially enhanced by identifying the eutomer configuration at the stereocenter. Moreover, the introduction of an amide bond proved to be an effective strategy to eliminate the metabolic hotspot. The most potent compounds, (*R*)-3-(3-((7-chloro-9*H*-pyrimido[4,5-*b*]indol-4-yl)(methyl)amino)piperidin-1-yl)-3-oxopropanenitrile (**(*R*)-2**) and (*R*)-1-(3-((7-bromo-9*H*pyrimido[4,5-*b*]indol-4-yl)(methyl)amino)piperidin-1-yl)propan-1-one (**(*R*)-28**), exhibited IC_{50} values of 480 nM and 360 nM, respectively, and displayed improved metabolic stability. Their favorable biological profile is complemented by minimal cytotoxicity and neuroprotective properties.

Keywords: protein kinase; kinase inhibitor; 9*H*-pyrimido[4,5-*b*]indole; glycogen synthase kinase-3β; metabolic stability

1. Introduction

Glycogen synthase kinase-3 (GSK-3) is a ubiquitously expressed protein existing in two highly related isoforms, GSK-3α and GSK-3β [1]. This serine/threonine kinase is involved in several signal cascades and is assumed to phosphorylate more than 30 different substrates, highlighting its multifaceted role in intracellular processes [1,2]. Under physiological conditions, complex mechanisms ensure a strict regulation and proper functionality of this highly multitasking enzyme. In turn, aberrant activity of GSK-3 is assumed to be a critical factor for the development of diverse pathologies, including diabetes, cancer, bipolar disorder, and especially Alzheimer's disease (AD) [3]. In particular, GSK-3β is implicated in crucial mechanisms associated with AD pathology. These include tau hyperphosphorylation and Aβ generation, the two major histopathological hallmarks of the disease [4]. Therefore, GSK-3β is a potential target for novel disease-modifying AD therapeutics motivating drug discovery efforts in the field of small molecule kinase inhibitors.

Recently, we reported on the optimization of a novel class of 7-chloro-9*H*-pyrimido[4,5-*b*] indole-based glycogen synthase kinase-3β (GSK-3β) inhibitors, including compound **1** (Figure 1a) [5]. This tertiary alicyclic amine with a promising biological activity on the target enzyme, however, suffered from poor metabolic stability when exposed to human liver microsomes (HLMs). In the HLM stability assay, inhibitor **1** underwent rapid biotransformation, resulting in a limited half-life of approximately 30 min (Figure 1b).
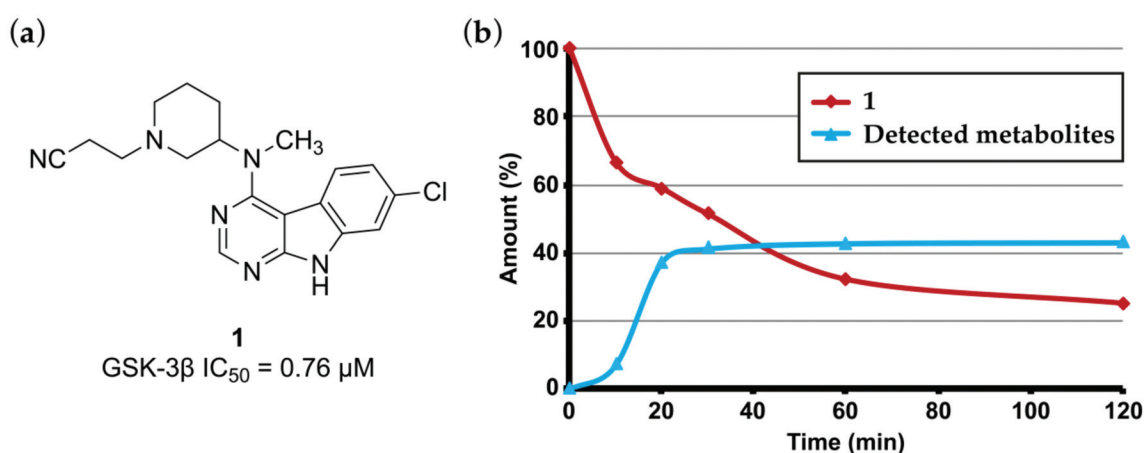
Figure 1. (**a**) Structure and biological activity of compound **1**; (**b**) metabolic degradation and formation of detected metabolites of **1**.

Tertiary alicyclic amines represent common yet metabolically vulnerable motifs in pharmaceutical agents. Their oxidative metabolization typically includes chemical modifications such as α-carbonyl introduction and ring opening as well as oxygenation or dealkylation of the nitrogen atom [6]. Correspondingly, the observed metabolic lability of **1** can be ascribed to the (2-cyanoethyl)piperidine substructure of the molecule. The mass spectrometry-based profiling of the metabolites formed from **1** in the HLM experiment indicated an extensive elimination of the cyanoethyl substituent through C–N bond cleavage. However, we found this moiety to be of utmost importance for the biochemical activity of **1** in our preliminary optimization study. This suggests that its removal would compromise the activity of this compound.

Herein, we present a strategy to improve the metabolic stability of this class of 9*H*-pyrimido[4,5-*b*] indole-based GSK-3β inhibitors while maintaining the biological activity. We hypothesized that the introduction of an acyl substituent on the piperidine nitrogen atom was a suitable approach to eliminate the potential metabolic hotspot. To this end, we refocused our attention on the reported

amide derivative **2**, which was 2.5-fold less active than **1** [5]. We used this compound as a template in order to design and optimize a series of novel amide-based GSK-3β inhibitors by applying a variety of structural modifications (Scheme 1). The obtained biological data established structure–activity relationships (SARs), which were substantiated by in silico approaches. The most promising candidates were assessed for their metabolic stability in the HLM experiment and further were characterized in cellular assays.

2

GSK-3β IC$_{50}$ = 1.86 µM

48 derivatives
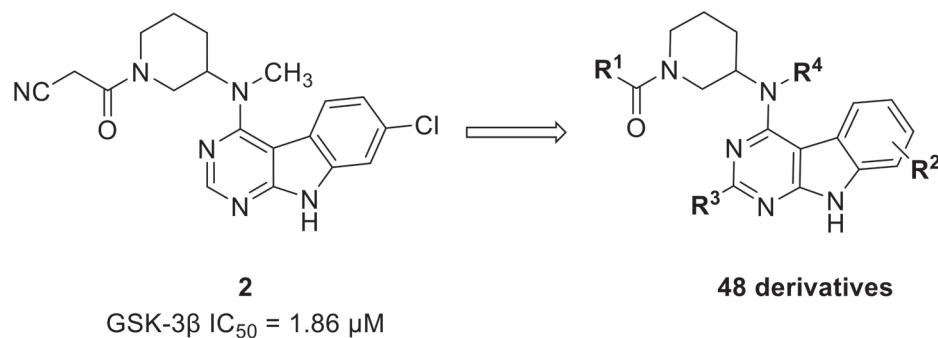
Scheme 1. Development of novel amide-based Glycogen synthase kinase-3β (GSK-3β) inhibitors; IC$_{50}$: halfmaximal inhibitory concentration.
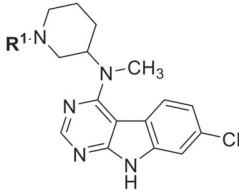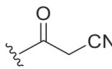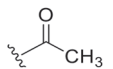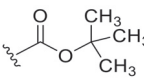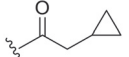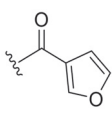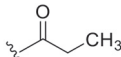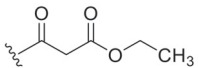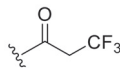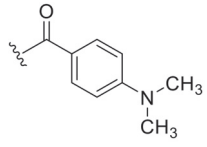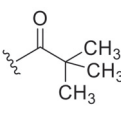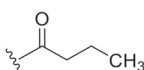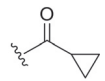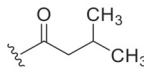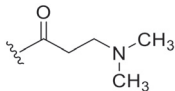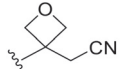
2. Results and Discussion

2.1. Biological Evaluation

In our initial attempts to optimize **2** for GSK-3β inhibition, we focused on the piperidine nitrogen substituent and evaluated its effect on the compound potency (Table 1). The application of bulky moieties including aromatic rings (**8** and **10**), an ethyl ester function (**9**), or a *tert*-butyloxy group (**6c**) led to inactive compounds. Analogs carrying substituents with longer aliphatic moieties such as butanoyl- (**11**), isovaleryl- (**12**), or cyclopropylacetyl- (**15**) were inactive or exhibited significantly higher IC$_{50}$ values than **2**. Derivatives with shorter hydrocarbon chains, i.e., cyclopropanoyl- (**39**), acryloyl- (**40**), 3-(dimethylamino)propanoyl- (**13**), and *tert*-butanoyl- (**38**), were found to retain moderate biological activity. In agreement with this trend, a slight potency improvement was seen with the acetyl- and propanoyl-substituted compounds **14** and **16** compared to their cyanoacetyl counterpart. Perhaps surprisingly, the 3,3,3-trifluoropropanoyl derivative **17** was clearly less active than its propanoyl congener **16**. This dramatical difference in potency can be rationalized by the larger van der Waals volume of the CF$_3$ group as compared to a CH$_3$ group [7]. These results indicate that only short-chained substituents such as acetyl-, cyanoacetyl-, or propanoyl- are tolerated in this position.

To assess the effect of the carbonyl group functionality, we replaced it with an oxetane ring (**41**). This four-membered heterocyclic motif has been successfully applied in medicinal chemistry programs in order to improve the metabolic stability of drug candidates [8]. The resulting compound **41**, however, displayed a 4-fold higher IC$_{50}$ value than **2**. An oxetane is considered to form weaker hydrogen bonds than an amide carbonyl group [9]. Thus, we ascertain that carbonyl group-mediated interactions are important for the binding affinity of **2**.
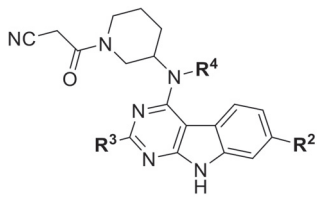
Table 1. Structures and biological activities of compounds **2**, **6c**, **8–17**, and **38–41**.

Cpd.	R^1	IC$_{50}$ (µM) Mean ± SEM GSK-3β [a]	Cpd.	R^1	IC$_{50}$ (µM) Mean ± SEM GSK-3β [a]
2		1.86 ± 0.11 [b]	14		1.57 ± 0.30
6c		≥10	15		≥10
8		5.46 ± 1.03	16		1.71 ± 0.52
9		≥10	17		≥10
10		≥10	38		4.39 ± 0.09
11		7.07 ± 1.03	39		3.49 ± 0.66
12		≥10	40		3.92 ± 0.56
13		3.83 ± 0.08	41		6.70 [c]

[a] IC$_{50}$ values were determined in an ADP Glo™ Kinase assay [10,11] (for details, see the Supplementary Materials) and are the means of at least two independent experiments; [b] data taken from [5]; [c] *n* = 1.

The results obtained from the piperidine substituent series highlighted the suitability of both the cyanoacetyl and propanoyl substituent in this position. Based on these results, we elected to maintain both moieties for further optimization and shifted our focus to other positions of the scaffold that are amenable to modification (Table 2).

Table 2. Structures and biological activities of compounds **2**, **18–24**, and **45–50**.
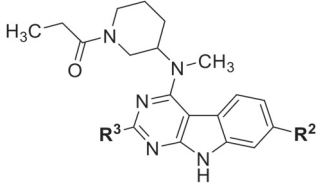
Cpd.	R^2	R^3	R^4	IC$_{50}$ (µM) Mean ± SEM GSK-3β [a]
18	–H	–H	–CH$_3$	1.73 ± 0.03
45			–H	2.17 ± 0.02
19	–F	–H	–CH$_3$	1.79 ± 0.18
46			–H	≥10
2	–Cl	–H	–CH$_3$	1.86 ± 0.11 [b]
47			–H	1.29 ± 0.27
20	–Br	–H	–CH$_3$	1.42 ± 0.16
48			–H	1.94 ± 0.72
21	–I	–H	–CH$_3$	0.94 ± 0.17
22	–OCH$_3$	–H	–CH$_3$	≥10
49			–H	≥10
23	–CF$_3$	–H	–CH$_3$	≥10
50			–H	≥10
24	–Cl	–CH$_3$	–CH$_3$	≥10

[a] IC$_{50}$ values were determined in an ADP Glo™ Kinase assay and are the means of at least two independent experiments; [b] data taken from [5].

Replacement of the chlorine atom in the 7-position of the tricyclic core (R^2 in Table 2) with different halides, i.e., fluorine (**19**), bromine (**20**), and iodine (**21**), as well as removal of this substituent (**18**) was well tolerated. In fact, the inhibitory potency within these compounds marginally increased alongside the van der Waals radii of the halogens. In contrast, the introduction of a methoxy (**22**) or CF$_3$ (**23**) group in this position gave inactive derivatives, presumably due to a steric clash at the target binding site. Similarly, the addition of a methyl group in the 2-position of the 7-chloro-9H-pyrimido[4,5-b]indole (**24**) resulted in a substantial loss in potency. Within this series, the removal of the N-methyl group (R^4 in Table 2) typically proved unfavorable to the activity (**45–50**), which prompted us to maintain this substituent.

Accordingly, the activity trend observed for the halogen series in Table 2 was maintained with the propionamides (Table 3). The only exception was the iodine derivative (**29**), which exhibited a 5-fold reduced potency compared to its bromine counterpart **28**. Unfortunately, no inhibition data could be generated for the methylated propionamide **27** due to insufficient aqueous solubility.

The relocation of the R^2 substituent to the adjacent 6-position retained potency in the case of chlorine (**30** and **34**) and bromine (**31** and **35**) (Table 4). In contrast to compound **22**, the methoxy substituent was also tolerated in this position (**32** and **36**). However, compounds **33** and **37** carrying chlorine in the 5-position of the tricyclic scaffold suffered from a decrease in activity relative to their regioisomers **2** and **15**.

Table 3. Structures and biological activities of compounds **16** and **25–29**.

Cpd.	R²	R³	IC₅₀ (μM) Mean ± SEM GSK-3β ᵃ
25	–H	–H	4.58 ± 0.74
26	–F	–H	4.81 ± 0.61
16	–Cl	–H	1.71 ± 0.52
27	–Cl	–CH₃	n.d. ᵇ
28	–Br	–H	0.71 ± 0.02
29	–I	–H	3.75 ± 0.65

ᵃ IC50 values were determined in an ADP Glo™ Kinase assay and are the means of at least two independent experiments; ᵇ not determined.

Table 4. Structure and biological activities of compounds **16** and **30–37** as well as **2**, **20**, and **28** and their enantiopure analogs.

Cpd.	R²	IC₅₀ (μM) Mean ± SEM GSK-3β ᵃ	Cpd.	R²	IC₅₀ (μM) Mean ± SEM GSK-3β ᵃ
2		1.86 ± 0.11 ᵇ			
***(R)*-2**	7-Cl	0.48 ± 0.04	**16**	7-Cl	1.71 ± 0.52
***(S)*-2**		≥10			
20		1.42 ± 0.16	**28**		0.71 ± 0.02
***(R)*-20**	7-Br	0.84 ± 0.07	***(R)*-28**	7-Br	0.36 ± 0.05
***(S)*-20**		≥10	***(S)*-28**		n.d. ᶜ
30	6-Cl	2.30 ± 0.07	**34**	6-Cl	1.25 ± 0.03
31	6-Br	2.01 ± 0.20	**35**	6-Br	1.27 ± 0.47
32	6-OCH₃	2.54 ± 0.11	**36**	6-OCH₃	1.18 ± 0.03
33	5-Cl	8.20 ± 1.27	**37**	5-Cl	≥10

ᵃ IC50 values were determined in an ADP Glo™ Kinase assay and are the means of at least two independent experiments; ᵇ data taken from [5]; ᶜ not determined.

As observed in several instances [12,13], the bioactivity of enantiomers may be strikingly different. The compounds presented in this work have a stereocenter in the 3-position of the piperidine ring. We expected the conformations of the different enantiomers to be unidentical, which motivated us to examine the influence of stereochemistry on the compound activity. To this end, we prepared the enantiopure analogs *(R)-2/(S)-2* and *(R)-20/(S)-20* of inhibitors **2** and **20**, respectively, and determined their IC₅₀ values. Within these two matched pairs, the respective *(S)*-configured enantiomers showed a dramatic loss in activity, while their *(R)*-configured stereoisomers displayed IC₅₀ values in the nanomolar

range. Having identified the eutomer configuration, we also prepared *(R)-28*, which followed the same trend and exhibited an improved IC_{50} value of 360 nM. These findings demonstrated that only the *(R)*-enantiomer displays GSK3β inhibition among these compounds.

2.2. Molecular Modeling

To gain insight into the binding interactions of these amide-based compounds within the ATP site of GSK-3β, we performed 1 µs molecular dynamics (MD) simulations for the most potent inhibitors *(R)-2* and *(R)-28*. The observed binding modes for *(R)-2* and *(R)-28* are highly similar and provide plausible explanations for structure–activity relationships of the compound series (Figure 2a,b). Both compounds display extremely stable hydrogen bonding interactions to the hinge region residues Asp133 and Val135 (>95% frequency, Figure S1). The halogen substituent in the 7-position of the tricyclic scaffold (chlorine in *(R)-2* and bromine in*(R)-28*) is pointing towards the hydrophobic region I of the kinase. Furthermore, the observed low values of ligand root-mean-square deviation (RMSD) highlight the stable binding conformation of both ligands.
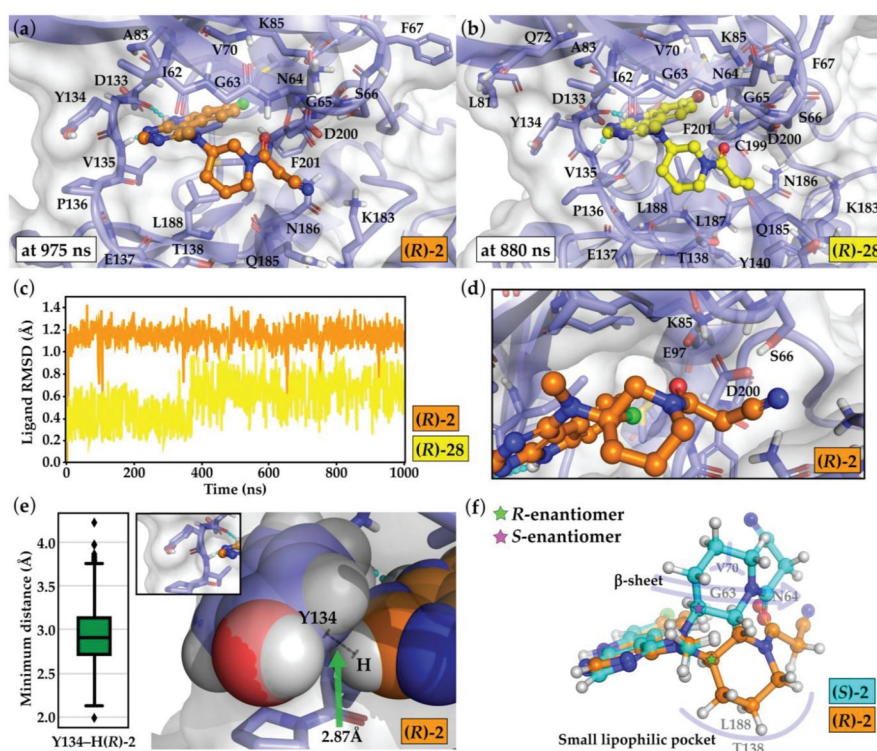
Figure 2. Putative binding mode of the described GSK3β inhibitors: (**a**) representative snapshot of the *(R)-2* binding conformation during the 1 µs molecular dynamics (MD) simulation. All residues located within 4 Å of the ligand during the simulation are shown as sticks. Hydrogen bonds are depicted with cyan dashed lines; (**b**) representative snapshot of the *(R)-28* binding conformation during the 1 µs MD simulation; (**c**) the ligands appear extremely stable in the shown conformation throughout the simulations as demonstrated by their root-mean-square deviation (RMSD) values; (**d**) the carbonyl oxygen points towards the polar residues Asp200, Lys85, Ser66, and Glu97 but does not form any specific direct interactions with GSK-3β; (**e**) the proton in the 2-position of the pyrimidine ring is in close proximity to the side chain of Tyr134. Here, the conformation of (**a**) is illustrated, where the distance is 2.87 Å. The *(R)-2* and Tyr134 atoms are shown as spheres representing their van der Waals radius; and (**f**) comparison of the preferred quantum mechanics (QM)-derived conformations of the different enantiomers of **2**. *(S)-2* is unable to obtain the binding conformation as observed for *(R)-2*. In the preferred *(S)-2* conformation, the piperidine ring would clash with the β-sheet and Val70 and would not occupy the small lipophilic pocket formed by Leu188 and Thr138.

The carbonyl oxygen, which points towards the polar residues Asp200, Lys85, Ser66, and Glu87, does not form any direct interactions to any residues of GSK3β throughout the simulations (Figure 2d). Nevertheless, water-mediated interactions are evident for the carbonyl group (Figure S1), which might explain the enhanced activity of **2** compared to its oxetane bioisoster **41**.

The piperidine ring of both compounds occupies a small lipophilic pocket formed by Leu188 (and Thr138) in the bottom of the binding site (Figure 2a,b). The amide substituent on the piperidine nitrogen atom is oriented towards the solvent interface with polar residues, e.g., Lys183. We postulate that this space, which does not present any suitable binding sites for accommodation, especially of bulkier lipophilic substituents, provides an explanation for the observed activity trends in Table 1.

The proton in the 2-position of the pyrimidine ring is in close proximity and in contact with the side chain of hinge residue Tyr134 (Figure 2e). This observation offers an explanation for the inactivity of 2-methyl derivative **24**, as this substitution would result in a steric clash with the side chain of Tyr134.

The remarkable activity difference among the stereoisomers can be realized via the comparison of the preferred quantum mechanics (QM)-derived conformations of *(R)*-**2** and *(S)*-**2** (Figure 2f). The superimposition of the enantiomers clearly demonstrates that a favorable configuration of the piperidine is not possible for *(S)*-**2**. This enantiomer not only would be unable to occupy the small lipophilic pocket but also would clash with the β-sheet next to the G-loop (Figure 2f).

2.3. Microsomal Stability

As our initial aim was to improve the metabolic stability of the compounds, we evaluated the most potent eutomers *(R)*-**2** and *(R)*-**28** in our in-house microsomal stability assay. To this end, the compounds were incubated with pooled male and female HLM for 120 min, and the compound degradation as well as the formation of metabolites was monitored by liquid chromatography-mass spectrometry (LC-MS) analysis.

In contrast to the labile tertiary amine **1**, the enantiopure cyanoacetamide compound *(R)*-**2** displayed a favorable metabolic profile in the microsomal stability assay (Figure 3a). The metabolization of this inhibitor was characterized by a slower degradation rate and consequently a larger fraction of intact compound after the time span of 120 min. Some metabolites with an *m/z* ratio of 399 were detected in the LC-MS analysis and likely result from monooxygenation of the parent compound. However, no elimination of the piperidine nitrogen substituent was seen, which supports our initial hypothesis concerning stability of the amide bond.

The propanoyl analog *(R)*-**28** even showed a slightly enhanced stability compared to its cyanoacetamide counterpart. Nearly 70% of unchanged inhibitors was detected after the incubation time of 120 min (Figure 3b). We assume that this noticeable decrease in decomposition can be attributed to the lack of the metabolically vulnerable nitrile group. Similar to *(R)*-**2**, the LC-MS-based metabolite profiling indicates formation of oxygenated derivatives of *(R)*-**28** yet no cleavage of the piperidine amide bond.

2.4. Cell Data

To extend the biological profile of inhibitor *(R)*-**28**, we evaluated the in vitro cytotoxic potential of this compound on a variety of cell lines. These included two wild-type cell lines (human lung fibroblast cell line MRC-5 and Chinese hamster ovary cell line CHO-K1) as well as three cancer cell lines (hepatocellular carcinoma cell line HepG2, human breast adenocarcinoma cell line MCF-7, and human neuroblastoma cell line SH-SY5Y). The cells were treated with different concentrations of *(R)*-**28**, and their viability was assessed by the 3-(4,5-dimethylthiazol-2-yl)-2,5-diphenyltetrazolium bromide (MTT) colorimetric assay (for details, see Supplementary Materials). Even at the highest tested concentration of 10 μM, minimal to no cytotoxic effects were seen for *(R)*-**28** on all cell lines, demonstrating a highly favorable cytotoxicity profile (Figures S2 and S3).
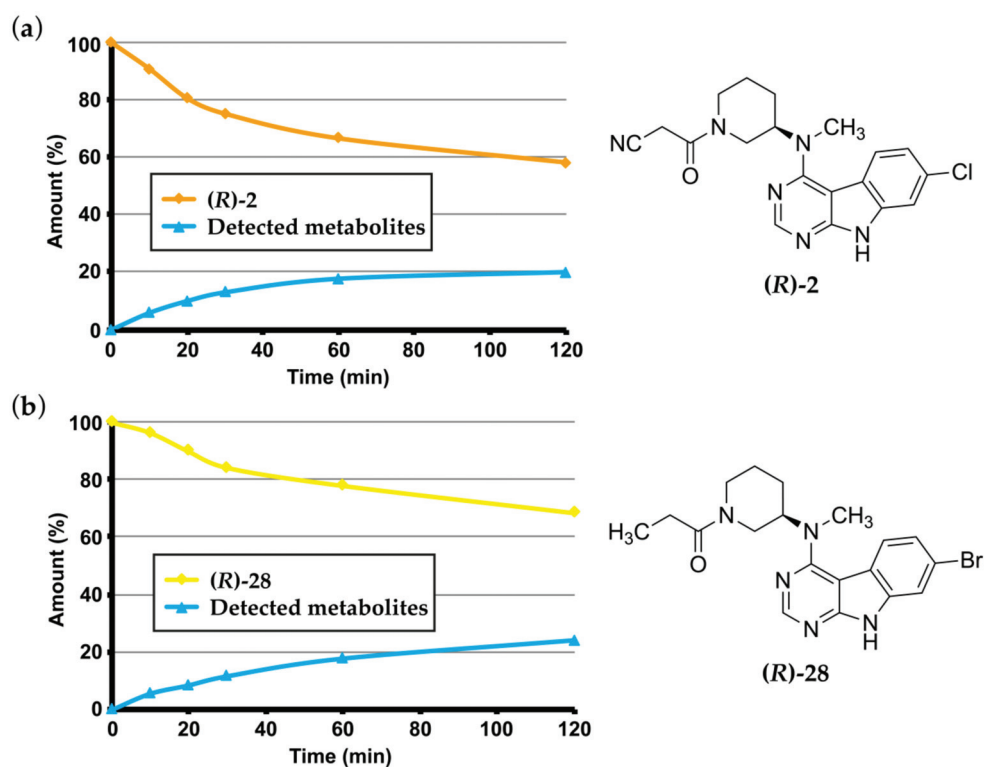
Figure 3. Microsomal degradation and formation of detected metabolites of (**a**) *(R)*-**2** and (**b**)*(R)*-**28** during the incubation time of 120 min.

These results motivated us to further characterize compound *(R)*-**28** by its ability to inhibit GSK-3β and to exert neuroprotective effects in neuronal SH-SY5Y cells (for details, see Supplementary Materials). Initially, we determined the concentrations of *(R)*-**28** not associated to neurotoxicity by the MTT assay [14]. Therefore, concentrations of 1 and 5 μM were selected for the assays in SH-SY5Y cells, which were performed according to previously described protocols [15–17]. At the tested concentration of 1 μM, *(R)*-**28** inhibited GSK3β activity in terms of inactive phospho-GSK3α/β (Ser21/9) increase and active phospho-GSK3α/β (Tyr279/Tyr216) decrease after 1 h of treatment in neuronal SH-SY5Y cells (Figure S4).

Next, we investigated the neuroprotective effects of *(R)*-**28** in SH-SY5Y cells against the neurotoxicity induced by neurotoxins. These included hydrogen peroxide (H_2O_2, 100 μM) and amyloid-β 1–42 oligomers ($OA\beta_{1-42}$, 10 μM), that mimic general oxidative stress and Alzheimer's disease (AD), respectively. In these experiments, the concomitant treatment of 5 μM *(R)*-**28** with neurotoxins significantly decreased the neurotoxicity elicited by H_2O_2 but not $OA\beta_{1-42}$ (Figure S5). Still, these neuroprotective effects against the oxidative stress underline the potential usefulness of inhibitor *(R)*-**28** in the AD therapeutic area.

2.5. Chemistry

We previously reported a synthetic route for the preparation of compound **2** [5]. This strategy demonstrated broad applicability within the herein presented study, as it provided access to the majority of final compounds with only minor alterations in the experimental protocols (Scheme 2). 4-Chloro-9*H*-pyrimido[4,5-*b*]indoles **3a–l** were prepared in four steps from commercially available *o*-halonitrobenzenes according to modified literature procedures (for details, see Supplementary Materials) [5,18–20]. These tricyclic intermediates were protected by a tosyl group on the indole nitrogen, resulting in **4a–l**. The aliphatic side chain was then introduced by treatment of **4a–l** with appropriate amines under basic conditions. In the case of **6a–l**, we used racemic 1-Boc-3-(methylamino)piperidine, which was prepared as described previously [5]. For the synthesis of

analogs *(R)*-**5c,d** and *(S)*-**5c,d**, enantiopure 1-Boc-3-aminopiperidine building blocks were utilized. This demanded an additional methylation step, which was carried out with methyl iodide under strictly anhydrous, basic conditions [21]. Subsequent cleavage of the orthogonal protecting groups furnished precursors **7a–l**, *(R)*-**7c,d**, and *(S)*-**7c,d**, which were acylated on the piperidine nitrogen to access the final compounds.
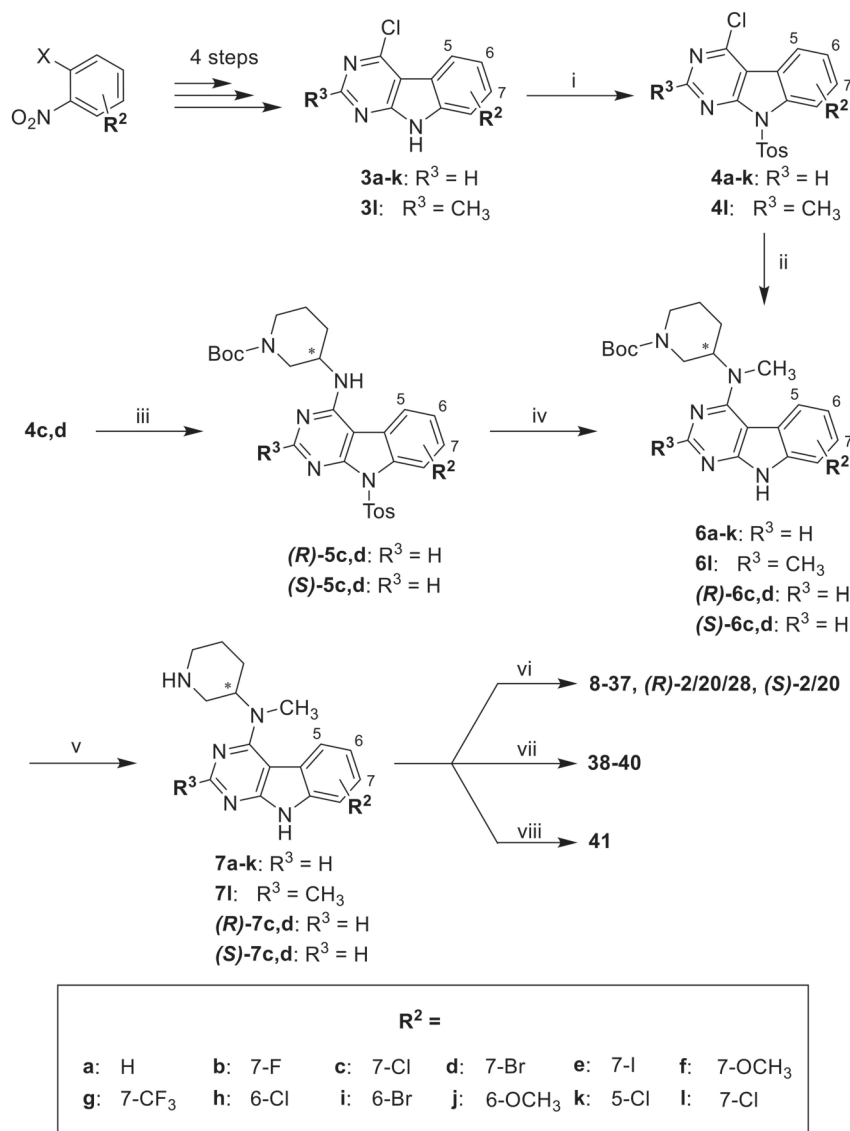
Scheme 2. Synthetic route to final compounds **8–41**, *(R)*-**2/20/28**, and *(S)*-**2/20** listed with their structures in Tables 1–4. Reagents and conditions: (i) *p*-toluenesulfonyl chloride, NaH, THF, rt (82%-quant.); (ii) (1) 1-Boc-3-(methylamino)piperidine, DIPEA, DMF, 70 °C, (2) K*t*BuO or Na*t*BuO, THF or DMF, rt (43–74% over two steps); (iii) *(R)*-1-Boc-3-aminopiperidine in case of *(R)*-**5c,d** or *(S)*-1-Boc-3-aminopiperidine in case of *(S)*-**5c,d**, DIPEA, DMF, 70 °C (62–80%); (iv) (1) methyl iodide, NaH, DMF, −10 °C to rt, (2) K*t*BuO, THF, rt (24–70% over two steps); (v) TFA, DCM, rt (76%-quant.); (vi) corresponding carboxylic acid, appropriate amide coupling reagent, DIPEA or TEA, DCM, rt (22–83%); and (vii) **7c**, corresponding acid chloride, DIPEA, THF or DCM, 0 °C to rt (47–76%); (viii) **7c**, 2-(oxetan-3-yliden)acetonitrile, EtOH, 70 °C (76%). Abbreviations: THF: tetrahydrofurane; DMF: dimethylformamide; DIPEA: *N,N*-diisopropylethylamine; TFA: trifluoroacetic acid; DCM: dichloromethane; DCC: *N,N′*-dicyclohexylcarbodiimide; TEA: triethylamine; rt: room temperature.

Searching for a generally applicable and regioselective amide coupling procedure, various reagents including 3-(ethyliminomethylidenamino)-*N*,*N*-dimethyl-propan-1-amine (EDCI), benzotriazol-1-yl-oxytripyrrolidinophosphonium hexafluorophosphate (PyBOP), and *O*-(benzotriazol-1-yl)-*N*,*N*,*N*′,*N*′-tetramethyluronium tetrafluoroborate (TBTU) were tested. The application of EDCI suffered from a slow and inefficient conversion, while utilizing PyBOP required a laborious separation of the liberated tri(pyrrolidin-1-yl)phophine oxide. In contrast, the use of TBTU conveniently provided the final compounds in short reaction times and high purity and thus became the method of choice in the course of the project. In addition, compounds **38**, **39**, and **40** were prepared using commercially available acid chlorides applying common procedures. Compound **41** was accessible via Michael reaction of **7c** with 2-(oxetan-3-yliden)acetonitrile (synthesized from (triphenylphosphoranyliden)acetonitrile [22] and oxetan-3-one according to the literature [9]) [23].

For convenient access to the *N*-desmethyl analogs **45–50**, a 3-aminopiperidine building block with a preinstalled cyanoacetyl substituent (**44**) was synthesized (Scheme 3). Following a published protocol, 3-(Boc-amino)piperidine (**42**) was coupled with cyanoacetic acid in the presence of *N*,*N*′-dicyclohexylcarbodiimide (DCC) furnishing **43**, which was Boc-deprotected with HCl in dioxane to afford the hydrochloride salt of **44** [21]. This precursor was reacted with the appropriate 4-chloro-9-tosyl-9*H*-pyrimido[4,5-*b*]indoles (**4a–d** and **4f,g**), and the resulting S$_N$Ar products were finally detosylated to obtain **45–50**.
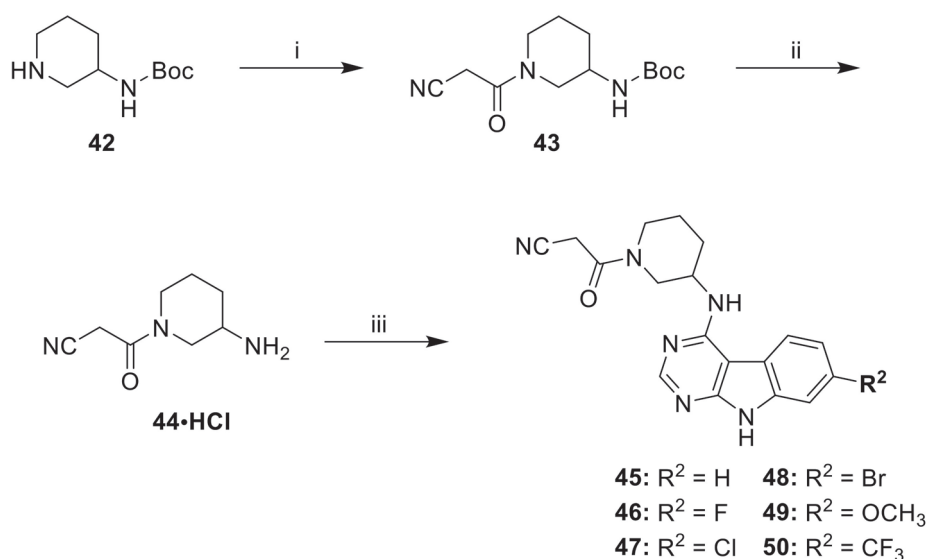
Scheme 3. Synthetic route to final compounds **45–50** listed with their structures in Table 2. Reagents and conditions: (i) cyanoacetic acid, DCC, DCM, 0 °C to rt (71%); (ii) 4N HCl in dioxane, THF, rt (96%); and (iii) (1) corresponding 4-chloro-9-tosyl-9*H*-pyrimido[4,5-*b*]indole (**4a–d** and **4f–g**), DIPEA, DMF, 70 °C and (2) K*t*BuO or Na*t*BuO, THF or DMF, rt (7–53% over two steps). Abbreviations: THF: tetrahydrofurane; DMF: dimethylformamide; DIPEA: *N*,*N*-diisopropylethylamine; TFA: trifluoroacetic acid; DCM: dichloromethane; DCC: *N*,*N*′-dicyclohexylcarbodiimide; TEA: triethylamine; rt: room temperature.

2.6. Conclusion

We used the moderately potent 9*H*-pyrimido[4,5-*b*]indole **2** as a lead structure to design a series of novel amide-based GSK-3β inhibitors. The newly synthesized compounds were evaluated for their biological activity on the targeted kinase in an ADP Glo™ assay. Compounds **2** and **28** demonstrated an optimized scaffold decoration pattern for GSK-3β inhibition. Remarkably, we observed a strong influence of the stereoconfiguration on the activity of this compound series. The *(R)*-enantiomers were found to be nanomolar inhibitors of GSK-3β, while a substantial loss in activity was seen with the *(S)*-configured counterparts. Furthermore, the most potent nanomolar inhibitors *(R)*-**2** and *(R)*-**28** and

their binding modes were examined by 1 μs molecular dynamics simulations, rationalizing the SARs of the series. Most importantly, these inhibitors exhibited enhanced stability in the HLM assay as well as a minimal toxicity along with neuroprotective effects in a cellular context. The favorable properties of these compounds motivate additional studies to further assess the biological effects of this class of GSK-3β inhibitors and to finally elucidate the binding mode to the target enzyme.

3. Materials and Methods

3.1. Molecular Modelling

All in silico work was conducted with Maestro (Schrödinger Release 2019-3/4: Maestro, Schrödinger, LLC, New York, NY, USA, 2019) using OPLS3e force field [24]. Illustrations were made with PyMOL (The PyMOL Molecular Graphics System, Version 2.2.3 Schrödinger, LLC, New York, NY, USA, 2020). First, we prepared the ligands *(R)-2* and *(R)-28* with LigPrep (Schrödinger, LLC) and then optimized their conformations with the QM Conformer & Tautomer Predictor tool (Schrödinger, LLC), which utilizes Jaguar [25]. In short, this tool optimizes conformations of the compounds with increasing levels of theory, starting with semiempirical method and using density functional theory (DFT) with M06-2X/cc-pVTZ(-f) in the final step. For more detailed description of the QM Conformer & Tautomer Predictor protocol, see the supplementary information in [26]. Next, the ligand of the Protein preparation wizard [27] prepared and energy-minimized GSK-3β structure (PDB ID: 4PTC) [28] was manually replaced with the lowest energy QM-derived structure of *(R)-2* or *(R)-28*. After this, the new complex was prepared for simulations with the Protein preparation wizard [27]. For MD simulations, we used Desmond [29]. The systems were solvated in the cubic box with the minimum distance to the edges of 13 Å from the protein and neutralized with Cl⁻ions, adding a total of 0.15 M KCl salt. The water molecules were described with the TIP3P water model [30]. The production simulations of 1000 ns were run with NpT ensemble (*T* = 310 K, Nosé–Hoover method; *p* = 1.01325 bar, Martyna–Tobias–Klein method) with the default Desmond settings as described previously [5]. Before the actual production run, the default Desmond relaxation protocol was applied for both systems. For the conformation comparison of different enantiomers of **2** (in Figure 2f), *(S)-2* was also prepared with the QM Conformer & Tautomer Predictor tool with the same default settings as *(R)-2*, and they were superimposed by their hinge binding moieties.

3.2. Chemistry

3.2.1. General Information

All solvents and reagents were purchased from commercial sources and used without further purification, if not stated otherwise. Organic solvents used for analytical chromatography were generally of HPLC grade.

High performance liquid chromatography (HPLC) was performed on a Hewlett Packard HP1090 series II HPLC system (Hewlett-Packard, Palo Alto, CA, USA) or an Agilent 1100 series HPLC system (Agilent, Santa Clara, CA, USA) equipped with a diode array detector detecting at 230 nm and 254 nm. Method A consisted of elution using mobile phase A (MeOH) and mobile phase B (aqueous 0.01 M KH_2PO_4 buffer, pH 2.3) in a flow of 1.5 mL/min on a Phenomenex Luna 5 μm C8(2) 100 Å RP column (150 × 4.6 mm) (Phenomenex, Torrance, CA, USA) and the gradient as follows: mobile phase A 40% to 85% during 8 min, mobile phase A 85% constant for 5 min, mobile phase A 85% to 40% during 1 min, mobile phase A 40% constant for 2 min; complete run time 16 min; injection volume 5 μL. Method B consisted of elution using the same mobile phases in a flow of 1.5 mL/min on an XBridge C18 5 μm RP column (150 × 4.6 mm) (Waters, Milford, MA, USA) and the gradient as follows: mobile phase A 45% to 85% during 10 min, mobile phase A constant for 6 min; complete run time 16 min; injection volume 10 μL. The purity of the final compounds was determined at 254 nm and was >95%.

Final compounds *(R)*-2/*(S)*-2, *(R)*-20/*(S)*-20, and *(R)*-28 were evaluated for their enantiomeric purity by chiral chromatography, which was performed on an Agilent 1290 Infinity series LC system (Agilent, Santa Clara, CA, USA) consisting of a binary pump, a thermostatted column compartment, an autosampler, and a diode array detector. The system was provided with an ultralow dispersion kit (including a Max-Light ultralow dispersion cartridge flow cell with an inner volume of 0.6 μL, an ultralow dispersion needle seat, and capillaries with 0.075-mm inner diameter from autosampler to column compartment (350 mm length) and from column compartment to DAD (220 mm length)) to minimize extra column volume. The method consisted of elution using the mobile phase (64% n-heptane/36% isopropanol) in a flow of 0.4 mL/min on a Chiralpak IA-U 1.6 μm column (100 × 3.0 mm) (Daicel, Osaka/Tokyo, Japan); injection volume was 5 μL. Samples of the stereoisomers and racemates were prepared by diluting 10 mM aliquotes in dimethyl sulfoxide (DMSO) by the factor 10 with the mobile phase to a total concentration of 1 mM. The purity was determined at 254 nm. The enantiomeric excess (ee) was >98% in all cases.

Thin layer chromatography—electrospray ionization—mass spectrometry coupled analysis (TLC-ESI-MS) was performed on an Advion expression^s CMS coupling system (Advion, Ithaca, NY, USA). The parameters of the ESI+ mode were as follows: capillary temperature 250 °C, capillary voltage 180 V, source gas temperature 250 °C, and ESI voltage 3500 V. The parameters of the ESI− mode were as follows: capillary temperature 250 °C, capillary voltage 180 V, source gas temperature 250 °C, and ESI voltage 2500 V. The compounds were eluted from the TLC plate with MeOH.

Flash column chromatography was performed on an Interchim puriflash 430 or XS 420 (Interchim, Montluçon, France) on Grace Davison Discovery Sciences Davisil Chromatographic Silica Media LC60A (20–45 μm) (Grace Davison Discovery Sciences, MD, USA) or Interchim puriflash prepacked silica columns (SIHP-JP, 30 μm) (Interchim, Montluçon, France). For preparation of pre-columns, Merck Geduran Si60 63–200 μm silica gel (Merck, Darmstadt, Germany) was used. Mobile phases for each compound were described in the respective experimental procedure.

^{1}H and ^{13}C Nuclear magnetic resonance (NMR) analysis was performed on 200, 300, and 400 MHz Bruker Avance and 400 MHz Bruker Ascend spectrometers (Bruker, Billerica, MA, USA). Spectra were calibrated to residual peaks of the utilized deuterated solvents. Chemical shifts were reported in parts per million (ppm) relative to tetramethylsilane ($\delta = 0$). NMR spectra of compounds with acyl substituents on the piperidine nitrogen frequently showed mixtures of amide bond rotamers resulting in complex reports. The ratio of rotamers was estimated from the respective integrals in the ^{1}H-NMR spectra.

Thin layer chromatography (TLC) was performed on silica gel coated aluminum sheets (Merck TLC Silica gel F$_{254}$, Merck, Darmstadt, Germany or Macherey-Nagel Alugram Sil G/UV$_{254}$, Macherey-Nagel, Düren, Germany), detected under UV light (254 nm).

3.2.2. General Procedures

(1) General Procedure A

The appropriate intermediate (**3a,b** and **3d–l**) was suspended in dry tetrahydrofurane (THF). NaH was added, and the mixture was stirred at room temperature (rt) and under N$_2$ atmosphere for 15–30 min. *p*-Toluenesulfonyl chloride was added, and the mixture was stirred at rt and under N$_2$ atmosphere until reaction control by TLC indicated complete consumption of the starting material. The reaction mixture was poured into ice-cold, water and saturated NH$_4$Cl solution was added. The precipitate was filtered off, rinsed with fresh demineralized water, and dried over P$_2$O$_5$ in vacuo. The crude product was used in the next step without further purification.

(2) General Procedure B

The appropriate intermediate (**4a–l**) was suspended in dry dimethylformamide (DMF). *N,N*-diisopropylethylamine (DIPEA) and the appropriate Boc protected secondary amine were added,

and the mixture was stirred at 70–80 °C until reaction control by HPLC indicated sufficient consumption of the starting material. After cooling down to rt, the mixture was poured into ice-cold water and saturated NH$_4$Cl solution was added. The resulting precipitate was filtered off, rinsed with fresh demineralized water, and dried over P$_2$O$_5$ in vacuo. The crude product was used in the next step without further purification, if not stated otherwise.

(3) General Procedure C

A solution of the appropriate intermediate (**(R)-5c,d** and **(S)-5c,d**) in dry DMF was stirred in a flame-dried Schlenk tube under Ar atmosphere and ice-cooling. NaH was added, and the mixture was left to stir for 30 min for deprotonation. Cooling was then switched to a MeOH ice bath prior to adding methyl iodide. The mixture was left to warm to 0 °C and then to rt and stirred under Ar atmosphere until HPLC indicated sufficient consumption of the starting material. The mixture was then poured into ice-cold saturated NH$_4$Cl solution. The resulting precipitate was filtered off, washed with demineralized, and dried over P$_2$O$_5$ in vacuo. The crude product was used in the next step without further purification, if not stated otherwise.

(4) General Procedure D

The appropriate intermediate was dissolved in THF (dry or HPLC grade). K*t*BuO was added, and the mixture was stirred at rt and under N$_2$ atmosphere until reaction control by HPLC indicated complete consumption of the starting material. Saturated NH$_4$Cl solution and ethyl acetate (EtOAc) were added to the reaction mixture, and phases were separated. The aqueous layer was extracted with EtOAc (2–3×). Combined organic layers were dried over Na$_2$SO$_4$ and concentrated under reduced pressure. The residue was purified by flash column chromatography.

(5) General Procedure E

The appropriate intermediate (**6a,b**, **6d–l**, **(R)-6c,d**, and **(S)-6c,d**) was stirred in a 17% (*v/v*) mixture of dry dichloromethane (DCM) and trifluoroacetic acid (TFA) at rt and under N$_2$ atmosphere until reaction control by HPLC indicated complete consumption of the starting material. The mixture was concentrated under reduced pressure, and saturated NaHCO$_3$ solution was added to neutralize residual TFA. The mixture was then extracted repeatedly with EtOAc. MeOH was added to improve the solubility of the product in the organic layer. Combined organic layers were washed with saturated NaHCO$_3$ solution (3×), dried over Na$_2$SO$_4$, and evaporated to dryness. The crude product was used in the next step without further purification, if not stated otherwise.

(6) General Procedure F

The appropriate carboxylic acid and PyBOP or TBTU were stirred in dry DCM for 15–30 min at rt and under N$_2$ atmosphere. A mixture of the appropriate intermediate (**7a–l**, **(R)-7c,d**, and **(S)-7c,d**) and DIPEA in dry DCM was added to the activated carboxylic acids and the reaction mixture stirred at rt and under N$_2$ atmosphere until reaction control by HPLC indicated complete consumption of the starting material. The mixture was diluted with DCM, washed with saturated NaHCO$_3$ solution (2–3×) and saturated NH$_4$Cl solution (2–3×), dried over Na$_2$SO$_4$, and concentrated under reduced pressure. The residue was purified by flash column chromatography.

(7) General Procedure G

The appropriate intermediate (**4a–d** and **4f,g**), **44·HCl**, and DIPEA were stirred in dry DMF at 70 °C overnight. After cooling down to rt, Na*t*BuO was added and the mixture was stirred at rt overnight. Saturated NH$_4$Cl solution was added, and the mixture was extracted thrice with EtOAc. Combined organic layers were dried over Na$_2$SO$_4$ and concentrated under reduced pressure. The residue was purified by flash column chromatography.

3.2.3. Detailed Procedures

(1) Detailed Procedures for the Preparation of Intermediates **4a–l**

4-Chloro-9-tosyl-9*H*-pyrimido[4,5-*b*]indole (**4a**)

The title compound was prepared from **3a** (500.0 mg, 2.45 mmol), *p*-toluenesulfonyl chloride (585.0 mg, 3.07 mmol), and NaH (147.3 mg of a 60% in mineral oil, 3.68 mmol) in dry THF (16 mL) according to general procedure A (reaction time 2 h); 753 mg of a yellow solid was yielded (82% crude yield) and used in the next step without further purification. ESI-MS: (*m/z*) 380.3 [M + Na]$^+$, 356.3 [M − H]$^-$.

4-Chloro-7-fluoro-9-tosyl-9*H*-pyrimido[4,5-*b*]indole (**4b**)

The title compound was prepared from **3b** (250.0 mg, 2.05 mmol), *p*-toluenesulfonyl chloride (268.8 mg, 1.41 mmol), and NaH (67.7 mg of a 60% dispersion in mineral oil, 1.69 mmol) in dry THF (7.5 mL) according to general procedure A (reaction time 1.5 h); 412 mg of a yellow solid was yielded (97% crude yield) and used in the next step without further purification. ESI-MS: (*m/z*) 398.2 [M + Na]$^+$, 374.1 [M − H]$^-$.

4,7-Dichloro-9-tosyl-9H-pyrimido[4,5-*b*]indole (**4c**)

The title compound was prepared from **3c** as described previously [5].

7-Bromo-4-chloro-9-tosyl-9*H*-pyrimido[4,5-*b*]indole (**4d**)

The title compound was prepared from **3d** (560.0 mg, 1.98 mmol), *p*-toluenesulfonyl chloride (472.4 mg, 2.48 mmol), and sodium hydride (118.9 mg of a 60% dispersion in mineral oil, 2.97 mmol) in dry THF (15 mL) according to general procedure A (reaction time 20 min); 834 mg of a yellow solid was yielded (96% crude yield) and used in the next step without further purification. ESI-MS: (*m/z*) 457.8 [M + Na]$^+$, 433.9 [M − H]$^-$.

4-Chloro-7-iodo-9-tosyl-9*H*-pyrimido[4,5-*b*]indole (**4e**)

The title compound was prepared from **3e** (421.0 mg, 1.35 mmol), *p*-toluenesulfonyl chloride (322.5 mg, 1.69 mmol), and sodium hydride (81.2 mg of a 60% dispersion in mineral oil, 2.03 mmol) in dry THF (10 mL) according to general procedure A (reaction time 1 h); 606 mg of a dark yellow solid was yielded (93% crude yield) and used in the next step without further purification. ESI-MS: (*m/z*) 506.3 [M + Na]$^+$; 482.4 [M − H]$^-$.

4-Chloro-7-methoxy-9-tosyl-9*H*-pyrimido[4,5-*b*]indole (**4f**)

The title compound was prepared from **3f** (710.0 mg, 3.03 mmol) and NaH (182.3 mg of a 60% dispersion in mineral oil, 4.56 mmol) in dry THF (10 mL) according to general procedure A (reaction time 30 min). *p*-Toluenesulfonyl chloride (695.1 mg, 3.65 mmol) was added as solution in THF (2 mL); 1.15 g was yielded (98% yield) and used in the next step without further purification.

4-Chloro-9-tosyl-7-(trifluoromethyl)-9*H*-pyrimido[4,5-*b*]indole (**4g**)

NaH (176.7 mg of a 60% dispersion in mineral oil, 4.42 mmol) was added portion-wise to an ice-cooled stirring suspension of **3g** (800.0 mg, 2.95 mmol) in dry THF (10 mL). The mixture was stirred under ice-cooling for 30 min. A solution of *p*-toluenesulfonyl chloride (673.8 mg, 3.53 mmol) in dry THF (2 mL) was drop-added, while the mixture was left to warm to rt and stirring continued at rt for 30 min. The mixture was poured into saturated NH$_4$Cl solution (100 mL). The resulting precipitate was filtered off, washed with demineralized water, and dried over P$_2$O$_5$ in vacuo; 1.2 g was yielded (96% crude yield) and used in the next step without further purification. ESI-MS: (*m/z*) 448.0 [M + H]$^+$, 424.0 [M − H]$^-$.

4,6-Dichloro-9-tosyl-9*H*-pyrimido[4,5-*b*]indole (**4h**)

The title compound was prepared from **3h** (550.0 mg, 2.31 mmol), *p*-toluenesulfonyl chloride (550.2 mg, 2.89 mmol). and NaH (138.6 mg of a 60% dispersion in mineral oil, 3.47 mmol) in dry THF (18 mL) according to general procedure A (reaction time 40 min); 890 mg of a yellow solid was yielded (98% crude yield) and used in the next step without further purification. ESI-MS: (*m/z*) 413.9 [M + Na]$^+$, 390.0 [M − H]$^-$.

6-Bromo-4-chloro-9-tosyl-9*H*-pyrimido[4,5-*b*]indole (**4i**)

The title compound was prepared from **3i** (740.0 mg, 2.62 mmol), *p*-toluenesulfonyl chloride (624.2 mg, 3.27 mmol), and NaH (157.2 mg of a 60% dispersion in mineral oil, 3.93 mmol) in dry THF (33 mL) according to general procedure A (reaction time 1.5 h); 1.1 g was yielded (96% crude yield) and used in the next step without further purification. ESI-MS: (*m/z*) 457.7 [M + Na]$^+$, 433.8 [M − H]$^-$.

4-Chloro-6-methoxy-9-tosyl-9*H*-pyrimido[4,5-*b*]indole (**4j**)

The title compound was prepared from **3j** (480.0 mg, 2.05 mmol), *p*-toluenesulfonyl chloride (489.6 mg, 2.57 mmol), and sodium hydride (123.3 mg of a 60% dispersion in mineral oil, 3.08 mmol) in dry THF (16 mL) according to general procedure A in a (reaction time 30 min); 750 mg of a brown solid was yielded (94% crude yield) and used in the next step without further purification. ESI-MS: (*m/z*) 410.7 [M + Na]$^+$, 386.7 [M − H]$^-$.

4,5-Dichloro-9-tosyl-9*H*-pyrimido[4,5-*b*]indole (**4k**)

3k (600.0 mg, 2.52 mmol) was suspended in dry THF (20 mL), and NaH (151.2 mg of a 60% dispersion in mineral oil, 3.78 mmol) was added. The mixture was stirred at rt and under N$_2$ atmosphere for 15 min. *p*-Toluenesulfonyl chloride (600.6 mg, 3.15 mmol) was added and the mixture stirred at rt and under N$_2$ atmosphere for 40 min. Saturated NH$_4$Cl solution (50 mL), EtOAc (30 mL), and some MeOH were added, and phases were separated. The aqueous layer was extracted with DCM (4 × 30 mL). Combined organic layers were dried over Na$_2$SO$_4$. Volatiles were removed under reduced pressure to yield 1.1 g of a brown solid (>100% crude yield), which contained excessive *p*-toluenesulfonyl chloride. The crude product was used in the next step without further purification. ESI-MS: (*m/z*) 414.7 [M + Na]$^+$, 390.7 [M − H]$^-$.

4,7-Dichloro-2-methyl-9-tosyl-9*H*-pyrimido[4,5-*b*]indole (**4l**)

The title compound was prepared from **3l** (470.0 mg, 1.86 mmol), *p*-toluenesulfonyl chloride (444.3 mg, 2.33 mmol), and NaH (111.9 mg of a 60% dispersion in mineral oil, 2.80 mmol) in dry THF (16 mL) according to general procedure A (reaction time 20 min); 759 mg of a beige solid was yielded (100% crude yield) and used in the next step without further purification.

(2) Detailed Procedures for the Preparation of Enantiopure Intermediates **(R)-5c,d** and **(S)-5c,d**

tert-Butyl (*R*)-3-((7-chloro-9-tosyl-9*H*-pyrimido[4,5-*b*]indol-4-yl)amino)piperidine-1-carboxylate (**(R)-5c**)

The title compound was prepared from **4c** (465.0 mg, 1.19 mmol), (*R*)-1-Boc-3-aminopiperidine (284.9 mg, 1.42 mmol), and DIPEA (444.3 mg, 3.44 mmol) in dry DMF (11 mL) according to general procedure B (reaction time 16 h). Purification by flash column chromatography (SiO$_2$, hexane–EtOAc–MeOH 60:38:2) gave 462 mg of a pale yellow solid (69% yield). ^{1}H-NMR (300 MHz, CDCl$_3$) δ 8.60 (s, 1H), 8.49 (s, 1H), 8.05 (d, *J* = 7.9 Hz, 2H), 7.68 (s, 1H), 7.35 (d, *J* = 7.5 Hz, 1H), 7.25 (d, *J* = 8.9 Hz, 2H, overlap with CHCl$_3$ signal), 6.44–4.91 (m, 1H), 4.55–4.31 (m, 1H), 4.23–3.66 (m, 2H), 3.54–2.97 (m, 2H), 2.46–2.01 (m, 4H), 1.97–1.79 (m, 1H), 1.75–1.30 (m, 11H); ESI-MS: (*m/z*) 578.0 [M + Na]$^+$, 553.9 [M − H]$^-$; HPLC method A: t$_r$ = 10.118 min.

tert-Butyl (*R*)-3-((7-bromo-9-tosyl-9*H*-pyrimido[4,5-*b*]indol-4-yl)amino)piperidine-1-carboxylate (**(R)-5d**)

The title compound was prepared from **4d** (465.0 mg, 1.07 mmol), *(R)*-1-Boc-3-aminopiperidine (277.2 mg, 1.38 mmol), and DIPEA (412.9 mg, 3.19 mmol) in dry DMF (12 mL) according to general procedure B (reaction time 7 h). Purification by flash column chromatography (SiO$_2$, hexane–EtOAc–MeOH 67:31.5:1.5) gave 400 mg of a light yellow solid (62% yield). ESI-MS: (*m/z*) 599.8 [M + H]$^+$, 621.7 [M + Na]$^+$, 597.7 [M − H]$^-$; HPLC method A: t$_r$ = 10.848 min.

tert-Butyl (*S*)-3-((7-chloro-9-tosyl-9*H*-pyrimido[4,5-*b*]indol-4-yl)amino)piperidine-1-carboxylate (**(S)-5c**)

The title compound was prepared from **4c** (460.0 mg, 1.17 mmol), *(S)*-1-Boc-3-aminopiperidine (305.3 mg, 1.53 mmol), and DIPEA (444.8 mg, 3.44 mmol) in dry DMF (11 mL) according to general procedure B (reaction time 9 h). Purification by flash column chromatography (SiO$_2$, DCM–MeOH 97.5:2.5) gave 523 mg of a yellow solid (80% yield). ESI-MS: (*m/z*) 578.8 [M + Na]$^+$, 554.8 [M − H]$^-$; HPLC method A: t$_r$ = 10.577 min.

tert-Butyl (*S*)-3-((7-bromo-9-tosyl-9*H*-pyrimido[4,5-*b*]indol-4-yl)amino)piperidine-1-carboxylate (**(S)-5d**)

The title compound was prepared from **4d** (510.0 mg, 1.17 mmol), *(S)*-1-Boc-3-aminopiperidine (315.8 mg, 1.58 mmol), and DIPEA (452.9 mg, 3.50 mmol) in dry DMF (14 mL) according to general procedure B (reaction time 6 h). Purification by flash column chromatography (SiO$_2$, hexane–EtOAc–MeOH 67:31.5:1.5) gave 462 mg of a light yellow solid (66% yield). ^{1}H-NMR (300 MHz, CDCl$_3$) δ 8.67 (s, 1H), 8.60 (s, 1H), 8.06 (d, *J* = 8.4 Hz, 2H), 7.62 (br s, 1H), 7.49 (dd, *J* = 8.1, 1.3 Hz, 1H), 7.25 (d, 2H, overlap with CHCl$_3$ signal), 6.14–5.03 (m, 1H), 4.45–4.32 (m, 1H), 4.20–3.72 (m, 2H), 3.47–2.98 (m, 2H), 2.42–2.02 (m, 4H), 1.92–1.78 (m, 1H), 1.75–1.32 (m, 11H); ESI-MS: (*m/z*) 599.8 [M + H]$^+$, 621.8 [M + Na]$^+$, 597.9 [M − H]$^-$; HPLC method A: t$_r$ = 10.767 min.

(3) Detailed Procedures for the Preparation of Intermediates **6a,b** and **6d–l**

tert-Butyl 3-(methyl(9*H*-pyrimido[4,5-*b*]indol-4-yl)amino)piperidine-1-carboxylate (**6a**)

The title compound was prepared by a two-step procedure. In the first step, **4a** (100.0 mg, 0.28 mmol), 1-Boc-3-(methylamino)piperidine (71.9 mg, 0.34 mmol), and DIPEA (108.4 mg, 0.84 mmol) were reacted in dry DMF (3 mL) according to general procedure B (reaction time 16 h) to afford 145 mg of crude *tert*-butyl 3-(methyl(9-tosyl-9*H*-pyrimido[4,5-*b*]indol-4-yl)amino)piperidine-1-carboxylate (97% crude yield), used in the second step without further purification. ESI-MS: (*m/z*) 558.1 [M + Na]$^+$, 533.9 [M − H]$^-$; HPLC method B: 10.875 min. The crude material obtained from the first step was reacted with Na*t*BuO (182.1 mg, 1.89 mmol) in dry THF (5 mL) according to general procedure D (reaction time 1 h). Purification by flash column chromatography (SiO$_2$, DCM–EtOH 95:5) gave 60 mg of the title compound (58% yield). ^{1}H-NMR (300 MHz, DMSO-*d$_6$*) δ 12.10 (s, 1H), 8.42 (s, 1H), 7.76 (br s, 1H), 7.50 (d, *J* = 7.7 Hz, 1H), 7.43–7.35 (m, 1H), 7.25 (t, *J* = 7.4 Hz, 1H), 4.30–3.72 (m, 3H), 3.20–3.04 (m, 4H), 2.79–2.60 (m, 1H), 2.09–1.71 (m, 3H), 1.51–0.99 (m, 10H); HPLC method B: t$_r$ = 8.335 min.

tert-Butyl 3-((7-fluoro-9*H*-pyrimido[4,5-*b*]indol-4-yl)(methyl)amino)piperidine-1-carboxylate (**6b**)

The title compound was prepared by a two-step procedure. In the first step, **4b** (420.0 mg, 1.12 mmol), 1-Boc-3-(methylamino)piperidine (287.4 mg, 1.34 mmol), and DIPEA (433.0 mg, 3.35 mmol) were reacted in dry DMF (15 mL) according to general procedure B (reaction time 16 h) to afford 549 mg of crude *tert*-butyl 3-((7-fluoro-9-tosyl-9*H*-pyrimido[4,5-*b*]indol-4-yl) (methyl)amino)piperidine-1-carboxylate as a yellow solid (89% crude yield), used in the second step without further purification. Purification of a small portion for analytical purposes was performed by flash column chromatography (SiO$_2$, petroleum ether–EtOAc gradient elution from 2:1 to 1:1). ^{1}H-NMR (400 MHz, CDCl$_3$) δ 8.63 (s, 1H), 8.26 (dd, *J* = 10.2, 2.4 Hz, 1H), 8.10 (d, *J* = 8.4 Hz, 2H), 7.65 (s, 1H), 7.26 (d, *J* = 8.2 Hz, 2H, overlap with CHCl$_3$ signal), 7.17 (td, *J* = 8.7, 2.4 Hz, 1H), 4.49–3.89 (m, 3H), 3.13 (s, 3H), 3.11–3.02 (m, 1H), 2.76–2.65 (m, 1H), 1.99–1.70 (m, 3H), 1.67–1.29 (m, 10H); ESI-MS: (*m/z*) 554.7 [M + H]$^+$, 576.7 [M + Na]$^+$, 552.7 [M − H]$^-$; HPLC method A: t$_r$ = 10.806 min.

The crude material obtained from the first step was reacted with K*t*BuO (780.0 mg, 6.95 mmol) in HPLC grade THF (28 mL) according to general procedure D. Purification by flash column chromatography (SiO$_2$, DCM–MeOH gradient elution from 97.5:2.5 to 93:7) gave 191 mg of a beige solid (48% yield). ^{1}H-NMR (400 MHz, CDCl$_3$) δ 11.48 (s, 1H), 8.54 (s, 1H), 7.79–7.69 (m, 1H), 7.24 (dd, *J* = 8.9, 2.3 Hz, 1H), 7.05 (td, *J* = 9.1, 2.4 Hz, 1H), 4.59–3.98 (m, 3H), 3.27 (s, 3H), 3.12–3.02 (m, 1H), 2.77–2.60 (m, 1H), 2.08–1.77 (m, 3H), 1.69–1.54 (m, 1H), 1.43 (s, 9H); ESI-MS: (*m/z*) 422.5 [M + Na]$^+$, 398.5 [M − H]$^-$; HPLC method A: t$_r$ = 9.140 min.

tert-Butyl 3-((7-bromo-9*H*-pyrimido[4,5-*b*]indol-4-yl)(methyl)amino)piperidine-1-carboxylate (**6d**)

The title compound was prepared by a two-step procedure. In the first step, **4d** (752.0 mg, 1.73 mmol), 1-Boc-3-(methylamino)piperidine (479.4 mg, 2.23 mmol), and DIPEA (667.4 mg, 5.17 mmol) were reacted in dry DMF (22 mL) according to general procedure B (reaction time 6 h) to afford 1.2 g of crude *tert*-butyl 3-((7-bromo-9-tosyl-9*H*-pyrimido[4,5-*b*]indol-4-yl)(methyl)amino)piperidine-1-carboxylate as a yellow solid (>100% crude yield), used in the second step without further purification. A small portion was purified for analytical purposes by flash column purification (SiO$_2$; DCM–EtOH 97.5:2.5). ^{1}H-NMR (300 MHz, CDCl$_3$) δ 8.75–8.55 (m, 2H), 8.17–8.03 (m, 2H), 7.61–7.46 (m, 2H), 7.31–7.21 (m, 2H, overlap with CHCl$_3$ signal), 4.46–3.93 (m, 3H), 3.20–2.95 (m, 4H), 2.75–2.61 (m, 1H), 2.37 (s, 3H), 2.00–1.71 (m, 3H), 1.62–1.32 (m, 10H); ^{13}C NMR (50 MHz, CDCl$_3$) δ 160.5, 157.2, 154.8, 154.3, 145.8, 136.3, 135.4, 129.8, 128.2, 127.3, 123.7, 120.7, 120.5, 117.5, 101.2, 80.0, 55.6, 46.7, 44.0 (br), 33.7 (br), 28.5, 28.0, 24.8, 21.8; ESI-MS: (*m/z*) 636.1 [M + Na]$^+$, 612.2 [M − H]$^-$; HPLC method *A*: t$_r$ = 11.296 min. The crude material obtained from the first step was reacted with K*t*BuO (1.4 g, 12.05 mmol) in dry THF (50 mL) according to general procedure D (reaction time 1 h). Purification by flash column chromatography (SiO$_2$, DCM:MeOH gradient elution from 97.5:2.5 to 93:7) gave 488 mg of a light brown solid (62% yield). ^{1}H-NMR (300 MHz, CDCl$_3$) δ 11.46 (br s, 1H), 8.56 (s, 1H), 7.71–7.62 (m, 2H), 7.40 (dd, *J* = 8.6, 1.8 Hz, 1H), 4.52–4.01 (m, 3H), 3.27 (s, 3H), 3.13–3.01 (m, 1H), 2.77–2.62 (m, 1H), 2.09–1.77 (m, 3H), 1.72–1.56 (m, 1H), 1.43 (s, 9H); ESI-MS: (*m/z*) 481.9 [M + Na]$^+$, 458.0 [M − H]$^-$; HPLC method A: t$_r$ = 9.546 min.

tert-Butyl 3-((7-iodo-9*H*-pyrimido[4,5-*b*]indol-4-yl)(methyl)amino)piperidine-1-carboxylate (**6e**)

The title compound was prepared by a two-step procedure. In the first step, **4e** (590.0 mg, 1.22 mmol), 1-Boc-3-(methylamino)piperidine (339.8 mg, 1.59 mmol), and DIPEA (473.0 mg, 3.66 mmol) were reacted in dry DMF (16 mL) according to general procedure B. Dissident from the general procedure, the mixture was stirred at 60 °C for 2 h; 779 mg of crude *tert*-butyl 3-((7-iodo-9-tosyl-9*H*-pyrimido[4,5-*b*]indol-4-yl)(methyl)amino)piperidine-1-carboxylate as a beige solid (97% crude yield) was used in the second step without further purification. Purification of a small portion for analytical purposes was performed by flash column chromatography (SiO$_2$, petroleum ether–EtOAc gradient elution from 3:2 to 1:1). ^{1}H-NMR (300 MHz, CDCl$_3$) δ 8.86 (d, *J* = 1.4 Hz, 1H), 8.62 (s, 1H), 8.09 (d, *J* = 8.4 Hz, 2H), 7.74 (dd, *J* = 8.4, 1.4 Hz, 1H), 7.41 (d, *J* = 7.9 Hz, 1H), 7.27 (d, *J* = 8.1 Hz, 2H; overlap with CHCl$_3$ signal), 4.47–3.90 (m, 3H), 3.11 (s, 3H), 3.08–2.98 (m, 1H), 2.77–2.60 (m, 1H), 2.37 (s, 3H), 2.01–1.71 (m, 3H), 1.64–1.29 (m, 10H); ^{13}C NMR (50 MHz, CDCl$_3$) δ 160.5, 157.0, 154.8, 154.4, 145.8, 136.4, 135.4, 133.2, 129.8, 128.2, 124.0, 123.1, 121.3, 101.2, 91.3, 80.0, 55.6 (br), 46.7, 44.1 (br), 33.7 (br), 28.5, 28.1, 24.8, 21.8; ESI-MS: (*m/z*) 684.7 [M + Na]$^+$, 660.8 [M − H]$^-$; HPLC method A: t$_r$ = 10.993 min.

The crude material obtained from the first step was reacted with K*t*BuO (807.4 mg, 7.2 mmol) in dry THF (30 mL) according to general procedure D (reaction time 1 h). Purification twice by flash column chromatography (SiO$_2$, DCM–MeOH 95:5 and SiO$_2$, DCM–MeOH gradient elution from 97.5:2.5 to 93:7) gave 292 mg of a beige solid (56% yield). ^{1}H-NMR (300 MHz, CDCl$_3$) δ 11.30 (s, 1H), 8.52 (s, 1H), 7.92 (d, *J* = 1.1 Hz, 1H), 7.61 (dd, *J* = 8.5, 1.4 Hz, 1H), 7.53 (d, *J* = 8.5 Hz, 1H), 4.55–4.04 (m, 3H), 3.29 (s, 3H), 3.11–2.98 (m, 1H), 2.78–2.61 (m, 1H), 2.10–1.76 (m, 3H), 1.74–1.30 (m, 10H); ESI-MS: (*m/z*) 530.6 [M + Na]$^+$, 506.6 [M − H]$^-$; HPLC method A: t$_r$ = 9.541 min.

tert-Butyl 3-((7-methoxy-9*H*-pyrimido[4,5-*b*]indol-4-yl)(methyl)amino)piperidine-1-carboxylate (**6f**)

4f (250.0 mg, 0.64 mmol), 1-Boc-3-(methylamino)piperidine (165.8, 0.77 mmol), and DIPEA (249.5 mg, 1.93 mmol) were stirred in dry DMF (10 mL) at 70 °C overnight. After cooling down to rt, Na*t*BuO (433.6 mg, 4.51 mmol) was added and stirring continued at rt for 1 h. Saturated NH₄Cl solution (150 mL) was added. The resulting precipitate was filtered off, washed with water, and dried over P₂O₅ in vacuo. Purification by flash column chromatography (SiO₂, DCM–EtOH 97:3) gave 172 mg (64% yield). ¹H-NMR (300 MHz, DMSO-*d₆*) δ 12.00 (s, 1H), 8.37 (s, 1H), 7.64 (br s, 1H), 6.98 (d, *J* = 2.3 Hz, 1H), 6.85 (dd, *J* = 8.7, 1.6 Hz, 1H), 4.24–3.80 (m, 6H), 3.19–3.03 (m, 4H), 2.79–2.60 (m, 1H), 2.05–1.70 (m, 3H), 1.47–1.02 (m, 10H); ESI-MS: (*m/z*) 412.0 [M + H]⁺, 433.9 [M + Na]⁺, 410.1 [M − H]⁻; HPLC method B: t_r = 8.342 min.

tert-Butyl 3-(methyl(7-(trifluoromethyl)-9*H*-pyrimido[4,5-*b*]indol-4-yl)amino)piperidine-1-carboxylate (**6g**)

4g (600.0 mg, 1.41 mmol), 1-Boc-3-(methylamino)piperidine (362.4 mg, 1.69 mmol), and DIPEA (546.7 mg, 4.23 mmol) were stirred in dry DMF (20 mL) at 70 °C overnight. After cooling down to rt, Na*t*BuO (947.9 mg, 9.86 mmol) was added and stirring continued at rt for 1 h. Saturated NH₄Cl solution (200 mL) was added. The resulting precipitate was filtered off, washed with water, and dried over P₂O₅ in vacuo. Purification by flash column chromatography (SiO₂, DCM–EtOH 97:3) gave 280 mg (44% yield). ¹H-NMR (300 MHz, DMSO-*d₆*) δ 12.48 (s, 1H), 8.47 (s, 1H), 7.97 (br s, 1H), 7.75 (s, 1H), 7.54 (d, *J* = 8.3 Hz, 1H), 4.39–3.83 (m, 3H), 3.21 (s, 3H), 3.18–3.06 (m, 1H), 2.81–2.61 (m, 1H), 2.12–1.71 (m, 3H), 1.53–1.01 (m, 10H); HPLC method B: t_r = 10.213 min.

tert-butyl 3-((6-chloro-9*H*-pyrimido[4,5-*b*]indol-4-yl)(methyl)amino)piperidine-1-carboxylate (**6h**)

The title compound was prepared by a two-step procedure. In the first step, **4h** (450.0 mg, 1.15 mmol), 1-Boc-3-(methylamino)piperidine (368.8 mg, 1.72 mmol), and DIPEA (444.7 mg, 3.44 mmol) were reacted in dry DMF (17 mL) according to general procedure B (reaction time 14 h) to afford 682 mg of crude *tert*-butyl 3-((6-chloro-9-tosyl-9*H*-pyrimido[4,5-*b*]indol-4-yl)(methyl)amino)piperidine-1-carboxylate as a beige solid (>100% crude yield), used in the second step without further purification. Purification of a small portion for analytical purposes was performed by flash column chromatography (SiO₂, petroleum ether–EtOAc gradient elution from 65:35 to 1:1). ¹H-NMR (300 MHz, CDCl₃) δ 8.61 (s, 1H), 8.43 (d, *J* = 9.0 Hz, 1H), 8.05 (d, *J* = 8.4 Hz, 2H), 7.58 (d, *J* = 2.0 Hz, 1H), 7.46 (dd, *J* = 9.0, 2.1 Hz, 1H), 7.24 (d, *J* = 9.2 Hz, 2H; overlapping with CHCl₃ signal), 4.30–3.94 (m, 3H), 3.13 (s, 3H), 3.07–2.94 (m, 1H), 2.75–2.61 (m, 1H), 2.35 (s, 3H), 2.16–2.04 (m, 1H), 1.98–1.78 (m, 2H), 1.74–1.55 (m, 1H), 1.38 (s, 9H); ESI-MS: (*m/z*) 592.0 [M + Na]⁺, 568.1 [M − H]⁻; HPLC method A: t_r = 10.903 min.

The crude material obtained from the first step was reacted with K*t*BuO (774.5 mg, 6.91 mmol) in HPLC grade THF (29 mL) according to general procedure D (reaction time 2.5 h). Purification by flash column chromatography (SiO₂, DCM–MeOH gradient elution from 97.5:2.5 to 93:7) gave 252 mg of a yellow solid (61% yield). ¹H-NMR (300 MHz, CDCl₃) δ 11.46 (br s, 1H), 8.54 (s, 1H), 7.73 (d, *J* = 1.6 Hz, 1H), 7.45 (d, *J* = 8.5 Hz, 1H), 7.38 (dd, *J* = 8.6, 1.8 Hz, 1H), 4.54–4.40 (m, 1H), 4.38–4.01 (m, 2H), 3.30 (s, 3H), 3.10–2.97 (m, 1H), 2.77–2.62 (m, 1H), 2.22–2.11 (m, 1H), 2.03–1.84 (m, 2H), 1.81–1.63 (m, 1H), 1.40 (s, 9H); ESI-MS: (*m/z*) 416.1 [M + H]⁺, 438.1 [M + Na]⁺, 414.1 [M − H]⁻; HPLC method A: t_r = 9.385 min.

tert-Butyl 3-((6-bromo-9*H*-pyrimido[4,5-*b*]indol-4-yl)(methyl)amino)piperidine-1-carboxylate (**6i**)

The title compound was prepared by a two-step procedure. In the first step, **4i** (650 mg, 1.49 mmol), 1-Boc-3-(methylamino)piperidine (415.1 mg, 1.94 mmol), and DIPEA (576.5 mg, 4.46 mmol) were reacted in dry DMF (20 mL) according to procedure B (reaction time 5 h) to yield 871 mg of crude *tert*-butyl 3-((6-bromo-9-tosyl-9*H*-pyrimido[4,5-*b*]indol-4-yl)(methyl)amino)piperidine-1-carboxylate as a dark yellow solid (95% crude yield), used in the second step without further purification. Purification of a small portion for analytical purposes was performed by flash column chromatography (SiO₂,

petroleum ether–EtOAc gradient elution from 2:1 to 1:1). ^{1}H-NMR (300 MHz, CDCl$_3$) δ 8.61 (s, 1H), 8.39 (d, *J* = 9.0 Hz, 1H), 8.05 (d, *J* = 8.3 Hz, 2H), 7.73 (d, *J* = 1.9 Hz, 1H), 7.60 (dd, *J* = 9.0, 1.9 Hz, 1H), 7.25 (d, *J* = 8.4 Hz, 2H, overlap with CHCl$_3$ signal), 4.30–3.96 (m, 3H), 3.13 (s, 3H), 3.06–2.93 (m, 1H), 2.75–2.60 (m, 1H), 2.36 (s, 3H), 2.16–2.07 (m, 1H), 1.98–1.80 (m, 2H), 1.75–1.58 (m, 1H), 1.37 (s, 9H); ^{13}C NMR (50 MHz, CDCl$_3$) δ 160.6, 157.5, 155.0, 154.6, 145.7, 135.4, 134.4, 129.8, 129.4, 128.0, 125.3, 123.7, 117.3, 115.8, 100.5, 79.9, 55.2, 46.4 (br), 44.0 (br), 34.3, 28.4, 28.1, 24.8, 21.8; ESI-MS: (*m/z*) 614.2 [M + H]$^+$, 636.1 [M + Na]$^+$, 612.2 [M − H]$^-$; HPLC method A: t$_r$ = 11.194 min.

The crude material obtained from the first step was reacted with K*t*BuO (976.5 mg, 8.70 mmol) in dry THF (36 mL) according to general procedure D (reaction time 1 h). Purification by flash column chromatography (SiO$_2$, DCM–MeOH gradient elution from 97.5:2.5 to 93:7) gave 364 mg of a beige solid (64% yield). ^{1}H-NMR (300 MHz, CDCl$_3$) δ 11.26 (br s, 1H), 8.53 (s, 1H), 7.87 (d, *J* = 0.8 Hz, 1H), 7.52 (dd, *J* = 8.5, 1.6 Hz, 1H), 7.40 (d, *J* = 8.5 Hz, 1H), 4.54–4.40 (m, 1H), 4.35–4.03 (m, 2H), 3.30 (s, 3H), 3.09–2.96 (m, 1H), 2.77–2.63 (m, 1H), 2.24–2.13 (m, 1H), 2.04–1.67 (m, 3H), 1.40 (s, 9H); ^{13}C NMR (50 MHz, CDCl$_3$) δ 160.2, 157.1, 155.1, 152.8, 135.5, 127.8, 125.4, 121.9, 113.7, 112.8, 98.0, 79.9, 54.8, 46.6 (br), 44.1 (br), 33.8, 28.5, 28.3, 24.9; ESI-MS: (*m/z*) 482.3 [M + Na]$^+$, 458.3 [M − H]$^-$; HPLC method A: t$_r$ = 9.550 min.

tert-Butyl 3-((6-methoxy-9*H*-pyrimido[4,5-*b*]indol-4-yl)(methyl)amino)piperidine-1-carboxylate (**6j**)

The title compound was prepared by a two-step procedure. In the first step, **4j** (730.0 mg, 1.88 mmol), 1-Boc-3-(methylamino)piperidine (524.4 mg, 2.45 mmol), and DIPEA (729.8 mg, 5.65 mmol) were reacted in dry DMF (22 mL) according to general procedure B (reaction time 6.5 h) to afford 975 mg of crude *tert*-butyl 3-((6-methoxy-9-tosyl-9*H*-pyrimido[4,5-*b*]indol-4-yl)(methyl)amino)piperidine-1-carboxylate as a beige solid (92% crude yield), used in the next step without further purification. Purification of a small portion for analytical purposes was performed by flash column chromatography (SiO$_2$). ^{1}H-NMR (400 MHz, CDCl$_3$) δ 8.63 (s, 1H), 8.40 (d, *J* = 9.0 Hz, 1H), 8.03 (d, *J* = 7.8 Hz, 2H), 7.22 (d, *J* = 7.9 Hz, 2H), 7.16–7.07 (m, 2H), 4.24–3.98 (m, 3H), 3.89 (s, 3H), 3.14 (s, 3H), 3.08–2.99 (m, 1H), 2.75–2.64 (m, 1H), 2.34 (s, 3H), 2.10–2.02 (m, 1H), 1.95–1.76 (m, 2H), 1.69–1.57 (m, 1H), 1.45–1.22 (m, 9H); ESI-MS: (*m/z*) 588.5 [M + Na]$^+$, 564.6 [M − H]$^-$; HPLC method A: t$_r$ = 10.013 min.

The crude material obtained from the first step was reacted with K*t*BuO (1180.2 mg, 10.52 mmol) in dry THF (45 mL) according to general procedure D (reaction time 30 min). Purification by flash column chromatography (SiO$_2$, DCM–MeOH gradient elution from 97.5:2.5 to 93:7) gave 369 mg of a beige solid (60% yield). ^{1}H-NMR (400 MHz, DMSO-*d$_6$*) δ 11.95 (s, 1H), 8.40 (s, 1H), 7.41 (d, *J* = 8.7 Hz, 1H), 7.19 (s, 1H), 7.06 (dd, *J* = 8.8, 2.4 Hz, 1H), 4.25–4.15 (m, 1H), 4.06–3.57 (m, 5H), 3.15 (s, 3H), 3.11–3.01 (m, 1H), 2.80–2.61 (m, 1H), 2.20–1.89 (m, 2H), 1.87–1.77 (m, 1H), 1.55–1.43 (m, 1H), 1.39–0.91 (m, 9H); ESI-MS: (*m/z*) 412.4 [M + H]$^+$, 434.5 [M + Na]$^+$, 410.4 [M − H]$^-$; HPLC method A: t$_r$ = 8.549 min.

tert-Butyl 3-((5-chloro-9*H*-pyrimido[4,5-*b*]indol-4-yl)(methyl)amino)piperidine-1-carboxylate (**6k**)

The title compound was prepared by a two-step procedure. In the first step, **4k** (675.0 mg, 1.72 mmol), 1-Boc-3-(methylamino)piperidine (516.3 mg, 2.41 mmol), and DIPEA (667.3 mg, 5.16 mmol) were reacted in dry DMF (25 mL) according to general procedure B. Purification of a small portion for analytical purposes was performed by flash column chromatography (SiO$_2$; DCM–MeOH gradient elution from 96.5:3.5 to 92.5:7.5). ^{1}H-NMR (300 MHz, CDCl$_3$) δ 8.51 (s, 1H), 8.38 (d, *J* = 7.8 Hz, 1H), 8.08 (d, *J* = 6.6 Hz, 2H), 7.45–7.30 (m, 2H), 7.25 (d, 2H, overlap with CHCl$_3$ signal), 4.60–3.88 (m, 3H), 3.25–2.55 (m, 5H), 2.36 (s, 3H), 2.19–1.62 (m, 4H), 1.42 (s, 9H); ESI-MS: (*m/z*) 592.1 [M + Na]$^+$, 568.1 [M − H]$^-$; HPLC method A: 10.604 min. The crude material obtained from the first step was reacted with K*t*BuO (1.2 g, 10.71 mmol) in HPLC grade THF (45 mL) according to general procedure D (reaction time 2 h). Purification by flash column chromatography (SiO$_2$, DCM–MeOH gradient elution from 96.5:3.5 to 92.5:7.5) gave 379 mg of a beige solid (53% yield over two steps). ^{1}H-NMR (400 MHz, DMSO-*d$_6$*) δ 12.35 (s, 1H), 8.41 (s, 1H), 7.44 (d, *J* = 7.5 Hz, 1H), 7.38 (t, *J* = 7.8 Hz, 1H), 7.28 (d, *J* = 7.5 Hz, 1H), 4.35–3.65 (m, 3H), 3.09–2.87 (m, 4H), 2.84–2.63 (m, 1H), 2.18–1.66 (m, 3H), 1.50–1.09 (m, 10H); ESI-MS: (*m/z*) 438.1 [M + Na]$^+$, 414.1 [M − H]$^-$; HPLC method A: t$_r$ = 9.317 min.

tert-Butyl 3-((7-chloro-2-methyl-9*H*-pyrimido[4,5-*b*]indol-4-yl)(methyl)amino)piperidine-1-carboxylate (**6l**)

The title compound was prepared by a two-step procedure. In the first step, **4l** (535.0 mg, 1.32 mmol), 1-Boc-3-(methylamino)piperidine (423.3 mg, 1.98 mmol), and DIPEA (510.6 mg, 3.95 mmol) were reacted in dry DMF (20 mL) according to general procedure B (reaction time 6.5 h) to afford 750 mg of crude *tert*-butyl-3-((7-chloro-2-methyl-9-tosyl-9*H*-pyrimido[4,5-*b*]indol-4-yl)(methyl)amino)piperidine-1-carboxylate as a beige solid (98% crude yield), used in the next step without further purification. Purification of a small portion for analytical purposes was performed by flash column chromatography (SiO$_2$, petroleum ether–EtOAc gradient elution from 7:3 to 3:7). ^{1}H-NMR (300 MHz, CDCl$_3$) δ 8.52 (d, *J* = 1.8 Hz, 1H), 8.12 (d, *J* = 8.3 Hz, 2H), 7.55 (d, *J* = 8.2 Hz, 1H), 7.35 (dd, *J* = 8.5, 1.9 Hz, 1H), 7.26 (d, *J* = 8.1 Hz, 2H, overlap with CHCl$_3$ signal), 4.45–3.91 (m, 3H), 3.15–2.96 (m, 4H), 2.75–2.59 (m, 4H), 2.37 (s, 3H), 1.98–1.70 (m, 3H), 1.64–1.31 (m, 10H); ESI-MS: (*m/z*) 606.5 [M + Na]$^+$, 582.5 [M − H]$^−$; HPLC method A: t$_r$ = 12.593 min.

The crude material obtained from the first step was reacted with K*t*BuO (874.0 mg, 7.79 mmol) in dry THF (32 mL) according to general procedure D (reaction time 2.5 h). Purification by flash column chromatography (SiO$_2$, DCM–MeOH gradient elution from 97.5:2.5 to 93:7) gave 358 mg of a light yellow solid (75% yield). ^{1}H-NMR (400 MHz, DMSO-*d*$_6$) δ 12.03 (s, 1H), 7.78–7.60 (m, 1H), 7.45 (d, *J* = 1.8 Hz, 1H), 7.26–7.13 (m, 1H), 4.30–3.78 (m, 3H), 3.12 (s, 3H), 3.09–3.01 (m, 1H), 2.80–2.57 (m, 1H), 2.50 (s, 3H, overlap with DMSO-*d*$_5$ signal), 2.08–1.68 (m, 3H), 1.54–0.99 (m, 10H); ^{13}C NMR (101 MHz, DMSO-*d*$_6$) δ 162.5, 159.6, 158.4, 153.9, 137.4, 128.8, 123.3, 120.2, 118.6, 110.8, 95.2, 78.7, 54.5, 46.0 (br), 43.3 (br), 32.5, 27.8, 27.4, 25.8, 24.6; ESI-MS: (*m/z*) 430.5 [M + H]$^+$, 452.5 [M + Na]$^+$; 428.6 [M − H]$^−$; HPLC method A: t$_r$ = 10.332 min.

(4) Detailed Procedures for the Preparation of Enantiopure Intermediates *(R)*-**6c,d** and *(S)*-**6c,d**

tert-Butyl *(R)*-3-((7-chloro-9*H*-pyrimido[4,5-*b*]indol-4-yl)(methyl)amino)piperidine-1-carboxylate (*(R)*-**6c**)

The title compound was prepared by a two-step procedure. In the first step, *(R)*-**5c** (350.0 mg, 0.63 mmol), methyl iodide (134.0 mg, 0.94 mmol), and NaH (37.7 mg of a 60% dispersion in mineral oil, 0.94 mmol) were reacted in dry DMF (15 mL) according to general procedure C (reaction time of 3 h) to afford 346 mg of crude *tert*-butyl *(R)*-3-((7-chloro-9-tosyl-9*H*-pyrimido[4,5-*b*]indol-4-yl) (methyl)amino)piperidine-1-carboxylate as an off-white solid (96% crude yield), used in the next step without further purification. Purification for analytical purposes was performed by flash column chromatography (SiO$_2$, DCM–MeOH gradient elution from 98:2 to 97.5:2.5). ^{1}H-NMR (200 MHz, CDCl$_3$) δ 8.61 (s, 1H), 8.52 (d, *J* = 1.6 Hz, 1H), 8.09 (d, *J* = 8.2 Hz, 2H), 7.60 (d, *J* = 8.6 Hz, 1H), 7.38 (dd, *J* = 8.5, 1.6 Hz, 1H), 7.26 (d, *J* = 8.1 Hz, 2H, overlap with CHCl$_3$ signal), 4.56–3.88 (m, 3H), 3.18–2.94 (m, 4H), 2.79–2.57 (m, 1H), 2.35 (s, 3H), 2.07–1.68 (m, 3H), 1.66–1.51 (m, 1H), 1.40 (s, 9H).; ^{13}C NMR (50 MHz, CDCl$_3$) δ 160.2, 157.3, 154.8, 154.0, 145.8, 136.2, 135.4, 132.8, 129.8, 128.2, 124.6, 123.4, 120.2, 114.7, 101.2, 80.0, 55.7, 46.7, 44.0 (br), 33.8, 28.5, 28.1, 24.8, 21.8; ESI-MS: (*m/z*) 591.8 [M + Na]$^+$, 567.7 [M − H]$^−$; HPLC method A: t$_r$ = 10.548 min.

The crude material obtained from the first step was reacted with K*t*BuO (476.7 mg, 4.25 mmol) in dry THF (19 mL) according to general procedure D (reaction time 1 h). Purification by flash column chromatography (DCM–MeOH gradient elution from 96.5:3.5 to 93:7) gave 183 mg of an off-white solid (73% yield). ^{1}H-NMR (200 MHz, CDCl$_3$) δ 11.91 (br s, 1H), 8.53 (s, 1H), 7.65 (d, *J* = 8.6 Hz, 1H), 7.46 (s, 1H), 7.21 (d, *J* = 8.3 Hz, 1H, overlap with CHCl$_3$ signal), 4.75–3.89 (m, 3H), 3.24 (s, 3H), 3.15–2.95 (m, 1H), 2.82–2.53 (m, 1H), 2.21–1.59 (m, 4H), 1.51 (s, 9H); ^{13}C NMR (50 MHz, CDCl$_3$) δ 160.1, 156.8, 154.9, 152.1, 137.5, 131.1, 123.6, 121.5, 118.7, 111.7, 98.6, 80.0, 55.1, 46.8 (br), 44.0 (br), 33.4, 28.5, 28.2, 24.9; ESI-MS: (*m/z*) 416.0 [M + H]$^+$, 437.9 [M + Na]$^+$, 413.8 [M − H]$^−$; HPLC method A: t$_r$ = 9.052 min.

tert-Butyl *(R)*-3-((7-bromo-9*H*-pyrimido[4,5-*b*]indol-4-yl)(methyl)amino)piperidine-1-carboxylate (*(R)*-**6d**)

The title compound was prepared by a two-step procedure. In the first step, *(R)*-**5d** (400.0 mg, 0.67 mmol), methyl iodide (141.8 mg, 1.0 mmol), and NaH (40.0 mg of a 60% dispersion in mineral

oil, 1.0 mmol) were reacted in dry DMF (14 mL) according to general procedure C (reaction time 2.5 h) to afford 382 mg of crude *tert*-butyl *(R)*-3-((7-bromo-9-tosyl-9*H*-pyrimido[4,5-*b*]indol-4-yl) (methyl)amino)piperidine-1-carboxylate as an off-white solid (93% crude yield), used in the next without further purification. Purification of a small portion for analytical purposes was performed by flash column chromatography (SiO$_2$, hexane–EtOAc 3:2). ^{1}H-NMR (300 MHz, CDCl$_3$) δ 8.68 (s, 1H), 8.62 (s, 1H), 8.10 (d, *J* = 8.4 Hz, 2H), 7.60–7.48 (m, 2H), 7.27 (d, *J* = 8.0 Hz, 2H, overlap with CHCl$_3$ signal), 4.45–3.97 (m, 3H), 3.11 (s, 3H), 3.09–2.98 (m, 1H), 2.75–2.61 (m, 1H), 2.37 (s, 3H), 1.95–1.72 (m, 3H), 1.59–1.31 (m, 10H); ^{13}C NMR (75 MHz, CDCl$_3$) δ 160.41, 157.10, 154.69, 154.23, 145.69, 136.14, 135.26, 129.70, 128.02, 127.23, 123.66, 120.65, 120.32, 117.28, 101.06, 79.80, 55.48, 46.56, 43.99 (br), 33.71 (br), 28.36, 27.93, 24.75, 21.68. ESI-MS: (*m/z*) 635.9 [M + Na]$^+$, 612.1 [M − H]$^−$; HPLC method A: t$_r$ = 11.342 min.

The crude material obtained from the first step was reacted with K*t*BuO (488.0 mg, 4.35 mmol) in dry THF (20 mL) according to general procedure D (reaction time 45 min). Purification by flash column chromatography (SiO$_2$, DCM–MeOH 96:4) gave 175 mg of a white solid (61% yield). ^{1}H-NMR (300 MHz, CDCl$_3$) δ 11.59 (br s, 1H), 8.58 (s, 1H), 7.72–7.62 (m, 2H), 7.40 (dd, *J* = 8.6, 1.8 Hz, 1H), 4.48–4.02 (m, 3H), 3.26 (s, 3H), 3.14–3.00 (m, 1H), 2.77–2.61 (m, 1H), 2.11–1.75 (m, 3H), 1.70–1.54 (m, 1H), 1.43 (s, 9H); ESI-MS: (*m/z*) 482.0 [M + Na]$^+$, 458.2 [M − H]$^−$; HPLC method A: t$_r$ = 9.693 min.

tert-Butyl *(S)*-3-((7-chloro-9*H*-pyrimido[4,5-*b*]indol-4-yl)(methyl)amino)piperidine-1-carboxylate (**(S)-6c**)

The title compound was prepared by a two-step procedure. In the first step, **(S)-5c** (465.0 mg, 0.84 mmol), methyl iodide (178.0 mg, 1.25 mmol), and NaH (50.2 mg of a 60% dispersion in mineral oil, 1.25 mmol) were reacted in dry DMF (15 mL) according to general procedure C (reaction time 3.5 h) to afford 440 mg of crude *tert*-Butyl *(S)*-3-((7-chloro-9-tosyl-9*H*-pyrimido[4,5-*b*]indol-4-yl) (methyl)amino)piperidine-1-carboxylate as a yellow solid (92% crude yield), used in the next step without further purification. ESI-MS: (*m/z*) 591.8 [M + Na]$^+$, 567.7 [M − H]$^−$; HPLC method A: t$_r$ = 11.053 min.

The crude material obtained from the first step was reacted with K*t*BuO (606.2 mg, 5.40 mmol) in dry THF (24 mL) according to general procedure D (reaction time 1 h). Purification by flash column chromatography (SiO$_2$, DCM–MeOH gradient elution from 96.5:3.5 to 92.5:7.5) gave 203 mg of a white solid (63% yield). ^{1}H-NMR (300 MHz, CDCl$_3$) δ 11.71 (br s, 1H), 8.57 (s, 1H), 7.71 (d, *J* = 8.6 Hz, 1H), 7.53 (d, *J* = 1.7 Hz, 1H), 7.26 (dd, *J* = 8.6, 1.9 Hz, 1H, overlap with CHCl$_3$ signal), 4.59–3.97 (m, 3H), 3.27 (s, 3H), 3.16–2.99 (m, 1H), 2.83–2.58 (m, 1H), 2.11–1.54 (m, 4H), 1.43 (s, 9H); ESI-MS: (*m/z*) 437.9 [M + Na]$^+$, 413.8 [M − H]$^−$; HPLC method A: t$_r$ = 9.451 min.

tert-Butyl *(S)*-3-((7-bromo-9*H*-pyrimido[4,5-*b*]indol-4-yl)(methyl)amino)piperidine-1-carboxylate (**(S)-6d**)

The title compound was prepared by a two-step procedure. In the first step, **(S)-5d** (585.0 mg, 0.97 mmol), NaH (58.4 mg of a 60% dispersion in mineral oil, 1.46 mmol), and methyl iodide (207.4 mg, 1.46 mmol) were reacted in dry DMF (10 mL) according to general procedure C (reaction time 3 h) to afford 578 mg of crude *tert*-butyl *(S)*-3-((7-bromo-9-tosyl-9*H*-pyrimido[4,5-*b*]indol-4-yl) (methyl)amino)piperidine-1-carboxylate as a light yellow solid (96% crude yield), used in the next step without further purification.

The crude material obtained from the first step was reacted with K*t*BuO (639.1 mg, 5.70 mmol) in dry THF (25 mL) according to general procedure D (reaction time 2 h). Purification by flash column chromatography (SiO$_2$, DCM–MeOH 96:4) gave 214 mg of a white solid (57% yield). ^{1}H-NMR (400 MHz, CDCl$_3$) δ 12.09 (s, 1H), 8.56 (s, 1H), 7.66 (d, *J* = 1.6 Hz, 1H), 7.64 (d, *J* = 8.6 Hz, 1H), 7.38 (dd, *J* = 8.6, 1.8 Hz, 1H), 4.61–3.96 (m, 1H), 3.26 (s, 1H), 3.11–3.01 (m, 1H), 2.78–2.61 (m, 1H), 2.09–1.75 (m, 1H), 1.72–1.55 (m, 1H), 1.44 (s, 1H).

(5) Detailed Procedures for the Preparation of Intermediates **7a–l**

N-methyl-*N*-(piperidin-3-yl)-9*H*-pyrimido[4,5-*b*]indol-4-amine (**7a**)

The title compound was prepared from **6a** (60.0 mg, 0.16 mmol) in dry DCM (1 mL) and TFA (0.2 mL) according to general procedure E (reaction time 1.5 h); 36 mg of a light brown solid was yielded (81% crude yield) and used in the next step without further purification. ^{1}H-NMR (400 MHz, MeOD) δ 8.36 (s, 1H), 7.84 (d, *J* = 8.0 Hz, 1H), 7.52 (d, *J* = 8.0 Hz, 1H), 7.41 (td, *J* = 7.7, 1.0 Hz, 1H), 7.34–7.27 (m, 1H), 3.30–3.23 (m, 4H), 3.14–3.07 (m, 1H), 3.07–3.00 (m, 1H), 2.72–2.63 (m, 1H), 2.20–1.94 (m, 3H), 1.83–1.70 (m, 1H); ESI-MS: (*m/z*) 282.3 [M + H]$^+$, 280.3 [M − H]$^−$; HPLC method A: t_r = 2.232 min.

7-Fluoro-*N*-methyl-*N*-(piperidin-3-yl)-9*H*-pyrimido[4,5-*b*]indol-4-amine (**7b**)

The title compound was prepared from **6b** (170.0 mg, 0.43 mmol) in dry DCM (5 mL) and TFA (1 mL) according to general procedure E (reaction time 1.5 h); 119 mg of a beige solid was yielded (93% crude yield) and used in the next step without further purification. ^{1}H-NMR (200 MHz, MeOD) δ 8.33 (s, 1H), 7.78 (dd, *J* = 8.8, 5.2 Hz, 1H), 7.22 (dd, *J* = 9.3, 2.4 Hz, 1H), 7.06 (td, *J* = 9.3, 2.5 Hz, 1H), 4.54–4.37 (m, 1H), 3.24 (s, 3H), 3.17–2.83 (m, 3H), 2.62–2.45 (m, 1H), 2.16–1.55 (m, 4H); ESI-MS: (*m/z*) 300.3 [M + H]$^+$, 298.3 [M − H]$^−$; HPLC method A: t_r = 3.036 min.

7-Chloro-*N*-methyl-*N*-(piperidin-3-yl)-9*H*-pyrimido[4,5-*b*]indol-4-amine (**7c**)

The title compound was prepared as described previously [5].

7-Bromo-*N*-methyl-*N*-(piperidin-3-yl)-9*H*-pyrimido[4,5-*b*]indol-4-amine (**7d**)

6d (425.0 mg, 0.92 mmol) was stirred in dry DCM (9 mL) and TFA (1.5 mL) at rt for 1 h. The mixture was concentrated under reduced pressure. Residual TFA was neutralized by addition of saturated NaHCO$_3$ solution, resulting in a precipitate which was filtered off and washed with saturated NaHCO$_3$ solution and demineralized water and was then dried over P$_2$O$_5$ in vacuo; 285 mg of an off-white solid was yielded (86% crude yield) and used in the next step without further purification. ^{1}H-NMR (300 MHz, MeOD) δ 8.35 (s, 1H), 7.70 (d, *J* = 8.6 Hz, 1H), 7.65 (d, *J* = 1.7 Hz, 1H), 7.40 (dd, *J* = 8.6, 1.9 Hz, 1H), 4.55–4.37 (m, 1H), 3.24 (s, 3H), 3.15–3.06 (m, 1H), 3.02–2.95 (m, 1H), 2.95–2.85 (m, 1H), 2.61–2.48 (m, 1H), 2.15–1.84 (m, 3H), 1.78–1.60 (m, 1H); ^{13}C NMR (75 MHz, DMSO-*d$_6$*) δ 159.6, 157.3, 153.8, 137.7, 124.1, 123.1, 118.9, 117.2, 113.7, 97.1, 55.9, 48.7, 45.5, 32.7, 28.3, 26.5; ESI-MS: (*m/z*) 360.1 [M + H]$^+$, 358.1 [M − H]$^−$; HPLC method A: t_r = 4.033 min.

7-Iodo-*N*-methyl-*N*-(piperidin-3-yl)-9*H*-pyrimido[4,5-*b*]indol-4-amine (**7e**)

6e (240.0 mg, 0.473 mmol) was suspended in dry DCM (7 mL), and TFA was added (1.5 mL). The mixture was stirred at rt for 30 min and then concentrated under reduced pressure. Residual TFA was neutralized by addition of saturated NaHCO$_3$ solution (30 mL), which resulted in a precipitate. The precipitate was filtered off, washed with saturated NaHCO$_3$ solution and demineralized water, and dried over P$_2$O$_5$ in vacuo; 199 mg of a beige solid was yielded (>100% crude yield) and used in the next step without further purification. ^{1}H-NMR (300 MHz, MeOD) δ 8.35 (s, 1H), 7.86 (s, 1H), 7.65–7.52 (m, 2H), 4.55–4.40 (m, 1H), 3.24 (s, 3H), 3.14–3.05 (m, 1H), 3.02–2.84 (m, 2H), 2.60–2.47 (m, 1H), 2.15–1.84 (m, 3H), 1.77–1.59 (m, 1H); ESI-MS: (*m/z*) 408.3 [M + H]$^+$, 406.3 [M − H]$^−$; HPLC method A: t_r = 4.563 min.

7-methoxy-*N*-methyl-*N*-(piperidin-3-yl)-9*H*-pyrimido[4,5-*b*]indol-4-amine (**7f**)

TFA (0.4 mL) was added to a solution of **6f** (126.0 mg, 0.31 mmol) in dry DCM (10 mL). The mixture was stirred at rt for 1.5 h and then concentrated under reduced pressure. Saturated NaHCO$_3$ solution was added to the residue, and the mixture was extracted with EtOAc (3 × 20 mL). Combined organic layers were dried over Na$_2$SO$_4$ and evaporated to dryness to afford 90 mg (95% crude yield). ^{1}H-NMR (300 MHz, DMSO-*d$_6$*) δ 11.95 (s, 1H), 8.33 (s, 1H), 7.68 (d, *J* = 8.8 Hz, 1H), 6.97 (d, *J* = 2.4 Hz, 1H), 6.88 (dd, *J* = 8.8, 2.4 Hz, 1H), 4.40–4.26 (m, 1H), 3.84 (s, 3H), 3.13 (s, 3H), 3.06–2.80 (m, 3H), 2.51–2.41 (m, 1H, overlap with DMSO-*d$_5$* signal), 2.00–1.71 (m, 3H), 1.60–1.39 (m, 1H); ESI-MS: (*m/z*) 312.0 [M + H]$^+$, 310.1 [M − H]$^−$; HPLC method B: t_r = 2.684 min.

N-Methyl-*N*-(piperidin-3-yl)-7-(trifluoromethyl)-9*H*-pyrimido[4,5-*b*]indol-4-amine (**7g**)

TFA (1 mL) was added to a solution of **6g** (237.0 mg, 0.53 mmol) in dry DCM (10 mL). The mixture was stirred at rt for 2 h and then concentrated under reduced pressure. Saturated NaHCO₃ solution was added to the residue, and the mixture was then extracted with EtOAc (3 × 20 mL). Combined organic layers were dried over Na₂SO₄ and evaporated to dryness; 194 mg was yielded (100% crude yield) and used in the next step without further purification. ¹H-NMR (300 MHz, DMSO-d_6) δ 12.30 (br s, 1H), 8.44 (s, 1H), 8.01 (d, *J* = 8.5 Hz, 1H), 7.74 (s, 1H), 7.56 (dd, *J* = 8.5, 1.2 Hz, 1H), 4.54–4.40 (m, 1H), 3.22 (s, 3H), 3.12–3.05 (m, 1H), 3.01–2.86 (m, 2H), 2.58–2.49 (m, 1H, overlap with DMSO-d_5 signal), 2.01–1.75 (m, 3H), 1.66–1.49 (m, 1H); HPLC method B: t_r = 4.956 min.

6-Chloro-*N*-methyl-*N*-(piperidin-3-yl)-9*H*-pyrimido[4,5-*b*]indol-4-amine (**7h**)

The title compound was prepared from **6h** (215.0 mg, 0.52 mmol) in dry DCM (5.6 mL) and TFA (1.1 mL) according to general procedure E (reaction time 1 h); 163 mg of a yellow solid (100% crude yield) was yielded, used in the next step without further purification. ¹H-NMR (300 MHz, MeOD) δ 8.35 (s, 1H), 7.76 (d, *J* = 1.8 Hz, 1H), 7.48 (d, *J* = 8.6 Hz, 1H), 7.38 (dd, *J* = 8.6, 2.0 Hz, 1H), 4.54–4.39 (m, 1H), 3.25 (s, 3H), 3.11–2.95 (m, 2H), 2.95–2.85 (m, 1H), 2.63–2.49 (m, 1H), 2.23–1.88 (m, 3H), 1.83–1.65 (m, 1H); ¹³C NMR (101 MHz, DMSO-d_6) δ 159.6, 157.5, 153.9, 135.1, 124.6, 124.3, 121.6, 120.9, 112.5, 96.8, 55.8, 48.8, 45.5, 32.5, 28.4, 26.3; ESI-MS: (*m/z*) 316.1 [M + H]⁺, 314.0 [M − H]⁻; HPLC method A: t_r = 4.102 min.

6-Bromo-*N*-methyl-*N*-(piperidin-3-yl)-9*H*-pyrimido[4,5-*b*]indol-4-amine (**7i**)

The title compound was prepared from **6i** in dry DCM (6.3 mL) and TFA (1 mL) according to general procedure E (reaction time 1 h). Purification by flash column chromatography (SiO₂, DCM–(2N NH₃ in MeOH) 9:1) gave 218 mg of a beige solid (93% yield). ¹H-NMR (300 MHz, MeOD) δ 8.35 (s, 1H), 7.91 (d, *J* = 1.6 Hz, 1H), 7.52 (dd, *J* = 8.6, 1.8 Hz, 1H), 7.43 (d, *J* = 8.6 Hz, 1H), 4.51–4.40 (m, 1H), 3.24 (s, 3H), 3.08–2.95 (m, 2H), 2.94–2.85 (m, 1H), 2.61–2.48 (m, 1H), 2.22–1.89 (m, 3H), 1.84–1.66 (m, 1H); ¹³C NMR (75 MHz, DMSO-d_6) δ 159.6, 157.4, 154.0, 135.4, 127.1, 124.6, 121.6, 113.1, 112.5, 96.7, 56.0, 48.9, 45.5, 32.5, 28.6, 26.5; ESI-MS: (*m/z*) 360.1 [M + H]⁺, 358.1 [M − H]⁻; HPLC method A: t_r = 4.058 min.

6-Methoxy-*N*-methyl-*N*-(piperidin-3-yl)-9*H*-pyrimido[4,5-*b*]indol-4-amine (**7j**)

The title compound was prepared from **6j** (325.0 mg, 0.78 mmol) in dry DCM (10 mL) and TFA (2 mL) according to general procedure E (reaction time 2 h); 207 mg of a beige solid (84% yield) was yielded. ¹H-NMR (200 MHz, MeOD) δ 8.32 (s, 1H), 7.43 (d, *J* = 8.8 Hz, 1H), 7.29 (d, *J* = 2.4 Hz, 1H), 7.07 (dd, *J* = 8.9, 2.3 Hz, 1H), 4.48–4.29 (m, 1H), 3.89 (s, 3H), 3.22 (s, 3H), 3.13–2.81 (m, 3H), 2.60–2.44 (m, 1H), 2.23–1.84 (m, 3H), 1.82–1.58 (m, 1H); ESI-MS: (*m/z*) 312.2 [M + H]⁺, 310.2 [M − H]⁻; HPLC method A: t_r = 2.084 min.

5-Chloro-*N*-methyl-*N*-(piperidin-3-yl)-9*H*-pyrimido[4,5-*b*]indol-4-amine (**7k**)

The title compound was prepared from **6k** (340.0 mg, 0.82 mmol) in dry DCM (9 mL) and TFA (1.8 mL) according to general procedure E (reaction time 2 h); 244 mg of a beige solid (95% crude yield) was yielded, used in the next step without further purification. ¹H-NMR (300 MHz, MeOD) δ 8.31 (s, 1H), 7.43 (dd, *J* = 7.9, 1.2 Hz, 1H), 7.35 (t, *J* = 7.8 Hz, 1H), 7.26 (dd, *J* = 7.7, 1.2 Hz, 1H), 4.52–4.33 (m, 1H), 3.19–2.90 (m, 5H), 2.89–2.68 (m, 1H), 2.57–2.41 (m, 1H), 2.20–1.97 (m, 1H), 1.96–1.74 (m, 2H), 1.73–1.56 (m, 1H); ESI-MS: (*m/z*) 316.1 [M + H]⁺, 314.1 [M − H]⁻; HPLC method A: t_r = 3.814 min.

7-Chloro-*N*,2-dimethyl-*N*-(piperidin-3-yl)-9*H*-pyrimido[4,5-*b*]indol-4-amine (**7l**)

The title compound was prepared from **6l** (310.0 mg, 0.72 mmol) in TFA (2 mL) and dry DCM (10 mL) according to general procedure E (reaction time 2.5 h); 239 mg of a yellow solid (100% crude yield) was yielded, used in the next step without further purification. ¹H-NMR (300 MHz, MeOD)

δ 7.70 (d, *J* = 8.6 Hz, 1H), 7.46 (d, *J* = 1.9 Hz, 1H), 7.22 (dd, *J* = 8.6, 2.0 Hz, 1H), 4.57–4.44 (m, 1H), 3.23 (s, 3H), 3.15–3.06 (m, 1H), 3.02–2.93 (m, 1H), 2.93–2.84 (m, 1H), 2.59–2.47 (m, 4H), 2.13–1.84 (m, 3H), 1.77–1.59 (m, 1H); ^{13}C NMR (101 MHz, DMSO-d_6) δ 162.5, 159.6, 158.4, 137.3, 128.6, 123.3, 120.2, 118.8, 110.7, 94.9, 55.8, 48.8, 45.5, 32.4, 28.3, 26.4, 25.9; ESI-MS: (*m/z*) 330.1 [M + H]$^+$, 328.1 [M − H]$^-$; HPLC method A: t_r = 4.602 min.

(6) Detailed Procedures for the Preparation of Enantiopure Intermediates *(R)*-7c,d and *(S)*-7c,d

(R)-7-Chloro-*N*-methyl-*N*-(piperidin-3-yl)-9*H*-pyrimido[4,5-*b*]indol-4-amine (*(R)*-7c)

The title compound was prepared from *(R)*-6c (160.0 mg, 0.39 mmol) in dry DCM (5 mL) and TFA (1 mL) according to general procedure E (reaction time 45 min); 120 mg of a yellow solid (99% crude yield) was yielded, used in the next step without further purification. ^{1}H-NMR (400 MHz, MeOD) δ 8.35 (s, 1H), 7.78 (d, *J* = 8.6 Hz, 1H), 7.50 (d, *J* = 1.9 Hz, 1H), 7.28 (dd, *J* = 8.6, 2.0 Hz, 1H), 4.56–4.47 (m, 1H), 3.26 (s, 3H), 3.20–3.13 (m, 1H), 3.06–3.00 (m, 1H), 2.99–2.92 (m, 1H), 2.64–2.55 (m, 1H), 2.16–1.90 (m, 3H), 1.78–1.65 (m, 1H); ESI-MS: (*m/z*) 316.0 [M + H]$^+$, 338.0 [M + Na]$^+$, 313.9 [M − H]$^-$; HPLC method A: t_r = 3.411 min.

(R)-7-Bromo-*N*-methyl-*N*-(piperidin-3-yl)-9*H*-pyrimido[4,5-*b*]indol-4-amine (*(R)*-7d)

The title compound was prepared from *(R)*-6d (175.0 mg, 0.38 mmol) in dry DCM (5 mL) and TFA (1 mL) according to general procedure E (reaction time 2.5 h); 135 mg of a beige solid (99% crude yield) was yielded, used in the next step without further purification. ^{1}H-NMR (300 MHz, MeOD) δ 8.35 (s, 1H), 7.70 (d, *J* = 8.6 Hz, 1H), 7.65 (d, *J* = 1.8 Hz, 1H), 7.40 (dd, *J* = 8.6, 1.9 Hz, 1H), 4.54–4.41 (m, 1H), 3.24 (s, 3H), 3.15–3.06 (m, 1H), 3.02–2.95 (m, 1H), 2.94–2.84 (m, 1H), 2.61–2.48 (m, 1H), 2.15–1.85 (m, 3H), 1.77–1.60 (m, 1H); ESI-MS: (*m/z*) 360.0 [M + H]$^+$, 358.1 [M − H]$^-$; HPLC method A: t_r = 3.985 min.

(S)-7-Chloro-*N*-methyl-*N*-(piperidin-3-yl)-9*H*-pyrimido[4,5-*b*]indol-4-amine (*(S)*-7c)

The title compound was prepared from *(S)*-6c (180.0 mg, 0.43 mmol) in dry DCM (5 mL) and TFA (1 mL) according to general procedure E (reaction time 1.5 h); 142 mg of a beige solid (>100% crude yield) was yielded, used in the next step without further purification. ^{1}H-NMR (300 MHz, MeOD) δ 8.34 (s, 1H), 7.76 (d, *J* = 8.6 Hz, 1H), 7.49 (d, *J* = 1.9 Hz, 1H), 7.27 (dd, *J* = 8.6, 2.0 Hz, 1H), 4.58–4.41 (m, 1H), 3.25 (s, 3H), 3.19–3.09 (m, 1H), 3.05–2.97 (m, 1H), 2.97–2.86 (m, 1H), 2.64–2.50 (m, 1H), 2.19–1.83 (m, 3H), 1.80–1.59 (m, 1H); ESI-MS: (*m/z*) 316.0 [M + H]$^+$, 338.0 [M + Na]$^+$, 313.9 [M − H]$^-$; HPLC method A: t_r = 3.897 min.

(S)-7-Bromo-*N*-methyl-*N*-(piperidin-3-yl)-9*H*-pyrimido[4,5-*b*]indol-4-amine (*(S)*-7d)

The title compound was prepared from *(S)*-6d (190.0 mg, 0.41 mmol) in dry DCM (5 mL) and TFA (1 mL) according to general procedure E (reaction time 1 h); 141 mg of a beige solid (95% crude yield) was yielded, used in the next step without further purification. ^{1}H-NMR (400 MHz, MeOD) δ 8.35 (s, 1H), 7.69 (d, *J* = 8.6 Hz, 1H), 7.65 (d, *J* = 1.8 Hz, 1H), 7.40 (dd, *J* = 8.6, 1.9 Hz, 1H), 4.53–4.43 (m, 1H), 3.24 (s, 3H), 3.14–3.08 (m, 1H), 3.02–2.95 (m, 1H), 2.95–2.87 (m, 1H), 2.59–2.50 (m, 1H), 2.12–1.86 (m, 3H), 1.75–1.62 (m, 1H); ESI-MS: (*m/z*) 360.2 [M + H]$^+$, 358.2 [M − H]$^-$; HPLC method A: t_r = 4.025 min.

(7) Detailed Procedures for the Preparation of Final Compounds **8–41**

(3-((7-Chloro-9*H*-pyrimido[4,5-*b*]indol-4-yl)(methyl)amino)piperidin-1-yl)(furan-3-yl)methanone (**8**)

The title compound was prepared from **7c** (64.0 mg, 0.20 mmol), 3-furoic acid (27.3 mg, 0.24 mmol), PyBOP (130.8 mg, 0.24 mmol), and DIPEA (78.6 mg, 0.61 mmol) in dry DCM (total amount 10 mL) according to general procedure F (reaction time 1.5 h). Purification by flash column chromatography (SiO$_2$, DCM–MeOH gradient elution from 96.5:3.5 to 93.5:6.5) gave 50 mg of a white solid (60% yield). ^{1}H-NMR (400 MHz, DMSO-d_6) δ 12.25 (s, 1H), 8.38 (s, 1H), 8.26–7.97 (m, 1H), 7.92–7.77 (m, 1H),

7.73 (t, *J* = 1.7 Hz, 1H), 7.48 (d, *J* = 2.0 Hz, 1H), 7.24 (dd, *J* = 8.6, 2.1 Hz, 1H), 6.85–6.58 (m, 1H), 4.81–3.79 (m, 3H), 3.30–2.56 (m, 5H), 2.15–1.94 (m, 2H), 1.94–1.74 (m, 1H), 1.63–1.47 (m, 1H); ESI-MS: (m/z) 410.0 [M + H]$^+$, 432.0 [M + Na]$^+$, 407.9 [M − H]$^−$; HPLC method A: t$_r$ = 7.624 min.

Ethyl 3-(3-((7-chloro-9*H*-pyrimido[4,5-*b*]indol-4-yl)(methyl)amino)piperidin-1-yl)-3-oxopropanoate (**9**)

The title compound was prepared from **7c** (70.0 mg, 0.22 mmol), ethyl potassium malonate (45.3 mg, 0.27 mmol), PyBOP (138.4 mg, 0.27 mmol), and DIPEA (86.0 mg, 0.67 mmol) in dry DCM (total amount 10 mL) according to general procedure F. Additional ethyl potassium malonate (5.7 mg, 0.03 mmol) and PyBOP (17.3 mg, 0.03 mmol) were added after a reaction time of 2.5 h, and then stirring continued for 1 h. Purification twice by flash column chromatography (SiO$_2$, DCM–MeOH gradient elution from 97.5:2.5 to 93.5:6.5 and SiO$_2$, DCM–EtOH gradient elution from 95:5 to 93:7) gave 50 mg of a white solid (53% yield). ^{1}H-NMR shows a 3:2 mixture of amide bond rotamers. ^{1}H-NMR (400 MHz, DMSO-*d$_6$*) δ 12.32–12.14 (m, 1H), 8.46–8.34 (m, 1H), 7.86–7.77 (m, 1H), 7.52–7.44 (m, 1H), 7.32–7.16 (m, 1H), 4.61–4.50 (m, 0.6H), 4.42–4.34 (m, 0.4H), 4.33–4.16 (m, 1H), 4.10–3.95 (m, 2H), 3.95–3.90 (m, 0.4H), 3.79–3.68 (m, 0.6H), 3.64–3.47 (m, 2H), 3.33–3.28 (m, 0.4H, overlap with water signal), 3.28–3.15 (m, 3H), 3.08–2.95 (m, 1.2H), 2.63–2.54 (m, 0.4H), 2.10–1.74 (m, 3H), 1.58–1.40 (m, 1H), 1.17–1.08 (m, 3H); ^{13}C NMR (101 MHz, DMSO-*d$_6$*) δ 167.7, 167.6, 164.5, 164.4, 159.43, 159.40, 157.51, 157.48, 153.7, 153.6, 137.44, 137.40, 129.3, 124.03, 123.97, 120.5, 120.4, 118.4, 118.3, 110.83, 110.81, 97.4, 97.2, 60.5, 60.4, 54.7, 54.5, 47.6, 45.7, 44.0, 41.5, 40.9, 40.8, 33.9, 32.6, 27.2, 27.1, 24.8, 24.3, 13.89, 13.86; ESI-MS: (*m/z*) 430.0 [M + H]$^+$, 451.9 [M + Na]$^+$, 427.8 [M − H]$^−$; HPLC method A: t$_r$ = 7.274 min.

(3-((7-Chloro-9*H*-pyrimido[4,5-*b*]indol-4-yl)(methyl)amino)piperidin-1-yl)(4-(dimethylamino)phenyl) methanone (**10**)

The title compound was prepared from **7c** (60.0 mg, 0.19 mmol), 4-(dimethylamino) benzoic acid (37.7 mg, 0.22 mmol), PyBOP (118.6 mg, 0.22 mmol), and DIPEA (73.7 mg, 0.57 mmol) in dry DCM (total amount 7 mL) according to general procedure F (reaction time 40 min). Purification by flash column chromatography (SiO$_2$, DCM–MeOH gradient elution from 95.5:4.5 to 93.5:6.5) gave 70 mg of an off-white solid (80% yield). ^{1}H-NMR (400 MHz, DMSO-*d$_6$*) δ 12.25 (s, 1H), 8.39 (s, 1H), 7.80 (d, *J* = 8.0 Hz, 1H), 7.50 (d, *J* = 1.9 Hz, 1H), 7.25 (dd, *J* = 8.6, 2.0 Hz, 1H), 7.17 (d, *J* = 7.8 Hz, 2H), 6.60 (d, *J* = 7.4 Hz, 2H), 4.50–3.85 (m, 3H), 3.28–3.13 (m, 4H), 3.04–2.78 (m, 7H), 2.12–1.99 (m, 2H), 1.93–1.76 (m, 1H), 1.65–1.46 (m, 1H); ESI-MS: (*m/z*) 463.9 [M + H]$^+$, 485.9 [M + Na]$^+$, 461.8 [M − H]$^−$; HPLC method A: t$_r$ = 8.928 min.

1-(3-((7-Chloro-9*H*-pyrimido[4,5-*b*]indol-4-yl)(methyl)amino)piperidin-1-yl)butan-1-one (**11**)

The title compound was prepared from **7c** (60.0 mg, 0.19 mmol), butyric acid (20.9 mg, 0.24 mmol), TBTU (76.3 mg, 0.24 mmol), and DIPEA (73.7 mg, 0.57 mmol) in dry DCM (total amount 10 mL) according to general procedure F (reaction time 1 h). Purification by flash column chromatography (SiO$_2$, DCM–MeOH 94.5:5.5) gave 54 mg of a white solid (74% yield). ^{1}H-NMR shows a 5:4 mixture of amide bond rotamers. ^{1}H-NMR (400 MHz, CDCl$_3$) δ 12.42 (br s, 1H), 8.58–8.42 (m, 1H), 7.74–7.59 (m, 1H), 7.51–7.38 (m, 1H), 7.25–7.16 (m, 1H), 5.05–4.86 (m, 0.45H), 4.81–4.65 (m, 0.55H), 4.53–4.29 (m, 1H), 4.28–4.16 (m, 0.55H), 3.97–3.81 (m, 0.45H), 3.37–3.19 (m, 3H), 3.19–3.10 (m, 0.55H), 3.05–2.89 (m, 0.9H), 2.57–2.30 (m, 2.55H), 2.22–1.85 (m, 3H), 1.82–1.53 (m, 3H), 0.98 (t, *J* = 7.3 Hz, 3H); ^{13}C NMR (101 MHz, CDCl$_3$) δ 172.4, 171.9, 160.1, 157.7, 157.3, 152.8, 152.6, 137.6, 137.5, 131.2, 131.1, 123.8, 123.7, 121.5, 121.4, 118.7, 111.7, 111.5, 98.8, 98.5, 55.3, 55.2, 47.8, 46.0, 45.0, 42.2, 35.7, 34.4, 33.4, 28.8, 28.0, 25.6, 25.0, 19.0, 14.3, 14.2; ESI-MS: (*m/z*) 408.3 [M + Na]$^+$, 384.3 [M − H]$^−$; HPLC method A: t$_r$ = 8.285 min.

1-(3-((7-Chloro-9*H*-pyrimido[4,5-*b*]indol-4-yl)(methyl)amino)piperidin-1-yl)-3-methylbutan-1-one (**12**)

The title compound was prepared from **7c** (60.0 mg, 0.19 mmol), isovaleric acid (22.3 mg, 0.22 mmol), TBTU (76.3 mg, 0.24 mmol), and DIPEA (73.7 mg, 0.57 mmol) in dry DCM (total amount 10 mL) according to general procedure F (reaction time 1 h). Purification by flash column chromatography

(SiO$_2$, DCM–MeOH 95:5) gave 61 mg of a white solid (80% yield). ^{1}H-NMR shows a 5:4 mixture of amide bond rotamers. ^{1}H-NMR (400 MHz, CDCl$_3$) δ 12.30 (br s, 1H), 8.56–8.47 (m, 1H), 7.73–7.63 (m, 1H), 7.50–7.41 (m, 1H), 7.25–7.19 (m, 1H), 5.04–4.93 (m, 0.45H), 4.80–4.70 (m, 0.55H), 4.52–4.29 (m, 1H), 4.28–4.20 (m, 0.55H), 3.97–3.85 (m, 0.45H), 3.34–3.20 (m, 3H), 3.18–3.10 (m, 0.55H), 3.05–2.91 (m, 0.9H), 2.55–2.46 (m, 0.55H), 2.45–2.24 (m, 2H), 2.23–1.86 (m, 4H), 1.75–1.54 (m, 1H), 1.01–0.93 (m, 6H); ^{13}C NMR (101 MHz, CDCl$_3$) δ 171.9, 171.4, 160.1, 157.7, 157.3, 152.8, 152.6, 137.6, 137.5, 131.22, 131.15, 123.8, 123.7, 121.6, 121.4, 118.7, 111.7, 111.5, 98.9, 98.6, 55.4, 55.3, 48.0, 46.2, 45.1, 42.5, 42.3, 34.4, 33.4, 28.8, 28.0, 26.0, 25.9, 25.7, 25.0, 22.93, 22.89; ESI-MS: (*m/z*) 422.3 [M + Na]$^+$, 398.3 [M − H]$^-$; HPLC method A: t$_r$ = 8.646 min.

1-(3-((7-Chloro-9*H*-pyrimido[4,5-*b*]indol-4-yl)(methyl)amino)piperidin-1-yl)-3-(dimethylamino) propan-1-one (**13**)

The title compound was prepared from **7c** (75.0 mg, 0.24 mmol), 3-(dimethylamino) propionic acid hydrochloride (47.4 mg, 0.31 mmol), PyBOP (160.7 mg, 0.31 mmol), and TEA (72.1 mg, 0.71 mmol) in dry DCM (total amount 10 mL) according to general procedure F (reaction time 1.5 h). During the extractive work-up the organic layer was not washed with saturated NH$_4$Cl solution due to the basic amino function of the introduced substituent. Purification twice by flash column chromatography (SiO$_2$, DCM–(2N NH$_3$ in MeOH) gradient elution from 95:5 to 9:1 and SiO$_2$, DCM:(2N NH$_3$ in MeOH) gradient elution from 92.5:7.5 to 9:1) gave 60 mg of a white solid (61% yield). ^{1}H-NMR shows a 3:2 mixture of amide bond rotamers. ^{1}H-NMR (400 MHz, CDCl$_3$) δ 13.05–12.30 (m, 1H), 8.52–8.41 (m, 1H), 7.65–7.56 (m, 1H), 7.44–7.36 (m, 1H), 7.21–7.11 (m, 1H), 4.96–4.83 (m, 0.4H), 4.76–4.62 (m, 0.6H), 4.47–4.20 (m, 1.6H), 3.95–3.84 (m, 0.4H), 3.32–3.17 (m, 3H), 3.17–3.08 (m, 0.6H), 3.03–2.95 (m, 0.4H), 2.93–2.86 (m, 0.4H), 2.85–2.57 (m, 4H), 2.55–2.45 (m, 0.6H), 2.32 (s, 6H), 2.18–1.83 (m, 3H), 1.73–1.52 (m, 1H); ^{13}C NMR (101 MHz, CDCl$_3$) δ 170.7, 170.2, 160.1, 160.0, 157.8, 157.7, 153.0, 137.7, 137.6, 131.0, 130.9, 123.7, 123.6, 121.22, 121.15, 118.7, 118.6, 111.6, 111.4, 98.8, 98.5, 55.3, 55.2, 54.9, 47.6, 46.0, 45.4, 45.3, 44.9, 42.3, 34.4, 33.4, 31.8, 31.5, 28.7, 27.9, 25.5, 24.8; ESI-MS: (*m/z*) 415.4 [M + H]$^+$, 413.2 [M − H]$^-$; HPLC *method A*: t$_r$ = 4.833 min.

1-(3-((7-Chloro-9*H*-pyrimido[4,5-*b*]indol-4-yl)(methyl)amino)piperidin-1-yl)ethan-1-one (**14**)

The title compound was prepared from **7c** (70.0 mg, 0.22 mmol), acetic acid (20.0 mg, 0.33 mmol), PyBOP (144.4 mg, 0.28 mmol), and DIPEA (86.1 mg, 0.67 mmol) in dry DCM (total amount 12 mL) according to general procedure F (reaction time 1.5 h). Purification twice by flash column chromatography (SiO$_2$, DCM–MeOH gradient elution from 96:4 to 93.5:6.5 and SiO$_2$, EtOAc/MeOH 9:1) gave 44 mg of an off-white solid (55% yield). ^{1}H-NMR shows a 5:4 mixture of amide bond rotamers. ^{1}H-NMR (300 MHz, DMSO-*d$_6$*) δ 12.30–12.14 (m, 1H), 8.41 (s, 1H), 7.87–7.78 (m, 1H), 7.51–7.44 (m, 1H), 7.30–7.17 (m, 1H), 4.57–4.47 (m, 0.55H), 4.43–4.12 (m, 1.45H), 4.07–3.95 (m, 0.45H), 3.84–3.72 (m, 0.55H), 3.33–3.16 (m, 3.45H), 3.07–2.85 (m, 1.1H), 2.57–2.44 (m, 0.45H, overlap with DMSO-*d$_5$* signal), 2.10–1.86 (m, 5H), 1.86–1.73 (m, 1H), 1.58–1.35 (m, 1H); ^{13}C NMR (101 MHz, DMSO-*d$_6$*) δ 168.3, 168.2, 159.5, 159.4, 157.50, 157.47, 153.7, 153.6, 137.4, 129.2, 124.0, 123.9, 120.4, 120.3, 118.4, 118.3, 110.8, 97.4, 97.1, 54.7, 54.5, 47.6, 45.7, 43.6, 41.0, 33.8, 32.6, 27.3, 27.1, 25.1, 24.4, 21.3; ESI-MS: (*m/z*) 380.4 [M + Na]$^+$, 356.5 [M − H]$^-$; HPLC method A: t$_r$ = 6.993 min.

1-(3-((7-Chloro-9*H*-pyrimido[4,5-*b*]indol-4-yl)(methyl)amino)piperidin-1-yl)-2-cyclopropylethan-1-one (**15**)

The title compound was prepared from **7c** (50.0 mg, 0.16 mmol), 2-cyclopropylacetic acid (19.8 mg, 0.20 mmol), TBTU (63.6 mg, 0.20 mmol), and DIPEA (61.4 mg, 0.48 mmol) in dry DCM (total amount 10 mL) according to general procedure F (reaction time 1.5 h). Purification by flash column chromatography (SiO$_2$, DCM–MeOH gradient elution from 96:4 to 93.5:6.5) gave 52 mg of a beige solid (83% yield). ^{1}H-NMR shows a 5:4 mixture of amide bond rotamers. ^{1}H-NMR (300 MHz, CDCl$_3$) δ 12.20 (br s, 1H), 8.72–8.27 (m, 1H), 7.79–7.59 (m, 1H), 7.56–7.39 (m, 1H), 7.29–7.17 (m, 1H, overlap with CHCl$_3$ signal), 5.07–4.88 (m, 0.45H), 4.81–4.66 (m, 0.55H), 4.58–4.30 (m, 1H), 4.27–4.12

(m, 0.55H), 3.94–3.79 (m, 0.45H), 3.38–2.91 (m, 4.55H), 2.60–2.29 (m, 2.45H), 2.25–1.83 (m, 3H), 1.81–1.52 (m, 1H), 1.18–0.96 (m, 1H), 0.65–0.40 (m, 2H), 0.34–0.08 (m, 2H); ^{13}C NMR (101 MHz, CDCl$_3$) δ 172.0, 171.5, 160.0, 157.6, 157.0, 152.7, 152.4, 137.6, 131.2, 123.9, 123.6, 121.6, 121.4, 118.7, 111.7, 98.8, 55.3, 55.2, 47.9, 46.2, 45.1, 42.2, 38.9, 38.8, 34.4, 33.5, 28.8, 28.0, 25.6, 24.9, 7.5, 4.70, 4.66; ESI-MS: (*m/z*) 398.3 [M + H]$^+$, 420.3 [M + Na]$^+$, 396.3 [M − H]$^−$; HPLC method A: t$_r$ = 8.031 min.

1-(3-((7-Chloro-9*H*-pyrimido[4,5-*b*]indol-4-yl)(methyl)amino)piperidin-1-yl)propan-1-one (**16**)

The title compound was prepared from **7c** (60.0 mg, 0.17 mmol), propionic acid (16.9 mg, 0.23 mmol), PyBOP (118.6 mg, 0.23 mmol). and DIPEA (73.7 mg, 0.57 mmol) in dry DCM (total amount 10 mL) according to general procedure F (reaction time 40 min). Purification by flash column chromatography (SiO$_2$, DCM–MeOH gradient elution from 96:4 to 93.5:6.5) gave 38 mg of a white solid (54% yield). ^{1}H-NMR shows a 5:4 mixture of amide bond rotamers. ^{1}H-NMR (400 MHz, CDCl$_3$) δ 12.58 (br s, 1H), 8.59–8.37 (m, 1H), 7.74–7.58 (m, 1H), 7.52–7.40 (m, 1H), 7.24–7.15 (m, 1H), 5.02–4.88 (m, 0.45H), 4.81–4.67 (m, 0.55H), 4.52–4.30 (m, 1H), 4.29–4.18 (m, 0.55H), 3.95–3.81 (m, 0.45H), 3.37–3.19 (m, 3H), 3.19–3.07 (m, 0.55H), 3.07–2.85 (m, 1H), 2.65–2.34 (m, 2.45H), 2.21–1.83 (m, 3H), 1.76–1.54 (m, 1H), 1.26–1.12 (m, 3H); ^{13}C NMR (101 MHz, CDCl$_3$) δ 173.2, 172.7, 159.92, 159.88, 157.2, 156.5, 152.4, 151.8, 137.6, 137.5, 131.1, 123.8, 123.6, 121.5, 121.3, 118.6, 111.72, 111.68, 98.5, 98.4, 55.2, 55.1, 47.5, 45.8, 44.9, 42.2, 34.5, 33.5, 28.7, 28.0, 26.9, 26.8, 25.5, 24.9, 9.8; ESI-MS: (*m/z*) 393.9 [M + Na]$^+$, 369.8 [M − H]$^−$; HPLC method A: t$_r$ = 7.599 min.

1-(3-((7-Chloro-9*H*-pyrimido[4,5-*b*]indol-4-yl)(methyl)amino)piperidin-1-yl)-3,3,3-trifluoropropan-1-one (**17**)

The title compound was prepared from **7c** (65.0 mg, 0.21 mmol), trifluoropropionic acid (33.0 mg, 0.26 mmol), TBTU (82.6 mg, 0.26 mmol), and DIPEA (79.8 mg, 0.62 mmol) in dry DCM (total amount 10 mL) according to general procedure F (reaction time 2 h). Purification by flash column chromatography (SiO$_2$, DCM–MeOH 95:5) gave 44 mg of a light yellow solid (50% yield). ^{1}H-NMR shows a 3:2 mixture of amide bond rotamers. ^{1}H-NMR (300 MHz, DMSO-*d$_6$*) δ 12.23 (s, 1H), 8.44–8.33 (m, 1H), 7.89–7.76 (m, 1H), 7.54–7.44 (m, 1H), 7.30–7.16 (m, 1H), 4.65–4.52 (m, 0.6H), 4.43–4.16 (m, 1.4H), 4.05–3.95 (m, 0.4H), 3.84–3.62 (m, 2.6H), 3.34–3.17 (m, 3.4H), 3.08–2.93 (m, 1.2H), 2.68–2.54 (m, 0.4H), 2.11–1.72 (m, 3H), 1.62–1.40 (m, 1H); ESI-MS: (*m/z*) 447.8 [M + Na]$^+$, 423.8 [M − H]$^−$; HPLC method A: t$_r$ = 8.124 min.

1-(3-((7-chloro-9*H*-pyrimido[4,5-*b*]indol-4-yl)(methyl)amino)piperidin-1-yl)-2,2-dimethylpropan-1-one (**38**)

7c (60.0 mg, 0.19 mmol), pivalic acid (24.3 mg, 0.24 mmol), TBTU (70.3 mg, 0.24 mmol), and DIPEA (73.7 mg, 0.57 mmol) were stirred in dry DCM (10 mL) at rt and under N$_2$ atmosphere, but no conversion was observed. Therefore, the stirring mixture was cooled down to 0 °C, and pivaloyl chloride (237 µL of a freshly prepared 1-M solution in dry DCM, 0.24 mmol) was added. The cooling was removed, and the mixture was stirred for 45 min under N$_2$ atmosphere. Saturated NH$_4$Cl solution (20 mL) was added, and the mixture was diluted with DCM. Phases were separated, and the organic layer was washed with saturated NH$_4$Cl solution (20 mL) and saturated NaHCO$_3$ solution (2 × 20 mL), then dried over Na$_2$SO$_4$, and concentrated under reduced pressure. Purification of the residue by flash column chromatography (DCM–MeOH 95:5) gave 36 mg of a white solid (47% yield). ^{1}H-NMR (300 MHz, CDCl$_3$) δ 12.39 (br s, 1H), 8.49 (s, 1H), 7.67 (d, *J* = 8.5 Hz, 1H), 7.46 (s, 1H), 7.21 (d, *J* = 8.3 Hz, 1H), 4.85–4.68 (m, 1H), 4.59–4.37 (m, 2H), 3.29 (s, 3H), 3.12–3.00 (m, 1H), 2.82–2.67 (m, 1H), 2.17–1.85 (m, 3H), 1.75–1.57 (m, 1H), 1.31 (s, 9H); ^{13}C NMR (101 MHz, CDCl$_3$) δ 177.0, 160.0, 157.4, 152.5, 137.6, 131.1, 123.7, 121.3, 118.7, 111.6, 98.6, 55.2, 47.8, 45.7, 39.0, 33.9, 28.6, 28.5, 25.2; ESI-MS: (*m/z*) 400.5 [M + H]$^+$, 422.5 [M + Na]$^+$, 398.5 [M − H]$^−$; HPLC method A: t$_r$ = 8.748 min.

(3-((7-chloro-9*H*-pyrimido[4,5-*b*]indol-4-yl)(methyl)amino)piperidin-1-yl)(cyclopropyl)methanone (**39**)

Cyclopropanecarbonyl chloride (190 µL of a freshly prepared 1M solution in dry THF, 0.19 mmol) was slowly added to an ice-cooled stirring solution of **7c** (50.0 mg, 0.16 mmol) and TEA (32.0 mg,

0.32 mmol) in dry THF (10 mL) under N_2 atmosphere. The mixture was left to warm to rt and stirred under N_2 atmosphere. Additional cyclopropanecarbonyl chloride solution was added after 1 h (79 µL, 0.08 mmol) and 2 h (158 µL, 0.16 mmol) after cooling down the mixture each time; however, full consumption of the starting material was not achieved. The mixture was evaporated to dryness. Purification of the residue by flash column chromatography (DCM–MeOH 95:5) gave 46 mg of a white solid (76% yield). ^{1}H-NMR shows a 5:4 mixture of amide bond rotamers. ^{1}H-NMR (400 MHz, DMSO-d_6) δ 12.23 (s, 1H), 8.41 (s, 1H), 7.86–7.76 (m, 1H), 7.48 (s, 1H), 7.32–7.14 (m, 1H), 4.63–4.48 (m, 0.55H), 4.44–4.14 (m, 2.45H), 3.30–3.14 (m, 3H), 3.12–2.92 (m, 1H), 2.64–2.54 (m, 0.45H), 2.12–1.74 (m, 4H), 1.56–1.38 (m, 1H), 0.78–0.55 (m, 4H), missing 0.45H below water signal; ^{13}C NMR (101 MHz, CDCl$_3$) δ 172.5, 160.1, 157.2 (br), 152.5 (br), 137.6, 131.1, 123.7, 121.4, 118.7, 111.6, 98.7, 55.3, 47.9 (br), 45.9 (br), 42.9 (br), 34.2 (br), 28.7 (br), 24.9 (br), 11.4, 7.6, 7.4; ESI-MS: (*m/z*) 384.2 [M + H]$^+$, 406.2 [M + Na]$^+$, 382.2 [M − H]$^-$; HPLC method A: t_r = 7.837 min.

1-(3-((7-Chloro-9*H*-pyrimido[4,5-*b*]indol-4-yl)(methyl)amino)piperidin-1-yl)prop-2-en-1-one (**40**)

Acryloyl chloride (228 µL of a freshly prepared 1M solution in dry THF, 0.23 mmol) was slowly added to a stirring solution of **7c** (60.0 mg, 0.19 mmol) and TEA (38.5 mg, 0.38 mmol) in dry THF (10 mL) under N_2 atmosphere and ice/MeOH cooling. The mixture was left to warm to rt and stirred until reaction control indicated sufficient conversion. Extractive work-up followed by flash column chromatography (DCM–MeOH 95:5) gave 50 mg of a white solid (71% yield). ^{1}H-NMR shows a 5:4 mixture of amide bond rotamers. ^{1}H-NMR (400 MHz, DMSO-d_6) δ 12.23 (s, 1H), 8.41 (s, 1H), 7.88–7.75 (m, 1H), 7.48 (d, *J* = 1.8 Hz, 1H), 7.22 (d, *J* = 8.3 Hz, 1H), 6.94–6.74 (m, 1H), 6.15–6.03 (m, 1H), 5.74–5.62 (m, 1H), 4.65–4.54 (m, 0.55H), 4.50–4.38 (m, 0.45H), 4.34–4.19 (m, 1.45H), 4.10–3.98 (m, 0.55H), 3.29–3.16 (m, 3H), 3.10–2.97 (m, 1.1H), 2.70–2.58 (m, 0.45H), 2.10–1.78 (m, 3H), 1.53–1.37 (m, 1H), missing 0.45H below water signal; ^{13}C NMR (101 MHz, DMSO-d_6) δ 164.49, 159.40, 157.45, 153.58, 137.40, 129.23, 128.45, 126.98, 123.91, 120.33, 118.34, 110.81, 97.33, 55.07, 54.43, 47.22, 45.09, 44.16, 41.65, 33.63, 32.67, 27.22, 25.37, 24.31; ESI-MS: (*m/z*) 370.1 [M + H]$^+$, 392.2 [M + Na]$^+$, 368.1 [M − H]$^-$; HPLC method A: t_r = 7.384 min.

2-(3-(3-((7-Chloro-9*H*-pyrimido[4,5-*b*]indol-4-yl)(methyl)amino)piperidin-1-yl)oxetan-3-yl)acetonitrile (**41**)

7c (60.0 mg, 0.19 mmol) and 2-(oxetan-3-ylidene)acetonitrile (36.1 mg, 0.38 mmol) were stirred in EtOH at 70 °C for 6 d. The mixture was concentrated under reduced pressure. Purification of the residue by flash column chromatography (SiO$_2$, DCM–MeOH gradient elution from 96:4 to 93.5:6.5) gave 59 mg of a beige solid (76% yield). ^{1}H-NMR (400 MHz, DMSO-*d6*) δ 12.21 (s, 1H), 8.41 (s, 1H), 7.79 (d, *J* = 8.6 Hz, 1H), 7.48 (d, *J* = 1.5 Hz, 1H), 7.27 (dd, *J* = 8.6, 1.6 Hz, 1H), 4.52–4.31 (m, 5H), 3.17 (s, 3H), 3.01 (s, 2H), 2.82–2.73 (m, 1H), 2.61–2.54 (m, 1H), 2.49–2.44 (m, 1H, overlap with DMSO-*d5* signal), 2.18–2.06 (m, 1H), 1.93–1.69 (m, 3H), 1.60–1.47 (m, 1H); ^{13}C NMR (50 MHz, DMSO-*d6*) δ 159.5, 157.5, 153.8, 137.4, 129.2, 123.8, 120.3, 119.3, 118.5, 110.9, 97.1, 78.1, 61.0, 55.1, 48.0, 45.0, 33.1, 27.3, 24.7, 17.4; ESI-MS: (*m/z*) 411.0 [M + H]$^+$, 433.0 [M + Na]$^+$, 409.0 [M − H]$^-$; HPLC method A: t_r = 7.888 min.

3-(3-(methyl(9*H*-pyrimido[4,5-*b*]indol-4-yl)amino)piperidin-1-yl)-3-oxopropanenitrile (**18**)

Cyanoacetic acid (36.7 mg, 0.31 mmol) and PyBOP (179.8 mg, 0.34 mmol) were stirred in dry DCM (3 mL) at rt for 20 min. A solution of **7a** (80.4 mg, 0.29 mmol) and DIPEA (43.9 mg, 0.34 mmol) in dry DCM (2 mL) was drop-added. The mixture was stirred at rt for 2 h and then concentrated under reduced pressure. Saturated NaHCO$_3$ solution was added to the residue, and the mixture was extracted with EtOAc (3 × 10 mL). Combined organic layers were dried over Na$_2$SO$_4$ and concentrated under reduced pressure. Purification of the residue by flash column chromatography (SiO$_2$, DCM–EtOH gradient elution from 98:2 to 9:1) gave 55 mg (55% yield). ^{1}H-NMR shows a 3:2 mixture of amide bond rotamers: (300 MHz, DMSO-d_6) δ 12.19–11.99 (m, 1H), 8.47–8.36 (m, 1H), 7.90–7.78 (m, 1H), 7.54–7.45 (m, 1H), 7.44–7.34 (m, 1H), 7.31–7.19 (m, 1H), 4.55–4.43 (m, 0.6H), 4.39–4.21 (m, 1.4H), 4.18–3.97 (m, 2H), 3.94–3.84 (m, 0.4H), 3.69–3.56 (m, 0.6H), 3.31–3.14 (m, 3.4H), 3.10–2.93 (m, 1.2H), 2.70–2.56 (m, 0.4H),

2.10–1.74 (m, 3H), 1.66–1.42 (m, 1H); ^{13}C NMR (101 MHz, DMSO-d_6) δ 161.6, 161.4, 159.6, 159.5, 157.0, 153.3, 136.7, 124.8, 122.7, 122.6, 120.4, 120.3, 119.32, 119.28, 116.1, 116.0, 111.2, 97.9, 97.7, 54.6, 54.2, 47.4, 45.5, 44.2, 42.1, 34.0, 32.7, 27.1, 26.9, 24.8, 24.7, 24.1; ESI-MS: (*m/z*) 370.9 [M + Na]$^+$, 346.9 [M − H]$^-$; HPLC method B: t$_r$ = 3.316 min.

3-(3-((7-Fluoro-9*H*-pyrimido[4,5-*b*]indol-4-yl)(methyl)amino)piperidin-1-yl)-3-oxopropanenitrile (**19**)

7b (80.0 mg, 0.27 mmol) and DIPEA (51.7 mg, 0.40 mmol) were stirred in dry DCM (3 mL). A suspension of cyanoacetic acid (25.0 mg, 0.29 mmol) and PyBOP (166.9 mg, 0.32 mmol) in dry DCM (3 mL) was drop-added. The mixture was stirred at rt for 2 h and then concentrated under reduced pressure. Saturated NaHCO$_3$ solution (10 mL) was added to the residue, and the mixture was extracted with EtOAc (3 × 10 mL). Combined organic layers were dried over Na$_2$SO$_4$ and concentrated under reduced pressure. Purification of the residue by flash column chromatography (SiO$_2$, DCM–EtOH gradient elution from 98:2 to 90:10 (twice)) gave 28 mg (29% yield); ^{1}H-NMR shows a 5:4 mixture of amide bond rotamers. ^{1}H-NMR (300 MHz, DMSO-d_6) δ 12.28–12.15 (m, 1H), 8.45–8.37 (m, 1H), 7.90–7.77 (m, 1H), 7.30–7.21 (m, 1H), 7.16–7.01 (m, 1H), 4.53–4.44 (m, 0.55H), 4.40–4.17 (m, 1.45H), 4.15–3.98 (m, 2H), 3.92–3.84 (m, 0.45H), 3.66–3.58 (m, 0.55H), 3.30–3.16 (m, 3H), 3.09–2.96 (m, 1.1H), 2.69–2.57 (m, 0.45H), 2.09–1.89 (m, 2H), 1.88–1.75 (m, 1H), 1.67–1.41 (m, 1H), missing 0.45H below water signal; ESI-MS: (*m/z*) 389.2 [M + Na]$^+$, 365.1 [M − H]$^-$; HPLC method B: t$_r$ = 4.514 min.

3-(3-((7-bromo-9*H*-pyrimido[4,5-*b*]indol-4-yl)(methyl)amino)piperidin-1-yl)-3-oxopropanenitrile (**20**)

Cyanoacetic acid (31.8 mg, 0.37 mmol) and PyBOP (213.3 mg, 0.4 mmol) were stirred in dry DCM (5 mL) at rt. A suspension of **7d** (120.0 mg, 0.33 mmol) and DIPEA (66.0 mg, 0.5 mmol) in dry DCM (5 mL) was added. The mixture was stirred at rt for 2 h and then concentrated under reduced pressure. Saturated NaHCO$_3$ solution was added to the residue, and the mixture was extracted with EtOAc (3 × 10 mL). Combined organic layers were dried over Na$_2$SO$_4$ and concentrated under reduced pressure. Purification of the residue by flash column chromatography (SiO$_2$, DCM–EtOH gradient elution from 98:2 to 9:1) gave 72 mg (51% yield). ^{1}H-NMR shows a 5:4 mixture of amide bond rotamers. ^{1}H-NMR (300 MHz, DMSO-d_6) δ 12.29–12.17 (m, 1H), 8.47–8.38 (m, 1H), 7.82–7.73 (m, 1H), 7.65–7.59 (m, 1H), 7.43–7.33 (m, 1H), 4.54–4.45 (m, 0.55H), 4.40–4.18 (m, 1.45H), 4.14–3.98 (m, 2H), 3.92–3.82 (m, 0.45H), 3.68–3.57 (m, 0.55H), 3.29–3.17 (m, 3H), 3.09–2.95 (m, 1.1H), 2.70–2.57 (m, 0.45H), 2.08–1.74 (m, 3H), 1.67–1.41 (m, 1H), missing 0.45H below water signal; ESI-MS: (*m/z*) 448.9 [M + Na]$^+$, 424.8 [M − H]$^-$; HPLC method B: t$_r$ = 6.305 min.

3-(3-((7-Iodo-9*H*-pyrimido[4,5-*b*]indol-4-yl)(methyl)amino)piperidin-1-yl)-3-oxopropanenitrile (**21**)

The title compound was prepared from **7e** (75 mg, 0.18 mmol), cyanoacetic acid (19.6 mg, 0.23 mmol), TBTU (73.9 mg, 0.23 mmol), and DIPEA (71.4 mg, 0.55 mmol) in dry DCM (total amount 12 mL) according to general procedure F (reaction time 2 h). Purification by flash column chromatography (SiO$_2$, DCM–MeOH 96:4) gave 61 mg of a white solid (70% yield); ^{1}H-NMR shows a 3:2 mixture of amide bond rotamers. ^{1}H-NMR (400 MHz, DMSO-d_6) δ 12.24–12.12 (m, 1H), 8.47–8.38 (m, 1H), 7.79 (s, 1H), 7.68–7.59 (m, 1H), 7.58–7.47 (m, 1H), 4.55–4.42 (m, 0.6H), 4.40–4.19 (m, 1.4H), 4.19–3.98 (m, 2H), 3.92–3.82 (m, 0.4H), 3.69–3.56 (m, 0.6H), 3.32–3.13 (m, 3H), 3.09–2.95 (m, 1.2H), 2.68–2.57 (m, 0.4H), 2.09–1.89 (m, 2H), 1.89–1.75 (m, 1H), 1.67–1.44 (m, 1H), missing 0.4H below water signal; ^{13}C NMR (101 MHz, DMSO-d_6) δ 161.6, 161.5, 159.5, 159.4, 156.9, 153.8, 138.0, 128.8, 128.7, 124.6, 124.5, 119.6, 119.02, 118.96, 116.1, 116.0, 97.4, 97.2, 89.5, 89.4, 54.6, 54.2, 47.3, 45.5, 44.1, 42.0, 34.0, 32.7, 27.0, 26.9, 24.8, 24.6, 24.1. ESI-MS: (*m/z*) 497.2 [M + Na]$^+$, 473.2 [M − H]$^-$; HPLC method A: t$_r$ = 7.258 min.

3-(3-((7-methoxy-9*H*-pyrimido[4,5-*b*]indol-4-yl)(methyl)amino)piperidin-1-yl)-3-oxopropanenitrile (**22**)

7f (120.0 mg, 0.39 mmol) and DIPEA (99.6 mg, 0.77 mmol) were stirred in dry DCM (5 mL) at rt. A suspension of cyanoacetic acid (36.1 mg, 0.42 mmol) and PyBOP (240.7 mg, 0.46 mmol) in dry DCM

(5 mL) was drop-added. The mixture was stirred at rt for 2 h and then concentrated under reduced pressure. Saturated NaHCO$_3$ solution (10 mL) was added to the residue, and the mixture was extracted with EtOAc (3 × 10 mL). Combined organic layers were dried over Na$_2$SO$_4$ and concentrated under reduced pressure. Purification of the residue by flash column chromatography (SiO$_2$, DCM–EtOH gradient elution from 98:2 to 9:1 (twice)) gave 62 mg (43% yield). ^{1}H-NMR shows a 3:2 mixture of amide bond rotamers. ^{1}H-NMR (300 MHz, DMSO-d_6) δ 12.05–11.88 (m, 1H), 8.43–8.28 (m, 1H), 7.79–7.61 (m, 1H), 7.02–6.92 (m, 1H), 6.92–6.79 (m, 1H), 4.52–4.40 (m, 0.6H), 4.38–4.16 (m, 1.4H), 4.15–3.97 (m, 2H), 3.93–3.77 (m, 3.4H), 3.68–3.56 (m, 0.6H), 3.27–3.12 (m, 3H), 3.08–2.93 (m, 1.2H), 2.69–2.58 (m, 0.4H), 2.10–1.74 (m, 3H), 1.65–1.41 (m, 1H), missing 0.4H below water signal; ESI-MS: (*m/z*) 379.0 [M + H]$^+$, 400.9 [M + Na]$^+$, 378.0 [M − H]$^-$; HPLC method B: t$_r$ = 3.635 min.

3-(3-(Methyl(7-(trifluoromethyl)-9*H*-pyrimido[4,5-*b*]indol-4-yl)amino)piperidin-1-yl)-3-oxopropanenitrile (**23**)

7g (100.0 mg, 0.29 mmol) and DIPEA (54.3 mg, 0.42 mmol) were stirred in dry DCM (5 mL) at rt. A suspension of cyanoacetic acid (26.8 mg, 0.31 mmol) and PyBOP (178.7 mg, 0.36 mmol) in dry DCM (5 mL) was drop-added. The mixture was stirred at rt for 2 h and then concentrated under reduced pressure. Saturated NaHCO$_3$ solution (10 mL) was added to the residue, and the mixture was extracted with EtOAc (3 × 10 mL). Combined organic layers were dried over Na$_2$SO$_4$ and concentrated under reduced pressure. Purification of the residue twice by flash column chromatography (SiO$_2$, DCM–EtOH gradient elution from 97:3 to 4:1 and SiO$_2$, DCM–(2N NH$_3$ in MeOH) gradient elution from 99:1 to 92:8) gave 28 mg (23% yield); ^{1}H-NMR shows a 3:2 mixture of amide bond rotamers. ^{1}H-NMR (300 MHz, DMSO-d_6) δ 12.45 (s, 1H), 8.50–8.43 (m, 1H), 8.09–7.99 (m, 1H), 7.74 (s, 1H), 7.59–7.48 (m, 1H), 4.58–4.49 (m, 0.6H), 4.41–4.27 (m, 1.4H), 4.16–4.00 (m, 2H), 3.93–3.84 (m, 0.4H), 3.71–3.60 (m, 0.6H), 3.33–3.21 (m, 3.4H), 3.10–2.95 (m, 1.2H), 2.69–2.58 (m, 0.4H), 2.11–1.76 (m, 3H), 1.70–1.45 (m, 1H); ESI-MS: (*m/z*) 438.9 [M + Na]$^+$, 415.0 [M − H]$^-$; HPLC method B: t$_r$ = 6.640 min.

3-(3-((7-Chloro-2-methyl-9*H*-pyrimido[4,5-*b*]indol-4-yl)(methyl)amino)piperidin-1-yl)-3-oxopropanenitrile (**24**)

The title compound was prepared from **7l** (65.0 mg, 0.20 mmol), cyanoacetic acid (21.0 mg, 0.25 mmol), TBTU (79.1 mg, 0.25 mmol), and DIPEA (76.4 mg, 0.59 mmol) in dry DCM (total amount 10 mL) according to general procedure F (reaction time 2 h). Purification by flash column chromatography (SiO$_2$, DCM–MeOH gradient elution from 95.5:4.5 to 93:7) gave 48 mg of a grey-yellow solid (61% yield). ^{1}H-NMR shows a 1:1 mixture of amide bond rotamers. ^{1}H-NMR (300 MHz, DMSO-d_6) δ 12.02 (s, 1H), 7.84–7.71 (m, 1H), 7.45 (d, *J* = 2.0 Hz, 1H), 7.28–7.15 (m, 1H), 4.57–4.48 (m, 0.5H), 4.39–4.30 (m, 0.5H), 4.29–3.97 (m, 3H), 3.95–3.86 (m, 0.5H), 3.67–3.58 (m, 0.5H), 3.34–3.27 (m, 0.5H), 3.26–3.14 (m, 3H), 3.08–2.92 (m, 1H), 2.70–2.58 (m, 0.5H), 2.53–2.47 (m, 3H, overlap with DMSO-d_5 signal), 2.13–1.72 (m, 3H), 1.67–1.43 (m, 1H); ^{13}C NMR (101 MHz, DMSO-d_6) δ 162.6, 162.5, 161.7, 161.5, 159.5, 159.4, 158.5, 158.4, 137.5, 137.4, 128.8, 123.7, 123.5, 120.3, 118.6, 118.5, 116.2, 116.0, 110.8, 95.2, 95.0, 54.5, 54.3, 47.2, 45.6, 44.1, 42.3, 34.2, 32.7, 27.4, 27.0, 25.8, 25.7, 25.0, 24.9, 24.7, 24.3; ESI-MS: (*m/z*) 396.9 [M + H]$^+$, 418.9 [M + Na]$^+$, 394.9 [M − H]$^-$; HPLC method A: t$_r$ = 7.427 min.

1-(3-(methyl(9*H*-pyrimido[4,5-*b*]indol-4-yl)amino)piperidin-1-yl)propan-1-one (**25**)

The title compound was prepared from **7a** (60.0 mg, 0.21 mmol), propionic acid (19.8 mg, 0.27 mmol), TBTU (85.6 mg, 0.27 mmol), and DIPEA (82.7 mg, 0.64 mmol) in dry DCM (total amount 10 mL) according to general procedure F (reaction time 1 h). Purification by flash column chromatography (SiO$_2$; DCM–MeOH 94:6) gave 45 mg of a beige solid (63% yield). ^{1}H-NMR shows a 5:4 mixture of amide bond rotamers. ^{1}H-NMR (400 MHz, DMSO-d_6) δ 12.08 (s, 1H), 8.43–8.36 (m, 1H), 7.88–7.78 (m, 1H), 7.52–7.45 (m, 1H), 7.43–7.35 (m, 1H), 7.30–7.17 (m, 1H), 4.62–4.49 (m, 0.55H), 4.45–4.37 (m, 0.45H), 4.35–4.27 (m, 0.45H), 4.26–4.16 (m, 0.55H), 4.08–4.00 (m, 0.45H), 3.88–3.75 (m, 0.55H), 3.29–3.15 (m, 3.45H), 3.02–2.87 (m, 1.1H), 2.56–2.46 (m, 0.45H, overlap with DMSO-d_6 signal), 2.46–2.26

(m, 2H), 2.07–1.87 (m, 2H), 1.85–1.75 (m, 1H), 1.52–1.37 (m, 1H), 1.02–0.92 (m, 3H); ESI-MS: (*m/z*) 338.7 [M + H]$^+$, 360.7 [M + Na]$^+$, 336.7 [M − H]$^-$; HPLC method A: t$_r$ = 6.107 min.

1-(3-((7-Fluoro-9*H*-pyrimido[4,5-*b*]indol-4-yl)(methyl)amino)piperidin-1-yl)propan-1-one (**26**)

The title compound was prepared from **7b** (50.0 mg, 0.17 mmol), propionic acid (15.5 mg, 0.21 mmol), TBTU (67.5 mg, 0.21 mmol), and DIPEA (64.8 mg, 0.50 mmol) in dry DCM (total amount 15 mL) according to general procedure F (reaction time 45 min). Purification by flash column chromatography (SiO$_2$; DCM–MeOH 95:5) gave 50 mg of a white solid (84% yield). ^{1}H-NMR (400 MHz, DMSO-*d$_6$*) δ 12.28–12.14 (m, 1H), 8.44–8.34 (m, 1H), 7.86–7.76 (m, 1H), 7.30–7.20 (m, 1H), 7.13–6.99 (m, 1H), 4.60–4.51 (m, 0.55H), 4.45–4.36 (m, 0.45H), 4.32–4.23 (m, 0.45H), 4.21–4.11 (m, 0.55H), 4.08–3.98 (m, 0.45H), 3.87–3.74 (m, 0.55H), 3.28–3.14 (m, 3.45H), 3.00–2.85 (m, 1.1H), 2.54–2.46 (m, 0.45H, overlap with DMSO-*d$_5$* signal), 2.44–2.26 (m, 2H), 2.05–1.86 (m, 2H), 1.83–1.75 (m, 1H), 1.52–1.37 (m, 1H), 1.03–0.92 (m, 3H); ^{13}C NMR (101 MHz, DMSO-*d$_6$*) δ 171.54, 171.37, 160.25 (d, *J* = 240.1 Hz), 159.33, 159.21, 157.72, 153.12, 153.03, 137.47 (d, *J* = 12.5 Hz), 124.14–123.87 (m), 116.17, 108.07 (d, *J* = 23.5 Hz), 97.80 (d, *J* = 26.1 Hz), 54.80, 54.55, 46.74, 44.79, 43.87, 41.22, 33.75, 32.55, 27.52, 27.24, 25.65, 25.15, 24.46, 9.43. ESI-MS: (*m/z*) 378.3 [M + Na]$^+$, 354.4 [M − H]$^-$; HPLC method B: t$_r$ = 7.075 min.

1-(3-((7-Chloro-2-methyl-9*H*-pyrimido[4,5-*b*]indol-4-yl)(methyl)amino)piperidin-1-yl)propan-1-one (**27**)

The title compound was prepared from **7l** (28.0 mg, 0.09 mmol), propionic acid (7.9 mg, 0.11 mmol), TBTU (34.1 mg, 0.11 mmol), and DIPEA (32.9 mg, 0.26 mmol) in dry DCM (total amount 5 mL) according to general procedure F (reaction time 2 h). Purification by flash column chromatography (SiO$_2$, DCM–MeOH gradient elution from 96:4 to 94:6) gave 20 mg of a beige solid (61% yield). ^{1}H-NMR shows a 3:2 mixture of amide bond rotamers. ^{1}H-NMR (400 MHz, DMSO-*d$_6$*) δ 12.02 (s, 1H), 7.85–7.71 (m, 1H), 7.48–7.40 (m, 1H), 7.29–7.13 (m, 1H), 4.64–4.53 (m, 0.4H), 4.49–4.37 (m, 0.6H), 4.34–4.23 (m, 0.6H), 4.20–4.06 (m, 1H), 3.89–3.77 (m, 0.4H), 3.29–3.14 (m, 3.6H), 3.02–2.86 (m, 0.8H), 2.63–2.54 (m, 0.6H), 2.47–2.29 (m, 2H), 2.10–1.75 (m, 3H), 1.54–1.39 (m, 1H), 1.08–0.92 (m, 3H); ESI-MS: (*m/z*) 408.2 [M + Na]$^+$, 384.2 [M − H]$^-$; HPLC method A: t$_r$ = 7.761 min.

1-(3-((7-Bromo-9*H*-pyrimido[4,5-*b*]indol-4-yl)(methyl)amino)piperidin-1-yl)propan-1-one (**28**)

The title compound was prepared from **7d** (115.0 mg, 0.32 mmol), propionic acid (29.6 mg, 0.40 mmol), TBTU (128.1 mg, 0.40 mmol), and DIPEA (123.8 mg, 0.96 mmol) in dry DCM (total amount 15 mL) according to general procedure F (reaction time 30 min). Purification by flash column chromatography (SiO$_2$, DCM–MeOH 94:6) gave 48 mg of an off-white solid (36% yield). ^{1}H-NMR shows a 5:4 mixture of amide bond rotamers. ^{1}H-NMR (400 MHz, CDCl$_3$) δ 12.75–12.17 (m, 1H), 8.58–8.47 (m, 1H), 7.67–7.53 (m, 2H), 7.40–7.30 (m, 1H), 5.01–4.90 (m, 0.45H), 4.80–4.68 (m, 0.55H), 4.54–4.40 (m, 0.55H), 4.38–4.29 (m, 0.45H), 4.28–4.20 (m, 0.55H), 3.95–3.82 (m, 0.45H), 3.36–3.20 (m, 3H), 3.19–3.09 (m, 0.55H), 3.05–2.88 (m, 0.9H), 2.67–2.36 (m, 2.55H), 2.21–1.86 (m, 3H), 1.76–1.56 (m, 1H), 1.28–1.13 (m, 3H); ^{13}C NMR (101 MHz, CDCl$_3$) δ 173.2, 172.6, 160.1, 160.0, 157.54, 157.46, 153.0, 137.9, 124.0, 123.92, 123.88, 119.1, 119.0, 118.73, 118.68, 114.6, 114.4, 98.4, 55.2, 55.0, 47.5, 45.8, 45.0, 42.2, 34.4, 33.4, 28.8, 28.0, 26.9, 26.8, 25.6, 24.9, 9.8; ESI-MS: (*m/z*) 438.0 [M + Na]$^+$, 414.0 [M − H]$^-$; HPLC method A: t$_r$ = 8.212 min.

1-(3-((7-Iodo-9*H*-pyrimido[4,5-*b*]indol-4-yl)(methyl)amino)piperidin-1-yl)propan-1-one (**29**)

The title compound was prepared from **7e** (43.0 mg, 0.11 mmol), propionic acid (9.8 mg, 0.13 mmol), TBTU (42.4 mg, 0.13 mmol), and DIPEA (40.9 mg, 0.32 mmol) in dry DCM (total amount 8 mL) according to general procedure F (reaction time 2 h). Purification by flash column chromatography (SiO$_2$, DCM–MeOH 95:5) gave 25 mg of an off-white solid (51% yield). ^{1}H-NMR shows a 1:1 mixture of amide bond rotamers. ^{1}H-NMR (400 MHz, DMSO-*d$_6$*) δ 12.20–12.11 (m, 1H), 8.43–8.37 (m, 1H), 7.82–7.76 (m, 1H), 7.67–7.60 (m, 1H), 7.56–7.47 (m, 1H), 4.59–4.52 (m, 0.5H), 4.44–4.37 (m, 0.5H), 4.35–4.26 (m, 0.5H), 4.23–4.14 (m, 0.5H), 4.07–3.98 (m, 0.5H), 3.85–3.79 (m, 0.5H), 3.26–3.15 (m, 3.5H), 3.01–2.87

(m, 1H), 2.54–2.46 (m, 0.5H, overlap with DMSO-d_5 signal), 2.45–2.25 (m, 2H), 2.05–1.75 (m, 3H), 1.53–1.37 (m, 1H), 1.02–0.93 (m, 3H); ESI-MS: (*m/z*) 464.9 [M + H]$^+$, 486.9 [M + Na]$^+$, 462.8 [M − H]$^-$; HPLC method A: t_r = 8.443 min.

3-(3-((6-Chloro-9*H*-pyrimido[4,5-*b*]indol-4-yl)(methyl)amino)piperidin-1-yl)-3-oxopropanenitrile (**30**)

Cyanoacetic acid (16.8 mg, 0.20 mmol) and TBTU (63.5 mg, 0.20 mmol) were stirred in dry DCM (5 mL) at rt and under N$_2$ atmosphere for 15 min. A suspension of **7h** (50.0 mg, 0.16 mmol) and DIPEA (61.4 mg, 0.48 mmol) in dry DCM (5 mL) was added to the activated acid, and the mixture was stirred at rt and under N$_2$ atmosphere for 2.5 h. A precipitate formed. The mixture was diluted with DCM, and MeOH was added to dissolve the precipitate. The solution was washed with saturated NaHCO$_3$ solution (2 × 20 mL) and saturated NH$_4$Cl solution (2 × 20 mL). The organic layer was dried over Na$_2$SO$_4$ and concentrated under reduced pressure. Purification of the residue by flash column chromatography (SiO$_2$, DCM–MeOH gradient elution from 95:5 to 92:8) gave 34 mg of a white solid (56% yield); ^{1}H-NMR shows a 5:4 mixture of amide rotamers. ^{1}H-NMR (400 MHz, DMSO-d_6) δ 12.32–12.18 (m, 1H), 8.46–8.36 (m, 1H), 7.83–7.73 (m, 1H), 7.53–7.45 (m, 1H), 7.44–7.36 (m, 1H), 4.51–4.42 (m, 0.55H), 4.40–4.25 (m, 1.45H), 4.17–3.99 (m, 2H), 3.93–3.85 (m, 0.45H), 3.69–3.60 (m, 0.55H), 3.29–3.19 (m, 3H), 3.07–2.91 (m, 1.1H), 2.68–2.57 (m, 0.45H), 2.10–1.94 (m, 2H), 1.89–1.79 (m, 1H), 1.71–1.42 (m, 1H), missing 0.45H below water signal; ^{13}C NMR (101 MHz, DMSO-d_6) δ 161.6, 161.5, 159.5, 157.5, 153.8, 135.20, 135.18, 124.7, 124.6, 121.8, 121.7, 120.72, 120.71, 116.02, 115.97, 112.6, 97.0, 96.9, 54.6, 53.8, 47.4, 45.4, 43.9, 42.0, 34.1, 33.1, 27.0, 26.9, 24.9, 24.6, 24.1; ESI-MS: (*m/z*) 405.4 [M + Na]$^+$, 381.4 [M − H]$^-$; HPLC method A: t_r = 6.666 min.

3-(3-((6-Bromo-9*H*-pyrimido[4,5-*b*]indol-4-yl)(methyl)amino)piperidin-1-yl)-3-oxopropanenitrile (**31**)

A mixture of cyanoacetic acid (21.3 mg, 0.25 mmol) and EDCI·HCl (47.9 mg, 0.25 mmol) was stirred in dry DCM (6 mL) at rt and under N$_2$ atmosphere for 20 min. A suspension of **7i** (60.0 mg, 0.17 mmol) and DIPEA (64.6 mg, 0.51 mmol) in dry DCM (4 mL) was added, and the mixture was stirred at rt and under N$_2$ atmosphere. Due to slow conversion, reactants were added repeatedly: EDCI·HCl (47.9 mg, 0.25 mmol) after 3 h of stirring, cyanoacetic acid (21.3 mg, 0.25 mmol) after 5 h of stirring, and again EDCI·HCl (63.9 mg, 0.33 mmol) after 20 h of stirring. Sufficient conversion was achieved after a reaction time of 2 days. The mixture was diluted with DCM, washed with saturated NH$_4$Cl solution and saturated NaHCO$_3$ solution, dried over Na$_2$SO$_4$, and concentrated under reduced pressure. Purification of the residue by flash column chromatography (SiO$_2$, DCM–MeOH 95:5) gave 16 mg of an off-white solid (22% yield). ^{1}H-NMR shows a 5:4 mixture of amide bond rotamers. ^{1}H-NMR (400 MHz, DMSO-d_6) δ 12.34–12.22 (m, 1H), 8.44 (s, 0.45H), 8.40 (s, 0.55H), 7.96–7.87 (m, 1H), 7.57–7.50 (m, 1H), 7.48–7.41 (m, 1H), 4.49–4.41 (m, 0.55H), 4.40–4.24 (m, 1.45H), 4.15–3.99 (m, 2H), 3.92–3.84 (m, 0.45H), 3.70–3.60 (m, 0.55H), 3.29–3.19 (m, 3H), 3.07–2.92 (m, 1.1H), 2.69–2.57 (m, 0.45H), 2.11–1.95 (m, 2H), 1.90–1.80 (m, 1H), 1.72–1.43 (m, 1H), missing 0.45H below water signal; ^{13}C NMR (101 MHz, DMSO-d_6) δ 161.6, 161.5, 159.5, 159.4, 157.4, 153.9, 135.5, 127.3, 127.2, 124.7, 124.6, 121.4, 121.3, 116.1, 116.0, 113.1, 112.5, 112.4, 96.8, 96.8, 54.7, 53.9, 47.4, 45.4, 43.9, 42.0, 34.0, 33.1, 27.0, 26.9, 24.9, 24.6, 24.1. ESI-MS: (m/z) 449.4 [M + Na]$^+$, 425.5 [M − H]$^-$; HPLC method A: t_r = 6.749 min.

3-(3-((6-Methoxy-9*H*-pyrimido[4,5-*b*]indol-4-yl)(methyl)amino)piperidin-1-yl)-3-oxopropanenitrile (**32**)

The title compound was prepared from **7j** (60.0 mg, 0.19 mmol), cyanoacetic acid (20.5 mg, 0.24 mmol), TBTU (77.3 mg, 0.24 mmol), and DIPEA (74.7 mg, 0.58 mmol) in dry DCM (total amount 10 mL) according to general procedure F (reaction time 0.5 h). Purification by flash column chromatography (SiO$_2$; DCM–MeOH 95:5) gave 38 mg of a beige solid (52% yield). ^{1}H-NMR shows a 5:4 mixture of amide bond rotamers. ^{1}H-NMR (400 MHz, DMSO-d_6) δ 12.00–11.87 (m, 1H), 8.43–8.36 (m, 1H), 7.44–7.37 (m, 1H), 7.34–7.20 (m, 1H), 7.09–7.01 (m, 1H), 4.40–3.97 (m, 4H), 3.92–3.80 (m, 3.45H), 3.65–3.57 (m, 0.55H), 3.30–3.17 (m, 3H), 3.06–2.92 (m, 1.1H), 2.69–2.57 (m, 0.4H), 2.15–1.98 (m, 2H), 1.90–1.79 (m, 1H), 1.71–1.44 (m, 1H), missing 0.45H below water signal; ^{13}C NMR (101 MHz, DMSO-d_6)

δ 161.6, 161.4, 159.9, 159.6, 157.3, 157.2, 154.0, 153.9, 153.1, 131.4, 131.3, 119.9, 119.7, 116.00, 115.96, 113.6, 112.9, 111.9, 111.8, 106.8, 106.0, 98.3, 97.9, 55.6, 55.5, 54.7, 54.3, 47.4, 45.4, 44.0, 42.0, 34.0, 32.7, 27.2, 27.1, 24.9, 24.8, 24.6, 24.1; ESI-MS: (*m/z*) 379.1 [M + H]$^+$, 401.2 [M + Na]$^+$, 377.2 [M − H]$^-$; HPLC method A: t_r = 4.053 min.

3-(3-((5-Chloro-9*H*-pyrimido[4,5-*b*]indol-4-yl)(methyl)amino)piperidin-1-yl)-3-oxopropanenitrile (**33**)

The title compound was prepared from **7k** (55.0 mg, 0.17 mmol), cyanoacetic acid (18.5 mg, 0.22 mmol), TBTU (69.9 mg, 0.22 mmol), and DIPEA (67.5 mg, 0.52 mmol) in dry DCM (total amount 10 mL) according to general procedure F (reaction time 1 h). A precipitate formed during the reaction and was dissolved by adding DCM and MeOH prior to the extractive work-up. Repeated purification by flash column chromatography (SiO$_2$, DCM–MeOH 94:6; SiO$_2$, DCM–MeOH gradient elution from 96:4 to 92:8; SiO$_2$, DCM–MeOH gradient elution from 96:4 to 92:8; and SiO$_2$, DCM–EtOH 95:5) gave 35 mg of a beige solid (52% yield). ^{1}H-NMR shows a 1:1 mixture of amide bond rotamers. ^{1}H-NMR (300 MHz, DMSO-*d$_6$*) δ 12.35 (s, 1H), 8.50–8.32 (m, 1H), 7.50–7.34 (m, 2H), 7.33–7.25 (m, 1H), 4.42–3.95 (m, 4H), 3.92–3.80 (m, 0.5H), 3.66–3.55 (m, 0.5H), 3.09–2.89 (m, 4H), 2.71–2.58 (m, 0.5H), 2.07–1.73 (m, 3H), 1.71–1.42 (m, 1H), missing 0.5H below water signal; ESI-MS: (*m/z*) 405.4 [M + Na]$^+$, 381.3 [M − H]$^-$; HPLC method A: t_r = 6.396 min.

1-(3-((6-Chloro-9*H*-pyrimido[4,5-*b*]indol-4-yl)(methyl)amino)piperidin-1-yl)propan-1-one (**34**)

The title compound was prepared from **7h** (50.0 mg, 0.16 mmol), propionic acid (14.7 mg, 0.20 mmol), TBTU (63.5 mg, 0.20 mmol), and DIPEA (61.4 mg, 0.48 mmol) in dry DCM (10 mL) according to general procedure F (reaction time 45 min). Purification by flash column chromatography (SiO$_2$, DCM–MeOH gradient elution from 96.5:3.5 to 92.5: 7.5) gave 42 mg of an off-white solid (71% yield); ^{1}H-NMR shows a 1:1 mixture of amide bond rotamers. ^{1}H-NMR (400 MHz, DMSO-*d$_6$*) δ 12.25 (s, 1H), 8.39 (s, 1H), 7.84–7.69 (m, 1H), 7.52–7.45 (m, 1H), 7.43–7.37 (m, 1H), 4.55–4.46 (m, 0.5H), 4.46–4.38 (m, 0.5H), 4.35–4.19 (m, 1H), 4.12–4.00 (m, 0.5H), 3.89–3.77 (m, 0.5H), 3.31–3.18 (m, 3.5H), 3.02–2.92 (m, 0.5H), 2.92–2.83 (m, 0.5H), 2.55–2.26 (m, 2.5H, overlap with DMSO-*d$_5$* signal), 2.08–1.93 (m, 2H), 1.90–1.75 (m, 1H), 1.60–1.35 (m, 1H), 1.04–0.91 (m, 3H); ^{13}C NMR (101 MHz, DMSO-*d$_6$*) δ 171.5, 171.4, 159.5, 157.5, 153.8, 153.8, 135.2, 124.7, 124.6, 124.5, 121.8, 121.6, 120.7, 112.6, 96.9, 96.8, 54.8, 54.1, 46.8, 44.7, 43.6, 41.1, 33.8, 32.9, 27.4, 27.2, 25.6, 25.0, 24.4, 9.3; ESI-MS: (*m/z*) 394.4 [M + Na]$^+$, 370.4 [M − H]$^-$; HPLC method A: t_r = 7.789 min.

1-(3-((6-Bromo-9*H*-pyrimido[4,5-*b*]indol-4-yl)(methyl)amino)piperidin-1-yl)propan-1-one (**35**)

Propionic acid (16.7 mg, 0.23 mmol) and TBTU (72.4 mg, 0.23 mmol) were stirred in dry DCM (4 mL) at rt and under N$_2$ atmosphere for 15 min. A suspension of **7i** (65.0 mg, 0.18 mmol) in dry DCM (8 mL) was added to the activated acid, followed by addition of DIPEA (70.0 mg, 0.54 mmol). The mixture was stirred at rt and under N$_2$ atmosphere for 50 min; then diluted with DCM; and washed with saturated NaHCO$_3$ solution (2 × 25 mL), saturated NH$_4$Cl solution (2 × 25 mL), and saturated NaCl solution (25 mL). The organic layer was dried over Na$_2$SO$_4$ and concentrated under reduced pressure. Purification of the residue by flash column chromatography (DCM–MeOH 95:5) gave 24 mg of an off-white solid (32% yield); ^{1}H-NMR shows a 1:1 mixture of amide bond rotamers. ^{1}H-NMR (400 MHz, DMSO-*d$_6$*) δ 12.26 (s, 1H), 8.39 (s, 1H), 7.96–7.81 (m, 1H), 7.56–7.48 (m, 1H), 7.48–7.40 (m, 1H), 4.50–4.36 (m, 1H), 4.34–4.16 (m, 1H), 4.08–4.01 (m, 0.5H), 3.87–3.77 (m, 0.5H), 3.31–3.18 (m, 3.5H), 3.02–2.92 (m, 0.5H), 2.92–2.82 (m, 0.5H), 2.54–2.26 (m, 2.5H, overlap with DMSO-*d$_5$* signal), 2.09–1.96 (m, 2H), 1.92–1.76 (m, 1H), 1.60–1.36 (m, 1H), 1.02–0.90 (m, 3H); ^{13}C NMR (101 MHz, DMSO-*d$_6$*) δ 171.6, 171.5, 159.5, 157.4, 153.9, 153.8, 135.5, 127.3, 124.7, 124.5, 121.4, 113.2, 112.5, 96.8, 96.7, 54.9, 54.1, 46.9, 44.7, 43.7, 41.2, 33.8, 32.9, 27.4, 27.3, 25.7, 25.1, 24.4, 9.4; ESI-MS: (*m/z*) 438.0 [M + Na]$^+$, 414.0 [M − H]$^-$; HPLC method A: t_r = 8.360 min.

1-(3-((6-Methoxy-9*H*-pyrimido[4,5-*b*]indol-4-yl)(methyl)amino)piperidin-1-yl)propan-1-one (**36**)

The title compound was prepared from **7j** (60.0 mg, 0.19 mmol), cyanoacetic acid (17.9 mg, 0.24 mmol), TBTU (77.3 mg, 0.24 mmol), and DIPEA (74.7 mg, 0.58 mmol) in dry DCM (total amount 10 mL) according to general procedure F (reaction time 2 h). Purification by flash column chromatography (SiO$_2$; DCM–MeOH 95:5) gave 43 mg of a beige solid (61% yield). ^{1}H-NMR (300 MHz, DMSO-d_6) δ 12.03–11.84 (m, 1H), 8.45–8.31 (m, 1H), 7.46–7.36 (m, 1H), 7.33–7.19 (m, 1H), 7.12–6.99 (m, 1H), 4.50–4.34 (m, 1H), 4.33–4.09 (m, 1H), 4.06–3.96 (m, 0.45H), 3.90–3.74 (m, 3.55H), 3.30–3.14 (m, 3.45H), 3.03–2.81 (m, 1.1H), 2.57–2.44 (m, 0.45H, overlap with DMSO-d_5 signal), 2.41–2.23 (m, 2H), 2.12–1.77 (m, 3H), 1.62–1.37 (m, 1H), 1.01–0.86 (m, 3H); ^{13}C NMR (101 MHz, DMSO-d_6) δ 171.42, 171.38, 159.9, 159.6, 157.3, 157.2, 154.0, 153.9, 153.1, 131.3, 119.8, 119.8, 113.5, 113.0, 111.9, 111.8, 106.7, 105.9, 98.3, 97.8, 55.6, 55.5, 54.9, 54.5, 46.8, 44.6, 43.6, 41.2, 33.6, 32.6, 27.6, 27.3, 25.6, 25.1, 24.4, 9.3; ESI-MS: (*m/z*) 390.2 [M + Na]$^+$, 366.2 [M − H]$^-$; HPLC method A: t$_r$ = 5.463 min.

1-(3-((5-Chloro-9*H*-pyrimido[4,5-*b*]indol-4-yl)(methyl)amino)piperidin-1-yl)propan-1-one (**37**)

The title compound was prepared from **7k** (55.0 mg, 0.17 mmol), propionic acid (16.2 mg, 0.22 mmol), TBTU (69.9 mg, 0.22 mmol), and DIPEA (67.5 mg, 0.52 mmol) in dry DCM (total amount 10 mL) according to general procedure F (reaction time 2 h). Purification by flash column chromatography (SiO$_2$, DCM–MeOH 94:6) gave 46 mg of a light beige solid (71% yield). NMR shows a 5:4 mixture of amide rotamers. ^{1}H-NMR (300 MHz, Pyr-d_5) δ 14.06–13.63 (m, 1H), 8.88–8.80 (m, 1H), 7.70–7.61 (m, 1H), 7.50–7.36 (m, 2H), 4.87–4.77 (m, 0.55H), 4.69–4.55 (m, 0.45H), 4.55–4.42 (m, 0.55H), 4.27–4.15 (m, 0.55H), 3.73–3.58 (m, 0.45H), 3.23–2.95 (m, 4H), 2.95–2.78 (m, 0.45H), 2.72–2.22 (m, 2.55H), 2.17–1.96 (m, 1H), 1.95–1.42 (m, 3H), 1.31–1.11 (m, 3H), missing 0.45H below water signal; ESI-MS: (*m/z*) 372.3 [M + H]$^+$, 394.4 [M + Na]$^+$, 370.3 [M − H]$^-$; HPLC method A: t$_r$ = 7.646 min.

(8) Detailed Procedures for the Preparation of Enantiopure Final Compounds *(R)*-**2**, *(R)*-**20** and *(R)*-**28**

(R)-3-(3-((7-Chloro-9*H*-pyrimido[4,5-*b*]indol-4-yl)(methyl)amino)piperidin-1-yl)-3-oxopropanenitrile (*(R)*-**2**)

The title compound was prepared from *(R)*-**7c** (50.0 mg, 0.16 mmol), cyanoacetic acid (16.2 mg, 0.19 mmol), PyBOP (98.9 mg, 0.19 mmol), and DIPEA (61.4 mg, 0.48 mmol) in dry DCM (total amount 10 mL) according to general procedure F (reaction time 2 h). Purification twice by flash column chromatography (SiO$_2$, DCM–MeOH gradient elution from 1:0 to 92:8 and SiO$_2$, DCM–EtOH gradient elution from 96.5:3.5 to 92:8) gave 33 mg of a white solid (54% yield). ^{1}H-NMR shows a 3:2 mixture of amide bond rotamers. ^{1}H-NMR (400 MHz, DMSO-d_6) δ 12.33–12.17 (m, 1H), 8.48–8.36 (m, 1H), 7.90–7.77 (m, 1H), 7.53–7.45 (m, 1H), 7.31–7.18 (m, 1H), 4.55–4.46 (m, 0.6H), 4.39–4.20 (m, 1.4H), 4.18–4.00 (m, 2H), 3.94–3.83 (m, 0.4H), 3.69–3.58 (m, 0.6H), 3.29–3.17 (m, 3H), 3.09–2.97 (m, 1.2H), 2.70–2.58 (m, 0.4H), 2.12–1.74 (m, 3H), 1.68–1.43 (m, 1H), missing 0.4H below water signal; ^{13}C NMR (101 MHz, DMSO-d_6) δ 161.6, 161.5, 159.4, 159.3, 157.5, 153.7, 137.4, 129.3, 129.2, 124.1, 124.0, 120.4, 118.4, 118.3, 116.14, 116.08, 110.8, 97.3, 97.2, 54.6, 54.2, 47.3, 45.5, 44.1, 42.0, 34.1, 32.8, 27.0, 26.9, 24.9, 24.7, 24.2; ESI-MS: (*m/z*) 404.9 [M + Na]$^+$, 380.8 [M − H]$^-$; HPLC method A: t$_r$ = 6.644 min.

(R)-3-(3-((7-Bromo-9*H*-pyrimido[4,5-*b*]indol-4-yl)(methyl)amino)piperidin-1-yl)-3-oxopropanenitrile (*(R)*-**20**)

The title compound was prepared from *(R)*-**7d** (70.0 mg, 0.19 mmol), cyanoacetic acid (20.7 mg, 0.24 mmol), TBTU (78.0 mg, 0.24 mmol), and DIPEA (75.3 mg, 0.58 mmol) in dry DCM (total amount 12 mL) according to general procedure F (reaction time 30 min). Purification by flash column chromatography (SiO$_2$, DCM–MeOH 94.5:5.5) gave 63 mg of a white solid (76% yield); ^{1}H-NMR shows a 3:2 mixture of amide bond rotamers. ^{1}H-NMR (300 MHz, DMSO-d_6) δ 12.30–12.14 (m, 1H), 8.49–8.37 (m, 1H), 7.82–7.72 (m, 1H), 7.66–7.58 (m, 1H), 7.44–7.31 (m, 1H), 4.55–4.44 (m, 0.6H), 4.40–4.19 (m, 1.4H), 4.16–3.98 (m, 2H), 3.93–3.82 (m, 0.4H), 3.68–3.57 (m, 0.6H), 3.28–3.14 (m, 3.4H), 3.09–2.94 (m, 1.2H), 2.70–2.56 (m, 0.4H), 2.09–1.74 (m, 3H), 1.67–1.41 (m, 1H); ^{13}C NMR (101 MHz, DMSO-d_6) δ 161.6, 161.4, 159.44, 159.36, 157.3, 153.7, 137.7, 124.4, 124.2, 123.1, 123.0, 118.7, 118.6, 117.38, 117.35, 116.1, 116.0,

113.7, 97.3, 97.2, 54.6, 54.2, 47.3, 45.5, 44.1, 42.0, 34.0, 32.8, 27.0, 26.9, 24.8, 24.6, 24.1; ESI-MS: (*m/z*) 449.4 [M + Na]$^+$, 425.5 [M − H]$^−$; HPLC method A: t_r = 6.672 min.

(R)-1-(3-((7-bromo-9*H*-pyrimido[4,5-*b*]indol-4-yl)(methyl)amino)piperidin-1-yl)propan-1-one (*(R)*-**28**)

The title compound was prepared from *(R)*-**7d** (45.0 mg, 0.13 mmol), propionic acid (11.6 mg, 0.16 mmol), TBTU (50.1 mg, 0.16 mmol), and DIPEA (48.4 mg, 0.38 mmol) in dry DCM (total amount 10 mL) according to general procedure F (reaction time 40 min). Purification by flash column chromatography (SiO$_2$, DCM–MeOH gradient elution from 96:4 to 92:8) gave 28 mg (54% yield). ^{1}H-NMR shows a 5:4 mixture of amide bond rotamers. ^{1}H-NMR (400 MHz, CDCl$_3$) δ 12.89–12.09 (m, 1H), 8.52 (s, 1H), 7.73–7.55 (m, 2H), 7.43–7.29 (m, 1H), 5.01–4.88 (m, 0.45H), 4.80–4.67 (m, 0.55H), 4.55–4.41 (m, 0.55H), 4.39–4.29 (m, 0.45H), 4.28–4.18 (m, 0.55H), 3.94–3.80 (m, 0.45H), 3.35–3.19 (m, 3H), 3.18–3.09 (m, 0.55H), 3.04–2.87 (m, 0.9H), 2.64–2.35 (m, 2.55H), 2.20–1.84 (m, 3H), 1.75–1.54 (m, 1H), 1.26–1.17 (m, 3H); ^{13}C NMR (101 MHz, CDCl$_3$) δ 173.2, 172.6, 160.1, 157.6, 157.4, 153.0, 137.84, 137.76, 124.1, 124.03, 123.96, 119.2, 119.1, 118.84, 118.79, 114.6, 114.4, 98.8, 98.5, 55.2, 55.1, 47.5, 45.8, 45.0, 42.3, 34.5, 33.4, 29.8, 28.8, 28.0, 26.9, 25.6, 24.9, 9.8; ESI-MS: (*m/z*) 416.0 [M + H]$^+$, 438.0 [M + Na]$^+$, 414.0 [M − H]$^−$; HPLC method A: t_r = 8.046 min.

(9) Detailed Procedures for the Preparation of Enantiopure Final Compounds *(S)*-**2** and *(S)*-**20**

(S)-3-(3-((7-Chloro-9*H*-pyrimido[4,5-*b*]indol-4-yl)(methyl)amino)piperidin-1-yl)-3-oxopropanenitrile (*(S)*-**2**)

The title compound was prepared from *(S)*-**7c** (64.0 mg, 0.20 mmol), cyanoacetic acid (20.7 mg, 0.24 mmol), PyBOP (126.6 mg, 0.24 mmol), and DIPEA (78.6 mg, 0.61 mmol) in dry DCM (total amount 10 mL) according to general procedure F (reaction time 3 h). Purification by flash column chromatography (SiO$_2$, DCM–MeOH gradient elution from 95.5:4.5 to 92:8) gave 54 mg of a white solid (70% yield). ^{1}H-NMR shows a 3:2 mixture of amide bond rotamers: (300 MHz, DMSO-*d$_6$*) δ 12.31–12.16 (m, 1H), 8.48–8.37 (m, 1H), 7.89–7.77 (m, 1H), 7.53–7.43 (m, 1H), 7.32–7.18 (m, 1H), 4.58–4.44 (m, 0.6H), 4.41–4.19 (m, 1.4H), 4.16–3.98 (m, 2H), 3.93–3.81 (m, 0.4H), 3.71–3.56 (m, 0.6H), 3.29–3.17 (m, 3H), 3.10–2.94 (m, 1.2H), 2.70–2.56 (m, 0.4H), 2.10–1.73 (m, 3H), 1.68–1.42 (m, 1H), missing 0.4H below water signal; ESI-MS: (*m/z*) 405.1 [M + Na]$^+$, 380.9 [M − H]$^−$; HPLC method A: t_r = 6.679 min.

(S)-3-(3-((7-Bromo-9*H*-pyrimido[4,5-*b*]indol-4-yl)(methyl)amino)piperidin-1-yl)-3-oxopropanenitrile (*(S)*-**20**)

The title compound was prepared from *(S)*-**7d** (65.0 mg, 0.18 mmol), cyanoacetic acid (19.2 mg, 0.23 mmol), TBTU (72.4 mg, 0.23 mmol), and DIPEA (70.0 mg, 0.54 mmol) in dry DCM (total amount 12 mL) according to general procedure F (reaction time 30 min). Purification by flash column chromatography (SiO$_2$, DCM–MeOH 94.5:5.5) gave 48 mg of an off-white solid (62% yield). ^{1}H-NMR shows a 3:2 mixture of amide bond rotamers. ^{1}H-NMR (300 MHz, DMSO-*d$_6$*) δ 12.32–12.12 (m, 1H), 8.49–8.37 (m, 1H), 7.83–7.72 (m, 1H), 7.67–7.57 (m, 1H), 7.44–7.30 (m, 1H), 4.56–4.44 (m, 0.6H), 4.41–4.19 (m, 1.4H), 4.17–3.99 (m, 2H), 3.93–3.81 (m, 0.4H), 3.69–3.58 (m, 0.6H), 3.32–3.14 (m, 3.4H), 3.11–2.95 (m, 1.2H), 2.70–2.56 (m, 0.4H), 2.10–1.73 (m, 3H), 1.67–1.41 (m, 1H); ESI-MS: (*m/z*) 449.3 [M + Na]$^+$, 425.3 [M − H]$^−$; HPLC method A: t_r = 6.649 min.

(10) Detailed Procedures for the Preparation of Intermediates **43** and **44·HCl**

tert-Butyl (1-(2-cyanoacetyl)piperidin-3-yl)carbamate (**43**)

tert-Butyl piperidin-3-yl-carbamate (**42**) (1.0 g, 4.99 mmol) and cyanoacetic acid (470.0 mg, 5.49 mmol) were stirred in dry DCM (15 mL) at 0°C and under N$_2$ atmosphere. A solution of DCC (1.1 g, 5.49 mmol) in dry DCM (11 mL) was drop-added. The mixture was stirred at rt overnight and then filtered rinsing the residue with fresh DCM. The filtrate was concentrated under reduced pressure. Purification of the residue by flash column chromatography (SiO$_2$, DCM–EtOAc 7:3) gave 942 mg (71% yield); ^{1}H-NMR shows a 3:2 mixture of amide bond rotamers. ^{1}H-NMR (300 MHz, DMSO-*d6*) δ 7.08–6.49 (m, 1H), 4.10–3.88 (m, 2.6H), 3.81–3.67 (m, 0.4H), 3.53–3.19 (m, 2H, overlap with water signal), 3.06–2.91 (m, 1.4H), 2.69–2.58 (m, 0.6H), 1.85–1.36 (m, 13H).

1-(2-Cyanoacetyl)piperidin-3-amine hydrochloride (**44·HCl**)

4N HCl in dioxane (2.1 mL) was added to a solution of **43** (200.0 mg, 0.75 mmol) in dry THF (2 mL). The mixture was stirred at rt overnight. The resulting precipitate was filtered off, washed with Et$_2$O, and dried under reduced pressure. The yield was 130 mg (96% crude yield), used in the next step without further purification. ^{1}H-NMR shows a 3:2 mixture of amide bond rotamers. ^{1}H-NMR (400 MHz, DMSO-d_6) δ 8.61–8.25 (m, 3H), 4.26–3.95 (m, 2.4H), 3.70–3.64 (m, 0.6H), 3.55–3.50 (m, 0.4H), 3.45–3.36 (m, 1H), 3.31–3.04 (m, 2.6H), 2.03–1.89 (m, 1H), 1.77–1.62 (m, 2H), 1.54–1.36 (m, 1H); ^{13}C NMR (101 MHz, DMSO-d_6) δ 162.1, 161.7, 116.2, 116.1, 47.7, 46.1, 46.0, 45.3, 43.9, 41.6, 27.4, 27.1, 25.3, 25.2, 25.1, 22.0, 21.1.

(11) Detailed Procedures for the Preparation of Final Compounds **45–50**

3-(3-((9*H*-Pyrimido[4,5-*b*]indol-4-yl)amino)piperidin-1-yl)-3-oxopropanenitrile (**45**)

The title compound was prepared from **4a** (100.0 mg, 0.27 mmol), **44·HCl** (113.8 mg, 0.56 mmol), DIPEA (181.0 mg, 1.40 mmol), and Na*t*BuO (188.0 mg, 1.96 mmol) in dry DMF (5 mL) according to general procedure G. Purification by flash column chromatography (SiO$_2$, DCM–EtOH gradient elution from 97:3 to 85:15) gave 34 mg (36% yield). ^{1}H-NMR shows a 5:4 mixture of amide bond rotamers. ^{1}H-NMR (300 MHz, DMSO-$d6$) δ 11.98–11.84 (m, 1H), 8.42–8.34 (m, 1H), 8.33–8.26 (m, 2H), 7.50–7.43 (m, 1H), 7.42–7.33 (m, 1H), 7.29–7.20 (m, 1H), 6.86–6.63 (m, 1H), 4.51–4.23 (m, 2H), 4.16–3.98 (m, 2H), 3.93–3.83 (m, 0.45H), 3.69–3.57 (m, 0.55H), 3.21–3.11 (m, 0.45H), 3.08–2.97 (m, 0.55H), 2.94–2.84 (m, 0.55H), 2.73–2.60 (m, 0.45H), 2.13–1.97 (m, 1H), 1.92–1.72 (m, 2H), 1.69–1.42 (m, 1H); ESI-MS: (*m/z*) 335.1 [M + H]$^+$, 357.0 [M + Na]$^+$, 332.9 [M − H]$^-$; HPLC method B: t$_r$ = 2.649 min.

3-(3-((7-Fluoro-9*H*-pyrimido[4,5-*b*]indol-4-yl)amino)piperidin-1-yl)-3-oxopropanenitrile (**46**)

The title compound was prepared from **4b** (100.0 mg, 0.27 mmol), **44·HCl** (81.3 mg, 0.40 mmol), DIPEA (171.9 mg, 1.33 mmol), and Na*t*BuO (179.0 mg, 1.86 mmol) in dry DMF (5 mL) according to general procedure G. The precipitate formed upon addition of saturated NH$_4$Cl solution was not extracted with EtOAc but instead filtered off, washed with water, and dried over P$_2$O$_5$ in vacuo. Purification by flash column chromatography (SiO$_2$, DCM–EtOH gradient elution from 94:6 to 9:1) gave 29 mg (31% yield). ^{1}H-NMR shows a 5:4 mixture of amide bond rotamers. ^{1}H-NMR (300 MHz, DMSO-$d6$) δ 12.14–11.96 (m, 1H), 8.41–8.27 (m, 2H), 7.26–7.18 (m, 1H), 7.17–7.06 (m, 1H), 6.92–6.73 (m, 1H), 4.49–4.23 (m, 2H), 4.16–3.97 (m, 2H), 3.93–3.83 (m, 0.45H), 3.70–3.59 (m, 0.55H), 3.20–3.08 (m, 0.45H), 3.08–2.95 (m, 0.55H), 2.90–2.80 (m, 0.55H), 2.72–2.61 (m, 0.45H), 2.13–1.95 (m, 1H), 1.88–1.74 (m, 2H), 1.68–1.42 (m, 1H); ^{13}C NMR (101 MHz, DMSO-$d6$) δ 161.59, 161.56, 161.5, 161.4, 159.1, 159.1, 156.1, 155.6, 155.6, 154.4, 154.4, 137.1, 137.0, 122.9, 122.83, 122.80, 122.7, 116.2, 116.1, 116.02, 115.99, 107.9, 107.6, 97.9, 97.6, 95.7, 95.5, 50.0, 47.5, 46.4, 46.3, 45.8, 42.2, 29.83, 29.75, 24.94, 24.86, 24.3, 23.7; ESI-MS: (m/z) 375.3 [M + Na]$^+$, 351.1 [M − H]$^-$; HPLC method B: t$_r$ = 3.525 min.

3-(3-((7-Chloro-9*H*-pyrimido[4,5-*b*]indol-4-yl)amino)piperidin-1-yl)-3-oxopropanenitrile (**47**)

The title compound was prepared by a two-step procedure.
In the first step **4c** (200.0 mg, 0.51 mmol), **44·HCl** (135.0 mg, 0.66 mmol), and DIPEA (197.7 mg, 1.53 mmol) were reacted in dry DMF (3.5 mL) at 70 °C for 19 h. Additional **44·HCl** (26.0 mg, 0.128 mmol) was added, and stirring at 70 °C continued for 6 h. After cooling down to rt, the mixture was poured into ice-cold water and saturated NH$_4$Cl solution was added (30 mL). The resulting precipitate was filtered off, washed with water, and dried over P$_2$O$_5$ in vacuo. Purification by flash column chromatography (SiO$_2$, DCM–MeOH 96.5:3.5) gave 104 mg of 3-(3-((7-Chloro-9-tosyl-9*H*-pyrimido[4,5-*b*]indol-4-yl)amino)piperidin-1-yl)-3-oxopropanenitrile as a pale yellow solid (39% yield). ^{1}H-NMR shows a 5:4 mixture of amide bond rotamers. ^{1}H-NMR (300 MHz, DMSO-$d6$) δ 8.55–8.44 (m, 1H), 8.42–8.30 (m, 2H), 8.00 (d, *J* = 8.4 Hz, 2H), 7.64–7.52 (m, 1H), 7.39 (d, *J* = 8.3 Hz, 2H), 7.22–7.05 (m, 1H), 4.44–4.19 (m, 2H), 4.15–3.92 (m, 2H), 3.84–3.74

(m, 0.45H), 3.67–3.57 (m, 0.55H), 3.16–3.06 (m, 0.45H), 3.05–2.92 (m, 0.55H), 2.87–2.75 (m, 0.55H), 2.70–2.55 (m, 0.45H), 2.32 (s, 3H), 2.07–1.90 (m, 1H), 1.90–1.68 (m, 2H), 1.68–1.35 (m, 1H); ESI-MS: (*m/z*) 544.8 [M + Na]$^+$, 520.7 [M − H]$^-$; HPLC method A: t_r = 8.439 min.

The purified material obtained from the first step (91.0 mg, 0.17 mmol) was reacted with K*t*BuO (136.7 mg, 1.22 mmol) in dry THF (10 mL) according to general procedure D (reaction time 2 h). Purification by flash column chromatography (SiO$_2$, DCM–MeOH gradient elution from 95:5 to 92:8) gave 41 mg of a white solid (64% yield). ^{1}H-NMR shows a 5:4 mixture of amide bond rotamers. ^{1}H-NMR (300 MHz, DMSO-*d6*) δ 12.07 (s, 1H), 8.49–8.26 (m, 2H), 7.54–7.41 (m, 1H), 7.36–7.21 (m, 1H), 6.99–6.78 (m, 1H), 4.51–4.24 (m, 2H), 4.17–3.97 (m, 2H), 3.93–3.82 (m, 045H), 3.72–3.57 (m, 0.55H), 3.20–3.09 (m, 0.45H), 3.08–2.95 (m, 0.55H), 2.90–2.79 (m, 0.55H), 2.74–2.59 (m, 0.45H), 2.15–1.96 (m, 1H), 1.91–1.72 (m, 2H), 1.71–1.38 (m, 1H); ^{13}C NMR (101 MHz, DMSO-*d6*) δ 161.6, 161.4, 155.90, 155.85, 155.8, 155.03, 154.99, 137.0, 129.1, 129.0, 122.9, 122.8, 120.0, 118.22, 118.18, 116.2, 116.1, 110.7, 95.6, 95.4, 49.9, 47.5, 46.5, 46.2, 45.8, 42.2, 29.8, 29.7, 24.94, 24.86, 24.3, 23.7; ESI-MS: (*m/z*) 391.0 [M + Na]$^+$, 366.9 [M − H]$^-$; HPLC method A: t_r = 6.023 min.

3-(3-((7-Bromo-9*H*-pyrimido[4,5-*b*]indol-4-yl)amino)piperidin-1-yl)-3-oxopropanenitrile (**48**)

4d (50.0 mg, 0.11 mmol), **44·HCl** (35.0 mg, 0.17 mmol), and DIPEA (73.7 mg, 0.57 mmol) were stirred in a solvent mixture of dry dioxane (1 mL) and dry DMF (0.1 mL) at 70 °C overnight. Additional **44·HCl** (35.0 mg, 0.17 mmol) and DIPEA (73.7 mg, 0.57 mmol) were added, and stirring at 70 °C continued overnight. The mixture was concentrated under reduced pressure, the residue diluted with dry THF (4 mL). Na*t*BuO (77.0 mg, 0.80 mmol) was added, and the mixture was stirred at rt for 1 h. Saturated NH$_4$Cl solution (30 mL) was added, and the mixture was extracted with EtOAc (3 × 20 mL). Combined organic layers were dried over Na$_2$SO$_4$ and concentrated under reduced pressure. Purification of the residue by flash column chromatography (SiO$_2$, DCM–EtOH gradient elution from 97:3 to 4:1) gave 25 mg (53% yield). ^{1}H-NMR shows a 5:4 mixture of amide bond rotamers. ^{1}H-NMR (400 MHz, DMSO-*d6*) δ 12.11–12.03 (m, 1H), 8.43–8.34 (m, 1H), 8.33–8.26 (m, 1H), 7.60 (s, 1H), 7.45–7.38 (m, 1H), 6.99–6.80 (m, 1H), 4.49–4.41 (m, 0.55H), 4.39–4.26 (m, 1.45H), 4.15–3.99 (m, 2H), 3.90–3.83 (m, 0.45H), 3.68–3.61 (m, 0.55H), 3.19–3.10 (m, 0.45H), 3.05–2.96 (m, 0.55H), 2.87–2.79 (m, 0.55H), 2.70–2.61 (m, 0.45H), 2.12–1.97 (m, 1H), 1.87–1.75 (m, 2H), 1.67–1.40 (m, 1H); ^{13}C NMR (101 MHz, DMSO-*d6*) δ 161.5, 161.4, 155.9, 155.8, 155.7, 155.13, 155.09, 137.3, 123.2, 123.1, 122.7, 118.51, 118.47, 117.2, 117.1, 116.2, 116.1, 113.6, 95.6, 95.4, 49.9, 47.5, 46.5, 46.2, 45.8, 42.2, 29.8, 29.7, 24.9, 24.9, 24.3, 23.7; ESI-MS: (*m/z*) 434.8 [M + Na]$^+$, 410.7 [M − H]$^-$; HPLC method B: t_r = 5.144 min.

3-(3-((7-Methoxy-9*H*-pyrimido[4,5-*b*]indol-4-yl)amino)piperidin-1-yl)-3-oxopropanenitrile (**49**)

The title compound was prepared from **4f** (496.0 mg, 1.28 mmol), **44·HCl** (392.2 mg, 1.92 mmol), DIPEA (828.5 mg, 6.41 mmol), and Na*t*BuO (863.7 mg, 8.97 mmol) in dry DMF (20 mL) according to general procedure G but was stirred at rt for 3 d after addition of Na*t*BuO. Purification by flash column chromatography (SiO$_2$, DCM–EtOH gradient elution from 97:3 to 4:1) gave 70 mg (15% yield). ^{1}H-NMR shows a 5:4 mixture of amide bond rotamers. ^{1}H-NMR (400 MHz, DMSO-*d6*) δ 11.88–11.77 (m, 1H), 8.37–8.27 (m, 1H), 8.22–8.16 (m, 1H), 6.98–6.94 (m, 1H), 6.90–6.84 (m, 1H), 6.74–6.57 (m, 1H), 4.48–4.24 (m, 2H), 4.15–4.00 (m, 2H), 3.91–3.81 (m, 3.45H), 3.67–3.59 (m, 0.55H), 3.18–3.09 (m, 0.45H), 3.06–2.96 (m, 0.55H), 2.89–2.82 (m, 0.55H), 2.71–2.61 (m, 0.45H), 2.11–1.98 (m, 1H), 1.88–1.74 (m, 2H), 1.66–1.40 (m, 1H); ^{13}C NMR (101 MHz, DMSO-*d6*) δ 161.5, 161.4, 157.7, 157.6, 155.4, 155.2, 155.1, 153.5, 153.4, 137.7, 122.4, 122.2, 116.2, 116.1, 112.9, 112.8, 108.8, 96.1, 95.9, 95.0, 55.3, 50.1, 47.5, 46.3, 45.8, 42.2, 29.84, 29.76, 24.9, 24.8, 24.2, 23.7; ESI-MS: (*m/z*) 387.0 [M + Na]$^+$, 363.1 [M − H]$^-$; HPLC method B: t_r = 2.768 min.

3-Oxo-3-(3-((7-(trifluoromethyl)-9*H*-pyrimido[4,5-*b*]indol-4-yl)amino)piperidin-1-yl)propanenitrile (**50**)

The title compound was prepared from **4g** (180.0 mg, 0.42 mmol), **44·HCl** (129.1 mg, 0.63 mmol), DIPEA (272.7 mg, 2.11 mmol), and Na*t*BuO (284.4 mg, 2.96 mmol) in dry DMF (10 mL) according

to general procedure G. Purification by flash column chromatography (SiO$_2$, 1.DCM–EtOH gradient elution from 97:3 to 4:1, 2.DCM–(2N NH$_3$ in MeOH) gradient elution from 99:1 to 92:8) gave 12 mg (7% yield). ^{1}H-NMR shows a 5:4 mixture of amide bond rotamers. ^{1}H-NMR (300 MHz, DMSO-*d6*) δ 12.31 (s, 1H), 8.60–8.51 (m, 1H), 8.50–8.39 (m, 1H), 7.73 (s, 1H), 7.62–7.53 (m, 1H), 7.17–6.98 (m, 1H), 4.52–4.24 (m, 2H), 4.16–3.97 (m, 2H), 3.93–3.83 (m, 1H), 3.71–3.61 (m, 1H), 3.22–3.12 (m, 1H), 3.08–2.96 (m, 1H), 2.92–2.82 (m, 1H), 2.73–2.62 (m, 1H), 2.15–1.97 (m, 1H), 1.92–1.74 (m, 2H), 1.70–1.40 (m, 1H); ESI-MS: (*m/z*) 424.9 [M + Na]$^+$, 401.0 [M − H]$^-$; HPLC method B: t$_r$ = 5.880 min.

Conflicts of Interest: The authors declare no conflict of interest.

References

1. Kaidanovich-Beilin, O.; Woodgett, J. GSK-3: Functional Insights from Cell Biology and Animal Models. *Front. Mol. Neurosci.* **2011**, *4*, 40. [CrossRef]

2. Sutherland, C. What are the bona fide GSK3 Substrates? *Int. J. Alzheimer's Dis.* **2011**, *2011*, 23.

3. Beurel, E.; Grieco, S.F.; Jope, R.S. Glycogen synthase kinase-3 (GSK3): Regulation, actions, and diseases. *Pharmacol. Ther.* **2015**, *148*, 114–131. [CrossRef]

4. Lauretti, E.; Dincer, O.; Praticò, D. Glycogen synthase kinase-3 signaling in Alzheimer's disease. *Biochim. Biophys. Acta* **2020**, *1867*, 118664. [CrossRef] [PubMed]

5. Andreev, S.; Pantsar, T.; Ansideri, F.; Kudolo, M.; Forster, M.; Schollmeyer, D.; Laufer, S.A.; Koch, P. Design, Synthesis and Biological Evaluation of 7-Chloro-9H-pyrimido[4,5-b]indole-based Glycogen Synthase Kinase-3β Inhibitors. *Molecules* **2019**, *24*, 2331. [CrossRef] [PubMed]

6. Gorrod, J.W.; Aislaitner, G. The metabolism of alicyclic amines to reactive iminium ion intermediates. *Eur. J. Drug Metab. Pharmacokinet.* **1994**, *19*, 209–217. [CrossRef]

7. Meanwell, N.A. Fluorine and Fluorinated Motifs in the Design and Application of Bioisosteres for Drug Design. *J. Med. Chem.* **2018**, *61*, 5822–5880. [CrossRef]

8. Bull, J.A.; Croft, R.A.; Davis, O.A.; Doran, R.; Morgan, K.F. Oxetanes: Recent Advances in Synthesis, Reactivity, and Medicinal Chemistry. *Chem. Rev.* **2016**, *116*, 12150–12233. [CrossRef]

9. Wuitschik, G.; Carreira, E.M.; Wagner, B.; Fischer, H.; Parrilla, I.; Schuler, F.; Rogers-Evans, M.; Müller, K. Oxetanes in Drug Discovery: Structural and Synthetic Insights. *J. Med. Chem.* **2010**, *53*, 3227–3246. [CrossRef]

10. Heider, F.; Ansideri, F.; Tesch, R.; Pantsar, T.; Haun, U.; Döring, E.; Kudolo, M.; Poso, A.; Albrecht, W.; Laufer, S.A.; et al. Pyridinylimidazoles as dual glycogen synthase kinase 3β/p38α mitogen-activated protein kinase inhibitors. *Eur. J. Med. Chem.* **2019**, *175*, 309–329. [CrossRef]

11. Zegzouti, H.; Zdanovskaia, M.; Hsiao, K.; Goueli, S.A. ADP-Glo: A Bioluminescent and Homogeneous ADP Monitoring Assay for Kinases. *Assay Drug Dev. Technol.* **2009**, *7*, 560–572. [CrossRef] [PubMed]

12. Pantsar, T.; Singha, P.; Nevalainen, T.J.; Koshevoy, I.; Leppänen, J.; Poso, A.; Niskanen, J.M.A.; Pasonen-Seppänen, S.; Savinainen, J.R.; Laitinen, T.; et al. Design, synthesis, and biological evaluation of 2,4-dihydropyrano[2,3-c]pyrazole derivatives as autotaxin inhibitors. *Eur. J. Pharm. Sci.* **2017**, *107*, 97–111. [CrossRef] [PubMed]

13. Laufer, S.A.; Hauser, D.R.J.; Domeyer, D.M.; Kinkel, K.; Liedtke, A.J. Design, Synthesis, and Biological Evaluation of Novel Tri- and Tetrasubstituted Imidazoles as Highly Potent and Specific ATP-Mimetic Inhibitors of p38 MAP Kinase: Focus on Optimized Interactions with the Enzyme's Surface-Exposed Front Region. *J. Med. Chem.* **2008**, *51*, 4122–4149. [CrossRef] [PubMed]

14. Di Martino, R.M.C.; Pruccoli, L.; Bisi, A.; Gobbi, S.; Rampa, A.; Martinez, A.; Pérez, C.; Martinez-Gonzalez, L.; Paglione, M.; Di Schiavi, E.; et al. Novel Curcumin-Diethyl Fumarate Hybrid as a Dualistic GSK-3β Inhibitor/Nrf2 Inducer for the Treatment of Parkinson's Disease. *ACS Chem. Neurosci.* **2020**, *11*, 2728–2740. [CrossRef] [PubMed]

15. Tarozzi, A.; Morroni, F.; Merlicco, A.; Hrelia, S.; Angeloni, C.; Cantelli-Forti, G.; Hrelia, P. Sulforaphane as an inducer of glutathione prevents oxidative stress-induced cell death in a dopaminergic-like neuroblastoma cell line. *J. Neurochem.* **2009**, *111*, 1161–1171. [CrossRef] [PubMed]

16. Tarozzi, A.; Bartolini, M.; Piazzi, L.; Valgimigli, L.; Amorati, R.; Bolondi, C.; Djemil, A.; Mancini, F.; Andrisano, V.; Rampa, A. From the dual function lead AP2238 to AP2469, a multi-target-directed ligand for the treatment of Alzheimer's disease. *Pharmacol. Res. Perspect.* **2014**, *2*, e00023. [CrossRef]

17. Pruccoli, L.; Morroni, F.; Sita, G.; Hrelia, P.; Tarozzi, A. Esculetin as a Bifunctional Antioxidant Prevents and Counteracts the Oxidative Stress and Neuronal Death Induced by Amyloid Protein in SH-SY5Y Cells. *Antioxidants* **2020**, *9*, 551. [CrossRef]

18. Showalter, H.D.H.; Bridges, A.J.; Zhou, H.; Sercel, A.D.; McMichael, A.; Fry, D.W. Tyrosine Kinase Inhibitors. 16. 6,5,6-Tricyclic Benzothieno[3,2-d]pyrimidines and Pyrimido[5,4-b]- and -[4,5-b]indoles as Potent Inhibitors of the Epidermal Growth Factor Receptor Tyrosine Kinase. *J. Med. Chem.* **1999**, *42*, 5464–5474. [CrossRef]

19. Tichý, M.; Pohl, R.; Xu, H.Y.; Chen, Y.-L.; Yokokawa, F.; Shi, P.-Y.; Hocek, M. Synthesis and antiviral activity of 4,6-disubstituted pyrimido[4,5-b]indole ribonucleosides. *Bioorganic Med. Chem.* **2012**, *20*, 6123–6133. [CrossRef]

20. Tichý, M.; Pohl, R.; Tloušt'ová, E.; Weber, J.; Bahador, G.; Lee, Y.-J.; Hocek, M. Synthesis and biological activity of benzo-fused 7-deazaadenosine analogues. 5- and 6-substituted 4-amino- or 4-alkylpyrimido[4,5-b]indole ribonucleosides. *Bioorganic Med. Chem.* **2013**, *21*, 5362–5372.

21. Gehringer, M.; Forster, M.; Pfaffenrot, E.; Bauer, S.M.; Laufer, S.A. Novel Hinge-Binding Motifs for Janus Kinase 3 Inhibitors: A Comprehensive Structure–Activity Relationship Study on Tofacitinib Bioisosteres. *ChemMedChem* **2014**, *9*, 2516–2527. [CrossRef] [PubMed]

22. Manley, D.W.; McBurney, R.T.; Miller, P.; Walton, J.C.; Mills, A.; O'Rourke, C. Titania-Promoted Carboxylic Acid Alkylations of Alkenes and Cascade Addition–Cyclizations. *J. Org. Chem.* **2014**, *79*, 1386–1398. [CrossRef] [PubMed]

23. Gehringer, M.; Pfaffenrot, E.; Bauer, S.; Laufer, S.A. Design and Synthesis of Tricyclic JAK3 Inhibitors with Picomolar Affinities as Novel Molecular Probes. *ChemMedChem* **2014**, *9*, 277–281. [CrossRef] [PubMed]

24. Roos, K.; Wu, C.; Damm, W.; Reboul, M.; Stevenson, J.M.; Lu, C.; Dahlgren, M.K.; Mondal, S.; Chen, W.; Wang, L.; et al. OPLS3e: Extending Force Field Coverage for Drug-Like Small Molecules. *J. Chem. Theory Comput.* **2019**, *15*, 1863–1874. [CrossRef]

25. Bochevarov, A.D.; Harder, E.; Hughes, T.F.; Greenwood, J.R.; Braden, D.A.; Philipp, D.M.; Rinaldo, D.; Halls, M.D.; Zhang, J.; Friesner, R.A. Jaguar: A high-performance quantum chemistry software program with strengths in life and materials sciences. *Int. J. Quantum Chem.* **2013**, *113*, 2110–2142. [CrossRef]

26. Heider, F.; Pantsar, T.; Kudolo, M.; Ansideri, F.; De Simone, A.; Pruccoli, L.; Schneider, T.; Goettert, M.I.; Tarozzi, A.; Andrisano, V.; et al. Pyridinylimidazoles as GSK3β Inhibitors: The Impact of Tautomerism on Compound Activity via Water Networks. *ACS Med. Chem. Lett.* **2019**, *10*, 1407–1414. [CrossRef]

27. Madhavi Sastry, G.; Adzhigirey, M.; Day, T.; Annabhimoju, R.; Sherman, W. Protein and ligand preparation: Parameters, protocols, and influence on virtual screening enrichments. *J. Comput. Aided Mol. Des.* **2013**, *27*, 221–234. [CrossRef]

28. Sivaprakasam, P.; Han, X.; Civiello, R.L.; Jacutin-Porte, S.; Kish, K.; Pokross, M.; Lewis, H.A.; Ahmed, N.; Szapiel, N.; Newitt, J.A.; et al. Discovery of new acylaminopyridines as GSK-3 inhibitors by a structure guided in-depth exploration of chemical space around a pyrrolopyridinone core. *Bioorg. Med. Chem. Lett.* **2015**, *25*, 1856–1863. [CrossRef]

29. Bowers, K.J.; Chow, E.; Xu, H.; Dror, R.O.; Eastwood, M.P.; Gregersen, B.A.; Klepeis, J.L.; Kolossvary, I.; Moraes, M.A.; Sacerdoti, F.D.; et al. *Scalable Algorithms for Molecular Dynamics Simulations on Commodity Clusters, Proceedings of the 2006 ACM/IEEE Conference on Supercomputing, Tampa, FL, USA, 11–17 November 2006*; ACM: Tampa, FL, USA, 2006; p. 84.

30. Jorgensen, W.L.; Chandrasekhar, J.; Madura, J.D.; Impey, R.W.; Klein, M.L. Comparison of simple potential functions for simulating liquid water. *J. Chem. Phys.* **1983**, *79*, 926–935. [CrossRef]

Supplementary Materials

Discovery and Evaluation of Enantiopure 9*H*-pyrimido[4,5-*b*]indoles as Nanomolar GSK-3β Inhibitors with Improved Metabolic Stability

Stanislav Andreev [1], Tatu Pantsar [1,2], Ahmed El-Gokha [1,3], Francesco Ansideri [1], Mark Kudolo [1], Débora Bublitz Anton [4], Giulia Sita [5], Jenny Romasco [6], Christian Geibel [7], Michael Lämmerhofer [7], Márcia Ines Goettert [4], Andrea Tarozzi [6], Stefan A. Laufer [1] and Pierre Koch [1,8,*]

[1] Institute of Pharmaceutical Sciences, Department of Medicinal and Pharmaceutical Chemistry, Eberhard Karls University Tübingen, Auf der Morgenstelle 8, 72076 Tübingen, Germany; stanislav.andreev@uni-tuebingen.de (S.A.); tatu.pantsar@uni-tuebingen.de (T.P.); ahmed.abdelaleem@science.menofia.edu.eg (A.E.-G.); francesco.ansideri@uni-tuebingen.de (F.A.); mark.kudolo@uni-tuebingen.de (M.K.); stefan.laufer@uni-tuebingen.de (S.L.)

[2] School of Pharmacy, Faculty of Health Sciences, University of Eastern Finland, P.O. Box 1627, 70211 Kuopio, Finland

[3] Chemistry Department, Faculty of Science, Menoufia University, 32511 Shebin El-Kom, Egypt

[4] Cell Culture Laboratory, Postgraduate Program in Biotechnology, University of Vale do Taquari (Univates), 95914-014 Lajeado, Brazil; debora.anton@univates.br (D.B.A.); marcia.goettert@univates.br (M.I.)

[5] Department of Pharmacy and Biotechnology, Alma Mater Studiorum, University of Bologna, Via Irnerio, 48, 40126 Bologna, Italy; giulia.sita2@unibo.it

[6] Department for Life Quality Studies, Alma Mater Studiorum, University of Bologna, Corso D'Augusto, 237, 47921 Rimini, Italy; jenny.romasco@unibo.it (J.R.); andrea.tarozzi@unibo.it (A.T.)

[7] Institute of Pharmaceutical Sciences, Department of Pharmaceutical (Bio-)Analysis, Eberhard Karls University Tübingen, Auf der Morgenstelle 8, 72076 Tübingen, Germany; christian.geibel@uni-tuebingen.de (C.G.); michael.laemmerhofer@uni-tuebingen.de (M.L.)

[8] Department of Pharmaceutical/Medicinal Chemistry II, Institute of Pharmacy, University of Regensburg, Universitätsstraße 31, 93053 Regensburg, Germany

* Correspondence: pierre.koch@uni-tuebingen.de; Tel.: +49-(941)-943-2847

Table of Contents

1. ADP Glo™ Kinase Assay

The inhibitory activity of the final compounds on GSK-3β was determined by the Promega ADP-Glo™ Kinase assay (Promega Corporation, Madison, WI 53711, USA), which was performed in white, non-treated 384-well plates (Corning). The experiments were carried out as quadruplicates using a concentration of 0.58 ng/μL of recombinant human GSK-3β, 0.2 μg/μL GSK-3 substrate G50-58 (sequence: YRRAAVPPSPSLSRHSSPHQ(pS)EDEEE) and 25 μM ATP in the presence of serial dilutions of the final compounds. In addition, two control experiments with uninhibited kinase and two blank experiments with ATP/substrate solution were performed.

In detail, the kinase was pre-incubated with the final compounds for 10 min at rt. Then substrate/ATP was added to start the reaction, which was run for 1 h at rt. The next steps consisted of addition of ADP-Glo™ reagent (5 μL, then 1 h incubation) and Kinase detection reagent (10 μL, then 30 min incubation). Finally, the luminescence was measured on a FilterMax F5 microplate reader (Molecular Devices) (integration time 500 ms). GraphPad Prism v. 7.03. was used to normalize the raw data to the values of the control and blank experiments and generate absolute IC_{50} values.

2. Interaction Frequencies of *(R)*-2 and *(R)*-28 in the 1 μs Molecular Dynamics Simulations
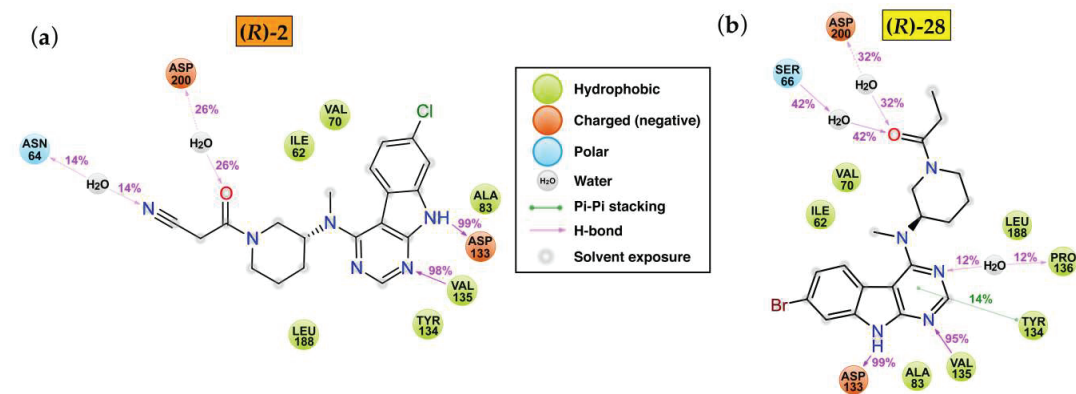
Figure S1. Observed interactions of *(R)*-2 **(a)** and *(R)*-28 **(b)** in the MD simulations. Both ligands demonstrate stable hinge binding (95–99% Asp133 and Val135 interactions). The carbonyl group mediates water-bridged interactions to Asp200 or Ser66. Interactions with >10% frequency are shown.

3. Microsomal Stability Assay

Pooled male and female human liver microsomes (HLMs) (Lot: SLBQ7487V) were purchased from Merck (Schnelldorf, Germany). The compounds (*(R)*-2 and *(R)*-28, respectively) (100 μM), 4 mM MgCl₂·6 H₂O in 0.1 M Tris buffer (pH 7.4) and an NADPH-regenerating system (5 mM glucose-6-phosphate, 5 U/mL glucose-6-phosphate dehydrogenase and 1 mM NADP⁺) were preincubated for 5 min at 37 °C and 750× rpm on a shaker. The HLMs were added to start the reaction. The reaction mixture was then split into triplicates of 50 μL. The reaction was quenched at six time points (0, 10, 20, 30, 60 and 120 min) by addition of 100 μL internal standard (30 μM in MeCN). The samples were vortexed for 30 s and centrifuged (19,800 relative centrifugal force/4 °C/10 min). The obtained supernatant was directly used for LC-MS analysis. A limit of 1% organic solvent was not exceeded.
Positive control: Propranolol
Negative control: Heat inactivated microsomes
The metabolite formation was analyzed with an Alliance 2695 Separations Module (Waters GmbH, Eschborn).
Sample temperature: 4 °C
Column: Phenomenex Kinetex C18 column (100 × 3 mm; 2.6 μm; 100 Å)
Column temperature: 40 °C

Injection volume: 5 μL
Flow rate: 0.6 mL/min
Gradient: see Table below

Table S1. Chromatographic gradient for separation of metabolism analytes.

Time (min)	Solvent A (%) (90% H_2O, 10% MeCN, 0.1% formic acid)	Solvent B (%) (MeCN, 0.1% formic acid)
0	90	10
2.5	90	10
10	45	55
12	45	55
12.01	90	10
15	90	10

The detection was performed on a Micromass Quattro micro triple quadrupole mass spectrometer (Waters GmbH, Eschborn).

Ionization mode: Electrospray ionization, positive mode
Spray voltage: 4.5 kV
Desolvation temperature: 250 °C
Desolvation gas flow: 600 L/h

4. Investigation of Cell Toxicity on Five Different Cell Lines

4.1. Maintenance of Cell Culture

The experiments were performed in an *in vitro* model of cell cytoxicity analyses on hepatocellular carcinoma (HepG2), human breast adenocarcinoma (MCF-7), human neuroblastoma (SH-SY5Y), human lung fibroblast (MRC-5) and chinese hamster ovary (CHO-K1). The cells lines were cultured in appropriate medium, supplemented with 10% (*v/v*) of fetal bovine serum (FBS) and 1% antibiotic/antimycotic solution. For subculture, cells were dissociated with trypsin-EDTA (Cultilab), split into a 1:3 ratio and subcultured into Petri dishes with 25 cm^2 growth area. Culture medium was replaced every 2 days until the cells reached the total confluence after 4–5 days of initial seeding. Cells were maintained in the following controlled conditions: 95% of humidified atmosphere, 5% of CO_2 and constant temperature of 37 °C.

4.2. Cytotoxicity

The assessment of cell viability was performed according to the MTT colorimetric assay. The cytotoxicity of the compounds was assessed on 5 different cell lines. Cells (5 × 10^3/well) in 200 μL appropriate medium containing 10% FBS were seeded on 96-well plates and incubated overnight. These cells were subsequently treated with different concentrations of compound *(R)*-**28** for 48 h. The effects were estimated by colorimetric assay based on the conversion of tetrazolium salts (MTT) after 3 h of incubation to a blue formazan product by active mitochondria. The absorbance was read at 570 nm using a Spectramax i5 microplate reader. Results were expressed as percentage of control.

Cell Lines
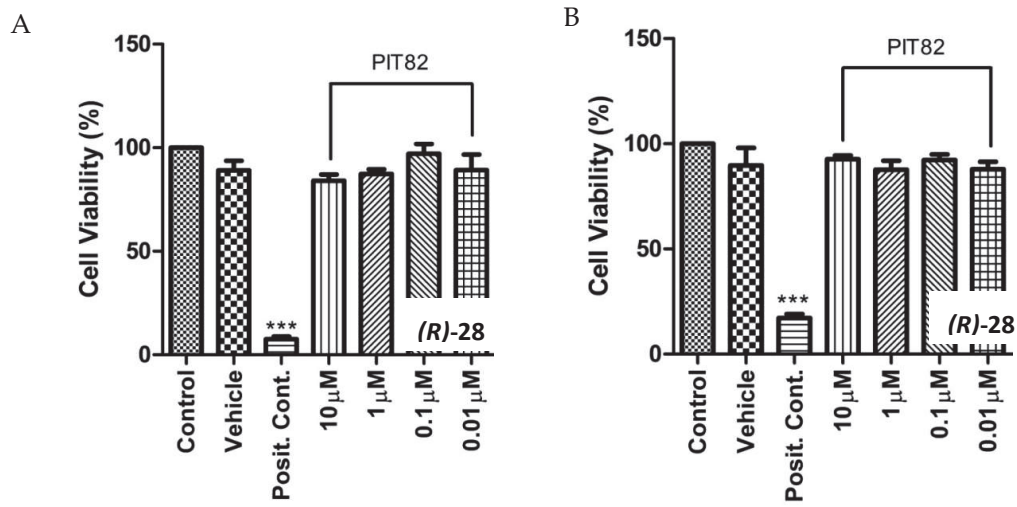
Figure S2. Evaluation of the cytotoxic potential of *(R)-28* on cell lines. (**A**) Human lung fibroblast cell line MRC-5 and (**B**) chinese hamster ovary cell line CHO-K1. Cell viability was evaluated by MTT assay, after 48 h treatment with *(R)-28*. Mean values ± SEM of three independent experiments are shown. *** $p < 0.001$ compared with control. *(R)-28*; Vehicle (DMSO); Positive Control (hydrogen peroxide).

Cancer Cell Lines
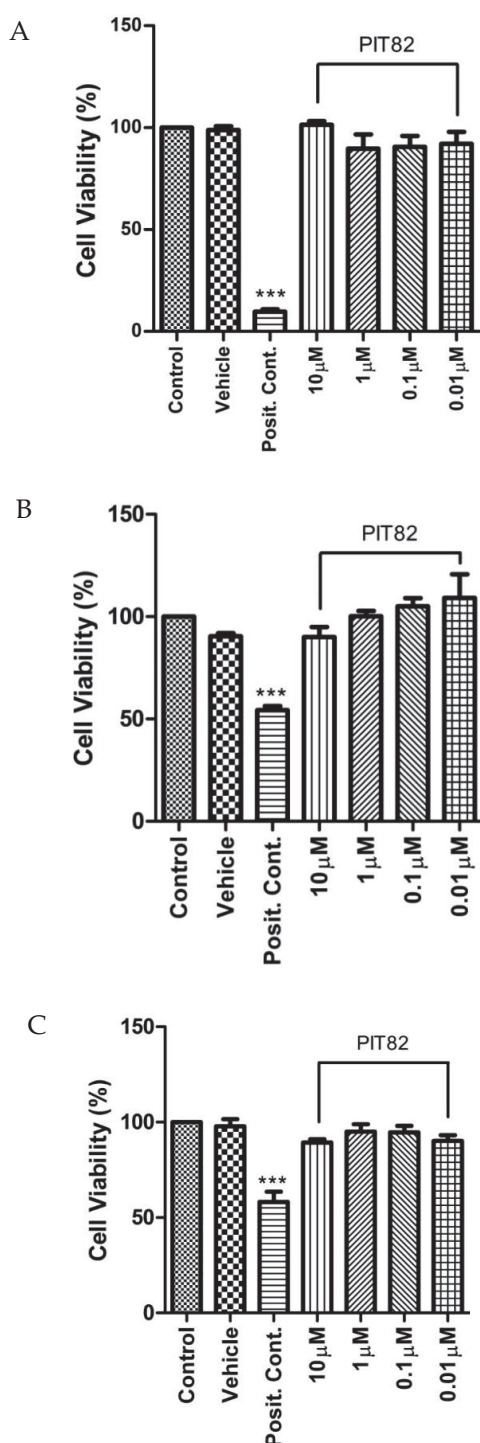
Figure S3. Evaluation of the cytotoxic potential of *(R)*-28 on cancer cell lines. (**A**) Hepatocellular carcinoma cell line HepG2, (**B**) human breast adenocarcinoma cell line MCF-7 and (**C**) human neuroblastoma cell line SH-SY5Y. Cell viability was evaluated by MTT assay, after 48 h treatment with *(R)*-28. Mean values ± SEM of three independent experiments are shown. *** $p < 0.001$ compared with control. *(R)*-28; Vehicle (DMSO); Positive Control (hydrogen peroxide).

5. Investigation of Cellular GSK-3α/β Inhibition by *(R)*-28 and Its Neuroprotective Effects

5.1. Cell Cultures

Human neuronal SH-SY5Y cells (Sigma Aldrich, St. Louis, MO, USA) were routinely grown in Dulbecco's modified Eagle's Medium supplemented with 10% fetal bovine serum, 2 mM L-glutamine, 50 U/mL penicillin and 50 μg/mL streptomycin at 37 °C in a humidified incubator with 5% CO_2.

5.2. Neuronal Viability

SH-SY5Y cells were seeded in a 96-well plate at 2×10^4 cells/well, incubated for 24 h and then treated with various concentrations (1.25–40 μM) of *(R)-28* for 24 h. Cell viability, in terms of mitochondrial activity, was evaluated by MTT assay, as previously described [14].

5.3. Neuroprotective Activity toward H_2O_2

SH-SY5Y cells were seeded in a 96-well plate at 2×10^4 cells/well, incubated for 24 h and subsequently treated with *(R)-28* (5 μM) and H_2O_2 (100 μM) for 1 h. Then, cells were starved in complete medium for 22 h. The neuroprotective activity was measured by using the MTT assay as previously described [15]. Data are expressed as a percentage of neurotoxicity versus untreated cells.

5.4. OAβ_{1-42} Preparation for the Determination of Neuroprotective Activity

Aβ_{1-42} peptide (AnaSpec, Fremont, CA, USA) was first dissolved in 1,1,1,3,3,3-hexafluoroisopropanol to 1 mg/mL, sonicated, incubated at rt for 24 h, and lyophilised to obtain an unaggregated Aβ_{1-42} peptide film that was solubilised with DMSO and stored at −20 °C until use. The aggregation of Aβ_{1-42} peptide into oligomers was performed as previously described [16].

5.5. Neuroprotective Activity toward OAβ_{1-42}

SH-SY5Y cells were seeded in a 96-well plate at 3×10^4 cells/well, incubated for 24 h, and subsequently treated with *(R)-28* (5 μM) and OAβ_{1-42} (10 μM) for 4 h. The neuroprotective activity was measured by using the MTT assay as previously described [17]. Data are expressed as a percentage of neurotoxicity versus untreated cells.

5.6. Western Blotting

SH-SY5Y cells were seeded in 60 mm dishes at 2×10^6 cells/dish, incubated for 24 h and subsequently treated with *(R)-28* (1 μM) for 1 h at 37 °C in 5% CO_2. At the end of incubation, cells were trypsinized and the cellular pellet was resuspended in complete lysis buffer containing leupeptin (2 μg/mL), PMSF (100 μg/mL) and cocktail of protease/phosphatase inhibitors (100×). Small amounts were removed for the determination of the protein concentration using the Bradford method. The samples (30 μg proteins) were run on 4–15% SDS polyacrylamide gels (Bio-rad Laboratories S.r.L., Hercules, CA, USA) and electroblotted onto 0.45 μm nitrocellulose membranes. The membranes were incubated at 4 °C overnight with primary antibody recognizing phospho-GSK3α/β (Ser21/9), (1:1000; Cell Signaling Technology Inc, Danvers, MA, USA), or anti-phospho-GSK3(Tyr279/Tyr216), (1:1000; EMD Millipore, Darmstadt, Germany). After washing with TBS-T (TBS +0.05% Tween20), the membranes were incubated with secondary antibodies (1:2000; GE Healthcare). Enhanced chemiluminescence was used to visualize the bands (ECL; Bio-rad Laboratories). The membranes were then reprobed with GSK3α/β, (1:1000; Cell Signaling Technology Inc.). The data were analyzed by densitometry, using Quantity One software (Bio-Rad Laboratories® S.r.L.). The values were normalized and expressed as mean ± SD of densitometry in each experimental group.

5.7. Statistical Analysis

Results are shown as mean ± standard deviation (SD) of three independent experiments. Statistical analysis was performed using Student's t-test. Differences were considered significant at $p < 0.05$. Analyses were performed using GraphPad PRISM software (v. 5.0; GraphPad Software, La Jolla, CA, USA) on a Windows platform.
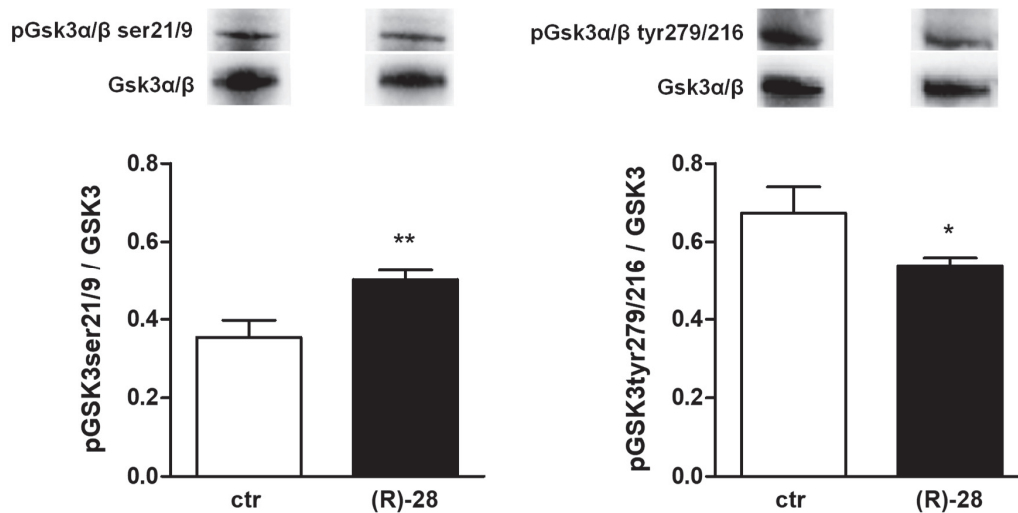
Figure S4. Compound *(R)-28* inhibits the GSK-3β activity in neuronal SH-SY5Y cells. Cells were incubated with *(R)-28* (1 µM) for 1 h. At the end of incubation, the phosphorylation of GSK-3α/β (Ser21/9) (inactive GSK-3α/β form) and GSK-3α/β (Tyr279/Tyr216) (active GSK-3α/β form) was determined by western blotting. Data are expressed as ratio between phospho-GSK-3α/β and total GSK-3β levels normalized against β-Actin. Mean values ± SD of at least three independent experiments are shown (* $p < 0.05$ and ** $p < 0.01$ vs untreated cells).
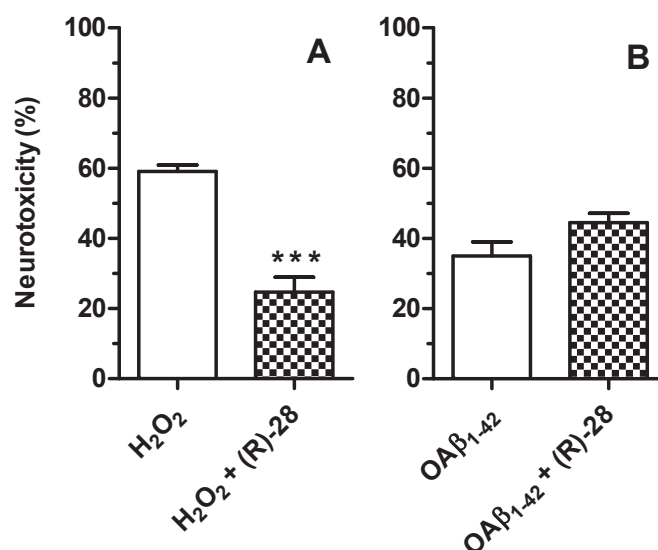
Figure S5. Neuroprotective effects of *(R)-28* against the neurotoxicity induced by H_2O_2 and $OA\beta_{1-42}$ in SH-SY5Y cells. **(A)** Cells were incubated with *(R)-28* (5 μM) and H_2O_2 (100 μM) for 1 h and then starved in complete medium for 22 h. **(B)** Cells were incubated with *(R)-28* (5 μM) and $OA\beta_{1-42}$ (10 μM) for 4 h. The neurotoxicity was evaluated by MTT assay as described above. Data are expressed as percentages of neurotoxicity versus untreated cells. Mean values ± SD of three independent experiments are shown (*** $p < 0.001$ vs cells treated with H_2O_2).

6. Preparation of 4-chloro-9*H*-pyrimido[4,5-*b*]indoles 3a–l

The substitution pattern of the non-aromatic ring in the 9*H*-pyrimido[4,5-*b*]indole core was defined by utilizing appropriate *o*-halonitrobenzenes (**S1a–k**) in the first step of the synthetic route (Scheme S1). These commercially available starting materials were reacted with ethyl cyanoacetate under highly basic conditions giving substitution products **S2a–k**. Reductive ring closure was then effected with elemental zinc in acetic acid and typically generated 2-aminoindoles **S3a–k** along with characteristic by-products, which presumably are the corresponding 1-hydroxy-2-aminoindoles [18]. However, a purification of these mixtures was unnecessary in most cases, as the following condensation with formamide predominently afforded the desired 3,9-dihydro-4*H*-pyrimido[4,5-*b*]indol-4-ones **S1a–k**. The introduction of a methyl group in the 2-position of the pyrimidine ring of **S4l** was achieved applying a protocol modified from Showalter et al. [18]. To this end, **S3c** was converted to an amidine intermediate with acetonitrile, which was then cyclized to **S4l** with aqueous NaOH in EtOH. The reaction of **S4a–l** with $POCl_3$ finally delivered 4-chloro-9*H*-pyrimido[4,5-*b*]indoles **3a–l**.
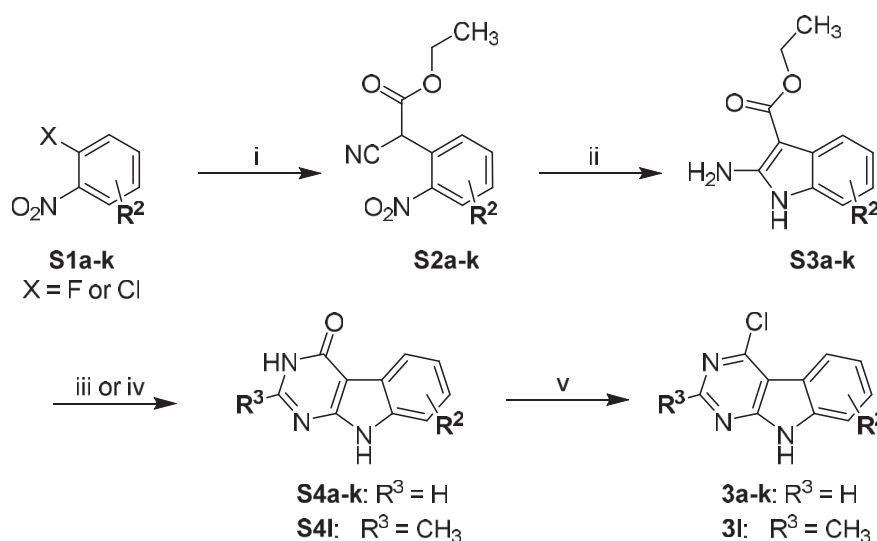
Scheme S1. Synthetic route to 4-chloro-9*H*-pyrimido[4,5-*b*]indoles **3a–l**. For the definition of R² see Scheme 1 in the main manuscript. Reagents and conditions: (i) ethyl cyanoacetate, NaH, DMF, 0 °C to rt or 75 °C in case of **S2a–g** or ethyl cyanoacetate, K*t*BuO, THF, 0 °C to 60 °C in case of **S2h–k** (ii) Zn⁰, AcOH, 90 °C; (iii) NH₄HCOO, formamide, 160 °C in case of **S4a–d** and **S4h–k** or formamide, 160–190 °C in case of **S4e–g**; (iv) (1) **S3c**, HCl, MeCN, rt to reflux, (2) NaOH₍aq₎, EtOH, reflux (in case of **S4l**); (v) POCl₃, DIPEA, chlorobenzene, rt to 80–100 °C in case of **3a, 3c–e**, **3h,i** and **3k,l** or DIPEA, POCl₃ (neat), rt to 80 °C in case of **3b**, **3f** and **3j** or POCl₃ (neat), rt to 80 °C in case of **3g**.

6.1. General Procedure H

The appropriate intermediate was dissolved in glacial AcOH. The solution was heated to 80–90 °C and zinc powder was added in portions. The suspension was stirred at 80–90 °C until reaction control by HPLC indicated complete consumption of the starting material. The suspension was left to cool down to rt and filtered rinsing the residue with glacial AcOH or EtOAc. The filtrate was concentrated under reduced pressure to leave a residue of AcOH which was neutralized by addition of saturated NaHCO₃ solution. The resulting precipitate was filtered off, washed with demineralised water and dried over P₂O₅ in vacuo. The crude material isolated from these reactions typically consisted of a mixture of the title compounds and the corresponding 1-hydroxyindoles. These crude mixtures were used in the next step without further purification.

6.2. General Procedure I

The appropriate intermediate was suspended in formamide and ammonium formate was added. The mixture was stirred at 160 °C until reaction control by HPLC indicated complete consumption of the starting material. The suspension was left to cool down to rt and poured into ice-cold water. The resulting precipitate was filtered off, rinsed thoroughly with demineralised water and dried over P₂O₅ in vacuo. The crude product was used in the next step without further purification.

6.3. General Procedure J

The appropriate intermediate was suspended in chlorobenzene. DIPEA was added followed by careful addition of POCl₃ (used in stochiometric amounts or as co-solvent). The mixture was stirred at 80–100 °C until reaction control by HPLC indicated complete consumption of the starting material. After cooling down to rt the mixture was carefully transferred into stirring demineralised water of rt. The highly acidic aqueous mixture was neutralized with aqueous NaOH solution. The resulting precipitate was filtered off, rinsed thoroughly with demineralised water and dried over P₂O₅ in

vacuo. If not stated otherwise, the crude material was purified by hot filtration from toluene as described previously [5].

Detailed Procedures for the Preparation of Intermediates S3a–k.

Ethyl 2-amino-1*H*-indole-3-carboxylate (**S3a**)

The title compound was prepared by a two-step procedure. In the first step ethyl cyanoacetate (32.1 g, 283.79 mmol) was drop-added to an ice-cooled stirring suspension of NaH (11.4 g of a 60% dispersion in mineral oil, 283.79 mmol) in dry DMF (20 mL) under N_2 atmosphere. The mixture was left to warm to rt for 30 min. A solution of 1-fluoro-2-nitrobenzene (**S1a**) (20.0 g, 141.74 mmol) in dry DMF (10 mL) was drop-added at 0 °C. The mixture was left to warm to rt for 30 min and then heated to 75 °C for 3 h. After cooling down to rt, 10% HCl(aq) (80 mL) was added to acidify the mixture, which was then extracted with EtOAc (3 × 80 mL). Combined organic layers were washed with saturated NaCl solution (2 × 100 mL), dried over Na_2SO_4 and concentrated under reduced pressure. The oily residue contained ethyl 2-cyano-2-(2-nitrophenyl)acetate (**S2a**), as well as the excessive ethyl cyanoacetate and was used in the next step without further purification; ESI-MS: (*m/z*) 257.0 [M + Na]$^+$, 232.9 [M − H]$^-$; HPLC method B: t_r = 3.399 min.

The crude material obtained from the first step was reacted with zinc powder (111.2 g, 1.70 mol) in glacial AcOH (50 mL) according to general procedure H (reaction time 2 h, after complete addition of zinc). The precipitate obtained during the aqueous work-up was not filtered off, but extracted repeatedly with EtOAc. Combined organic layers were dried over Na_2SO_4 and evaporated to dryness. 26.7 g of the crude product were yielded (92% crude yield over two steps) and used in the next step without further purification; HPLC method B: t_r = 5.176 min.

Ethyl 2-amino-6-fluoro-1*H*-indole-3-carboxylate (**S3b**)

The title compound was prepared by a two-step procedure. In the first step ethyl cyanoacetate (6.0 g, 52.80 mmol) was drop-added to an ice-cooled stirring suspension of NaH (2.1 g of a 60% dispersion in mineral oil, 52.80 mmol) in dry DMF (4 mL) under N_2 atmosphere. The mixture was left to warm to rt for 30 min. A solution of 1,4-difluoro-2-nitrobenzene (**S1b**) (4.0 g, 25.14 mmol) in dry DMF (4 mL) was drop-added and the mixture stirred at rt for 30 min and then heated to 75 °C for another 30 min. After cooling down to rt, 10% HCl(aq) (20 mL) was added to acidify the mixture, which was then extracted with EtOAc (3 × 20 mL). Combined organic layers were washed with saturated NaCl solution (2 × 40 mL), dried over Na_2SO_4 and concentrated under reduced pressure. The oily residue contained ethyl 2-cyano-2-(4-fluoro-2-nitrophenyl)acetate (**S2b**), as well as excessive ethyl cyanoacetate and was used in the next step without further purification.

The crude material obtained from the first step was reacted with zinc powder (19.7 g, 301.31 mmol) in glacial AcOH (50 mL) according to general procedure H (reaction time 1.5 h). 4.6 g of the crude product were yielded (82% crude yield over two steps) and used in the next step without further purification; ^{1}H NMR (300 MHz, DMSO-*d₆*) δ 10.70 (s, 1H), 7.48 (dd, *J* = 8.5, 5.6 Hz, 1H), 6.94 (dd, *J* = 9.7, 2.4 Hz, 1H), 6.78 (ddd, *J* = 10.2, 8.5, 2.5 Hz, 1H), 6.71 (s, 2H), 4.22 (q, *J* = 7.1 Hz, 2H), 1.31 (t, *J* = 7.1 Hz, 3H).

Ethyl 2-amino-6-bromo-1*H*-indole-3-carboxylate (**S3d**)

The title compound was prepared by a two-step procedure. In the first step ethyl cyanoacetate (8.1 g, 71.59 mmol) was drop-added to an ice-cooled stirring suspension of NaH (2.9 g of a 60% dispersion in mineral oil, 71.59 mmol) in dry DMF (15 mL) under N_2 atmosphere. The dropping funnel was purged with additional dry DMF (3 mL) and the mixture left to warm to rt for 10 min. A solution of 4-bromo-1-fluoro-2-nitrobenzene (**S1d**) (7.5 g, 34.01 mmol) in dry DMF (7.5 mL) was then drop-added to the stirring suspension. Again, the dropping funnel was purged with additional dry DMF (5 mL). The mixture was stirred at rt for 45 min. 10% HCl(aq) (40 mL) was added to acidify the mixture, which was then extracted with EtOAc (3 × 30 mL). Combined organic layers were washed

with saturated NaCl solution (5 × 30 mL), dried over Na_2SO_4 and concentrated under reduced pressure. The liquid residue was treated with ice-cold water resulting in a precipitate, which was filtered off and dried over P_2O_5 in vacuo. 10.7 g of crude ethyl 2-(4-bromo-2-nitrophenyl)-2-cyanoacetate (**S2d**) as a yellow solid (100% crude yield) were yielded and used in the next step without further purification. ^1H NMR (300 MHz, DMSO-d_6) δ 8.44 (d, *J* = 2.0 Hz, 1H), 8.13 (dd, *J* = 8.3, 2.1 Hz, 1H), 7.70 (d, *J* = 8.3 Hz, 1H), 6.25 (s, 1H), 4.22 (q, *J* = 7.1 Hz, 2H), 1.19 (t, *J* = 7.1 Hz, 3H); ^{13}C NMR (75 MHz, DMSO-d_6) δ 163.7, 147.4, 137.9, 134.7, 128.7, 124.9, 123.3, 115.0, 63.1, 40.8, 13.8; ESI-MS: (*m/z*) 310.8 [M − H]$^-$; HPLC method A: t_r = 6.985 min.

The crude material obtained from the first step (10.3 g, 32.81 mmol) was reacted with zinc powder (12.9 g, 196.83 mmol) in glacial AcOH (80 mL) according to general procedure H (reaction time 2.5 h). 9.4 g of the crude product as a grey-red solid were yielded (98% crude yield over two steps) and used in the next step without further purification.

Ethyl 2-amino-6-iodo-1*H*-indole-3-carboxylate (**S3e**)

The title compound was prepared by a two-step procedure. In the first step a solution of ethyl cyanoacetate (4.2 g, 36.97 mmol) in dry DMF (4 mL) was drop-added to an ice-cooled stirring suspension of NaH (1.48 g of a 60% dispersion in mineral oil, 36.97 mmol) in dry DMF (13 mL) under N_2 atmosphere. The dropping funnel was purged with additional dry DMF (2 mL) and the mixture left to warm to rt. A solution of 1-fluoro-4-iodo-2-nitrobenzene (**S1e**) (4.7 g, 17.60 mmol) in dry DMF (7 mL) was then drop-added to the stirring suspension during 15 min. The mixture was left stirring for 30 min at rt. 10% $HCl_{(aq)}$ (50 mL) was added to acidify the mixture, which was then extracted with EtOAc (3 × 60 mL). Combined organic layers were washed with saturated NaCl solution (3 × 60 mL), dried over Na_2SO_4 and concentrated under reduced pressure. The oily residue was treated with ice-cold water resulting in a yellow precipitate, which was filtered off and dried over P_2O_5 in vacuo. 6.5 g of crude ethyl 2-cyano-2-(4-iodo-2-nitrophenyl)acetate (**S2e**) as a yellow solid were yielded (>100% crude yield) and used in the next step without further purification; ^1H NMR (300 MHz, DMSO-d_6) δ 8.53 (d, *J* = 1.7 Hz, 1H), 8.27 (dd, *J* = 8.1, 1.7 Hz, 1H), 7.50 (d, *J* = 8.1 Hz, 1H), 6.21 (s, 1H), 4.22 (q, *J* = 7.1 Hz, 2H), 1.19 (t, *J* = 7.1 Hz, 3H); ^{13}C NMR (75 MHz, DMSO-d_6) δ 163.7, 147.1, 143.7, 134.5, 134.0, 125.1, 115.0, 96.5, 63.1, 40.9, 13.8. ESI-MS: (*m/z*) 359.2 [M − H]$^-$; HPLC method A: t_r = 6.970 min.

The crude material obtained from the first step (3.3 g, 9.08 mmol) was dissolved in glacial acetic acid (22 mL). Pronounced dehalogenation was observed when applying the general procedure H, therefore zinc powder (3.3 g, 49.94 mmol) was added in portions at rt and the mixture was then stirred at 80 °C for 30 min. The suspension was left to cool down to rt and filtered rinsing the residue with EtOAc. The filtrate was concentrated under reduced pressure to leave a residue of AcOH, which was neutralized by addition of saturated $NaHCO_3$ solution. The resulting precipitate was filtered off and washed with demineralised water. It was then redissolved in EtOAc and the solution was dried over Na_2SO_4 and evaporated to dryness. 2.5 g of the crude product as a black foam were yielded (85% crude yield over two steps) and used in the next step without further purification.

Ethyl 2-amino-6-methoxy-1*H*-indole-3-carboxylate (**S3f**)

The title compound was prepared by a two-step procedure. In the first step ethyl cyanoacetate (6.3 g, 55.98 mmol) was drop-added to an ice-cooled stirring suspension of NaH (2.2 g, 55.98 mmol) in dry DMF (35 mL) under N_2 atmosphere. The mixture was left to warm to rt for 30 min. A solution of 1-chloro-4-methoxy-2-nitrobenzene (**S1f**) (5.0 g, 26.66 mmol) in dry DMF (7 mL) was drop-added and the mixture stirred at rt for 30 min and then heated to 75 °C for 5 h. After cooling down to rt, 5N $HCl_{(aq)}$ was added to acidify the mixture followed by DCM (150 mL) and saturated NaCl solution (100 mL). The mixture was stirred at rt for 30 min and phases were separated. The aqueous layer was extracted with DCM (50 mL). Combined organic layers were dried over Na_2SO_4 and concentrated under reduced pressure. Purification of the residue by flash column chromatography (SiO$_2$, hexane:EtOAc gradient elution from 1:0 to 3:2) gave 4.3 g of ethyl 2-cyano-2-(4-methoxy-2-nitrophenyl)acetate (**S2f**); ^1H NMR (300 MHz, DMSO-d_6) δ 7.76 (d, *J* = 2.7 Hz, 1H), 7.65 (d, *J* = 8.7 Hz,

1H), 7.46 (dd, *J* = 8.6, 2.8 Hz, 1H), 6.13 (s, 1H), 4.21 (q, *J* = 7.0 Hz, 2H), 1.19 (t, *J* = 7.1 Hz, 3H); ESI-MS: (*m/z*) 287.3 [M + Na]$^+$, 263.1 [M − H]$^-$; HPLC method B: t$_r$ = 4.414 min.

The purified material from the first step (4.3 g, 16.27 mmol) was reacted with zinc powder (12.8 g, 195.8 mmol) in glacial AcOH (50 mL) according to general procedure H (reaction time 1.5 h). Purification by flash column chromatography (SiO$_2$, hexane:EtOAc gradient elution from 1:0 to 3:2) gave 1.6 g of the title compound (26% yield over two steps); ^{1}H NMR (300 MHz, DMSO-*d$_6$*) δ 10.49 (s, 1H), 7.40 (d, *J* = 8.4 Hz, 1H), 6.73 (d, *J* = 2.3 Hz, 1H), 6.62–6.46 (m, 3H), 4.20 (q, *J* = 7.1 Hz, 2H), 1.30 (t, *J* = 7.1 Hz, 3H); ESI-MS: (*m/z*) 234.3 [M + H]$^+$, 257.3 [M + Na]$^+$, 233.1 [M − H]$^-$; HPLC method B: t$_r$ = 4.805 min.

Ethyl 2-amino-6-(trifluoromethyl)-1*H*-indole-3-carboxylate (**S3g**)

The title compound was prepared by a two-step procedure. In the first step ethyl cyanoacetate (5.3 g, 46.55 mmol) was drop-added to an ice-cooled stirring suspension of NaH (1.9 g of a 60% dispersion in mineral oil, 46.55 mmol) in dry DMF (30 mL) under N$_2$ atmosphere. The mixture was left to warm to rt for 30 min. A solution of 1-chloro-2-nitro-4-(trifluoromethyl)benzene (**S1g**) (5.0 g, 22.17 mmol) in dry DMF (10 mL) was drop-added and the mixture stirred at rt for 30 min and then heated to 70 °C for 2 h. After cooling down to rt, 10% HCl$_{(aq)}$ was added to acidify the mixture, which was then extracted with EtOAc (3 × 50 mL). Combined organic layers were dried over Na$_2$SO$_4$ and concentrated under reduced pressure. The oily residue contained ethyl 2-cyano-2-(2-nitro-4-(trifluoromethyl)phenyl)acetate (**S2g**), as well as excessive ethyl cyanoacetate and was used in the next step without further purification; ESI-MS: (*m/z*) 301.1 [M − H]$^-$; HPLC method B: 6.395 min.

The crude material obtained from the first step was reacted with zinc powder (17.4 g, 266.04 mmol) in glacial AcOH (50 mL) according to general procedure G (reaction time 1.5 h). 6.8 g of the crude product were yielded (>100% crude yield over two steps) and used in the next step without further purification; ^{1}H NMR (300 MHz, DMSO-*d$_6$*) δ 10.91 (s, 1H), 7.67 (d, *J* = 8.2 Hz, 1H), 7.42 (d, *J* = 1.0 Hz, 1H), 7.26 (dd, *J* = 8.2, 1.0 Hz, 1H), 6.97 (br s, 2H), 4.24 (q, *J* = 7.1 Hz, 2H), 1.32 (t, *J* = 7.1 Hz, 3H); ESI-MS: (*m/z*) 270.9 [M − H]$^-$; HPLC method B: t$_r$ = 8.259 min.

Ethyl 2-amino-5-chloro-1*H*-indole-3-carboxylate (**S3h**)

The title compound was prepared by a two-step procedure. In the first step a solution of ethyl cyanoacetate (6.2 g, 54.69 mmol) in dry THF (35 mL) was drop-added to an ice-cooled stirring suspension of K*t*BuO (6.1 g, 54.69 mmol) in dry THF (115 mL) under N$_2$ atmosphere. The mixture was left to warm to rt and a solution of 2,4-dichloro-1-nitrobenzene (**S1h**) (5.0 g, 26.04 mmol) in dry THF (30 mL) was drop-added. The mixture was stirred at 60 °C for 20 h. After cooling down to rt, 10% HCl$_{(aq)}$ (50 mL) was added and the mixture extracted with EtOAc (3 × 30 mL). Combined organic layers were dried over Na$_2$SO$_4$ and concentrated under reduced pressure. The oily residue contained ethyl 2-(5-chloro-2-nitrophenyl)-2-cyanoacetate (**S2h**), as well as excessive ethyl cyanoacetate and was used in the next step without further purification. Purification of a small portion for analytical purposes was performed by flash column chromatography (SiO$_2$; petroleum ether:EtOAc gradient elution from 4:1 to 3:1); ^{1}H NMR (300 MHz, DMSO-*d$_6$*) δ 8.36–8.25 (m, 1H), 7.92–7.79 (m, 2H), 6.18 (s, 1H), 4.22 (q, *J* = 7.0 Hz, 2H), 1.19 (t, *J* = 7.1 Hz, 3H); ^{13}C NMR (75 MHz, DMSO-*d$_6$*) δ 163.7, 145.5, 139.8, 133.2, 131.3, 128.2, 127.8, 115.0, 63.3, 41.1, 13.9. ESI-MS: (*m/z*) 266.8 [M − H]$^-$; HPLC method A: t$_r$ = 6.130 min.

The crude material obtained from the first step was reacted with zinc powder (10.0 g, 152.32 mmol) in glacial AcOH (60 mL) according to general procedure G (reaction time 2 h). 7.0 g of the crude product as a dark red solid were yielded (>100% crude yield over two steps) and used in the next step without further purification.

Ethyl 2-amino-5-bromo-1*H*-indole-3-carboxylate (**S3i**)

The title compound was prepared by a two-step procedure. In the first step a solution of ethyl cyanoacetate (5.4 g, 47.73 mmol) in dry THF (30 mL) was drop-added to an ice-cooled stirring suspension of K*t*BuO (5.4 g, 47.73 mmol) in dry THF (100 mL) under N$_2$ atmosphere. The dropping funnel was purged with additional dry THF and the mixture left to warm to rt. A solution of 4-bromo-2-fluoro-1-nitrobenzene (**S1i**) (5.0 g, 22.73 mmol) in dry THF was then drop-added to the stirring suspension. The mixture was heated to reflux for 1.5 h. After cooling down to rt, 10% HCl$_{(aq)}$ (40 mL) was added followed by EtOAc (40 mL). Phases were separated and the aqueous layer was extracted with EtOAc (2 × 30 mL). Combined organic layers were dried over Na$_2$SO$_4$ and concentrated under reduced pressure. The oily residue contained ethyl 2-(5-bromo-2-nitrophenyl)-2-cyanoacetate (**S2i**), as well as the excessive ethyl cyanoacetate and was used in the next step without further purification. Purification of a small portion for analytical purposes was performed by flash column chromatography (SiO$_2$, petroleum ether:(EtOAc + MeOH 95+5) 3:1); ^{1}H NMR (300 MHz, DMSO-*d$_6$*) δ 8.25–8.17 (m, 1H), 8.05–7.96 (m, 2H), 6.19 (s, 1H), 4.23 (q, *J* = 7.1 Hz, 2H), 1.19 (t, *J* = 7.1 Hz, 3H); ^{13}C NMR (75 MHz, DMSO-*d$_6$*) δ 163.6, 145.8, 136.0, 134.2, 128.7, 128.0, 127.7, 114.9, 63.2, 40.9, 13.8; ESI-MS: (*m/z*) 311.0 [M − H]$^-$; HPLC method A: t$_r$ = 6.437 min.

The crude material obtained from the first step was reacted with zinc powder (8.9 g, 136.38 mmol) in glacial AcOH (55 mL) according to general procedure H. Heat was applied after the complete addition of the zinc powder. After a reaction time of 2 h HPLC indicated incomplete conversion, therefore additional zinc powder was added (1.5 g, 22.73 mmol) and stirring continued for 1.5 h. 7.1 g of the crude product were yielded (>100% crude yield over two steps) and used in the next step without further purification; HPLC method A: t$_r$ = 8.042 min.

Ethyl 2-amino-5-methoxy-1*H*-indole-3-carboxylate (**S3j**)

The title compound was prepared by a two-step procedure. In the first step a solution of ethyl cyanoacetate (6.9 g, 61.32 mmol) in dry THF (40 mL) was drop-added to an ice-cooled stirring suspension of K*t*BuO (6.87 g, 61.32 mmol) in dry THF (120 mL) under N$_2$ atmosphere. The mixture was left to warm to rt and a solution of 2-fluoro-4-methoxy-1-nitrobenzene (**S1j**) (5.0 g, 29.20 mmol) in dry THF (10 mL) was then drop-added to the stirring suspension. The mixture was heated to reflux for 5 h. After cooling down to rt, 10% HCl$_{(aq)}$ (50 mL) was added and the mixture extracted with EtOAc (2 × 30 mL). Combined organic layers were dried over Na$_2$SO$_4$ and concentrated under reduced pressure. The oily residue contained ethyl 2-cyano-2-(5-methoxy-2-nitrophenyl)acetate (**S2j**), as well as the excessive ethyl cyanoacetate and was used in the next step without further purification. Purification of a small portion for analytical purposes was performed by flash column chromatography (SiO$_2$, petroleum ether:EtOAc gradient elution from 3:1 to 3:2); ^{1}H NMR (200 MHz, DMSO-*d$_6$*) δ 8.39–8.29 (m, 1H), 7.34–7.22 (m, 2H), 6.14 (s, 1H), 4.21 (qd, *J* = 7.0, 0.8 Hz, 2H), 3.93 (s, 3H), 1.19 (t, *J* = 7.1 Hz, 3H); ^{13}C NMR (50 MHz, DMSO-*d$_6$*) δ 163.9, 139.2, 129.0, 128.7, 119.4, 115.3, 115.0, 62.8, 56.5, 41.8, 13.8; ESI-MS: (*m/z*) 286.9 [M + Na]$^+$, 262.9 [M − H]$^-$; HPLC method A: t$_r$ = 6.002 min.

The crude material obtained from the first step was reacted with zinc powder (11.5 g, 175.0 mmol) in glacial AcOH (66 mL) according to general procedure H (reaction time 3 h). 5.6 g of the crude product as a red-brown solid were yielded (82% crude yield over two steps) and used in the next step without further purification. Purification of a small portion for analytical purposes was performed by flash column chromatography (SiO$_2$, DCM:MeOH 97:3); ^{1}H NMR (200 MHz, DMSO-*d$_6$*) δ 10.45 (s, 1H), 7.13 (d, *J* = 2.4 Hz, 1H), 6.99 (d, *J* = 8.5 Hz, 1H), 6.60 (br s, 2H), 6.49 (dd, *J* = 8.5, 2.5 Hz, 1H), 4.21 (q, *J* = 7.1 Hz, 2H), 3.71 (s, 3H), 1.32 (t, *J* = 7.1 Hz, 3H); ^{13}C NMR (50 MHz, DMSO-*d$_6$*) δ 165.8, 154.5, 153.9, 127.7, 127.3, 110.0, 106.4, 103.0, 84.0, 58.0, 55.2, 14.7; ESI-MS: (*m/z*) 233.2 [M − H]$^-$; HPLC method A: t$_r$ = 5.545 min.

Ethyl 2-amino-4-chloro-1*H*-indole-3-carboxylate (**S3k**)

The title compound was prepared by a two-step procedure. In the first step a solution of ethyl cyanoacetate (8.6 g, 76.56 mmol) in dry THF (48 mL) was drop-added to an ice-cooled stirring suspension of K*t*BuO (8.6 g, 76.56 mmol) in dry THF (160 mL). The stirring suspension was left to warm to rt and a solution of 1,2-dichloro-3-nitrobenzene (**S1k**) (7.0 g, 36.46 mmol) in dry THF (44 mL) was drop-added. The mixture was stirred at 60 °C for 43 h, when additional K*t*BuO (1.6 g, 14.58 mmol) was added and stirring at 60 °C continued for another 34 h. After cooling down to rt, 10% HCl$_{(aq)}$ (70 mL) was added and the mixture extracted with EtOAc (3 × 30 mL). Combined organic layers were dried over Na$_2$SO$_4$ and concentrated under reduced pressure. The oily residue contained ethyl 2-(2-chloro-6-nitrophenyl)-2-cyanoacetate (**S2k**), as well as excessive ethyl cyanoacetate and was used in the next step without further purification. Purification of a small portion for analytical purposes was performed by flash column chromatography (SiO$_2$, petroleum ether:EtOAc gradient elution from 4:1 to 1:1); ^{1}H NMR (300 MHz, DMSO-d_6) δ 8.15 (dd, J = 8.2, 1.2 Hz, 1H), 8.06 (dd, J = 8.2, 1.2 Hz, 1H), 7.79 (t, J = 8.2 Hz, 1H), 6.37 (s, 1H), 4.23 (q, J = 6.9 Hz, 2H), 1.21 (t, J = 7.1 Hz, 3H), ^{13}C NMR (75 MHz, DMSO-d_6) δ 163.2, 149.7, 136.1, 135.5, 132.0, 124.8, 123.4, 114.3, 63.2, 38.2, 13.7; ESI-MS: (*m/z*) 266.9 [M − H]$^-$; HPLC method A: t$_r$ = 5.470 min.

The crude material obtained from the first step was reacted with zinc powder (14.1 g, 215.3 mmol) in glacial AcOH (87 mL) according to general procedure H (reaction time 1.5 h). 7.6 g of the crude product as a brown solid were yielded (87% crude yield over two steps) and used in the next step without further purification; HPLC method A: t$_r$ = 7.689 min.

Detailed Procedures for the Preparation of Intermediates S4a,b and S4d–l.

3,9-Dihydro-4*H*-pyrimido[4,5-*b*]indol-4-one (**S4a**)

S3a (26.7 g, 130.7 mmol) and ammonium formate (9.1 g, 144.3 mmol) were stirred in formamide (140 mL) at 170 °C for 18 h. After cooling down to rt, MeOH (150 mL) was added. The resulting precipitate was filtered off, washed with MeOH and dried under reduced pressure. 7.4 g of the crude product were yielded (30% crude yield) and used in the next step without further purification; ^{1}H NMR (300 MHz, DMSO-d_6) δ 12.31–12.04 (m, 2H), 8.12 (s, 1H), 7.98 (d, J = 7.7 Hz, 1H), 7.47 (d, J = 8.0 Hz, 1H), 7.36–7.29 (m, 1H), 7.23 (td, J = 7.6, 1.1 Hz, 1H); ESI-MS: (*m/z*) 183.8 [M − H]$^-$; HPLC method B: t$_r$ = 2.066 min.

7-Fluoro-3,9-dihydro-4*H*-pyrimido[4,5-*b*]indol-4-one (**S4b**)

The title compound was prepared from **S3b** (4.0 g, 18.00 mmol) and ammonium formate (1.3 g, 20.70 mmol) in formamide (40 mL) according to general procedure I (reaction time 28 h). 3.2 g of the crude product were yielded (86% crude yield) and used in the next step without further purification; ESI-MS: (*m/z*) 201.9 [M − H]$^-$.

7-Bromo-3,9-dihydro-4*H*-pyrimido[4,5-*b*]indol-4-one (**S4d**)

The title compound was prepared from **S3d** (9.0 g, 31.79 mmol) and ammonium formate (2.3 g, 36.56 mmol) in formamide (65 mL) according to general procedure I (reaction time 22 h). 8.7 g of the crude product as a brown solid were yielded (>100% crude yield) and used in the next step without further purification; ESI-MS: (*m/z*) 261.8 [M − H]$^-$; HPLC method B: t$_r$ = 4.027 min.

7-Iodo-3,9-dihydro-4H-pyrimido[4,5-b]indol-4-one (**S4e**)

The title compound was prepared from **S3e** (2.5 g, 6.83 mmol) in formamide (17 mL) according to general procedure I (reaction time 29 h). No ammonium formate was used for this reaction. 1.7 g of the crude product as a brown solid were yielded (73% crude yield) and used in the next step without further purification. Purification of a small portion for analytical purposes was performed by flash column chromatography (SiO$_2$, DCM:MeOH 9:1); 1H NMR (200 MHz, DMSO-d$_6$) δ 12.37–12.16 (m, 2H), 8.16 (s, 1H), 7.84–7.73 (m, 2H), 7.58–7.49 (m, 1H); 13C NMR (50 MHz, DMSO-d6) δ 158.1, 153.8, 148.2, 136.7, 129.6, 122.4, 121.5, 120.0, 100.1, 88.3; ESI-MS: (*m/z*) 310.2 [M − H]$^-$; HPLC method A: t$_r$ = 5.770 min.

7-Methoxy-3,9-dihydro-4*H*-pyrimido[4,5-*b*]indol-4-one (**S4f**)

The title compound was prepared from **S3f** (1.6 g, 6.83 mmol) in formamide (40 mL) according to general procedure I (reaction time 16 h). No ammonium formate was used for this reaction. 1.5 g of the crude product were yielded (97% crude yield) and used in the next step without further purification; ¹H NMR (300 MHz, DMSO-*d$_6$*) δ 12.15 (s, 1H), 12.04 (s, 1H), 8.05 (s, 1H), 7.84 (d, *J* = 8.6 Hz, 1H), 6.96 (d, *J* = 2.2 Hz, 1H), 6.86 (dd, *J* = 8.6, 2.3 Hz, 1H), 3.81 (s, 3H); ESI-MS: (*m/z*) 213.9 [M − H]$^-$.

7-(Trifluoromethyl)-3,9-dihydro-4*H*-pyrimido[4,5-*b*]indol-4-one (**S4g**)

A suspension of **S3g** (4.5 g, 16.53 mmol) in formamide (75 mL) was stirred at 190 °C for 3 h. After cooling down to rt, MeOH (700 mL) was added and stirring continued at rt overnight. The mixture was filtered rinsing with fresh MeOH. The filtrate was concentrated under reduced pressure to the half and the resulting precipitate filtered off. The filtrate was then concentrated under reduced pressure to afford a dark brown oil. Water (300 mL) was added and the mixture stirred at rt for 1 h resulting in a precipitate, which was filtered off, washed with water and dried over P$_2$O$_5$ in vacuo. 1 g of the crude product were yielded (24% crude yield) and used in the next step without further purification; ESI-MS: (*m/z*) 251.9 [M − H]$^-$; HPLC method B: t$_r$ = 5.113 min.

6-Chloro-3,9-dihydro-4*H*-pyrimido[4,5-*b*]indol-4-one (**S4h**)

The title compound was immediately converted into **3h** (see the detailed procedure for the preparation of **3h**).

6-Bromo-3,9-dihydro-4*H*-pyrimido[4,5-*b*]indol-4-one (**S4i**)

The title compound was prepared from **S3i** (7.1 g, 25.2 mmol) and ammonium formate (1.6 g, 25.9 mmol) in formamide (65 mL) according to general procedure I (reaction time 24 h). 7.3 g of the crude product as a brown solid were yielded (>100% crude yield) and used in the next step without further purification. Purification of a small portion by flash column chromatography for analytical purposes (SiO$_2$, petroleum ether:(EtOAc + MeOH 95+5) gradient elution from 3:2 to 1:4); ¹H NMR (300 MHz, DMSO-*d$_6$*) δ 12.49–12.19 (m, 2H), 8.16 (s, 1H), 8.06 (s, 1H), 7.54–7.36 (m, 2H); ¹³C NMR (50 MHz, DMSO-*d$_6$*) δ 158.1, 154.3, 148.3, 134.2, 126.7, 123.9, 122.5, 113.8, 113.4, 99.6; HPLC method A: t$_r$ = 5.689 min.

6-Methoxy-3,9-dihydro-4*H*-pyrimido[4,5-*b*]indol-4-one (**S4j**)

The title compound was prepared from **S3j** (5.3 g, 22.62 mmol) and ammonium formate (1.6 g, 26.02 mmol) in formamide (46 mL) according to general procedure I. Purification of a small portion for analytical purposes was performed by flash column chromatography (SiO$_2$, DCM:MeOH 9:1). 3.9 g of the crude product were yielded (80% crude yield) and used in the next step withour further purification; ¹H NMR (200 MHz, DMSO-*d$_6$*) δ 12.16 (s, 1H), 12.04 (s, 1H), 8.08 (s, 1H), 7.48 (d, *J* = 2.4 Hz, 1H), 7.38 (d, *J* = 8.8 Hz, 1H), 6.95 (dd, *J* = 8.9, 2.6 Hz, 1H), 3.80 (s, 3H); ¹³C NMR (50 MHz, DMSO-

d$_6$) δ 158.5, 154.7, 153.8, 147.2, 130.0, 122.7, 113.6, 112.5, 102.8, 100.2, 55.4; ESI-MS: (*m/z*) 214.1 [M − H]⁻; HPLC method A: t$_r$ = 3.430 min.

5-Chloro-3,9-dihydro-4*H*-pyrimido[4,5-*b*]indol-4-one (**S4k**)

The title compound was prepared from **S3k** (7.0 g, 29.33 mmol) and ammonium formate (2.4 g, 38.13 mmol) in formamide (60 mL) according to general procedure I (reaction time 24 h). 5.5 g of the crude product as a brown solid were yielded (85% crude yield) and used in the next step without further purification. Purification of a small portion for analytical purposes was performed by flash column chromatography (SiO₂, DCM:MeOH 9:1). ¹H NMR (200 MHz, DMSO-*d*$_6$) δ 12.49 (s, 1H), 12.16 (s, 1H), 8.13 (s, 1H), 7.40 (dd, *J* = 7.4, 1.7 Hz, 1H), 7.35–7.18 (m, 2H); ¹³C NMR (50 MHz, DMSO-*d*$_6$) δ 156.9, 154.3, 148.4, 136.9, 125.7, 125.0, 122.3, 120.7, 110.4, 99.4. ESI-MS: (*m/z*) 242.0 [M + Na]⁺, 218.0 [M − H]⁻; HPLC method A: t$_r$ = 4.214 min.

7-Chloro-2-methyl-3,9-dihydro-4*H*-pyrimido[4,5-*b*]indol-4-one (**S4l**)

Ethyl 2-amino-6-chloro-1*H*-indole-3-carboxylate (**S3c**) was prepared by a two-step procedure from 1,4-dichloro-2-nitrobenzene (**S1c**) as described previously [5] and purified by flash column chromatography (SiO₂, DCM:MeOH 97.5:2.5). Purified **S3c** (400.0 mg, 1.68 mmol) was dissolved in dry acetonitrile (22 mL). The stirring solution was treated with hydrogen chloride gas at rt for 45 min and then refluxed for 2.5 h. After cooling the mixture overnight the formed precipitate was filtered off, washed with cold acetonitrile and dried under reduced pressure to yield 240 mg of the amidine intermediate. EtOH (50 mL) and 10% NaOH$_{(aq)}$ (5 mL) were added and the suspension refluxed for 3.5 h. After cooling down to rt the mixture was concentrated under reduced pressure. 10% HCl$_{(aq)}$ (5 mL) was added to the aqueous residue. The resulting precipitate was filtered off, washed with demineralised water and dried under reduced pressure. 127 mg of a white solid were yielded (32% crude yield) and used in the next step without further purification; ¹H NMR (300 MHz, DMSO-*d*$_6$) δ 12.20 (s, 1H), 12.12 (s, 1H), 7.90 (d, *J* = 8.3 Hz, 1H), 7.44 (d, *J* = 1.7 Hz, 1H), 7.22 (dd, *J* = 8.3, 1.9 Hz, 1H), 2.40 (s, 3H); ESI-MS: (*m/z*) 232.0 [M − H]⁻.

Detailed Procedures for the Preparation of Intermediates 3a–l.

4-Chloro-9*H*-pyrimido[4,5-*b*]indole (**3a**)

The title compound was prepared from **S4a** (2.2 g, 11.61 mmol), DIPEA (2.3 g, 17.40 mmol) in POCl₃ (11 mL) and chlorobenzene (24 mL) according to general procedure J (reaction time 20 h at a temperature of 100°C). 1.8 g of the crude product as a brown solid were obtained (76% crude yield) and purified by hot filtration from toluene to yield 524 mg of a dark yellow solid; ¹H NMR (400 MHz, DMSO-*d*$_6$) δ 12.76 (s, 1H), 8.78 (s, 1H), 8.28 (d, *J* = 7.9 Hz, 1H), 7.68–7.60 (m, 2H), 7.46–7.40 (m, 1H); ESI-MS: (*m/z*) 202.0 [M − H]⁻; HPLC method A: t$_r$ = 7.570 min.

4-Chloro-7-fluoro-9*H*-pyrimido[4,5-*b*]indole (**3b**)

The title compound was prepared from **S4b** (1.5 g, 7.38 mmol) and DIPEA (1.9 g, 14.77 mmol) according to general procedure J (reaction time 4 h), but using POCl₃ (20 mL) as only solvent. 1.6 g of the crude product were obtained (98% crude yield) and purified by hot filtration from toluene in portions; ¹H NMR (300 MHz, DMSO-*d*$_6$) δ 12.91 (s, 1H), 8.78 (s, 1H), 8.27 (dd, *J* = 8.7, 5.4 Hz, 1H), 7.42 (dd, *J* = 9.5, 2.3 Hz, 1H), 7.33–7.22 (m, 1H); ¹³C NMR (50 MHz, DMSO-*d*$_6$) δ 162.1 (d, *J* = 243.7 Hz), 156.5 (d, *J* = 1.2 Hz), 153.6, 150.8 (d, *J* = 1.4 Hz), 139.5 (d, *J* = 13.2 Hz), 124.0 (d, *J* = 10.7 Hz), 114.3 (d, *J* = 1.2 Hz), 110.8, 109.9 (d, *J* = 24.3 Hz), 99.1 (d, *J* = 26.6 Hz); ESI-MS: (*m/z*) 219.8 [M − H]⁻; HPLC method B: t$_r$ = 7.001 min.

4,7-Dichloro-9*H*-pyrimido[4,5-*b*]indole (**3c**)

The title compound was prepared in four steps from 1,4-dichloro-2-nitrobenzene (**S1c**) as described previously [5].

7-Bromo-4-chloro-9*H*-pyrimido[4,5-*b*]indole (**3d**)

The title compound was prepared from **S4d** (8.0 g, 30.3 mmol) and DIPEA (5.9 g, 45.44 mmol) in POCl$_3$ (24 mL) and chlorobenzene (60 mL) according to general procedure J (reaction time 7 h). 6.9 g of the crude product as a brown solid were obtained (81% crude yield) and purified by hot filtration in toluene in portions; ^{1}H NMR (200 MHz, DMSO-d_6) δ 12.86 (s, 1H), 8.78 (s, 1H), 8.09 (d, *J* = 8.5 Hz, 1H), 7.73 (d, *J* = 1.2 Hz, 1H), 7.51 (dd, *J* = 8.5, 1.5 Hz, 1H); ^{13}C NMR (50 MHz, DMSO-d_6) δ 156.1, 154.3, 151.4, 139.3, 124.6, 123.9, 121.1, 116.8, 114.9, 110.7; ESI-MS: (*m/z*) 280.0 [M − H]$^-$; HPLC method A: t$_r$ = 8.804 min.

4-Chloro-7-iodo-9*H*-pyrimido[4,5-*b*]indole (**3e**)

S4e (1.8 g, 5.82 mmol) was suspended in chlorobenzene (12 mL) and POCl$_3$ (5 mL) was added carefully. DIPEA (1.1 g, 8.73 mmol) was added portionwise to the stirring suspension and the mixture then stirred at 80 °C for 7 h. The mixture was stirred at rt overnight and then carefully transferred into stirring demineralised water of rt. The stirring mixture was cooled by ice and neutralized with 50% NaOH$_{(aq)}$. The brown precipitate was filtered off and stirred in hot toluene (600 mL) for 1 h. The hot suspension was filtered rinsing with additional hot toluene. The filtrate was concentrated under reduced pressure resulting in a precipitate. The suspension was cooled by ice and filtered off rinsing with cold toluene. The residue was dried under reduced pressure. 843 mg of a brown solid were obtained (44% yield); ^{1}H NMR (200 MHz, DMSO-d_6) δ 12.82 (s, 1H), 8.79 (s, 1H), 7.99 (d, *J* = 8.3 Hz, 1H), 7.94 (d, *J* = 1.0 Hz, 1H), 7.70 (dd, *J* = 8.3, 1.5 Hz, 1H); ^{13}C NMR (50 MHz, DMSO-d_6) δ 155.9, 154.5, 151.5, 139.5, 130.4, 124.0, 120.8, 117.2, 110.9, 94.0; ESI-MS: (*m/z*) 328.0 [M − H]$^-$; HPLC method A: t$_r$ = 9.375 min.

4-Chloro-7-methoxy-9*H*-pyrimido[4,5-*b*]indole (**3f**)

The title compound was prepared from **S4f** (1.4 g, 5.99 mmol) and DIPEA (1.8 g, 13.70 mmol) according to general procedure J (reaction time 5 h), but using POCl$_3$ (25 mL) as only solvent. 1.3 g of the crude product were obtained (87% crude yield) and purified by hot filtration in toluene; ^{1}H NMR (300 MHz, DMSO-d_6) δ 12.65 (s, 1H), 8.69 (s, 1H), 8.11 (d, *J* = 8.7 Hz, 1H), 7.08 (d, *J* = 2.2 Hz, 1H), 7.02 (dd, *J* = 8.7, 2.3 Hz, 1H), 3.89 (s, 3H); ESI-MS: (*m/z*) 231.9 [M − H]$^-$; HPLC method B: t$_r$ = 6.760 min.

4-Chloro-7-(trifluoromethyl)-9*H*-pyrimido[4,5-*b*]indole (**3g**)

A suspension of **S4g** (1.0 g, 3.95 mmol) in POCl$_3$ (50 mL) was stirred at 80°C for 6 h. After cooling down to rt, the mixture was carefully transferred into stirring water of rt and then neutralized with 50% NaOH$_{aq}$. The precipitate was filtered off, washed with water and dried over P$_2$O$_5$ in vacuo. 845 mg of the crude product were obtained (79% crude yield). The crude material was not purified by hot filtration from toluene, but used in the next step without further purification; ^{1}H NMR (300 MHz, DMSO-d_6) δ 13.13 (s, 1H), 8.85 (s, 1H), 8.39 (d, *J* = 8.3 Hz, 1H), 7.87 (s, 1H), 7.69 (dd, *J* = 8.3, 1.0 Hz, 1H); ESI-MS: (*m/z*) 269.9 [M − H]$^-$; HPLC method B: t$_r$ = 9.071 min.

4,6-Dichloro-9*H*-pyrimido[4,5-*b*]indole (**3h**)

The title compound was prepared by a two-step procedure. In the first step crude **S3h** (5.8 g) was reacted with ammonium formate (4.2 g, 66.19 mmol) in formamide (50 mL) according to general procedure I (reaction time 35 h). The solvent was replenished in between, as the reaction had dried out. Drying procedures gave 9.5 g of 6-chloro-3,9-dihydro-4*H*-pyrimido[4,5-*b*]indol-4-one (**S4h**) as a crude brown material with residual formamide. Purification of a small portion for analytical purposes was performed by flash column chromatography (SiO$_2$, DCM:MeOH 9:1); ^{1}H NMR (300

MHz, DMSO-*d₆*) δ 12.49–12.21 (m, 2H), 8.16 (s, 1H), 7.91 (d, *J* = 2.0 Hz, 1H), 7.49 (d, *J* = 8.6 Hz, 1H), 7.34 (dd, *J* = 8.6, 2.1 Hz, 1H); ESI-MS: (*m/z*) 218.0 [M − H]⁻; HPLC method A: t$_r$ = 5.251 min. The crude material obtained from the first step (4.4 g) was reacted with DIPEA (3.8 g, 30.05 mmol) and POCl₃ (17 mL) in chlorobenzene (40 mL) according to general procedure J (reaction time 24 h). The reaction mixture was additionally stirred at rt overnight. The reaction seized at 85% conversion as calculated by HPLC and was therefore worked up according to the general procedure. 4.4 g of a brown solid were obtained and purified by hot filtration from toluene in portions to yield a total 600 mg of a dark yellow solid (25% yield over 4 steps); ¹H NMR (300 MHz, DMSO-*d₆*) δ 12.91 (s, 1H), 8.80 (s, 1H), 8.21–8.14 (m, 1H), 7.63 (d, *J* = 1.3 Hz, 2H); ESI-MS: (*m/z*) 235.9 [M − H]⁻; HPLC method A: t$_r$ = 8.583 min.

6-Bromo-4-chloro-9*H*-pyrimido[4,5-*b*]indole (**3i**)

The title compound was prepared from **S4i** (4.6 g, 17.42 mmol) and DIPEA (3.4 g, 26.13 mmol) in chlorobenzene (35 mL) and POCl₃ (15 mL) according to general procedure J (reaction time 20 h). 3.7 g of the crude product as a brown solid were obtained (75% crude yield) and purified by hot filtration from toluene in portions; ¹H NMR (300 MHz, DMSO-*d₆*) δ 12.91 (s, 1H), 8.79 (s, 1H), 8.29 (d, *J* = 2.0 Hz, 1H), 7.73 (dd, *J* = 8.7, 2.0 Hz, 1H), 7.61–7.53 (m, 1H); ¹³C NMR (50 MHz, DMSO-*d₆*) δ 156.1, 154.5, 151.8, 137.3, 130.9, 124.4, 119.5, 114.4, 113.7, 110.3; ESI-MS: (*m/z*) 280.0 [M − H]⁻; HPLC method A: t$_r$ = 8.963 min.

4-Chloro-6-methoxy-9*H*-pyrimido[4,5-*b*]indole (**3j**)

The title compound was prepared from **S4j** (2.0 g, 9.29 mmol) and DIPEA (1.8 g, 13.93 mmol) according to general procedure J, but using POCl₃ (17.5 mL) as only solvent. 1.7 g of a brown solid were obtained (80% crude yield) and purified by hot filtration from toluene in portions; ¹H NMR (200 MHz, DMSO-*d₆*) δ 12.58 (s, 1H), 8.71 (s, 1H), 7.65 (d, *J* = 2.4 Hz, 1H), 7.52 (d, *J* = 8.8 Hz, 1H), 7.22 (dd, *J* = 8.8, 2.5 Hz, 1H), 3.85 (s, 3H); ¹³C NMR (50 MHz, DMSO-*d₆*) δ 155.9, 154.7, 153.6, 151.2, 132.9, 118.2, 117.4, 113.1, 111.0, 104.8, 55.6; ESI-MS: (*m/z*) 231.8 [M − H]⁻; HPLC method A: t$_r$ = 7.566 min.

4,5-Dichloro-9*H*-pyrimido[4,5-*b*]indole (**3k**)

The title compound was prepared from **S4k** (5.2 g, 23.68 mmol), DIPEA (4.6 g, 35.5 mmol) and POCl₃ (20 mL) in chlorobenzene (47 mL) according to general procedure J (reaction time 24 h). The wet crude material obtained was directly purified by hot filtration from toluene to yield 2.4 g (43% yield); ¹H NMR (400 MHz, DMSO-*d₆*) δ 13.12 (s, 1H), 8.77 (s, 1H), 7.57–7.55 (m, 2H), 7.40 (dd, *J* = 5.1, 3.7 Hz, 1H); ¹³C NMR (101 MHz, DMSO-*d₆*) δ 156.2, 153.9, 151.3, 140.2, 129.2, 127.0, 123.6, 115.5, 111.2, 110.2; ESI-MS: (*m/z*) 236.0 [M − H]⁻; HPLC method A: t$_r$ = 8.664 min.

4,7-Dichloro-2-methyl-9*H*-pyrimido[4,5-*b*]indole (**3l**)

The title compound was prepared from **S4l** (810.0 mg, 3.51 mmol), DIPEA (680.0 mg, 5.26 mmol) and POCl₃ (3 mL) in chlorobenzene (7 mL) according to general procedure J. The reaction mixture was left to stir at rt overnight after heating to 80°C for 6 h. The wet crude material obtained was directly purified by hot filtration in toluene to yield 512 mg of a beige solid (59% yield); ¹H NMR (400 MHz, DMSO-*d₆*) δ 12.62 (s, 1H), 8.15–8.09 (m, 1H), 7.56 (dd, *J* = 1.9, 0.4 Hz, 1H), 7.37 (dd, *J* = 8.4, 1.9 Hz, 1H), 2.67 (s, 3H); ¹³C NMR (101 MHz, DMSO-*d₆*) δ 164.0, 157.1, 151.1, 139.0, 132.1, 123.2, 121.7, 116.7, 111.9, 108.1, 25.5; ESI-MS: (*m/z*) 251.8 [M + H]⁺, 249.8 [M − H]⁻; HPLC method A: t$_r$ = 9.012 min.

7.3 Publikation III

**Addressing a Trapped High-Energy Water: Design and Synthesis of
Highly Potent 9*H*-pyrimido[4,5-*b*]indole-based GSK-3β Inhibitors**

Stanislav Andreev, Tatu Pantsar, Roberta Tesch, Niclas Kahlke, Ahmed El-Gokha,

Francesco Ansideri, Lukas Grätz, Jenny Romasco, Giulia Sita, Christian Geibel,

Michael Lämmerhofer, Andrea Tarozzi, Stefan Knapp, Stefan Laufer und Pierre Koch

Manuskript wurde beim Journal of Medicinal Chemistry eingereicht.

Addressing a Trapped High-Energy Water: Design and Synthesis of Highly Potent 9H-pyrimido[4,5-b]indole-based GSK-3β inhibitors

SCHOLARONE™
Manuscripts

1 **Addressing a Trapped High-Energy Water: Design and Synthesis of Highly**

2 **Potent 9*H*-pyrimido[4,5-*b*]indole-based GSK-3β inhibitors.**

3 Stanislav Andreev [1,‡], Tatu Pantsar [1,2,‡], Roberta Tesch [3,4], Niclas Kahlke [1], Ahmed El-

4 Gokha [1,5], Francesco Ansideri [1], Lukas Grätz [6], Jenny Romasco [7], Giulia Sita [8],

5 Christian Geibel [9], Michael Lämmerhofer [9], Andrea Tarozzi [7], Stefan Knapp [3,4], Stefan

6 A. Laufer [1,10] and Pierre Koch [1,6,*]

7 [1] Institute of Pharmaceutical Sciences, Department of Medicinal and Pharmaceutical

8 Chemistry, Eberhard Karls University Tübingen, Auf der Morgenstelle 8, 72076 Tübingen,

9 Germany

10 [2] School of Pharmacy, Faculty of Health Sciences, University of Eastern Finland, P.O. Box

11 1627, 70211 Kuopio, Finland

12 [3] Institute for Pharmaceutical Chemistry, Johann Wolfgang Goethe-University, Max-von-

13 Laue-Str. 9, 60438 Frankfurt am Main, Germany

14 [4] Structural Genomics Consortium, Buchmann Institute for Life Sciences, Johann Wolfgang

15 Goethe-University, Max-von-Laue-Str. 15, 60438 Frankfurt am Main, Germany

16 [5] Chemistry Department, Faculty of Science, Menoufia University, Gamal Abdel-Nasser

17 Street, 32511 Shebin El-Kom, Egypt

18 [6] Department of Pharmaceutical/Medicinal Chemistry II, Institute of Pharmacy, University

19 of Regensburg, Universitätsstraße 31, 93053 Regensburg, Germany

20 [7] Department for Life Quality Studies, Alma Mater Studiorum, University of Bologna,

21 Corso D'Augusto 237, 47921 Rimini, Italy

22 [8] Department of Pharmacy and Biotechnology, Alma Mater Studiorum, University of

23 Bologna, Via Irnerio 48, 40126 Bologna, Italy

24 [9] Institute of Pharmaceutical Sciences, Department of Pharmaceutical (Bio-)Analysis,

25 Eberhard Karls University Tübingen, Auf der Morgenstelle 8, 72076 Tübingen, Germany

26 [10] Tübingen Center for Academic Drug Discovery (TüCAD2), Auf der Morgenstelle 8,

27 72076 Tübingen, Germany

28

29 ‡ These authors contributed equally.

30

31 **Abstract**

32 In small molecule binding, water is not a passive bystander but rather takes an active role in the

33 binding site that may be decisive for inhibitor potency. Here, by addressing a high-energy water,

34 we improved the IC_{50} value of our co-crystallized glycogen synthase kinase-3β (GSK-3β)

35 inhibitor by nearly two-orders of magnitude. Surprisingly, our results demonstrate that this

36 high-energy water was not displaced by our potent inhibitor *(S)*-3-(3-((7-ethynyl-9*H*-

37 pyrimido[4,5-*b*]indol-4-yl)(methyl)amino)piperidin-1-yl)propanenitrile (*(S)*-15, IC_{50} value of

38 6 nM). Instead, the location of this water molecule was slightly shifted. The shift resulted in a

39 dramatic decrease in energy of this high-energy hydration site based on the WaterMap analysis,

40 which was well in line with the observed IC_{50} values. Our results indicate that combining

41 WaterMap with microsecond timescale molecular dynamics simulations is essential when

42 evaluating ligand-shifted hydration site energies. Overall, these findings highlight that even a

43 slight adjustment in a high-energy water location can be decisive for the ligand binding and

44 underlines the importance of taking water into account in the ligand design process.

45

48

1
2
3
4
5
6
7
8
9
10
11
12
13
14
15
16
17
18
19
20
21
22
23
24
25
26
27
28
29
30
31
32
33
34
35
36
37
38
39
40
41
42
43
44
45
46
47
48
49
50
51
52
53
54
55
56
57
58
59
60

49   **Introduction**

50   Protein kinases are important regulators in the cellular signaling machinery.[1] Aberrations in

51   their activity can lead to disease, and they are considered as potential drug targets in many

52   therapeutical areas, including cancer, degenerative disorders as well as autoimmune and

53   inflammatory diseases.[2] Therefore, perhaps unsurprisingly, protein kinases are currently the

54   most pursued drug targets in the pharmaceutical industry.[3]

55   During the last decades, in particular glycogen synthase kinase-3β (GSK-3β) has

56   received extensive attention both from academia and industry. This serine/threonine kinase is a

57   highly multitasking enzyme that contributes to several key signaling pathways in cells.[4] GSK-

58   3β dysregulation has been associated with various pathologies such as type II diabetes mellitus,

59   various types of cancer and Alzheimer's disease.[5-7] Therefore, determined efforts are ongoing

60   to develop selective inhibitors against GSK-3β.

61   We recently reported optimization of a novel class of 7-chloro-9H-

62   pyrimido[4,5-b]indole-based inhibitors of GSK-3β.[8] In this study, we revealed the cyanoethyl

63   substituted piperidine (**1**) as an essential motif for the compound activity, which was further

64   improved by a rigidification approach (**2**). Having identified the optimal structural features for

65   the aliphatic side chain of the molecules, we herein pursued to optimize decorations at the 9H-

66   pyrimido[4,5-b]indole core.

2
IC_{50} GSK-3β = 0.13 μM ^{a}

1
IC_{50} GSK-3β = 0.76 μM ^{a}

23 derivatives
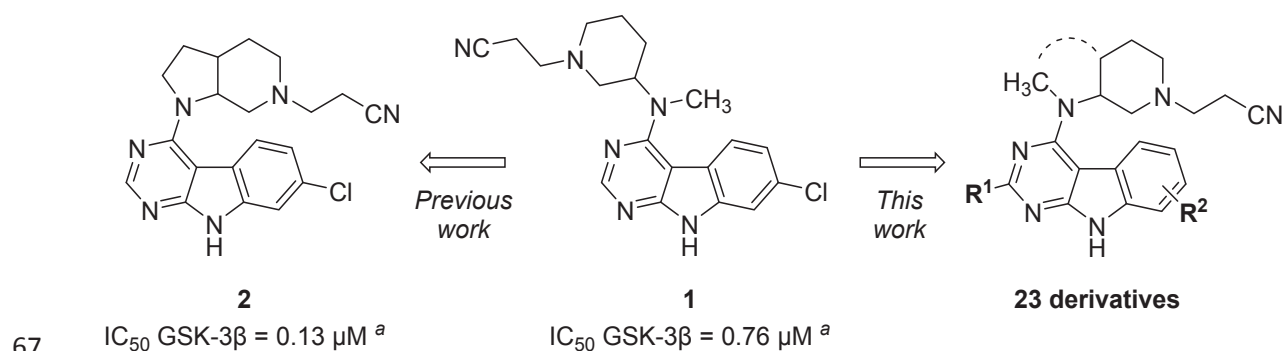
67   **Scheme 1**. Previously reported optimization of the aliphatic side chain. ^{a} Data taken from

68   Andreev *et al.*[8]

70   Water is a vital component in the biological matrix that plays various important roles in

71   molecular biology.[9] This is especially true at the protein interface, as water plays a pivotal role

72   in ligand binding thermodynamics.[10-15] As solvent organization may be decisive for the binding

73   affinity,[16-17] exploiting water offers an excellent opportunity to optimize ligand binding.

74   However, not all waters are equal at the protein interface. While a displacement of an

75   energetically favorable water from the binding site by the ligand has a negative impact on

76   binding affinity, it is highly beneficial in the case of energetically unfavorable water molecules.

77   Therefore, it is essential to estimate the energies of these molecules before aiming for their

78   displacement. There are a rising number of computational methods that aim to predict water

79   energies and thereby guide the decision for a beneficial water displacement.[18-19] One such

80   method is WaterMap,[20-21] which evaluates the water energies based on a short molecular

81   dynamics (MD) simulation. This method has been successfully applied in several instances

82   related to protein kinases, such as with Platelet Derived Growth Factor Receptor-β (PDGF-

83   Rβ),[22] p38α MAP kinase,[23] Dual-specificity tyrosine phosphorylation-regulated kinase

84   (DYRK),[24] kinase inhibitor selectivity among four kinases,[25] inhibitor selectivity among

85   phosphoinositide 3-kinases (PI3Ks),[26] Cyclin G-Associated Kinase (GAK),[27] Janus kinases

86   (JAKs),[28] and Interleukin-1 Receptor Associated Kinase 4 (IRAK4).[29]
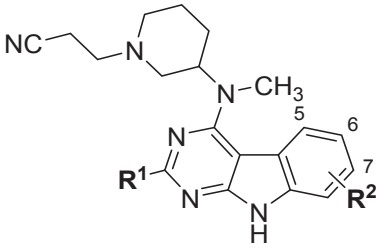
87   Here we applied a water-guided ligand-design approach in the development of highly

88   potent inhibitors of GSK-3β. By exploiting a new co-crystal structure in combination with

89   WaterMap and MD simulations, we were able to improve the potency of our 9*H*-pyrimido[4,5-

90   *b*]indole based compounds by almost two orders of magnitude, resulting in single-digit

91   nanomolar IC_{50} values. Remarkably, our results demonstrate how a small shift in the location

92   of a high-energy water by the ligand was highly beneficial. This strategy offers a new approach

93   to the ligand design in addition to the typical solvent displacement, replacement or interaction.[30]

94

95

96   **Results**

97   Our initial structural modifications on the tricyclic scaffold of **1** were mainly focused on the

98   third non-heteroaromatic ring of the 9*H*-pyrimido[4,5-*b*]indole tricycle (Table 1). The

99   exchange of the chlorine atom in the 7-position with fluorine or bromine as well as its complete

100   removal were well tolerated and generally provided triple-digit nanomolar GSK-3β inhibitors

101   (**5a-d**). Only the corresponding 7-iodine derivative (**11**) displayed diminished activity. In

102   contrast, the relocation of the chlorine or bromine substituent to the 6-position (**5g** and **5h**) or

103   5-position (**5i**) was associated with a substantial (5–10 fold) decrease in potency. Furthermore,

104   the introduction of a methyl group in the pyrimidine 2-position of parent compound **1** afforded

105   a completely inactive derivative (**5j**). As we recently observed a strong influence of the

106   stereoconfiguration on the bioactivity of structurally related GSK-3β inhibitors,[31] we also

107   decided to evaluate the activity of enantiopure compounds within this series. Here, the

108   respective *S*-enantiomers of **1** (= *rac*-**5c**) and **5d** displayed slightly improved IC$_{50}$ values.

109

110   **Table 1. Structures and biological activities of halogen substituted compounds.**

No.	R^1		R^2	GSK-3β IC$_{50}$ ± SEM [μM] ^{a}	pIC$_{50}$	clogP ^{c}	LLE ^{d}
5a	—H	-	—H	0.480 ± 0.076	6.3	2.6	3.7
5b	—H	7-	—F	0.973 ± 0.276	6.0	2.8	3.2
1 (= *rac*-**5c**)	—H	7-	—Cl	0.764 ± 0.203 ^{b}	6.1	3.3	2.9
(R)-5c	—H	7-	—Cl	0.712 ± 0.176	6.1	3.3	2.9
(S)-5c	—H	7-	—Cl	0.489 ± 0.119	6.3	3.3	3.0
5d	—H	7-	—Br	0.388 ± 0.080	6.4	3.3	3.1
(R)-5d	—H	7-	—Br	0.408 ± 0.099	6.4	3.3	3.1

(S)-5d	—H	7-	—Br	0.319 ± 0.066	6.5	3.3	3.2
11	—H	7-	—I	1.382 ± 0.394	5.9	3.2	2.7
5g	—H	6-	—Cl	3.811 ± 0.118	5.4	3.2	2.2
5h	—H	6-	—Br	6.096 ± 0.654	5.2	3.3	1.9
5i	—H	5-	—Cl	8.042 ± 0.617	5.1	3.2	1.9
5j	—CH₃	7-	—Cl	>10	-	3.2	-

[a] IC_{50} values were determined in an ADP Glo™ kinase assay (for details see Supporting Information (SI)).[32] The reported data are mean values ± SEM from at least two independent experiments; [b] data taken from Andreev *et al*.[8]; [c] AlogP calculated with Canvas (Schrödinger LLC)[33], [d] Lipophilic ligand efficiency (LLE) = pIC_{50} – clogP.[34]

Considering these results, we next set out to resolve the binding mode of the eutomer *(S)*-5c to GSK-3β by X-ray crystallography (PDB 7B6F). As we anticipated, the crystal structure confirmed interactions of the 9*H*-pyrimido[4,5-*b*]indole core to the hinge region of the kinase (Figure 1). In particular, two hydrogen-bonds were formed with the backbone of hinge residues Asp133 and Val135. Moreover, a water bridge was observed between the N-3 atom of the pyrimidine ring and Pro136, an interaction which was also suggested by our earlier MD simulations.[8] The third aromatic ring of the tricyclic core is located deeper in the pocket and the chlorine substituent is oriented towards the hydrophobic region I (HR-I) of the kinase, while the piperidine ring is accommodated in the sugar pocket. This allows the flexible cyanoethyl substituent to obtain a folded conformation under Phe67. The nitrile group displays a hydrogen bond to the side chain of Lys85. Notably, the obtained conformation of the inhibitor would be disturbed by larger substituents in the 5- or 6-position of the 9*H*-pyrimido[4,5-*b*]indole core, explaining the decreased activity of 5g-i. The inactivity of 5j is evident from the apparent clash caused by the methyl group in the 2-position of the pyrimidine with the protein.

1
2
3
4
5
6
7
8
9
10
11
12
13
14
15
16
17
18
19
20
21
22
23
24
25
26
27
28
29
30
31
32
33
34
35
36
37
38
39
40
41
42
43
44
45
46
47
48
49
50
51
52
53
54
55
56
57
58
59
60
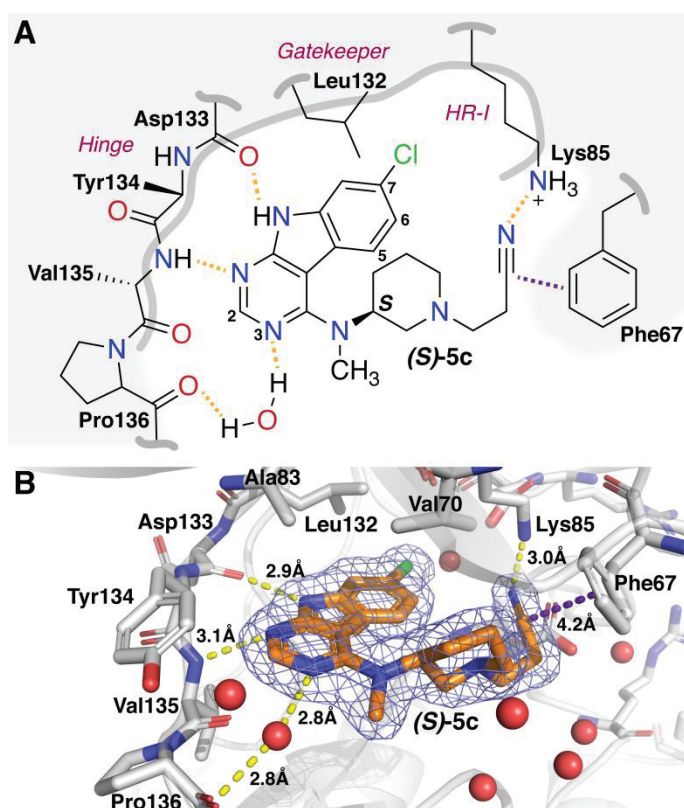
129

130 **Figure 1.** Co-crystal structure of *(S)*-5c in complex with GSK-3β (PDB 7B6F). (**A**) 2D-
131 depiction of the observed binding mode observed in the crystal structure. (**B**) The hinge-binder
132 of *(S)*-5c is stabilized by two direct and one water-bridged interaction to the protein. The
133 chlorine atom is located near the gatekeeper residue Leu132 and the nitrile group is close
134 proximity to Lys85. GSK-3β residues making close contacts with *(S)*-5c are shown in stick
135 representation, and water molecules are illustrated as red spheres. Blue mesh surface on the
136 ligand displays a 2Fo–Fc map contoured at 1σ. H-bonds are indicated by yellow dashed lines,
137 and distance from the Phe67 aromatic ring center to the carbon of the nitrile group is depicted
138 as a purple dashed line.

139

140 During a closer examination of the crystal structure, we noticed that a single water molecule is

141 trapped in the HR-I and the chlorine atom of the ligand is pointing towards it (Figure 2A).

142 Intrigues by this finding, we decided to evaluate the solvent organization near the ligand using

143 WaterMap.[20-21] This analysis, which provides an estimate of the hydration sites and their

144 energies, revealed both low- and high-energy hydration sites (Figure 2B, 2C). The hydration

145 site related to the water-bridge located between the N-3 atom of the pyrimidine ring and GSK-

146 3β was characterized as a low energy site (+0.13 kcal/mol). Importantly, we noticed that the

147 trapped water molecule in the HR-I was indeed identified as a high-energy hydration site
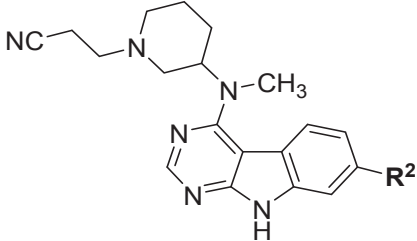
148 (+6.71 kcal/mol). Therefore, our subsequent ligand design aimed for the displacement of this

149 high-energy water. To this end, we installed a variety of substituents at the 7-position of the

150 9*H*-pyrimido[4,5-*b*]indole core. Our initial efforts introducing considerably bulkier residues

151 (**5k**, **5l**) or with a methoxy group (**5e**) resulted in compounds with decreased activity (Table 2).

152 Also, perhaps surprisingly, the trifluoromethyl derivative (**5f**) appeared inactive. However,

153 even the trifluoromethyl group is substantially bulkier in its radius compared to chlorine

154 (Figure S1A, SI). Therefore, we ascertained a clear limitation on the substituent's radius in this

155 area, most likely caused by the steric hindrance of the gatekeeper residue Leu132 (Figure 2D).

156 We speculate that this also applied to the observed slight decrease in activity seen for derivative

157 **11**, which carried the considerably larger iodine substituent (Figure S1A, SI). Based on these

158 initial results, addressing this high-energy water required a long and narrow substituent.

159 Correspondingly, we next tested a nitrile derivative (**5m**), as this moiety has been demonstrated

160 earlier as a successful approach to displace a water molecule in the design of the autotaxin

161 inhibitor GLPG1690 and Hsp90 inhibitors.[35-36] The nitrile group is comparable to the chlorine

162 substituent in terms of its van der Waals radius, but it is longer and reaches deeper towards the

163 HR-I (Figure S1B, SI). Unfortunately, in this case this approach was unsuccessful as **5m**

164 displayed even lower activity compared to the parent compound **5c**. Next, we introduced an

165 ethinyl substituent (**15**), which is even longer than the nitrile group while maintaining a similar

166 radius (Figure S1B, SI). To our astonishment, **15** displayed a remarkable increase in activity

167 with an IC_{50} value of 23 nM. Since we initially identified *(S)*-**5c** as the eutomer, we assumed

168 that higher activity would be observed for the corresponding stereoisomer of **15**. Indeed,

169 compound *(S)*-**15** displayed an improved IC_{50} value of 6 nM.
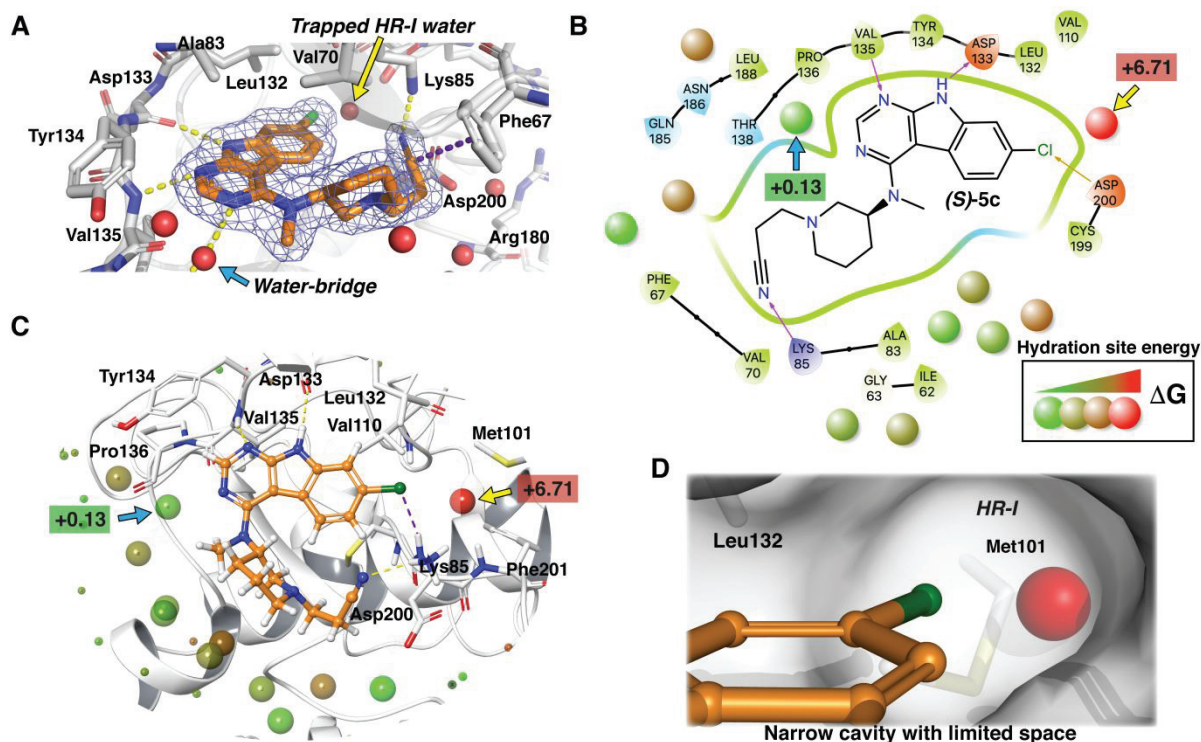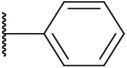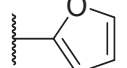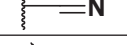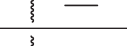
Figure 2. The WaterMap analysis of the GSK-3β–*(S)*-5c crystal structure revealed a high-energy water in the HR-I region. (**A**) In the crystal structure, a trapped water molecule was found in the HR-I region (indicated by a yellow arrow). The water molecule which forms the water bridge is indicated by a blue arrow. (**B**) 2D- and (**C**) 3D-depiction of the WaterMap analysis. The hydration site related to the water bridge was identified as a low energy water (+0.13 kcal/mol), whereas the estimated free energy for the trapped water in HR-I is high (+6.71 kcal/mol). All other hydration sites near the ligand located in the solvent interface displayed low or medium energy values. (**D**) The chlorine atom of *(S)*-5c is pointing towards the HR-I, where the high-energy water is located. The gatekeeper residue Leu132 sterically restricts the access of the ligand to the HR-I.

182 **Table 2. Structures and biological activities of compounds addressing the high-energy**
183 **hydration site.**

| No.	R²	GSK-3β IC$_{50}$ ± SEM [μM] ^{a}	pIC$_{50}$	clogP ^{b}	LLE ^{c}
5k	phenyl	5.112 ± 0.270	5.3	4.1	1.2
5l	furan	5.299 ± 0.145	5.3	3.3	2.0
5e	—OCH$_3$	8.690 ± 0.057	5.1	2.6	2.5
5f	—CF$_3$	> 10	-	3.5	-
5m	≡N	1.204 ± 0.146	5.9	2.5	3.4
15	≡	0.023 ± 0.008	7.6	3.7	3.9
***(S)*-15**	≡	0.006 ± 0.003	8.2	3.7	4.5

184 ^{a} IC$_{50}$ values were determined in an ADP Glo^{TM} kinase assay.[32] The reported data are mean
185 values ± SEM from at least two independent experiments; ^{b} AlogP calculated with Canvas
186 (Schrödinger LLC)[33]; ^{c} LLE = pIC$_{50}$ – clogP.[34]

187   We were puzzled about the remarkable activity differences among the ethinyl (**15**) and

188 the nitrile (**5m**) derivatives. To further rationalize this finding, we ran additional WaterMap

189 analyses for both compounds, using them as ligands in the simulations. Interestingly, with the

190 nitrile (**5m**) the high-energy hydration site appeared at the same location as with *(S)*-**5c**, whereas

191 this hydration site was shifted with the highly active ethinyl analog *(S)*-**15** (Figure S2, SI).

192 These results demonstrated that adequate length of the ethinyl substituent was required to push

193 the water, with the nitrile group being "too short" in this case. The evaluated energy for this

194 hydration site was slightly lower with the nitrile (+6.21 kcal/mol) compared to the chlorine

195 (+6.71 kcal/mol). Even though the electrostatic potential among these compounds was notably

196 different in their high-energy water facing apical site (Figure S3, SI), no interactions between

197 the water and the ligand were observed. Therefore, the decreased biological activity of **5m** most

198   likely arose from its lower lipophilicity (see LLE in Table 2). For the shifted hydration site with

199   *(S)*-**15**, however, even higher energy (+7.97 kcal/mol) was estimated by the WaterMap.

200   Therefore, this approach failed to provide us further rationale for the remarkable activity of *(S)*-

201   **15**.

202   To further investigate the water behaviour in this high-energy site, we conducted

203   10 x 1 µs MD simulations for both compounds, *(S)*-**5c** and *(S)*-**15**, in complex with GSK-3β.

204   Throughout the simulations the two inhibitors displayed nearly identical interaction patterns,

205   demonstrating that the ethinyl substituent does not affect the direct interactions of the ligand

206   with GSK-3β (Figure S4, SI). Comprehensive protein sidechain conformational sampling

207   occurs within a microsecond timescale [37]; therefore, these simulations would be expected to

208   reveal the putative water displacement if it occurred. Interestingly, these longer simulations

209   agreed with the notably shorter (2 ns) WaterMap simulations: the water position was shifted,

210   and it was not displaced from the HR-I site. We further evaluated the water location as well as

211   the solvent exposure of the lipophilic residue sidechains in this region. There were in total five

212   lipophilic residues found in this area: gatekeeper Leu132 and Val110 that were in close contact

213   with the ligand, Leu112 and Leu130 located deep in the pocket, and Met101 protruding from

214   the αC-helix (Figure 3A). Leu132 was almost fully shielded from the solvent exposure by *(S)*-

215   **15**, which clearly pushed the water molecule away from the gatekeeper (Figure 3B, 3C). A

216   similar trend was also evident in the case of Val110, while only marginal changes were

217   observed for the other lipophilic residues. There is virtually no change in the water exposure of

218   Leu112 with *(S)*-**15**. Met101 appeared somewhat less exposed to water with *(S)*-**15**, whereas a

219   slight increase in the water exposure of Leu130 was observed. These findings clearly

220   demonstrated that the hydration site was shifted away from the gatekeeper Leu132, but the

221   water remained in the HR-I (Figure 3D). Next, we wanted to re-evaluate the energy of this

222   shifted high-energy hydration site. To this end, we selected five conformations (at 1 µs) of the

223　*(S)*-15 MD simulations. Of note, one should always use caution when applying WaterMap for

224　an MD simulation derived structure, as the method has been originally developed to be applied

225　for crystal structures and is highly sensitive to changes in sidechain conformations. In other

226　words, the thermodynamic quantities calculated by WaterMap only apply to the input

227　conformation. Intriguingly, even though the slightly shifted water was still trapped in the

228　hydrophobic environment, WaterMap now demonstrated significantly decreased energy of this

229　high energy hydration site (Figure 3E). The estimated hydration site energy (average difference

230　of 2.302 kcal/mol compared to *(S)*-5c) was in line with the observed biological activities, as a

231　free energy difference of 2.6 kcal/mol would be expected in their binding affinity (80-fold

232　difference).
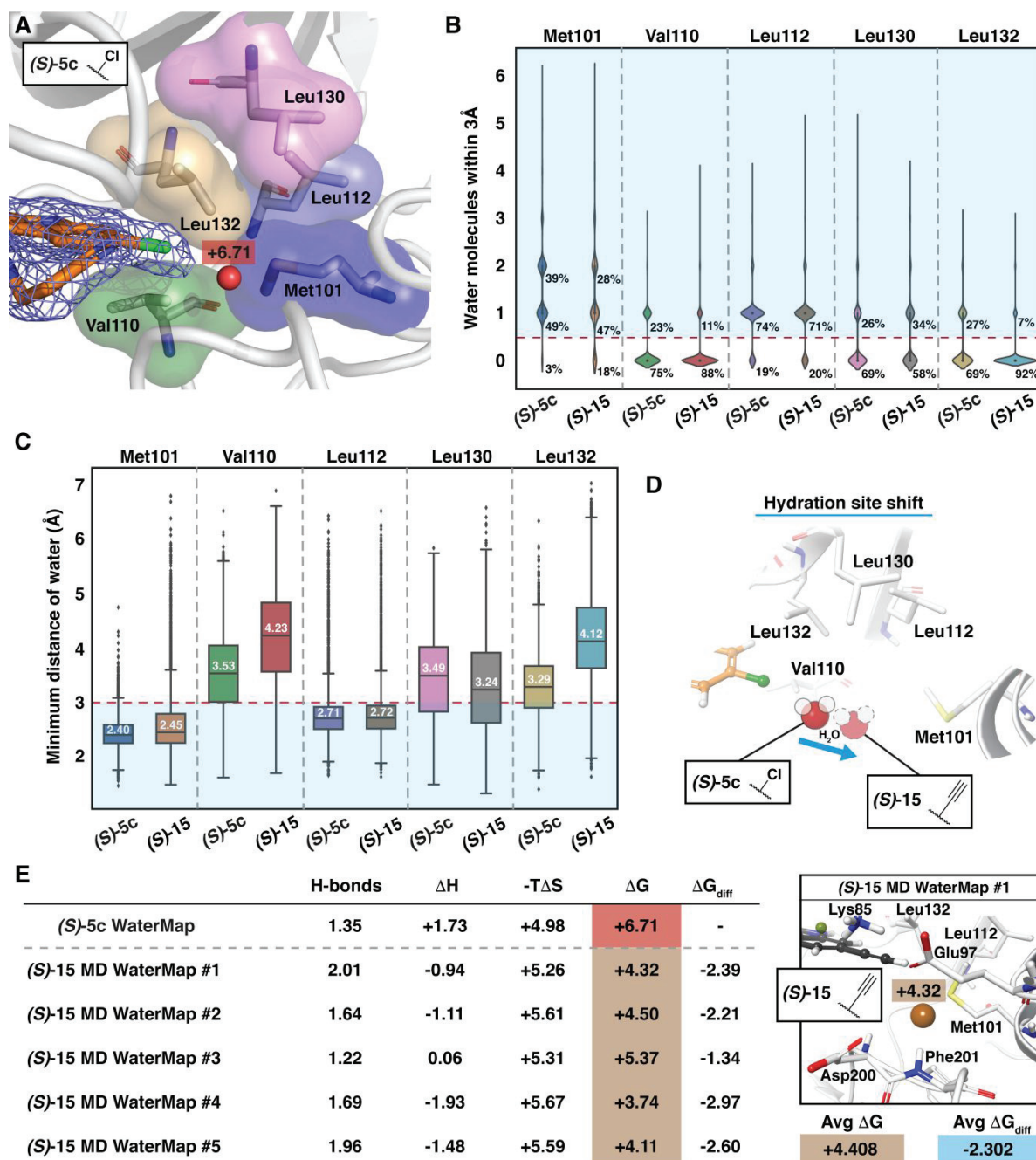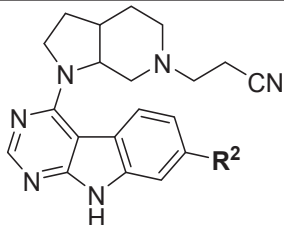
Figure 3. Molecular dynamics simulations reveal the high-energy hydration site shift that is accompanied with decreased energy. (**A**) Lipophilic residues Met101, Val110, Leu112, Leu130 and Leu132 are flanking the high-energy water in the HR-I. (**B**) Quantitation of the observed water molecules within 3Å of the sidechains of the selected lipophilic residues during the simulations (a total simulation time of 10 μs for each ligand). Light-blue shaded area indicates water exposure of the lipophilic sidechains. (**C**) Observed minimum distance of water to the sidechain of the selected lipophilic residues during the simulations. Light-blue shaded area indicates water exposure of the lipophilic sidechains. In the boxplots, the box indicates quartiles of the dataset (25–75%) and whiskers the rest of the data within 1.5 times the interquartile range (IQR) (outliers are shown with black diamonds). Median values are provided as horizontal lines in the boxes. (**D**) Schematic depiction of the hydration site movement based on the data in **B** and **C**. (**E**) The WaterMap analysis of the MD simulation output structures for five replicates of (*S*)-**15** demonstrate that the shifted hydration site has lower energy compared to (*S*)-**5c**.

247   To examine if our earlier successful rigidification approach on this compound series

248   also applies here (Scheme 1), we evaluated a set of rigidified congeners (Table 3). Indeed, most

249   of these compounds displayed enhanced IC$_{50}$ values compared to their nonrigid counterparts.

250   Importantly, the ethinyl derivative **22** exhibited outstanding potency (IC$_{50}$ value of 2 nM),

251   confirming the highly beneficial effect of this substituent. We also observed a clear trend of

252   enhanced activity alongside the increasing size of the halogens (**2**, **19-21**). The results of this

253   rigidified compound set imply a similar impact of the substituent in the 7-position on the high-

254   energy hydration site as observed with the nonrigid analogs.

255   **Table 3. Structures and biological activities of rigid compounds.**

No.	R^2	GSK-3β IC$_{50}$ ± SEM [μM] [a]	(IC$_{50}$ nonrigid)	pIC$_{50}$	clogP [d]	LLE [e]
19	—F	2.668 ± 1.488	(0.973)	5.6	2.7	2.9
2	—Cl	0.130 ± 0.008 [b]	(0.764 [b])	6.9	3.2	3.7
20	—Br	0.066 ± 0.015	(0.388)	7.2	3.2	3.9
21	—I	0.132 ± 0.036	(1.382)	6.9	3.1	3.8
22	≡	0.002 ± 0.000	(0.023)	8.7	3.6	5.1

256   [a] IC$_{50}$ values were determined in an ADP Glo^{TM} kinase assay.[32] The reported data are mean

257   values ± SEM from at least two independent experiments. [b] data taken from Andreev *et al*.[8], [c]

258   IC$_{50}$ values of the corresponding non-rigid compounds from Tables 1 and 2; [d] AlogP calculated

259   with Canvas (Schrödinger LLC)[33]; [e] LLE = pIC$_{50}$ – clogP.[34]

260

261   Next, we set out to evaluate the cellular target engagement of *(S)*-**5c**, *(S)*-**15**, **20** and **22**.

262   In a NanoBRET assay, these inhibitors generally demonstrated GSK-3β binding affinities in

263   the single-digit micromolar range (for details see SI and Table S1, SI). Importantly, this data

264   correlates well with the IC$_{50}$ values determined in the kinase activity assay with *(S)*-**15**

265   displaying the highest affinity to GSK-3β in cells.

266	These results motivated us to further characterize *(S)*-**15** along with **20** in terms of their

267	intracellular GSK-3 inhibition and neuroprotective effects in neuronal SH-SY5Y cells. The

268	treatment of SH-SY5Y cells with *(S)*-**15** and **20** at concentrations lower than 10 μM and 20 μM,

269	respectively, did not affect cell viability (3-(4,5-dimethylthiazol-2-yl)-2,5-diphenyltetrazolium

270	bromide (MTT) assay,[38] data not shown). Therefore, we selected the concentration of 5 μM to

271	perform an immunoblotting assay monitoring the phosphorylation status of GSK-3 in the

272	presence of the inhibitors. While both *(S)*-**15** and **20** increased the phospho-GSK-3α/β (Ser21/9)

273	(inactive GSK-3α/β form), only *(S)*-**15** decreased the phospho-GSK-3α/β (Tyr279/Tyr216)

274	(active GSK-3α/β form), after 3 h of treatment in neuronal SH-SY5Y cells (Figure S5, SI). As

275	Tyr279 and Tyr216 are autophosphorylation sites of GSK-3α and GSK-3β, respectively, the

276	phosphorylation status of these residues reflected the enzymatic activity of the kinase.[39-41]

277	Accordingly, these results demonstrate that *(S)*-**15** inhibits GSK-3 activity in cells targeting the

278	ATP binding pocket of both GSK-3α and GSK-3β and rendering its inhibition selective and

279	persistent. Furthermore, we investigated the neuroprotective effects of *(S)*-**15** and **20** against

280	the neurotoxicity induced by hydrogen peroxide (H_2O_2, 100 μM), that mimics general oxidative

281	stress.[42] The concomitant treatment of the SH-SY5Y cells with H_2O_2 and the compounds (5 μM)

282	significantly decreased the neurotoxicity elicited by oxidative stress on a neuronal level (Figure

283	S6, SI). Interestingly, the neuroprotective effect of *(S)*-**15** was significantly higher than of **20**

284	corroborating the ability of *(S)*-**15** to promote the neuronal survival through the strong

285	inhibition of GSK-3β.

286	Finally, to assess the kinome selectivity of the inhibitors *(S)*-**15** and **22**, we evaluated

287	their biological activity on a subset of 57 kinases. At an inhibitor concentration of 500 nM only

288	few kinases were substantially inhibited by *(S)*-**15** and **22** (Figure 4; see full list in Table S2,

289	SI). These data suggested a similar off-target profile for these two compounds. Notably, the

290	more potent rigid inhibitor **22** consistently exhibited stronger inhibition on all off-target kinases

291	compared to its non-rigid counterpart *(S)*-**15**. Even though the off-targets appeared only

292 remotely related, they share structural similarities in residues near the HR-I that participate in

293 the accommodation of the ethinyl substituent in the 7-position of the 9*H*-pyrimido[4,5-*b*]indole

294 core (Figure 4C). In particular, they mostly harbor a branched gatekeeper residue (Ile, Leu, Thr

295 and Val) as well as a large lipophilic amino acid protruding from the αC helix (Met, Leu and

296 Phe). Thus, we anticipate that these residues together with a suitable overall binding site

297 topology allow binding of *(S)*-15 or 22, offering a putative explanation to the observed off-

298 target activity.
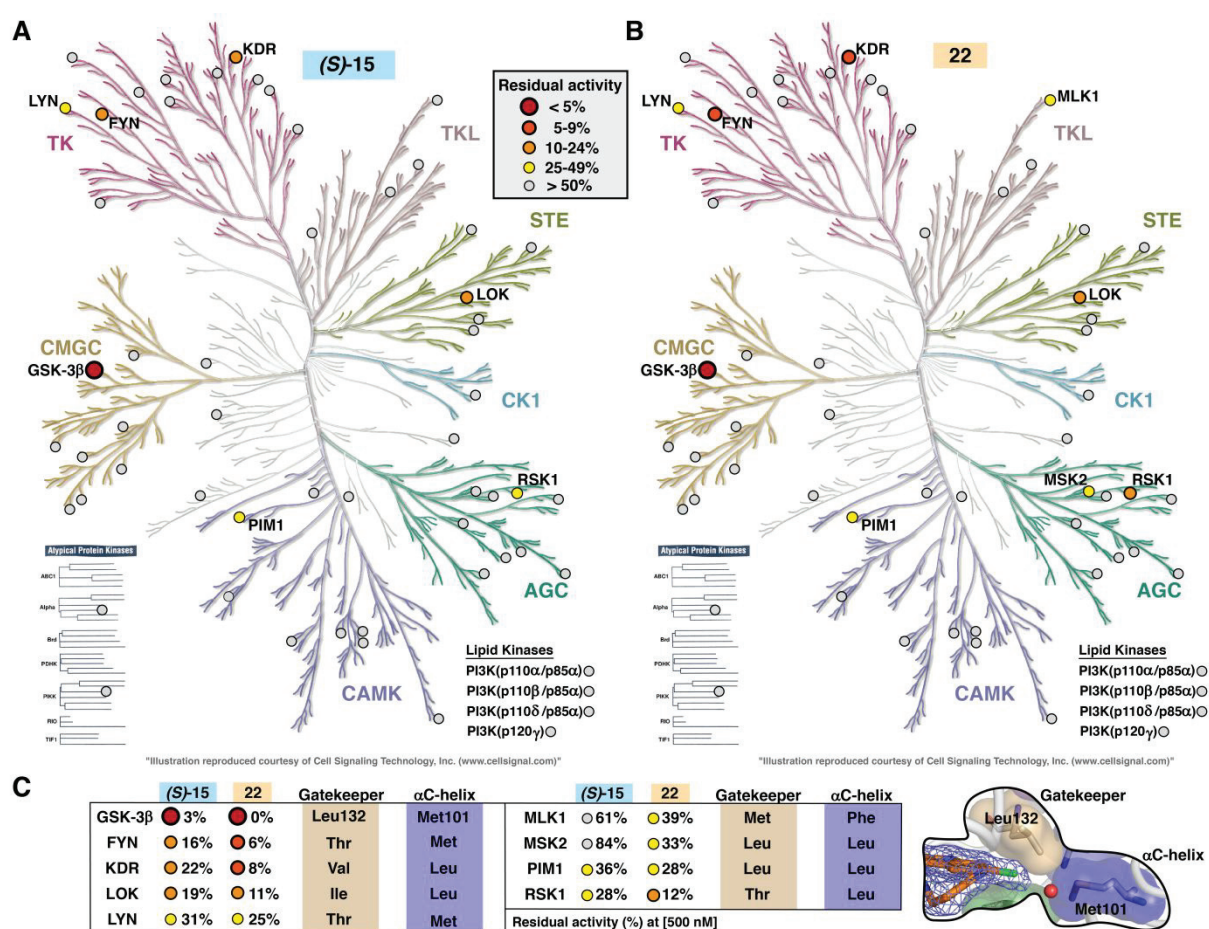
299 **Figure 4.** Selectivity of the *(S)*-15 and 22 within the human kinome. (**A**) Selectivity of
300 compound *(S)*-15. All tested kinases are highlighted with circles and colored according to their
301 residual activity at 500 nM inhibitor concentration. (**B**) Selectivity of compound 22. (**C**) The
302 residual activities of the off-targets which display <50% residual activity for *(S)*-15 or 22. The
303 corresponding gatekeeper and αC-helix residues are listed for each kinase. The figures **A** and
304 **B** were generated with the help of the KinMap.[43]

305

306

307

1
2
3   308   **Chemistry**
4
5   309   We recently reported the synthetic preparation of piperidines **4a-j** and the enantiopure analogs
6
7   310   *(R)*-**4c,d** and *(S)*-**4c,d** from 9-tosyl-9*H*-pyrimido[4,5-*b*]indoles **3a-j** (Scheme 2).[31] These
8
9   311   piperidine intermediates display diverse substitution patterns of the tricyclic core and served as
10
11   312   precursors to prepare the final compounds **5a-j** as well as *(R)*-**5c,d** and *(S)*-**5c,d** within the
12
13
14   313   herein reported study. As previously described in the synthesis of inhibitor **1**, the cyanoethyl
15
16   314   substituent was installed on the piperidine nitrogen by Michael reaction with acrylonitrile.[8]
17
18
19
20
21
22
23
24
25
26
27
28
29   **3a-i**: R^1 = H   **4a-i**: R^1 = H   **5a-i**: R^1 = H
30   **3j**: R^1 = CH$_3$ *(R)*-**4c,d**: R^1 = H   *(R)*-**5c,d**: R^1 = H
31   *(S)*-**4c,d**: R^1 = H   *(S)*-**5c,d**: R^1 = H
32   **4j**: R^1 = CH$_3$ **5j**: R^1 = CH$_3$
33
34
35
36   **R^2 =**
37
38   **a**:   H   **b**:   7-F   **c**:   7-Cl   **d**:   7-Br   **e**:   7-OCH$_3$
39   **f**:   7-CF$_3$ **g**:   6-Cl   **h**:   6-Br   **i**:   5-Cl   **j**:   7-Cl
40   315
41

42   316   **Scheme 2.** Synthetic route towards compounds **5a-j** and the enantiopure analogs *(R)*-**5c,d** and
43
44   317   *(S)*-**5c,d** listed in Tables 1 and 2. Reagents and conditions: (i) acrylonitrile, MeOH, rt (37-84%).
45
46   318   Moreover, our established synthetic methodologies were successfully applied to the
47
48
49   319   corresponding 7-iodine derivatives (Scheme 3).[31] In detail, previously reported 7-iodo-9-tosyl-
50
51   320   9*H*-pyrimido[4,5-*b*]indole (**6**) was reacted with *N*-Boc-3-(methylamino)piperidine in a
52
53   321   nucleophilic aromatic substitution (S$_N$Ar) giving intermediate **8**. In case of the enantiopure
54
55   322   analog *(S)*-**8**, commercially available *(S)*-*N*-Boc-3-aminopiperidine was used in the S$_N$Ar
56
57   323   resulting in *(S)*-**7**, which was subsequently methylated with iodomethane under strictly
58
59   324   anhydrous basic conditions. Intermediates **8** and *(S)*-**8** were then subjected to deprotection
60

325   procedures to generate piperidines **10** and *(S)*-**10**, which were similarly reacted with

326   acrylonitrile to form final compound **11** and intermediate *(S)*-**11**.

327
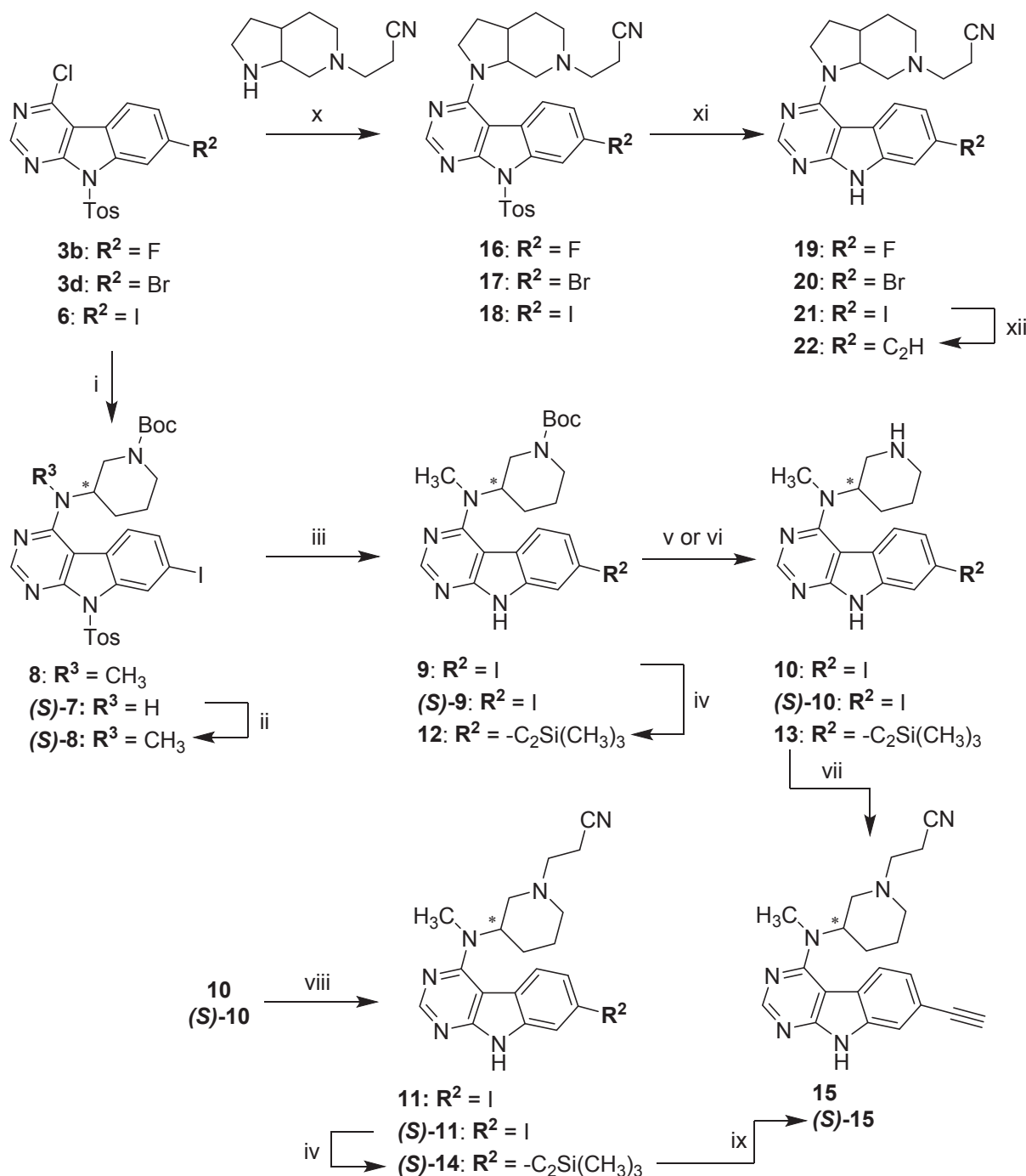
329   **Scheme 3.** Synthetic route towards compounds **11, 15, (S)-15** and **19-21** listed in Tables 2

330   and 3. Reagents and conditions: (i) **6**, DIPEA, DMF, 70 °C (54% for *(S)*-**7**); (ii) iodomethane,

331   NaH, DMF, -10 °C to rt (5); (iii) K*t*BuO, THF, rt (54-58% over two steps); (iv) TMS-acetylene,

332   Pd(PPh$_3$)$_4$ or PdCl$_2$(PPh$_3$)$_2$, CuI, TEA, DMF, rt or 50 °C (86-96%); (v) **9** or *(S)*-**9**, TFA, DCM,

333   rt (quant.); (vi) **12**, 4N HCl in 1,4-dioxane, rt (42%); (vii) (1) acrylonitrile, MeOH, rt, (2)

334   K$_2$CO$_3$, MeOH, rt (41% over two steps); (viii) acrylonitrile, MeOH, rt (44-74%); (ix) K$_2$CO$_3$,

335   MeOH, rt (68%); (x) DIPEA, DMF, 70 °C (41-62%); (xi) KtBuO, THF, rt (40-62%); (xii) (1)

336   TMS-acetylene, PdCl$_2$(PPh$_3$)$_2$, CuI, TEA, DMF, rt, (2) K$_2$CO$_3$, MeOH, rt (41% over two steps).

337   For the synthesis of the racemic ethinyl derivative **15**, a Sonogashira cross coupling

338   reaction was initially performed with the Boc-protected intermediate **9** and

339   trimethylsilylacetylene (TMS-acetylene) following a modified literature protocol (Scheme 3).[44]

340   The treatment of the Sonogashira product **12** with TFA in DCM, however, resulted in

341   simultaneous Boc and TMS deprotection along with pronounced by-product formation. While

342   the application of 4N HCl in 1,4-dioxane allowed for a selective Boc cleavage, it still suffered

343   from a poor yield in the synthesis of **13**. Nevertheless, this intermediate was converted into the

344   racemic final compound **15** in a one-pot two-step reaction, including introduction of the

345   cyanoethyl substituent followed by TMS deprotection with K$_2$CO$_3$.

346   In order to avoid an acidic Boc deprotection in presence of the alkyne substituent in the

347   synthesis of the *S*-configured analog *(S)*-**15**, the Pd-catalyzed alkynylation was instead carried

348   out with *(S)*-**11**. The TMS protecting group of *(S)*-**14** was then smoothly cleaved with K$_2$CO$_3$

349   to obtain *(S)*-**15** in a 2.5-fold higher yield over four steps compared to the initial approach.

350   Compounds **5k-l** bearing a nitrile substituent or aryl moieties in the 7-position of the

351   9*H*-pyrimido[4,5-*b*]indole core were prepared by cross coupling reactions from the already

352   reported compound **1** (Scheme 4). In the case of **5m**, precursor **1** was subjected to a palladium-

353   catalyzed cyanation procedure using K$_4$[Fe(CN)$_6$] as cyanide source,[45] whereas **5k** and **5l** were

354   synthesized *via* Suzuki coupling with the appropriate aryl boronic acids applying common

355   procedures.
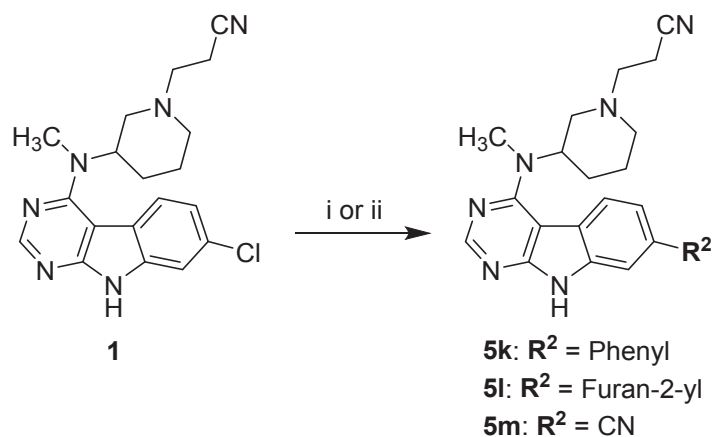
Scheme 4. Synthetic route towards compounds **5k-m** listed in Table 2. Reagents and conditions: (i) $K_4[Fe(CN)_6] \cdot 3H_2O$, BrettPhos Pd G3, BrettPhos, KOAc, 1,4-dioxane:H_2O (1:1, v/v), 100 °C (26%); (ii) appropriate aryl boronic acid, XPhos Pd G3, K_3PO_4, 1,4-dioxane:H_2O (4:1, v/v), 100 °C (60-66%).

The rigidized compounds **19-21** were accessible by a two-step synthetic route starting from the corresponding 9-tosyl-9*H*-pyrimido[4,5-*b*]indoles **3b**, **3d** and **6** (Scheme 3). The required 3-(octahydro-6*H*-pyrrolo[2,3-*c*]pyridin-6-yl)propanenitrile building block was prepared as described previously and introduced under S_NAr conditions.[8] Application of the tosyl deprotection protocol on intermediates **16-18** eventually furnished **19-21**. In addition, the iodine derivative **21** was subjected to the established methodology to introduce the ethinyl substituent to afford inhibitor **22**. We previously confirmed by X-ray crystallographic analysis of **2** that the protocols for the preparation of the 3-(octahydro-6*H*-pyrrolo[2,3-*c*]pyridin-6-yl)propanenitrile building block and its use in the subsequent steps deliver a mixture of the (3a*R*, 7a*S*) and (3a*S*, 7a*R*) enantiomers of the respective final compound.[8]

Conclusion

We utilized a newly obtained co-crystal structure of the moderately potent GSK-3β inhibitor *(S)*-**5c** to identify highly potent compounds. The binding affinity of these compounds was improved by addressing a trapped high-energy water molecule in the HR-I. Here, the ethinyl substituent proved highly beneficial, affording an up to 80-fold increase in potency. The improved inhibitory activity of *(S)*-**15** towards GSK-3β (IC$_{50}$ value of 6 nM) translated also into a cellular context, as the target engagement was demonstrated in a NanoBRET assay together with the neuroprotective effects against H$_2$O$_2$ and reduced autophosphorylation of GSK-3 in neuronal SH-SY5Y cells. In addition, the ethinyl substituted compounds displayed favorable kinome selectivity profiles. Based on our MD simulations and WaterMap analysis, this ethinyl substituent induced only a slight shift in the position of the trapped water molecule, which resulted in a decreased energy of the hydration site that is in line with the observed biological activity. The nearly identical interactions of *(S)*-**5c** and *(S)*-**15** to GSK-3β and improved LLE values of the ethinyl derivatives suggested that it is mainly the subtle change in the high-energy hydration site location that influences the ligand binding. To the best of our knowledge, these results demonstrate for the first time that a high-energy water does not necessarily need to be fully displaced, replaced or interacted by the ligand to alter its energy in a beneficial manner for the ligand binding. Moreover, we noted that a short (ns) simulation appears to be insufficient for the energy evaluation of a shifted hydration site, whereas a combination of longer (μs) MD simulations with WaterMap can be useful. Interestingly, in a completely different compound series we observed that stabilizing a dynamic water network and avoiding unfavorable water exposure related to the HR-I of GSK-3β is also crucial for the inhibitor activity.[46] Overall, these results highlight the importance of considering even subtle changes of hydration site positions in the ligand design process.

403 **Experimental**

404

405 **Chemistry**

406 *General information*

407   All solvents and reagents were obtained from commercial sources and utilized without

408 additional purification. Solvents used for analytical chromatography were of HPLC grade.

409 3-(octahydro-6*H*-pyrrolo[2,3-*c*]pyridin-6-yl)propanenitrile was prepared according to modified

410 reported procedures and obtained as free base or TFA salt.[8] High performance liquid

411 chromatography (HPLC) was carried out on an HP1090 series II HPLC system from Hewlett-

412 Packard (Palo Alto, CA, USA) or an 1100 series HPLC system from Agilent Technologies

413 (Santa Clara, CA, USA). The systems consisted of a binary pump, a column compartment

414 equipped with a Luna C8(2) 100 Å RP column (4.6 mm inner diameter × 150 mm length, 5 μm

415 particle size) from Phenomenex (Torrance, CA, USA), an autosampler and a diode array

416 detector (DAD) (purity of test compounds determined at 254 nm). The mobile phases A

417 (MeOH) and B (aqueous 0.01M KH_2PO_4 buffer, pH 2.3) were used in the following gradient:

418 mobile phase A 40% to 85% during 8 min, mobile phase A 85% constant for 5 min, mobile

419 phase A 85% to 40% during 1 min, mobile phase A 40% constant for 2 min; complete run time

420 16 min; flow rate 1.5 mL/min. Sample injection volume was 5 μL.

421   Chiral chromatographic analysis was performed on a 1290 Infinity series LC system from

422 Agilent Technologies (Santa Clara, CA, USA). The system consisted of a binary pump, a

423 thermostatted column compartment equipped with a Chiralpak IB-U column (3.0 mm inner

424 diameter x 100 mm length, 1.6 μm particle size) from Daicel (Osaka and Tokyo, Japan), an

425 autosampler and a DAD (chiral purity of test compounds determined at 254 nm). To minimize

426 extra column volume, the system was provided with an ultralow dispersion kit (including a

427 Max-Light ultralow dispersion cartridge flow cell with an inner volume of 0.6 μL, an ultralow

428 dispersion needle seat and capillaries with 0.075 mm inner diameter from autosampler to

429 column compartment (350 mm length) and from column compartment to DAD (220 mm

430 length)). The mobile phase was composed of 90% n-heptane, 10% isopropanol and 0.1%

431 diethylamine, flow rate 0.15 mL/min. Samples were prepared by diluting 10 mM aliquotes in

432 DMSO by the factor 10 with the mobile phase to a total concentration of 1 mM and injected

433 with a volume of 5 μL. The enantiomeric excess (ee) of the enantiopure final compounds was

434 >98% in all cases.

435   Thin layer chromatography (TLC) was carried out on TLC Silica gel F254 sheets from

436 Merck (Darmstadt, Germany) or Alugram Sil G/UV254 sheets from Macherey-Nagel (Düren,

437 Germany). Bands were visualized under UV light at 254 nm.

438   Electrospray ionization mass spectrometry (ESI-MS) was performed on an Advion

439 expressions CMS TLC-ESI-MS coupling system from Advion (Ithaca, NY, USA) operating in

440 positive ESI mode (capillary temperature 250 °C, capillary voltage 180 V, source gas

441 temperature 250 °C, ESI voltage 3500 V) and negative ESI mode (capillary temperature

442 250 °C, capillary voltage 180V, source gas temperature 250 °C, ESI voltage 2500 V), elution

443 with LCMS grade MeOH.

444   Flash column chromatography was performed on a Puriflash 430 or XS 420 from Interchim

445 (Montluçon, France) on Davisil Chromatographic Silica Media LC60A (20–45 μm) from Grace

446 Davison Discovery Sciences (MD, USA) or Interchim Puriflash prepacked silica columns

447 (SIHP-JP, 30 μm) from Interchim (Montluçon, France) and Geduran Si60 63200 μm silica gel

448 from Merck (Darmstadt, Germany) for pre-column preparation. Mobile phases are described in

449 the detailed procedures for each purified compound.

450   Nuclear magnetic resonance (NMR) analysis was carried out on 200, 300, and 400 MHz

451 Avance and 400 MHz Ascend spectrometers from Bruker (Billerica, MA, USA). Spectra were

452 calibrated to residual peaks of utilized solvents. The chemical shifts are reported in parts per

453 million (ppm) relative to tetramethylsilane ($\delta = 0$).

454

455   *Experimental procedures*

456   *General Procedure A for the preparation of final compounds* **5a,b** *and* **5d-j** *and the enantiopure*

457   *analogs (R)-***5c,d** *and (S)-***5c,d**

458   The appropriate secondary amine intermediate was dissolved in MeOH (HPLC grade or dry)

459   and acrylonitrile was added. The mixture was stirred at rt and under N_2 atmosphere for 16 h and

460   concentrated under reduced pressure. The residue was purified by flash column

461   chromatography.

462

463   *Detailed procedures for the preparation of final compounds* **5a,b** *and* **5d-j** *and the enantiopure*

464   *analogs (R)-***5c,d** *and (S)-***5c,d**

465   3-(3-(Methyl(9*H*-pyrimido[4,5-*b*]indol-4-yl)amino)piperidin-1-yl)propanenitrile (**5a**)

466   The title compound was prepared from *N*-methyl-*N*-(piperidin-3-yl)-9*H*-pyrimido[4,5-*b*]indol-

467   4-amine (36.0 mg, 0.13 mmol) and acrylonitrile (10.1 mg, 0.19 mmol) in dry MeOH (5 mL)

468   according to general procedure A. Purification by flash column chromatography (SiO$_2$;

469   DCM:EtOH gradient elution from 98:2 to 9:1) gave 26 mg (61% yield); ^{1}H NMR (400 MHz,

470   DMSO-d_6) δ 12.07 (s, 1H), 8.39 (s, 1H), 7.80 (d, J = 8.0 Hz, 1H), 7.48 (d, J = 7.8 Hz, 1H), 7.39

471   (t, J = 7.5 Hz, 1H), 7.33 – 7.27 (m, 1H), 4.52 – 4.41 (m, 1H), 3.15 (s, 3H), 3.07 – 2.99 (m, 1H),

472   2.90 – 2.80 (m, 1H), 2.73 – 2.66 (m, 2H), 2.65 – 2.58 (m, 2H), 2.41 – 2.34 (m, 1H), 1.99 – 1.90

473   (m, 1H), 1.86 – 1.67 (m, 3H), 1.57 – 1.44 (m, 1H); ^{13}C NMR (101 MHz, DMSO-d_6) δ 159.6,

474   157.0, 153.4, 136.6, 124.7, 122.5, 120.5, 120.0, 119.5, 111.2, 97.6, 55.7, 54.8, 53.0, 52.2, 32.5,

475   27.3, 24.4, 14.9; ESI-MS: (m/z) 335.1 [M+H]$^+$, 357.0 [M+Na]$^+$, 333.0 [M-H]$^-$; HPLC *method*

476   *B*: t$_r$ = 2.391 min.

477   3-(3-((7-Fluoro-9*H*-pyrimido[4,5-*b*]indol-4-yl)(methyl)amino)piperidin-1-yl)propanenitrile

478   (**5b**)

479   The title compound was prepared from 7-fluoro-*N*-methyl-*N*-(piperidin-3-yl)-9*H*-

480   pyrimido[4,5-*b*]indol-4-amine (80.0 mg, 0.27 mmol) and acrylonitrile (28.1 mg, 0.53 mmol) in

481   dry MeOH (7 mL) according to general procedure A. Purification by flash column

482   chromatography (SiO$_2$, DCM:EtOH gradient elution from 98:2 to 9:1) gave 44 mg (47% yield);

483   ^{1}H NMR (400 MHz, DMSO-d_6) δ 12.21 (s, 1H), 8.38 (s, 1H), 7.78 (dd, *J* = 8.8, 5.3 Hz, 1H),

484   7.24 (dd, *J* = 9.4, 2.4 Hz, 1H), 7.15 (td, *J* = 9.4, 2.4 Hz, 1H), 4.50 – 4.35 (m, 1H), 3.13 (s, 3H),

485   3.09 – 3.02 (m, 1H), 2.90 – 2.81 (m, 1H), 2.74 – 2.66 (m, 2H), 2.65 – 2.58 (m, 2H), 2.42 – 2.33

486   (m, 1H), 1.99 – 1.89 (m, 1H), 1.81 – 1.65 (m, 3H), 1.55 – 1.42 (m, 1H); ^{13}C NMR (101 MHz,

487   DMSO-d_6) δ 160.2 (d, *J* = 239.8 Hz), 159.3, 157.6, 153.2, 137.4 (d, *J* = 12.6 Hz), 123.9 (d, *J* =

488   10.0 Hz), 120.0, 116.3, 108.3 (d, *J* = 23.5 Hz), 97.7 (d, *J* = 26.0 Hz), 97.3, 55.7, 54.8, 53.0,

489   52.2, 32.5, 27.2, 24.3, 15.0; ESI-MS: (m/z) 353.2 [M+H]$^+$, 375.2 [M+Na]$^+$, 351.1 [M-H]$^-$;

490   HPLC *method B*: t$_r$ = 2.804 min.

491   (*R*)-3-(3-((7-Chloro-9*H*-pyrimido[4,5-*b*]indol-4-yl)(methyl)amino)piperidin-1-

492   yl)propanenitrile (**(R)-5c**)

493   *(R)*-7-chloro-*N*-methyl-*N*-(piperidin-3-yl)-9*H*-pyrimido[4,5-*b*]indol-4-amine (50.0 mg, 0.16

494   mmol) and acrylonitrile (12.6 mg, 0.24 mmol) were stirred in dry MeOH (15 mL) at rt and

495   under N$_2$ atmosphere for 6 h. DIPEA (24.6 mg, 0.19 mmol) was added to promote conversion

496   and stirring continued overnight. The mixture was concentrated under reduced pressure. The

497   residue was dissolved in DCM and the solution washed with saturated NH$_4$Cl solution (3 x 10

498   mL), dried over Na$_2$SO$_4$ and concentrated under reduced pressure. Purification of the residue

499   twice by flash column chromatography (SiO$_2$, DCM:MeOH gradient elution from 95.5:4.5 to

500   93.5:6.5 and SiO$_2$, DCM:EtOH gradient elution from 1:0 to 93:7) gave 30 mg of a white solid

501   (51% yield); ^{1}H NMR (400 MHz, DMSO-d_6) δ 12.22 (s, 1H), 8.40 (s, 1H), 7.78 (d, *J* = 8.7 Hz,

502   1H), 7.48 (d, J = 2.0 Hz, 1H), 7.34 (dd, J = 8.6, 2.0 Hz, 1H), 4.52 – 4.40 (m, 1H), 3.14 (s, 3H),

503   3.11 – 3.03 (m, 1H), 2.91 – 2.82 (m, 1H), 2.76 – 2.69 (m, 2H), 2.66 – 2.59 (m, 2H), 2.43 – 2.34

504   (m, 1H), 2.02 – 1.89 (m, 1H), 1.82 – 1.66 (m, 3H), 1.57 – 1.42 (m, 1H); ^{13}C NMR (101 MHz,

505   DMSO-d_6) δ 159.4, 157.4, 153.8, 137.4, 129.2, 123.9, 120.7, 120.1, 118.6, 110.8, 97.0, 55.7,

506   54.8, 53.1, 52.3, 32.6, 27.3, 24.4, 15.1; ESI-MS: (m/z) 369.0 [M+H]$^+$, 390.9 [M+Na]$^+$, 366.8

507   [M-H]$^-$; HPLC *method A*: t_r = 4.329 min.

508   (*S*)-3-(3-((7-Chloro-9*H*-pyrimido[4,5-*b*]indol-4-yl)(methyl)amino)piperidin-1-

509   yl)propanenitrile (*(S)*-**5c**)

510   The title compound was prepared from *(S)*-7-chloro-*N*-methyl-*N*-(piperidin-3-yl)-9*H*-

511   pyrimido[4,5-*b*]indol-4-amine (65.0 mg, 0.21 mmol) and acrylonitrile (21.8 mg, 0.41 mmol) in

512   dry MeOH (20 mL) according to general procedure A. Purification by flash column

513   chromatography (SiO$_2$, DCM:MeOH gradient elution from 95.5:4.5 to 93.5:6.5) gave 53 mg of

514   a white solid (70% yield); ^{1}H NMR (200 MHz, DMSO-d_6) δ 12.21 (s, 1H), 8.40 (d, J = 0.4 Hz,

515   1H), 7.78 (d, J = 8.7 Hz, 1H), 7.47 (d, J = 2.0 Hz, 1H), 7.34 (dd, J = 8.7, 1.8 Hz, 1H), 4.57 –

516   4.36 (m, 1H), 3.15 (s, 3H), 3.12 – 3.01 (m, 1H), 2.94 – 2.80 (m, 1H), 2.78 – 2.68 (m, 2H), 2.67

517   – 2.57 (m, 2H), 2.46 – 2.30 (m, 1H), 2.05 – 1.86 (m, 1H), 1.85 – 1.37 (m, 4H); ^{13}C NMR (50

518   MHz, DMSO-d_6) δ 159.4, 157.4, 153.8, 137.3, 129.1, 123.9, 120.6, 120.1, 118.5, 110.8, 97.0,

519   55.7, 54.8, 53.0, 52.2, 32.6, 27.2, 24.3, 15.0; ESI-MS: (m/z) 369.1 [M+H]$^+$, 391.0 [M+Na]$^+$,

520   366.9 [M-H]$^-$; HPLC *method A*: t_r = 4.724 min.

521   3-(3-((7-Bromo-9*H*-pyrimido[4,5-*b*]indol-4-yl)(methyl)amino)piperidin-1-yl)propanenitrile

522   (**5d**)

523   The title compound was prepared from 7-bromo-*N*-methyl-*N*-(piperidin-3-yl)-9*H*-

524   pyrimido[4,5-*b*]indol-4-amine (120.0 mg, 0.33 mmol) and acrylonitrile (26.5 mg, 0.50 mmol)

525   in dry MeOH (10 mL) according to general procedure A. Purification by flash column

526   chromatography (SiO$_2$, DCM:EtOH gradient elution from 98:2 to 9:1) gave 90 mg (65% yield);

527   ^{1}H NMR (300 MHz, DMSO-d_6) δ 12.20 (s, 1H), 8.40 (s, 1H), 7.73 (d, J = 8.7 Hz, 1H), 7.61 (d,

528   J = 1.9 Hz, 1H), 7.46 (dd, J = 8.6, 1.9 Hz, 1H), 4.51 – 4.39 (m, 1H), 3.14 (s, 3H), 3.10 – 3.03

529   (m, 1H), 2.90 – 2.81 (m, 1H), 2.76 – 2.67 (m, 2H), 2.67 – 2.58 (m, 2H), 2.44 – 2.33 (m, 1H),

530   2.01 – 1.88 (m, 1H), 1.80 – 1.64 (m, 3H), 1.58 – 1.41 (m, 1H); ESI-MS: (m/z) 412.9 [M+H]$^+$,

531   434.9 [M+Na]$^+$, 410.7 [M-H]$^-$; HPLC *method B*: t$_r$ = 5.272 min.

532   (*R*)-3-(3-((7-Bromo-9*H*-pyrimido[4,5-*b*]indol-4-yl)(methyl)amino)piperidin-1-

533   yl)propanenitrile (*(R)*-5d)

534   The title compound was prepared from *(R)*-7-bromo-*N*-methyl-*N*-(piperidin-3-yl)-9*H*-

535   pyrimido[4,5-*b*]indol-4-amine (65.0 mg, 0.18 mmol) and acrylonitrile (21.1 mg, 0.4 mmol) in

536   HPLC grade MeOH (30 mL) according to general procedure A. Purification by flash column

537   chromatography (SiO$_2$, DCM:MeOH 95:5) gave 65 mg of a white solid (87% yield); ^{1}H NMR

538   (300 MHz, DMSO-d_6) δ 12.20 (s, 1H), 8.40 (s, 1H), 7.73 (d, J = 8.7 Hz, 1H), 7.61 (d, J = 1.9

539   Hz, 1H), 7.46 (dd, J = 8.6, 1.9 Hz, 1H), 4.52 – 4.39 (m, 1H), 3.14 (s, 3H), 3.11 – 3.04 (m, 1H),

540   2.91 – 2.81 (m, 1H), 2.76 – 2.68 (m, 2H), 2.67 – 2.59 (m, 2H), 2.44 – 2.33 (m, 1H), 2.02 – 1.89

541   (m, 1H), 1.82 – 1.64 (m, 3H), 1.58 – 1.40 (m, 1H); ESI-MS: (m/z) 413.5 [M+H]$^+$, 435.5

542   [M+Na]$^+$, 411.5 [M-H]$^-$; HPLC *method A*: t$_r$ = 4.038 min.

543   (*S*)-3-(3-((7-Bromo-9*H*-pyrimido[4,5-*b*]indol-4-yl)(methyl)amino)piperidin-1-

544   yl)propanenitrile (*(S)*-5d)

545   The title compound was prepared from *(S)*-7-bromo-*N*-methyl-*N*-(piperidin-3-yl)-9*H*-

546   pyrimido[4,5-*b*]indol-4-amine (55.0 mg, 0.15 mmol) and acrylonitrile (17.8 mg, 0.34 mmol) in

547   HPLC grade MeOH (25 mL) according to general procedure A. Purification by flash column

548   chromatography (SiO$_2$, DCM:MeOH 95:5) gave 28 mg of a white solid (44% yield); ^{1}H NMR

549   (300 MHz, DMSO-d_6) δ 12.20 (s, 1H), 8.40 (s, 1H), 7.73 (d, J = 8.7 Hz, 1H), 7.61 (d, J = 1.9

550　Hz, 1H), 7.46 (dd, J = 8.6, 1.9 Hz, 1H), 4.52 – 4.38 (m, 1H), 3.14 (s, 3H), 3.11 – 3.02 (m, 1H),

551　2.92 – 2.81 (m, 1H), 2.76 – 2.68 (m, 2H), 2.68 – 2.57 (m, 2H), 2.45 – 2.31 (m, 1H), 2.03 – 1.88

552　(m, 1H), 1.83 – 1.63 (m, 3H), 1.60 – 1.40 (m, 1H); ESI-MS: (m/z) 413.3 [M+H]$^+$, 435.3

553　[M+Na]$^+$, 411.3 [M-H]$^-$; HPLC *method A*: t_r = 4.099 min.

554　3-(3-((7-Methoxy-9*H*-pyrimido[4,5-*b*]indol-4-yl)(methyl)amino)piperidin-1-yl)propanenitrile

555　(**5e**)

556　The title compound was prepared from 7-methoxy-*N*-methyl-*N*-(piperidin-3-yl)-9*H*-

557　pyrimido[4,5-*b*]indol-4-amine (90.0 mg, 0.29 mmol) and acrylonitrile (23.0 mg, 0.43 mmol) in

558　dry MeOH (7 mL) according to general procedure A. Purification by flash column

559　chromatography (SiO$_2$, DCM:EtOH gradient elution from 98:2 to 9:1) gave 60 mg (57% yield);

560　^{1}H NMR (300 MHz, DMSO-d_6) δ 11.96 (s, 1H), 8.34 (s, 1H), 7.67 (d, J = 8.7 Hz, 1H), 7.01 –

561　6.89 (m, 1H), 4.52 – 4.35 (m, 1H), 3.83 (s, 3H), 3.11 (s, 3H), 3.06 – 2.98 (m, 1H), 2.90 – 2.81

562　(m, 1H), 2.76 – 2.57 (m, 4H), 2.43 – 2.32 (m, 1H), 2.00 – 1.87 (m, 1H), 1.83 – 1.63 (m, 3H),

563　1.59 – 1.40 (m, 1H); ^{13}C NMR (101 MHz, DMSO-d_6) δ 158.8, 157.6, 157.0, 152.3, 138.0,

564　123.3, 119.9, 113.1, 109.2, 97.9, 95.1, 55.7, 55.2, 54.5, 53.0, 52.2, 32.2, 27.2, 24.3, 14.9; ESI-

565　MS: (m/z) 365.0 [M+H]$^+$, 387.0 [M+Na]$^+$, 363.1 [M-H]$^-$; HPLC *method B*: t_r = 2.744 min.

566　3-(3-(Methyl(7-(trifluoromethyl)-9*H*-pyrimido[4,5-*b*]indol-4-yl)amino)piperidin-1-yl)-

567　propanenitrile (**5f**)

568　The title compound was prepared from *N*-methyl-*N*-(piperidin-3-yl)-7-(trifluoromethyl)-9*H*-

569　pyrimido[4,5-*b*]indol-4-amine (85.0 mg, 0.24 mmol) and acrylonitrile (19.1 mg, 0.36 mmol) in

570　dry MeOH (3 mL) according to general procedure A. Purification twice by flash column

571　chromatography (SiO$_2$, DCM:EtOH gradient elution from 97:3 to 4:1 and SiO$_2$, DCM:(2N NH$_3$

572　in MeOH) gradient elution from 99:1 to 92:8) gave 36 mg (37% yield); ^{1}H NMR (300 MHz,

573　DMSO-d_6) δ 12.44 (s, 1H), 8.44 (s, 1H), 8.00 (d, J = 8.5 Hz, 1H), 7.74 (s, 1H), 7.64 (d, J = 8.5

574 Hz, 1H), 4.59 – 4.45 (m, 1H), 3.19 (s, 3H), 3.15 – 3.07 (m, 1H), 2.92 – 2.83 (m, 1H), 2.77 –

575 2.69 (m, 2H), 2.68 – 2.60 (m, 2H), 2.46 – 2.35 (m, 1H), 2.02 – 1.91 (m, 1H), 1.84 – 1.66 (m,

576 3H), 1.60 – 1.42 (m, 1H); ESI-MS: (m/z) 403.1 [M+H]$^+$, 425.0 [M+Na]$^+$, 401.0 [M-H]$^-$; HPLC

577 *method B*: t$_r$ = 5.218 min.

578 3-(3-((6-Chloro-9*H*-pyrimido[4,5-*b*]indol-4-yl)(methyl)amino)piperidin-1-yl)propanenitrile

579 (**5g**)

580 The title compound was prepared from 6-chloro-*N*-methyl-*N*-(piperidin-3-yl)-9*H*-

581 pyrimido[4,5-*b*]indol-4-amine (45.0 mg, 0.14 mmol) and acrylonitrile (16.6 mg, 0.31 mmol) in

582 HPLC grade MeOH (13 mL) according to general procedure A. Purification by flash column

583 chromatography (SiO$_2$, DCM:MeOH gradient elution from 95.5:4.5 to 93.5:6.5) gave 44 mg of

584 a white solid (84% yield); ^{1}H NMR (400 MHz, DMSO-d_6) δ 12.23 (s, 1H), 8.40 (s, 1H), 7.73

585 (d, *J* = 1.4 Hz, 1H), 7.49 (d, *J* = 8.6 Hz, 1H), 7.41 (dd, *J* = 8.5, 1.5 Hz, 1H), 4.48 – 4.36 (m,

586 1H), 3.17 (s, 3H), 3.03 – 2.94 (m, 1H), 2.90 – 2.81 (m, 1H), 2.72 – 2.61 (m, 4H), 2.43 – 2.34

587 (m, 1H), 2.05 – 1.94 (m, 1H), 1.92 – 1.70 (m, 3H), 1.63 – 1.49 (m, 1H); ^{13}C NMR (101 MHz,

588 DMSO-d_6) δ 159.5, 157.5, 153.9, 135.1, 124.6, 124.4, 121.6, 120.8, 119.8, 112.6, 96.8, 55.4,

589 54.7, 52.9, 51.9, 32.8, 27.2, 24.3, 14.7; ESI-MS: (m/z) 369.4 [M+H]$^+$, 391.4 [M+Na]$^+$, 367.4

590 [M-H]$^-$; HPLC *method A*: t$_r$ = 6.421 min.

591 3-(3-((6-Bromo-9*H*-pyrimido[4,5-*b*]indol-4-yl)(methyl)amino)piperidin-1-yl)propanenitrile

592 (**5h**)

593 The title compound was prepared from 6-bromo-*N*-methyl-*N*-(piperidin-3-yl)-9*H*-

594 pyrimido[4,5-*b*]indol-4-amine (55.0 mg, 0.15 mmol) and acrylonitrile (17.8 mg, 0.34 mmol) in

595 HPLC grade MeOH (25 mL) according to general procedure A. Purification by flash column

596 chromatography (SiO$_2$, DCM:MeOH gradient elution from 95.5:4.5 to 93.5:6.5) gave 48 mg of

597 a white solid (76% yield); ^{1}H NMR (300 MHz, DMSO-d_6) δ 12.25 (s, 1H), 8.40 (s, 1H), 7.86

598 (d, J = 1.5 Hz, 1H), 7.53 (dd, J = 8.6, 1.7 Hz, 1H), 7.44 (d, J = 8.5 Hz, 1H), 4.48 – 4.35 (m,

599 1H), 3.16 (s, 3H), 3.02 – 2.91 (m, 1H), 2.91 – 2.81 (m, 1H), 2.75 – 2.59 (m, 4H), 2.46 – 2.34

600 (m, 1H), 2.05 – 1.70 (m, 4H), 1.65 – 1.49 (m, 1H); ^{13}C NMR (101 MHz, DMSO-d_6) δ 159.5,

601 157.3, 154.0, 135.4, 127.1, 124.5, 121.4, 119.9, 113.1, 112.5, 96.7, 55.4, 54.8, 52.9, 51.9, 32.7,

602 27.3, 24.3, 14.7; ESI-MS: (m/z) 413.1 [M+H]$^+$, 435.0 [M+Na]$^+$, 411.1 [M-H]$^-$; HPLC *method*

603 *A*: t$_r$ = 4.195 min.

604 3-(3-((5-Chloro-9*H*-pyrimido[4,5-*b*]indol-4-yl)(methyl)amino)piperidin-1-yl)propanenitrile

605 (**5i**)

606 The title compound was prepared from 5-chloro-*N*-methyl-*N*-(piperidin-3-yl)-9*H*-

607 pyrimido[4,5-*b*]indol-4-amine (47.0 mg, 0.15 mmol) and acrylonitrile (17.4 mg, 0.33 mmol) in

608 HPLC grade MeOH (13.5 mL) according to general procedure A (reaction time 20 h).

609 Purification by flash column chromatography (SiO$_2$, DCM:MeOH 94.5:5.5) gave 38 mg of a

610 white solid; ^{1}H NMR (400 MHz, DMSO-d_6) δ 12.26 (s, 1H), 8.37 (s, 1H), 7.45 – 7.34 (m, 2H),

611 7.27 (dd, J = 7.5, 0.8 Hz, 1H), 4.49 – 4.33 (m, 1H), 3.03 – 2.76 (m, 5H), 2.71 – 2.54 (m, 4H),

612 2.37 – 2.19 (m, 1H), 2.01 – 1.46 (m, 5H); ESI-MS: (m/z) 369.3 [M+H]$^+$, 391.3 [M+Na]$^+$, 367.3

613 [M-H]$^-$; HPLC *method A*: t$_r$ = 3.343 min.

614 3-(3-((7-Chloro-2-methyl-9*H*-pyrimido[4,5-*b*]indol-4-yl)(methyl)amino)piperidin-1-

615 yl)propanenitrile (**5j**)

616 The title compound was prepared from 7-chloro-*N*,2-dimethyl-*N*-(piperidin-3-yl)-9*H*-

617 pyrimido[4,5-*b*]indol-4-amine (60.0 mg, 0.18 mmol) and acrylonitrile (21.2 mg, 0.40 mmol) in

618 HPLC grade MeOH (17 mL) according to general procedure A. Purification by flash column

619 chromatography (SiO$_2$, DCM:MeOH gradient elution from 96:4 to 94:6) gave 55 mg of a beige

620 solid (79% yield); ^{1}H NMR (300 MHz, DMSO-d_6) δ 11.99 (s, 1H), 7.72 (d, J = 8.7 Hz, 1H),

621 7.44 (d, J = 2.0 Hz, 1H), 7.30 (dd, J = 8.6, 2.1 Hz, 1H), 4.49 – 4.35 (m, 1H), 3.11 (s, 3H), 3.09

622   – 3.02 (m, 1H), 2.90 – 2.80 (m, 1H), 2.75 – 2.67 (m, 2H), 2.66 – 2.55 (m, 2H), 2.48 (s, 3H),

623   2.41 – 2.29 (m, 1H), 2.02 – 1.89 (m, 1H), 1.82 – 1.63 (m, 3H), 1.58 – 1.43 (m, 1H); ^{13}C NMR

624   (50 MHz, DMSO-d_6) δ 162.6, 159.4, 158.4, 137.4, 128.7, 123.5, 120.5, 120.2, 118.8, 110.8,

625   94.8, 55.6, 54.8, 53.1, 52.5, 32.4, 27.4, 25.9, 24.4, 15.1; ESI-MS: (m/z) 382.9 [M+H]$^+$, 404.9

626   [M+Na]$^+$, 380.9 [M-H]$^-$; HPLC *method A*: t$_r$ = 5.951 min.

627

628   *Detailed procedures for the preparation of final compound* **11**

629   *tert*-Butyl 3-((7-iodo-9*H*-pyrimido[4,5-*b*]indol-4-yl)(methyl)amino)piperidine-1-carboxylate

630   **(9)**

631   The title compound was prepared by a two-step procedure. In the first step 4-chloro-7-iodo-9-

632   tosyl-9*H*-pyrimido[4,5-*b*]indole (**6**) (590.0 mg, 1.22 mmol), *N*-Boc-3-(methylamino)piperidine

633   (339.8 mg, 1.59 mmol) and DIPEA (473.0 mg, 3.66 mmol) were stirred in dry DMF (16 mL)

634   at 60°C for 2 h. After cooling down to rt, the mixture was poured into ice-cold and saturated

635   NH$_4$Cl solution (50 mL) was added. The resulting precipitate was filtered off and dried over

636   P$_2$O$_5$ in vacuo to yield 779 mg of crude *tert*-butyl 3-((7-iodo-9-tosyl-9*H*-pyrimido[4,5-*b*]indol-

637   4-yl)(methyl)amino)piperidine-1-carboxylate (**8**) as a beige solid (97% crude yield), used in the

638   second step without further purification. A small portion was purified by flash column

639   chromatography for analytical purposes (SiO$_2$, petroleum ether:EtOAc gradient elution from

640   3:2 to 1:1); ^{1}H NMR (300 MHz, CDCl$_3$) δ 8.86 (d, *J* = 1.4 Hz, 1H), 8.62 (s, 1H), 8.09 (d, *J* =

641   8.4 Hz, 2H), 7.74 (dd, *J* = 8.4, 1.4 Hz, 1H), 7.41 (d, *J* = 7.9 Hz, 1H), 7.27 (d, *J* = 8.1 Hz, 2H;

642   overlap with CHCl$_3$ signal), 4.47 – 3.90 (m, 3H), 3.11 (s, 3H), 3.08 – 2.98 (m, 1H), 2.77 – 2.60

643   (m, 1H), 2.37 (s, 3H), 2.01 – 1.71 (m, 3H), 1.64 – 1.29 (m, 10H); ^{13}C NMR (50 MHz, CDCl$_3$)

644   δ 160.5, 157.0, 154.8, 154.4, 145.8, 136.4, 135.4, 133.2, 129.8, 128.2, 124.0, 123.1, 121.3,

645   101.2, 91.3, 80.0, 55.6 (br), 46.7, 44.1 (br), 33.7 (br), 28.5, 28.1, 24.8, 21.8; ESI-MS: (m/z)

646   684.7 [M+Na]$^+$, 660.8 [M-H]$^-$; HPLC *method A*: t$_r$ = 10.993 min.

647 Crude *tert*-butyl 3-((7-iodo-9-tosyl-9*H*-pyrimido[4,5-*b*]indol-4-yl)(methyl)amino)piperidine-

648 1-carboxylate (**8**) (680 mg) was dissolved in dry THF (30 mL). K*t*BuO (807.4 mg, 7.2 mmol)

649 was added and the mixture stirred at rt for 1 h. Saturated NH$_4$Cl solution (50 mL) was added

650 and the mixture was extracted with EtOAc (3 x 30 mL). Combined organic layers were dried

651 over Na$_2$SO$_4$ and concentrated under reduced pressure. Purification of the residue twice by flash

652 column chromatography (SiO$_2$, DCM:MeOH 95:5 and SiO$_2$, DCM:MeOH gradient elution

653 from 97.5:2.5 to 93:7) gave 292 mg of a beige solid (56% yield); ^{1}H NMR (300 MHz, CDCl$_3$)

654 δ 11.30 (s, 1H), 8.52 (s, 1H), 7.92 (d, *J* = 1.1 Hz, 1H), 7.61 (dd, *J* = 8.5, 1.4 Hz, 1H), 7.53 (d, *J*

655 = 8.5 Hz, 1H), 4.55 – 4.04 (m, 3H), 3.29 (s, 3H), 3.11 – 2.98 (m, 1H), 2.78 – 2.61 (m, 1H), 2.10

656 – 1.76 (m, 3H), 1.74 – 1.30 (m, 10H); ESI-MS: (m/z) 530.6 [M+Na]$^+$, 506.6 [M-H]$^-$; HPLC

657 *method A*: t$_r$ = 9.541 min.

658 7-Iodo-*N*-methyl-*N*-(piperidin-3-yl)-9*H*-pyrimido[4,5-*b*]indol-4-amine (**10**)

659 *tert*-Butyl 3-((7-iodo-9*H*-pyrimido[4,5-*b*]indol-4-yl)(methyl)amino)piperidine-1-carboxylate

660 (**9**) (240.0 mg, 0.473 mmol) was suspended in dry DCM (7 mL) and TFA was added (1.5 mL).

661 The mixture was stirred at rt for 30 min and then concentrated under reduced pressure. Residual

662 TFA was neutralised by addition of saturated NaHCO$_3$ solution (30 mL) which resulted in a

663 precipitate. The precipitate was filtered off, washed with saturated NaHCO$_3$ solution and

664 demineralised water and dried over P$_2$O$_5$ *in vacuo*. 199 mg of a beige solid were yielded (>100%

665 crude yield) and used in the next step without further purification; ^{1}H NMR (300 MHz, MeOD)

666 δ 8.35 (s, 1H), 7.86 (s, 1H), 7.65 – 7.52 (m, 2H), 4.55 – 4.40 (m, 1H), 3.24 (s, 3H), 3.14 – 3.05

667 (m, 1H), 3.02 – 2.84 (m, 2H), 2.60 – 2.47 (m, 1H), 2.15 – 1.84 (m, 3H), 1.77 – 1.59 (m, 1H);

668 ESI-MS: (m/z) 408.3 [M+H]$^+$, 406.3 [M-H]$^-$; HPLC *method A*: t$_r$ = 4.563 min.

669 3-(3-((7-Iodo-9*H*-pyrimido[4,5-*b*]indol-4-yl)(methyl)amino)piperidin-1-yl)propanenitrile (**11**)

670 The title compound was prepared from 7-Iodo-*N*-methyl-*N*-(piperidin-3-yl)-9*H*-pyrimido[4,5-

671 *b*]indol-4-amine (**10**) (70.0 mg, 0.17 mmol) and acrylonitrile (20.1 mg, 0.38 mmol) in HPLC

672 grade MeOH (30 mL) according to general procedure A. Purification by flash column

673 chromatography (SiO$_2$, DCM:MeOH 95:5) gave 35 mg of a white solid (44% yield); ^{1}H NMR

674 (400 MHz, DMSO-*d$_6$*) δ 12.15 (s, 1H), 8.40 (s, 1H), 7.79 (s, 1H), 7.67 – 7.53 (m, 2H), 4.51 –

675 4.37 (m, 1H), 3.13 (s, 3H), 3.09 – 3.01 (m, 1H), 2.90 – 2.80 (m, 1H), 2.76 – 2.67 (m, 2H), 2.67

676 – 2.58 (m, 2H), 2.42 – 2.31 (m, 1H), 2.01 – 1.89 (m, 1H), 1.82 – 1.63 (m, 3H), 1.58 – 1.41 (m,

677 1H); ^{13}C NMR (101 MHz, DMSO-*d$_6$*) δ 159.5, 156.9, 153.9, 137.9, 128.9, 124.4, 120.0, 119.5,

678 119.2, 97.1, 89.3, 55.6, 54.7, 53.0, 52.2, 32.5, 27.2, 24.3, 15.0; ESI-MS: (m/z) 461.2 [M+H]$^+$,

679 483.2 [M+Na]$^+$, 459.2 [M-H]$^-$; HPLC *method A*: t$_r$ = 5.555 min.

680

681 *Detailed procedures for the preparation of final compound* **15**

682 *tert*-Butyl 3-(methyl(7-((trimethylsilyl)ethynyl)-9*H*-pyrimido[4,5-*b*]indol-4-

683 yl)amino)piperidine-1-carboxylate (**12**)

684 A mixture of *tert*-butyl 3-((7-iodo-9*H*-pyrimido[4,5-*b*]indol-4-yl)(methyl)amino)piperidine-1-

685 carboxylate (**9**) (310.0 mg, 0.61 mmol), CuI (23.3 mg, 0.12 mmol) and Pd(PPh$_3$)$_4$ (70.6 mg,

686 0.06 mmol) in dry DMF was degassed under reduced pressure by sonication and subsequently

687 set under Ar atmosphere. TMS-acetylene (180.0 mg, 1.83 mmol) and TEA (123.0 mg, 1.22

688 mmol) were added and the mixture stirred at 50°C and under Ar atmosphere overnight. After

689 cooling down to rt, saturated NH$_4$Cl solution (3 mL) was added and the mixture was extracted

690 with EtOAc (5 x 3 mL). Combined organic layers were washed with saturated NaCl solution (4

691 x 7 mL), dried over Na$_2$SO$_4$ and concentrated under reduced pressure. Purification of the residue

692 by flash column chromatography (SiO$_2$, DCM:MeOH gradient elution from 30:1 to 93:7) gave

693 280 mg of a brown solid (96% yield) containing approx. 10% of an impurity, which was

694 detected in the ^{1}H NMR and is assumed to be triphenylphosphine oxide; ^{1}H NMR (400 MHz,

695   CDCl$_3$) δ 11.81 (s, 1H), 8.61 (s, 1H), 7.72 (d, *J* = 8.3 Hz, 1H), 7.64 (s, 1H), 7.39 (dd, *J* = 8.3,

696   1.4 Hz, 1H), 4.55 – 4.02 (m, 3H), 3.28 (s, 3H), 3.11 – 3.00 (m, 1H), 2.75 – 2.60 (m, 1H), 2.11

697   – 2.04 (m, 1H), 1.97 – 1.77 (m, 2H), 1.70 – 1.57 (m, 1H), 1.42 (s, 9H), 0.29 (s, 9H); ESI-MS:

698   (m/z) 500.4 [M+Na]$^+$, 476.5 [M-H]$^-$; HPLC *method A*: t$_r$ = 11.448 min.

699   *N*-Methyl-*N*-(piperidin-3-yl)-7-((trimethylsilyl)ethynyl)-9*H*-pyrimido[4,5-*b*]indol-4-amine

700   (**13**)

701   *tert*-Butyl 3-(methyl(7-((trimethylsilyl)ethynyl)-9*H*-pyrimido[4,5-*b*]indol-4-

702   yl)amino)piperidine-1-carboxylate (**12**) (115.2 mg, 0.24 mmol) was suspended in dry 4N HCl

703   in 1,4-dioxane (6 mL). The mixture was stirred at rt for 20 min (the reaction time was strictly

704   kept short to prevent by-product formation). Saturated NaHCO$_3$ solution (20 mL) was added

705   for neutralisation and the mixture extracted with EtOAc (10 x 20 mL). Combined organic layers

706   were dried over Na$_2$SO$_4$ and concentrated under reduced pressure. Purification of the residue

707   by flash column chromatography (SiO$_2$, DCM:(2N NH$_3$ in MeOH) 9:1) gave 38 mg of a solid

708   (42% yield); ^{1}H NMR (400 MHz, MeOD) δ 8.33 (s, 1H), 7.76 (d, *J* = 8.4 Hz, 1H), 7.56 (s, 1H),

709   7.35 (d, *J* = 8.3 Hz, 1H), 4.54 – 4.45 (m, 1H), 3.26 (s, 3H), 3.13 – 3.07 (m, 1H), 3.02 – 2.95 (m,

710   1H), 2.94 – 2.86 (m, 1H), 2.59 – 2.49 (m, 1H), 2.14 – 1.87 (m, 3H), 1.76 – 1.63 (m, 1H), 0.26

711   (s, 9H); HPLC *method A*: t$_r$ = 7.008 min.

712   3-(3-((7-Ethynyl-9*H*-pyrimido[4,5-*b*]indol-4-yl)(methyl)amino)piperidin-1-yl)propanenitrile

713   (**15**)

714   Acrylonitrile (8.0 mg, 0.15 mmol) and TEA (15.3 mg, 015 mmol) were added to a stirring

715   solution of *N*-methyl-*N*-(piperidin-3-yl)-7-((trimethylsilyl)ethynyl)-9*H*-pyrimido[4,5-*b*]indol-

716   4-amine (**13**) in HPLC grade MeOH (20 mL) and the mixture was stirred at rt and under N$_2$

717   atmosphere. Due to slow conversion, reactands were added repeatedly: acrylonitrile (8.0 mg,

718   0.15 mmol) and TEA (15.3 mg, 015 mmol) after 3 h of stirring and additional acrylonitrile (4.0

719   mg, 0.08 mmol) and TEA (7.7 mg, 0.08 mmol) after 6 h of stirring. After stirring at rt and under

720 N$_2$ atmosphere overnight, K$_2$CO$_3$ (16.7 mg, 0.12 mmol) was added to initiate the TMS

721 deprotection and stirring continued. Additional K$_2$CO$_3$ (10.0 mg, 0.07 mmol) was added and

722 stirring continued for 2 days. The mixture was concentrated under reduced pressure and the

723 residue was purified three times by flash column chromatography (1.SiO$_2$, DCM:MeOH 95:5,

724 2.SiO$_2$, DCM:(2N NH3 in MeOH) gradient elution from 96.5:3.5 to 93:7 and 3.SiO$_2$,

725 DCM:MeOH gradient elution from 96.5:3.5 to 93:7) to yield 15 mg of a light beige solid (41%

726 yield); ^{1}H NMR (400 MHz, DMSO-d_6) δ 12.18 (s, 1H), 8.39 (s, 1H), 7.79 (d, J = 8.4 Hz, 1H),

727 7.54 (d, J = 1.1 Hz, 1H), 7.40 (dd, J = 8.3, 1.4 Hz, 1H), 4.56 − 4.41 (m, 1H), 4.19 (s, 1H), 3.16

728 (s, 3H), 3.13 − 3.06 (m, 1H), 2.94 − 2.84 (m, 1H), 2.80 − 2.59 (m, 4H), 2.47 − 2.35 (m, 1H),

729 2.06 − 1.90 (m, 1H), 1.89 − 1.67 (m, 3H), 1.60 − 1.45 (m, 1H); ^{13}C NMR (101 MHz, DMSO-

730 d_6) δ 159.5, 157.6, 153.9, 136.2, 124.0, 122.7, 120.1, 117.4, 114.3, 97.2, 84.2, 80.4, 55.6, 54.6,

731 53.0, 52.2, 32.7, 27.1, 24.2, 14.9; ESI-MS: (m/z) 359.1 [M+H]$^+$, 381.1 [M+Na]$^+$, 357.0 [M-H]$^-$;

732 HPLC *method A*: t$_r$ = 3.865 min.

733

734 *Detailed procedures for the preparation of final compound (S)-15*

735 *tert*-Butyl (S)-3-((7-iodo-9-tosyl-9*H*-pyrimido[4,5-*b*]indol-4-yl)amino)piperidine-1-

736 carboxylate (*(S)*-7)

737 4-Chloro-7-iodo-9-tosyl-9*H*-pyrimido[4,5-*b*]indole (**6**) (500.0 mg, 1.03 mmol), *(S)*-*N*-Boc-3-

738 aminopiperidine (288.8 mg, 1.45 mmol) and DIPEA (399.3 mg, 3.09 mmol) were stirred in dry

739 DMF (14 mL) at 80°C for 16 h. After cooling down to rt, the mixture was poured into ice-cold

740 water and saturated NH$_4$Cl solution (75 mL) was added. The mixture was extracted twice with

741 EtOAc (175 mL and 25 mL). Combined organic layers were washed with saturated NaCl

742 solution (3 x 30 mL), dried over Na$_2$SO$_4$ and concentrated under reduced pressure. Purification

743 of the residue by flash column chromatography (SiO$_2$, petroleum ether:(EtOAc+MeOH 95+5)

744   2:1) gave 360 mg of a yellow solid (54% yield); ESI-MS: 671.0 [M+Na]⁺, 646.9 [M-H]⁻; HPLC

745   *method A*: t_r = 11.182 min.

746   *tert*-Butyl (*S*)-3-((7-iodo-9*H*-pyrimido[4,5-*b*]indol-4-yl)(methyl)amino)piperidine-1-

747   carboxylate (*(S)*-**9**)

748   The title compound was prepared by a two-step procedure. In the first step a solution of *tert*-

749   butyl   (*S*)-3-((7-iodo-9-tosyl-9*H*-pyrimido[4,5-*b*]indol-4-yl)amino)piperidine-1-carboxylate

750   (*(S)*-**7**) (342.0 mg, 0.53 mmol) in dry DMF (6 mL) was stirred in a flame-dried Schlenk tube

751   under Ar atmosphere and cooled to 0 °C. NaH (31.0 mg of a 60% dispersion in mineral oil,

752   0.752 mmol) was added and the mixture stirred for 30 minutes for deprotonation. The mixture

753   was then cooled by an MeOH/ice bath before iodomethane (112.5 mg, 0.79 mmol) was added.

754   Stirring was continued under Ar atmosphere for 2.5 h leaving the mixture to warm to rt.

755   Saturated NH₄Cl solution (5 mL) was added and the mixture poured into ice-cold water, which

756   was then extracted with EtOAc (3 x 50 mL). Combined organic layers were dried over Na₂SO₄

757   and concentrated under reduced pressure to afford 368 mg of crude (*S*)-3-((7-iodo-9-tosyl-9*H*-

758   pyrimido[4,5-*b*]indol-4-yl)(methyl)amino)piperidine-1-carboxylate (*(S)*-**8**), which was used in

759   the second step without further purification. The crude material was dissolved in dry THF (15

760   mL). K*t*BuO (414.7 mg, 3.70 mmol) was added and the mixture stirred at rt for 2.5 h. Saturated

761   NH₄Cl solution (20 mL) was added and the mixture extracted with EtOAc (3 x 20 mL).

762   Combined organic layers were dried over Na₂SO₄ and concentrated under reduced pressure.

763   Purification of the residue by flash column chromatography (SiO₂, DCM:MeOH gradient

764   elution from 97.5:2.5 to 96.5:3.5) gave 157 mg of a white solid (59% yield); ¹H NMR (400

765   MHz, CDCl₃) δ 11.58 (br s, 1H), 8.55 (s, 1H), 7.89 (s, 1H), 7.59 (dd, *J* = 8.5, 1.3 Hz, 1H), 7.53

766   (d, *J* = 8.5 Hz, 1H), 4.52 – 4.00 (m, 3H), 3.27 (s, 3H), 3.10 – 3.00 (m, 1H), 2.76 – 2.60 (m, 1H),

767   2.10 – 1.77 (m, 3H), 1.71 – 1.56 (m, 1H), 1.43 (s, 9H).; ESI-MS: 508.9 [M+H]⁺, 530.9 [M+Na]⁺,

768   506.9 [M-H]⁻; HPLC *method A*: t_r = 10.246 min.

769   *(S)*-7-Iodo-*N*-methyl-*N*-(piperidin-3-yl)-9*H*-pyrimido[4,5-*b*]indol-4-amine (*(S)*-**10**)

770   *tert*-Butyl (*S*)-3-((7-iodo-9*H*-pyrimido[4,5-*b*]indol-4-yl)(methyl)amino)piperidine-1-

771   carboxylate (*(S)*-**9**) (140.0 mg, 0.28 mmol) was stirred in a mixture of dry DCM (4 mL) and

772   TFA (0.8 mL) at rt for 1 h. The mixture was concentrated under reduced pressure and residual

773   TFA was neutralized by addition of saturated NaHCO$_3$ solution (30 mL). The mixture was then

774   extracted with EtOAc (3 x 25 mL), adding MeOH to improve the solubility of the product in

775   the organic layer. Combined organic layers were washed with saturated NaHCO$_3$ solution (3 x

776   30 mL), dried over Na$_2$SO$_4$ and evaporated to dryness to afford 113 mg of a beige solid (100%

777   yield); ^{1}H NMR (400 MHz, MeOD) δ 8.35 (s, 1H), 7.85 (s, 1H), 7.61 − 7.54 (m, 2H), 4.53 −

778   4.44 (m, 1H), 3.24 (s, 3H), 3.15 − 3.08 (m, 1H), 3.03 − 2.96 (m, 1H), 2.95 − 2.87 (m, 1H), 2.61

779   − 2.50 (m, 1H), 2.13 − 1.86 (m, 3H), 1.76 − 1.63 (m, 1H); ESI-MS: (m/z) 408.5 [M+H]$^+$, 406.5

780   [M-H]$^-$; HPLC *method A*: t$_r$ = 5.134 min.

781   *(S)*-3-(3-((7-Iodo-9*H*-pyrimido[4,5-*b*]indol-4-yl)(methyl)amino)piperidin-1-yl)propanenitrile

782   (*(S)*-**11**)

783   Acrylonitrile (16.6 mg, 0.31 mmol) and triethylamine (26.5 mg, 0.26 mmol) were added to a

784   stirring solution of *(S)*-7-iodo-*N*-methyl-*N*-(piperidin-3-yl)-9*H*-pyrimido[4,5-*b*]indol-4-amine

785   (*(S)*-**10**) (107.0 mg, 0.26 mmol) in HPLC grade MeOH (45 mL). The mixture was stirred at rt

786   for 16 h and then concentrated under reduced pressure. Purification of the residue by flash

787   column chromatography (SiO$_2$, DCM:MeOH gradient elution from 95:5 to 92.5:7.5) gave

788   89 mg of a white solid (74% yield); ^{1}H NMR (400 MHz, DMSO-*d$_6$*) δ 12.15 (s, 1H), 8.40 (s,

789   1H), 7.79 (d, *J* = 1.2 Hz, 1H), 7.62 (dd, *J* = 8.5, 1.5 Hz, 1H), 7.58 (d, *J* = 8.5 Hz, 1H), 4.51 −

790   4.38 (m, 1H), 3.13 (s, 3H), 3.09 − 3.02 (m, 1H), 2.89 − 2.81 (m, 1H), 2.75 − 2.67 (m, 2H), 2.67

791   − 2.58 (m, 2H), 2.41 − 2.32 (m, 1H), 2.00 − 1.88 (m, 1H), 1.81 − 1.65 (m, 3H), 1.56 − 1.42 (m,

792   1H); ^{13}C NMR (101 MHz, DMSO-*d$_6$*) δ 159.5, 156.9, 154.0, 137.9, 129.0, 124.4, 120.1, 119.6,

793   119.2, 97.1, 89.4, 55.7, 54.8, 53.0, 52.2, 32.6, 27.3, 24.3, 15.0.

794   *(S)*-3-(3-(Methyl(7-((trimethylsilyl)ethynyl)-9*H*-pyrimido[4,5-*b*]indol-4-yl)amino)piperidin-

795   1-yl)propanenitrile (*(S)*-14)

796   A   solution   of   *(S)*-3-(3-((7-iodo-9*H*-pyrimido[4,5-*b*]indol-4-yl)(methyl)amino)piperidin-1-

797   yl)propanenitrile (*(S)*-11) (40.0 mg, 0.09 mmol) and CuI (1.65 mg, 0.009 mmol) in dry DMF

798   (1.5 mL) was degassed and stirred in a Schlenk tube under Ar atmosphere. Triethylamine (17.6

799   mg, 0.17 mmol) and trimethylsilylacetylen (25.6 mg, 0.26 mmol) were added under Ar flow,

800   followed by a small amount of bis(triphenylphosphine)palladium(II) dichloride (5 mg, 0.007

801   mmol). The mixture was stirred at rt for 2 h, then diluted with EtOAc and washed with saturated

802   NaHCO$_3$ solution (2 x 10 mL). The organic layer was dried over Na$_2$SO$_4$ and concentrated

803   under reduced pressure. Purification of the residue by flash column chromatography (SiO$_2$,

804   DCM:MeOH 95:5) gave 32 mg of a yellow solid (86% yield); ^{1}H NMR (400 MHz, CDCl$_3$) δ

805   12.49 (br s, 1H), 8.59 (br s, 1H) 7.69 (d, *J* = 8.4 Hz, 1H), 7.63 (s, 1H), 7.40 (dd, *J* = 8.3, 0.8 Hz,

806   1H), 4.71 − 4.58 (m, 1H), 3.27 (s, 3H), 3.19 − 3.12 (m, 1H), 2.98 − 2.91 (m, 1H), 2.85 − 2.74

807   (m, 2H), 2.58 (t, *J* = 7.0 Hz, 2H), 2.50 − 2.41 (m, 1H), 2.15 − 2.07 (m, 1H), 2.03 − 1.94 (m, 1H),

808   1.90 − 1.71 (m, 3H), 0.35 − 0.21 (m, 9H); ^{13}C NMR (101 MHz, CDCl$_3$) δ 160.2, 157.8, 153.0,

809   136.4, 124.9, 122.6, 120.5, 119.5, 118.8, 115.0, 105.8, 98.8, 94.5, 56.1, 55.1, 53.8, 53.1, 33.6,

810   27.9, 24.6, 16.0, 0.2; ESI-MS: (m/z) 431.7 [M+H]$^+$, 453.7 [M+Na]$^+$, 429.7 [M-H]$^-$, HPLC

811   *method A*: t$_r$ = 7.262 min.

812   *(S)*-3-(3-((7-Ethynyl-9*H*-pyrimido[4,5-*b*]indol-4-yl)(methyl)amino)piperidin-1-

813   yl)propanenitrile (*(S)*-15)

814   *(S)*-3-(3-(methyl(7-((trimethylsilyl)ethynyl)-9*H*-pyrimido[4,5-*b*]indol-4-yl)amino)piperidin-1-

815   yl)propanenitrile (*(S)*-14) (32.0 mg, 0.07 mmol) and K$_2$CO$_3$ (12.0 mg, 0.09 mmol) were stirred

816   in HPLC grade MeOH (4 mL) at rt and under N$_2$ atmosphere for 3 h. The mixture was

817   concentrated under reduced pressure and the residue redissolved in EtOAc. The solution was

818   washed with saturated NaHCO$_3$ solution (2 x 15 mL), dried over Na$_2$SO$_4$ and concentrated

819 under reduced pressure. Purification of the residue by flash column chromatography (SiO$_2$,

820 DCM:MeOH 95:5) gave 18 mg of a white solid (68% yield); ^{1}H NMR (400 MHz, DMSO-d_6)

821 δ 12.18 (s, 1H), 8.39 (s, 1H), 7.79 (d, J = 8.4 Hz, 1H), 7.54 (s, 1H), 7.40 (dd, J = 8.3, 1.1 Hz,

822 1H), 4.53 − 4.43 (m, 1H), 4.19 (s, 1H), 3.16 (s, 3H), 3.11 − 3.04 (m, 1H), 2.90 − 2.83 (m, 1H),

823 2.76 − 2.68 (m, 2H), 2.67 − 2.58 (m, 2H), 2.43 − 2.33 (m, 1H), 2.01 − 1.90 (m, 1H), 1.83 − 1.66

824 (m, 3H), 1.60 − 1.43 (m, 1H); ^{13}C NMR (101 MHz, DMSO-d_6) δ 159.5, 157.6, 153.8, 136.2,

825 124.0, 122.6, 120.0, 119.9, 117.3, 114.2, 97.2, 84.1, 80.2, 55.6, 54.7, 53.0, 52.2, 32.6, 27.2,

826 24.3, 15.0; ESI-MS: (m/z) 359.9 [M+H]$^+$, 381.9 [M+Na]$^+$, 357.8 [M-H]$^-$; HPLC *method A*: t$_r$ =

827 3.237 min.

828

829 *Detailed procedures for the preparation of final compounds* **5k-m**

830 3-(3-(Methyl(7-phenyl-9H-pyrimido[4,5-b]indol-4-yl)amino)piperidin-1-yl)propanenitrile

831 **(5k)**

832 Degassed dry dioxane (4 mL) and degassed 0.5M aq. K$_3$PO$_4$ solution (1 mL) were added to 3-

833 (3-((7-chloro-9H-pyrimido[4,5-b]indol-4-yl)(methyl)amino)piperidin-1-yl)propanenitrile **(1)**

834 (60.0 mg, 0.16 mmol), phenylboronic acid (31.7 mg, 0.26 mmol) and XPhos Pd G3 (4.1 mg,

835 0.005 mmol) under Ar atmosphere. The mixture was stirred at 100°C for 3 h. After cooling

836 down to rt, saturated NaCl solution (3 mL) was added and the mixture extracted with EtOAc (5

837 x 3 mL). DCM and MeOH were added to improve the solubility of the product in the organic

838 layer. Combined organic layers washed with saturated NaHCO$_3$ solution (3 x 20 mL), dried

839 over Na$_2$SO$_4$ and concentrated under reduced pressure. Purification of the residue by flash

840 column chromatography (SiO$_2$, DCM:MeOH gradient elution from 95:5 to 92.5:7.5) gave 40

841 mg of an off-white solid (60% yield); ^{1}H NMR (300 MHz, DMSO-d_6) δ 12.18 (s,

842 1H), 7.88 (d, J = 8.5 Hz, 1H), 7.78 − 7.68 (m, 3H), 7.64 (dd, J = 8.4, 1.5 Hz, 1H), 7.54 − 7.45

843 (m, 2H), 7.42 – 7.34 (m, 1H), 4.60 – 4.46 (m, 1H), 3.17 (s, 3H), 3.13 – 3.05 (m, 1H), 2.93 –

844 2.83 (m, 1H), 2.77 – 2.58 (m, 4H), 2.46 – 2.34 (m, 1H), 2.03 – 1.89 (m, 1H), 1.86 – 1.66 (m,

845 3H), 1.63 – 1.42 (m, 1H); ^{13}C NMR (101 MHz, DMSO-d_6) δ 159.4, 157.4, 153.4, 140.4, 137.3,

846 136.8, 129.0, 127.2, 126.7, 122.9, 120.0, 119.6, 118.9, 108.9, 97.4, 55.7, 54.7, 53.0, 52.2, 32.5,

847 27.3, 24.3, 15.0; ESI-MS: (m/z) 411.1 [M+H]$^+$, 433.1 [M+Na]$^+$, 409.2 [M-H]$^-$; HPLC *method*

848 *A*: t$_r$ = 5.034 min.

849 3-(3-((7-(Furan-2-yl)-9*H*-pyrimido[4,5-*b*]indol-4-yl)(methyl)amino)piperidin-1-

850 yl)propanenitrile (**5l**)

851 Degassed dry dioxane (4 mL) and degassed 0.5M aq. K$_3$PO$_4$ solution (1 mL) were added to 3-

852 (3-((7-chloro-9*H*-pyrimido[4,5-*b*]indol-4-yl)(methyl)amino)piperidin-1-yl)propanenitrile (**1**)

853 (60.0 mg, 0.16 mmol), 2-furanylboronic acid (29.1 mg, 0.26 mmol) and XPhos Pd G3 (4.1 mg,

854 0.005 mmol) in a reaction tube. The tube was sealed and the mixture stirred at 100°C for 3 h.

855 After cooling down to rt, saturated NaCl solution (3 mL) was added and the mixture extracted

856 with EtOAc (5 x 3 mL). DCM and MeOH were added to improve the solubility of the product

857 in the organic layer. Combined organic layers washed with saturated NaHCO$_3$ solution. The

858 combined NaHCO$_3$ solution layers were extracted once more with DCM. The organic layers

859 were unified, dried over Na$_2$SO$_4$ and concentrated under reduced pressure. Purification of the

860 residue by flash column chromatography (SiO$_2$, DCM:MeOH gradient elution from 96:4 to

861 93:7) gave 43 mg of a beige solid (66% yield); ^{1}H NMR (400 MHz, DMSO-d_6) δ 12.17 (s, 1H),

862 8.39 (s, 1H), 7.82 (d, *J* = 8.5 Hz, 1H), 7.79 – 7.72 (m, 2H), 7.68 (dd, *J* = 8.4, 1.1 Hz, 1H), 6.96

863 (d, *J* = 3.2 Hz, 1H), 6.62 (dd, *J* = 3.2, 1.7 Hz, 1H), 4.56 – 4.43 (m, 1H), 3.16 (s, 3H), 3.11 –

864 3.02 (m, 1H), 2.92 – 2.82 (m, 1H), 2.78 – 2.58 (m, 4H), 2.45 – 2.34 (m, 1H), 2.03 – 1.90 (m,

865 1H), 1.86 – 1.68 (m, 3H), 1.60 – 1.45 (m, 1H); ^{13}C NMR (101 MHz, DMSO-d_6) δ 159.3, 157.5,

866 153.5, 153.4, 142.8, 137.0, 126.9, 122.9, 120.0, 118.8, 116.7, 112.1, 105.6, 105.5, 97.5, 55.6,

867   54.7, 53.0, 52.1, 32.5, 27.2, 24.3, 14.9; ESI-MS: (m/z) 401.1 [M+H]$^+$, 423.1 [M+Na]$^+$, 399.1

868   [M-H]$^-$; HPLC *method A*: t$_r$ = 4.069 min.

869   4-((1-(2-Cyanoethyl)piperidin-3-yl)(methyl)amino)-9*H*-pyrimido[4,5-*b*]indole-7-carbonitrile

870   (**5m**)

871   Degassed dry 1,4-dioxane (2 mL) and degassed 0.01M aq. KOAc solution (2 mL) were added

872   to 3-(3-((7-chloro-9*H*-pyrimido[4,5-*b*]indol-4-yl)(methyl)amino)piperidin-1-yl)propanenitrile

873   (**1**) (60.0 mg, 0.16 mmol), K$_4$[Fe(CN)$_6$]·3H$_2$O (41.2 mg, 0.10 mmol), BrettPhos Pd G3 (5.2 mg,

874   0.006 mmol) and BrettPhos (3.1 mg, 0.006 mmol) under Ar atmosphere. The mixture was

875   stirred at 100°C and under Ar atmosphere for 2.5 h. Additional BrettPhos Pd G3 and BrettPhos

876   catalysts were added (1.0 mg each) to promote conversion and stirring continued at 10 0°C for

877   2 h, but the conversion seized at 85%. After cooling down to rt, saturated NaCl solution (3

878   mL) was added and the mixture extracted with EtOAc (6 x 3 mL). Combined organic layers

879   were dried over Na$_2$SO$_4$ and concentrated under reduced pressure. Purification of the residue

880   twice by flash column chromatography (1.SiO$_2$, petroleum ether:(EtOAc+MeOH 95+5)

881   gradient elution from 1:1 to 0:1 and 2.SiO$_2$, DCM:MeOH gradient elution from 95.5:4.5 to

882   93.5:6.5) gave 15 mg of an off-white solid (26% yield); ^{1}H NMR (400 MHz, DMSO-d_6) δ 12.50

883   (s, 1H), 8.44 (s, 1H), 7.95 (d, *J* = 8.4 Hz, 1H), 7.88 (s, 1H), 7.67 (dd, *J* = 8.4, 1.2 Hz, 1H), 4.58

884   − 4.41 (m, 1H), 3.19 (s, 3H), 3.14 − 3.06 (m, 1H), 2.96 − 2.82 (m, 1H), 2.79 − 2.56 (m, 4H),

885   2.47 − 2.31 (m, 1H), 2.06 − 1.89 (m, 1H), 1.87 − 1.65 (m, 3H), 1.61 − 1.47 (m, 1H); ^{13}C NMR

886   (101 MHz, DMSO-d_6) δ 159.8, 158.2, 154.7, 135.8, 123.5, 123.4, 123.3, 119.6, 114.9, 105.9,

887   96.8, 55.4, 54.8, 52.9, 52.1, 32.9, 27.0, 24.2, 15.0; ESI-MS: (m/z) 360.1 [M+H]$^+$, 382.1

888   [M+Na]$^+$, 358.1 [M-H]$^-$; HPLC *method A*: t$_r$ = 3.062 min.

889   *Detailed procedures for the preparation of intermediates* **16-18**

890   3-(1-(7-Fluoro-9-tosyl-9*H*-pyrimido[4,5-*b*]indol-4-yl)octahydro-6*H*-pyrrolo[2,3-*c*]pyridin-6-

891   yl)propanenitrile (**16**)

892   4-Chloro-7-fluoro-9-tosyl-9*H*-pyrimido[4,5-*b*]indole (**3b**) (200.0 mg, 0.53 mmol), 3-

893   (octahydro-6*H*-pyrrolo[2,3-*c*]pyridin-6-yl)propanenitrile (used as TFA salt and calculated to

894   37.2 mg of the free base, 0.21 mmol,) and DIPEA (275.3 mg, 2.13 mmol) were stirred in dry

895   DMF (6 mL) at 70 °C for 2.5 h. Additional 3-(octahydro-6*H*-pyrrolo[2,3-*c*]pyridin-6-

896   yl)propanenitrile (used as TFA salt and calculated to 71.0 mg of the free base, 0.40 mmol) and

897   DIPEA (137.7 mg, 1.07 mmol) were added and stirring at 70 °C continued for 5 h. After cooling

898   down to rt, saturated NaCl solution (15 mL) was added and the mixture extracted with EtOAc

899   (3 x 25 mL). Combined organic layers were washed with saturated NaCl solution (3 x 25 mL),

900   dried over Na_2SO_4 and concentrated under reduced pressure. Purification of the residue by flash

901   column chromatography (SiO_2, petroleum ether:(EtOAc+MeOH 95+5) gradient elution from

902   2:1 to 1:3) gave 113 mg of a solid (41% yield); ^{1}H NMR (400 MHz, $CDCl_3$) δ 8.51 (s, 1H),

903   8.22 (d, J = 9.8 Hz, 1H), 8.10 (d, J = 8.4 Hz, 2H), 7.82 (br s, 1H), 7.26 (d, J = 8.2 Hz, 2H,

904   overlap with $CHCl_3$ signal), 7.14 (td, J = 8.7, 2.0 Hz, 1H), 4.67 – 4.50 (m, 1H), 4.28 – 4.08 (m,

905   1H), 3.50 – 3.41 (m, 1H), 3.19 – 2.98 (m, 1H), 2.91 – 2.53 (m, 4H), 2.52 – 2.13 (m, 7H), 1.99

906   – 1.81 (m, 3H), 1.69 – 1.56 (m, 1H); ESI-MS: (m/z) 519.5 [M+H]$^+$, 541.5 [M+Na]$^+$, 517.6 [M-

907   H]$^-$; HPLC *method A*: t_r = 6.594 min.

908   3-(1-(7-Bromo-9-tosyl-9*H*-pyrimido[4,5-*b*]indol-4-yl)octahydro-6*H*-pyrrolo[2,3-*c*]pyridin-6-

909   yl)propanenitrile (**17**)

910   7-Bromo-4-chloro-9-tosyl-9*H*-pyrimido[4,5-*b*]indole (**3d**) (92.0 mg, 0.21 mmol), 3-

911   (octahydro-6*H*-pyrrolo[2,3-*c*]pyridin-6-yl)propanenitrile (41.5 mg of the free base, 0.23 mmol)

912   and DIPEA (81.7 mg, 0.63 mmol) were stirred in dry DMF (2.5 mL) at 75 °C for 1.5 h.

913   Additional 3-(octahydro-6*H*-pyrrolo[2,3-*c*]pyridin-6-yl)propanenitrile (10.0 mg of the free

914   base, 0.06 mmol) was added and stirring at 75 °C continued for 3 h. Saturated NaCl solution

915   (10 mL) was added and the mixture extracted with EtOAc (3 x 20 mL). Combined organic

916   layers were washed with saturated NaCl solution (3 x 20 mL), dried over Na_2SO_4 and

917   concentrated under reduced pressure. Purification of the residue by flash column

918   chromatography (SiO$_2$, petroleum ether:(EtOAc + MeOH 95+5) gradient elution from 2:1 to

919   1:3) gave 66 mg of an off-white solid (54% yield); ESI-MS: 579.7 [M+H]$^+$, 601.7 [M+Na]$^+$;

920   HPLC *method A*: t$_r$ = 7.363 min.

921   3-(1-(7-Iodo-9-tosyl-9*H*-pyrimido[4,5-*b*]indol-4-yl)octahydro-6*H*-pyrrolo[2,3-*c*]pyridin-6-

922   yl)propanenitrile (**18**)

923   4-Chloro-7-iodo-9-tosyl-9*H*-pyrimido[4,5-*b*]indole (**6**) (200.0 mg, 0.41 mmol), 3-(octahydro-

924   6*H*-pyrrolo[2,3-*c*]pyridin-6-yl)propanenitrile (used as TFA salt and calculated to 83.8 mg of

925   the free base, 0.47 mmol) and DIPEA (213.7 mg, 1.65 mmol) were stirred in dry DMF (6 mL)

926   at 75 °C for 2.5 h. After cooling down to rt, saturated NaCl solution (15 mL) was added and the

927   mixture extracted with EtOAc (3 x 25 mL). Combined organic layers were washed with

928   saturated NaCl solution (3 x 20 mL), dried over Na_2SO_4 and concentrated under reduced

929   pressure. Purification of the residue by flash column chromatography (SiO$_2$, petroleum

930   ether:(EtOAc+MeOH 95+5) gradient elution from 2:1 to 1:3) gave 158 mg of a solid (61%

931   yield); ^{1}H NMR (400 MHz, CDCl$_3$) δ 8.84 (s, 1H), 8.53 (s, 1H), 8.09 (d, *J* = 8.4 Hz, 2H), 7.69

932   (d, 1H), 7.66 − 7.51 (br s, 1H), 7.27 (d, *J* = 7.3 Hz, 2H, overlap with CHCl$_3$ signal), 4.62 − 4.45

933   (m, 1H), 4.29 − 4.02 (m, 1H), 3.49 − 3.41 (m, 1H), 3.21 − 3.00 (m, 1H), 2.81 − 2.48 (m, 4H),

934   2.47 − 2.23 (m, 7H), 1.95 − 1.80 (m, 3H), 1.72 − 1.61 (m, 1H); ESI-MS: (m/z) 627.2 [M+H]$^+$,

935   649.2 [M+Na]$^+$, 625.0 [M-H]$^-$; HPLC *method A*: t$_r$ = 7.423 min.

936

937   *Detailed procedures for the preparation of final compounds* **19-22**

938 3-(1-(7-Fluoro-9*H*-pyrimido[4,5-*b*]indol-4-yl)octahydro-6*H*-pyrrolo[2,3-*c*]pyridin-6-

939 yl)propanenitrile (**19**)

940 The title compound was prepared from 3-(1-(7-fluoro-9-tosyl-9*H*-pyrimido[4,5-*b*]indol-4-

941 yl)octahydro-6*H*-pyrrolo[2,3-*c*]pyridin-6-yl)propanenitrile (**16**) (100.0 mg, 0.19 mmol) and

942 K*t*BuO (151.4 mg, 1.35 mmol) were stirred in HPLC grade THF (10 mL) at rt for 1.5 h.

943 Saturated NaCl solution (10 mL) was added and the mixture extracted with EtOAc (4 x 25 mL).

944 Combined organic layers were dried over Na_2SO_4 and concentrated under reduced pressure.

945 Purification of the residue by flash column chromatography (SiO_2, DCM:MeOH gradient

946 elution from 95:5 to 91.5:8.5) gave 43 mg of a solid (61% yield); ^{1}H NMR (400 MHz, DMSO-

947 *d₆*) δ 12.12 (s, 1H), 8.28 (s, 1H), 8.04 (dd, *J* = 9.0, 5.3 Hz, 1H), 7.19 (dd, *J* = 9.3, 2.6 Hz, 1H),

948 7.05 (td, *J* = 9.3, 2.6 Hz, 1H), 4.66 – 4.58 (m, 1H), 4.21 – 4.11 (m, 1H), 3.86 – 3.77 (m, 1H),

949 2.94 – 2.84 (m, 1H), 2.67 – 2.46 (m, 6H, overlap with DMSO-*d₅* signal), 2.44 – 2.32 (m, 2H),

950 2.03 – 1.82 (m, 3H), 1.77 – 1.68 (m, 1H); ^{13}C NMR (101 MHz, DMSO-*d₆*) δ 159.9 (d, *J* = 239.5

951 Hz), 157.1, 156.4, 153.3, 137.3 (d, *J* = 12.5 Hz), 123.8 (d, *J* = 9.8 Hz), 119.9, 116.3, 107.9 (d,

952 *J* = 23.2 Hz), 97.5 (d, *J* = 25.8 Hz), 96.2, 56.5, 53.2, 52.9, 49.1, 48.5, 34.1, 26.7, 25.5, 14.8;

953 ESI-MS: (m/z) 387.0 [M+Na]$^+$, 363.0 [M-H]$^-$; HPLC *method A*: t$_r$ = 3.053 min.

954 3-(1-(7-Bromo-9*H*-pyrimido[4,5-*b*]indol-4-yl)octahydro-6*H*-pyrrolo[2,3-*c*]pyridin-6-

955 yl)propanenitrile (**20**)

956 The title compound was prepared from 3-(1-(7-bromo-9-tosyl-9*H*-pyrimido[4,5-*b*]indol-4-

957 yl)octahydro-6*H*-pyrrolo[2,3-*c*]pyridin-6-yl)propanenitrile (**17**) (66.0 mg, 0.11 mmol) and

958 K*t*BuO (89.5 mg, 0.80 mmol) were stirred in HPLC grade THF (4 mL) for 2 h. Saturated NH₄Cl

959 solution (25 mL) was added and the mixture was extracted with EtOAc (3 x 25 mL). Combined

960 organic layers were dried over Na_2SO_4 and concentrated under reduced pressure. Purification

961 of the residue by flash column chromatography (SiO_2, DCM:MeOH 95.5:4.5) gave 19 mg of a

962 beige solid (40% yield); ^{1}H NMR (400 MHz, DMSO-*d₆*) δ 12.13 (s, 1H), 8.30 (s, 1H), 7.99 (d,

J = 8.8 Hz, 1H), 7.57 (d, J = 2.0 Hz, 1H), 7.35 (dd, J = 8.7, 2.0 Hz, 1H), 4.68 − 4.58 (m, 1H),

4.21 − 4.10 (m, 1H), 3.89 − 3.77 (m, 1H), 2.96 − 2.86 (m, 1H), 2.66 − 2.48 (m, 6H, overlap with

DMSO-d_5 signal), 2.44 − 2.33 (m, 2H), 2.07 − 1.84 (m, 3H), 1.77 − 1.69 (m, 1H); ^{13}C NMR

(101 MHz, DMSO-d_6) δ 156.8, 156.6, 154.0, 137.6, 124.2, 123.0, 120.0, 118.9, 116.8, 113.6,

96.0, 56.7, 53.2, 52.9, 49.1, 48.5, 34.1, 26.7, 25.5, 14.9. ESI-MS: (m/z) 425.5 [M+H]$^+$, 447.5

[M+Na]$^+$, 423.4 [M-H]$^-$; HPLC *method A*: t_r = 3.996 min.

3-(1-(7-Iodo-9H-pyrimido[4,5-b]indol-4-yl)octahydro-6H-pyrrolo[2,3-c]pyridin-6-

yl)propanenitrile (**21**)

3-(1-(7-Iodo-9-tosyl-9H-pyrimido[4,5-b]indol-4-yl)octahydro-6H-pyrrolo[2,3-c]pyridin-6-

yl)propanenitrile (**18**) (100.0 mg, 0.16 mmol) and KtBuO (125.4 mg, 1.11 mmol) were stirred

in HPLC grade THF (10 mL) at rt for 2 h. Saturated NaCl solution (10 mL) was added and the

mixture extracted with EtOAc (4 x 20 mL). Combined organic layers were dried over Na$_2$SO$_4$

and concentrated under reduced pressure. Purification of the residue by flash column

chromatography (SiO$_2$, DCM:MeOH gradient elution from 95:5 to 91.5:8.5) gave 47 mg of a

light beige solid (62% yield); ^{1}H NMR (400 MHz, DMSO-d_6) δ 12.07 (s, 1H), 8.30 (s, 1H),

7.86 (d, J = 8.7 Hz, 1H), 7.74 (d, J = 1.4 Hz, 1H), 7.51 (dd, J = 8.6, 1.4 Hz, 1H), 4.66 − 4.58

(m, 1H), 4.20 − 4.10 (m, 1H), 3.87 − 3.77 (m, 1H), 2.95 − 2.86 (m, 1H), 2.68 − 2.47 (m, 6H,

overlap with DMSO-d_5 signal), 2.43 − 2.33 (m, 2H), 2.06 − 1.83 (m, 3H), 1.78 − 1.69 (m, 1H).

ESI-MS: (m/z) 473.2 [M+H]$^+$, 495.1 [M+Na]$^+$, 471.1 [M-H]$^-$; HPLC *method A*: t_r = 4.747 min.

3-(1-(7-Ethynyl-9H-pyrimido[4,5-b]indol-4-yl)octahydro-6H-pyrrolo[2,3-c]pyridin-6-

yl)propanenitrile (**22**)

A solution of 3-(1-(7-iodo-9H-pyrimido[4,5-b]indol-4-yl)octahydro-6H-pyrrolo[2,3-c]pyridin-

6-yl)propanenitrile (**21**) (22.0 mg, 0.05 mmol), triethylamine (11.9 mg, 0.12 mmol) and CuI

(0.89 mg, 0.005 mmol) in dry DMF (1.5 mL) was degassed and stirred in a Schlenk tube under

987   Ar atmosphere. More triethylamine (11.9 mg, 0.12 mmol) and trimethylsilylacetylen (13.8 mg,

988   0.14 mmol) were added under Ar flow, followed by a small amount of

989   bis(triphenylphosphine)palladium(II) dichloride (< 5 mg). The mixture was stirred at rt and

990   under Ar atmosphere for 2 h, then diluted with EtOAc (40 mL) and washed with saturated

991   NaHCO$_3$ solution (2 x 10 mL). The combined aqueous layers were re-extracted with EtOAc

992   (25 mL). The combined organic layers were dried over Na$_2$SO$_4$ and concentrated under reduced

993   pressure. Residual DMF was removed under oil pump vacuum. The brown oily residue was

994   mixed with HPLC MeOH (5 mL) and K$_2$CO$_3$ (7.8 mg, 0.06 mmol) was added. The mixture was

995   stirred at rt and under N$_2$ atmosphere for 3 h and then concentrated under reduced pressure. The

996   residue was dissolved in EtOAc (40 mL) and the solution was washed with saturated NaHCO$_3$

997   solution (2 x 15 mL), then dried over Na$_2$SO$_4$ and concentrated under reduced pressure.

998   Purification of the residue by flash column chromatography (SiO$_2$, DCM:MeOH gradient

999   elution from 95:5 to 92.5:7.5) gave 7 mg of a beige solid (41% yield); ^{1}H NMR (400 MHz,

1000   DMSO-d_6) δ 12.10 (s, 1H), 8.30 (s, 1H), 8.06 (d, J = 8.5 Hz, 1H), 7.50 (d, J = 1.5 Hz, 1H), 7.32

1001   (dd, J = 8.5, 1.5 Hz, 1H), 4.70 − 4.62 (m, 1H), 4.23 − 4.14 (m, 2H), 3.90 − 3.81 (m, 1H), 2.96

1002   − 2.88 (m, 1H), 2.67 − 2.51 (m, 6H, overlap with DMSO-d_5 signal), 2.46 − 2.36 (m, 2H), 2.08

1003   − 1.98 (m, 1H), 1.96 − 1.85 (m, 2H), 1.79 − 1.70 (m, 1H); ^{13}C NMR (101 MHz, DMSO-d_6) δ

1004   157.1, 156.7, 154.1, 136.2, 123.8, 122.7, 120.1, 120.4, 117.0, 114.3, 96.2, 84.2, 80.3, 56.7, 53.2,

1005   52.9, 49.2, 48.5, 34.2, 26.7, 25.5, 14.9; ESI-MS: (m/z) 393.8 [M+Na]$^+$; HPLC *method A*: t$_r$ =

1006   3.014 min.

1007   **Protein expression and purification**

1008   GSK-3β was expressed using a construct (pNIC-CH vector) containing residues 26-383

1009   followed by a C-terminal hexahistidine tag. The construct was transformed into BL21(D3)-R3-

1010   pRARE2 and the colonies were inoculated into 2X LB media containing 50 µg mL^{-1} kanamycin

1011   and 34 µg/mL chloramphenicol and cultured overnight at 37 °C. 10-12 mL of the overnight

1012   culture were inoculated in 1 L of TB media containing 50 µg/mL kanamycin and cultures were

1013   grown at 37 °C with shaking until OD600 of 1.5-1.8 was reached. After the temperature was

1014   reduced to 18 °C, IPTG was added at a final concentration of 0.5 mM to the cultures and left

1015   overnight. The cells were harvested on the next day by centrifugation at 5000 rpm for 10

1016   minutes and the pellet was collected for the purification steps.

1017   The pellet was resuspended in Lysis buffer containing 50 mM HEPES pH 7.5, 500 mM NaCl,

1018   30 mM imidazole, 5% glycerol and 0.5 mM TCEP. Protease inhibitor cocktail from Sigma was

1019   added to a dilution of 1:5000. The resuspended cells were lysed by sonication and cleared of

1020   DNA by addition of 0.15% polyethylenimine followed by centrifugation at 23000 rpm for 30

1021   minutes. The supernatant was added into a gravity column containing 5 mL of 50% Ni-NTA

1022   slurry (Qiagen) previously equilibrated with 40 mL of lysis buffer. Subsequently, 100 mL of

1023   lysis buffer was used for washing the column and GSK-3β was eluted with lysis buffer

1024   containing 50 mM, 100 mM, 200 mM and 300 mM imidazole. The eluted fractions containing

1025   the protein were pulled together and concentrated using a 10 kDa cutoff ultrafiltration unit until

1026   5 mL and further purified by fractionation on a size exclusion chromatography (SEC) using

1027   column Hiload 16/600 Superdex 200 pre-equilibrated with SEC buffer containing 25 mM

1028   HEPES pH 7.5, 200mM NaCl, 5% glycerol and 0.5 mM TCEP. The purified protein was

1029   concentrated to 12 mg/mL and snap frozen into liquid nitrogen. Protein identity was confirmed

1030   by electrospray ionization mass spectrometry (expected 41550.9 Da, observed 41552.0 Da).

Crystallization and structure determination

1032   The inhibitors were added at a final concentration of 1 mM to 10 mg/mL of protein (diluted

1033   from 12 mg/mL stock using SEC buffer) incubated for minimum 1 h at 4 °C. The mixture

1034   protein:inhibitor was centrifuged to separate any insoluble material and crystals were obtained

1035   by sitting drop vapor diffusion method at 20 °C using 12% PEG 8000, 1 mM $MgCl_2$, 0.5M

1036   NaCl and 0.1M Tris pH 8.0 into a 300 nl drop mixing protein and precipitant at 2:1 volume

1037 ratio. The crystals were cryoprotected with a solution of precipitant and 20% ethylene glycol

1038 and flash cooled to 100 K and diffraction data were collected at Swiss Light Source station PXI-

1039 X06SA. The data were processed with XDS package[47] and AIMLESS[48] and solved by

1040 molecular replacement using the program PHASER[49] implemented in the CCP4 suite[50] and the

1041 structure of GSK-3β (PDB ID 6GN1) as searching model.[51] The asymmetric unit contained one

1042 molecule and the electron density on the ATP binding site was clearly detected. The structure

1043 was further refined upon insertion of water molecules and the ligand using REFMAC5[52],

1044 PHENIX[53] COOT[54] and MOLPROBITY[55] was used for model validation. Data collection and

1045 refinement statistics are summarized in Table 4.

1046 **Table 4.** Data collection and refinement statistics.

GSK-3β and compound *(S)*-5c (PDB 7B6F)	
Data Collection	
Resolution range (Å) [a]	42.41-2.05 (2.11 - 2.05)
Space group	I 1 2 1
Cell dimensions a, b, c (Å), α, β, γ (°C)	57.7, 63.1, 132.2, 90.0, 97.4, 90.0
No. unique observations [a]	28973 (2204)
Completeness (%) [a]	97.7 (96.8)
Mean ($(I)/\sigma(I)$) [a]	11.1 (2.2)
R_{pim} [a]	0.036 (0.373)
Mean CC (1/2) [a]	0.998 (0.713)
Multiplicity [a]	2.7 (2.5)
Refinement	
No. atoms in refinement	2928
average B factor (Å^2)	43.0
R_{work} (%)	17.4
R_{free} (%)	20.9
r.m.s deviation from ideal bond length (Å)	0.86
r.m.s deviation from ideal bond angle (°)	0.008
Molprobity Ramachandran	
Favoured (%)	97
Outliers (%)	0

1047 [a] Values within parentheses refer to the highest-resolution shell.

1048

1049

1
2
3
4
5
6
7
8
9
10
11
12
13
14
15
16
17
18
19
20
21
22
23
24
25
26
27
28
29
30
31
32
33
34
35
36
37
38
39
40
41
42
43
44
45
46
47
48
49
50
51
52
53
54
55
56
57
58
59
60

1050   **Molecular Modeling**

1051   All modeling was conducted with Maestro version 2020-2 (Schrödinger LLC, New York, NY,

1052   2020) using OPLS3e force field,[56] unless otherwise stated.

1053   For WaterMap [20-21] calculations, the crystal structure was first prepared with Protein

1054   Preparation Wizard,[57] where *e.g.* hydrogen bonds were optimized and the structure was energy

1055   minimized (RMSD restrain of 0.3 Å was applied for heavy atoms convergence). For

1056   calculations with *(S)*-**15** and *(S)*-**5m**, the co-crystallized ligand *(S)*-**5** was first replaced with the

1057   aligned ligands that were prepared with LigPrep (Schrödinger LLC) and then the obtained

1058   protein–ligand structure was prepared with the Protein Preparation Wizard (as above). Waters

1059   within 10 Å of the retained ligand were included in the WaterMap analysis. Existing crystal

1060   structure waters were treated as regular solvent and simulation time of 2.0 ns was used. The

1061   WaterMap analysis for the MD derived structures were run with the same settings, and the

1062   protein-ligand complexes were taken from final frames (at 1000 ns) of five MD simulation

1063   replicas, where ions and water (except water within 4 Å from the ligand) were deleted before

1064   the system preparation with the Protein Preparation Wizard.

1065   QM calculation were conducted with Jaguar.[58] Geometry optimization was done for the aligned

1066   ligands, which were prepared with the LigPrep, using B3LYP-D3 theory with 6-31G** basis

1067   set in gas-phase (except LACVP** for *(S)*-**11** with iodine). Atomic electrostatic potential (ESP)

1068   charges were calculated for the optimized geometries using 6-31G**++ using the PBF water as

1069   solvent model.

1070   MD simulations we run in NPT ensemble (310 K; 1.01325 bar) using Desmond engine.[59]

1071   Simulation settings were as described earlier.[60] Protein Preparation Wizard prepared GSK-3β–

1072   *(S)*-**15** complexes were solvated in a cubic box (min. distance of 15 Å from the protein to the

1073   box edges) including K^+ and Cl^- ions in 0.15 M concentration with a neutral net charge for the

1074   final system. The water was described with TIP3P model.[61] Final systems consisted of 76,109

1075   atoms. Ten replica simulations were run using a different seed for each simulation. A default

1076   Desmond relaxation protocol was applied before the 1000 ns production simulations. Water

1077   distances and locations were analysed with trajectory_asl_monitor.py script (Schrödinger

1078   LLC).

1079   Maestro and PyMOL Molecular Graphics System (Version 2.2.3 Schrödinger, LLC) were used

1080   for visualization.

1081

ASSOCIATED CONTENTS

Supporting Information

1084   ADP Glo™ kinase assay protocol, Figures S1-S6, nanoBRET™ target engagement assay

1085   protocol and results, materials and methods for cellular assays in neuronal SH-SY5Y cells,

1086   kinome screening data (PDF).

1087   SMILES strings of tested compounds (CSV).

1088   This material is available free of charge via the Internet at http://pubs.acs.org.

1089   The raw concatenated trajectories of the MD simulations of compounds (*S*)-5c and (*S*)-15 are

1090   freely available at https://doi.org/10.5281/zenodo.4314272.

1091

Acknowledgments

1110

Abbreviations

1112   BRET, bioluminescence resonance energy transfer; GSK-3β, glycogen synthase kinase-3β;

1113   HPLC, high-performance liquid chromatography; HR-I, hydrophobic region I; MS, mass

1114   spectrometry; MD, molecular dynamics; S_NAr, nucleophilic aromatic substitution.

1115

1116

1117

1118

1119   **AUTHOR INFORMATION**

1120   **Corresponding Author**

1121   *Corresponding author: pierre.koch@uni-tuebingen.de, pierre.koch@ur.de; Tel.: +49 941 943

1122   4827

1123   Notes

1124   The authors declare no competing financial interest.

1125

1126   **References**

1127   1.   Taylor, S. S.; Meharena, H. S.; Kornev, A. P., Evolution of a dynamic molecular switch.

1128   *IUBMB Life* **2019**, *71*, 672-684.

1129   2.   Ferguson, F. M.; Gray, N. S., Kinase inhibitors: the road ahead. *Nature Reviews Drug*

1130   *Discovery* **2018**, *17*, 353-377.

1131   3.   Shih, H.-P.; Zhang, X.; Aronov, A. M., Drug discovery effectiveness from the

1132   standpoint of therapeutic mechanisms and indications. *Nature Reviews Drug Discovery* **2018**,

1133   *17*, 19-33.

1134   4.   Patel, P.; Woodgett, J. R., Chapter Eight - Glycogen Synthase Kinase 3: A Kinase for

1135   All Pathways? *Current Topics in Developmental Biology* **2017**, *123*, 277-302.

1136   5.   Phukan, S.; Babu, V.; Kannoji, A.; Hariharan, R.; Balaji, V., GSK3β: role in therapeutic

1137   landscape and development of modulators. *British Journal of Pharmacology* **2010**, *160*, 1-19.

1138   6.   Lauretti, E.; Dincer, O.; Praticò, D., Glycogen synthase kinase-3 signaling in

1139   Alzheimer's disease. *Biochimica et Biophysica Acta (BBA) - Molecular Cell Research* **2020**,

1140   *1867*, 118664.

1141   7.   Ding, L.; Billadeau, D. D., Glycogen synthase kinase-3β: a novel therapeutic target for

1142   pancreatic cancer. *Expert Opinion on Therapeutic Targets* **2020**, *24*, 417-426.

1143   8.   Andreev, S.; Pantsar, T.; Ansideri, F.; Kudolo, M.; Forster, M.; Schollmeyer, D.; Laufer,

1144   S. A.; Koch, P., Design, Synthesis and Biological Evaluation of 7-Chloro-9H-pyrimido[4,5-

1145   b]indole-based Glycogen Synthase Kinase-3β Inhibitors. *Molecules* **2019**, *24*, 2331.

1146   9.   Ball, P., Water is an active matrix of life for cell and molecular biology. *Proceedings of*

1147   *the National Academy of Sciences* **2017**, *114*, 13327-13335.

1148   10.   Snyder, P. W.; Mecinović, J.; Moustakas, D. T.; Thomas, S. W.; Harder, M.; Mack, E.

1149   T.; Lockett, M. R.; Héroux, A.; Sherman, W.; Whitesides, G. M., Mechanism of the

1150   hydrophobic effect in the biomolecular recognition of arylsulfonamides by carbonic anhydrase.

1151   *Proceedings of the National Academy of Sciences* **2011**, *108*, 17889-17894.

1152   11.   Breiten, B.; Lockett, M. R.; Sherman, W.; Fujita, S.; Al-Sayah, M.; Lange, H.; Bowers,

1153   C. M.; Heroux, A.; Krilov, G.; Whitesides, G. M., Water Networks Contribute to

1154   Enthalpy/Entropy Compensation in Protein–Ligand Binding. *Journal of the American*

1155   *Chemical Society* **2013**, *135*, 15579-15584.

1156   12.   Michel, J.; Tirado-Rives, J.; Jorgensen, W. L., Energetics of Displacing Water

1157   Molecules from Protein Binding Sites: Consequences for Ligand Optimization. *Journal of the*

1158   *American Chemical Society* **2009**, *131*, 15403-15411.

1159   13.   Spyrakis, F.; Ahmed, M. H.; Bayden, A. S.; Cozzini, P.; Mozzarelli, A.; Kellogg, G. E.,

1160   The Roles of Water in the Protein Matrix: A Largely Untapped Resource for Drug Discovery.

1161   *Journal of Medicinal Chemistry* **2017**, *60*, 6781-6827.

1162   14.   Ladbury, J. E., Just add water! The effect of water on the specificity of protein-ligand

1163   binding sites and its potential application to drug design. *Chemistry & Biology* **1996**, *3*, 973-

1164   980.

1165   15.   Maurer, M.; Oostenbrink, C., Water in protein hydration and ligand recognition. *Journal*

1166   *of Molecular Recognition* **2019**, *32*, e2810.

1167   16.   Darby, J. F.; Hopkins, A. P.; Shimizu, S.; Roberts, S. M.; Brannigan, J. A.; Turkenburg,

1168   J. P.; Thomas, G. H.; Hubbard, R. E.; Fischer, M., Water Networks Can Determine the Affinity

1169   of Ligand Binding to Proteins. *Journal of the American Chemical Society* **2019**, *141*, 15818-

1170   15826.

1171   17.   Krimmer, S. G.; Cramer, J.; Betz, M.; Fridh, V.; Karlsson, R.; Heine, A.; Klebe, G.,

1172   Rational Design of Thermodynamic and Kinetic Binding Profiles by Optimizing Surface Water

1173   Networks Coating Protein-Bound Ligands. *Journal of Medicinal Chemistry* **2016**, *59*, 10530-

1174   10548.

1175   18.   Nittinger, E.; Gibbons, P.; Eigenbrot, C.; Davies, D. R.; Maurer, B.; Yu, C. L.; Kiefer,

1176   J. R.; Kuglstatter, A.; Murray, J.; Ortwine, D. F.; Tang, Y.; Tsui, V., Water molecules in

1177   protein–ligand interfaces. Evaluation of software tools and SAR comparison. *Journal of*

1178   *Computer-Aided Molecular Design* **2019**, *33*, 307-330.

1179   19.   Bucher, D.; Stouten, P.; Triballeau, N., Shedding Light on Important Waters for Drug

1180   Design: Simulations versus Grid-Based Methods. *Journal of Chemical Information and*

1181   *Modeling* **2018**, *58*, 692-699.

1182   20.   Abel, R.; Young, T.; Farid, R.; Berne, B. J.; Friesner, R. A., Role of the Active-Site

1183   Solvent in the Thermodynamics of Factor Xa Ligand Binding. *Journal of the American*

1184   *Chemical Society* **2008**, *130*, 2817-2831.

1185   21.   Young, T.; Abel, R.; Kim, B.; Berne, B. J.; Friesner, R. A., Motifs for molecular

1186   recognition exploiting hydrophobic enclosure in protein–ligand binding. *Proceedings of the*

1187   *National Academy of Sciences* **2007**, *104*, 808-813.

1188   22.   Horbert, R.; Pinchuk, B.; Johannes, E.; Schlosser, J.; Schmidt, D.; Cappel, D.; Totzke,

1189   F.; Schächtele, C.; Peifer, C., Optimization of Potent DFG-in Inhibitors of Platelet Derived

1190   Growth Factor Receptorβ (PDGF-Rβ) Guided by Water Thermodynamics. *Journal of*

1191   *Medicinal Chemistry* **2015**, *58*, 170-182.

1192   23.   Pearlstein, R. A.; Sherman, W.; Abel, R., Contributions of water transfer energy to

1193   protein-ligand association and dissociation barriers: Watermap analysis of a series of p38α

1194   MAP kinase inhibitors. *Proteins: Structure, Function, and Bioinformatics* **2013**, *81*, 1509-1526.

1195   24.   Myrianthopoulos, V.; Kritsanida, M.; Gaboriaud-Kolar, N.; Magiatis, P.; Ferandin, Y.;

1196   Durieu, E.; Lozach, O.; Cappel, D.; Soundararajan, M.; Filippakopoulos, P.; Sherman, W.;

1197   Knapp, S.; Meijer, L.; Mikros, E.; Skaltsounis, A.-L., Novel Inverse Binding Mode of Indirubin

1198   Derivatives Yields Improved Selectivity for DYRK Kinases. *ACS Medicinal Chemistry Letters*

1199   **2013**, *4*, 22-26.

1200   25.   Robinson, D. D.; Sherman, W.; Farid, R., Understanding Kinase Selectivity Through

1201   Energetic Analysis of Binding Site Waters. *ChemMedChem* **2010**, *5*, 618-627.

1202   26.   Robinson, D.; Bertrand, T.; Carry, J.-C.; Halley, F.; Karlsson, A.; Mathieu, M.; Minoux,

1203   H.; Perrin, M.-A.; Robert, B.; Schio, L.; Sherman, W., Differential Water Thermodynamics

1204   Determine PI3K-Beta/Delta Selectivity for Solvent-Exposed Ligand Modifications. *Journal of*

1205   *Chemical Information and Modeling* **2016**, *56*, 886-894.

1206   27.   Asquith, C. R. M.; Tizzard, G. J.; Bennett, J. M.; Wells, C. I.; Elkins, J. M.; Willson, T.

1207   M.; Poso, A.; Laitinen, T., Targeting the Water Network in Cyclin G-Associated Kinase (GAK)

1208   with 4-Anilino-quin(az)oline Inhibitors. *ChemMedChem* **2020**, *15*, 1200-1215.

1209   28.   Hamaguchi, H.; Amano, Y.; Moritomo, A.; Shirakami, S.; Nakajima, Y.; Nakai, K.;

1210   Nomura, N.; Ito, M.; Higashi, Y.; Inoue, T., Discovery and structural characterization of

1211   peficitinib (ASP015K) as a novel and potent JAK inhibitor. *Bioorganic & Medicinal Chemistry*

1212   **2018**, *26*, 4971-4983.

1213   29.   Lee, K. L.; Ambler, C. M.; Anderson, D. R.; Boscoe, B. P.; Bree, A. G.; Brodfuehrer, J.

1214   I.; Chang, J. S.; Choi, C.; Chung, S.; Curran, K. J.; Day, J. E.; Dehnhardt, C. M.; Dower, K.;

1215   Drozda, S. E.; Frisbie, R. K.; Gavrin, L. K.; Goldberg, J. A.; Han, S.; Hegen, M.; Hepworth,

1216   D.; Hope, H. R.; Kamtekar, S.; Kilty, I. C.; Lee, A.; Lin, L.-L.; Lovering, F. E.; Lowe, M. D.;

1217   Mathias, J. P.; Morgan, H. M.; Murphy, E. A.; Papaioannou, N.; Patny, A.; Pierce, B. S.; Rao,

1218   V. R.; Saiah, E.; Samardjiev, I. J.; Samas, B. M.; Shen, M. W. H.; Shin, J. H.; Soutter, H. H.;

1219   Strohbach, J. W.; Symanowicz, P. T.; Thomason, J. R.; Trzupek, J. D.; Vargas, R.; Vincent, F.;

1220   Yan, J.; Zapf, C. W.; Wright, S. W., Discovery of Clinical Candidate 1-{[(2S,3S,4S)-3-Ethyl-

1221   4-fluoro-5-oxopyrrolidin-2-yl]methoxy}-7-methoxyisoquinoline-6-carboxamide   (PF-

1222   06650833), a Potent, Selective Inhibitor of Interleukin-1 Receptor Associated Kinase 4

1223   (IRAK4), by Fragment-Based Drug Design. *Journal of Medicinal Chemistry* **2017**, *60*, 5521-

1224   5542.

1225   30.   Matricon, P.; Suresh, R. R.; Gao, Z.-G.; Panel, N.; Jacobson, K. A.; Carlsson, J., Ligand

1226   design by targeting a binding site water. *Chemical Science* **2021**.

1227   31.   Andreev, S.; Pantsar, T.; El-Gokha, A.; Ansideri, F.; Kudolo, M.; Anton, D. B.; Sita,

1228   G.; Romasco, J.; Geibel, C.; Lämmerhofer, M.; Goettert, M. I.; Tarozzi, A.; Laufer, S. A.; Koch,

1229   P., Discovery and Evaluation of Enantiopure 9H-pyrimido[4,5-b]indoles as Nanomolar GSK-

1230   3β Inhibitors with Improved Metabolic Stability. *International Journal of Molecular Sciences*

1231   **2020**, *21*, 7823.

1232   32.   Zegzouti, H.; Zdanovskaia, M.; Hsiao, K.; Goueli, S. A., ADP-Glo: A Bioluminescent

1233   and Homogeneous ADP Monitoring Assay for Kinases. *ASSAY and Drug Development*

1234   *Technologies* **2009**, *7*, 560-572.

1235   33.   Ghose, A. K.; Viswanadhan, V. N.; Wendoloski, J. J., Prediction of Hydrophobic

1236   (Lipophilic) Properties of Small Organic Molecules Using Fragmental Methods: An Analysis

1237   of ALOGP and CLOGP Methods. *The Journal of Physical Chemistry A* **1998**, *102*, 3762-3772.

1238   34.   Hopkins, A. L.; Keserü, G. M.; Leeson, P. D.; Rees, D. C.; Reynolds, C. H., The role of

1239   ligand efficiency metrics in drug discovery. *Nature Reviews Drug Discovery* **2014**, *13*, 105-

1240   121.

1241   35.   Desroy, N.; Housseman, C.; Bock, X.; Joncour, A.; Bienvenu, N.; Cherel, L.;

1242   Labeguere, V.; Rondet, E.; Peixoto, C.; Grassot, J.-M.; Picolet, O.; Annoot, D.; Triballeau, N.;

1243   Monjardet, A.; Wakselman, E.; Roncoroni, V.; Le Tallec, S.; Blanque, R.; Cottereaux, C.;

1244   Vandervoort, N.; Christophe, T.; Mollat, P.; Lamers, M.; Auberval, M.; Hrvacic, B.; Ralic, J.;

1245   Oste, L.; van der Aar, E.; Brys, R.; Heckmann, B., Discovery of 2-[[2-Ethyl-6-[4-[2-(3-

1246   hydroxyazetidin-1-yl)-2-oxoethyl]piperazin-1-yl]-8-methylimidazo[1,2-a]pyridin-3-

1247   yl]methylamino]-4-(4-fluorophenyl)thiazole-5-carbonitrile (GLPG1690), a First-in-Class

1248   Autotaxin Inhibitor Undergoing Clinical Evaluation for the Treatment of Idiopathic Pulmonary

1249   Fibrosis. *Journal of Medicinal Chemistry* **2017**, *60*, 3580-3590.

1250   36.   Kung, P.-P.; Sinnema, P.-J.; Richardson, P.; Hickey, M. J.; Gajiwala, K. S.; Wang, F.;

1251   Huang, B.; McClellan, G.; Wang, J.; Maegley, K.; Bergqvist, S.; Mehta, P. P.; Kania, R., Design

1252   strategies to target crystallographic waters applied to the Hsp90 molecular chaperone.

1253   *Bioorganic & Medicinal Chemistry Letters* **2011**, *21*, 3557-3562.

1254   37.   Henzler-Wildman, K.; Kern, D., Dynamic personalities of proteins. *Nature* **2007**, *450*,

1255   964-972.

1256   38.   Pruccoli, L.; Morroni, F.; Sita, G.; Hrelia, P.; Tarozzi, A., Esculetin as a Bifunctional

1257   Antioxidant Prevents and Counteracts the Oxidative Stress and Neuronal Death Induced by

1258   Amyloid Protein in SH-SY5Y Cells. *Antioxidants* **2020**, *9*, 551.

1259   39.   Lochhead, P. A.; Kinstrie, R.; Sibbet, G.; Rawjee, T.; Morrice, N.; Cleghon, V., A

1260   Chaperone-Dependent GSK3β Transitional Intermediate Mediates Activation-Loop

1261   Autophosphorylation. *Molecular Cell* **2006**, *24*, 627-633.

1262   40.   Cole, A.; Frame, S.; Cohen, P., Further evidence that the tyrosine phosphorylation of

1263   glycogen synthase kinase-3 (GSK3) in mammalian cells is an autophosphorylation event.

1264   *Biochem J* **2004**, *377*, 249-255.

1265   41.   Wagner, F. F.; Benajiba, L.; Campbell, A. J.; Weïwer, M.; Sacher, J. R.; Gale, J. P.;

1266   Ross, L.; Puissant, A.; Alexe, G.; Conway, A.; Back, M.; Pikman, Y.; Galinsky, I.; DeAngelo,

1267   D. J.; Stone, R. M.; Kaya, T.; Shi, X.; Robers, M. B.; Machleidt, T.; Wilkinson, J.; Hermine,

1268   O.; Kung, A.; Stein, A. J.; Lakshminarasimhan, D.; Hemann, M. T.; Scolnick, E.; Zhang, Y.-

1269   L.; Pan, J. Q.; Stegmaier, K.; Holson, E. B., Exploiting an Asp-Glu "switch" in glycogen

1270 synthase kinase 3 to design paralog-selective inhibitors for use in acute myeloid leukemia.

1271 *Science Translational Medicine* **2018**, *10*, eaam8460.

1272 42. Tarozzi, A.; Morroni, F.; Merlicco, A.; Hrelia, S.; Angeloni, C.; Cantelli-Forti, G.;

1273 Hrelia, P., Sulforaphane as an inducer of glutathione prevents oxidative stress-induced cell

1274 death in a dopaminergic-like neuroblastoma cell line. *Journal of Neurochemistry* **2009**, *111*,

1275 1161-1171.

1276 43. Eid, S.; Turk, S.; Volkamer, A.; Rippmann, F.; Fulle, S., KinMap: a web-based tool for

1277 interactive navigation through human kinome data. *BMC Bioinformatics* **2017**, *18*, 16.

1278 44. Young, J. R.; Lim, J.; Machacek, M. R.; Taoka, B. M.; Otte, R. D. Inhibitors of Janus

1279 Kinases. WO2009075830, 2009.

1280 45. Senecal, T. D.; Shu, W.; Buchwald, S. L., A General, Practical Palladium-Catalyzed

1281 Cyanation of (Hetero)Aryl Chlorides and Bromides. *Angewandte Chemie International Edition*

1282 **2013**, *52*, 10035-10039.

1283 46. Heider, F.; Pantsar, T.; Kudolo, M.; Ansideri, F.; De Simone, A.; Pruccoli, L.;

1284 Schneider, T.; Goettert, M. I.; Tarozzi, A.; Andrisano, V.; Laufer, S. A.; Koch, P.,

1285 Pyridinylimidazoles as GSK3β Inhibitors: The Impact of Tautomerism on Compound Activity

1286 via Water Networks. *ACS Medicinal Chemistry Letters* **2019**, *10*, 1407-1414.

1287 47. Kabsch, W., XDS. *Acta Crystallographica Section D* **2010**, *66*, 125-132.

1288 48. Evans, P., An introduction to data reduction: space-group determination, scaling and

1289 intensity statistics. *Acta Crystallographica Section D* **2011**, *67*, 282-292.

1290 49. McCoy, A. J.; Grosse-Kunstleve, R. W.; Adams, P. D.; Winn, M. D.; Storoni, L. C.;

1291 Read, R. J., Phaser crystallographic software. *Journal of Applied Crystallography* **2007**, *40*,

1292 658-674.

1293 50. Winn, M. D.; Ballard, C. C.; Cowtan, K. D.; Dodson, E. J.; Emsley, P.; Evans, P. R.;

1294 Keegan, R. M.; Krissinel, E. B.; Leslie, A. G. W.; McCoy, A.; McNicholas, S. J.; Murshudov,

1295 G. N.; Pannu, N. S.; Potterton, E. A.; Powell, H. R.; Read, R. J.; Vagin, A.; Wilson, K. S.,

1296   Overview of the CCP4 suite and current developments. *Acta Crystallographica Section D* **2011**,

1297   *67*, 235-242.

1298   51.   Tesch, R.; Becker, C.; Müller, M. P.; Beck, M. E.; Quambusch, L.; Getlik, M.; Lategahn,

1299   J.; Uhlenbrock, N.; Costa, F. N.; Polêto, M. D.; Pinheiro, P. d. S. M.; Rodrigues, D. A.;

1300   Sant'Anna, C. M. R.; Ferreira, F. F.; Verli, H.; Fraga, C. A. M.; Rauh, D., An Unusual

1301   Intramolecular Halogen Bond Guides Conformational Selection. *Angewandte Chemie*

1302   *International Edition* **2018**, *57*, 9970-9975.

1303   52.   Murshudov, G. N.; Skubak, P.; Lebedev, A. A.; Pannu, N. S.; Steiner, R. A.; Nicholls,

1304   R. A.; Winn, M. D.; Long, F.; Vagin, A. A., REFMAC5 for the refinement of macromolecular

1305   crystal structures. *Acta Crystallographica Section D* **2011**, *67*, 355-367.

1306   53.   Liebschner, D.; Afonine, P. V.; Baker, M. L.; Bunkoczi, G.; Chen, V. B.; Croll, T. I.;

1307   Hintze, B.; Hung, L. W.; Jain, S.; McCoy, A. J.; Moriarty, N. W.; Oeffner, R. D.; Poon, B. K.;

1308   Prisant, M. G.; Read, R. J.; Richardson, J. S.; Richardson, D. C.; Sammito, M. D.; Sobolev, O.

1309   V.; Stockwell, D. H.; Terwilliger, T. C.; Urzhumtsev, A. G.; Videau, L. L.; Williams, C. J.;

1310   Adams, P. D., Macromolecular structure determination using X-rays, neutrons and electrons:

1311   recent developments in Phenix. *Acta Crystallographica. Section D, Structural Biology* **2019**,

1312   *75*, 861-877.

1313   54.   Emsley, P.; Lohkamp, B.; Scott, W. G.; Cowtan, K., Features and development of Coot.

1314   *Acta Crystallographica Section D* **2010**, *66*, 486-501.

1315   55.   Chen, V. B.; Arendall, W. B., III; Headd, J. J.; Keedy, D. A.; Immormino, R. M.; Kapral,

1316   G. J.; Murray, L. W.; Richardson, J. S.; Richardson, D. C., MolProbity: all-atom structure

1317   validation for macromolecular crystallography. *Acta Crystallographica Section D* **2010**, *66*, 12-

1318   21.

1319   56.   Roos, K.; Wu, C.; Damm, W.; Reboul, M.; Stevenson, J. M.; Lu, C.; Dahlgren, M. K.;

1320   Mondal, S.; Chen, W.; Wang, L.; Abel, R.; Friesner, R. A.; Harder, E. D., OPLS3e: Extending

1321 Force Field Coverage for Drug-Like Small Molecules. *Journal of Chemical Theory and*

1322 *Computation* **2019**, *15*, 1863-1874.

1323 57.   Madhavi Sastry, G.; Adzhigirey, M.; Day, T.; Annabhimoju, R.; Sherman, W., Protein

1324 and ligand preparation: parameters, protocols, and influence on virtual screening enrichments.

1325 *Journal of Computer-Aided Molecular Design* **2013**, *27*, 221-234.

1326 58.   Bochevarov, A. D.; Watson, M. A.; Greenwood, J. R.; Philipp, D. M.,

1327 Multiconformation, Density Functional Theory-Based pKa Prediction in Application to Large,

1328 Flexible Organic Molecules with Diverse Functional Groups. *Journal of Chemical Theory and*

1329 *Computation* **2016**, *12*, 6001-6019.

1330 59.   Bowers, K. J.; Chow, E.; Xu, H.; Dror, R. O.; Eastwood, M. P.; Gregersen, B. A.;

1331 Klepeis, J. L.; Kolossvary, I.; Moraes, M. A.; Sacerdoti, F. D.; Salmon, J. K.; Shan, Y.; Shaw,

1332 D. E., Scalable algorithms for molecular dynamics simulations on commodity clusters. In

1333 *Proceedings of the 2006 ACM/IEEE conference on Supercomputing*, ACM: Tampa, Florida,

1334 2006; p 84.

1335 60.   Pantsar, T., KRAS(G12C)–AMG 510 interaction dynamics revealed by all-atom

1336 molecular dynamics simulations. *Scientific Reports* **2020**, *10*, 11992.

1337 61.   Jorgensen, W. L.; Chandrasekhar, J.; Madura, J. D.; Impey, R. W.; Klein, M. L.,

1338 Comparison of simple potential functions for simulating liquid water. *The Journal of Chemical*

1339 *Physics* **1983**, *79*, 926-935.

1340

1341

1342

1343

1344
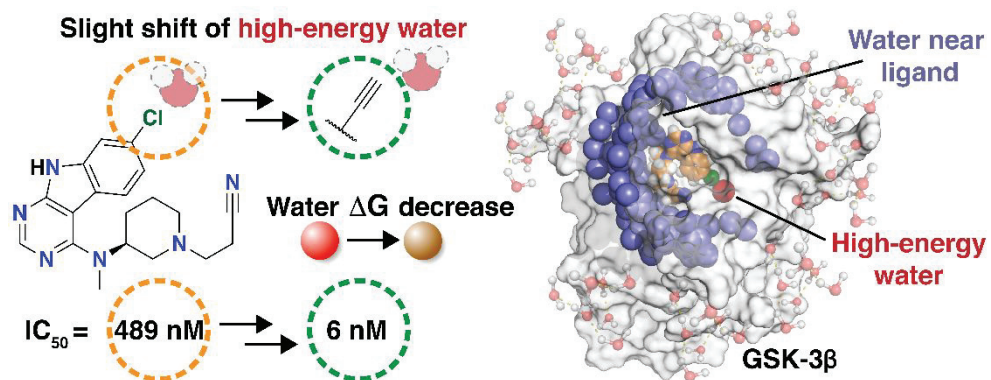
1
2
3 1345 **TOC graphic**
4
5 1346
6
7
8
9
10
11
12
13
14
15
16
17
18 1347
19
20 1348

Supporting Information

Addressing a Trapped High-Energy Water: Design and Synthesis of Highly Potent 9*H*-pyrimido[4,5-*b*]indole-based GSK-3β inhibitors.

Stanislav Andreev [1,‡], Tatu Pantsar [1,2,‡], Roberta Tesch [3,4], Niclas Kahlke [1], Ahmed El-Gokha [1,5], Francesco Ansideri [1], Lukas Grätz [6], Jenny Romasco [7], Giulia Sita [8], Christian Geibel [9], Michael Lämmerhofer [9], Andrea Tarozzi [7], Stefan Knapp [3,4], Stefan A. Laufer [1,10] and Pierre Koch [1,6,*]

[1] Institute of Pharmaceutical Sciences, Department of Medicinal and Pharmaceutical Chemistry, Eberhard Karls University Tübingen, Auf der Morgenstelle 8, 72076 Tübingen, Germany

[2] School of Pharmacy, Faculty of Health Sciences, University of Eastern Finland, P.O. Box 1627, 70211 Kuopio, Finland

[3] Institute for Pharmaceutical Chemistry, Johann Wolfgang Goethe-University, Max-von-Laue-Str. 9, 60438 Frankfurt am Main, Germany

[4] Structural Genomics Consortium, Buchmann Institute for Life Sciences, Johann Wolfgang Goethe-University, Max-von-Laue-Str. 15, 60438 Frankfurt am Main, Germany

[5] Chemistry Department, Faculty of Science, Menoufia University, Gamal Abdel-Nasser Street, 32511 Shebin El-Kom, Egypt

[6] Department of Pharmaceutical/Medicinal Chemistry II, Institute of Pharmacy, University of Regensburg, Universitätsstraße 31, 93053 Regensburg, Germany

[7] Department for Life Quality Studies, Alma Mater Studiorum, University of Bologna, Corso D'Augusto 237, 47921 Rimini, Italy

[8] Department of Pharmacy and Biotechnology, Alma Mater Studiorum, University of Bologna, Via Irnerio 48, 40126 Bologna, Italy

[9] Institute of Pharmaceutical Sciences, Department of Pharmaceutical (Bio-)Analysis, Eberhard Karls University Tübingen, Auf der Morgenstelle 8, 72076 Tübingen, Germany

[10] Tübingen Center for Academic Drug Discovery (TüCAD2), Auf der Morgenstelle 8, 72076 Tübingen, Germany

‡ These authors contributed equally.

* Correspondence: pierre.koch@uni-tuebingen.de, pierre.koch@ur.de; Tel.: +49 941 943-2847.

Table of Contents

ADP Glo™ Kinase Assay Protocol.

The IC$_{50}$-values of the final compounds for GSK-3β were determined in an ADP-Glo™ Kinase assay from Promega (Madison, WI, USA).

The assay was carried out in white, non-treated 384-well plates from Corning (Corning, NY, USA). The experiments were carried out as duplicates or quadruplicates using a concentration of 0.58 ng/μL of recombinant human GSK-3β, 0.2 μg/μL GSK-3 substrate G50-58 (sequence: YRRAAVPPSPSLSRHSSPHQ(pS)EDEEE) and 25 μM ATP in the presence of serial dilutions of the final compounds (six 1:3 or 1:4 dilution steps starting from 10 μM). Two control experiments with uninhibited kinase and blank experiments with ATP/substrate solution were performed and their results were used for the normalization of the raw data.

In detail, GSK-3β was pre-incubated with the final compounds for 10 min at rt. Then substrate/ATP was added to start the reaction, which was run for 1 h at rt. ADP-Glo™ reagent (5 μL, then 1 h incubation) and Kinase detection reagent (10 μL, then 30 min incubation) were subsequently added. The luminescence was finally measured on a FilterMax F5 microplate reader from Molecular Devices LLC (San José, CA, USA) (integration time 500 ms). The raw data was normalized and absolute IC$_{50}$-values were generated with PRISM v.7.03. from GraphPad Software (San Diego, CA, USA).
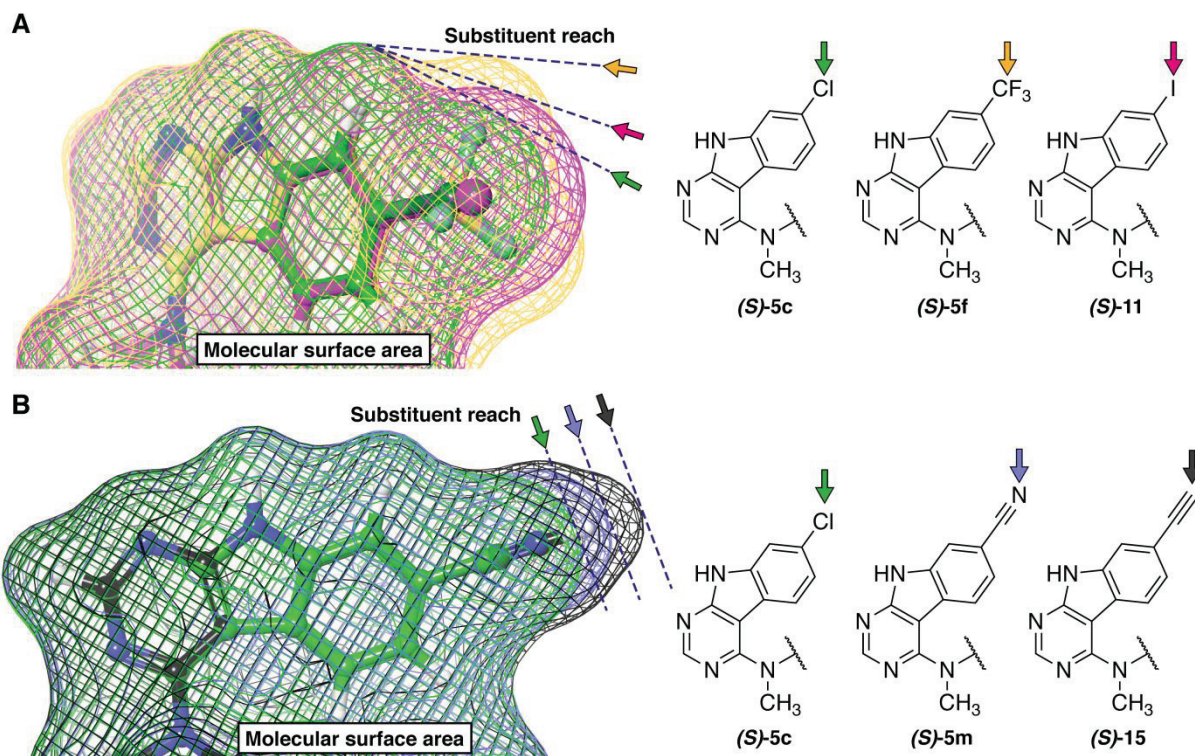
Figure S1. Comparison of molecular surface areas among selected compounds (*S*-isomers) based on Jaguar-optimized geometries. (**A**) Compared to *(S)*-5c, the substituents of *(S)*-5f and *(S)*-11 have considerably larger radii, which will most likely result in a clash with the gatekeeper residue Leu132. (**B**) Compared to *(S)*-5c, the substituents of *(S)*-5m and *(S)*-15 reach deeper towards the HR-I but do not significantly increase the molecular radius (compare to *(S)*-5f and *(S)*-11 in **A**).

S4
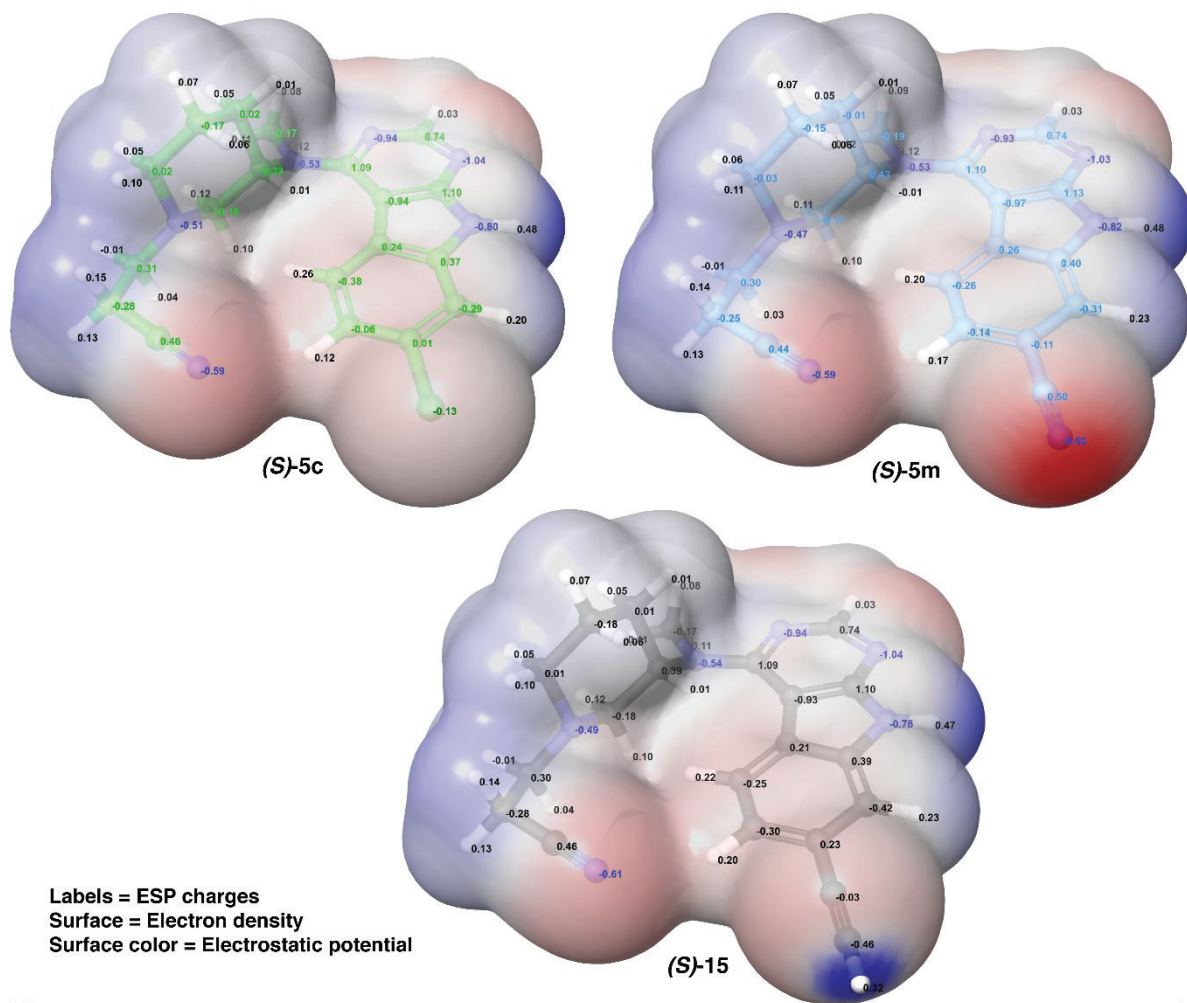
Figure S2. Comparison of the electrostatic potential and electron density of *(S)*-5c, *(S)*-15 and *(S)*-5m. Atomic electrostatic potential (ESP) charges were calculated with Jaguar (6-31G**++, PBF water solvent model).

WaterMap calculated hydration site energies

	● (S)-5c	▲ (S)-5m	■ (S)-15
ΔG	+6.71	+6.21	+7.97
ΔH	+1.73	+1.04	+2.68
-TΔS	+4.98	+5.17	+5.29
H-bonds	1.35	1.24	1.43
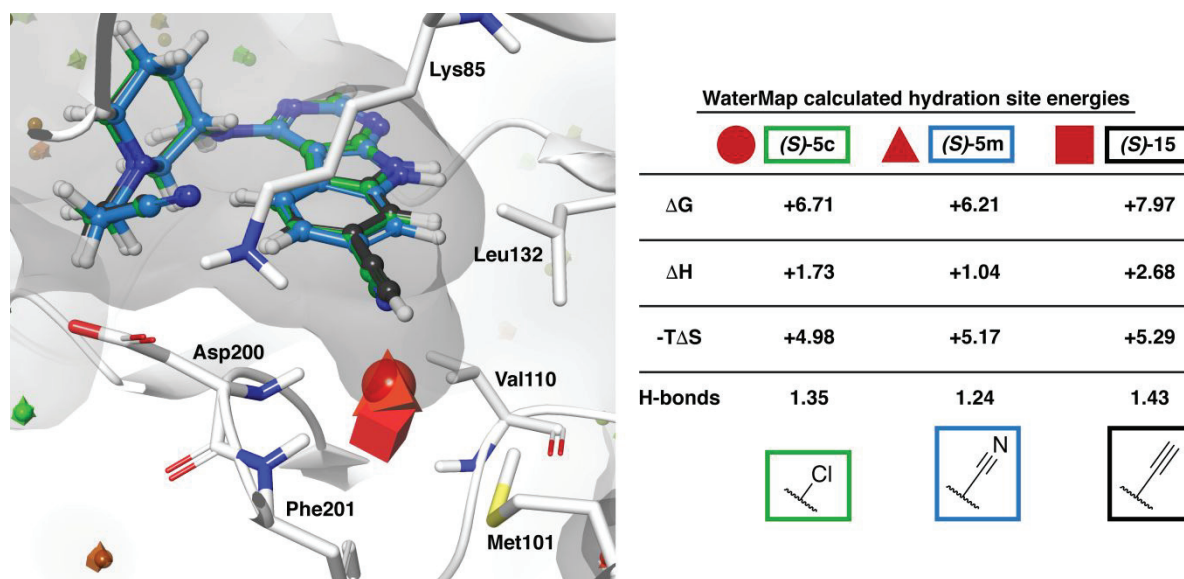
Figure S3. WaterMap analysis of *(S)*-5m and *(S)*-15 based on the *(S)*-5c crystal structure. No shift of the high-energy hydration site is observed with *(S)*-5m (pyramid) compared to *(S)*-5c (sphere), whereas *(S)*-15 clearly shifts the hydration site position (cube). A slightly lower free energy value is observed with *(S)*-5m compared to *(S)*-5c. The shifted hydration site of *(S)*-15 displays an extremely high free energy value.
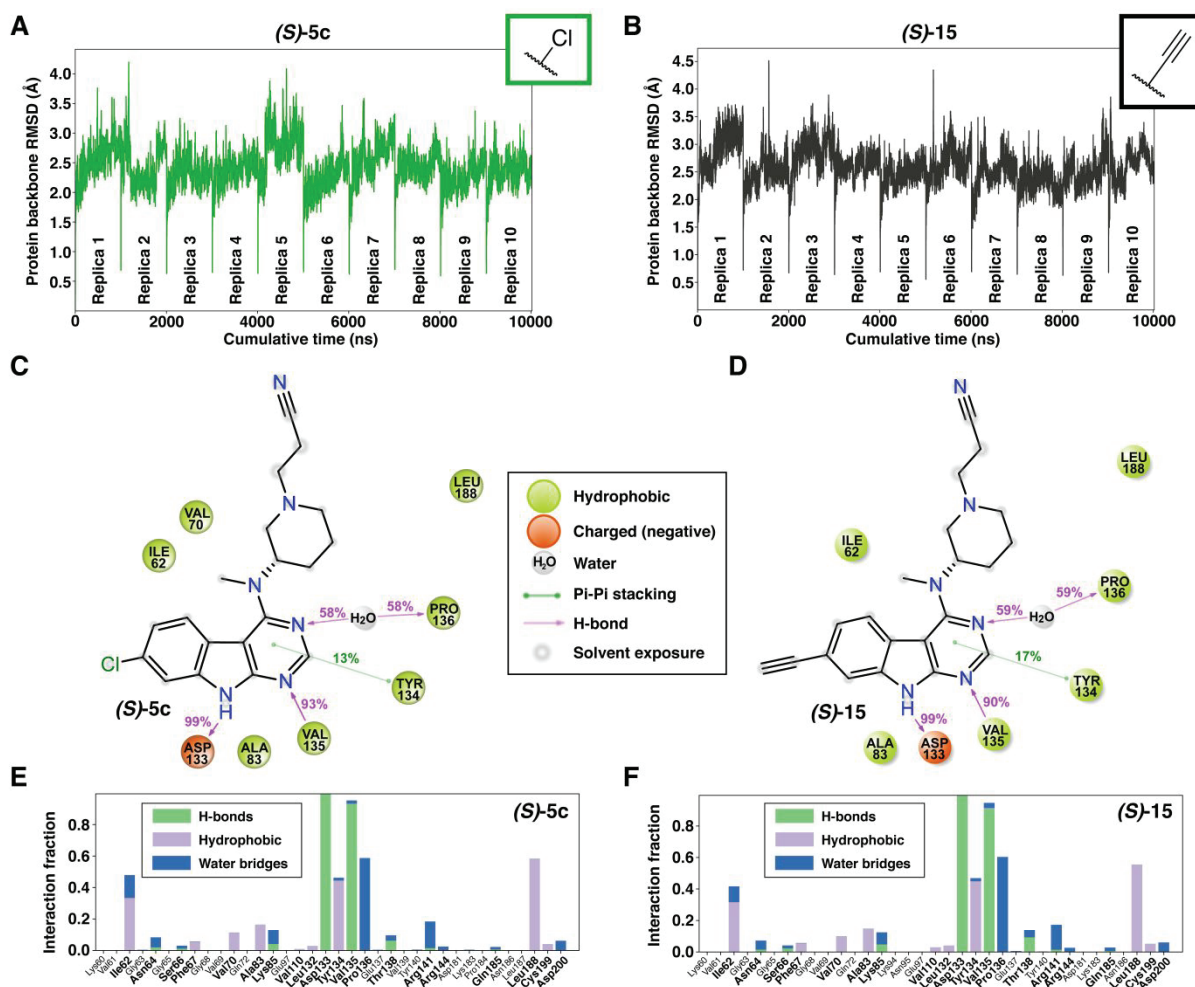
Figure S4. Molecular dynamics simulations of *(S)*-5c and *(S)*-15 suggest no shift in interactions with GSK-3β among these compounds. Root-mean-square deviation (RMSD) values of protein backbone atoms in ten 1 μs replica simulations of *(S)*-5c (**A**) and *(S)*-15 (**B**). Nearly identical interactions and their frequencies are observed with both compounds throughout the simulations. The observed main ligand–protein contacts are shown in the 2D-representations (**C**, **D**) and all contacts in the histogram-plots (**E**, **F**).

NanoBRET target engagement assay.

HEK293T cells (kind gift from Prof. Dr. Wulf Schneider, Institute for Medical Microbiology and Hygiene, University Hospital Regensburg, Germany) were routinely maintained in DMEM (Dulbecco's Modified Eagle's Medium, Sigma-Aldrich, Munich, Germany), supplemented with 10% FCS (Sigma-Aldrich, Munich, Germany), at 37 °C in a water-saturated atmosphere (5% CO_2). All cells were routinely checked for mycoplasma infection using the Venor GeM Mycoplasma Detection Kit (Minerva Biolabs, Berlin, Germany).

HEK293T cells stably expressing NLuc-GSK3β were generated according to a described procedure with the exception that the amount of transfected cDNA was reduced to 1 µg.[1] The cDNA encoding NLuc-GSK3β was kindly provided by Promega (Mannheim, Germany). Stably transfected cells were selected in the presence of 1 mg/mL G418 (Fisher Scientific, Nidderau, Germany). For further cultivation of the stable transfectants, the concentration of G418 was reduced to 600 µg/mL.

After reaching ≈ 80-90% confluency, the stably transfected cells were detached with trypsin/EDTA (0.05%/0.02%, Biochrom, Berlin, Germany) and centrifuged (500 g, 5 min). The cell pellet was resuspended in Leibovitz' L-15 medium (L-15, Fisher Scientific, Nidderau, Germany), supplemented with 5% FCS and 10 mM HEPES (Sigma-Aldrich, Munich, Germany). After adjusting the cell density to 6.25 x 10^5 cells/mL, 80 µL of the cell suspension were added to each well of a white 96-well plate (Brand, Wertheim, Germany) and incubated overnight at 37 °C (no additional CO_2).

On the day of the experiment, serial dilutions of the test compounds (10-fold more concentrated than the final assay concentration) were prepared in L-15 + 10 mM HEPES. The fluorescent tracer K-8 (Promega, Mannheim, Germany) was diluted in DMSO to a concentration of 4 µM (100-fold more concentrated than the final assay concentration). This was further diluted 10-fold using the Tracer Dilution Buffer (Promega, Mannheim, Germany) yielding a dilution, which was 10-fold concentrated to the final assay concentration. Next, 10 µL of the final fluorescent tracer dilution were added to the cells (final concentration of K-8 in the assay: 0.04 µM) and the plate was shaken for 10 seconds (orbital, 250 rpm). After adding 10 µL of the serial dilutions of the respective test compounds, the plate was shaken again for 10 seconds (orbital, 250 rpm). A solvent control (0%) and a positive control, which contained solely the fluorescent tracer K-8 but no test compound, were included in each experiment. After incubating the plate at 37 °C for 2 h, the plate was equilibrated to room temperature for 15 min.

Next, 10 µL of the detection reagent (consisting of 1192 µL L-15 + 6 µL NanoBRET NanoGlo Substrate + 2 µL Extracellular NanoLuc Inhibitor; substrate and inhibitor were purchased from Promega, Mannheim, Germany) were added to each well on the plate and the measurement was started. All measurements were performed at room temperature using a TECAN InfiniteLumi plate reader (TECAN Austria GmbH, Grödig, Austria). The bioluminescence of NLuc was detected using a 460/35 nm band-pass filter. The fluorescence of the fluorescent tracer K-8 was detected using a 610 nm long-pass filter. Integration times were set to 1000 ms for both channels. The raw BRET ratio was calculated by dividing the emission of the fluorescent acceptor (measured with the 610 nm long-pass filter) by the donor luminescence (measured with the 460/35 nm band-pass filter). The obtained data were analyzed by a four-parameter logistic equation (GraphPad Prism 8.0, GraphPad Software Inc., San Diego, CA, USA) yielding IC_{50} values, for which means and the SEM were calculated.

Table S1. Cellular target engagement of compounds **(*S*)-5c**, **(*S*)-15**, **20** and **22** determined by a nanoBRET assay (n = 3).

Compound	(*S*)-5c	(*S*)-15	20	22
$IC_{50} \pm$ SEM [µM]	10.31 ± 1.53	2.51 ± 0.16	5.27 ± 0.24	2.40 ± 0.017
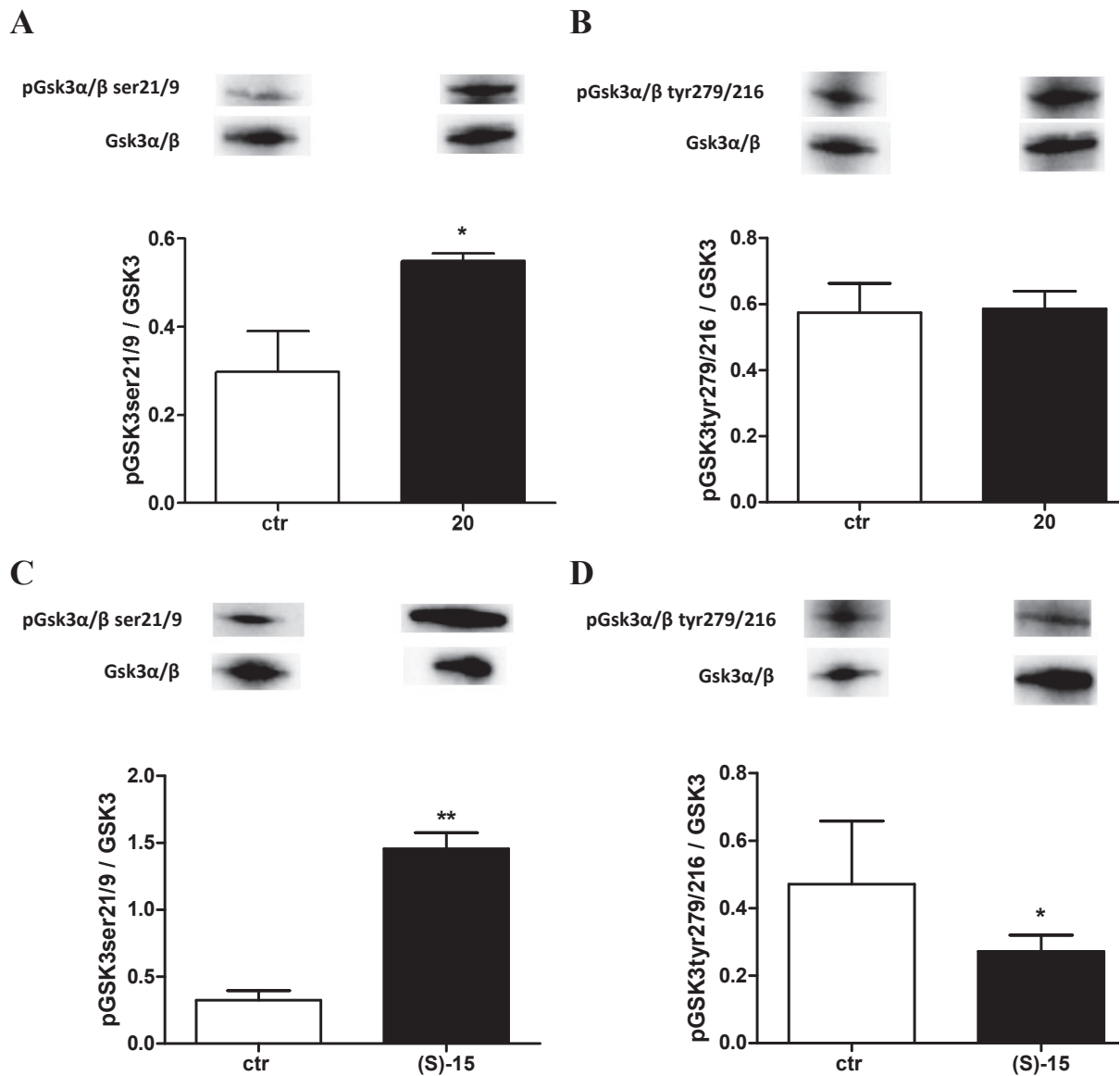
Figure S5. Effects of **20** and *(S)*-**15** on the GSK-3 activity in neuronal SH-SY5Y cells. Cells were incubated with **20** and *(S)*-**15** (5 μM) for 3 h. At the end of incubation, the phosphorylation of GSK3α/β on Ser21/9 (inactive GSK3α/β form) (**A** for **20**, **C** for *(S)*-**15**) and on Tyr279/Tyr216 (active GSK3α/β form) (**B** for **20**, **D** for *(S)*-**15**), respectively, was determined by western blotting. Data are expressed as ratio between phospho-GSK3α/β and total GSK-3 levels normalized against β-Actin and reported as mean ± SD of at least three independent experiments (*p < 0.05 and **p < 0.01 vs untreated cells).
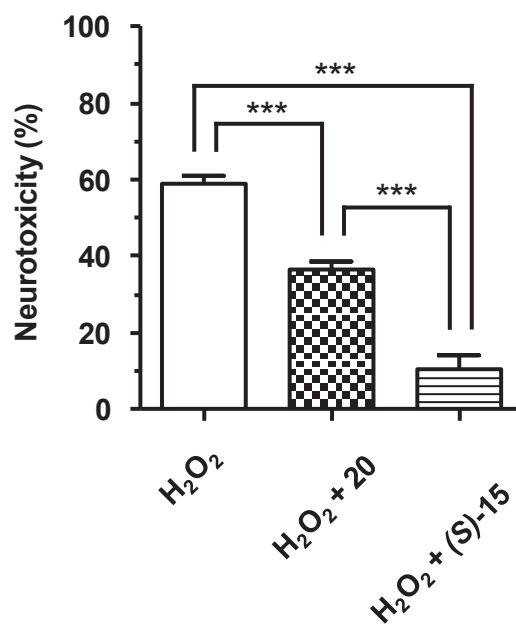
Figure S6. Neuroprotective effects of **20** and *(S)*-**15** against the neurotoxicity induced by H_2O_2 in neuronal SH-SY5Y cells. Cells were incubated with **20** and *(S)*-**15** (5 μM) and H_2O_2 (100 μM) for 1 h and then starved in complete medium for 22 h. The neurotoxicity was then evaluated by MTT assay as reported in materials and methods section. Data are expressed as percentages of neurotoxicity versus untreated cells and reported as mean ± SD of three independent experiments (***$p < 0.001$).

Materials and methods for cellular assays in neuronal SH-SY5Y cells.

Cell cultures. Human neuronal SH-SY5Y cells (Sigma Aldrich, St. Louis, MO, USA) were routinely grown in Dulbecco's modified Eagle's Medium supplemented with 10 % fetal bovine serum, 2 mM L-glutamine, 50 U/mL penicillin and 50 μg/mL streptomycin at 37 °C in a humidified incubator with 5 % CO_2.

Neuronal viability. SH-SY5Y cells were seeded in a 96-well plate at 2×10^4 cells/well, incubated for 24 h and then treated with various concentrations (1.25-40 μM) of **20** and *(S)*-**15** for 24 h. Cell viability, in terms of mitochondrial activity, was evaluated by MTT assay, as previously described.[2]

Neuroprotective activity toward H_2O_2. SH-SY5Y cells were seeded in a 96-well plate at 2×10^4 cells/well, incubated for 24 h and subsequently treated with **20** and *(S)*-**15** (5 μM) and H_2O_2 (100 μM) for 1 h. Then, cells were starved in complete medium for 22 h. The neuroprotective activity was measured by using the MTT assay as previously described.[3] Data are expressed as a percentage of neurotoxicity versus untreated cells.

Western blotting

SH-SY5Y cells were seeded in 60 mm dishes at 2×10^6 cells/dish, incubated for 24 h and subsequently treated with **20** and *(S)*-**15** (5 μM) for 3 h at 37°C in 5% CO_2. At the end of incubation, cells were trypsinized and the cellular pellet was resuspended in complete lysis buffer containing leupeptin (2μg/mL), PMSF (100μg/mL) and cocktail of protease/phosphatase inhibitors (100×). Small amounts were removed for the determination of the protein concentration using the Bradford method. The samples (30 μg proteins) were run on 4-15% SDS polyacrylamide gels (Bio-rad Laboratories S.r.L., Hercules, CA, USA) and electroblotted onto 0.45 μm nitrocellulose membranes. The membranes were incubated at 4 °C overnight with primary antibody recognizing phospho-GSK3α/β (Ser21/9), (1:1000; Cell Signaling Technology Inc, Danvers, MA, USA), or anti-phospho-GSK3(Tyr279/Tyr216), (1:1000; EMD Millipore, Darmstadt, Germany). After washing with TBS-T (TBS +0.05% Tween20), the membranes were incubated with secondary antibodies (1:2000; GE Healthcare). Enhanced chemiluminescence was used to visualized the bands (ECL; Bio-rad Laboratories). The membranes were then reprobed with GSK3α/β, (1:1000; Cell Signaling Technology Inc.). The data were analyzed by densitometry, using Quantity One software (Bio-Rad Laboratories®

S.r.L.). The values were normalized and expressed as mean ± SD of densitometry in each experimental group.

Statistical Analysis. Results are shown as mean ± standard deviation (SD) of three independent experiments. Statistical analysis was performed using Student's t-test and One-way ANOVA (post-hoc Bonferroni test). Differences were considered significant at $p < 0.05$. Analyses were performed using GraphPad PRISM software (version 5.0; GraphPad Software, La Jolla, CA, USA) on a Windows platform.

Kinome screening data for inhibitors *(S)*-15 and 22.

The selectivity of inhibitors *(S)*-15 and **22** was evaluated by the Eurofins KinaseProfiler[TM] (Eurofins Cerep, Celle l'Evescault, France) on 57 human kinases. The percentage residual activity of each kinase at an inhibitor concentration of 500 nM was determined and is reported in Table S2.

Table S2. Selectivity data of *(S)*-15 and **22** on 57 human kinases. Residual kinase activity is reported in percentage. Values below 50% are highlighted in red.

	(S)-15	22
Abl(h)	79	82
ALK(h)	71	90
AMPKα1(h)	103	95
ASK1(h)	94	122
Aurora-A(h)	80	97
CaMKI(h)	86	94
CDK1/cyclinB(h)	113	85
CDK2/cyclinA(h)	77	79
CDK6/cyclinD3(h)	100	85
CDK7/cyclinH/MAT1(h)	86	80
CDK9/cyclin T1(h)	75	76
CHK1(h)	86	99
CK1γ1(h)	123	115
CK2α2(h)	97	105
c-RAF(h)	80	98
DRAK1(h)	85	100
eEF-2K(h)	90	77
EGFR(h)	94	101
EphA5(h)	90	57
EphB4(h)	94	97
Fyn(h)	16	6
GSK3β(h)	3	-5
IGF-1R(h)	99	104
IKKα(h)	103	111
IRAK4(h)	97	118
JAK2(h)	129	79
KDR(h)	22	8
LOK(h)	19	11
Lyn(h)	31	25
MAPKAP-K2(h)	71	111
MEK1(h)	85	77
MLK1(h)	61	39
Mnk2(h)	82	92
MSK2(h)	84	33
MST1(h)	72	67
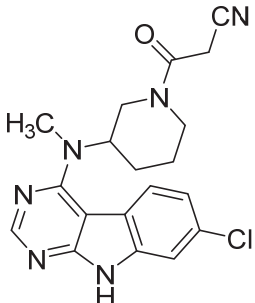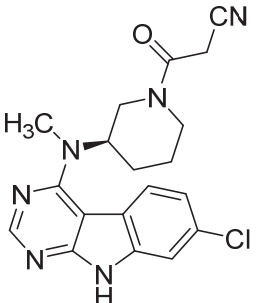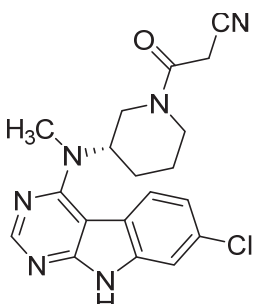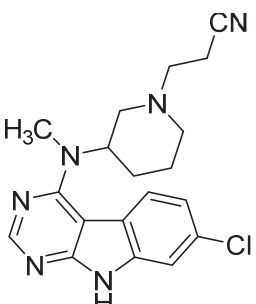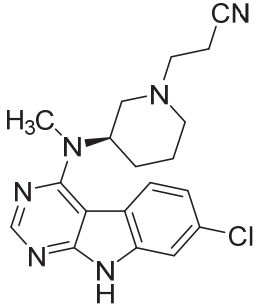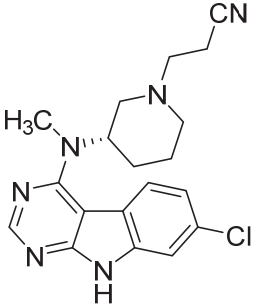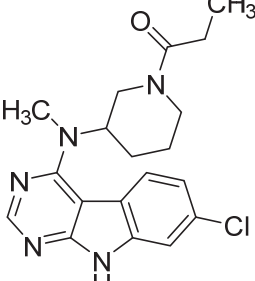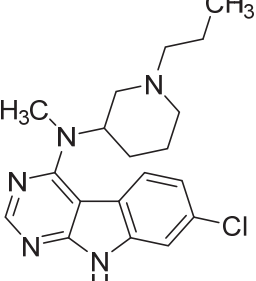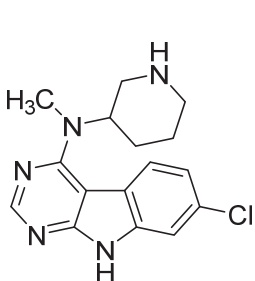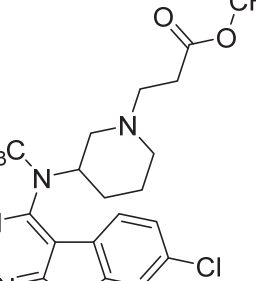
Table S2. continued.

	(S)-15	22
mTOR(h)	93	103
NEK2(h)	94	92
p70S6K(h)	99	79
PAK2(h)	77	83
PDGFRβ(h)	67	72
Pim-1(h)	36	28
PKA(h)	87	89
PKBα(h)	91	94
PKCα(h)	99	87
PKCθ(h)	82	75
PKG1α(h)	84	75
Plk3(h)	109	113
PRAK(h)	91	99
ROCK-I(h)	84	90
Rse(h)	99	78
Rsk1(h)	28	12
SAPK2a(h)	107	126
SRPK1(h)	109	121
TAK1(h)	53	88
PI3 Kinase (p110β/p85α)(h)	98	100
PI3 Kinase (p120γ)(h)	95	99
PI3 Kinase (p110δ/p85α)(h)	68	97
PI3 Kinase (p110α/p85α)(h)	96	100
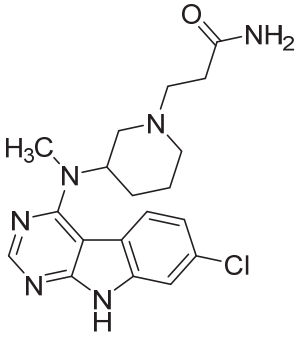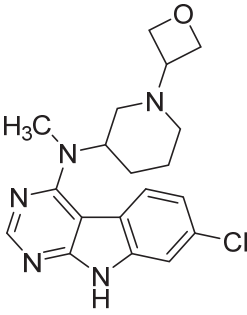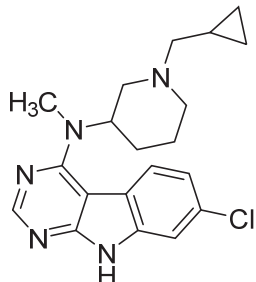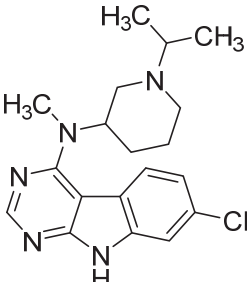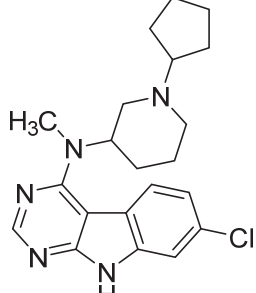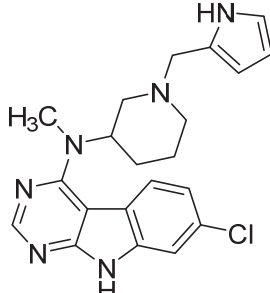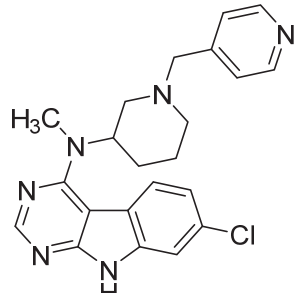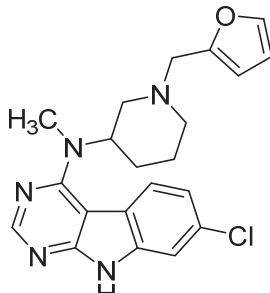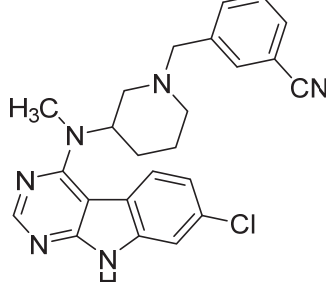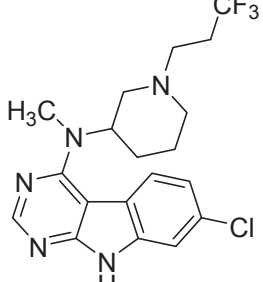
References
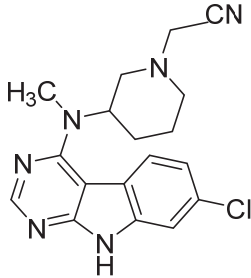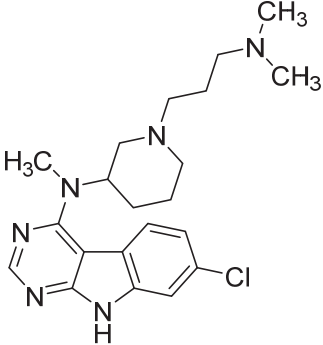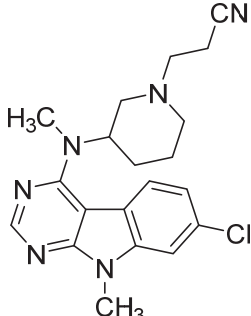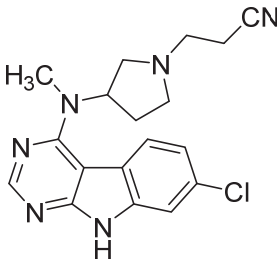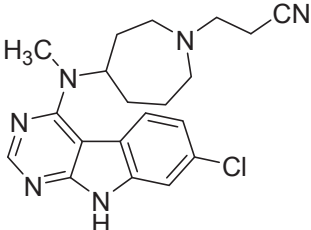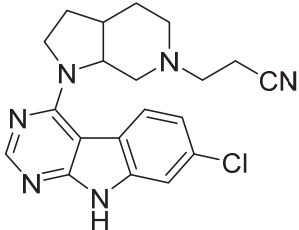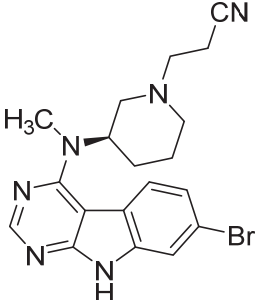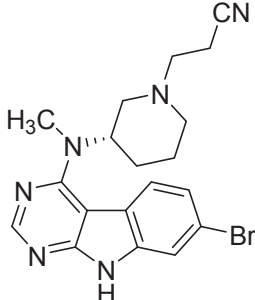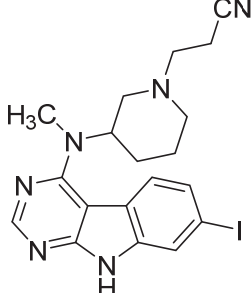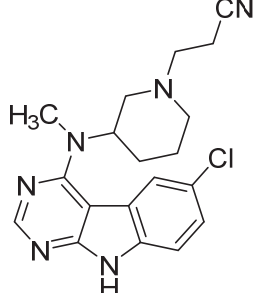
1. Bartole, E., Grätz, L., Littmann, T., Wifling, D., Seibel, U., Buschauer, A. & Bernhardt, G. UR-DEBa242: a Py-5-labeled fluorescent multipurpose probe for investigations on the histamine H$_3$ and H$_4$ receptors. *J. Med. Chem.* **2020**, *63*, 5297-5311.

2. Pruccoli, L., Morroni, F., Sita, G., Hrelia, P., Tarozzi, A. Esculetin as a bifunctional antioxidant prevents and counteracts the oxidative stress and neuronal death induced by amyloid protein in SH-SY5Y cells. *Antioxidants* **2020**, *9*, 551.

3. Tarozzi, A., Morroni, F., Merlicco, A., Hrelia, S., Angeloni, C., Cantelli-Forti, G. Hrelia P. Sulforaphane as an inducer of glutathione prevents oxidative stress-induced cell death in a dopaminergic-like neuroblastoma cell line. *J. Neurochem.* **2009**, *5*, 1161-1171.
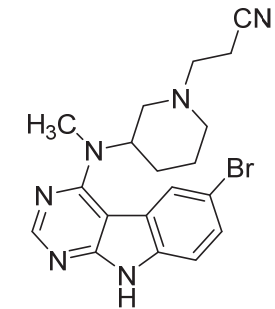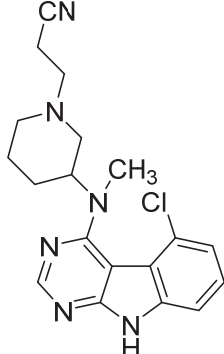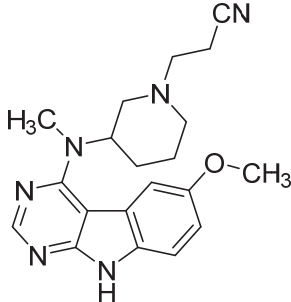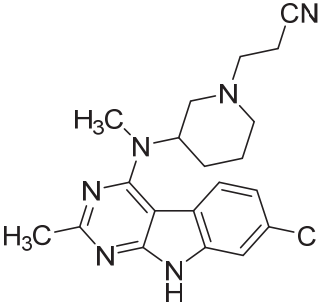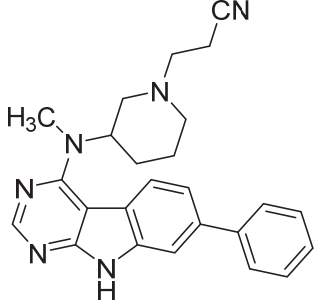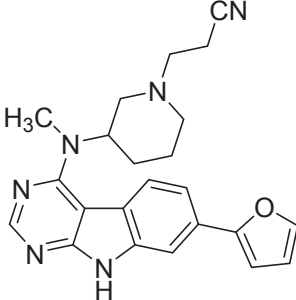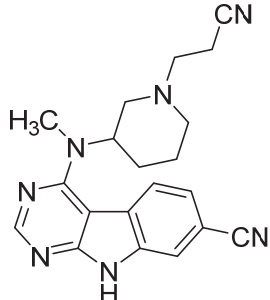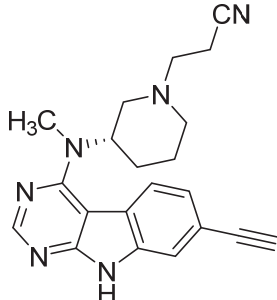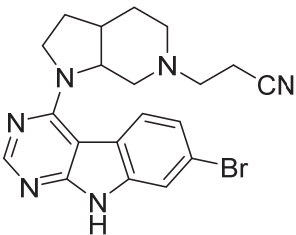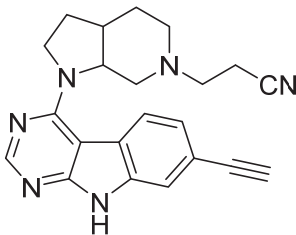
7.4 Testverbindungen
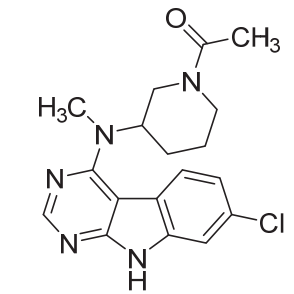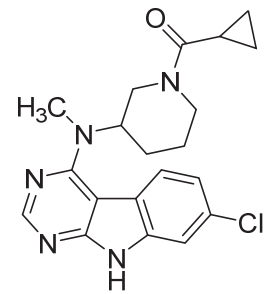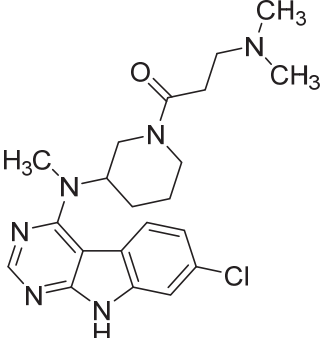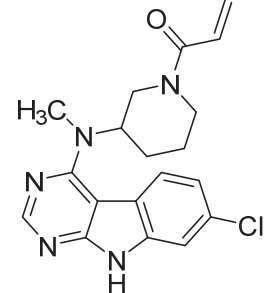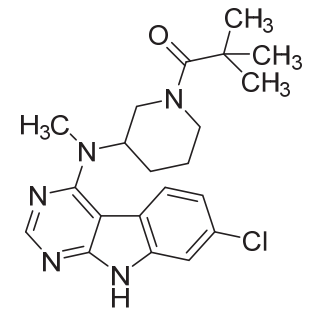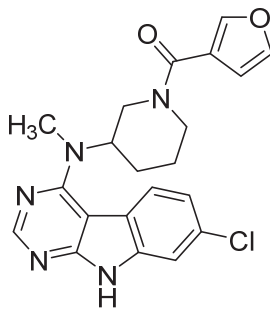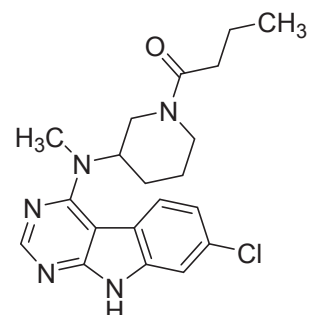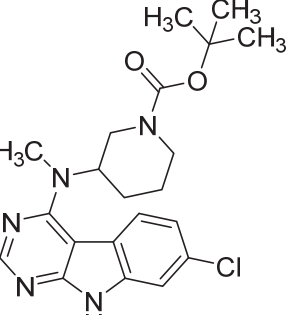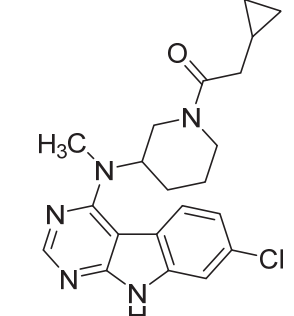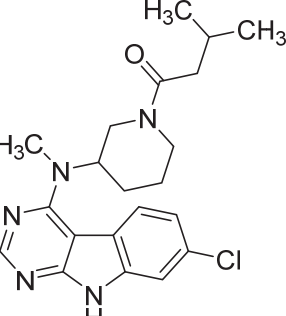
2		***(R)*-2**	
***(S)*-2**		**3**	
***(R)*-3**		***(S)*-3**	
4		**5**	
6		**7**	

8		**9**	
10		**11**	
12		**13**	
14		**15**	
16		**17**	

18	CN, H₃C–N, N, Cl	**19**	CH₃, CH₃, N, H₃C–N, N, Cl
20	CN, H₃C–N, N, Cl, CH₃	**21**	CN, H₃C–N, N, Cl
22	CN, H₃C–N, N, Cl	**23**	CN, N, Cl
(R)-26	CN, H₃C–N, N, Br	**(S)-26**	CN, H₃C–N, N, Br
27	CN, H₃C–N, N, I	**28**	CN, H₃C–N, N, Cl
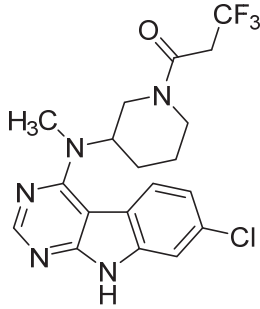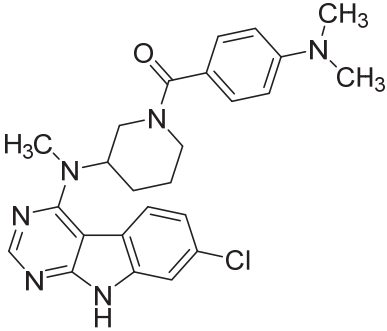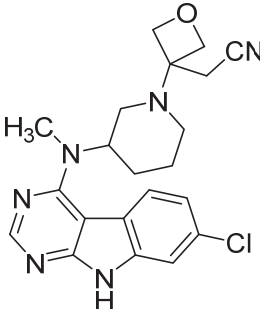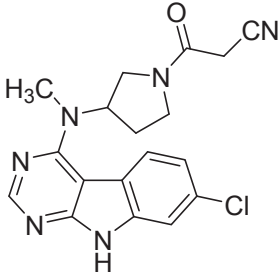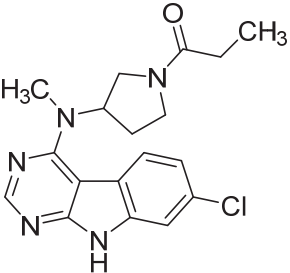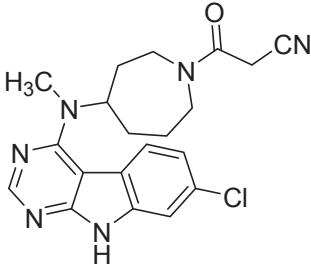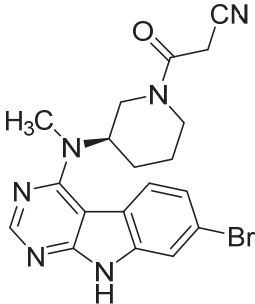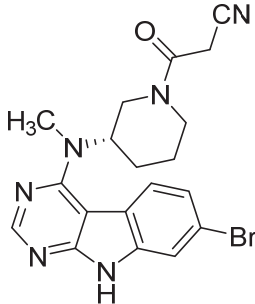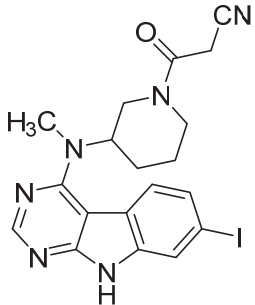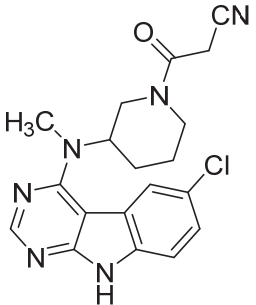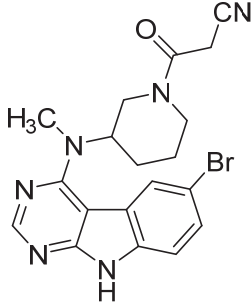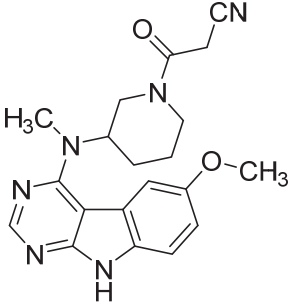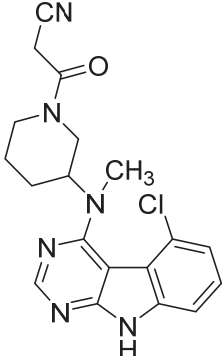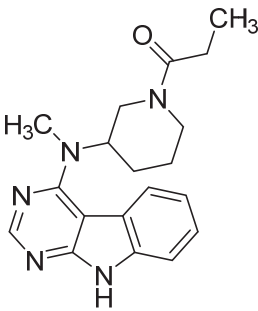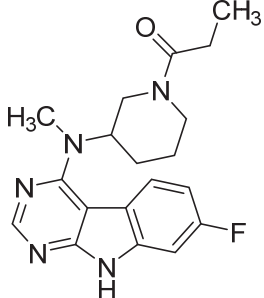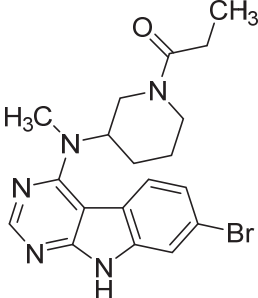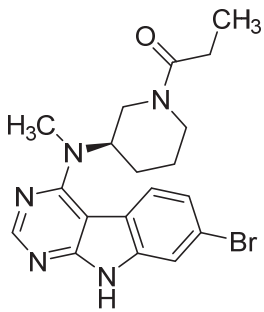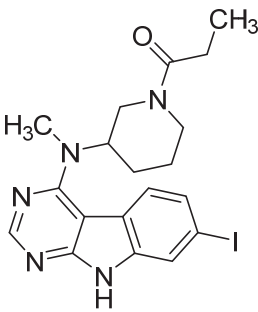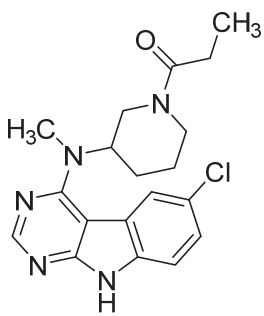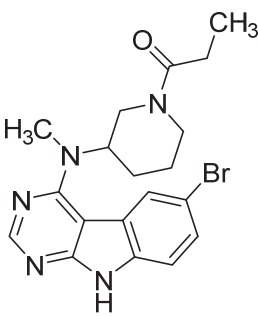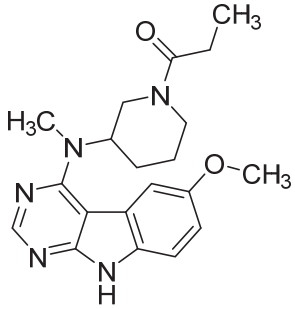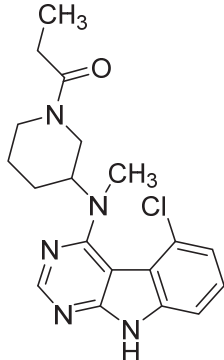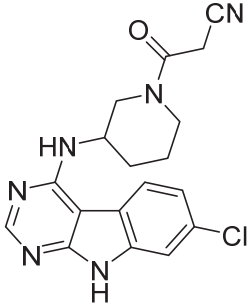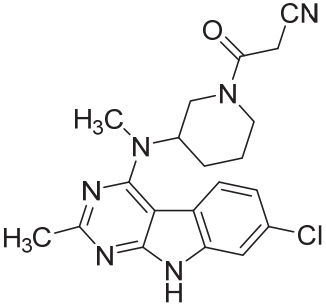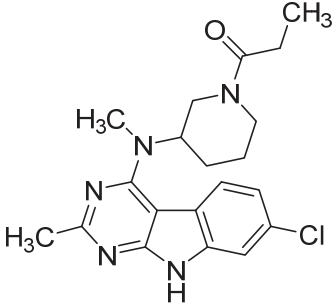
29		**30**	
31		**32**	
33		**34**	
37		*(S)*-**38**	
40		**42**	

43		**44**	
45		**46**	
47		**48**	
49		**50**	
51		**52**	

53		**54**	
55		**56**	
57		**58**	
(R)-62		**(S)-62**	
63		**66**	

67		68	
69		70	
71		72	
(R)-72		73	
74		75	

76		77	
78		79	
80			